

PALACKÝ UNIVERSITY OLOMOUC

FACULTY OF SCIENCE

Department of Physical Chemistry



**Application of green nanocomposites in enhanced oil  
recovery**

*Habilitation Thesis*

Jagar Ali, Ph.D.

Olomouc, 2023

## **Acknowledgment**

I would like to express my thanks and appreciation to the heads of departments of Geology and Physical Chemistry “prof. RNDr. Libor Kvítek and prof. M.Sc. Ondřej Bábek” for their trust and endless support in applying for the habilitation process to grant the associate professorship. I would like to thank all colleagues and faculty members in both departments and faculty of science at Palacky University Olomouc.

I would also like to express thanks to all members of my research group, especially Assistant Prof. Dr. Abbas Khaksar Manshad, Prof. Dr. Kamal Kolo, Assitant Prof. Dr. Karl Steppen and Prof. Dr. S.Mohammed Sajadi who always supported me in exploring new knowledge and innovations in my research works by creating a friendly research atmosphere.

I sincerely thank my family, friends and work colleagues who always supported me throughout my research projects and publications.

**Declaration of originality**

I hereby declare that I am the sole author of the submitted thesis, which, to the best of my knowledge and belief, contains no material previously published by another person, except where due acknowledgement has been made.

The author grants permission to Palacký University Olomouc to store and display this thesis and its electronic version in the university library and on the official website.

In Olomouc, 24.08.2023

Jagar Ali

## Abstract

Conventional chemical enhanced oil recovery (EOR) methods show a promising role in enhancing oil recovery from carbonate and sandstone reservoirs due to decreasing the interfacial tension (IFT), wettability alteration and mobility improvement. Nowadays, application of nanomaterials at different types and shapes in EOR are attracting researchers and companies because of their unique chemical and physical properties. This thesis focuses on the synthesis and application of green nanocomposites (NCs) in EOR. Several NCs were synthesized in a green way using the extracts of different sources of plants and characterized using ultraviolet–visible spectroscopy (UV–Vis), scanning electron microscopy (SEM), X-ray diffraction (XRD) and Fourier-transform infrared spectroscopy (FTIR). Nanofluids as EOR injection solutions are prepared from dispersing the synthesized green NCs (250 to 2000 ppm) within various aqueous phases including water at different salinity levels, surfactant and mutual solvents. The prepared nanofluids were then tested by various experimental studies related to the stability of injections fluids, IFT behavior, wettability alteration, oil/nanofluid emulsification and oil displacement. The pendant drop technique was used to measure the interfacial tension (IFT) of crude-oil/nanofluid systems, the wettability behavior of carbonate rock samples was studied using the contact angle (CA) measurement, and 26 core samples were used to observe the role of the synthesized NCs in improving oil recovery using oil displacement tests.

From the obtained results, it can be stated that the synthesized NCs are valid with applicable features of size, shape and crystallinity. A nanofluid prepared from dispersing 1000 ppm  $\text{TiO}_2$ /Quartz NCs within the distilled is the most effective green NCs in reducing the IFT which is by 96% from 28 to 1.141 mN/m. Meanwhile, ZnO/Montmorilant NCs enabled to alter the wettability of the carbonate rock to the strongest water wet state by reducing the CA from 134 to 19° when it is added to the natural surfactant extracted from *Cyclamen Persicum* plant. However, NCs-5-DW nanofluid formulated from mixing 2000 ppm ZnO/SiO<sub>2</sub>/bentonite NCs within the distilled water enabled to produce an additional 21.41% original oil in place (OOIP) after the waterflooding which is the highest oil recovery factor that was obtained among all synthesized NCs. In addition, these greenly synthesized NCs exhibited a good behavior in altering the relative permeability and emulsification.

**Keywords:** Green nanocomposites; plant extract; interfacial tension; wettability; oil recovery.

## Table of Contents

|   |            |
|---|------------|
| <b>Acknowledgment</b> .....                           | <b>ii</b>  |
| <b>Abstract</b> .....                                 | <b>iv</b>  |
| <b>1. Introduction</b> .....                          | <b>6</b>   |
| <b>2. Nanotechnology</b> .....                        | <b>10</b>  |
| 2.1. Nanocomposites .....                             | 13         |
| 2.2. Green synthesis of nanocomposites .....          | 15         |
| 2.2.1. Plant sources .....                            | 17         |
| 2.2.2. Preparation methods .....                      | 18         |
| 2.2.3. Characterization .....                         | 23         |
| 2.3. Nanofluid preparation and characterization ..... | 31         |
| <b>3. Interfacial tension reduction</b> .....         | <b>35</b>  |
| <b>4. Wettability alteration</b> .....                | <b>41</b>  |
| <b>5. Oil recovery</b> .....                          | <b>48</b>  |
| 5.1. Core plug preparation .....                      | 48         |
| 5.2. Oil displacement .....                           | 50         |
| 5.3. Relative permeability .....                      | 54         |
| 5.4. Emulsification .....                             | 56         |
| <b>6. Conclusions and future prospective</b> .....    | <b>58</b>  |
| <b>7. Abbreviations and nomenclature</b> .....        | <b>59</b>  |
| <b>8. References</b> .....                            | <b>61</b>  |
| <b>9. List of included publications</b> .....         | <b>73</b>  |
| <b>Appendix 1</b> .....                               | <b>75</b>  |
| <b>Appendix 2</b> .....                               | <b>89</b>  |
| <b>Appendix 3</b> .....                               | <b>103</b> |
| <b>Appendix 4</b> .....                               | <b>118</b> |
| <b>Appendix 5</b> .....                               | <b>134</b> |
| <b>Appendix 6</b> .....                               | <b>146</b> |
| <b>Appendix 7</b> .....                               | <b>166</b> |
| <b>Appendix 8</b> .....                               | <b>184</b> |
| <b>Appendix 9</b> .....                               | <b>207</b> |
| <b>Appendix 10</b> .....                              | <b>218</b> |

## 1. Introduction

Global energy's need will remain to rise with the growing population of the world. According to U.S. Energy Information Administration (EIA), the world will be needing over 47% more energy in 2050 compared to 2010 due to the population expansion and industrialization (Gordon and Weber, 2021). Despite that, renewable energy and nuclear power will assist us to face these difficulties, with about 2.5% increment per year. Nonetheless, fossil fuels will remain to provide approximately 70% of the globe energy use, which increases the world need for petroleum to 129 million barrels per day (mmbbl/day) depending on recent records from the US EIA (Gordon and Weber, 2021; Mirzavandi et al., 2023). This higher demand on petroleum has to be satisfied by locating new oilfields and/or expanding the life of current producing fields. New oil and gas fields have become significantly difficult to be discovered (Hama, 2023). The agreement in the petroleum industry is that most of the large, easily producible reservoirs were already found. The remaining unidentified reserves are either in difficult locations and environments or are energy-intensive to produce (Lashari and Ganat, 2020). Conventional technology focuses on producing hydrocarbons using the natural reservoir mechanisms including pressure variation, water aquifer and gas cap, or merely employs secondary energy by injecting water into the reservoir to push the oil towards the production wells. Although, above 50% OOIP remained stuck in the reservoir as a residual oil because of capillary forces (Udoh, 2021). Extracting the residual oil economically is the main concern and challenge of the industry. For this purpose, thermal, chemical and gas enhanced oil recovery (EOR) methods provided a remarkable enhancement in the oil recovery, which improved oil production by about 20% (Schramm, 2000; Schneider, 2023). However, the current EOR techniques are expensive and only accounted for less than 10% of the global production of 100 mmbbl/day. Thus, the oil and gas industry is currently focused on innovative strategies and techniques which can extract extra hydrocarbons from currently discovered reservoirs (Schneider, 2023).

Nowadays, the oil and gas industry has attracted much consideration on applications of nanomaterials with the size typically less than 100 nm. Nanomaterials have become widely used due to having unique optical, magnetic and electrical features (Torsater et al., 2012; Lau et al., 2017). Regardless of having this technology at the beginning stage, nanotechnology has shown a great potential in several applications of petroleum industry, such as increasing the quality and capacity of tools in hydrocarbon exploration (Torsater et al., 2012), enhancing oil recovery (Avendano et al., 2012; Behera and Sangwai, 2022), improving the rheological and filtration

properties of drilling mud (Ikram et al., 2021; Oseh et al., 2023), improving the strength and quality of drilling tools (Ismail et al., 2014), achieving cementing with better features (Maagi et al., 2020; Goyal et al., 2021), and developing the injection fluids with high stability and efficiency (Roustaei et al., 2013). Particularly, nanomaterials within different dispersion media, as shown in Figure 1a, can be easily transported through the porous media and reach to the oil bank because of possessing smaller sizes than micron-sized rock pores (see Figure 1b, d). As can be seen, the prepared nanofluids can be injected into the oil reservoir like the conventional methods of oil recovery and they displace hydrocarbon towards the production wells. However, the dispersion stability of NPs inside the nanofluids is crucial and it is usually reduced through the porous media as it is reported by Lashari et al. (2022) and Toma et al. (2022). Thus, dispersing nanoparticles within the polymer, surfactant and alkaline is recommended to provide better stability inside the porous media (Ali et al., 2019; Lashari et al., 2022; Toma et al., 2022; Hamdi et al., 2022; Roslan et al., 2023). Hamdi et al. (2022) and Roslan et al. (2023) were successful in improving the stability of injected nanofluids using polymer-NPs composites for EOR applications. In addition, nanomaterials can have the impact on the microscopic and macroscopic displacement efficiencies of oil recovery in the porous media, especially the polymer NCs or functionalized nanomaterials (ShamsiJazeyi et al., 2014; Kazemzadeh et al., 2018; Ali et al., 2018; Bila et al., 2019; Ali et al., 2019; Rezvani et al., 2020; Davoodi et al., 2022; Manshad et al., 2022). Figure 1c demonstrates the mechanism of improving the areal and vertical sweep efficiencies of the crude oil due to improving the mobility ratio under the influence of polymeric nanofluids. Meanwhile, these nanofluids can modify the IFT, wettability, capillary pressure and relative permeability due to their strong adsorption to the rock surface that makes crude oil free and entering the liquid-liquid interface which creates the disjoining pressure (see Figure 1d,f). Moreover, polymer NCs can provide a stronger emulsion between the crude oil and injected nanofluid through the porous media as shown in Figure 1g. Which is another reason behind the improvement of the oil recovery.

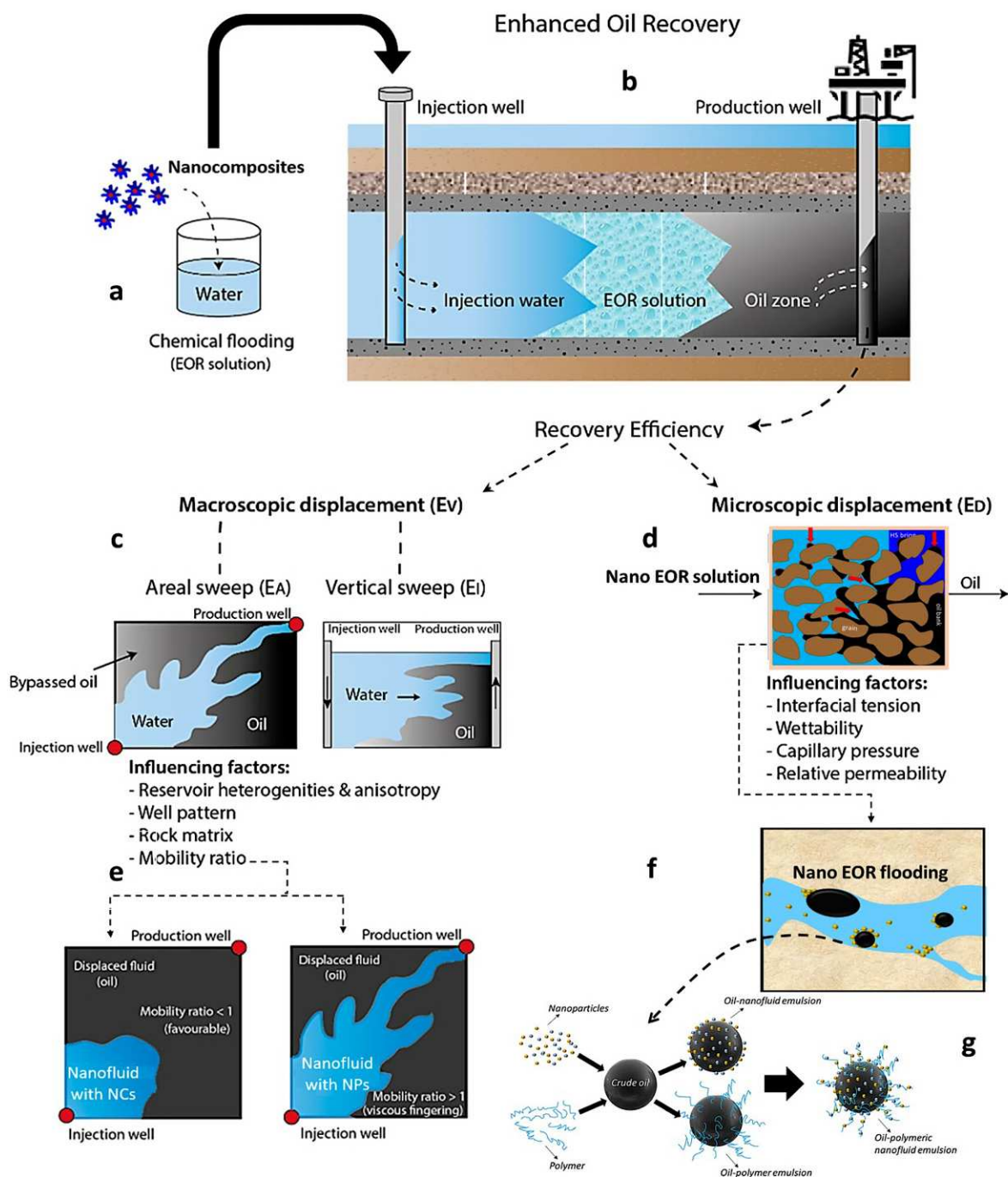


**Figure 1** Mechanistic illustration of nanofluid flooding considered in this study; a) dispersion of the synthesized NCs, b) nanofluid injection into the porous media, c) macroscopic displacement mechanisms including vertical and areal sweep efficiency, d) microscopic displacement mechanisms of recovery efficiency, e) mobility ratio behaviour under the impact of nanofluid, f) EOR mechanisms (IFT reduction and wettability alteration) that affect the microscopic displacement of oil, g) oil-nanofluid emulsion.

Oil recovery from EOR methods can be improved using new eco-friendly techniques. According to what have reported in the literature and presented in Figure 1, there are some main arguments behind the development of the green NCs and applying as chemical EOR agents to improve the oil recovery from the mature oil reservoirs:

- The surface area to volume ratio of nanomaterials (nanocomposites) is too large, which means that only a small concentration of them is needed to induce EOR injection fluids. Thus, the lower costs and better logistics can be achieved due to needing a smaller volume for transportation and storage compared to other additives.
- Nanomaterials can be dispersed in different aqueous phases to develop the EOR nanofluids, such as water, alcohols, glycols and surfactant solutions.
- Nanomaterials are small enough to pass through the reservoir's pore network. They might even be able to penetrate nanoscale pores that other additives cannot access.
- Combining nanoparticles with the natural polymer will result the development of the polymeric nanofluids with better stability of NPs, mobility of injection fluids and sweep efficiency.
- Many nanoparticles have passed ecotoxicity tests, for example titanium dioxide and silica nanoparticles are already used as food additives (Peters et al., 2012; Weir et al., 2012). So, adding the natural polymer to providing them more likely to be approved for field applications, will have no risks on the environment and underground waters.

The main objective of synthesizing the objective-oriented nanomaterials was to develop EOR agents with the capacity to cover the roles of conventional chemical methods (surfactant and polymer flooding), eco-friendly and environmentally friendly. We thus proposed several greenly synthesized nanocomposites (NCs) using the extract of plants and identified using various analytical methods in terms of size, morphology, composition and elemental analysis. The synthesized NCs were dispersed within different aqueous phases to develop nanofluids. The developed nanofluids were applied to reduce the IFT between oil and aqueous phases, alter the wettability of carbonate rocks, change the relative permeability curve, increase the viscosity of injected fluid, improve oil/aqueous phase emulsions, and improve oil recovery.

## 2. Nanotechnology

In the view of literature, nanomaterials possess an astonishing lengthy history (Heiligtag and Niederberger, 2013). Vollath (2013) declared that nanomaterials had already been used a long time ago by the Sumerians before the recent desire for the development and use of these tiny particles. In other words, after lots of years of intense and deep research, work, struggle and efforts, it turned out that nanomaterials were not the sole invention of humans even though there are many man-made and synthesized nanoparticles (Heiligtag and Niederberger, 2013). Nanomaterials are a wide class of materials which are substances, solid or colloidal particles with the size ranges from 1 to 100 nm in diameter or at list on of their dimensions is within the mentioned range (Hendraningrat and Torsæter, 2015; Khan et al., 2016; Subbenaik, 2016; Fakoya et al., 2017; Rizvi et al., 2018). As is obvious, nanomaterials can be different in size, shape, composition and originality. Thus, the classification of nanomaterials is crucial for better understanding of their use. Figure 2 illustrates the different types of the nanomaterials dependent on the composition (organic, inorganic, carbonaceous and composites), dispersion (isomeric and inhomogeneous), dimensionality (0D, 1D, 2D and 3D), phases (single and multi) and origin (natural, incidental and engineered), such as nanoparticles, composite nanoparticles, nanotube, nanowire, composite nanowire, nanoplates, nanobelts, nanosheets and microporous composite electrode (Harish et al., 2022).

Nanomaterials exhibit distinctive, unique and exceptional properties and features, which are tremendously different from others, due to their small sizes, larger surface area per unit volume and special higher chemical reactivity than that of other particles (Kamal et al., 2017; Fakoya et al., 2017; Kazemzadeh et al., 2018). It is worth mentioning nanomaterials are not, indeed, as simple as one might have thought of; rather they are comprised of three layers: <sup>(i)</sup> the core (the nanoparticle's principal part), <sup>(ii)</sup> the shell layer (unlike the core, it is a different material chemically in all features), and <sup>(iii)</sup> may have small the surface layer (a layer which molecules, surfactants, metal ions and/or polymers stuck to them) (Khan et al., 2016). In terms of the morphology, nanomaterials can be varied dependents on their high and low aspect ratio which is the ratio of their longest to shortest size; nanobelts, nanotubes and nanowires can be categorized within the long aspect ratio nanomaterials and short aspect ratio nanomaterials consist of nanocubes, nanoparticles and nanocomposites.

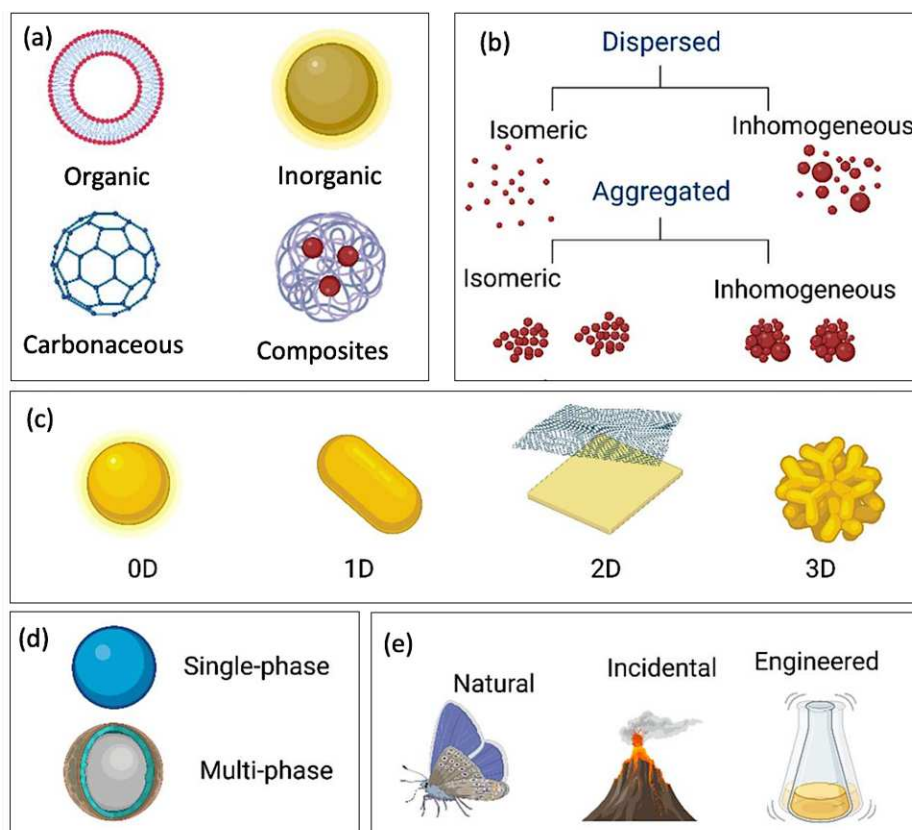


**Figure 2** Classification of the nanomaterial dependent on; a) composition, b) dispersion, c) dimensionality, d) phases, and e) origin.

A large number of methods are suggested by the scientists to synthesize a wide diversity of nanomaterials of different shape, size and chemical and/or physical properties as shown in Figure 3 (Abou El-Nour et al., 2010; Heiligtag and Niederberger, 2013; Kango et al., 2013; Subbenaik, 2016). As is clear, these methods and techniques of the nanomaterial preparation are generally divided into two groups including bottom-up and top-down. The top-down covers the procedural steps that convert the bulk materials to nanomaterials, such as lithography, ultrasonication and ball milling. However, synthesis of nanomaterials from atom to atom, cluster to cluster and molecule to molecule to assemble particles is called bottom-up method which includes sol-gel technique, chemical precipitation and biological methods.

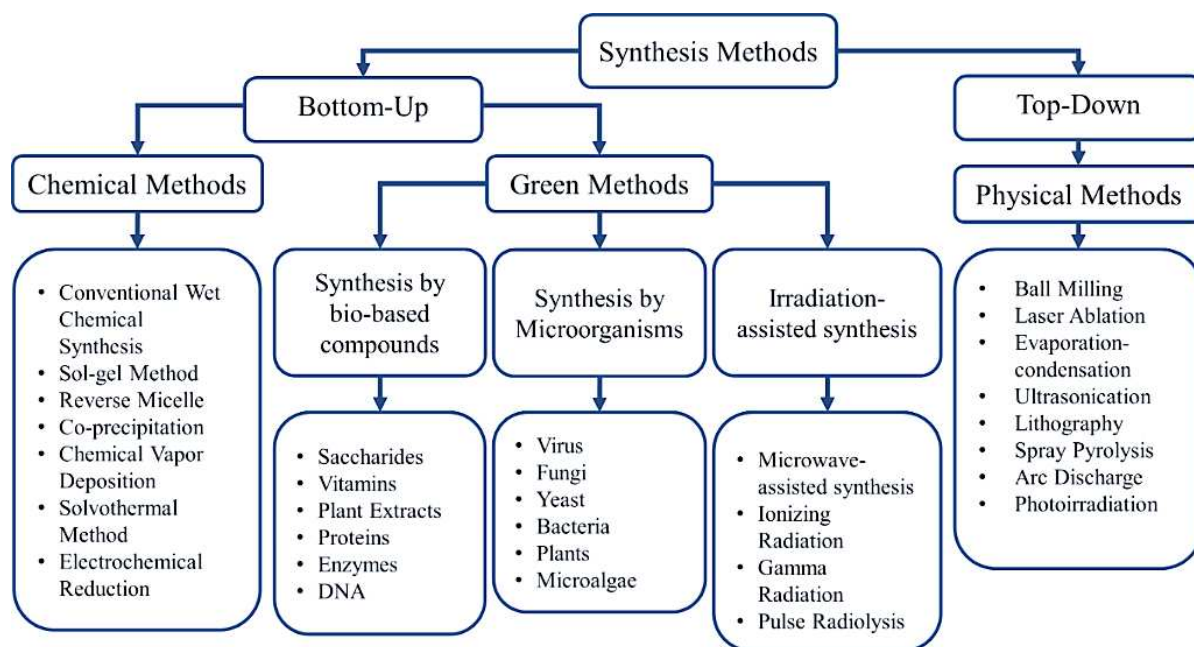


**Figure 3** Schematic illustration of the synthesis methods of nanomaterials; bottom-up and top-down categories (Srivastava et al., 2020).

Solvent evaporation, as a synthesis method from bio-based compounds, is the one of most common methods for the preparation of nanoparticles (Murakami et al., 1999; Desgouilles et al., 2003). During this process, compound solutions can be prepared in emulsions and advanced by exploitation of the chloride and chloroform (Bastos-Arrieta et al., 2014). However, this has currently been replaced with the organic compound that provides a higher pharmacological medicine profile and urges particles to be within the 500 nm in size. The prepared emulsions, oil-in-water as single emulsion and double emulsions including (water-in-oil)-in-water, are converted into a nanoparticle suspension by conducting a controlled evaporation of the dissolved solvents (Salager, 2000; Mendoza-Muñoz et al., 2016; Sharma et al., 2023). Such sort of process applies the high-speed homogenizations or ultrasonification, followed by evaporation of the solvent, either by continuous magnetic stirring at elevated temperatures, rotary evaporation, thin-film evaporation or spray drying. Afterwards, the nanosized particles can be collected and characterized using various analytical techniques. Figure 4 illustrates the general procedural steps of the nanomaterial synthesis using ball milling as the top-down method and sol gel solvent evaporation as the bottom-up method. As is obvious, ball milling method can produce nanomaterials from the bulk particles which convert to powder and then nano-sized particles under the mechanical processes (see Figure 4a). This process consists of a specialized milling machine that mill the powder to nanomaterials

by milling balls and a rotary motion mechanism (Salavati-Niasari et al., 2013; Wirunchit et al., 2023). On the other hand, nanomaterials are synthesized from the atoms and clusters using mixtures of aqueous phases, magnetic stirrer, ultrasonicate and then evaporation (see Figure 4b). As is clear, this process involves the transformation of a sol, a colloidal suspension of solid particles in a liquid medium, into a gel through a controlled chemical reaction. The gelation process leads to the formation of a three-dimensional network of nanoparticles or a continuous film structure. The sol-gel method provides precise control over composition, structure, and morphology, making it suitable for tailoring nanoparticles with specific properties (Alagiri and Hamid, 2015; Hasan and Azhdar, 2023).

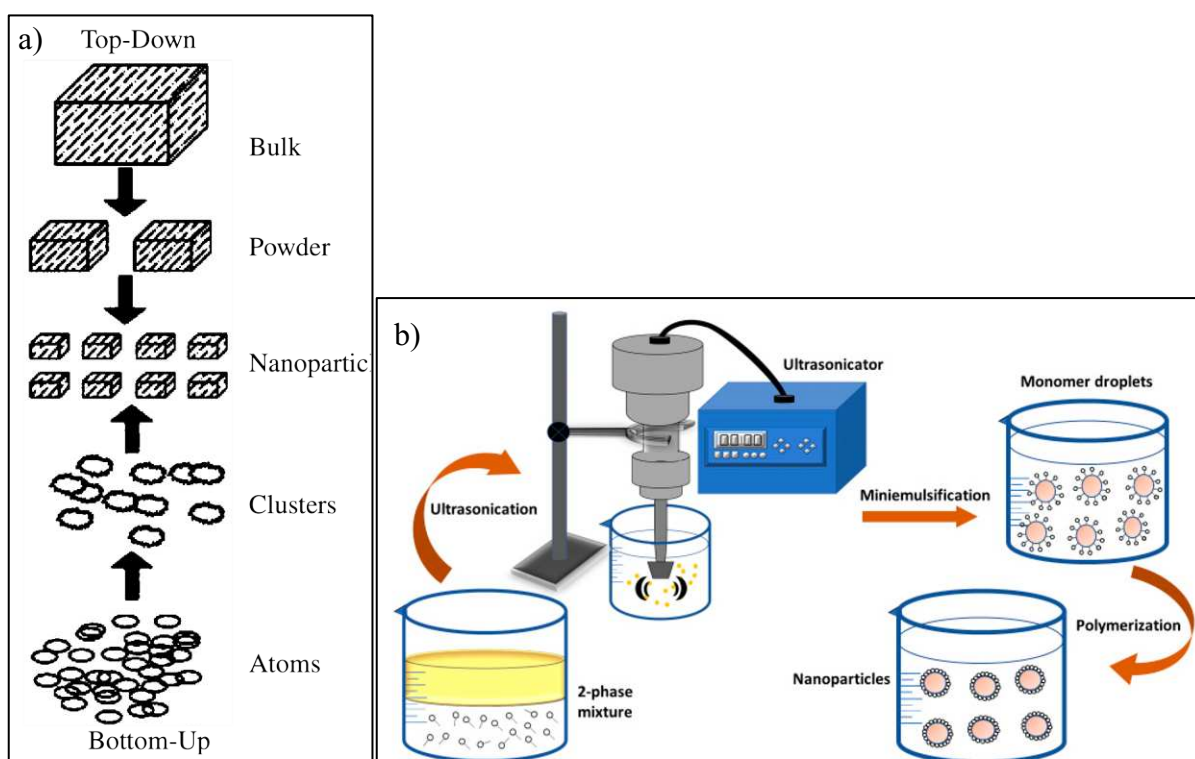


**Figure 4** Top-down and bottom-up methods of the nanomaterial synthesise: a) ball milling, and b) sol-gel solvent evaporation (Srivastava et al., 2020).

## 2.1. Nanocomposites

Composites are mixtures of two or more substances or layers of nanoparticles that are mixed to obtain a blend bearing the characteristics of the parental substances with enhanced performance. It is composed of two parts, a discontinuous phase called “reinforcement” and a continuous phase called “matrix”. However, according to Cammarata (2006), nanocomposites can be defined as a blend of several mixtures with different phases and one of those elementary particles must have

the scale of less than 100 nm. Okpala, (2014) stated that experiments have proved adding different types of nanocomposites to their macroscopic counterparts can efficiently yield new byproducts with enhanced qualities and higher surface area to volume ratios compared to conventional composites. The properties of nanocomposites are dependent on the morphology, dimension, agglomeration, diffusion and composition of materials (Kango et al., 2013).

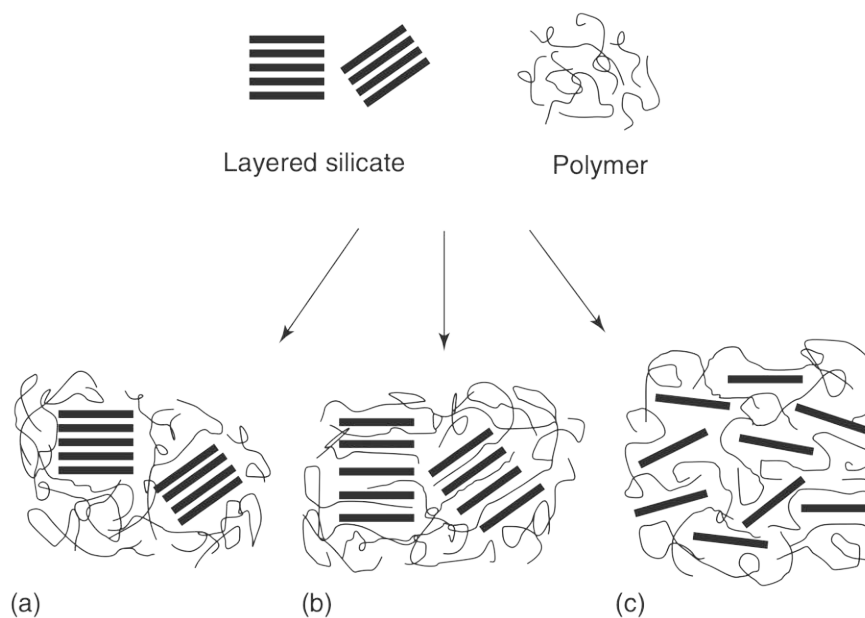


**Figure 5** Polymer matrix nanocomposites; a) unintercalated (micro-composite), b) intercalated, and c) exfoliated (Fawaz and Mittal, 2015).

Nanocomposites (NCs) are basically classified depending on their matrix material into three different groups; metal matrix nanocomposite, MMNC (Ceschini et al., 2016; Bhowmik and Arora, 2022), polymer matrix nanocomposite, PMNC (Mago et al., 2011; Guo et al., 2018), and ceramic matrix nanocomposite, CMNC (Low, 2018). Polymer matrix NCs is a combination of the nanoparticles and polymer in different manners including unintercalated (micro-composite), intercalated and exfoliated (see Figure 5). Polymer nanocomposites can be green NCs depends on the synthesis process and biodegradability of the materials used. This kind of NCs is cost-effective and eco-friendly along with providing an excellent performance in many engineering and medical issues, such construction, oil recovery, drug delivery ad vaccination. Well dispersion of the nanoparticles within NCs will improve the efficiency polymer matrix due to the ability of nanoparticles towards a strong interaction between two phases and having a large surface area. However, the formulation of polymer NCs with even distribution of nanoparticles is difficult

because of their high surface energy and tendency toward the agglomeration (Koo, 2019). According Fawaz and Mittal (2015), nanoparticles enable the adjustment of the configuration, function, and characteristics of nanocomposites wherein adding only one nanoparticle can introduce a particular functionality that is absent in natural polymers. Diverse combinations of natural polymers and particles at the nanoscale are tested to attain the targeted properties, expanding their potential applications.

## 2.2. Green synthesis of nanocomposites

Several physical and chemical methods can be used to synthesis nanoparticles, such as pyrolysis and attrition are the most common physical methods, and chemical techniques are photochemical, electrochemical and chemical reduction. As is stated by Nikolaidis (2020), the simplest and most widely used method for the fabrication of the metal oxide NPs with high stability is the chemical reduction. While, all these chemical and physical techniques have shown various disadvantages including high cost, toxicity, environmental hazardous and high energy consumption. Thus, introducing a new approach to replace integrating the toxic chemicals in the fabrication of the nanomaterials is necessary. This non-toxic, ecofriendly and low-cost approach was attracted by researchers which is based on the biological processes. They involved the plant extract in the process of developing the nanomaterials under different conditions of pH, oxygenation, temperature and time. Figure 6 illustrates the schematical diagram of the general procedural steps of synthesizing metallic nanomaterials from the plant extract when  $M^{n+}$  are dropped to  $M^0$  NPs (Bai and Zhang, 2009; Saratale et al., 2018). The green synthesis of nanomaterials from microorganisms (bacteria or fungi) to plant extracts can be addressed as a key part of the nanotechnology, which results in better energy efficiency, designing safer products, preventing the bio-based waste, eliminating the pollution and decreasing the accident potentiality (Schmidt, 2007).

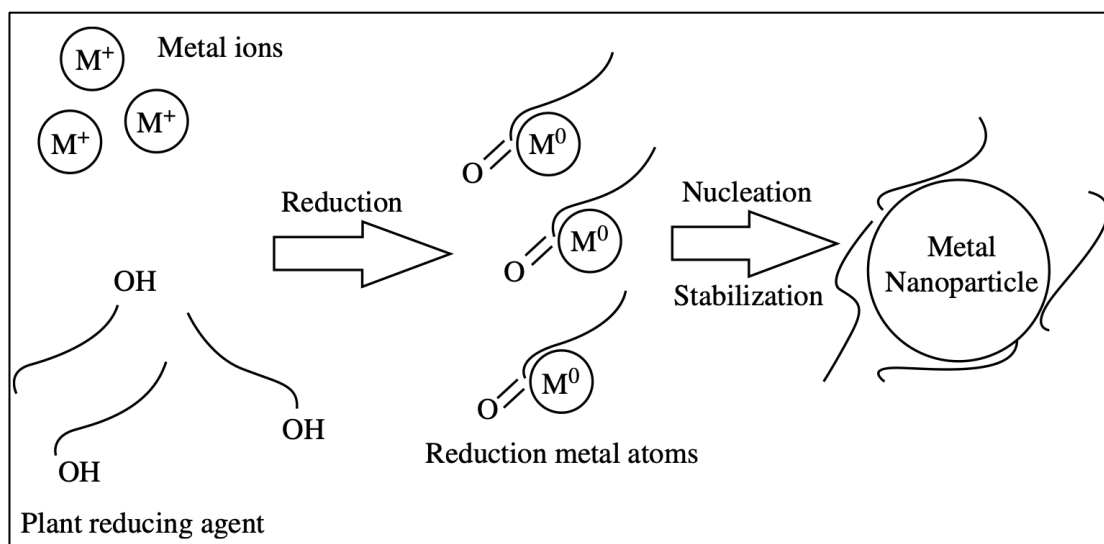


**Figure 6** Schematic illustration of the general procedure of green synthesis of metal nanoparticles from the plant extract (Keat et al., 2015)

Green synthesis of nanocomposites refers to a method of fabricating the nanomaterials in the same way of green nanoparticles but combining with, coating by or mixing within the matrix materials. Similarly, in this simple and eco-friendly approach, different biological sources can be used including bacteria, fungi, yeast, algae and plant. All these sources can be used to synthesis variety number of nanoparticles depends on the integrated salt base and experiment conditions (Herrera-Becerra et al., 2008; Gericke and Pinches, 2017). The production of nanomaterials using the green synthesis method can be influenced by several factors, such as pH, temperature and time. For instance, the shape and size of nanoparticles can be varied depends on the concentration of hydrogen ions. Lower acidic creates larger particles; a reaction medium with 2 pH produces nanorods and smaller NPs with the size of 5-20 nm can be produced at the pH above 5 (Armendariz et al., 2004; Sathishkumar et al., 2009). Similarly, the reaction temperature during the synthesis process has a vital role in controlling the shape and size of the produced nanoparticles. Raju et al. (2011) stated that the higher reaction temperature can lead producing more spherical nanoparticles, whereas triangular nanoparticles can be synthesized at lower reaction temperature when they synthesized gold NPs from leaf extract of *Cymbopogon flexuosus*. In addition, green synthesis of nanomaterials can be affected by time duration of the reaction media. With the variation in the time duration, nanomaterials can be synthesized at different quality, properties and morphology (Darroudi, 2011; Kuchibhatla et al., 2012). In this study project, different green nanocomposites

(NCs-1 to 8) were synthesized as shown in Table 1. As can be seen, these green nanocomposites were synthesized from different sources of the plant, salts and matrix materials. The selection of the types of metallic nanoparticles (ZnO, SiO<sub>2</sub>, TiO<sub>2</sub> and Fe<sub>2</sub>O<sub>3</sub>) and matrix materials (polyacrylamide, xanthan gum and bentonite) is based on the literature and their performance in oil and gas industry.

**Table 1** Synthesized nanocomposites and their plant source, salts and matrix materials.

| NCs   | Plant source            | Salts   | Matrix material            | Product                                      |
|-------|-------------------------|---|----------------------------|--|
| NCs-1 | Pomegranate seed        | ZnCl <sub>2</sub> & Na <sub>2</sub> SiO <sub>3</sub>    | Xantahn Gum                | ZnO/SiO <sub>2</sub> /Xanthan                |
| NCs-2 | Pomegranate seed        | Na <sub>2</sub> SiO <sub>3</sub> & TiO(OH) <sub>2</sub> | Polyacrylamide             | TiO <sub>2</sub> /SiO <sub>2</sub> /PAM      |
| NCs-3 | Euphorbia condylocarpa  | TiO(OH) <sub>2</sub>                                    | Quartz                     | TiO <sub>2</sub> /Quartz                     |
| NCs-4 | Adinandra dumosa leaves | Na <sub>2</sub> SiO <sub>3</sub>                        | Montmorilant & Xanthan gum | SiO <sub>2</sub> /Montmorilant/Xanthan       |
| NCs-5 | Cordyline fruticosa     | ZnCl <sub>2</sub> & Na <sub>2</sub> SiO <sub>3</sub>    | Bentonite                  | ZnO/SiO <sub>2</sub> /bentonite              |
| NCs-6 | A.conyzoides L          | ZnCl <sub>2</sub>                                       | Montmorilant               | ZnO/Montmorilant                             |
| NCs-7 | Euodia hortensis leaf   | FeCl <sub>3</sub> ·6H <sub>2</sub> O                    | Mineral–Soil               | Fe <sub>3</sub> O <sub>4</sub> /Mineral–Soil |
| NCs-8 | Euphorbia condylocarpa  | Na <sub>2</sub> SiO <sub>3</sub>                        | KCl & Xanthan Gum          | SiO <sub>2</sub> /KCl/Xanthan                |

### 2.2.1. Plant sources

Several types of the botanical sources which are locally exist can be used to synthesis green nanomaterials, such as the plant, leaf, seed, flower, marine plant, fruit, fruit peel, root, stolon waste and gum. Among these botanical sources, several plants can be found that can provide the active phytochemical antioxidants with high concentrations. From these phytochemical antioxidants, nanomaterials are produced in a green and economically feasible way which reduces the environmental pollution. Researchers applied various plant sources in their green synthesis protocols of fabricating nanomaterials, such as Aloe vera plant (Phumying et al., 2013), Alfalfa plant (Ramasahayam et al., 2012), Kappaphycus alvarezii plant (Yew et al., 2018), Syzygium cumini seed (Venkateswarlu et al., 2014), Green tea leaf (Xiao et al., 2016), Lagenaria siceraria leaf (Silveira et al., 2017), Eucalyptus leaf (Weng et al., 2017; Gan et al., 2018), Ananas comosus peel (Venkateswarlu and Yoon, 2015), Rice straw (Khatae et al., 2017), Arabic gum (Horst et al., 2017). In this research project, several plant sources were used including pomegranate seed, Euphorbia condylocarpa, Adinandra dumosa leaves, Cordyline fruticosa, A.conyzoides L and Euodia hortensis leaves as shown in Figure 7.



**Figure 7** Images of plant sources used in the preparation of the green nanocomposites.

### 2.2.2. Preparation methods

Synthesized NCs were designed in a way to deliver several functions in EOR, as shown in Figure 1, with improved nanoparticles performance, for instance  $\text{TiO}_2/\text{SiO}_2/\text{PAM}$  NCs that composed of the silica and titanium oxide nanoparticles and polyacrylamide polymer. When a nanofluid prepared from NPs flows through the porous media interfingering might occur and cause hydrocarbon to remain behind. However, when a polymeric nanofluid that contains NPs distributed on the surface (chains) of the polymer as the substrate, a continuous chain between nanoparticles is likely to make the nanofluid flow with an even displacement front in porous media. Thus, the inter-fingering of normal water that is expected within the oil phase may be prevented and better displacement efficiency can be achieved leading to much improved oil recovery from the reservoir as shown in Figure 8.

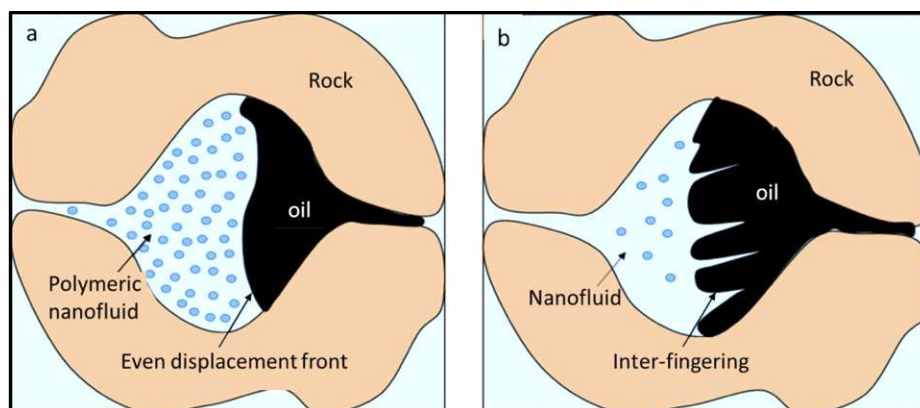


**Figure 8** Schematic illustration depicting the flow behaviour of nanofluids within the porous medium; a) polymeric-nanofluid made of polymer nanocomposites, and b) nanofluid made of nanoparticles (re-drawn after Afolabi and Yusuf, 2018).

The green nanocomposites mentioned in Table 1 were synthesized as follows:

▪ **ZnO/SiO<sub>2</sub>/xanthan nanocomposites (NCs-1)**

In a 500 mL beaker, 2 gm of ZnCl<sub>2</sub> and 5 gm of sodium metasilicate (Na<sub>2</sub>SiO<sub>3</sub>) were mixed with 200 mL pomegranate seed extract at 80 °C and 850 rpm stirring for 2 hr until the formation of a light black precipitate (Figure 9). The precipitate was then separated using filtration and heated up to 600 °C by furnace to burn all the remaining plant particles. Then, it was washed with hot distillate water many times to remove impurities. The clean temperature precipitate was then dried at room and mixed with 10 gm of Xanthan powder using mortar and pestle, and under reflux for 2 hr at 80°C. Finally, the dried and cleaned ZnO/SiO<sub>2</sub>/xanthan nanocomposites was collected and characterized as ready to be used for EOR applications (Ali et al., 2019)

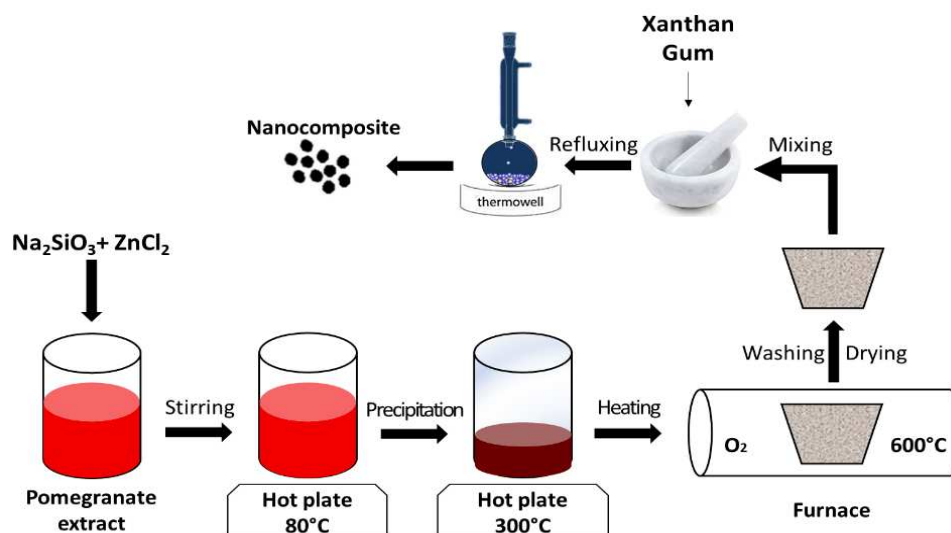


**Figure 9** A schematic diagram of the green synthesis ZnO/SiO<sub>2</sub>/xanthan NCs.

▪ **TiO<sub>2</sub>/SiO<sub>2</sub>/PAM nanocomposites (NCs-2)**

Multi-pots approach was used to synthesis TiO<sub>2</sub>/SiO<sub>2</sub>/PAM nanocomposites in an eco-friendly manner using the pomegranate seed extract (Ali et al., 2021). Polyacrylamide was used as a substrate for the NPs. This plant has a rich makeup of phytochemicals which are the source of many biologically active compounds such as phenolics, aromatic esters, steroids, terpenoids, essential oils and other bioactive constituents used in various applications (Islam et al. 2015; Sajadi et al., 2019; Nasrollahzadeh et al., 2019). Following the methodology of Nasrollahzadeh et al. (2019) and Sajadi et al. (2019), the extract of the pomegranate seeds was collected and filtered into two beakers of 500 mL size. In one beaker, 6 gm of Na<sub>2</sub>SiO<sub>3</sub> was added while 3 gm of TiO(OH)<sub>2</sub> was added to the other. Both were mixed with 200 mL of the filtered extract at 80 °C and 850 rpm and stirred until a dark greenish-brown formation precipitated. The precipitates for both nanoparticles were filtered, heated up to 600 °C, and washed to remove impurities. The obtained nanoparticles were mixed with 12 gm of polyacrylamide (PAM) powder under reflux conditions with ethanol solvent for 2 hours at 80 °C.

▪ **TiO<sub>2</sub>/quartz (NCs-3)**

Titanium oxide NPs was synthesized from euphoria condylocarpa extract in a green way then was combined in a composite with the quartz (Zargar et al., 2020). First, 400 mL of plant extract was collected in a beaker and 6 gm of TiO(OH)<sub>2</sub> was mixed with it by stirring until a dark brown-greenish formation became precipitated. The precipitate was then filtered from the solution and heated up to 600 °C using a furnace to burn all the remained plant particles. Afterwards, the burned precipitate was washed to remove the impurities and dried at room temperature. The clean obtained TiO<sub>2</sub> was mixed with 12 gm of quartz powder using mortar and pestle, and under reflux for 3 hr at 80 °C.

▪ **SiO<sub>2</sub>/Montmorilant/xanthan nanocomposites (NCs-4)**

100 gm of dried leaves of Adinandra dumosa plant were mixed with 500 mL of distilled water at 80 °C for 30 min under reflex conditions (Nazarahari et al., 2021). Then, the prepared aqueous extract was filtered and stored at 4 °C for further application. Afterwards, 1 gm of sodium metasilicate (Na<sub>2</sub>SiO<sub>3</sub>) and 4 gm of montmorillonite were mixed with 100 mL of the prepared extract by maintaining pH around 9 (adjusted by 0.1 mol/L of Na<sub>2</sub>CO<sub>3</sub>) during the stirring at 80

°C. This mixing process was continued for 5 hr until SiO<sub>2</sub>/montmorillonite precipitate was formed followed by the drying process at 80 °C for 24 hr. Thereafter, SiO<sub>2</sub>/montmorillonite precipitate was mixed with 10 gm of xanthan gum with the presence of 100 mL ethanol at 80 °C for 3 hr to form SiO<sub>2</sub>/Montmorilant/xanthan nanocomposites precipitate followed by filtration and drying process.

▪ **ZnO/SiO<sub>2</sub>/ bentonite nanocomposites (NCs-5)**

To create the extract of the plant, 50 gm of the dried powder of Cordyline fruticosa leaves mixed with 500 mL distilled water at 80 °C under continues stirring at 600 rpm for 30 min. Later, in a 250 mL flask, 2 gm ZnCl<sub>2</sub>, 5 gm Na<sub>2</sub>SiO<sub>3</sub> and 10 gm bentonite were mixed with 100 mL Cordyline fruticosa leaves extract under reflux condition at 9 pH (adjusted by 0.1 mg Na<sub>2</sub>CO<sub>3</sub>) and kept under the stirring at 60 °C for 24 hr until absolute formation of NPs and their deposition on the surface of bentonite. The reason of adding clay is due to its cheap cost to produce ZnO/SiO<sub>2</sub>/ bentonite NCs economically viable. In addition, it behaves as polymer chains in order to create a better distribution of nanoparticles rather than agglomeration. The mixture then filtered and obtained precipitate was dried and kept to identification and application processes (Manshad et al., 2022).

▪ **ZnO/montmorillonite nanocomposites (NCs-6)**

The prepared A. conyzoides L plant extract (100 mL) was placed within a beaker of 250 cm<sup>3</sup> volume to provide the stabilized reducing medium of synthesis. Chemical powders of zinc chloride and microscopic crystals of montmorillonite phyllosilicates were then added to the reducing environment for 2 and 8 gm, in turn. To increase the chemical reaction role-in surfaces, the solution was continuously stirred; also, to increase the reaction rate, the temperature increased to 80 °C and was kept constant. The used synthesized method was the precipitation method; therefore, the stirring process continued until a white precipitate was formed within the system. The precipitated materials were then screened from the synthesized environment through the filtration process. The product went under a 100 °C heating process and washing with distilled water for any elimination of purity inclusions in synthesized NCs (Nourinia et al., 2022).

- **Fe<sub>3</sub>O<sub>4</sub>/mineral–soil nanocomposites (NCs-7)**

The synthesis of Fe<sub>3</sub>O<sub>4</sub>/mineral–soil NCs was carried out in several steps: preparation of the plant extract, synthesis of Fe<sub>3</sub>O<sub>4</sub> nanoparticles, development of nanocomposites, and characterization of the synthesized NCs as shown in Figure 10. The *Euodia hortensis* leaves were dried at ambient temperature and powdered. In 500-mL flask, 50 gm of the dried powder was mixed within the distilled water using magnetic hot plate stirrer at 70 °C for 2 h. The achieved extract was then filtered using the centrifugation at 7000 rpm. After- ward, 5 gm of FeCl<sub>3</sub>·6H<sub>2</sub>O and a certain amount of Na<sub>2</sub>CO<sub>3</sub> to keep pH above 10 were mixed with 100 mL of the filtered extract in 250-mL flask. The mixture was well mixed until the dark color was obtained and filtered using the centrifuge to separate the precipitate. The collected precipitate was burned in an oven and then washed using ethanol to achieve the green iron oxide NPs. Lastly, the synthesized NPs were mixed with 12 gm of natural mineral soil using a refluxing system at 70 °C and 700 rpm for 12 h to obtain Fe<sub>3</sub>O<sub>4</sub>/mineral–soil NCs (Ali, 2022).

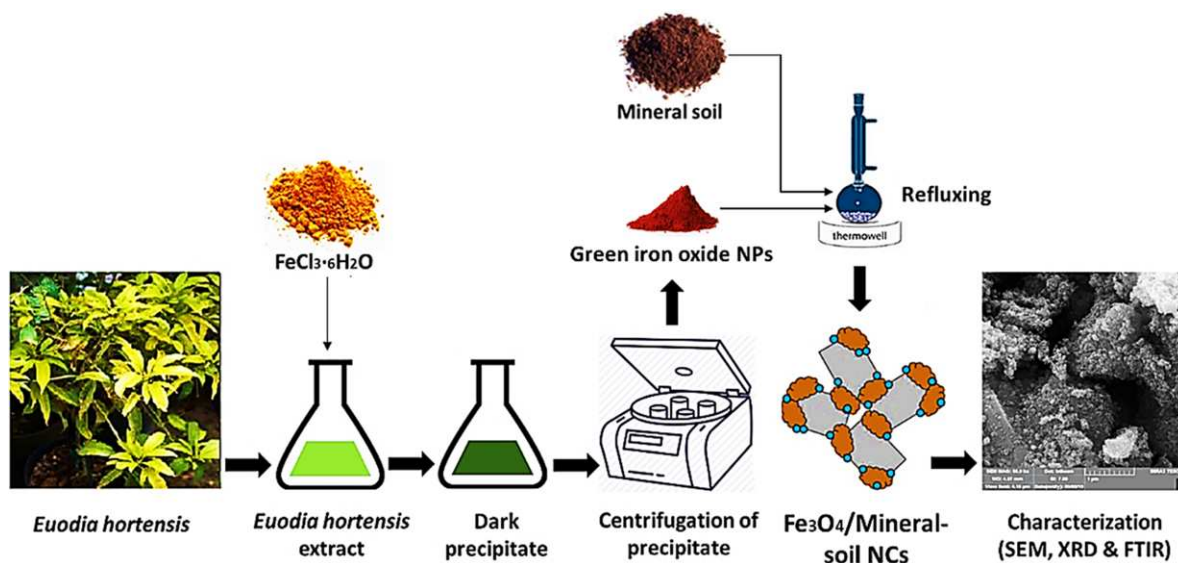


**Figure 10** Synthesis procedure of Fe<sub>3</sub>O<sub>4</sub>/mineral–soil nanocomposites from *Euodia hortensis* leaves.

- **SiO<sub>2</sub>/KCl/Xanthan nanocomposites (NCs-8)**

A composite of KCl (as a common salt), SiO<sub>2</sub> (as nanoparticles) and xanthan gum (as a natural stabilizing polymer) was synthesized from *euphorbia condylocarpa* plant (Motraghi et al., 2023). 100 mL of *euphorbia condylocarpa* plant extract was first mixed with 5 gm of Na<sub>2</sub>SiO<sub>3</sub>, while stirring at 80 °C for 10 hr at 10 pH. After the components were mixed together thoroughly,

precipitation was obtained. Then the obtained precipitation was separated and added to an ethanolic suspension of 10 gm of the xanthan gum as substrate at 80 °C for 5 hr under reflux conditions. Further, after drying and milling of the precipitate, the milled SiO<sub>2</sub>-xanthan nanocomposites was mixed with 100 mL KCl-hydroalcoholic solution at 100 °C and stirred for 4 hr. Finally, the SiO<sub>2</sub>/KCl/Xanthan nanocomposites was produced by drying and milling of the final precipitate (see Figure 11).

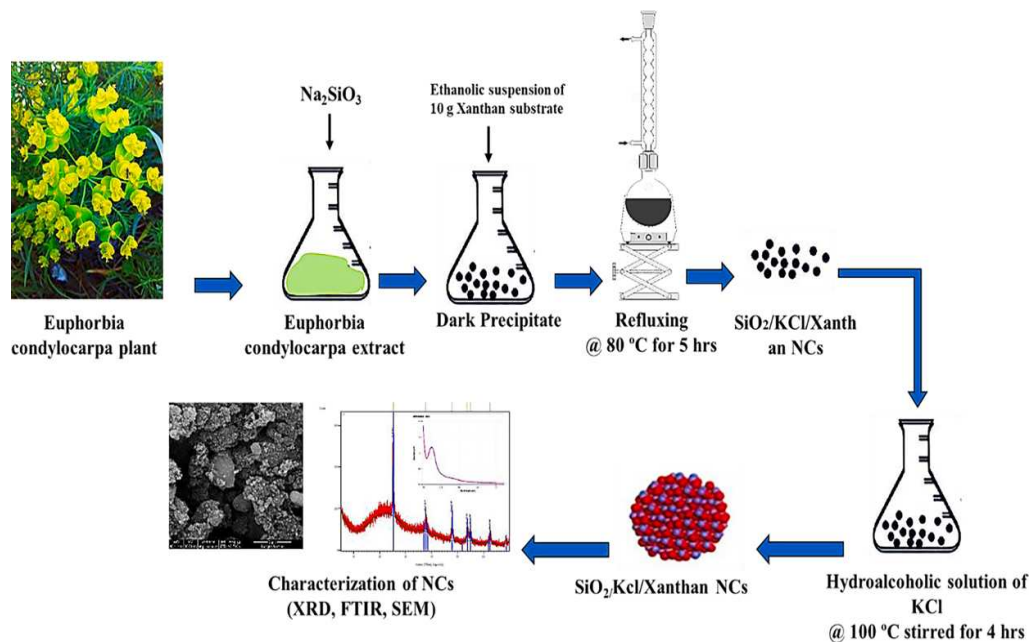


**Figure 11** A schematic diagram of the green synthesis of SiO<sub>2</sub>/KCl/xanthan NCs from euphorbia condylocarpa plant.

### 2.2.3. Characterization

Nanomaterials are available in many types, different shape and various dimensions; thus, the advanced techniques should be used to analysis their physical and chemical characteristics including the size, morphology, crystal structure and composition. The main techniques that are useable nowadays and used in this project are ultraviolet-visible (UV-Vis) spectroscopy, scanning electron microscopy (SEM), transmission electron microscopy (TEM), X-ray diffraction (XRD) and Fourier-transform infrared spectroscopy (FTIR).

- Ultraviolet-visible (UV-Vis) spectroscopy

When the salts were mixed with the plant extract and the colour of the colloidal solution is changed, the UV-Vis analysis was carried out for the solution to confirm the synthesis of

nanoparticles depends on the surface resonance of free electrons. Figure 12 shows the Uv-Vis spectrum of the colloidal solutions that contain the silica and titanium nanoparticles when were synthesized from the extract of pomegranate seeds. This technique is usually used in the nano science and technology for evaluating the optical properties of the particles. During the analysis, the absorption of radiations would be reported based on the concentration of the analyte within the solutions for different ultraviolets (near: 180-390 nm, and visible: 390-780 nm). Worsfold et al. (2019) stated that the radiation energy of organic solutions is absorbed in the near ultraviolet. Uv-Vis instrument can be single or double bema that mainly consists of the sample holder, detector, radiation source and output. For instance, the Uv-Vis spectrums shown in Figure 12, two bonds of phenolics around 300 nm wavelength with the absorbance of 1.9 and 2.8 were observed for TiO<sub>2</sub> and SiO<sub>2</sub>, respectively. Titanium and silica NPs bonds provide strong proof of the presence of potent antioxidants inside the pomegranate seed extract that led the synthesise of the nanoparticles in accordance with the results reported in the literature (Patil et al., 2018; Panda et al., 2018; Babu et al., 2018). In the same way, the Uv-Vis analysis was conducted for all mentioned NCs to confirm the synthesis of nanoparticles before further processing towards the fabrication of the NCs.

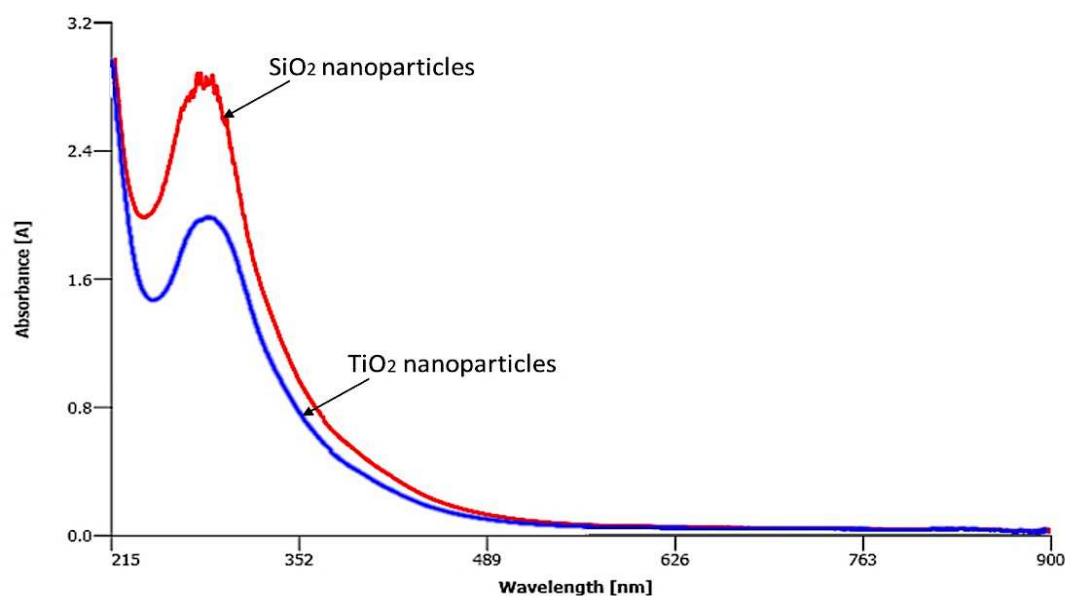


**Figure 12** Uv-Vis spectrum of pomegranate seeds extract to fabricate TiO<sub>2</sub> and SiO<sub>2</sub> NPs and finally TiO<sub>2</sub>/SiO<sub>2</sub>/PAM nanocomposites (NCs-2).

- X-ray diffraction (XRD)

After confirming the fabrication of the nanoparticles by Uv-Vis spectroscopy, the process of synthesizing NCs was continued until green composites of nanomaterials were obtained. The crystalline structure and chemical composition of the synthesized NCs were investigated using X-ray diffraction (XRD) technique. According to Kohli (2012) and Sima et al. (2016), this analysis can be used to estimate the features of crystallites including chemical composition, physical properties, structure and orientations. Since XRD analysis is dependent on the elastic scattering of X-ray photons by crystal planes, Bragg's formula shown in the below equation is used to determine the lattice spacings (Kacher et al., 2009).

$$n\lambda = 2d \sin(\theta) \quad (1)$$

where:

$n$ : order of reflection,

$\lambda$ : X-ray wavelengths,

$d$ : spacing between crystal planes, and

$\theta$ : angle between the reflected beam and the crystal plane.

To identify the composition of any unknown synthesized nanocomposites, its XRD pattern along with the position and intensity can be compared with reference patterns reported by international center for diffraction data (ICDD) and in the publications. For all eight green NCs mentioned in this study, the XRD analysis was performed, and the patterns are presented in Figure 13. As is obvious, any NCs demonstrated different pattern of XRD depends on the elastic scattering response of X-ray photons. For example, Figure 13a contains all the peaks associated with the crystalline planes of pure SiO<sub>2</sub> and ZnO concerning the crystallinity and phase purity of nanoparticles deposited on the surface of xanthan. Three XRD intense peaks were observed (labelled "010", "002" and "012") with the reflections from 31.5 to 36 degrees equivalent to the peaks of Zinc and silica NPs observed in previous studies (Khorsand et al., 2011; Zhang, 2011; Maqusood et al., 2012). In addition, a typical XRD pattern of TiO<sub>2</sub>/SiO<sub>2</sub>/PAM NCs is shown in Figure 13b. The presented pattern contains all the peaks associated with the crystalline planes of pure TiO<sub>2</sub> and SiO<sub>2</sub> nanoparticles deposited on the surface of polyacrylamide. Three major ("023", "032" and "043") and three minor ("051", "052" and "060") peaks were observed with the reflections about 25, 38 and 48 degrees, and 54, 55 and 63 degrees, respectively.

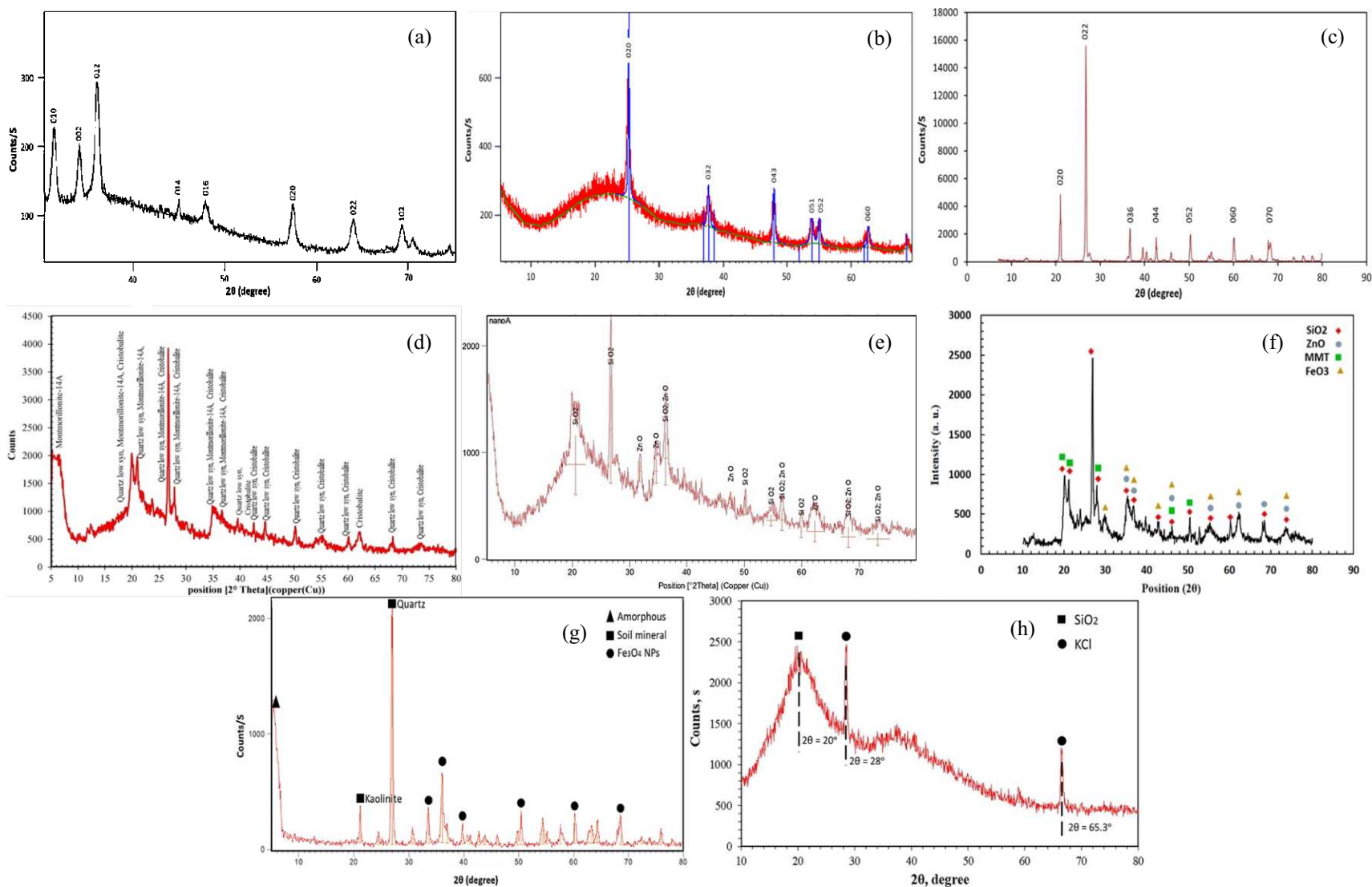


**Figure 13** XRD patterns of green synthesized NCs; a) ZnO/SiO<sub>2</sub>/Xanthan, b) TiO<sub>2</sub>/SiO<sub>2</sub>/PAM, c) TiO<sub>2</sub>/Quartz, d) SiO<sub>2</sub>/Montmorilant/Xanthan, e) ZnO/SiO<sub>2</sub>/bentonite, f) ZnO/Montmorilant, g) Fe<sub>3</sub>O<sub>4</sub>/Mineral–Soil, and h) SiO<sub>2</sub>/KCl/Xanthan NCs.

- Fourier-transform infrared spectroscopy (FTIR).

Furthermore, the molecular structure of all synthesized NCs was estimated using the Fourier transform infrared spectrometer (FTIR) analysis. This instrument consists of different components, such as interferometer, sample holder, radiation source, amplifier, data converter and detector. Basically, the source creates the radiation and send it to the detector through samples by interferometer. When the infrared radiation passes through the sample molecules (molecular bonds), wavelengths would be absorbed by molecules. This absorption makes sample molecules to transfer the vibrational energy due to changing their dipole moment. Finally, the received signals by detector will be converted to analog data and reported as the FTIR pattern by computer (Srivastava et al., 2020). The reported data as the intensity of absorption peaks for any molecule bond relies on the density of the that bond exist within the sample which is directly related to the dipole moment vibration and transition of the energy level. The FTIR spectrums of all synthesized NCs mentioned in Table 1 are shown in Figure 14. For example, the FTIR spectrum of Fe<sub>3</sub>O<sub>4</sub>/Mineral-soil NCs synthesized from the extract of *Euodia hortensis* plant is illustrated in Figure 14g. As is obvious, the intense peaks at 462.94, 1018.34, 1084.11, 3431.82 cm<sup>-1</sup> confirm the deposition if the phytochemicals on the surface of the nanostructure available in the synthesized of Fe<sub>3</sub>O<sub>4</sub> and mineral soil. The bending peak of S-O group can be seen at the wavenumber of 462 cm<sup>-1</sup> and the stretching vibration of S=O group is observed at 1018 cm<sup>-1</sup>. However, a very broad trough of O-H stretch is recognized at the wavenumber of 3431 cm<sup>-1</sup>. In addition, Figure 14e shows the FTIR spectrum of ZnO/SiO<sub>2</sub>/bentonite NCs synthesized from *Cordyline fruticose* extract. As can be seen, some main signals concerning the OH, C=O, C=C and C-C functional groups probably belonging to the antioxidant phenolics of the plant extract and the natural clay used (Tapondjou et al., 2016). Additionally, the main peaks of Zn-O and Si-O are also shown according to Kang et al. (2010) and Singh et al. (2019). These signals confirm the adsorption of plant phytochemicals on the surface of nanocomposite which beside showing the green synthesis of the system, they increase the stability of nano-surface against environmental decomposition and deformation side processes.



- Electron microscopy (SEM and TEM)

The scanning electron microscopy (SEM) and transmission electron microscopy (TEM) are common and advanced techniques of electron microscopies that nowadays researchers and technicians use for taking images of materials at the nanoscale with high resolution. Earlier, the optical microscopes were the only option for capturing material images using photons. However, introducing the electron microscopy gave the capability of observing nanomaterials with high resolution at large magnifications. SEM and TEM can observe the image of the samples with an atomic resolution due to having the shorter wavelength compared with the optical microscopy by photons. For SEM analysis, the sample is prepared simply and installed in a right place inside the SEM instrument to analyse the sample area at micron or nano sizes depends on the electron responses from a concentrated beam. When the electrons fired onto the sample area, they will be attracted by a positive charge detector that displace the morphology of the sample (Zhou and Li, 2015). On the other hand, with the same mechanism of SEM by spreading the electrons from a highly concentrated beam over the sample area, TEM is used to identify the internal structure of the materials. The only difference is that the electrons pass through the nano- or micro-sized particles by TEM; thus, it can identify the phase and internal structure of the materials (Ebnesajjad and Ebnesajjad, 2013). The morphological analysis of all synthesized NCs is shown in Figure 15. For example, the morphology of ZnO/SiO<sub>2</sub>/xanthan NCs synthesized from the extract of pomegranate seeds is illustrated by SEM and TEM images shown in Figure 15a and 15i, respectively. Similar morphology was observed elsewhere (Yeganeh-Faal et al., 2017; El Shafey, 2017; Azarshin et al., 2017) enabling the shapes of SiO<sub>2</sub> and ZnO, with sizes below 100 nm, to be identified. In figures, the particles were prepared with the formation of clusters with random distribution of the silica and zinc NPs on the xanthan surface for fabricating the nanocomposite. Also based on the SEM and TEM images, the synthesized was identified as being successfully prepared with the sizes of below 100 nm. Meanwhile, TEM results of TiO<sub>2</sub>/SiO<sub>2</sub>/PAM NCs synthesized in a green way from the same extract is shown in Figure 15j. As is clear, the prepared materials contain the particles with the size of nanometric around 10 nm. This has been also confirmed by SEM in accordance with the observed shapes of nanomaterials, which are very similar to shapes of TiO<sub>2</sub> and SiO<sub>2</sub> reported in the literature (Mahalingam, 2017; El Shafey, 2017; Azarshin, 2017). As can be seen, the particles were clustered together with random distribution of the silica and titanium NPs on the surface of the polyacrylamide (see Figure 15b).

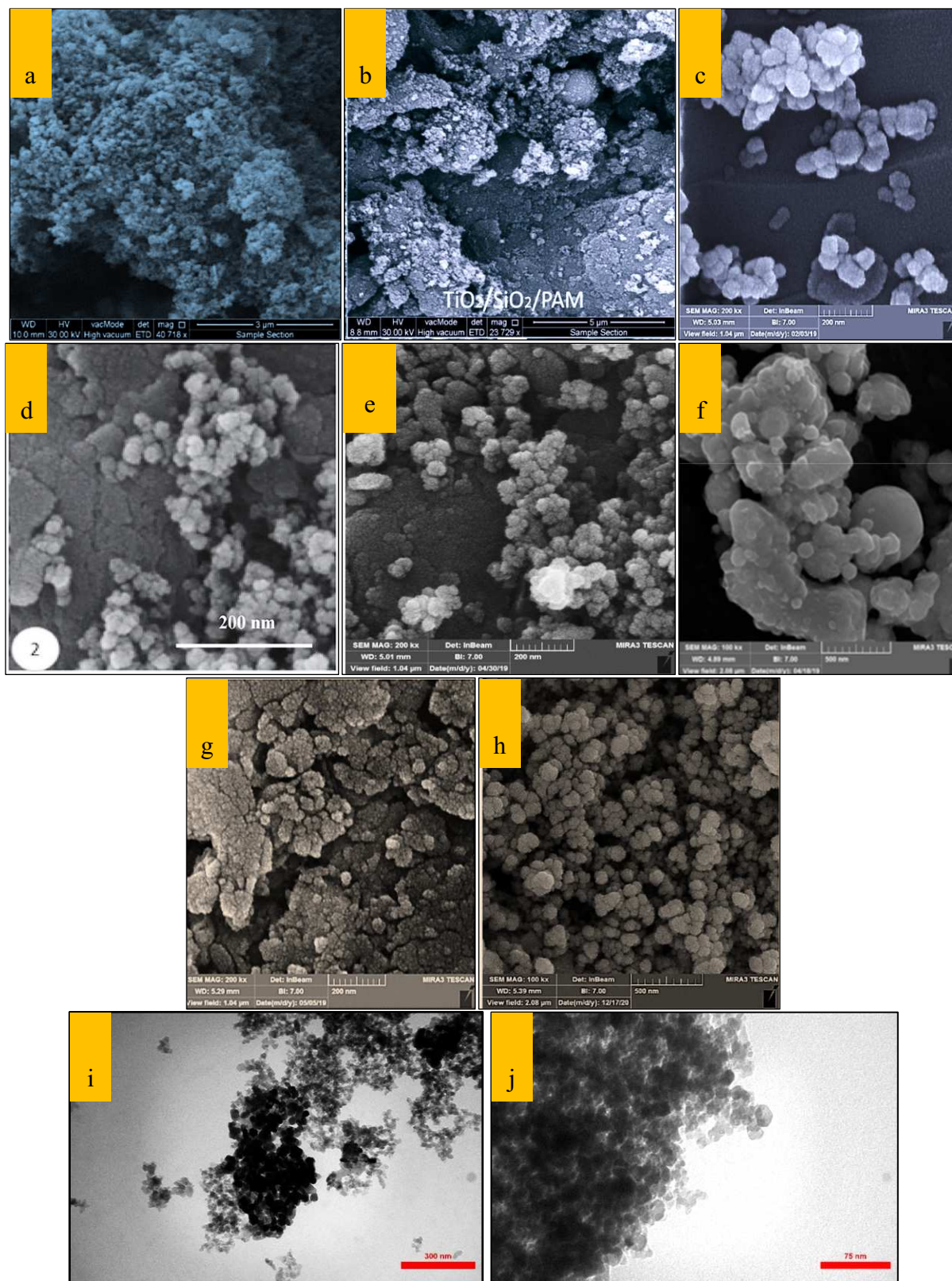


**Figure 15** Morphological analyses of green synthesized NCs; a) SEM of NCs-1, b) SEM of NCs-2, c) SEM of NCS-3, d) SEM of NCs-4, e) SEM of NCs-5, f) SEM of NCs-6, g) SEM of NCs-7, h) SEM of NCs-8, i) TEM of NCs-1, and j) TEM of NCs-2.

### 2.3. Nanofluid preparation and characterization

Nanofluid, as a crucial part of this research project, can be defined as a fluid that contains dispersed nanomaterials. Different types of aqueous phases including water, alcohol, surfactant and mutual solvents were used as the dispersion media for the green nanocomposites. Figure 16 illustrates the methods of the nanofluid preparation and characterization. As can be seen, nanomaterials can be dispersed within these aqueous phases of fluids at different concentrations varying from 100 to 5000 ppm using magnetic stirrer for a period of time between 4-8 hr at rotation speed of 600-800 rpm and room temperature (Sharma et al., 2016). The ultrasonic homogenizer is also used to obtain a good dispersion of the nanoparticles inside the liquid phase with high stability. The suspension stability is a major consideration of the nanofluid to exhibit its unique properties and functions over a certain time. Thus, several methods were used for characterization of the nanofluid, such as pH, conductivity, viscosity and visualization.

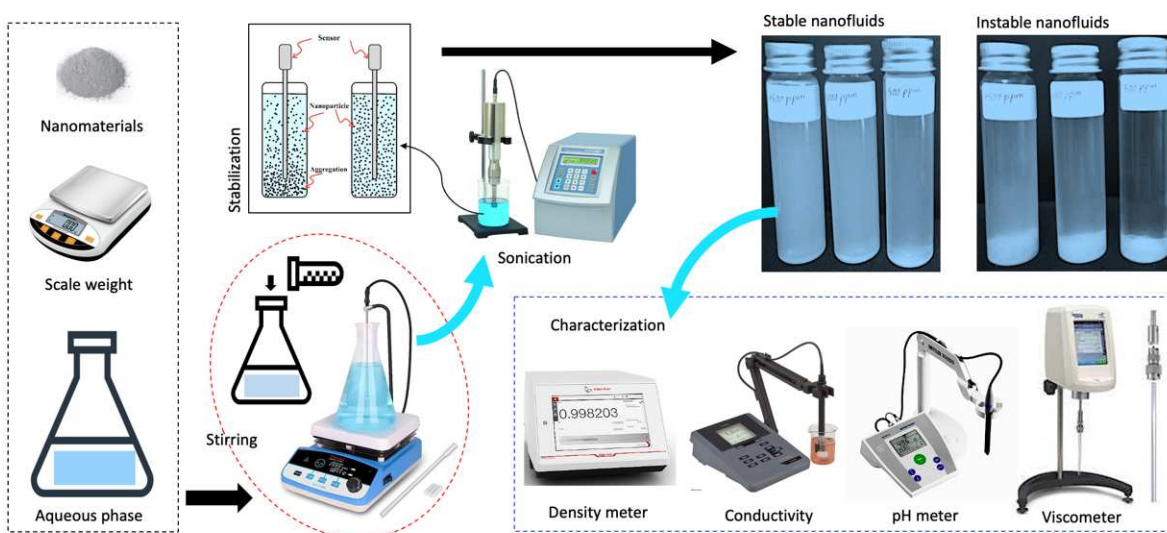


**Figure 16** Schematic illustration of nanofluid preparation and characterization including stirring, sonication, density meter, viscometer, conductivity meter and pH meter.

Table 2 shows the details of the nanofluids developed from the dispersing the synthesized nanocomposites (NCs-1 to NCs-8) at different concentrations with various aqueous phases. Nanofluids were prepared as follows:

- NCs 4 and 7 were mixed with the distilled water at different concentrations of 100 to 2000 and 250 to 1000 ppm, respectively.

- NCs 1, 3 and 5 were dispersed with water under the influence of different salinity levels (from low to high salinity) at concentrations of 500 to 2000, 250 to 1000 and 250 to 2000 ppm, respectively.
- NCs-2 is mixed with the smart water made of different dissolved ions including NaCl, KCl, MgCl<sub>2</sub>, CaCl<sub>2</sub>, Na<sub>2</sub>SO<sub>4</sub>, MgSO<sub>4</sub>, K<sub>2</sub>SO<sub>4</sub> and CaSO<sub>4</sub> at different concentrations of salts ranging from 2500 to 10000 ppm and NCs concentration of 500 to 1500 ppm.
- NCs-6 was mixed with the surfactant-based fluid extracted from *Cyclamen persicum* plant at concentration ranging from 250 to 2000 ppm.
- The last NCs was dispersed within the mutual solvents of ethanol and methyl ethyl ketone at concentrations ranging from 500 to 1500 ppm.

**Table 2** The recipe of the nanofluids prepared from dispersion of the synthesized NCs within different fluids, such as water, surfactant and alcohol.

| NCs   | Description                                  | Dispersion media | NCs concentration (ppm) | Condition  |
|-------|--|------------------|-------------------------|--|
| NCs-1 | ZnO/SiO <sub>2</sub> /Xanthan                | Water            | 500-2000                | Different salinity levels                              |
| NCs-2 | TiO <sub>2</sub> /SiO <sub>2</sub> /PAM      | Smart water      | 500-1500                | Various dissolved ions                                 |
| NCs-3 | TiO <sub>2</sub> /Quartz                     | Water            | 250-1000                | Different salinity levels                              |
| NCs-4 | SiO <sub>2</sub> /Montmorilant/Xanthan       | Water            | 100-2000                | Distilled water  |
| NCs-5 | ZnO/SiO <sub>2</sub> /bentonite              | Water            | 250-2000                | Different salinity levels                              |
| NCs-6 | ZnO/Montmorilant                             | Surfactant       | 250-2000                | Natural surfactant from <i>Cyclamen persicum</i> plant |
| NCs-7 | Fe <sub>3</sub> O <sub>4</sub> /Mineral–Soil | Water            | 250-1000                | Distilled water  |
| NCs-8 | SiO <sub>2</sub> /KCl/Xanthan NCs            | Mutual solvent   | 500-1500                | Ethanol and methyl ethyl ketone solvents               |

Visual observation of the developed nanofluids by naked eyes is one of the techniques that was used to evaluate the suspension stability of the greenly synthesized NCs over the time. Figure 17 illustrates the images of some samples of nanofluids prepared from mixing TiO<sub>2</sub>/SiO<sub>2</sub>/PAM NCs within water at different concentrations of 500, 1000 and 1500 ppm over the time period of six days. As can be seen, an excellent suspension stability of the of the nanofluids was obtained in first four days. This high stability might be due to the presence of PAM as a substrate in the synthesized NCs (Yang and Liu, 2010; Chen and Xie, 2010; Yu and Xie, 2012). However, the sedimentation of the dispersed NCs started to happen in day 5, and at the end of day 6, nanocomposites with the concentrations of 500 ppm were completely precipitated at the bottom of the vessels (Saw et al., 2023). Meanwhile, the nanocomposites of 1000 and 1500 ppm were

partially precipitated at the bottom of the vessels. Hence, it can be conducted that the nanofluids developed at higher concentrations of the nanocomposites provided better stability over the time.

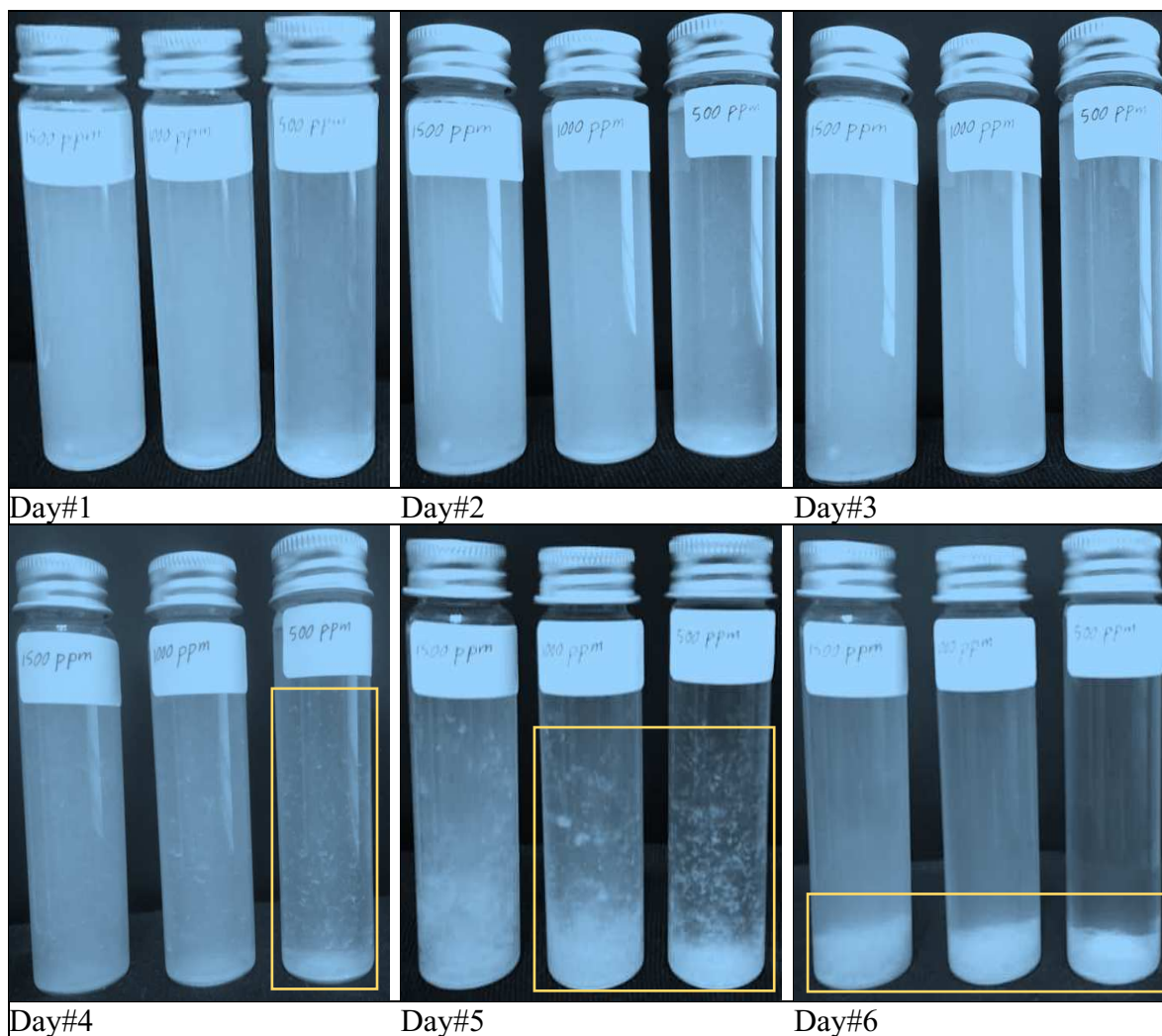


**Figure 17** Visual suspension stability observation of nanofluids prepared from NCs-2 at different concentrations of 500, 1000 and 1500 ppm over 6 days period of time.

Furthermore, Figure 18 illustrates the measured pH values, as one of the crucial physiochemical properties of nanofluids, formulated from the synthesized ZnO/SiO<sub>2</sub>/bentonite NCs depends on the NCs concentration and salinity of the dispersion media. As is obvious, pH has the direct influence on the aggregation and the suspension stability of nanoparticles within the colloidal solution (Fovet et al., 2001; Yu and Xie, 2012). The measured pH of all prepared nanofluids at different salinity level (HiSal: high salinity, LoSal: low salinity, MoSal: moderate salinity and distilled water) and various NCs concentrations are shown in Figure 18a. As can be

seen, the value of pH is in the range of 6.9 to 8.1 where a stable aqueous phase can be obtained. The pH is changed with changing the salinity and increasing the concentration of NCs; when the salinity of the aqueous phase is high, pH is increased with increasing the NCs concentration, however, the pH of the nanofluids in decreased with increasing the NCs concentration when the salinity is too low. Meanwhile, more stable trends of the conductivity and density of nanofluids were achieved (see Figures 18b,c). These two properties were more influenced by the effect of salinity compared with concentration of ZnO/SiO<sub>2</sub>/bentonite NCs. Generally, the density of the nanofluid was slightly increased from 0.995 to 1.028 gm/cm<sup>3</sup> which is belonged to the HiSal nanofluids. Nevertheless, the conductivity was highly changed from 30 mS/m to 284 mS/m under the impact of water salinity rather than NCs concentration.

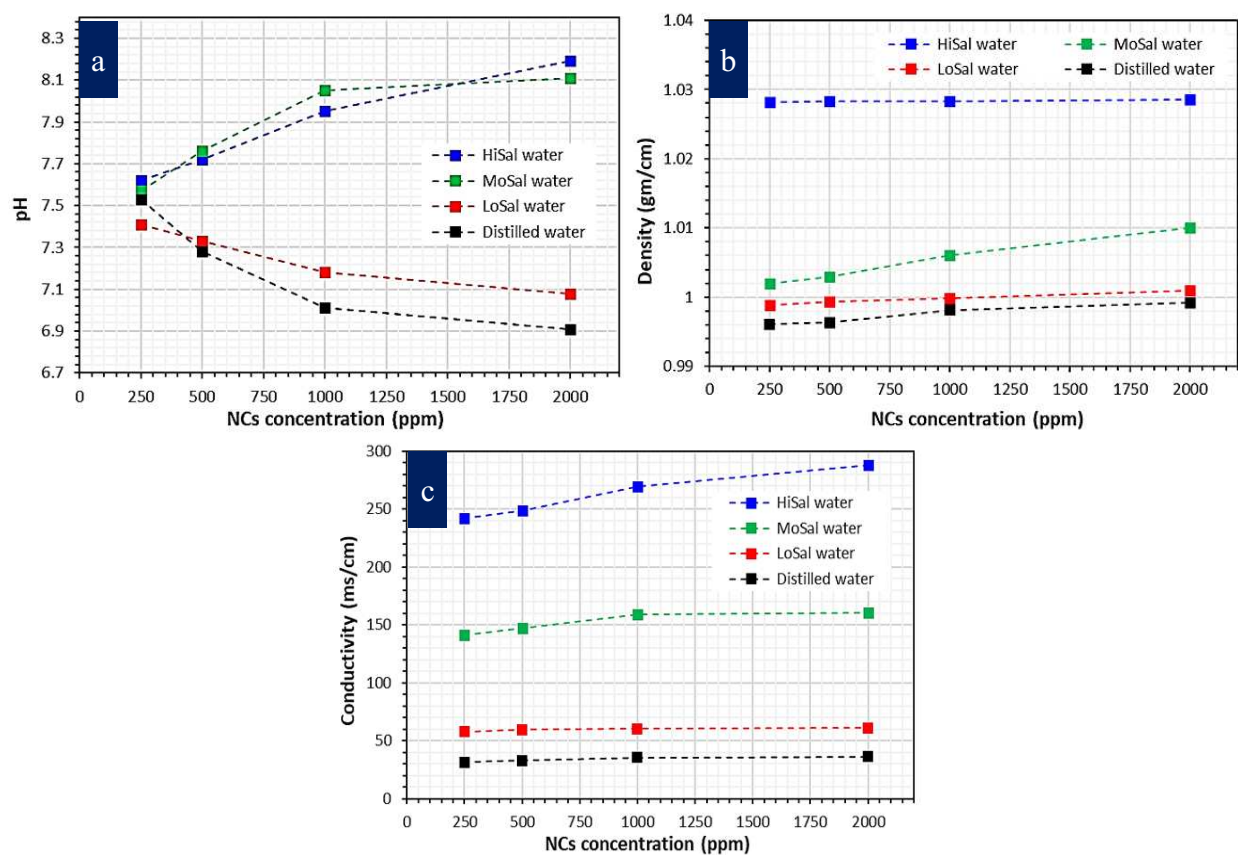


**Figure 18** Characteristics of nanofluids prepared from mixing 250, 500, 1000 and 2000 ppm ZnO/SiO<sub>2</sub>/bentonite NCs within HiSal, Mosal, LowSal and distilled water.

### 3. Interfacial tension reduction

Nanomaterials in the form of nanofluids have shown an effective role in EOR applications for improving oil recovery from oil reservoirs by activating the wettability alteration and interfacial tension reduction (Aurand et al., 2014; Ismailov and Veliyev, 2011; De Castro Dantas et al., 2017). IFT reduction is a critical mechanism of the chemical EOR that leads better oil efficiency by breaking the forces exist in an interference between crude oil and water inside porous spaces. Nanomaterials usually try to form a layer in the interface between water and crude oil (Dahle et al., 2013; Davoodi et al., 2022). This layer produces less interfacial tension between immiscible phases depends on the concentration of NPs dispersed within nanofluids (Hendraningrat et al., 2013; Roustaei et al., 2013). Thus, crude oil can be free to move easier towards the production well. Nanomaterials composed of nanoparticles and a matrix material (i.e., polymer) with better surface features can reduce the IFT greatly due to providing a withstanding impact on the interfacial interaction between the displacing fluid and crude oil (Garmroudi et al., 2022; Saw et al., 2023; Asl et al., 2023). In addition, nanocomposites can develop the nanofluid with better dispersion stability because of presence of polymer chains. The IFT between the crude oil and different aqueous phases is measured with an interfacial tension apparatus (VIT-6000) using a pendant drop method from estimating the dimensions of the suspended droplet of crude oil within the displacing fluid (Figure 19b). After receiving the image of the droplet from a camera, the software identified the value of IFT based using equation 2.

$$\gamma = \frac{\Delta\rho \cdot g \cdot D}{H} \quad (2)$$

where  $\Delta\rho$  is the difference between the density of the drop and bulk fluids ( $\text{gm/cm}^3$ ),  $g$  is the gravitational acceleration of the earth ( $\text{cm/sec}^2$ ),  $D$  is the large diameter of the droplet (cm), and  $H$  is the droplet shape factor. In our research studies, the IFT between the crude oil and nanofluids prepared from mixing the synthesized NCs within the distilled water, smart water, surfactant and mutual solvents at different concentrations under different temperature, pressure and salinity conditions as mentioned in was measured using pendant drop and ADSA (axisymmetric drop shape analysis) shape analysis technique (see Figure 19a). As can be seen, the setup consists of fluid pump, light panel, camera, fluid vessel and computer. The crude oil is injected into the view cell through a needle that can generate the oil droplet to be captured by a camera.

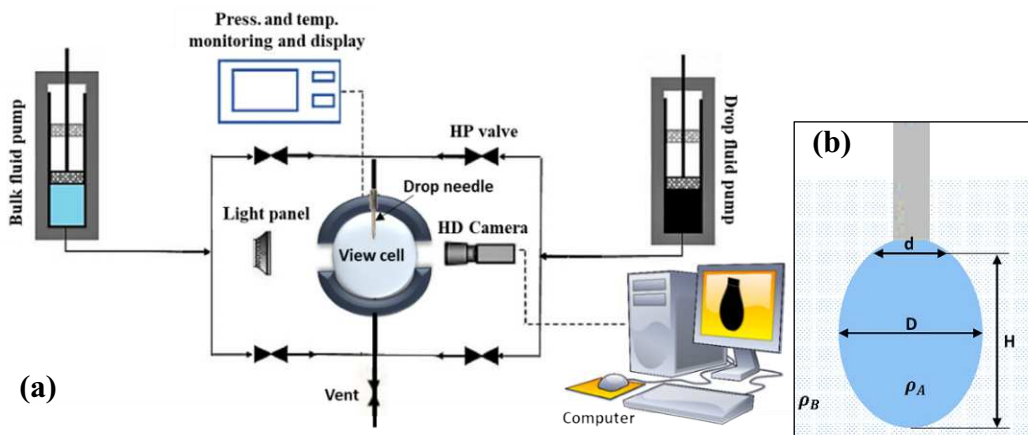


**Figure 19** Schematic presentation of high-pressure (HP) and high-temperature (HT) IFT measurement setup; a) pendant drop VIT-600 apparatus, and b) crude oil droplet.

IFT values measured from each system of crude-oil/aqueous phase is varied to another one dependent on the concentration of NCs, types of additives, temperature and salinity. The minimum IFTs obtained under the influence of each the prepared nanocomposites are shown in Table 3. As can be seen,  $\text{TiO}_2/\text{Quartz}$  NCs enabled to provide the minimum IFT between two immiscible phases when it is mixed with the distilled water, which is 1.141 mN/m. Generally, the synthesized NCs were highly effective when they dispersed with low salinity water (distilled water) and reduced IFT significantly, for example NCs-1 decreased IFT to 2.547 and 2.016 mN/m when it is mixed with the distilled water and low salinity water, respectively. However, the same nanocomposites created 9.85 mN/m as the minimum IFT at the same experimental condition when it is mixed with the high salinity water. This is true for the other green NCs (NCs-3, NCs-5 and NCs-7) when the same behavior was observed. In addition, mixing the synthesized NCs within the surfactant and methyl ethyl keton enabled high reduction in the value of IFT to 1.5-2.5 mN/m. Meanwhile, when  $\text{SiO}_2/\text{KCl}/\text{Xanthan}$  NCs is mixed with ethanol, it doesn't affect the value of IFT highly which is unfavorable. As is obvious, the initial IFT values between oil/seawater and oil/distilled water were measured to be about 31.8 and 28.312 mN/m, respectively.

**Table 3** IFT values measured under the effect of nanofluids developed from dispersing green polymer NCs within different aqueous phases.

| NCs   | Description                                  | Dispersion media | NCs conce. (ppm) | Condition   | Minimum IFT [mN/m] |
|-------|--|------------------|------------------|---|--------------------|
| NCs-1 | ZnO/SiO <sub>2</sub> /Xanthan                | Water            | 500-2000         | Distilled water   | 2.547              |
|       |  |                  |                  | Low salinity  | 2.016              |
|       |  |                  |                  | High salinity   | 9.85               |
| NCs-2 | TiO <sub>2</sub> /SiO <sub>2</sub> /PAM      | Smart water      | 500-1500         | KCl-5000  | 6.0                |
|       |  |                  |                  | K <sub>2</sub> SO <sub>4</sub> -5000                      | 8.9                |
|       |  |                  |                  | CaSO <sub>4</sub> +CaCl <sub>2</sub> (2500)               | 10.7               |
|       |  |                  |                  | K <sub>2</sub> SO <sub>4</sub> +CaCl <sub>2</sub> (25000) | 8.0                |
| NCs-3 | TiO <sub>2</sub> /Quartz                     | Water            | 250-1000         | Distilled water   | 1.141              |
|       |  |                  |                  | Low salinity  | 8.977              |
|       |  |                  |                  | High salinity   | 8.513              |
| NCs-4 | SiO <sub>2</sub> /Montmorilant/xanthan       | Water            | 100-2000         | Distilled water   | 15.42              |
| NCs-5 | ZnO/SiO <sub>2</sub> /bentonite              | Water            | 250-2000         | Distilled water   | 2.59               |
|       |  |                  |                  | Low salinity  | 3.1                |
|       |  |                  |                  | High salinity   | 5.59               |
| NCs-6 | ZnO/Montmorilant                             | Surfactant       | 250-2000         | Natural surfactant from Cyclamen persicum plant           | 2.46               |
| NCs-7 | Fe <sub>3</sub> O <sub>4</sub> /Mineral-Soil | Water            | 250-1000         | Distilled water   | 3.69               |
| NCs-8 | SiO <sub>2</sub> /KCl/Xanthan NCs            | Mutual solvent   | 500-1500         | Ethanol   | 6.4                |
|       |  |                  |                  | Methyl ethyl keton  | 1.51               |

As an example, the effect of ZnO/SiO<sub>2</sub>/Xanthan (NCs-1) and TiO<sub>2</sub>/SiO<sub>2</sub>/PAM (NCs-2) on IFT under different temperature, pressure and salinity conditions are presented below. It was identified that the IFT was reduced to its optimum value, 2.016 mN/m, by the influences of the synthesized NCs-1. When the salinity of water was decreased 20 times based on the salting-out approach, the IFT was reduced by 38% from 31.8 to 19.68 mN/m. Meanwhile, adding NCs-1 into the DW and LoSal water lead the IFT to be greatly decreased to its lowest values. The measured IFT values between the oil/nanofluid (DW) and oil/LoSal-nanofluid are 2.547 and 2.016 mN/m, respectively, at the same experimental conditions (see Figures 20-22). Figures 20-22 illustrate the effects of pressure and temperature on IFT reduction at different NCs-1 concentrations and water salinity ranges. In this work, the experiments were performed at 30, 50 and 70°C temperature and 500, 1000 and 1500 psi pressure. The effect of temperature on IFT reduction is strong compared with the impact of pressure. In all the cases, the IFT values were reduced more by increasing the temperature (part a on Figures 20-22). However, in some cases the pressure had an inverse relation with the IFT reduction but in others there is no clear trend of the impact of pressure (part b on Figures 20-22). In Figure 22, when the concentration of NCs is 2000 ppm and salinity of water is low; by increasing temperature from 30 to 70°C, the IFT of oil/optimum nanofluid was reduced

by 45% from 3.71 to 2.016 mN/m; while, the IFT was increased by about 40% from 2.215 to 3.71 mN/m when pressure was raised from 500 to 1500 psi.

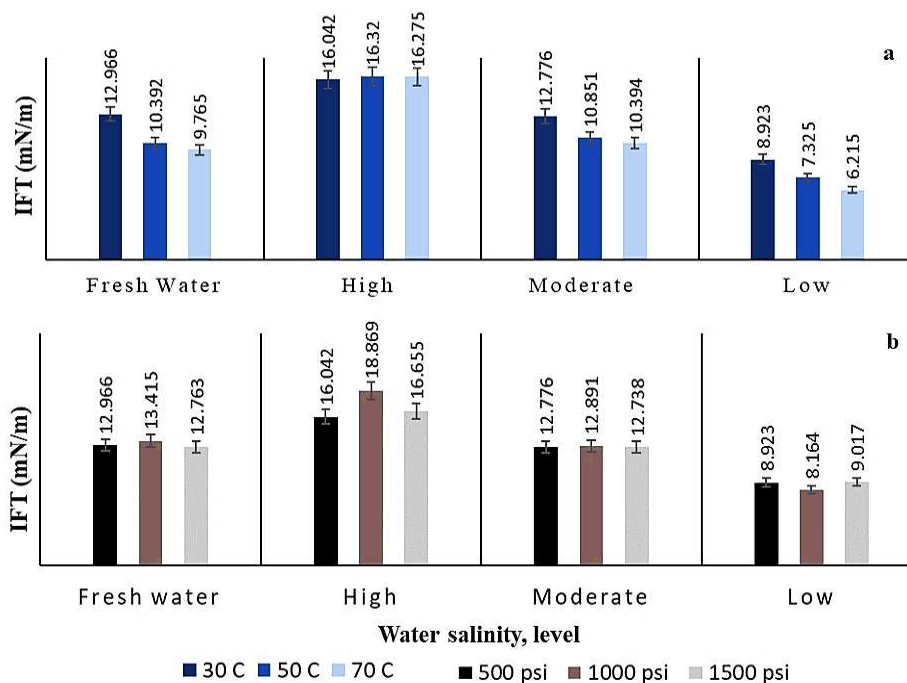


**Figure 20** IFT values measured at 500 ppm NCs-1 concentration (a) effect of temperature on IFT reduction at various salinity levels and ambient pressure (b) effect of pressure on IFT reduction at various salinity levels and room temperature.

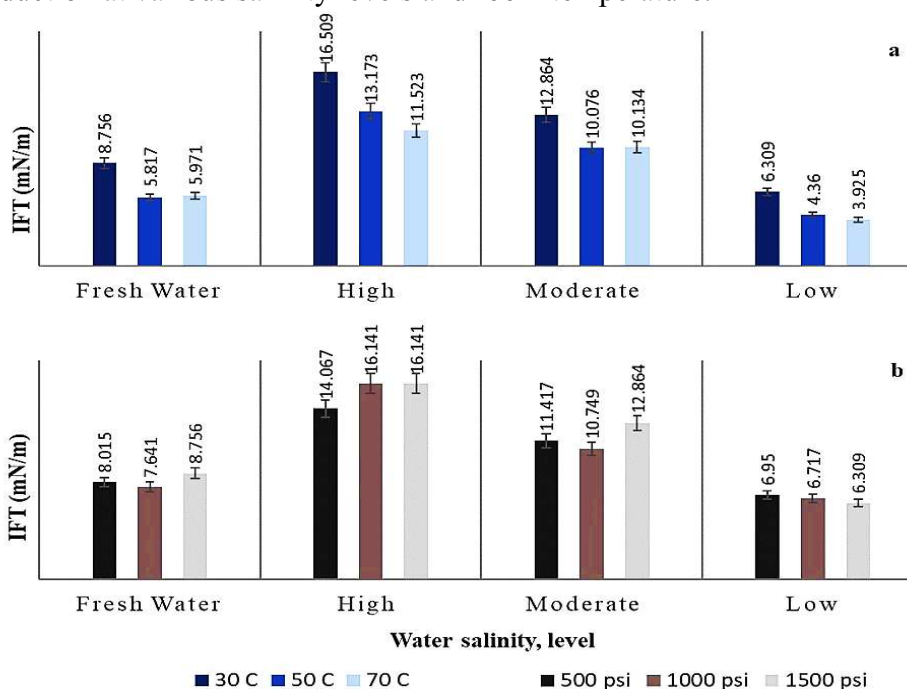


**Figure 21** IFT values measured at 1000 ppm NCs-1 concentration (a) effect of temperature on IFT reduction at various salinity levels and ambient pressure (b) effect of pressure on IFT reduction at various salinity levels and room temperature.

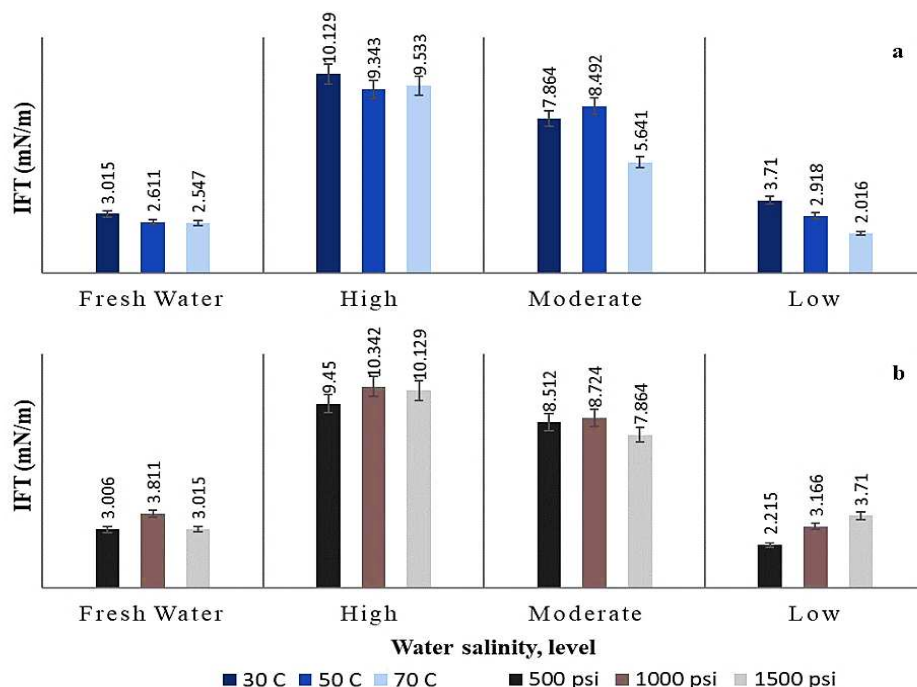


**Figure 22** IFT values measured at 1500 ppm NCs-1 concentration (a) effect of temperature on IFT reduction at various salinity levels and ambient pressure (b) effect of pressure on IFT reduction at various salinity levels and room temperature.

From carrying out all the IFT under the effect of smart water with the presence of the single dissolved-ion and binary dissolved ions, four optimal smart solutions were selected; OSS1 consists of 5000 ppm KCl, OSS2 made-up of 5000 ppm  $K_2SO_4$  dissolved in water, 5000+5000 ppm  $CaSO_4+CaCl_2$  was identified as the first optimal smart solution (OSS3) of binary-ion system, and the last optimal smart solution (OSS4) was with 2500+2500 ppm of  $K_2SO_4+CaCl_2$ . In order to study its effect on the IFT reduction and wettability alteration, smart nanofluids were prepared by adding  $TiO_2/SiO_2/PAM$  NCs to the optimal smart solutions at 500, 1000 and 1500 ppm concentrations. Figure 23 presents the results of the IFT measured under the influences of the smart nanofluids. As can be seen, the minimum IFT was achieved with the nano-KCl-5000 smart nanofluid prepared from dispersing 500 NCs within the OSS1. With this smart nanofluid, the IFT was reduced by 60.7% from 15.3 to 6 mN/m. This drop in IFT could be due to the accumulation of nanoparticles as a single-layer at the interface between two immiscible phases in the porous media, which provide a weak IFT compared with surfactants (Dahle et al., 2013). Additionally, Hendraningrat and Torsaeter (2014) stated that this force can be justified by managing the concentration of nanoparticles. For example, the same smart water (OSS1) increased the IFT by increasing the NCs concentration from 500 to 1000 and 1500 ppm, which is quite consistent with

the results reported by Bahraminejad et al. (2019). Similarly, when the NCs added to other optimal smart solutions (OSS2, OSS3 and OSS4) at different concentrations, different IFTs with the small variation were obtained from the smart nanofluids. The variation in the IFT value for all the studied nanofluids prepared from OSS2, OSS3 and OSS4 was ranged between 8 to 12 mN/m. Hence, we mostly focused on the CA results to select the optimum concentration of NCs.

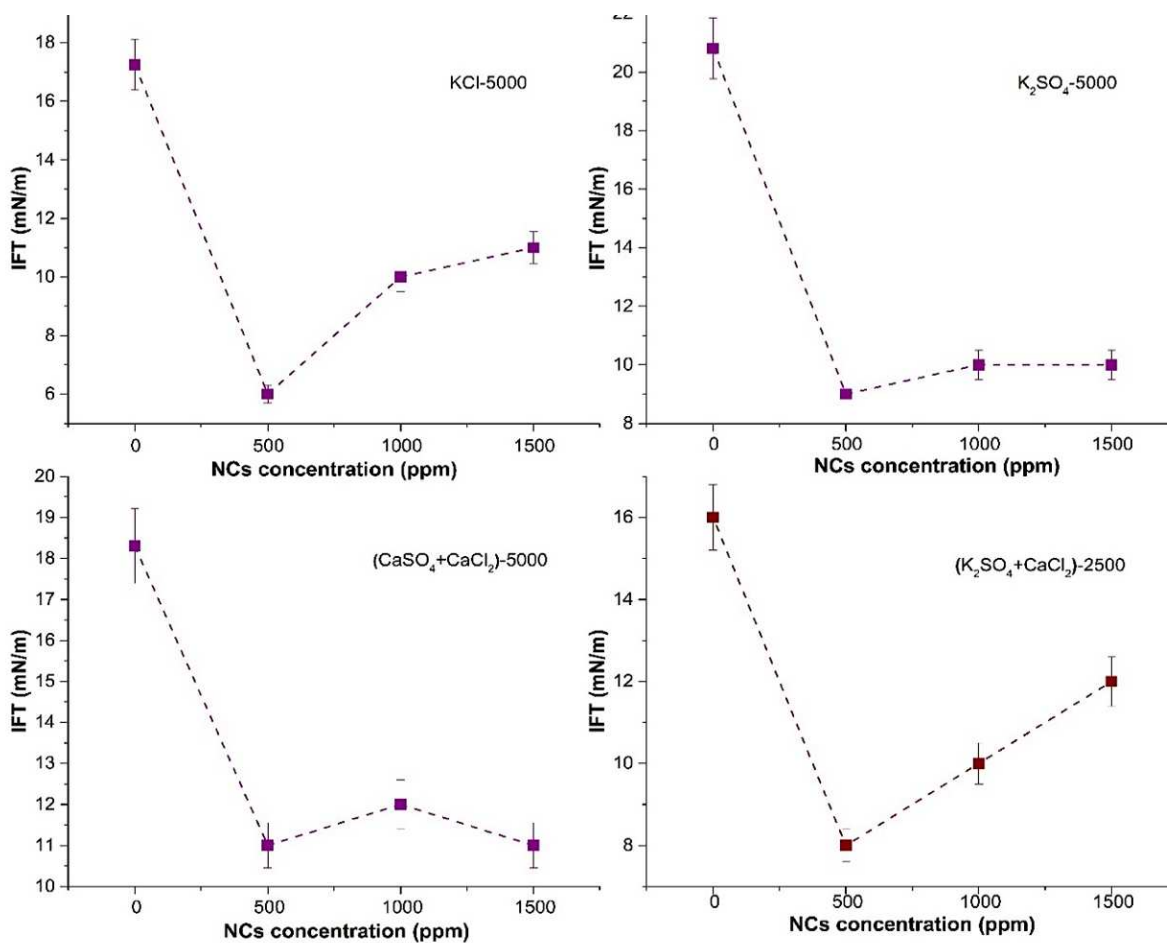


**Figure 23** IFTs measured between crude oil and smart nanofluids prepared from mixing  $TiO_2/SiO_2/PAM$  NCs with the optimal smart solutions ( $KCl$ -5000,  $K_2SO_4$ -5000,  $(CaSO_4+CaCl_2)$  - (2500+2500), and  $K_2SO_4+CaCl_2$  - (25000+25000) at 500, 1000 and 1500 ppm NCs concentration.

## 4. Wettability alteration

Wettability can be defined as the spreading tendency aqueous phases on solid surfaces in the porous media. The wettability as a crucial reservoir parameter plays a significant role in control the flow behavior of fluid phases inside the reservoir and affects the moveability of hydrocarbons toward the production wells (Lashari et al., 2022). The state of the fluids exist in the porous media can be classified into three states, such as water-wet, oil-wet and intermediate-wet sates as shown in Figure 24. As can be seen, water is absorbed onto the surface of the rock and is completely covering the solid surfaces in the porous media in a water-wet system. Thus, the crude oil is accumulated inside the pore spaces which can be easily produced by displacing fluids with a portion of trapped crude oil left in the reservoir. However, in the oil-wet system, crude oil is spreading on the solid surfaces and water is accumulated in the center of the pore spaces (Abdallah et al., 2007). To produce hydrocarbon from such wetting state, the displacing fluid should have a stronger adsorption ability to replace the crude oil and a portion of remaining crude oil is called residual (see Figure 24). Wettability alteration is a phenomenon of changing the state of the rock from water-wet to stronger water-wet or from oil-wet towards the water-wet to make hydrocarbons free for extraction. This phenomenon is conducted by different processes and chemical EOR is one the most common wherein some active agents with high adsorption adhesion are injected into the reservoir to replace the crude oil on solid surfaces (Yuan et al., 2019). The low salinity water and nanofluid as displacing fluids are highly attracted by the solid surfaces in the porous media, especially the carbonate rock (Yuan et al., 2019; Kumar et al., 2023).

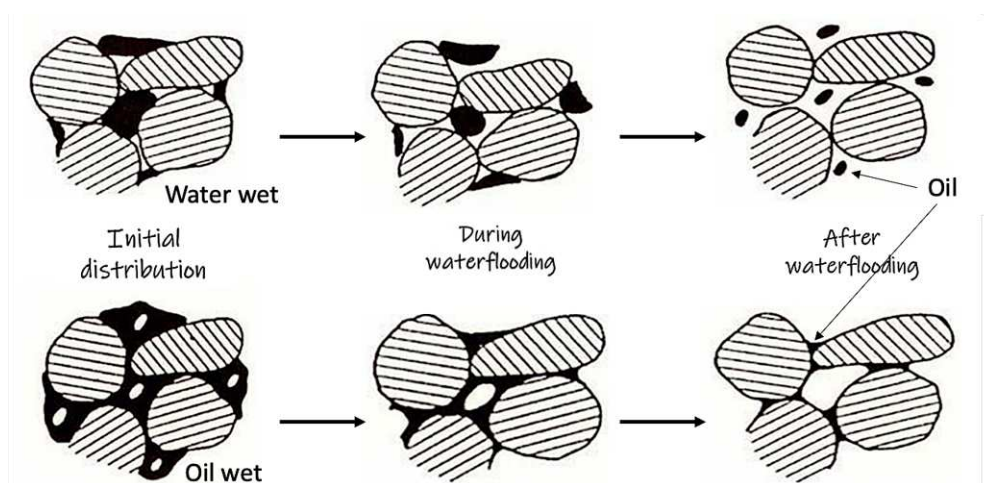


**Figure 24** Fluid distributions (water-wet and oil-wet) inside porous media before, during and after displacement of hydrocarbons (re-drawn after Abdallah et al., 2007).

For better understanding the mechanism of reducing the contact angle and altering the wettability of the reservoir from the oil-wet system towards the water wetting, it is necessary to consider the concept of disjoining pressure during nanofluid processes shown in Figure 25. Within this thin film, the NPs tend to arrange themselves in well-ordered layers. This arrangement increases the entropy of the nanofluids due to the greater freedom of the NPs in the nanofluids (Lashari et al., 2022). The result of this arrangement exerts additional disjoining pressure at that interface more than that in the bulk liquid. Paul et al. (2012) reported that a film of nanofluids on the surface of the rocks has the ability to separate and release the reservoir fluids. In this way, the wetting system can be changed from oil-wet to water wet. This can increase the displacement efficiency of crude oil through the porous media (Sun et al., 2017). Aveyard et al. (2003) explained that this film of nanofluids can be influenced by some parameters, such as nanoparticle concentrations and sizes, salinity, temperature and surface rock properties. Moslan et al. (2017) studied the effect of alumina NPs on wettability alteration in carbonate reservoir rock and identified that this nanomaterial is capable of altering the wettability system from the oil-wet to water-wet and increasing the recovery of oil by about 11.25%. Yuan et al. (2019) and Lashari et al. (2023) stated that from all the wettability systems, EOR nanofluids have shown a stable performance and altered the wettability on the quartz surface to strongly water-wet and improved the oil recovery better than the silica-based NPs due to the modification some properties including pH, conductivity and particle size distribution.

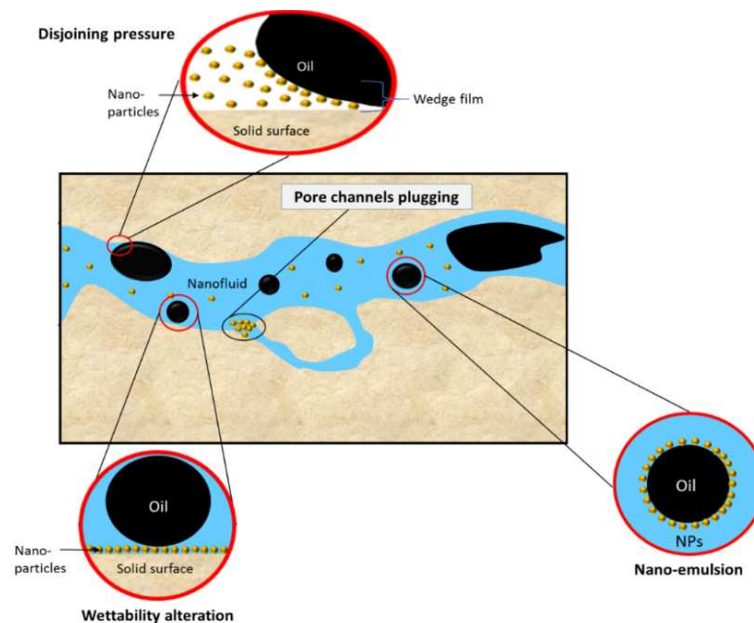


**Figure 25** The schematic of the EOR mechanisms of Nanofluids through the porous media.

In addition, the wettability of the used rock samples was determined by contact angle measurement when two immiscible liquids are presence, as shown in Figure 26a. The measurement consists of medium to hold the crude oil droplet on the surface of the rock with the presence of the aqueous phase, a camera, computer, illuminator and liquid storage vessels. When the snapshot of the crude oil droplet is captured, it will be sent to computer to estimate the right and left contact angle (CAs). According to the average value of CA, the wettability state can be defined as the oil-wet when the contact angle is higher  $90^\circ$ , neutral wet when the contact angle equals to  $90^\circ$ , or water-wet at the contact angle less than  $90^\circ$  (Tang et al., 2023). The experimental work of the contact angle measurements was started with preparing the rock plates of 2 mm from carbonate rock samples. After obtaining the smooth plates, they were cleaned using the toluene and distilled water. The smooth and cleaned sections were then submerged into the crude oil for the time period of 2-3 weeks at  $70^\circ\text{C}$  to achieve the oil-wet state (see Figure 26b). Afterwards, the aged rock slices were then dropped into the enclosed containers filled with different aqueous phases including distilled water, low-salinity water, seawater, smart water, mutual solvents, surfactant and nanofluids under the static condition of 3-7 days. Finally, the contact angle (CA) of the crude oil droplets on the surface of all aged slices were measured under the influences of synthesized green nanocomposites.

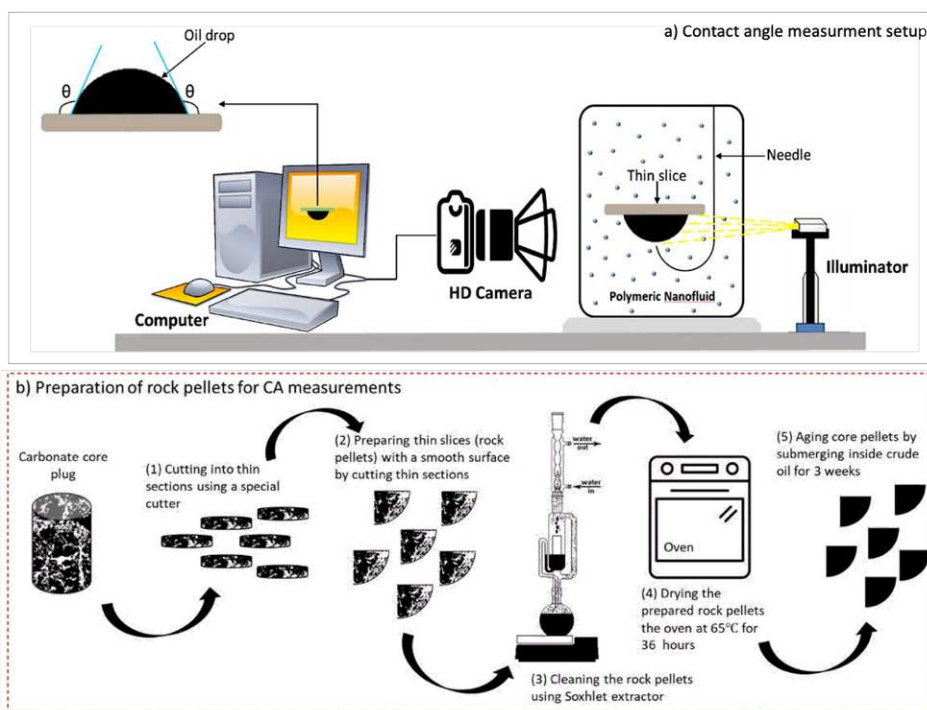


**Figure 26** Schematic illustration of the contact angle measurement; a) CA measurement setup, and b) preparation and aging of rock plates used in measuring contact angle.

All greenly synthesized nanocomposites including NCs-1, NCs-2, NCs-3, NCs-4, NCs-5, NCs-6, NCs-7 and NCs-8 are used in the contact angle (CA) measurement at different concentrations. Figure 27 shows the minimum obtained values of the contact angles of the crude oil droplets on the surface of the prepared rock plates obtained under the influence of the formulated nanofluids at different conditions (see Table 1). As can be seen, the minimum CA was obtained under the impact of nanofluid NCs-6-surfactant developed from mixing ZnO/Montmorillonite NCs with the extract of cyclamen persicum plant, which is  $19^\circ$  that presents a strong water-wet system. However, NCs-3-HSW and NCs-5-HSW nanofluids prepared from mixing TiO<sub>2</sub>/Quartz and ZnO/SiO<sub>2</sub>/bentonite NCs within the high salinity water exhibited the least performance in reducing the CA and recorded CAs of  $112^\circ$  and  $103.5^\circ$ , respectively. This confirms that both synthesized NCs were not applicable to be dispersed with water at high salinity level (HSW) and not able to alter the wettability of the rock from water-wet state. Overall, all synthesized NCs demonstrated a significant performance in altering the wettability of the rock samples at lower salinity levels of water. ZnO/SiO<sub>2</sub>/Xanthan NCs enabled to decline the CA of the crude oil on rock plates from its initial value above  $90^\circ$  to a favourable range between  $34^\circ$  to  $53^\circ$  under the influence of water salinity (see Figure 27). CAs with the range varied from  $44^\circ$  to  $50^\circ$  were obtained under the effect of TiO<sub>2</sub>/SiO<sub>2</sub>/PAM NCs dispersed within smart water contains various dissolved salts. In addition, TiO<sub>2</sub>/Quartz NCs was successful to alter the wettability from oil-wet towards water-wet when dispersed within the distilled water (DW) and low salinity water (LSW). Meanwhile, significantly low CAs of  $22^\circ$  and  $33^\circ$  were obtained by SiO<sub>2</sub>/KCl/Xanthan and Fe<sub>3</sub>O<sub>4</sub>/Mineral–Soil NCs when mixed within the distilled water (DW).

Furthermore, Figure 28 illustrates the snapshots of crude oil droplets on the prepared rock surfaces under the influences of the optimal smart solutions (OSS1-4) with and without the presence of TiO<sub>2</sub>/SiO<sub>2</sub>/PAM NCs. These optimal solutions of smart water were selected dependent on their efficiency in reducing the IFT and CA from several salts (NaCl, KCl, MgCl<sub>2</sub>, CaCl<sub>2</sub>, Na<sub>2</sub>SO<sub>4</sub>, MgSO<sub>4</sub>, K<sub>2</sub>SO<sub>4</sub> and CaSO<sub>4</sub>) when they mixed with the distilled water separately and together at different concentrations from 250 to 10000 ppm (see the included publication 6, Ali et al., 2021). OSS1 consists of 5000 ppm KCl, OSS2 made-up of 5000 ppm K<sub>2</sub>SO<sub>4</sub> dissolved in water, 5000+5000 ppm CaSO<sub>4</sub>+CaCl<sub>2</sub> was identified as the first optimal smart solution (OSS3) of binary-ion system, and the last optimal smart solution (OSS4) was with 2500+2500 ppm of K<sub>2</sub>SO<sub>4</sub>+CaCl<sub>2</sub>. As can be seen, different values of CAs were measured with various shapes of crude

oil droplets dependent on the type of the used dissolved ions and NCs concentrations, but entirely the variation was between 49 to 109° (Figure 28). This variation in the measured CAs is quite normal based on the reports of Azarshin et al. (2017). For instance, the CA value of the OSS1 (KCl-5000) was firstly increased from 65.7° to 70° by adding 500 ppm NCs, then reduced to 59° by increasing NCs concentration to 1000 ppm and raised again to 90° at 1500 ppm. The minimum CA of 48.3° was measured with the presence of the OSS2 (K<sub>2</sub>SO<sub>4</sub>-5000) at 1500 ppm NCs, which was reduced by 45% from 89°. Moreover, the lowest CAs measured with OSS3 ((CaSO<sub>4</sub>+CaCl<sub>2</sub>)-(2500)), and OSS4 ((K<sub>2</sub>SO<sub>4</sub>+CaCl<sub>2</sub>)-(25000)) were 62° and 57° at 1500 and 1000 ppm concentrations of green NCs, respectively. Generally, OSS2 consists of SO<sub>4</sub><sup>2-</sup> divalent ion and OSS3 solution contains the divalent ions (Ca<sup>2+</sup> and SO<sub>4</sub><sup>2-</sup>) together represented the best performance in proving a good water-wet state. Overall, the maximum CA of 109° was identified with the presence of Nano-OSS3-1500 nanofluid prepared from mixing 1500 ppm TiO<sub>2</sub>/SiO<sub>2</sub>/PAM NCs within a smart water that contains 2500 ppm of CaSO<sub>4</sub> and CaCl<sub>2</sub> salts. This nanofluid was unsuccessful in altering the water-wet wettability to oil-wet state. However, Nano-OSS2-1500 nanofluid enabled to alter the wettability greatly from oil-wet to water-wet system with a contact angle of 48.3°. In addition, some other nano-optimal smart solutions had an effective performance in decreasing the value of the CA, such as Nano-OSS2-100, Nano-OSS3-1000, Nano-OSS4-500 and Nano-OSS4-1000 (see Figure 28).

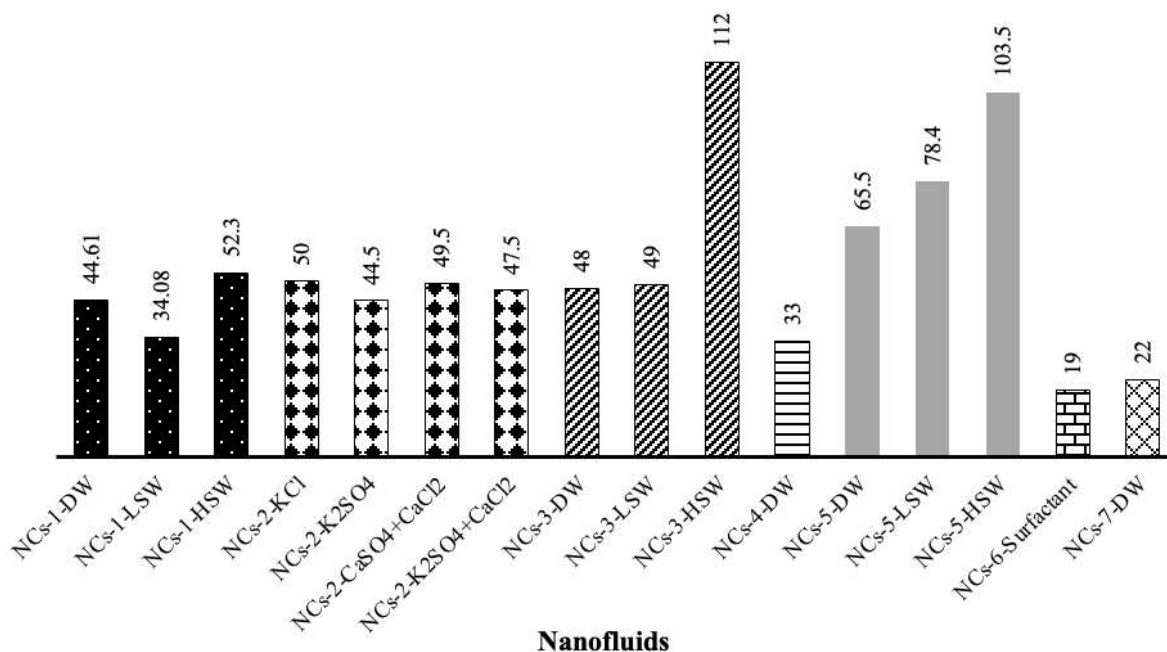


**Figure 27** Contact angles (CAs) of crude oil droplets on the surface of rock plates under the influence of nanofluids prepared from green NCs within various aqueous phases.

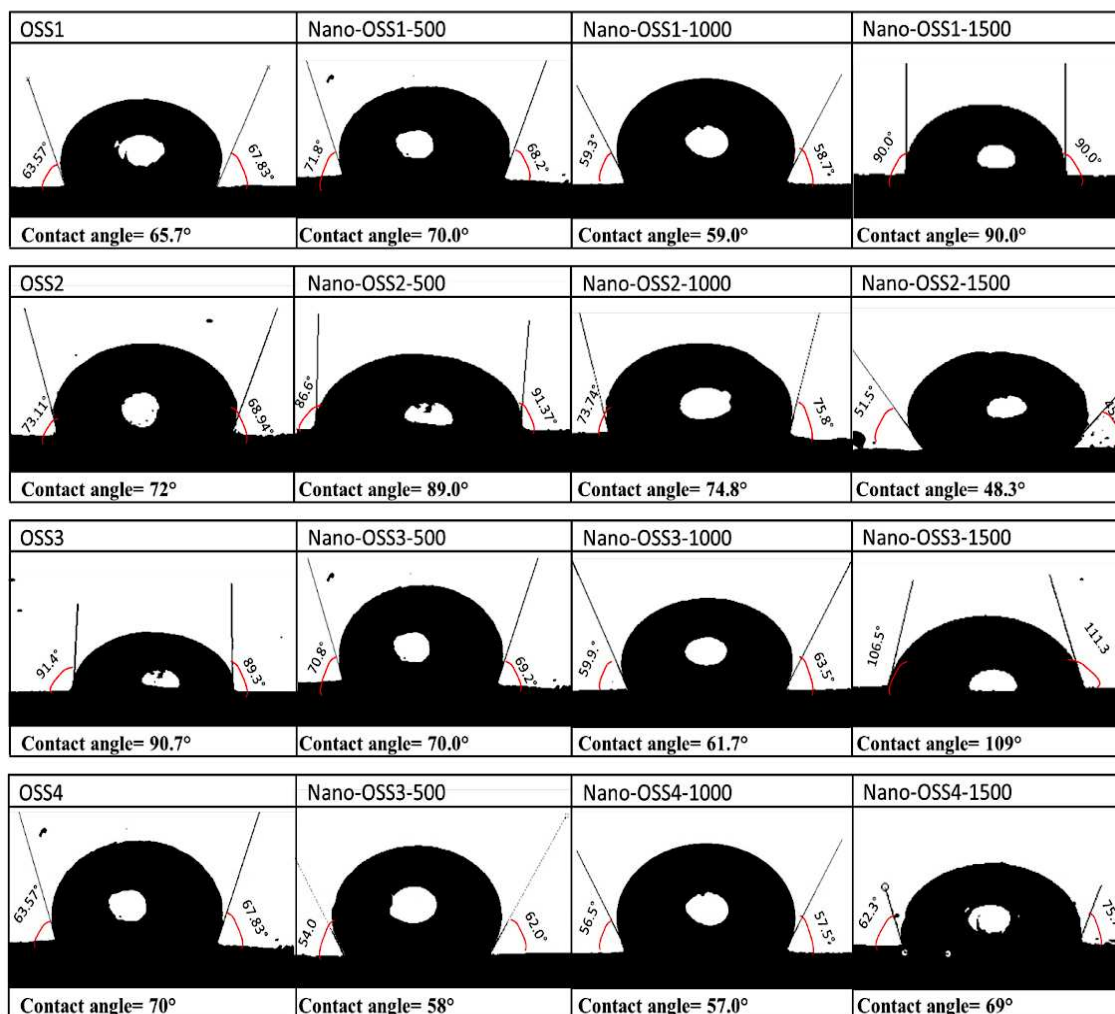


**Figure 28** Shapes of crude oil droplets on the carbonate surface under the influence of the optimal smart solutions (OSS1, OSS2, OSS3 and OSS4) and smart nanofluids (nano-OSS1, nano-OSS2, nano-OSS3 and nano-OSS4) at different concentrations of  $\text{TiO}_2/\text{SiO}_2/\text{PAM}$  NCs.

Furthermore, the mechanism of the wettability alteration in the porous media along with the distribution of the crude oil on the carbonate slices with the presence of nanofluids is shown in Figure 29. As is clear, the mechanism of wettability alteration is divided into three phases; oil blank when the system is oil-wet and crude oil is spread on the solid surface with no chemical influence on the crude oil/rock interaction (Figure 29c1,2), the mobile zone when the injected nanofluid is penetrating the oil blank and both aqueous phases are exist mobile oil and residual oil and wettability alteration started towards water-wet but not completely changed (Figure 29b1,2), and the nanofluid bank when the nanofluid already displaced crude oil and existing wetting state

is water-wet with minimum contact angle (Figure 29a1,2). The crude oil is spread completely on the solid surfaces in the oil bank with high contact angle above  $90^\circ$  that exhibits oil-wet state (see Figures 29c1,2). When the nanofluid injected to displace the crude oil, the contact angle affected to be decreased in the mobile zone due to demonstrating a high adhesion force between the nanofluid and the rock surface as shown in Figure 29b1. Thus, the injected nanofluid is flowing into the interface between the crude oil and rock surface which creates a disjoining pressure to alter the wettability with a CA of  $50-60^\circ$  (see Figure 29b2). Meanwhile, a significant change in the state of the wettability is obtained in the nanofluid bank when the crude oil is displaced by the injected nanofluid as shown in Figure 29a1,2. In this phase, the contact angle is minimal between  $20-40^\circ$  which exhibits a strong water-wet system with the presence of the residual oil saturation but most of the producible crude oil is displaced towards the production well.

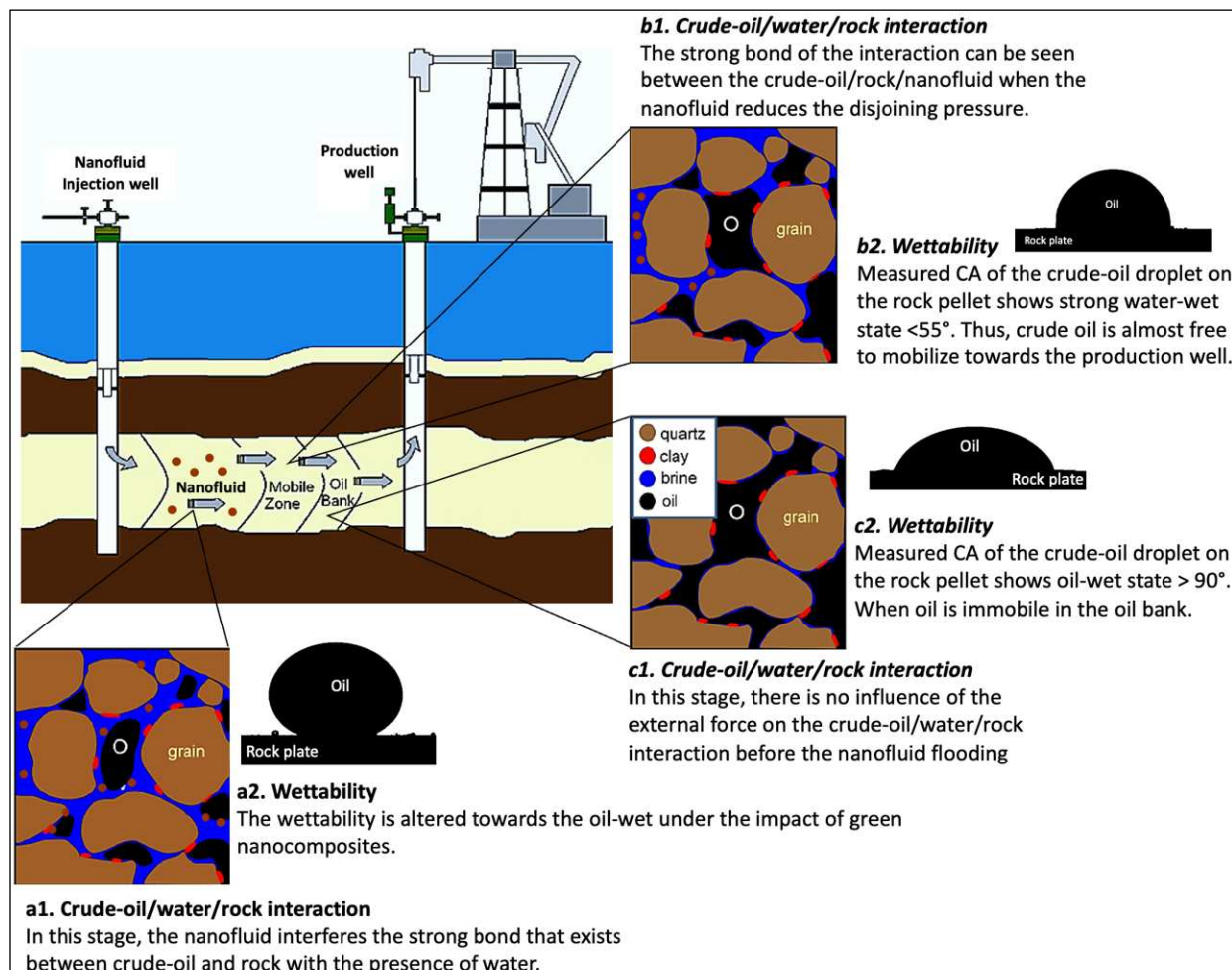


**Figure 29** The mechanism of wettability alteration of rock under the influence of green NCs in different stages; a) late stage with strong water-wet, b) early stage, and c) the strong oil-wet exists in the porous media without any alteration.

## 5. Oil recovery

### 5.1. Core plug preparation

Rock samples from outcrops were used to prepare the core plugs which were carefully cut in a desired length with a diameter of 1.5 in. The prepared plugs were cleaned by a Soxhlet extraction using ethanol and toluene at a temperature between 60-80°C for 1-5 days to remove all the presence water, oil and any other residues. The core plugs were then dried by placing into an oven at 70°C for 6 hours. The dry weight of the prepared core samples was measured. Then, the porosity and permeability of core samples were measured using the helium porosity meter and gas permeameter as shown in Figure 30a. A coreflooding device shown in Figure 30b was used to perform the oil displacement tests. As is clear, it consists of HPHT pump, liquid cylinders, core holder, pressure gauges, valves and hydraulic pump. In this study project, different phases of fluids were used to estimate the oil recovery factor (RF) including water (distilled or brine), crude oil and EOR injection solution. The distilled water and brine were used as the secondary oil recovery process and followed by injecting low salinity water, smart water, surfactant and nanofluid injection as the tertiary recovery process (enhanced oil recovery, EOR). The nanofluids prepared from the synthesized NCs were injected into all used core samples and the obtained results of oil recovery were compared with the results of other chemical solutions.

In order to establish the saturation profiles inside the prepared core plugs, initially, each core sample was placed inside the core holder and the brine accumulator was connected to the core holder, then a confining pressure of 1000 psi greater than the injection pressure was applied (see Figure 29b). After connecting the coreflooding system, the Brine was injected with 0.25 cm<sup>3</sup>/min rate by fluid injection pump. Before setting the cores inside the core holder, the dead volume of the core holder and tubes was measured. The saturation of the cores was achieved when the core produce brine and injection was stopped. Afterwards, oil accumulator was connected to the core holder instead of the brine accumulator and the confining pressure is applied to the core. Then, crude oil was injected into the core samples at different rates from 0.1 to 0.5 cm<sup>3</sup>/min and the produced water was measured in a graduated flask. After occurring the breakthrough, extra 2 pore volumes (PVs) of crude oil were injected to complete the saturation process. From the collected water in the graduated flask, the initial water saturation (Swi) was measured. Then, the saturated cores were kept for one week to achieve the complete and stable oil-wet state. In addition, in one of the cases, the performance of a synthesized NCs, named Fe<sub>3</sub>O<sub>4</sub>/Mineral–Soil, on the oil recovery

was evaluated using the spontaneous imbibition using Amott cell. Two imbibition tests were carried out under the effect of the brine and nanofluid and the test was monitored to determine the amount of the oil expelled from the core plugs and recorded as % of original oil in place (%OOIP) versus for 28 days at 50 °C.

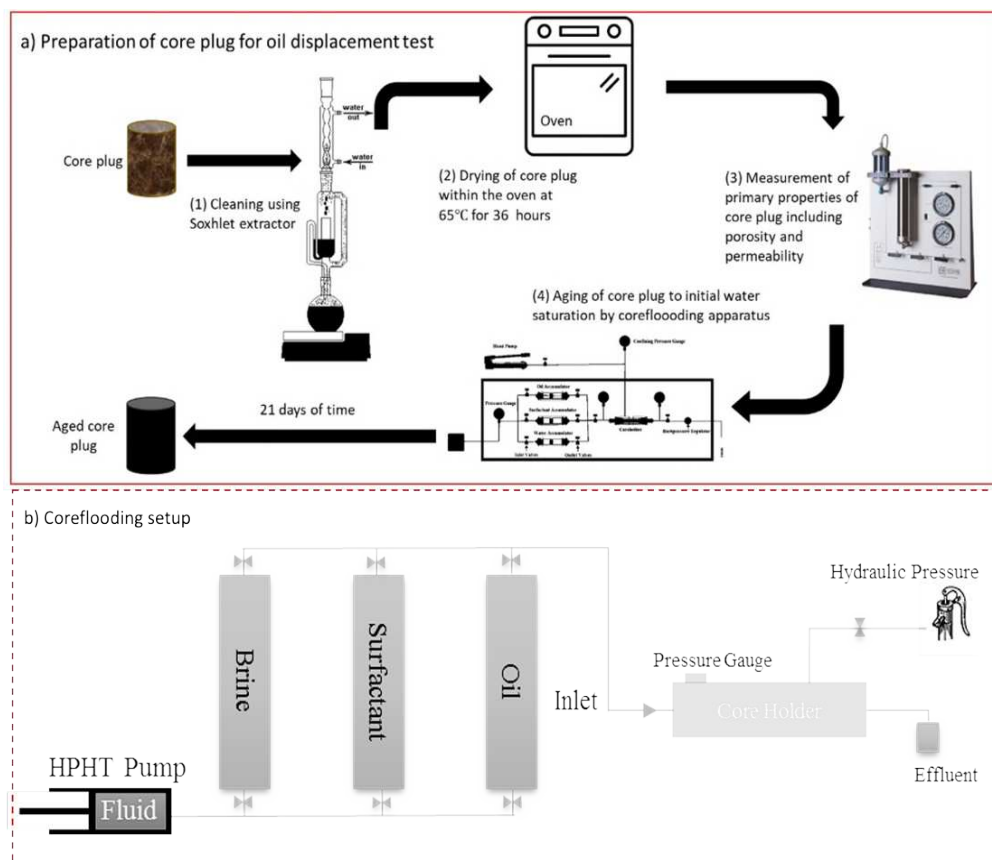


**Figure 30** Oil displacement test; a) core plug preparation, and b) coreflooding setup.

Overall, 25 different core samples mostly from carbonate rock and one core plug was prepared from the sandstone were used. The used rock samples were collected in the middle east mostly in south-east of Iran and north of Iraq. The prepared core plugs have different ranges of porosity from 7.75 to 18.41%, permeability is between 3.2 and 30 mD, the initial water saturation is from 21 to 45.3% and pore volume is about 5.3 to 14 cm<sup>3</sup> as shown in Figure 31. As can be seen, the permeability is mostly low for all samples, except the sandstone core plug which is the highest with 30 mD. In addition, the average porosity of all used core plugs is about 12.54% and the permeability is averagely equal to 7 mD. Meanwhile, the average value of the pore volume and the initial water saturation are 9.06 cm<sup>3</sup> and 33.6%, respectively.

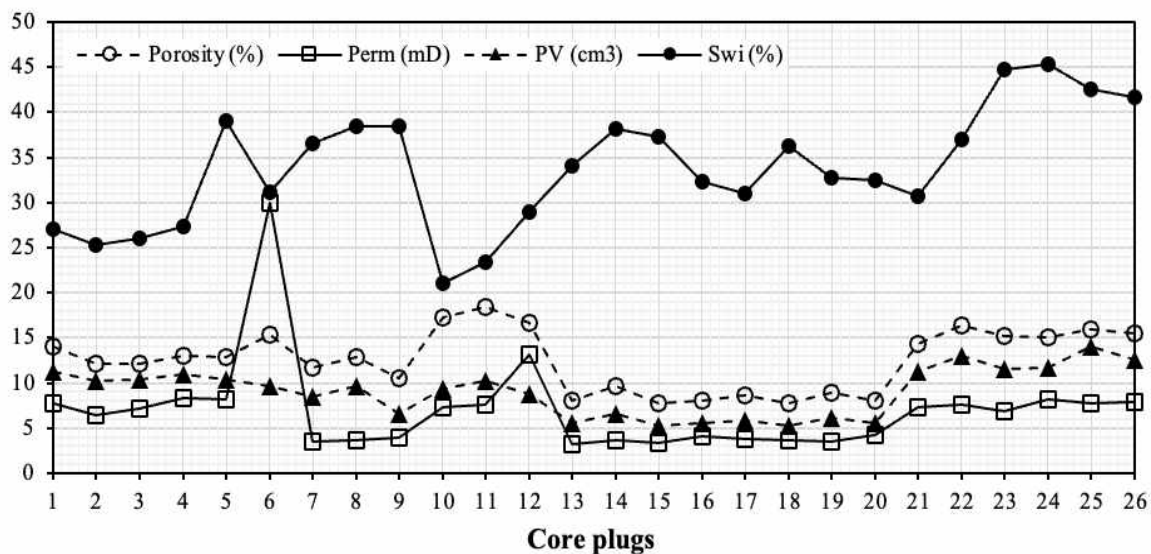


**Figure 31** Main characteristics of core plugs including porosity, permeability, initial water saturation and pore volume.

## 5.2. Oil displacement

Oil displacement experiments were started by injecting water as a secondary recovery process without the presence of any chemical additives including NCs. Afterwards, the performance of the synthesized NCs was tested by injecting the nanofluids prepared from different NCs at different concentrations within the different aqueous phases into core plugs. Meanwhile, other types of EOR solutions were injected after waterflooding to compare the outcome of the nanofluid EOR. The injection rate used to displace of the crude oil was ranged between 0.1 and 0.6 cm<sup>3</sup>/min during both phases of secondary and tertiary recoveries. These flooding tests were conducted under the temperature and pressure ranged between 1400 to 2000 psi and 50 to 75°C, respectively to represent the reservoir condition. Figure 32 illustrates the estimated values of oil recovery factories from the secondary and tertiary processes of the waterflooding and chemical injection. As can be see, the oil recovery factor of waterflooding varied between 36 to 51.05% original oil in place (OOIP). One sample of sandstone core plug was used with the porosity of 15.32% and permeability of 30 mD and enabled to expel the highest amount of the crude oil during the secondary phase of production due to having a good permeability. Otherwise, all other core plugs that are prepared from thee carbonate rock exhibited the almost the same behaviour in extracting the crude oil dependents on the permeability. While oil recovery factor during the tertiary phase is less compared with the oil recovery during waterflooding and ranged from 5.3 to 21.41% OOIP. This

situation is normal because from primary and secondary recovery un-trapped and non-residual crude oil is producing; however, the remaining trapped hydrocarbon is the target of the EOR techniques to break-down the crude-oil/water/rock bonds. The variation in the value of the recovery factor during this phase is dependent on the ability and performance of the injection solutions. NCs-1-DW nanofluid prepared from mixing 1500 ppm of ZnO/SiO<sub>2</sub>/Xanthan green NCs within the distilled water enabled to extract extra 19.28% OOIP. For the smart waters (OSS1, OSS2, OSS3 and OSS4 as the optimal smart solutions) prepared from mixing 5000 ppm KCl, 5000 ppm K<sub>2</sub>SO<sub>4</sub>, 2500 ppm CaSO<sub>4</sub> and CaCl<sub>2</sub> and 25000 ppm K<sub>2</sub>SO<sub>4</sub> and CaCl<sub>2</sub>, the oil recovery factor was around 5.3-8.1% OOIP. Meanwhile, after injecting the smart nanofluids prepared from dispersing TiO<sub>2</sub>/SiO<sub>2</sub>/PAM NCs within these smart waters, the oil recovery increased to 10.5% OOIP. In addition, when TiO<sub>2</sub>/Quartz NCs is applied with the salinity levels of distilled water, low salinity water and high salinity water as NCs-3-DW, NCs-3-LoSal and NCs-3-HiSal nanofluid, better oil recovery was obtained from 10 to 21% OOIP. The performance of NCs-5 was the highest with the presence of ZnO/SiO<sub>2</sub>/bentonite NCs within the distilled water which is 21.42% OOIP. However, the weakest performance of the synthesized green NCs was observed when ZnO/SiO<sub>2</sub>/xanthan is mixed with the surfactant and enabled 6% OOIP. Overall, mixing the green NCs within the distilled water exhibited the highest effectiveness in extracting the crude oil after waterflooding (see Figure 32).

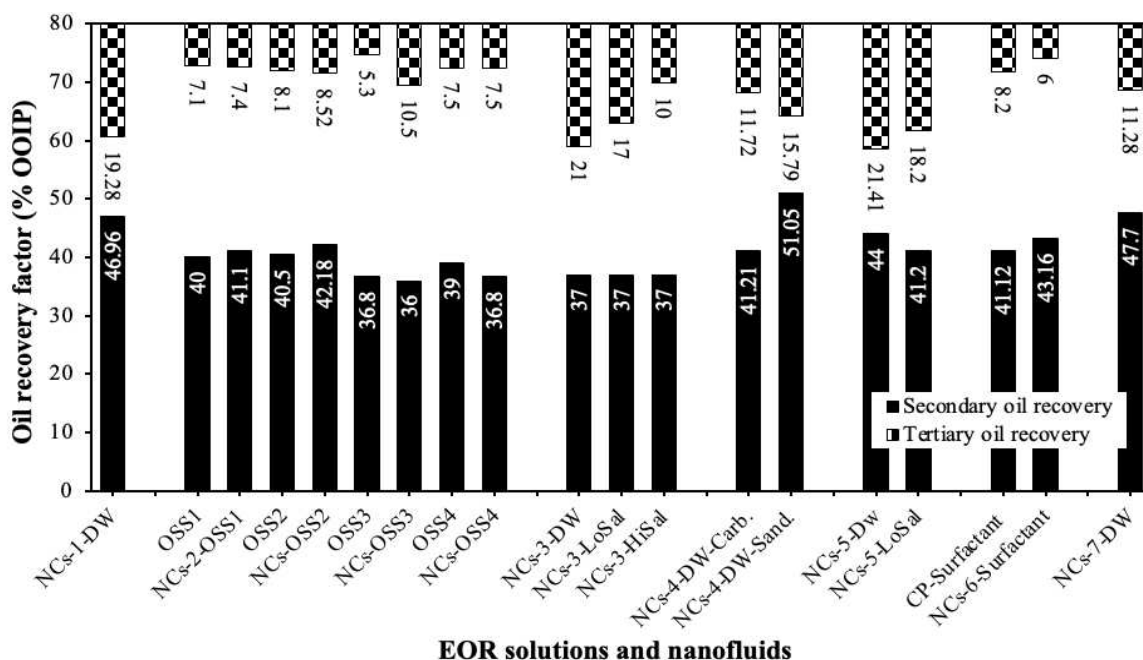


**Figure 32** Oil recovery factor obtained from waterflooding and tertiary recovery under the influence of the synthesized green NCs.

Furthermore, the oil recovery and pressure drop profiles of the secondary and tertiary processes obtained from the coreflooding by brine and chemical solutions contains the synthesized NCs are shown in Figure 33. For instance, the cumulative oil recovery improved steadily as more brine was injected before approaching a plateau at around 2 PVs. The waterflooding recovery factor was identified to be 46.96% original oil in place (OOIP). Then, the cumulative oil production was increased by 19.28% OOIP by injecting the NCs-1-LoSal nanofluid prepared from ZnO/SiO<sub>2</sub>/Xanth NCs. Again, the 2<sup>nd</sup> plateau value was arrived at after injecting roughly 2 PVs. At that point the total cumulative oil recovery from both of waterflooding and EOR nanofluid flooding was 66.24% OOIP (Figure 33a). In addition, Figure 33b-e demonstrate the flooding profiles of 8 core plugs used with NCs-2; wherein, the profile of each optimal smart solution with and without the presence of TiO<sub>2</sub>/SiO<sub>2</sub>/PAM NCs is shown on a separate figure. For instance, the flooding profiles of OSS1 and its performance under the impact of NCs from the core plugs 1 and 2 are shown together in Figure 33b. As is clear, the waterflooding from both plugs are almost similar, but nano-OSS1-1000 enabled to extract an extra 0.3% OOIP compared with the OSS1. While, Figure 33c presents the recovery profiles of OSS2 and its nanofluid. The performance of waterflooding through the plug#3 was higher compared with its performance through the plug#4 due to having better reservoir properties. Similarly, the ability of the smart water EOR was increased by 0.42% by adding NCs into the OSS2. The recovery profiles of binary-salt systems (CaSO<sub>4</sub>+CaCl<sub>2</sub>; K<sub>2</sub>SO<sub>4</sub>+ CaCl<sub>2</sub>) under the influences of the synthesized NCs are shown in Figure 32d,e. (CaSO<sub>4</sub>+CaCl<sub>2</sub>) and (K<sub>2</sub>SO<sub>4</sub>+ CaCl<sub>2</sub>) binary systems illustrate the low recovery efficiency of 5.3 and 6.1% OOIP, respectively, but their ability in enhancing oil recovery were improved to 10.5 and 7.5 % OOIP by adding 1500 and 500 ppm NCs, respectively. The pressure drop curve across a core plug during waterflooding is higher compared with the nanofluid injection because oil production is based on the pressure and displacement force during this stage (see Figure 33d). The pressure is highly increased after injecting 0.2 PV of water and then started to reduce due to the breakthrough of the injected water out of the core plu. Afterwards, the pressure continued in declining till the end of the displacement by injecting 4 PVs of water and nanofluid.

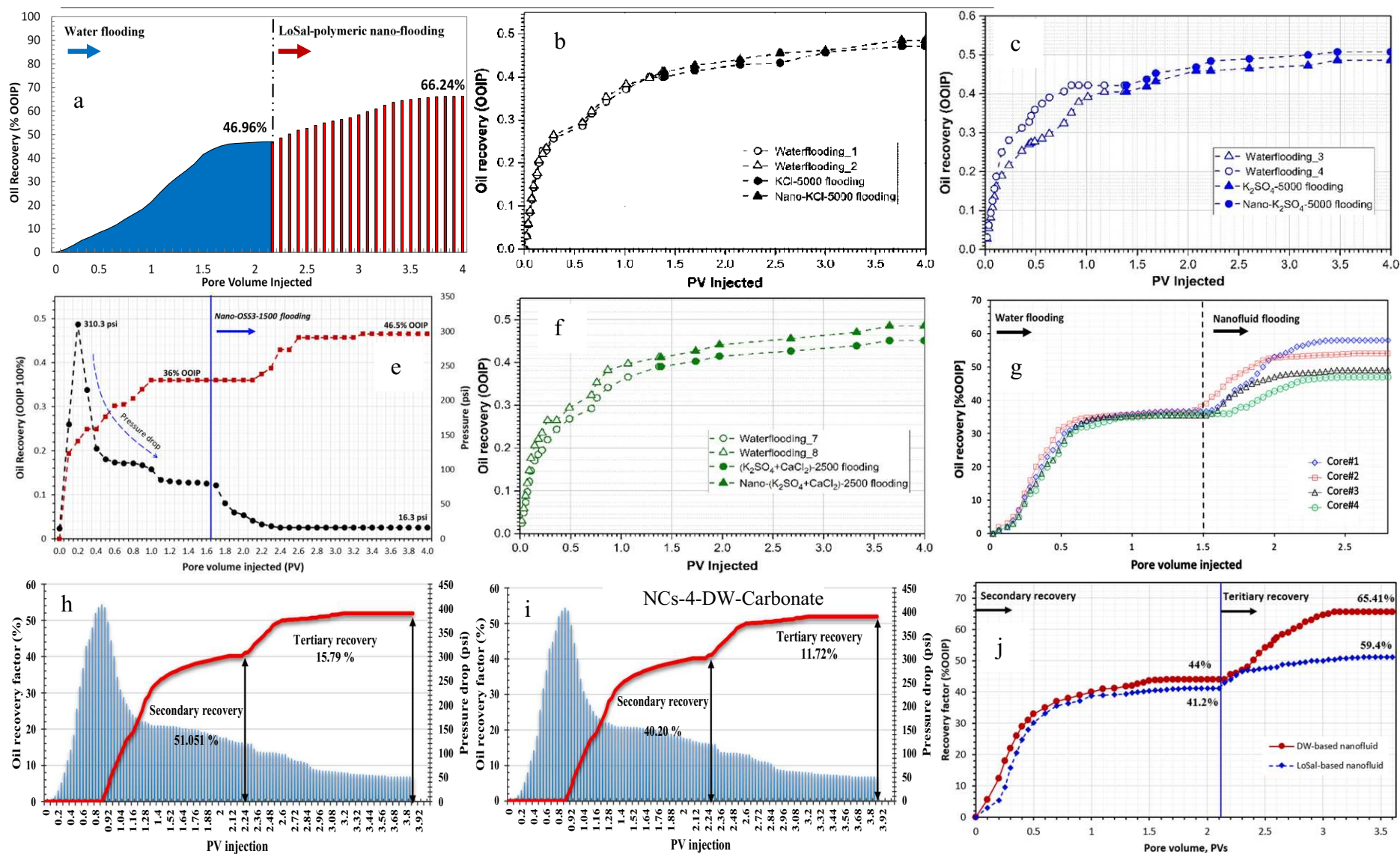


**Figure 33** Oil recovery and pressure drop profiles of some core plugs during secondary and tertiary recovery by injecting different types of water, surfactant and nanofluids prepared from NCs.; a) NCs-1, b-e) NCs-2, f) NCs-3, g) NCs-4, h) NCs-5, and i) NCs-6.

### 5.3. Relative permeability

Relative permeability is one of the crucial reservoir parameters that influence the flow behaviour of the fluids exists in the porous media. Changing the relative permeability is a key observation of improving the mobility of the crude oil over the brine towards the production well. Figure 34 represents the relative permeability curves ( $K_{ro}$  and  $K_{rw}$ ) of core plugs before and after the treatment tertiary recovery by nanofluids and other chemical solutions. In this study, oil displacement data were inserted in CYDAR software using Johnson, Bossler and Nauman (JBN) approach (Johnson et al., 1959). In this method, the obtained data of the oil displacement pressure drop and the ratio of extracted phase during time when two aqueous phases are existed. Generally, comparing the relative permeability curves before and after the nanofluid flooding, it can be observed that there are appropriate variations in the irreducible water saturation ( $S_{wir}$ ), the point where the water and oil relative permeabilities are equal and the relative permeability curves. Relative permeability curve of NCs-1-LoSal nanofluid whon in Figure 34a as an example, values of the irreducible water saturation, before ( $S_{wir} = 0.23$ ) and after treatment ( $S_{wir} = 0.47$ ), indicate that, according to the Craig's rules of thumb (Anderson, 1987), the wettability of the carbonate plug was changed from the oil-wet system to a strongly water-wet system. The most likely explanation for this considerable change in relative permeability curves is the adsorption of ZnO/SiO<sub>2</sub>/xanthan NCs on the surface of the carbonate. The oil relative permeability curve was considerably shifted to the right because of nanofluid flooding, which suggests that the oil effective permeability at a particular water saturation improved as the wettability system was changed to a stronger water-wet condition. Similar to the oil relative permeability curve, the crossover point was also moved to the right. After injecting the nanofluid, the water saturation at which the water and oil relative permeabilities become equal was changed from 0.4 to 0.6. According to the Craig's rules of thumb (Anderson, 1987), this value is typical of strongly water-wet cores.

In addition, the relative permeability curves estimated from NCs-4 nanofluid floodings through the sandstone and carbonate core plugs are shown in Figure 34c,d. As can be seen, the intersection point (at 57%) of water and oil permeability curves in the secondary recovery stage (located on the left side) indicates that the core is weakly water wet. In the tertiary recovery stage when NCs-4 nanofluid prepared from 1000 ppm SiO<sub>2</sub>/Montmorilant/xanthan NCs is injected, the intersection point (at 65%) of water and oil permeability curves moves toward the right side which confirms that the sandstone core plug became strongly water wet (see Figure 34c). This shifting in

wettability phase towards hydrophilic conditions is responsible for the decrease in residual oil saturation ( $S_{or}$ ) and increase in  $S_{wir}$ , hence resulting in enhancement of oil recovery. Meanwhile the same behavior of the relative permeability curves was observed when the same nanofluid was injected into the carbonate core plug but with weaker alteration (see Figure 34d).

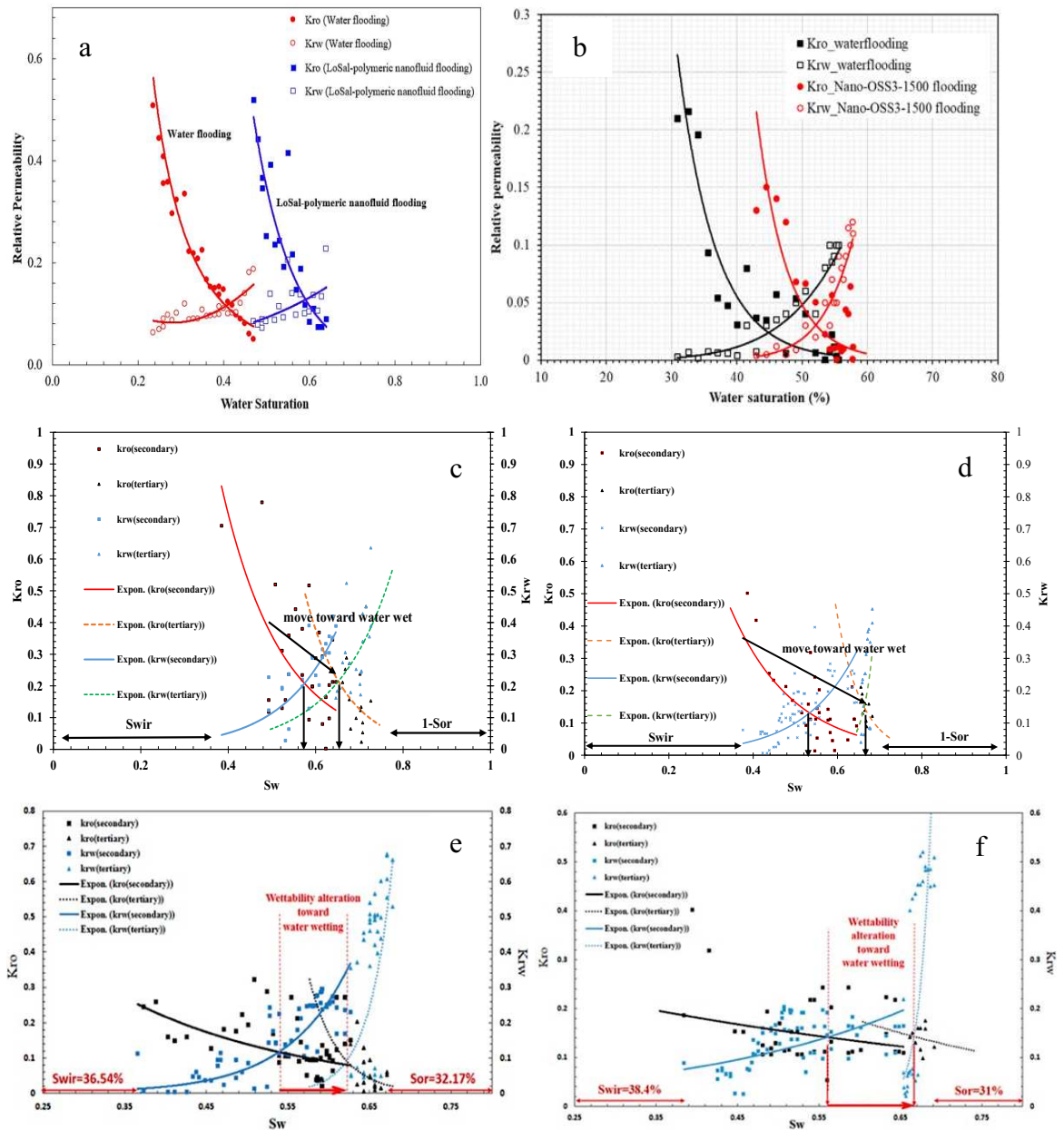


**Figure 34** Oil and water relative permeability curves before and after treatment of core plugs with nanofluids prepared from: a) ZnO/SiO<sub>2</sub>/xanthan NCs, b) TiO<sub>2</sub>/SiO<sub>2</sub>/PAM NCs, c) SiO<sub>2</sub>/Montmorilant/xanthan NCs, and d) ZnO/montmorilant NCs.

#### **5.4. Emulsification**

The emulsification stability analysis was carried out for the crude oil with different nanofluids prepared from ZnO/SiO<sub>2</sub>/Xanthan and TiO<sub>2</sub>/Quartz NCs at different concentrations. Figure 35 shows the emulsion behaviors of crude oil and NCs-1 nanofluids at concentrations ranged from 500 to 2000 ppm including nanofluids from mixing the NCs with the seawater (PN500, PN1000 and PN2000) and nanofluids prepared from mixing the nanocomposites with the LoSal water (LPN500, LPN1000 and LPN2000). Figure 35a-f presents the emulsification behavior of all fluid systems at different time steps, over 12 hours. On the whole, the stability varied between the time steps and across the NCs-1 concentration. As can be seen, after shaking the oil/nanofluid emulsions for 30 minutes, the coalescence of some mixtures was quickly occurred during the first two hours and increased (Figure 35b-d). On the other hand, the emulsion stability, with no flocculation and coalescence, for all other fluid systems was observed at 8 hrs and 12 hrs after settling (Figure 35e-f). At lower concentration of polymer coated ZnO/SiO<sub>2</sub> NCs, higher reduction of the emulsion stability was observed in both nanofluid and LoSal nanofluid systems. This is true according to the theory of Dickinson et al. (1994) in which they stated that oil droplets quickly experience coalescence to develop larger droplets with low polymer concentration which causes the emulsion stability to become decreased. However, with increasing the concentration of the synthesized NCs, better emulsion stability was obtained due to the better adsorption of the nanocomposites on oil droplets and occurring isolation between oil droplets (Ghosh, 2012). The emulsification stability of the nanofluids (PNs) developed from the high salinity seawater was gradually improved with increasing the NC concentration for all time steps as shown by purple line on Figure 35. The stability of the nanofluid emulsion formed with 500 ppm NCs was reduced very quickly after 1 hr of settling, and started to reduce after 4 hrs with 1000 ppm NCs concentration. However, a high stable emulsion of crude oil/PN2000 was observed through the all settling time-steps, which was inferred as an optimal nanofluid. However, there was no steady trend observed with the LoSal nanofluids (LPNs) with increasing the NC concentration. The stability of oil/LPN emulsion with 500, 1000 and 2000 ppm was started to reduce after 1-2 hrs of settling. In addition to this, better stability of LPN was identified with 2000 ppm NC concentration compared to 500 and 1000 ppm.



**Figure 35** Emulsification images of oil/polymeric and oil/low salinity-polymeric nanofluids over various time-steps.

## 6. Conclusions and future prospective

In this thesis, several nanocomposites which were synthesized greenly were evaluated in the EOR applications. These NCs were prepared from the extracts of plants and characterized using different analytical techniques. NCs dispersed within nanofluids were applied in IFT, contact angle and oil displacement tests, the outcomes of the current work can be summarized as follows:

- The synthesized NCs were evenly dispersed in water with high suspension stability for a certain period of time and an excellent rheology and interfacial activity.
- Synthesized NCs are more effective when mixed within the LoSal and distilled water compared with the HiSal water.
- $\text{TiO}_2/\text{Quartz}$  NCs made from euphoria condylocarpa extract reduced IFT from 28 to 1.141 mN/m when it is mixed with the distilled water; meanwhile, synthesized  $\text{SiO}_2/\text{KCl}/\text{Xanthan}$  NCs created the minimum IFT of 1.51 mN/m when it is dispersed within methyl ethyl keton.
- Nano-surfactant solution made up of  $\text{ZnO}/\text{Montmorilant}$  NCs and natural surfactant extracted from *Cyclamen persicum* plant provided the highest performance in altering the wettability towards strong water wet by decreasing the CA to  $19^\circ$ . In addition, NCs-1, 4,7 effectively reduced the CA to 34.08, 33 and  $22^\circ$ , respectively when mixed with LoSal and distilled water.
- Nanofluids prepared from mixing NCs-1, NCs-3 and NCs-5 within the distilled water enabled to improve oil recovery factor significantly by 19.28, 21 and 21.41% OOIP, respectively.

Despite the fact that the synthesized nanocomposites in this study demonstrated great potential for altering the wettability of oil-wet surfaces and reducing the interfacial tension of oil/water systems, more specific studies need to be studied to confirm their economical applicability in the real field. Consequently, it is critical to design a cheap nanosuspension with a controlled structure and stable formulation. Moreover, although this study investigated a comprehensive range of IFT, stability behaviour, wettability alteration, oil recovery, emulsification and relative permeability, there remain significant areas that need to covered in the future work. The performance of the distribution of the nanocomposites in the porous media must be studied visually using micro-models. Conducting the visualization study of the impact of nanofluid injection on clay the swelling, capillary continuity and capillary discontinuity phenomena in fracture medium in micromodels. In addition, the absorption behavior of the nanocomposites to the surface of the carbonate and sandstone rocks should be evaluated along with using simulation and modelling.

## 7. Abbreviations and nomenclature

|            |   |
|------------|---|
| EOR        | Enhanced oil recovery                     |
| IFT        | Interfacial tension                       |
| CA         | Contact angle                             |
| Kro        | Relative permeability for the oil phase   |
| Krw        | Relative permeability for the water phase |
| mD         | MilliDarcy                                |
| Nanofluid  | Nanoparticles dispersed in a fluid        |
| NCs        | Nanocomposites                            |
| NPs        | Nanoparticles                             |
| PV         | Pore volume                               |
| RF         | Recovery factor % OOIP                    |
| rpm        | Rotations per minute                      |
| SEM        | Scanning electron microscope              |
| So         | Oil saturation                            |
| Soi        | Initial oil saturation                    |
| Sor        | Residual oil saturation                   |
| Swi        | Initial water saturation                  |
| Swir       | Irreducible water saturation              |
| wt. %      | Weight percent                            |
| XRD        | X-ray diffraction                         |
| $\Delta P$ | Differential pressure over the core plug  |
| $\theta$   | Contact angle (CA)                        |
| $\mu$      | Viscosity                                 |
| $\sigma$   | Interfacial tension (IFT)                 |
| $\rho$     | Density                                   |
| OOIP       | Original oil in place                     |
| UV–Vis     | Ultraviolet–visible spectroscopy          |
| FT-IR      | Fourier-transform infrared spectroscopy   |
| TEM        | Transmission electron microscopy          |
| EIA        | Energy Information Administration         |

|       |   |
|-------|---|
| MMNC  | Metal matrix nanocomposite                |
| PMNC  | Polymer matrix nanocomposite              |
| CMNC  | Ceramic matrix nanocomposite              |
| ICDD  | International center for diffraction data |
| HiSal | High salinity                             |
| LoSal | Low salinity                              |
| MoSal | Moderate salinity                         |
| ADSA  | Axisymmetric Drop Shape Analysis          |
| DW    | Distilled water                           |
| OSS   | Optimal smart solution                    |
| HSW   | High salinity water                       |
| LSW   | Low salinity water                        |
| JBN   | Johnson, Bossler and Nauman               |
| PN    | Polymeric nanofluid                       |
| LPN   | Low salinity polymeric nanofluid          |

## 8. References

- Abdallah, W., Buckley, J.S., Carnegie, A., Edwards, J., Herold, B., Fordham, E., Graue, A., Habashy, T., Seleznev, N., Signer, C., Hussain, H., Montaron, B., Ziauddin, M. (2007) Fundamentals of Wettability. *Oilfield Rev.* 19, 4461.
- Abou El-Nour, K. M. M., Eftaiha, A., Al-Warthan, A., Ammar, R. A. A. (2010) Synthesis and applications of silver nanoparticles. *Arabian Journal of Chemistry*, 3(3), 135–140.
- Afolabi, R. O., Yusuf, E. O. (2018). Nanotechnology and global energy demand: Challenges and prospects for a paradigm shift in the oil and gas industry. *Journal of Petroleum Exploration and Production Technology*, 9(2), 1423-1441.
- Alagiri, M., Hamid, S. B. A. (2015). Sol–gel synthesis of  $\alpha$ -Fe<sub>2</sub>O<sub>3</sub> nanoparticles and its photocatalytic application. *Journal of Sol-Gel Science and Technology*, 74(3), 783-789.
- Ali, J. A., Kolo, K., Manshad, A. K., Mohammadi, A. H. (2018). Recent advances in application of nanotechnology in chemical enhanced oil recovery: Effects of nanoparticles on wettability alteration, interfacial tension reduction, and flooding. *Egyptian Journal of Petroleum*, 27(4), 1371-1383.
- Ali, J. A., Kolo, K., Manshad, A. K., Stephen, K. D. (2019). Potential application of low-salinity polymeric-nanofluid in carbonate oil reservoirs: IFT reduction, wettability alteration, rheology and emulsification characteristics. *Journal of Molecular Liquids*, 284, 735-747.
- Ali, J. A. (2022). Effect of Fe<sub>3</sub>O<sub>4</sub>/mineral–soil Nanocomposites on Wettability alteration and oil production under the spontaneous imbibition process. *Arabian Journal for Science and Engineering*, 48(7), 9259-9268.
- Armendariz V, Herrera I, Jose-yacaman M, Troiani H, Santiago P, Gardea-Torresdey JL. (2004) Size controlled gold nanoparticle formation by Avena sativa biomass: use of plants in nanobiotechnology. *J. Nanopart. Res.*, 6(4):377–82.
- Anderson, G.W. (1987) Wettability literature survey. Part 5: The effects of wettability on relative permeability. *J Pet. Technol.* 39(11), 1453–1468.
- Asl, FO, Zargar, G., Manshad, AK, Arif, M., Iglauer, S., Keshavarz, A. (2023). Impact of PAM-ZnO nanocomposite on oil recovery. *Fuel*, 332, 125941.
- Aurand, K. R. Dahle, G. S. Torsæter, O. (2014) Comparison of Oil Recovery for Six Nanofluids in Berea Sandstone Cores, SCA, A064 1-12.
- Aveyard, R. Binks, B. P. Clint, J. H. (2003) Emulsions stabilized solely by colloidal particles, *Adv. Colloid Interface Sci.* 100, 503–546.

- Avendano, C., Lee, S.S., Escalera, G., and Colvin, V. (2012) Magnetic characterization of nanoparticles designed for use as contrast agents for downhole measurements. Society of Petroleum Engineers.
- Azarshin, S. Moghadasi, J. Aboosadi, Z. (2017) Surface functionalization of silica Nanoparticles to improve the performance of waterflooding in oil wet reservoirs, *Energy Exploration & Exploitation* 35, 685-697.
- Babu RH, Yugandhar P, Savithamma N (2018) Synthesis, characterization and antimicrobial studies of bio silica nanoparticles prepared from *Cynodon dactylon* L.: a green approach. *Bulletin of Materials Science* 41(3).
- Bahraminejad, H., Khaksar Manshad, A., Riazi, M., Ali, J. A., Sajadi, S. M., Keshavarz, A. (2019). CuO/TiO<sub>2</sub>/PAM as a Novel Introduced Hybrid Agent for Water—Oil Interfacial Tension and Wettability Optimization in Chemical Enhanced Oil Recovery. *Energy & Fuels*, 33(11), 10547-10560.
- Bai, H.J., Zhang, Z.M. (2009). Microbial synthesis of semiconductor lead sulfide nanoparticles using immobilized *Rhodobacter sphaeroides*. *Mater. Lett.* 63 (9–10): 764–766.
- Bastos-Arrieta, J., Muñoz, M., Muraviev, D. N. (2014). Bi-Functional Polymer-Metal Nanocomposites: Modification of Ion-Exchange Materials with Silver Nanoparticles. *Solvent Extraction and Ion Exchange*, 33(2), 152-165.
- Behera, U. S., Sangwai, J. S. (2022). Silica nanofluid in low salinity seawater containing surfactant and polymer: Oil recovery efficiency, wettability alteration and adsorption studies. *Journal of Petroleum Science and Engineering*, 211, 110148.
- Bhowmik, P., Arora, G. (2022). Graphene/Metal Matrix Nanocomposites. *Metal Matrix Composites*, 109-148.
- Bila, A., Stensen, J. Åge, Torsæter, O. (2019). Experimental Investigation of Polymer-Coated Silica Nanoparticles for Enhanced Oil Recovery. *Nanomaterials*, 9(6), 822.
- Cammarata, R. (2006), *Introduction to nano scale science and technology*, Springer, USA.
- Ceschini, L., Dahle, A., Gupta, M., Jarfors, A. E. W., Jayalakshmi, S., Morri, A., Rotundo, F., Toschi, S., Singh, R. A. (2016). Metal Matrix Nanocomposites: An Overview. *Aluminum and Magnesium Metal Matrix Nanocomposites*, 1-17.
- Chen, L., Xie, H. (2010) Surfactant-free nanofluids containing double- and single-walled carbon nanotubes functionalized by a wet mechanochemical reaction, *Thermochimica Acta.* 497, 67–71.
- Dahle, S. G. (2013) *The Effect of Nanoparticles on Oil/Water Interfacial Tension*. Project thesis, NTNU.

- Davoodi, S., Al-Shargabi, M., Wood, D. A., Rukavishnikov, V. S., Minaev, K. M. (2022). Experimental and field applications of nanotechnology for enhanced oil recovery purposes: A review. *Fuel*, 324, 124669.
- Darroudi, M. (2011). Time-dependent effect in green synthesis of silver nanoparticles. *International Journal of Nanomedicine*, 677. <https://doi.org/10.2147/ijn.s17669>
- De Castro Dantas, T.N. De Souza, T. TDantas Neto, . A.A. Moura, M.C. De Barros Neto, E.L. (2017) Experimental Study of Nanofluids Applied in EOR Processes, *J. Surfactants and Detergents* 20,1095-1104.
- Desgouilles, S., Vauthier, C., Bazile, D., Vacus, J., Grossiord, J., Veillard, M., Couvreur, P. (2003). The Design of Nanoparticles Obtained by Solvent Evaporation: A Comprehensive Study. *Langmuir*, 19(22), 9504-9510.
- Dickinson, E. Ma, J. G. Povey, M. J. W. (1994) Creaming of concentrated oil in-water emulsions containing xanthan. *Food Hydrocolloids* 8 (1994) 481-497.
- Ebnesajjad, S. and C. Ebnesajjad (2013). *Surface treatment of materials for adhesive bonding*, William Andrew.
- El Shafey, A. M. (2017) Effect of Nanoparticles and polymer Nanoparticles implementation on chemical flooding, wettability and interfacial tension for the enhanced oil recovery processes, *African J. of Eng. Res.* 5, 35-53.
- Fakoya, M.F., Shah, S.N. (2017) Emergence of nanotechnology in the oil and gas industry: Emphasis on the application of silica nanoparticles. *Petroleum*, 3(4), 391-405.
- Fawaz, J., Mittal, V. (2015). Synthesis of Polymer Nanocomposites: Review of Various Techniques. In *Synthesis Techniques for Polymer Nanocomposites* (1st ed., pp. 19-30). John Wiley Sons.
- Fovet, Y. Gal, J.Y. Toumelin-Chemla, F. (2001) Influence of pH and fluoride concentration on titanium passivating layer: stability of titanium dioxide, *Talanta* 53 (2001) 1053–1063.
- Gan, L., Lu, Z., Cao, D., Chen, Z., (2018). Effects of cetyltrimethylammonium bromide on the morphology of green synthesized Fe<sub>3</sub>O<sub>4</sub> nanoparticles used to remove phosphate. *Mater. Sci. Eng. C* 82, 41e45.
- Garmroudi, A., Kheirollahi, M., Mousavi, S. A., Fattahi, M., Mahvelati, E. H. (2022). Effects of graphene oxide/TiO<sub>2</sub> nanocomposite, graphene oxide nanosheets and Cedar extraction solution on IFT reduction and ultimate oil recovery from a carbonate rock. *Petroleum*, 8(4), 476-482.
- Gericke M, Pinches A. (2006) *Biological synthesis of metal nanoparticles*. *Hydrometallurgy* 83(1-4):132–40.

- Ghosh, A. K. Bandyopadhyay, P. (2012) Polysaccharide-protein interactions and their relevance in food colloids. In *The complex world of polysaccharide*; Intech open science open minds 395–408.
- Gordon, M., Weber, M. (2021). Global energy demand to grow 47% by 2050, with oil still top source: US EIA. [www.spglobal.com/](http://www.spglobal.com/). July 24, 2023.
- Goyal, S., Joshi, P., Singh, R., Rohan. (2021). Applications and role of Nano-Silica particles on altering the properties and their usage for oil well cementing. *Materials Today: Proceedings*, 46, 10681-10686.
- Guo, J. Z., Song, K., Liu, C. (2018). *Polymer-Based Multifunctional Nanocomposites and Their Applications*. Elsevier.
- Hasan, S., Azhdar, B. (2023). NiFe<sub>2</sub>O<sub>4</sub> and ZnFe<sub>2</sub>O<sub>4</sub> nanoparticles synthesis by sol-gel auto-combustion for humidity sensor applications. *Journal of Sol-Gel Science and Technology*, 105(2), 416-429.
- Hama, S. M., Manshad, A. K., & Ali, J. A. (2023). Review of the Application of Natural Surfactants in Enhanced Oil Recovery: State-of-the-Art and Perspectives. *Energy & Fuels*, 37(14), 10061-10086.
- Hamdi, S. S., Al-Kayiem, H. H., Alsabah, M. S., Muhsan, A. S. (2022). A comparative study of dispersed and grafted nanofluids of graphene nanoplatelets with natural polymer in high salinity brine for enhanced oil recovery. *Journal of Petroleum Science and Engineering*, 210, 110004.
- Harish, V., Ansari, M. M., Tewari, D., Gaur, M., Yadav, A. B., García-Betancourt, M.-L., Abdel-Haleem, F. M., Bechelany, M., Barhoum, A. (2022). Nanoparticle and Nanostructure Synthesis and Controlled Growth Methods. *Nanomaterials*, 12(18), 3226.
- Heiligtag, F. J., Niederberger, M. (2013) The fascinating world of nanoparticle research. *Materials Today*, 16(7-8), 262-271.
- Hendraningrat, L., Li, S., Torsaeter, O. (2013) Enhancing Oil Recovery of Low-Permeability Berea Sandstone through Optimised Nanofluids Concentration. Presented at the SPE Enhanced Oil Recovery Conference, Society of Petroleum Engineers. doi:10.2118/165283-MS
- Hendraningrat, L., Torsæter, O. (2014) Effects of the Initial Rock Wettability on Silica-Based Nanofluid-Enhanced Oil Recovery Processes at Reservoir Temperatures. *Energy Fuels* 28, 62286241.
- Hendraningrat, L., Torsæter, O., (2015) A Stabilizer that Enhances the Oil Recovery Process Using Silica-Based Nanofluids. *Transp. Porous Media* 108, 679696.

- Herrera-Becerra R., Zorrilla C., Rius J.L., Ascencio J.A. (2008) Electron microscopy characterization of biosynthesized iron oxide nanoparticles. *Appl Phys A* 91(2):241–6.
- Horst, M.F., Coral, D.F., van Raap, M.B.F., Alvarez, M., Lassalle, V., (2017) Hybrid nanomaterials based on gum Arabic and magnetite for hyperthermia treatments. *Mater. Sci. Eng. C* 74, 443e450.
- Ikram, R., Jan, B. M., Vejpravova, J. (2021). Towards recent tendencies in drilling fluids: Application of carbon-based nanomaterials. *Journal of Materials Research and Technology*, 15, 3733-3758.
- Ismail, A.R., Rashid, N.M., Jaafar, M.Z., Sulaiman, W.R.W., Buang, N.A. (2014) Effect of nanomaterial on the rheology of drilling fluids. *Journal of Applied Sciences* 14(11): p. 1192-1197.
- Islam N.U., Khan I, Rauf A., Muhammad N., Shahid, M., Shah M.R. (2015) Antinociceptive, muscle relaxant and sedative activities of gold nanoparticles generated by methanolic extract of *Euphorbia milii*. *BMC Complementary and Alternative Medicine* 15(1).
- Ismailov, F.S., Veliyev, E.F. (2011) Nanofluid for Enhanced Oil Recovery. *JPSE*, 78, 431–437.
- Johnson, E.F., Bossler, D.P., Naumann, V.O. (1959) Calculation of relative permeability from displacement experiments. *Petroleum transactions, AIME* 216, 370-372.
- Kacher, J., Landon, C., Adams B.L., Fullwood, D. (2009). Bragg's Law diffractionsimulations for electron backscatter diffraction analysis. *Ultramicroscopy* 109(9): 1148–1156.
- Kamal, M.S., Adewunmi, A.A., Sultan, A.S., Al-Hamad, M.F., Mehmood, U. (2017). Recent advances in nanoparticles enhanced oil recovery: rheology, interfacial tension, oil recovery, and wettability alteration. *Journal of Nanomaterials*, 2017.
- Kang, S., Park, Y., Yang, J., Shin, Y., Yun, J. (2010). Fourier transform infrared studies of the aluminum chemical vapor deposition using aluminum Boro-hydride trimethylamine. *Thin Solid Films*, 518(8), 2228-2233.
- Kango, S., Kalia, S., Celli, A., Njuguna, J., Habibi, Y., Kumar, R. (2013). Surface modification of inorganic nanoparticles for development of organic–inorganic nanocomposites—A review. *Progress in Polymer Science*, 38(8), 1232-1261.
- Kazemzadeh, Y., Sharifi, M., Riazi, M., Rezvani, H., Tabaei, M. (2018) Potential effects of metal oxide/SiO<sub>2</sub> nanocomposites in EOR processes at different pressures. *Colloids and Surfaces A: Physicochemical and Engineering Aspects*, 559, 372-384.
- Keat, C.L., Aziz, A., Eid, A.M., and Elmarzugi, N.A. (2015). Biosynthesis of nanoparticles and silver nanoparticles. *Bioresour. Bioprocess* 2 (1): 47.

- Khan, I., Gothwal, A., Sharma, A.K., Qayum, A., Singh, S.K., Gupta, U. (2016) Biodegradable nano-architectural PEGylated approach for the improved stability and anticancer efficacy of bendamustine. *International Journal of Biological Macromolecules*, 92, 1242–1251.
- Khataee, A., Kayan, B., Kalderis, D., Karimi, A., Akay, S., Konsolakis, M. (2017). Ultra- sound assisted removal of Acid Red 17 using nanosized Fe<sub>3</sub>O<sub>4</sub>-loaded coffee waste hydrochar. *Ultrason. Sonochem.* 35, 72e80.
- Khorsand Z., Razali A., Abd Majid W.H., Darroudi M. (2011) Synthesis and characterization of a narrow size distribution of zinc oxide nanoparticles. *Int. J. Nanomedicine* 1399.
- Kohli, R. (2012). *Methods for monitoring and measuring cleanliness of surfaces. Developments in Surface Contamination and Cleaning*, Elsevier: 107–178.
- Koo, J. H. (2019). *Polymer Nanocomposites: Processing, Characterization, and Applications*, Second Edition. McGraw Hill Professional.
- Kuchibhatla S.V., Karakoti A.S., Baer D.R., Samudrala S., Engelhard M.H., Amonette J.E., Thevuthasan S., Seal S. (2012) Influence of aging and environment on nanoparticle chemistry: implication to confinement effects in nanoceria. *J Phys Chem C* 116(26):14108–14.
- Kumar, R. S., Sinha, A., Sharma, T., Arif, M. (2023). Nanocomposite of binary colloids in effective CO<sub>2</sub> utilization in porous media for enhanced oil production and wettability alteration. *Journal of Environmental Chemical Engineering*, 11(5), 110442.
- Lashari, N., Ganat, T. (2020). Emerging applications of nanomaterials in chemical enhanced oil recovery: Progress and perspective. *Chinese Journal of Chemical Engineering*, 28(8), 1995-2009.
- Lashari, N., Ganat, T., Elraies, K. A., Ayoub, M. A., Kalam, S., Chandio, T. A., Qureshi, S., Sharma, T. (2022). Impact of nanoparticles stability on rheology, interfacial tension, and wettability in chemical enhanced oil recovery: A critical parametric review. *Journal of Petroleum Science and Engineering*, 212, 110199.
- Lashari, N., Ganat, T., Ayoub, M. A., Kalam, S., Ali, I. (2023). Coreflood investigation of HPAM/GO-SiO<sub>2</sub> composite through wettability alteration. *Journal of Molecular Liquids*, 371, 121130.
- Lau, H. C., Yu, M., Nguyen, Q. P. (2017). Nanotechnology for oilfield applications: Challenges and impact. *Journal of Petroleum Science and Engineering*, 157, 1160-1169.
- Li, H., Xiao, H.-g., Yuan, J., Ou, J. (2004) Microstructure of cement mortar with nanoparticles. *Composites Part B: Engineering*, 35(2): p. 185-189.
- Low, I. M. (2018). *Advances in Ceramic Matrix Composites*. Woodhead Publishing.

- Maagi, M. T., Lupyana, S. D., Jun, G. (2020). Nanotechnology in the petroleum industry: Focus on the use of nanosilica in oil-well cementing applications - A review. *Journal of Petroleum Science and Engineering*, 193, 107397.
- Mahalingam T., Selvakumar C., Kumar R.E., Venkatachalam T (2017) Structural, optical, morphological and thermal properties of TiO<sub>2</sub>–Al and TiO<sub>2</sub>–Al<sub>2</sub>O<sub>3</sub> composite powders by ball milling. *Physics Letters A* 381(21):1815–1819
- Manshad, A. K., Ali, J. A., Haghighi, O. M., Mohammad Sajadi, S., Keshavarz, A. (2022). Oil recovery aspects of ZnO/SiO<sub>2</sub> nano-clay in carbonate reservoir. *Fuel*, 307, 121927.
- Mago, G., Kalyon, D. M., Jana, S. C. (2011). Polymer Nanocomposite Processing, Characterization and Applications 2011. *Journal of Nanomaterials*, 2011, 1-1.
- Maqsood A., Akhtar J., Majeed Khan A.K. (2012) Zinc oxide nanoparticles selectively induce apoptosis in human cancer cells through reactive oxygen species. *I. J. Nanomedicine* 845.
- Mendoza-Muñoz, N., Alcalá-Alcalá, S., Quintanar-Guerrero, D. (2016). Preparation of Polymer Nanoparticles by the Emulsification-Solvent Evaporation Method: From Vanderhoff's Pioneer Approach to Recent Adaptations. *Polymer Nanoparticles for Nanomedicines*, 87-121.
- Mirzavandi, M., Ali, J. A., Manshad, A. K., Majeed, B., Mahmood, B. S., Mohammadi, A. H., Iglauer, S., Keshavarz, A. (2023). Performance Evaluation of Silica–Graphene Quantum Dots for Enhanced Oil Recovery from Carbonate Reservoirs. *Energy & Fuels*, 37(2), 955-964.
- Moslan, M.S., Sulaiman, W.R.W., Ismail, A.R., Jaafar, M.Z. (2017) Applications of Aluminium Oxide and Zirconium Oxide Nanoparticles in Altering Dolomite Rock Wettability using Different Dispersing Medium, *Chemical Eng. Trans.* 65, 1339-1344.
- Motraghi, F., Khaksar Manshad, A., Akbari, M., Ali, J. A., Sajadi, S. M., Iglauer, S., Keshavarz, A. (2023). Interfacial tension reduction of hybrid crude-oil/mutual-solvent systems under the influence of water salinity, temperature and green SiO<sub>2</sub>/KCL/Xanthan nanocomposites. *Fuel*, 340, 127464
- Murakami, A., Kimura, K., Nakano, A. (1999). The Inactive Form of a Yeast Casein Kinase I Suppresses the Secretory Defect of the sec12 Mutant. *Journal of Biological Chemistry*, 274(6), 3804-3810.
- Nasrollahzadeh M, Sajjadi M, Maham M, Sajadi SM, Barzinjy A.A. (2019) Biosynthesis of the palladium/sodium borosilicate nanocomposite using *Euphorbia milii* extract and evaluation of its catalytic activity in the reduction of chromium(VI), nitro compounds and organic dyes. *Materials Research Bulletin* 102:24-35.

- Nazarahari, M. J., Manshad, A. K., Ali, M., Ali, J. A., Shafiei, A., Sajadi, S. M., Moradi, S., Iglauer, S., Keshavarz, A. (2021). Impact of a novel biosynthesized nanocomposite (SiO<sub>2</sub>@Montmorillonite@Xanthan) on wettability shift and interfacial tension: Applications for enhanced oil recovery. *Fuel*, 298, 120773.
- Nikolaidis, P. (2020). Analysis of Green Methods to Synthesize Nanomaterials. In *Green Synthesis of Nanomaterials for Bioenergy Applications* (1st ed., pp. 125-145). John Wiley & Sons.
- Nourinia, A., Manshad, A. K., Shadizadeh, S. R., Ali, J. A., Iglauer, S., Keshavarz, A., Mohammadi, A. H., Ali, M. (2022). Synergistic efficiency of zinc oxide/Montmorillonite Nanocomposites and a new derived saponin in liquid/Liquid/Solid interface-included systems: Application in nanotechnology-assisted enhanced oil recovery. *ACS Omega*, 7(29), 24951-24972.
- Okpala, C.C. (2014), The benefits and applications of nanocomposites, *International Journal of Advanced Engineering Technology*, 5(4), 12-18.
- Oseh, J. O., Mohd, N. M., Gbadamosi, A. O., Agi, A., Blkoor, S. O., Ismail, I., Igwilo, K. C., Igbafe, A. I. (2023). Polymer nanocomposites application in drilling fluids: A review. *Geoenergy Science and Engineering*, 222, 211416.
- Panda J, Singh UP, Sahu R (2018) Synthesis, characterization of TiO<sub>2</sub> nano particles for enhancement of electron transport application in DSSC with Cu-BPCA Dye. *IOP Conference Series: Materials Sci. Eng.* 410, 012008.
- Paul, M. Holcomb, M. Lee, D. Daniel, E. (2012) Application of nanofluid technology to improve recovery in oil and gas wells, *SPE Int. Oilfield Nanotechnology Conference*, Noordwijk, the Netherlands.
- Patil, N.B., Sharanagouda, H., Doddagoudar, S., Ramachandra, C., Ramappa, K. (2018). Biosynthesis and Characterization of Silica Nanoparticles from Rice (*Oryza sativa* L.) Husk. *International Journal of Current Microbiology and Applied Sciences*, 7(12), 2298-2306.
- Phumying, S., Labuayai, S., Thomas, C., Amornkitbamrung, V., Swatsitang, E., Maensiri, S., (2013). Aloe vera plant-extracted solution hydrothermal synthesis and magnetic properties of magnetite (Fe<sub>3</sub>O<sub>4</sub>) nanoparticles. *Appl. Phys. A* 111, 1187e1193.
- Peters, R., Kramer, E., Oomen, A.G., Herrera Rivera, Z.E., Oegema, G., Tromp, P.C., Fokkink, R., Rietveld, A., Marvin, H.J.P., Weigel, S., Peijnenburg, A.A.C.M., Bouwmeester, H. (2012). Presence of Nano-Sized Silica during In Vitro Digestion of Foods Containing Silica as a Food Additive. *ACS Nano* 6, 24412451.
- Raju D., Mehta U.J., Hazra S. (2011) Synthesis of gold nanoparticles by various leaf fractions of *Semecarpus anacardium* L. tree. *Trees* 25(2):145–51.

- Ramasahayam, S.K., Gunawan, G., Finlay, C., Viswanathan, T. (2012). Renewable resource-based magnetic nanocomposites for removal and recovery of phosphorous from contaminated waters. *Water, Air, Soil Pollut.* 223, 4853e4863.
- Rezvani, H., Panahpoori, D., Riazi, M., Parsaei, R., Tabaei, M., Cortés, F. B. (2020). A novel foam formulation by Al<sub>2</sub>O<sub>3</sub>/SiO<sub>2</sub> nanoparticles for EOR applications: A mechanistic study. *Journal of Molecular Liquids*, 304, 112730.
- Rizvi, S.A., Saleh, A.M. (2018). Applications of nanoparticle systems in drug delivery technology. *Saudi Pharmaceutical Journal*, 26(1), 64-70.
- Roslan, A. A., Zaine, S. N. A., Mohd Zaid, H., Umar, M., Beh, H. G. (2023). Nanofluids stability on amino-silane and polymers coating titanium dioxide and zinc oxide nanoparticles. *Engineering Science and Technology, an International Journal*, 37, 101318.
- Roustaei, A., Saffarzadeh, S., Mohammadi, M. (2013) An evaluation of modified silica nanoparticles' efficiency in enhancing oil recovery of light and intermediate oil reservoirs. *Egyptian Journal of Petroleum*, 22(3): p. 427-433.
- Salager, J. (2000). *Formulation Concepts for the Emulsion Maker*. *Drugs and the Pharmaceutical Sciences*, 19-72.
- Salavati-Niasari, M., Javidi, J., Dadkhah, M. (2013). Ball Milling Synthesis of Silica Nanoparticle from Rice Husk Ash for Drug Delivery Application. *Combinatorial Chemistry & High Throughput Screening*, 16(6), 458-462
- Sajadi S.M., Kolo K., Hamad S.M., Mahmud S.A., Barzinjy A.A., Hussein S.M. (2019) Green Synthesis of the Ag/Bentonite Nanocomposite Using *Euphorbia larica* Extract: A Reusable Catalyst for Efficient Reduction of Nitro Compounds and Organic Dyes. *ChemistrySelect* 3(43):12274-12280.
- Saratale, R. G., Karuppusamy, I., Saratale, G. D., Pugazhendhi, A., Kumar, G., Park, Y., Ghodake, G. S., Bharagava, R. N., Banu, J. R., Shin, H. S. (2018). A comprehensive review on green nanomaterials using biological systems: Recent perception and their future applications. *Colloids and Surfaces B: Biointerfaces*, 170, 20-35.
- Sathishkumar M., Sneha K., Won S.W., Cho C.W., Kim S., Yun Y.S. (2009) Cinnamon zeylanicum bark extract and powder mediated green synthesis of nano-crystalline silver particles and its bactericidal activity. *Colloids Surf B Biointerfaces* 73(2):332–8.
- Saw, R. K., Singh, A., Maurya, N. K., Mandal, A. (2023). A mechanistic study of low salinity water-based nanoparticle-polymer complex fluid for improved oil recovery in sandstone reservoirs. *Colloids and Surfaces A: Physicochemical and Engineering Aspects*, 666, 131308.

- Schramm, L.L. (2000) *Surfactants: Fundamentals and applications in the petroleum industry*. Cambridge: Cambridge University Press.
- Schmidt K.F., (2007). Green Nano Technology:it is Easier than you think. Technical Report. Project on Emerging Nanotechnologies (2007): 1-36.
- Schneider, M., Cesca, K., De Amorim, S. M., Hotza, D., Rodríguez-Castellón, E., Moreira, R. F. (2023). Synthesis and characterization of silica-based nanofluids for enhanced oil recovery. *Journal of Materials Research and Technology*, 24, 4143-4152.
- ShamsiJazeyi, H. Miller, C.A. Wong, M.S. Tour, J.M. Verduzco, R. (2014) Polymer-coated Nanoparticles for enhanced oil recovery. *J. App. Poly. Sci.* 131(15).
- Sharma, T., Iglauer, S., Sangwai, J.S. (2016) Silica Nanofluids in an Oilfield Polymer Polyacrylamide: Interfacial Properties, Wettability Alteration, and Applications for Chemical Enhanced Oil Recovery, *Industrial Eng. Chem. Res.* 55, 12387-12397.
- Sharma, A., Jain, P., Bajpai, R., Patel, P., Tiwari, A. (2023). Synthesis of ultra-thin graphene oxide/reduced graphene oxide nanocomposites and examine their properties. *Materials Today: Proceedings*. <https://doi.org/10.1016/j.matpr.2023.03.381>
- Silveira, C., Shimabuku, Q.L., Fernandes Silva, M., Bergamasco, R. (2017) Iron-oxide nanoparticles by green synthesis method using Moringa oleifera leaf extract for fluoride removal. *Environ. Technol.* 3330, 1e40.
- Sima, F., Ristoscu, C. Duta, L. Gallet, O. Anselme, K., Mihailescu, I. (2016). Laserthin films deposition and characterization for biomedical applications. *Laser Surface Modification of Biomaterials*, Elsevier: 77–125.
- Singh, J., Kaur, S., Kaur, G., Basu, S., Rawat, M. (2019). Biogenic ZnO nanoparticles: A study of blueshift of optical band gap and photocatalytic degradation of reactive yellow 186 dye under direct sunlight. *Green Processing and Synthesis*, 8(1), 272-280.
- Srivastava, N., Srivastava, M., Mishra, P. K., Gupta, V.K. (2020) *Green Synthesis of Nanomaterials for Bioenergy Applications*. John Wiley & Sons.
- Subbenaik, S.C. (2016) Physical and chemical nature of nanoparticles. *In Plant nanotechnology* (pp. 15-27). Springer, Cham.
- Sun, X. Zhang, Y. Chen, G. Gai, Z. (2017) Application of Nanoparticles in Enhanced Oil Recovery: A Critical Review of Recent Progress, *Energies* 10, 345.
- Tang, W., Wu, P., Da, C., Alzobaidi, S., Harris, J., Hallaman, B., Hu, D., Johnston, K. P. (2023). Synergy of surface modified nanoparticles and surfactant in wettability alteration of calcite at high salinity and temperature. *Fuel*, 331, 125752.
- Tapondjou, L.A., Fouedjou, R.T., Nguenefack, E.P., Ponou, B.K., Nguenefack, T.B., Barboni, L. (2016) Antioxidant activities and chemical constituents of extracts from cordyline

- fruticosa (L.) A. Chev. (Agavaceae) and Eriobotrya japonica (Thunb) Lindl, (Rosaceae). *Pharmacologia* 7(2);103-113.
- Toma, S. H., Santos, J. J., Da Silva, D. G., Huila, M. F., Toma, H. E., Araki, K. (2022). Improving stability of iron oxide nanofluids for enhanced oil recovery: Exploiting wettability modifications in carbonaceous rocks. *Journal of Petroleum Science and Engineering*, 212, 110311.
- Torsater, O., Engeset, B., Hendraningrat, L., Suwarno, S. (2012) Improved oil recovery by nanofluids flooding: An experimental study. *Society of Petroleum Engineers*.
- Udoh, T. H. (2021). Improved insight on the application of nanoparticles in enhanced oil recovery process. *Scientific African*, 13.
- Venkateswarlu, S., Kumar, B.N., Prasad, C., Venkateswarlu, P., Jyothi, N. (2014) Bio-inspired green synthesis of Fe<sub>3</sub>O<sub>4</sub> spherical magnetic nanoparticles using *Syzygium cumini* seed extract. *Phys. B Condens. Matter* 449, 67e71.
- Venkateswarlu, S., Yoon, M. (2015) Surfactant-free green synthesis of Fe<sub>3</sub>O<sub>4</sub> nanoparticles capped with 3,4-dihydroxyphenethylcarbamodithioate: stable recyclable magnetic nanoparticles for the rapid and efficient removal of Hg(II) ions from water. *Dalton Trans.* 44, 18427e18437.
- Vollath, D. (2013) *Nanoparticles-Nanocomposites-Nanomaterials: An Introduction for Beginners*. John Wiley & Sons.
- Weir, A., Westerhoff, P., Fabricius, L., von Goetz, N. (2012) Titanium Dioxide Nanoparticles 182 in Food and Personal Care Products. *Environ. Sci. Technol.* 46, 22422250.
- Weng, X., Guo, M., Luo, F., Chen, Z. (2017) One-step green synthesis of bimetallic Fe/Ni nanoparticles by eucalyptus leaf extract: biomolecules identification, characterization and catalytic activity. *Chem. Eng. J.* 308, 904e911.
- Xiao, Z., Yuan, M., Yang, B., Liu, Z., Huang, J., Sun, D. (2016) Plant-mediated synthesis of highly active iron nanoparticles for Cr(VI) removal: investigation of the leading biomolecules. *Chemosphere* 150, 357e364.
- Wirunchit, S., Gansa, P., Koetnuyom, W. (2021). Synthesis of ZnO nanoparticles by Ball-milling process for biological applications. *Materials Today: Proceedings*, 47, 3554-3559.
- Worsfold, P., Townshend, A., Poole C.F., Miró M. (2019) *Encyclopedia of analytical science*, Elsevier.
- Yang, X. Liu, Z. H. (2010) A kind of nanofluid consisting of surface -functionalized nanoparticles, *Nanoscale Research Letters* 5 (2010) 1324–1328.

- Yeganeh-Faal, A., Bordbar, M., Negahdar, N., Nasrollahzadeh, M. (2017) Green synthesis of the Ag/ZnO nanocomposite using *Valeriana officinalis* L. root extract: application as a reusable catalyst for the reduction of organic dyes in a very short time. *IET Nanobiotechnology* 11(6):669-676
- Yew, Y.P., Shameli, K., Miyake, M., Khairudin, N.B.B.A., Mohamad, S.E.B., Naiki, T., Lee, K.X. (2018) Green biosynthesis of superparamagnetic magnetite Fe<sub>3</sub>O<sub>4</sub> nanoparticles and biomedical applications in targeted anticancer drug delivery system: a review. *Arab. J. Chem.* 13 (1), 2287e2308.
- Yu, W., Xie, H. (2012) A review on nanofluids: preparation, stability mechanisms, and applications. *Journal of nanomaterials*, 2012, 1.
- Yuan, S., Liang, T., Zhou, F., Liang, X., Yu, F., Li, J. (2019). A Microfluidic Study of Wettability Alteration Rate on Enhanced Oil Recovery in Oil-Wet Porous Media. Day 3 Wed, November 13, 2019.
- Zargar, G., Arabpour, T., Khaksar Manshad, A., Ali, J. A., Mohammad Sajadi, S., Keshavarz, A., Mohammadi, A. H. (2020). Experimental investigation of the effect of green TiO<sub>2</sub>/Quartz nanocomposite on interfacial tension reduction, wettability alteration, and oil recovery improvement. *Fuel*, 263, 116599.
- Zhang, Q., Chen, C., Wang, M., Cai, J., Xu, J., Xia, C. (2011). Facile preparation of highly-dispersed cobalt-silicon mixed oxide nanosphere and its catalytic application in cyclohexane selective oxidation. *Nanoscale Research Letters*, 6(1)
- Zhou, X. Li Y. (2015) *Atlas of Oral Microbiology: From Healthy Microflora to Disease*, Academic Press.

## 9. List of included publications

1. **Ali, J. A.**, Kolo, K., Manshad, A. K., Mohammadi, A. H. (2018). Recent advances in application of nanotechnology in chemical enhanced oil recovery: Effects of nanoparticles on wettability alteration, interfacial tension reduction, and flooding. *Egyptian Journal of Petroleum*, 27(4), 1371-1383.
2. **Ali, J. A.**, Kolo, K., Khaksar Manshad, A., Stephen, K. D. (2019a). Low-salinity polymeric nanofluid-enhanced oil recovery using green polymer-coated ZnO/SiO<sub>2</sub>/Nanocomposites in the upper Qamchuqa formation in Kurdistan region, Iraq. *Energy & Fuels*, 33(2), 927-937.
3. **Ali, J. A.**, Kolo, K., Manshad, A. K., Stephen, K. D. (2019b). Potential application of low-salinity polymeric-nanofluid in carbonate oil reservoirs: IFT reduction, wettability alteration, rheology and emulsification characteristics. *Journal of Molecular Liquids*, 284, 735-747.
4. Zargar, G., Arabpour, T., Khaksar Manshad, A., **Ali, J. A.**, Mohammad Sajadi, S., Keshavarz, A., Mohammadi, A. H. (2020). Experimental investigation of the effect of green TiO<sub>2</sub>/Quartz nanocomposite on interfacial tension reduction, wettability alteration, and oil recovery improvement. *Fuel*, 263, 116599.
5. Nazarahari, M. J., Manshad, A. K., Ali, M., **Ali, J. A.**, Shafiei, A., Sajadi, S. M., Moradi, S., Iglauer, S., Keshavarz, A. (2021). Impact of a novel biosynthesized nanocomposite (SiO<sub>2</sub>@Montmorilant@Xanthan) on wettability shift and interfacial tension: Applications for enhanced oil recovery. *Fuel*, 298, 120773.
6. **Ali, J. A.**, Kolo, K., Manshad, A. K., Stephen, K. D. (2021). Emerging applications of TiO<sub>2</sub>/SiO<sub>2</sub>/poly(acrylamide) nanocomposites within the engineered water EOR in carbonate reservoirs. *Journal of Molecular Liquids*, 322, 114943.
7. Manshad, A. K., **Ali, J. A.**, Haghghi, O. M., Mohammad Sajadi, S., Keshavarz, A. (2022). Oil recovery aspects of ZnO/SiO<sub>2</sub> nano-clay in carbonate reservoir. *Fuel*, 307, 121927.

8. **Ali, J. A.** (2022). Effect of Fe<sub>3</sub>O<sub>4</sub>/mineral–soil Nanocomposites on Wettability alteration and oil production under the spontaneous imbibition process. *Arabian Journal for Science and Engineering*, 48(7), 9259-9268.
9. Nourinia, A., Manshad, A. K., Shadizadeh, S. R., **Ali, J. A.**, Iglauer, S., Keshavarz, A., Mohammadi, A. H., Ali, M. (2022). Synergistic efficiency of zinc oxide/Montmorillonite Nanocomposites and a new derived saponin in liquid/Liquid/Solid interface-included systems: Application in nanotechnology-assisted enhanced oil recovery. *ACS Omega*, 7(29), 24951-24972.
10. Motraghi, F., Khaksar Manshad, A., Akbari, M., **Ali, J. A.**, Sajadi, S. M., Iglauer, S., Keshavarz, A. (2023). Interfacial tension reduction of hybrid crude-oil/mutual-solvent systems under the influence of water salinity, temperature and green SiO<sub>2</sub>/KCL/Xanthan nanocomposites. *Fuel*, 340, 127464.

## Appendix 1

*Recent advances in application of nanotechnology in chemical enhanced oil recovery: Effects of nanoparticles on wettability alteration, interfacial tension reduction, and flooding*

**Jagar A. Ali**, Kamal Kolo, Abbas Khaksar Manshad, Amir H. Mohammadi

Egyptian Journal of Petroleum 27 (2018) 1371–1383



Contents lists available at ScienceDirect

Egyptian Journal of Petroleum

journal homepage: www.sciencedirect.com



Review

Recent advances in application of nanotechnology in chemical enhanced oil recovery: Effects of nanoparticles on wettability alteration, interfacial tension reduction, and flooding



Jagar A. Ali <sup>a,b,\*</sup>, Kamal Kolo <sup>b</sup>, Abbas Khaksar Manshad <sup>a,c</sup>, Amir H. Mohammadi <sup>d</sup>

<sup>a</sup> Department of Petroleum Engineering, Faculty of Engineering, Soran University, Kurdistan Region, Iraq

<sup>b</sup> Scientific Research Centre, Soran University, Kurdistan Region, Iraq

<sup>c</sup> Department of Petroleum Engineering, Abadan Faculty of Petroleum Engineering, Petroleum University of Technology (PUT), Abadan, Iran

<sup>d</sup> Institut de Recherche en Génie Chimique et Pétrolier (IRGCP), Paris Cedex, France

ARTICLE INFO

Article history:

Received 16 April 2018  
 Revised 25 July 2018  
 Accepted 26 September 2018  
 Available online 9 November 2018

Keywords:

Nanoparticles  
 Chemical EOR  
 Interfacial Tension  
 Wettability alteration  
 Nanofluid

ABSTRACT

Chemical methods of enhanced oil recovery (CEOR) are applied for improving oil recovery from different kinds of oil reservoirs due to their ability for modifying some crucial parameters in porous media, such as mobility ratio ( $M$ ), wettability, spreading behavior of chemical solutions on rock surface and the interfacial tension (IFT) between water and oil. Few decades ago, the surfactant and polymer flooding were the most common CEOR methods have been applied for producing the remained hydrocarbon after primary and secondary recovery techniques. Recently, more attention has been focused on the potential applications of the nanotechnology in enhanced oil recovery (EOR). For this purpose, many studies reported that nanoparticles (NPs) have promising roles in CEOR processes due to their ability in changing oil recovery mechanisms and unlocking the trapped oil in the reservoir pore system. This paper presents a comprehensive and up-to-date review of the latest studies about various applications of nanoparticles (NPs) within the surfactant (S), polymer (P), surfactant-polymer (SP), alkaline-surfactant-polymer (ASP) and low salinity waterflooding processes, which exhibits the way for researchers who are interested in investigating this technology. The review covers the effects of nanoparticles on wettability alteration, interfacial tension reduction and oil recovery improvement, and discusses the factors affecting the rock/fluid interaction behavior in porous media through the nanofluid flooding.

© 2018 Egyptian Petroleum Research Institute. Production and hosting by Elsevier B.V. This is an open access article under the CC BY-NC-ND license (<http://creativecommons.org/licenses/by-nc-nd/4.0/>).

Contents

|   |      |
|---|------|
| 1. Introduction . . . . .   | 1372 |
| 2. Nano-chemical EOR flooding . . . . .                                 | 1374 |
| 2.1. Nano-polymer flooding . . . . .                                    | 1375 |
| 2.2. Nano-surfactant flooding . . . . .                                 | 1375 |
| 2.3. Nano-surfactant-polymer flooding . . . . .                         | 1376 |
| 2.4. Smart-nano-waterflooding . . . . .                                 | 1376 |
| 3. Wettability . . . . .  | 1377 |
| 3.1. Effect of nanoparticles on wettability alteration . . . . .        | 1377 |
| 4. Interfacial tension (IFT) . . . . .                                  | 1378 |
| 4.1. Effect of nanoparticles on interfacial tension reduction . . . . . | 1379 |
| 5. Conclusions . . . . .  | 1380 |
| References . . . . .  | 1380 |

Peer review under responsibility of Egyptian Petroleum Research Institute.

\* Corresponding author.

E-mail address: [jagar.ali@soran.edu.iq](mailto:jagar.ali@soran.edu.iq) (J.A. Ali).

<https://doi.org/10.1016/j.ejpe.2018.09.006>

1110-0621/© 2018 Egyptian Petroleum Research Institute. Production and hosting by Elsevier B.V.

This is an open access article under the CC BY-NC-ND license (<http://creativecommons.org/licenses/by-nc-nd/4.0/>).

## 1. Introduction

Most of the oil-producing fields in the world have reached or are approaching the stage where the rate of total oil-field production is at or close to the decline phase regardless of oil companies' efforts to delay this phase by using different enhanced oil recovery (EOR) techniques including polymerchemical flooding, gas injection, surfactant, low salinity water and thermal methods [1]. Even though about 50% of the initial oil-in-place is still trapped in the reservoir as a bypassed and/or as a residual oil, but some older fields are faced with abandonment [2]. Since the last decade, numerous researchers are attempting to recover more oil commercially and to delay the abandonment of oil fields by innovating some newly techniques from utilizing the nanotechnology in oil and gas industry [3]. Nanotechnology, as the latest worldwide industrial innovation, uses nanoparticles with the size of 1–100 nm to enhance the rheological properties of fluids at different temperatures. This technology covers the construction, characterization and application of materials, systems and devices of an element at the nanometer scale [4,5]. By adding these nanoscale materials (nanoparticles) into various base fluids, different nanofluids can be designed and produced with different physical properties [6]. Specialized literature covers a wide range of research topics regarding how the various types of nanoparticles (NPs) are targeting the alteration of specific parameters and rock-fluid properties in order to enhance the oil recovery (Table 1). The SEM morphologies of the most used nanoparticles in EOR processes are shown in Fig. 1. Generally, there are some favorable outcomes behind the use of the nanoparticles in EOR applications (Fig. 2), such as the IFT reduction [7–9], wettability alteration

[10,11], heavy oil swelling [12], asphaltene stabilization [13], reducing the viscosity of oil [14–16], increasing the viscosity of injecting fluid [17,18], nano-emulsion creation [19], pore channel plugging [20,21], and disjoining pressure [22,23]. In some cases, the dispersion of nanoparticles into the reservoir fluids might lead to multiple positive results. For instance, disjoining pressure, as an EOR mechanism, can influence favorably other mechanisms such as wettability alteration and increasing the sweep efficiency [24,25].

In addition to their roles in recovery enhancement mechanisms, the transportation efficiency of nanoparticles in the porous media also matters and has been investigated. Rodriguez et al. [26], concluded that besides the ability of nanoparticles to pass easily through the pore throats in the porous media due to their small sizes, they can also stay dispersed within the solutions due to their active surface and high stability [26]. Kanj et al. [27] quantified the applicable sizes of nanoparticles which are feasible to be transported through the porous media, and reported that particles with the size up to 200  $\mu\text{m}$  can be easily transported with high dispersion stability. In addition, Li and Torsæter [28] studied the transportation and adsorption behaviors of various types of silica NPs through the porous media. From their results, it was found that the hydrophilic silica non-structure particles (NSP) have a better adsorption ability compared to hydrophilic silica colloidal nanoparticles (CNP) [28]. While, Aurand and Torsæter [29] claimed that the adsorption efficiency and recovery performance of nanofluids with the use of fumed silica NPs is better than with colloidal silica NPs.

Recently, several research studies indicated that different types of nanoparticles have promising roles in enhanced oil recovery,

**Table 1**

List of different classes and types of nanoparticles which can be used in EOR applications including IFT reduction, wettability alteration, emulsion stabilization, mobility ratio and viscosity modification.

| Type of NPs   | Subject of study               | Reference | Outcomes  |
|---|--------------------------------|-----------|---|
| <i>Metal Oxide Nanoparticles</i>                                |                                |           |   |
| Al <sub>2</sub> O <sub>3</sub>                                  | IFT & viscosity                | [43,158]  | Viscosity reduction is the dominant effect                          |
| CuO   | Viscosity of fluids            | [170]     | Reduced oil viscosity and increased the viscosity of injected fluid |
| Fe <sub>2</sub> O <sub>3</sub> , Fe <sub>3</sub> O <sub>4</sub> | Mobility ratio                 | [43,84]   | Not strongly effective  |
| Ni <sub>2</sub> O <sub>3</sub>                                  | Viscosity of fluids            | [43,171]  | Reduced oil viscosity & increased the viscosity of injected fluid   |
| MgO   | Fines migration                | [43,139]  | Improved the fine migration without any effects on oil recovery     |
| SnO <sub>2</sub>  | Oil recovery                   | [172,173] | Not effective for oil recovery but rarely altered the wettability   |
| TiO <sub>2</sub>  | Wettability & IFT modification | [174,187] | Very effective  |
| ZnO   | Oil recovery                   | [43]      | Negatively affected the permeability                                |
| ZrO <sub>2</sub>  | Oil recovery                   | [43]      | Lower oil recovery than injecting only water                        |
| <i>Magnetic NPs</i>   |                                |           |   |
| Ferro nanofluids  | IFT reduction                  | [84]      | Reduced IFT for both oil-wet and water-wet                          |
| CoFe <sub>2</sub> O <sub>4</sub>                                | Oil recovery                   | [175]     | Reduced residual oil from 31.5% to 8.7%                             |
| <i>Organic NPs</i>  |                                |           |   |
| Carbon NPs  | Oil recovery                   | [27]      | Improved oil recovery up to 96%                                     |
| CNTs  | EOR agent in HPHT              | [176]     | Effective for viscosity reduction                                   |
| <i>Inorganic NPs</i>  |                                |           |   |
| SiO <sub>2</sub>  | Wettability & IFT              | [177,178] | Very effective modifying IFT and wettability                        |
| Hydrophobic SiO <sub>2</sub>                                    | Oil recovery                   | [43,179]  | Very effective in improving oil recovery                            |
| Fumed SiO <sub>2</sub>  | Oil/water emulsion             | [179]     | Only changed the wettability.                                       |
| Silica-core/polymer   | High temp & high salinity      | [180]     | Reduced IFT and improved oil recovery                               |
| Silane SiO <sub>2</sub>   | Sandstone reservoir            | [43,181]  | Effective in increasing oil recovery                                |
| HLP   | Wettability & IFT              | [32,37]   | Very effective in modifying IFT and wettability                     |
| LHP   | Wettability alteration         | [32,38]   | Increased oil recovery by wettability alteration                    |
| NWP   | Wettability & IFT              | [32,37]   | Stronger impact on the wettability than IFT                         |
| <i>Non-silica NPs</i>   |                                |           |   |
| Zeolite   | –                              | [49]      | Effective in absorbing captions                                     |
| Nano-sensors  | –                              | [182]     | NO DISCOVERY  |
| Nano-sized colloidal disp. gels                                 | Sweep efficiency               | [183,184] | Increased oil recovery, moderately                                  |
| Polymer NPs   | Oil recovery                   | [185]     | Still not investigated  |
| Polymer coated NPs (PNP)  | Oil recovery                   | [186]     | Improved the mobility, wettability, emulsion and IFT                |
| PAM nano-spheres  | IFT reduction                  | [49]      | Reduced IFT and highly improved oil recovery                        |

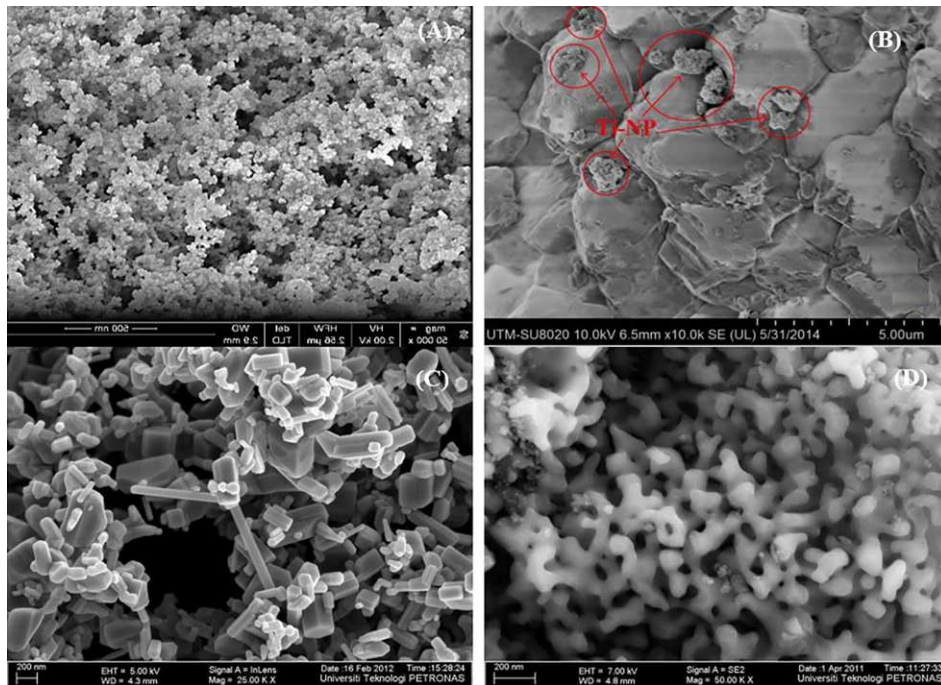


Fig. 1. SEM morphologies of various nanoparticles; (A) SiO<sub>2</sub> at 1.0 um, (B) TiO<sub>2</sub> at 5.0 um, (C) ZnO at 200 nm, and (D) Al<sub>2</sub>O<sub>3</sub> at 200 nm [116,125].

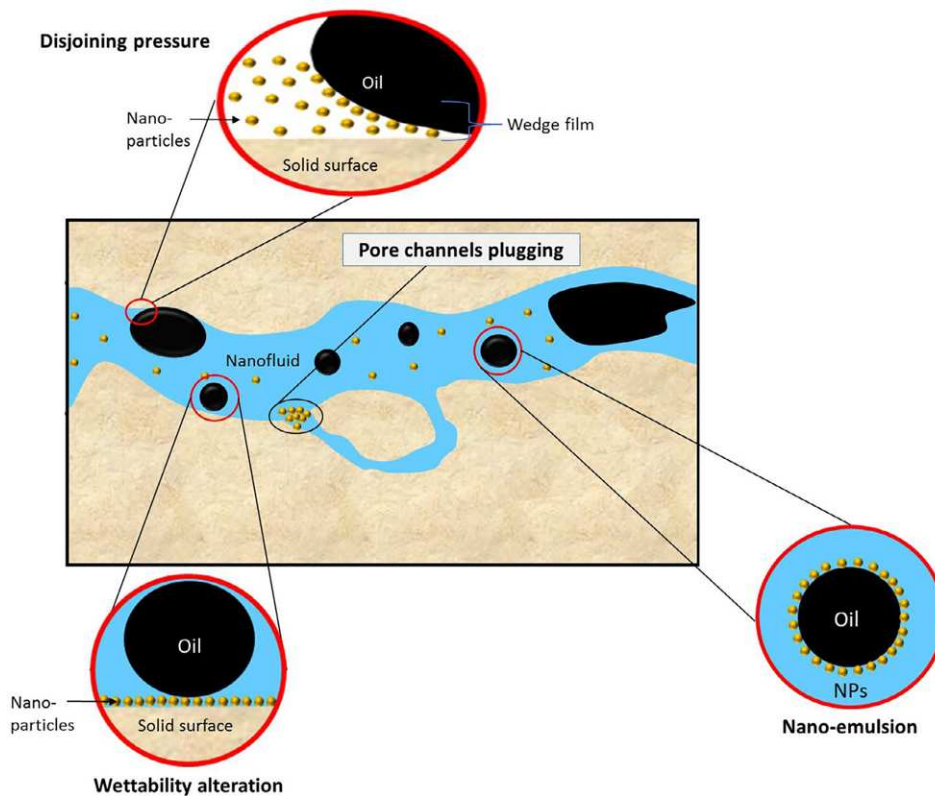


Fig. 2. EOR mechanisms of Nanofluids within the porous media.

particularly, the silica-based NPs because of their ability to alter wettability, and reduce the interfacial tension (IFT) and improve the mobility ratio [30,31,39]. In their attempt, Onyekonwu and Ogolo [32] investigated the ability of various polysilicon NPs (PSNP), such as lipophobic and hydrophilic (LHPN), hydrophilic and lipophobic (LHPN) and neutrally wet PSNP (NWPN) to enhance oil recovery; they found that all the three NPs were efficient for altering the wettability of the reservoir rocks to strongly water-wet system [32]. In various experimental studies, Hendraningrat et al. [33–36,41] verified that the silica-based NPs have a great impact on increasing oil recovery by changing the surface forces of reservoir rocks. Their results illustrated that the capability of the NPs in most nanofluid flooding processes was driven by some important parameters, such as the size of NPs, the initial wettability of rocks, the concentration of NPs, injection rate and temperature [33–36]. Additionally, Shahrabadi et al. [37] studied the effect of hydrophobic and lipophilic polysilicon (HLP) nanofluids on oil recovery with considering the IFT reduction and wettability alteration. The result of their study showed that the wettability changed from  $123.34^\circ$  to  $95.44^\circ$  contact angle and IFT reduced from 25.6 to 1.75 mN/m with an optimum concentration of 4 gr/lit of HLP NP [37]. From their experimental study, Mohammadi et al. [38] identified that  $Al_2O_3$  NP can also work as an active EOR agent for improving oil recovery in the sandstone reservoir. Later, as a novel EOR method, Tarek [40] reported that a nanofluid composed of different kinds of NPs, such as aluminum oxide ( $Al_2O_3$ ), iron oxide ( $Fe_2O_3$ ) and silicon oxide ( $SiO_2$ ) can provide better oil recovery than a nanofluid prepared only by one type of nanoparticle.

This review will analyze and discuss an up-to-date published literature on the efficiency of nanoparticles in chemical enhanced oil recovery. Particularly, we aim to explain the effect of nanoparticles within the polymer, surfactant, and smart waterflooding on the modification of wettability and interfacial tension.

## 2. Nano-chemical EOR flooding

In order to produce oil with a maximum recovery factor, the production life of a hydrocarbon reservoir has been classified into three phases; primary, secondary and tertiary production (EOR). During the primary phase, oil can be produced only by utilizing the natural energy sources of the reservoir, which includes solution gas, water aquifer, gas cap, rock and fluid expansion and gravity drainage. As oil production continues, the reservoir pressure decli-

nes and reaches a point at which there will be insufficient pressure to support oil production to the surface. Thus, as a secondary recovery method, gas or water can be injected into the reservoir in order to maintain its pressure and displace oil toward the producing wells. Even though waterflooding has been used as a promising and effective recovery process, but still part of crude oil remains as a residue and trapped due to the low viscosity of the injected water. In order to produce the residual and trapped crude oil, some more advanced chemical and thermal processes need to be applied, which are called EOR methods. Published studies of up to 2000 articles, showed that a thermal technique was more common EOR method than the chemical flooding, but now chemical methods are more widely applied in large-scale projects [3,42].

The Chemical EOR comprises alkaline, surfactant, and polymer fluid injections. Each of these fluids provides a specific function and can be used in a combination, for instance surfactant-polymer (SP) and alkaline-surfactant-polymer (ASP) mixtures. The rheological properties of these chemical solutions need to be well assessed in order to reduce the interfacial tension (IFT), decrease capillary pressure and increase the sweep efficiency. Thus, the residual and trapped oil can be displaced from the injection well into the production well. With polymer flooding, the mobility ratio ( $M$ ) could be changed to a favorable ratio, which improves sweep efficiency. On the other hand, surfactant flooding could alter the wettability and reduce IFT between the displacing fluid and the oil [42].

Recently, many research studies indicated that by adding nanoparticles (NPs) into chemical solutions, better performance of chemical EOR can be achieved [7,29–31]. Ogolo et al. [43] performed some EOR experiments using different types of NPs, with various sizes, in the different dispersing media including the distilled water, brine, ethanol and diesel. They reported that alumina NPs dispersed in distilled water and brine has a high tendency to increase oil recovery due to the reduction in oil viscosity [43]. While, the ability of both types of silica-based NPs dispersed in ethanol to increase oil recovery was due to wettability alteration. However, some permeability problems were found when magnesium oxide and zinc oxide were dispersed in distilled water and brine; and this resulted in a poor oil recovery [43]. In order to add NPs into the chemical flooding and investigate their effects on wettability alteration, IFT reduction and oil recovery, an experimental procedure shown in Fig. 3 can be applied. This figure demonstrates all the required steps for conducting an

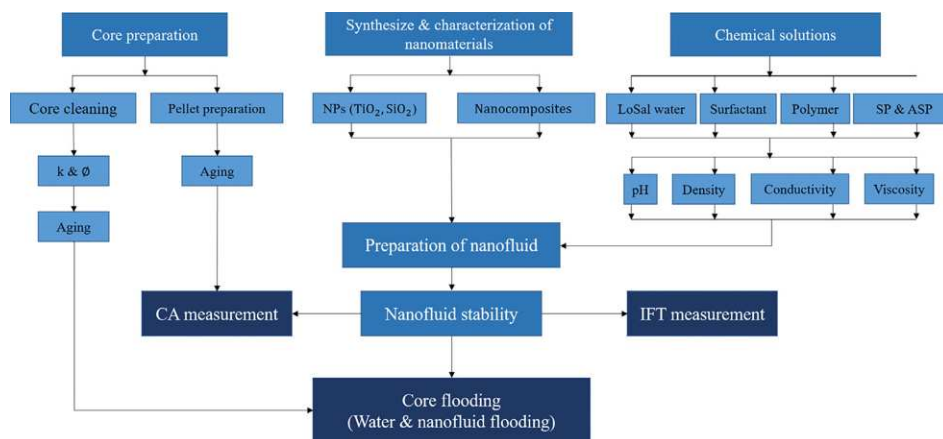


**Fig. 3.** Flow-chart shows the experimental procedure for studying the effect of nanoparticles on IFT reduction, wettability alteration and oil recovery during nano-chemical EOR injection.

experimental work about examining the effect of NPs on the oil recovery factor, and EOR mechanisms including IFT reduction and wettability.

### 2.1. Nano-polymer flooding

In order to improve the efficiency of waterflooding, polymers can be added to the injected water. This is called polymer flooding, which is one of the most common chemical EOR methods. By injecting polymer solutions, the mobility of water can be reduced, better sweep efficiency can be achieved, and more oil can be recovered [43]. Du and Guan [44] reported that the polymer flooding is unable in reducing the residual oil saturation but it can be reached in a shorter time. The ability of the injected polymer to increase the viscosity of water and to reduce the effective permeability to water varies according to the types of polymers [43]. The main types of polymers used in polymer flooding are poly(acrylamide), partially hydrolyzed poly(acrylamide), poly(dimethyl diallyl ammonium chloride), biopolymers, exopoly (saccharide), xanthan and welan [45–47]. In many EOR projects, the efficiency of polymer flooding was technically and economically confirmed, which increases the recovery by about 12–15% [42,48]. Wang et al. [49] investigated the actual data of polymer and waterflooding from an oilfield in China; they claimed that the polymer injection is economically more viable compared to water injection. For about two decades, the polymer flooding was considered as one of the most effective and promising EOR technique, especially, after applying the largely scaled polymer flooding in some fields around the world. For instance, daily oil production increased to about 300,000 bbls/day in Daqing oilfield in China after applying the polymer flooding [50,51].

Polymers are generally divided into two groups: synthetic polymers and biopolymers. Synthetic usually means polyacrylamides and biopolymers are formed from the fermentation process [44]. In practice, xanthan gums and hydrolyzed polyacrylamides (HPAM) are the two most common types of commercial polymers, which are used in oilfield operations [52]. Xanthan gums are polysaccharides polymers that have the ability to provide a favorable viscosity, high tolerance to salinity and temperature. While, the HPAM is a water-soluble polyelectrolyte that provides the negative charges on the polymer chains [53,54]. However, polyacrylamide (PAM) and partially hydrolyzed polyacrylamide (HPAM) are unable entirely to meet the EOR needs because of hydrolysis and degradation under high temperature and/or high salinity [55,56]. When PAM and HPAM polymers flow through the pump, pipeline and porous media, their polymer chains might be cut off due to their poor shear resistance [57–59]. Thus, the viscosity of the polymer would be highly decreased [59]. The viscosity behavior of polymer solutions in a reservoir might change, compared to water, due to shear thinning and shear thickening influences [60,61]. Amongst all polyacrylamide based solutions, a high molecular weight is widely used in oilfield EOR projects. On the other hand, the applicability and efficiency of these polymers can be influenced by their adsorption characteristics [62]. Moradi [63] studied the effect of Newtonian behavior, salinity, viscosity and shear thinning on the flow of hydrolyzed polyacrylamides through the porous media, and he found that the salinity has a great effect on these polymers [63].

In order to obtain a better flow behavior of polymer flooding, using NPs has recently acquired an excessive interest. Cheraghian et al. [64] studied the role of NPs in the adsorption of water-soluble polymers onto the surface of the carbonate and sandstone rocks. They found that the adsorption of polymer solution reduced by using nano-clay and nano-silica in both carbonate and sandstone rocks [64]. Cheraghian [65] investigated the impact of titanium oxide (TiO<sub>2</sub>) in different concentrations on the viscosity of

the polymer for improving the oil recovery from the heavy oil reservoir. His results showed that the polymer solution with NPs about 2.3 wt% concentration have a direct impact on fluid shear stress and caused oil recovery to be increased by about 3.9% compared to polymer flooding alone [65]. More recently, Khalilinezhad et al. [66] investigated the impact of hydrophilic silica NPs on heavy oil recovery during polymer flooding. They found that the silica NPs could increase the viscosity of the solution and reduces the adsorption of the polymer. They also stated that the recovery of heavy oil and breakthrough time for dispersed silica NPs in polymer (DSNP) flood would be improved in comparison with the conventional polymer flood [66].

### 2.2. Nano-surfactant flooding

After waterflooding, injecting the chemical surfactant is mostly applied to recover the trapped and residual oil bypassed by water due to its ability to reduce the IFT between oil and water and decrease the capillary pressure in porous media [67]. The injected surfactant could also lift off the connected oil film from the pore walls as a result of wettability alteration of the reservoir to strong water-wet [68]. For these purposes, the surfactant is generally used in two different ways: first, injecting large pore volumes (up to 60%) of a low concentration surfactant solution into reservoir, and second, injecting a small pore volume (up to 20%) of a higher surfactant concentration solution into the reservoir [52]. Among different types of surfactants include the anionic, cationic, nonionic and zwitterionic, anionic surfactants are most widely used in chemical EOR techniques due to their low adsorption behavior on sandstone rocks. However, cationic surfactants can be applied to alter the wettability of carbonate rocks from oil-wet to water-wet [42]. From the literature, it has been reported that the efficiency of the surfactant flooding is influenced by several factors including chemical types, phase behavior, chemistry, adsorption, stability, convection, dispersion, optimum formulation, pore morphology, rock wettability, etc. [69,70]. Karnanda et al. [71] reported that the temperature could have a negative impact on the surfactant flooding process if it reaches a point beyond a cloud point temperatures and at Krafft point temperature for anionic surfactants. A surfactant will become cloudy and insufficient due to dropping out of the aqueous solution [72–74]. Moreover, the performance of the surfactant flooding is also significantly affected by salinity. Bera et al. [75] outlined that high salinity has a negative impact on the efficiency of surfactant due to producing an unequal solubility of water and oil within the surfactant micro-emulsion and resulting unbalanced IFT between the micro-emulsion phase and presence oil or water phase.

Furthermore, the loss of costly surfactant due to the adsorption onto the rock surface is one of the main important aspects in surfactant-based EOR. Numerous studies have been performed on the adsorption and retention of different types of surfactant-based chemicals in various types of reservoir rocks [76–82,188]. Austad et al. [83] stated that the adsorption of surfactant has an inverse effect on the recovery efficiency, and it will be increased by increasing the surfactant concentration within the injected chemical solution.

In order to perform the surfactant flooding with a better performance, many researchers studied the effect of surfactant and nanoparticles together. Kothari et al. [84] studied the application of ferrofluid magnetic NPs with the surfactant flooding for improving oil recovery; their results showed that a better sweep efficiency can be achieved compared to the conventional surfactant flooding due to more reduction of IFT [84]. Le et al. [85] also studied the efficiency of a combination of silica NPs and surfactants as nano-surfactant flooding for reducing the IFT; their results showed that the nano-silica had a great influence on EOR mechanisms including

the reduction of adsorption of surfactant onto the rock surface, IFT reduction between crude oil and brine and oil displacement efficiency [85]. Furthermore, Zargartalebi et al., [86] used two silica-based NPs include hydrophilic and slightly hydrophobic fumed in combination with the sodium dodecyl sulfate (SDS) solution, and observed that the adsorption of surfactant to the rock surface was reduced due to the formation of the negatively charged clusters by NPs which retains the surfactant molecules in the bulk solution and prevents their adsorption on the rock surface because of electrostatic repulsion between the clusters and charged solid surface [86].

In their investigations regarding the effect of NPs on the adsorption of the surfactant, Ahmadi and Shadizadeh [76,77,81] illustrated that the nano-silica has a direct impact on surfactant adsorption in which by adding the silica NPs into the natural surfactant solution, its adsorption to the carbonate, sandstone and shale rocks has been reduced. At the same time, Cheraghian [51] studied the impact of TiO<sub>2</sub> on the efficiency of the surfactant chemical flooding in the heavy oil reservoir. They outlined that the oil recovery increased by about 4.85% during injecting the nano-titanium surfactant solution compared to the surfactant flooding alone. Moreover, Emadi et al. [87] reported that adding silica NPs into Cedar Extraction (CE) surfactant can have a great impact on the performance of surfactant flooding in terms of improving the oil recovery and reducing the IFT.

### 2.3. Nano-surfactant-polymer flooding

Most of the residual oil cannot be displaced by primary and secondary recovery methods. Thus, chemical EOR techniques, as effective recovery methods, are applied to increase the oil production, such as alkaline, surfactant and polymer flooding [42]. In the 1980s, the theory of combining the functions of these chemical solutions ended in the creation of the most important strategies of chemical EOR known as surfactant-polymer (SP) and alkaline-surfactant-polymer (ASP). Subsequently, many investigations have been conducted on designing, developing and applications of these techniques [88–94].

The saturation of residual oil can be effectively reduced during injecting the alkaline-surfactant-polymer (ASP) solution by reducing IFT and the mobility ratio between the water and oil phases [95]. Pope [96] reported that the alkali can be added into the SP solution for reducing the amount of adsorptive surfactant within the porous media and preventing the surfactant from being reacted with acid exits within the crude oil. Nevertheless, from results of some other studies, it has been shown that the use of alkali within SP flooding can introduce some problems, such as the deposition of alkali scales in the bottom of the hole and within the reservoir, which makes the treatment of produced water more difficult and reduces the viscosity of the injection solution [97–101]. In order to prevent these problems, some methods have been proposed, such as replacing the strong alkali with the weaker alkali, or applying the combination of surfactant and polymer without adding alkalis. Hence, Elraies [102] performed a series of experiments to evaluate the performance of surfactant and polymer solution in the absence and presence of alkali, and later Maolei and Yunhong [103] used weaker alkalis, such as organic and alkaline sodium carbonate to reduce their impact on the viscosity of the ASP solution. From the lab experience, it has been approved that these limitations of alkalis can be prevented by flooding the alkali-free SP flooding [104,105].

SP flooding, alkali-free, technique consists of the injection of a surfactant solution and followed by a polymer slug includes a polymer buffer and injected water [88]. It has been identified that the SP flooding can provide a better recovery performance compared to other chemical methods; this is because the polymer slug can improve the sweep efficiency and reduces the mobility ratio, and

surfactant increases the capillary number which is a significant factor for enhancing oil recovery [106]. In addition, the interactions of surfactant-polymer in flooding solution within the porous media are crucial for some scopes concerning the flow behavior, the oil displacement ability, and chemical losses by adsorption. One of the main factors that prohibited the use of surfactant in oilfield operations is the loss of this chemical solution by adsorption onto the surface of reservoir rocks [107–109]. Although it is possible to achieve an ultra-low IFT by a high concentration surfactant which is higher than the critical micelle concentration (CMC) but remain expensive.

However, the use of a mixture of hydrophilic and lipophilic surfactants has been studied experimentally to improve oil recovery due to its high ability in preventing the fingering and reducing the IFT [110–113]. During the injection of SP solution into a high permeability and low temperature reservoir, the highest oil recovery was obtained at the optimum value of IFT, not a minimum value [104]. This fact is true only for the light oil-heterogeneous reservoir with high permeability and low temperature [104]. In most investigations on the SP flooding, only the screening and evaluation of the surfactant and polymer have been considered. However, Ferdous et al. [114] and Cao et al. [115] stated that the salinity of the brine, reservoir temperature and chemical concentrations have also impacted the mobility ratio and IFT reduction [114,115].

Currently, the performance of SP chemical flooding is improved by adding nanoparticles. The results of laboratory work of many researchers highlighted that the use of NPs within the surfactant-polymer flooding improved the oil recovery greatly [116,117]. Sharma et al. [118] performed a comparative investigation to evaluate the recovery efficiency of nano-SP flooding and SP flooding concerning the Pickering emulsion stabilization. They reported that the cumulative oil recovery was increased up to 60% using Pickering emulsion compared to conventional SP flooding [118]. Later, Sedaghat et al. [119] examined the effect of SiO<sub>2</sub> and TiO<sub>2</sub> NPs on the efficiency of polymer-surfactant flooding in heavy oil reservoir. From the results of their study, it has been concluded that both types of NPs had a valuable impact on wettability alteration, IFT reduction and increasing the oil production. However, the silica NPs was more effective compared to the nano-titanium in terms of contact angle reduction and recovery efficiency [119]. Sharma and Sangawi [120] also studied the application of silica NP in SP flooding, and they outlined that the silica-SP nanofluid significantly improved oil recovery due to the reduction of IFT, increasing the viscosity of the flooding solution and changing the wettability from intermediate-wet to strongly water-wet. More recently, Cheraghian [121], in his laboratory work about the effect of NPs on recovery efficiency, stated that the efficiency of oil recovery by SP flooding can greatly be improved by adding NPs, and the adsorption of the SP solution reduces with increasing the concentration of NPs [121]. This is because of having such small size, high surface and contact area which prevents surfactant-polymer molecules to be in contact with the rock surface.

### 2.4. Smart-nano-waterflooding

In the late 1800s, when the oil reservoirs were depleted in any oilfields around the world, water injection was started as a secondary oil recovery method. At the beginning, the amount of the injected water was considered as the only factor that influences the oil recovery during waterflooding. However, researchers eventually found out that the quality and composition of the injected water were the most important factors in achieving the highest oil recovery. The formation brine has usually been used as injection water in the earlier waterfloods. Reduction of injected water salinity to improve the oil recovery was experimentally first introduced by Bernard [122]. By the late 1900s, Morrow and co-researchers [123–127] broadly investigated the effect of the low salinity

waterflooding on oil recovery. In field scale, the impact of low salinity (LoSal) water injection on oil recovery was also studied by the British Petroleum (BP) Company [128]. Since then, studying the effect of the low salinity waterflooding on oil recovery was been considered by many researchers as one of the best recovery methods due to its low cost and being environmentally safe [129–133]. In their studies, Gamage and Thyne [134] proposed different microscopic mechanisms behind the effect of the low salinity water, such as fine migration, pH variation, multi-component ion exchange, double layer effect, osmotic pressure and wettability alteration [134]. Furthermore, Collins [135] highlighted some other benefits of this recovery approach that includes scaling and corrosion reduction of the equipment involved in the recovery process. According to the outcomes of many experimental studies, the low salinity waterflooding is capable of increasing oil recovery by about 2–42%. This depends on the composition of the injected brine, the properties of the crude oil and reservoir rock [136]. Nowadays, there are great attention on the effect of LoSal-nanofluids on oil recovery as EOR method. Haroun et al. [137] investigated the effect of the various NPs on oil recovery during smart waterflooding for carbonate reservoirs. Their results showed that the oil recovery increased from 63% to about 85% by injecting the smart nanofluids [137]. Assef et al. [138] worked experimentally on the effect of MgO on LoSal waterflooding; they highlighted that the zeta potential of the porous medium became more positive by adding MgO NPs into the LoSal solution [138]. Thus, the fines migration in the presence of both divalent and monovalent salts was reduced and the performance of LoSal waterflooding was improved [138]. Huang et al. [139] investigated the effect of combining the NPs with waterflooding to improve the sweep efficiency of water in the reservoir containing the high amount of fines. Their results showed a stabilized formation of clays and fines during flooding operation, and the oil recovery was significantly improved by about 37% [139]. Additionally, Yuan et al. [140–142] studied the effect of various NPs in LoSal waterflooding, experimentally and analytically. They concluded that the pre-injection of the nanofluid prior to the flooding of the LoSal water can improve the well injectivity and reduces the side effects of fine migration [140–142]. More recently, the capability of silica NPs within the LoSal waterflooding was investigated by Zallaghi et al. [143], experimentally. They reported that the silica hydrophilic NPs have a positive impact on EOR and can recover more oil due to the modification of rock/fluid and fluid/fluid interactions at certain range of salinities and NPs concentrations [143].

### 3. Wettability

The tendency of a fluid to spread on or adhere to a solid surface in the presence of other immiscible fluids is known as wettability

[144]. Wettability affects the relative permeability curves, capillary pressure, dispersion, irreducible water saturation, oil displacement, and reducible oil saturation. In this way, it plays an important role in oil recovery mechanisms and the productivity of the reservoir. Recognizing the relationships between wettability, capillary pressure, and fluid distribution within the pore spaces is crucial for optimizing the oil recovery factor. Such relationships within crude oil-brine-rock (COBR) system are complicated due to the complexity of the rock mineralogy and pore structures [5]. The wettability inside the reservoir can be water-wet, oil-wet, or intermediate wet systems according to the distribution of the fluids around the rock grains as shown in Fig. 4 [144].

#### 3.1. Effect of nanoparticles on wettability alteration

Wettability alteration, as an important EOR mechanism, from water-wetting system to a strongly water-wet has a significant role in increasing oil production [5]. It is well known that there are some active agents and techniques which can be used to alter the wettability of rock surface to a favorable condition such as surfactants, low salinity brine, and selective ions [5]. Few years ago, many researchers identified that there is a strong effect of NPs on the wettability alteration (Table 2). For better understanding the mechanism of reducing the contact angle and altering the wettability of the reservoir from the oil-wet system towards the water wetting, it is necessary to consider the concept of disjoining pressure during nanofluid flooding. Disjoining pressure can directly increase the displacement efficiency of crude oil in the porous media [145]. This is mostly due to the wettability alteration, but ineffective in changing the interfacial tension. Chengara et al. [146] stated that nanoparticles form a thin film on a rock surface which is forced by injection pressure, and tend to arrange themselves in well-ordered layers. Consequently, an additional disjoining pressure would be exerted in an interface more than that in the bulk liquid. Additionally, Mc-Elfresh et al. [147] reported that a developed film of nanofluids on the surface of the rocks has the ability to separate and release the reservoir hydrocarbon. Hence, the wetting system can be changed from oil-wet to water wet. On the other hand, Aveyard et al. [148] explained that this film can be influenced by some parameters, such as NPs concentrations and sizes, salinity, temperature and surface rock properties. Hence, in their numerical study, Ju et al. [149] identified that increasing oil-wetting wettability control nanopowders (IOWCA) have better ability to improve oil recovery than increasing water-wetting wettability control agents (IWWCA), which is up to 66.41%. However, the effect of adding zirconium oxide ( $ZrO_2$ ) NPs on the wettability alteration in the carbonate rock was investigated by Karimi et al. [150], experimentally. They reported that the  $ZrO_2$  nanofluid is effective for modifying the wettability of carbonate rocks from strongly oil-wet to the strongly water-wet system due to the

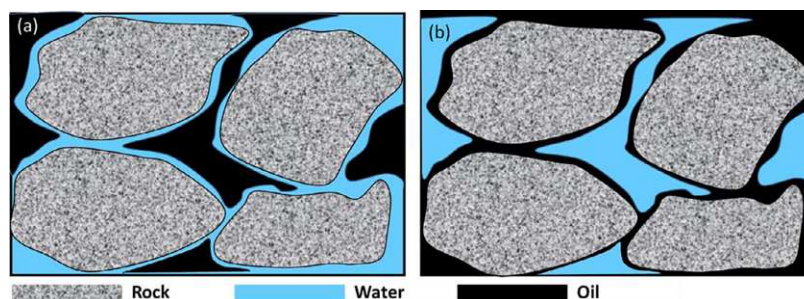


Fig. 4. Fluid distributions in (a) water-wet and (b) oil-wet rock.

**Table 2**  
A summary of previous works on effects of nanoparticles on contact angle.

| NPs                                      | NPs size (nm) | NPs Conc.     | Dispersion medium       | Porous media       | Contact angle (°) |          | Ref.  |
|--|---------------|---------------|-------------------------|--------------------|-------------------|----------|-------|
|  |               |               |                         |                    | Clean             | With NPs |       |
| NSP                                      | 7             | 0.05–0.5 wt%  | Brine (3 wt% NaCl)      | Sandstone cores    | 166               | 130      | [28]  |
| CNP                                      | 18            | 0.05–0.5 wt%  | Brine (3 wt% NaCl)      | Sandstone cores    | 166               | 124      | [28]  |
| $\gamma$ -Al <sub>2</sub> O <sub>3</sub> | 10–20         | 0.5–1.5 wt%   | Brine (180 K ppm NaCl)  | Carbonate rocks    | 119.8             | 40       | [38]  |
| ZrO <sub>2</sub>                         | 24            | 0–0.1 g/cc    | Surfactant              | Carbonate cores    | 180               | 40       | [150] |
| Al <sub>2</sub> O <sub>3</sub>           | 4             | 100–1000 ppm  | Anionic surfactant      | Sandstone cores    | 142               | ~0       | [152] |
| SiO <sub>2</sub>                         | 40            | 0.05 wt%      | Brine (3 wt% NaCl)      | Quartz plates      | 131.2             | 38.82    | [153] |
| TiO <sub>2</sub>                         | 21            | 0.05 wt%      | Brine (3 wt% NaCl)      | Quartz plates      | 131.2             | 21.64    | [153] |
| Al <sub>2</sub> O <sub>3</sub>           | 17            | 0.05 wt%      | Brine (3 wt% NaCl)      | Quartz plates      | 131.2             | 28.6     | [153] |
| ZrO <sub>2</sub>                         | >35           | 0.05 g/100 ml | Tween80/Span85          | Carbonate cores    | 140.2             | 59.7     | [155] |
| MgO                                      | >40           | 0.05 g/10 ml  | LA3 + Tween80/Span83    | Carbonate cores    | 140.2             | 98.2     | [155] |
| SiO <sub>2</sub>                         | 30–40         | 0.3 g/105 ml  | Ethylene/glycol + LA3EO | Carbonate cores    | 140.2             | 68.5     | [155] |
| TiO <sub>2</sub>                         | >35           | 0.05 g/10 ml  | LA-7EO                  | Carbonate cores    | 140.2             | 51.2     | [155] |
| Al <sub>2</sub> O <sub>3</sub>           | >40           | 0.03 g/100 ml | SDS                     | Carbonate cores    | 140.2             | 103.5    | [155] |
| SiO <sub>2</sub>                         | 12            | 1–4 g/L       | Brine (5 wt% NaCl)      | Sandstone cores    | 135.5             | 66       | [155] |
| SiO <sub>2</sub>                         | 10–15         | 10gr/200 ml   | Ethanol                 | Glass micromodel   | 134.4             | 54.52    | [159] |
| FSPNs <sup>+</sup>                       | 10–15         | 10gr/200 ml   | Ethanol                 | Glass micromodel   | 134.4             | 23.71    | [159] |
| SiO <sub>2</sub>                         | 14            | 0.1–5 wt%     | Distilled water         | Glass micromodel   | 100               | ~0       | [156] |
| Al <sub>2</sub> O <sub>3</sub>           | 20            | 0.05 wt%      | CTAB                    | Carbonate dolomite | 70                | 52       | [151] |
| Al <sub>2</sub> O <sub>3</sub>           | 20            | 0.05 wt%      | SDS                     | Carbonate dolomite | 92                | 75       | [151] |
| Al <sub>2</sub> O <sub>3</sub>           | 20            | 0.05 wt%      | TX-100                  | Carbonate dolomite | 85                | 62       | [151] |
| ZrO <sub>2</sub>                         | 40            | 0.05 wt%      | CTAB                    | Carbonate dolomite | 70                | 60       | [151] |
| ZrO <sub>2</sub>                         | 40            | 0.05 wt%      | SDS                     | Carbonate dolomite | 92                | 84       | [151] |
| ZrO <sub>2</sub>                         | 40            | 0.05 wt%      | TX-100                  | Carbonate dolomite | 85                | 71       | [151] |
| TiO <sub>2</sub>                         | 10–30         | 50 mg/L       | DIW                     | Limestone rocks    | 90                | 46       | [154] |
| HLP                                      | 10–40         | 4 gr/L        | Ethanol                 | Sandstone cores    | 135.5             | 95.44    | [153] |
| NWP                                      | 10–20         | 4 gr/L        | Ethanol                 | Sandstone cores    | 135.5             | 81.88    | [163] |
| Al <sub>2</sub> O <sub>3</sub>           | ~60           | 0.5–3 g/L     | Propanol                | Sandstone cores    | 131               | 92       | [164] |
| Fe <sub>2</sub> O <sub>3</sub>           | 40–60         | 0.5–3 g/L     | Propanol                | Sandstone cores    | 132.5             | 101      | [164] |
| SiO <sub>2</sub>                         | 10–30         | 0.5–3 g/L     | Propanol                | Sandstone cores    | 134               | 82       | [164] |

adsorption of NPs by the surface of nanostructured ribbons [150]. In addition, Moslan et al. [151] studied the effect of alumina NPs on wettability alteration in carbonate reservoir rock, and identified that this nanomaterial was enabled to alter the wettability system from the oil-wet to water-wet and increase oil recovery by about 11.25% [151]. Meanwhile, Giraldo et al. [152] injected the alumina nanofluid into the sandstone reservoir with eight different surfactant solutions and different NP concentrations. They indicated that the alumina-based NPs can improve the efficiency of the nonionic surfactants with the low concentration of 100 ppm, and alters the oil-wet wettability to strongly water-wet form. Thus, the oil recovery from the oil-wet sandstone reservoir was significantly improved [152]. On the other hand, the ability of metal oxide NPs to enhance oil recovery with different wettability conditions was also investigated [152]. For all various wetting systems, nanofluids had a stable performance and enabled in altering the wettability on the quartz surface to strongly water-wet and improved the oil recovery better than conventional chemical flooding [153,154]. At the same time, Moghaddam et al. [155] investigated the influences of various NPs such as ZeO<sub>2</sub>, CaCO<sub>3</sub>, TiO<sub>2</sub>, SiO<sub>2</sub>, MgO, Al<sub>2</sub>O<sub>3</sub>, CeO<sub>2</sub> and CNT on the wettability of carbonate rocks; among all of the nanoparticles, SiO<sub>2</sub>, TiO<sub>2</sub> and CaCO<sub>3</sub> were selected as the best candidates dependent on qualitative and quantitative results of wettability [155]. Furthermore, many researchers were studying the effect of silica-based NPs on wettability alteration including Ju et al. [38], Maghzi et al. [156], Yousefvand & Jafari [157], Hendraningrat & Torsæter [158], and Azarshin et al. [159], and they claimed that these kinds of NPs are highly efficient in changing the wettability of the porous media [38,156–159]. Yousefvand and Jafari [157] studied the effect polymeric silica-nanofluid on the oil recovery in a strongly oil-wet system, and highlighted that the oil production was greatly improved by developing a water-wet or partially water-wet on the rock surface [157]. In their investigation regarding the effect of smart nanofluid using silica NP on oil recovery, Hendraningrat and Torsæter [158] highlighted that

by changing the monovalent (Na<sup>+</sup> and K<sup>+</sup>) and divalent (Ca<sup>2+</sup> and Mg<sup>2+</sup>) cations, smart nanofluid resulted wettability alteration towards a stronger water-wet system compared to the nanofluid and smart water flooding separately [158]. All experimental steps required for studying the effect of nanoparticles on wettability alteration is shown in Fig. 6.

#### 4. Interfacial tension (IFT)

The co-presence of crude oil and water as immiscible fluids in oil reservoirs produces an interfacial tension force (IFT) as shown in Fig. 5. IFT is the energy that forces the molecule toward the surface from the bulk phase per unit area and it is usually measured in dynes/cm (milli-Newtons/meter). As one of the main parameters, IFT can be used to estimate the distribution and movement of fluids in porous media. Hence, IFT has an effective impact on the efficiency of the reservoir to produce the hydrocarbons. Therefore, for

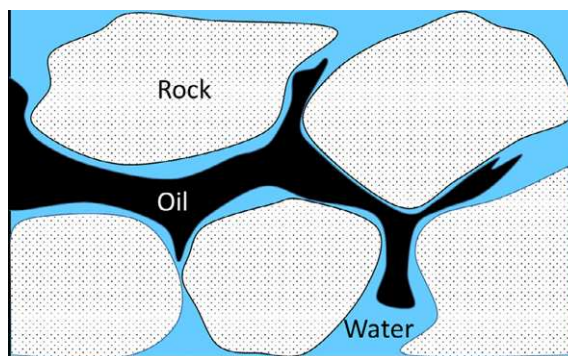


Fig. 5. An interface between oil and water in porous media.

evaluation of enhanced oil recovery techniques, it is crucial to determine the IFT between oil/brine or oil/injected fluids [82]. For measuring IFT between brine and oil phases, a spinning drop tensiometer can be used. If a micro-emulsion as a third phase is identified to be present in any cases, the oil phase can be considered as a middle phase in order to achieve the IFT measurements with more accuracy in [113]. In order to reduce the saturation of residual oil, it is essential to have a high capillary number and low IFT between water/oil [82].

#### 4.1. Effect of nanoparticles on interfacial tension reduction

Interfacial tension (IFT) reduction between oil and water in the oil reservoir is an important mechanism and target of EOR, which directly affects the capillary pressure, permeability and flow behavior of fluids in porous media. This was usually done using chemical which are very costly. Therefore, nanofluid EOR technique as a novel technology has been developed to reduce the IFT more effectively. Thus, some nanoparticles have been highlighted as efficient EOR agents for IFT reduction, such as silicon dioxide ( $\text{SiO}_2$ ), aluminum oxide ( $\text{Al}_2\text{O}_3$ ), and titanium dioxide ( $\text{TiO}_2$ ) as shown in Table 3 [160–168]. Nanoparticles usually try to form a layer in the interface between water and crude oil [160,161]. This layer produces less interfacial tension between immiscible phases depends on the concentration of NPs dispersed in nanofluids [162,160]. In 2012, Roustaei et al. in their experimental attempt to study impacts of different polysilicon NPs including hydrophobic and lipophilic polysilicon (HLP) and neutrally wet polysilicon (NWP) on IFT reduction and improving oil recovery, they stated that both HLP and NWP improved oil recovery. But from their results, it can be seen that the HLP NPs had a higher impact on the IFT and the NWP nanofluid influenced the wettability alteration more strongly [163].

Afterward, influences  $\text{Fe}_3\text{O}_4$ ,  $\text{Al}_2\text{O}_3$  and  $\text{SiO}_2$  NPs within the propanol on EOR recovery performance was investigated by Joonaki

and Ghanaatian [164]. Both alumina and silica NPs acted as efficient agents for improving oil recovery due to their ability to change the wettability and reduce IFT, while the iron oxide was less effective. At the same time, Bayat et al. [154] studied the use of metal oxide NPs within the deionized water (DIW) to improve oil recovery through limestone cores at various temperatures, and claimed that alumina is the most efficient NPs for EOR application through limestone reservoirs at all various temperatures due to reducing IFT and oil viscosity [154]. Later, Moradi et al. [39] added silica NP into water-alternating-gas (WAG) to improve the recovery efficiency. Their results showed that the IFT was greatly reduced because of NP adsorption at the interface between oil and water, and higher oil recovery factor obtained using NPs with smaller sizes [39]. While, Saigal et al. [165] used silica NP for stabilizing the polymer flooding emulsions, such as xylene and cyclohexane in water. The most efficient and stable emulsions were identified at lower grafting density of 0.077 chains/nm<sup>2</sup> for only about 0.05 wt% of particles [165].

Furthermore, the effects of NPs on IFT reduction have also been observed with the surfactant flooding process. Esmailzadeh et al., [166] conducted an experimental work to study the effect of zirconium oxide NPs on IFT between air-water and oil-water for different types of surfactant solutions include anionic surfactant (sodium dodecyl sulfate, SDS), cationic surfactant (Dodecyl trimethyl ammonium bromide, CTAB), and nonionic surfactant (Lauryl alcohol 7 mol ethoxylate, LA7). For all surfactant solutions, the IFT was effectively decreased between n-heptane and water, and air-water. But above micelle concentration (CMC) of surfactants,  $\text{ZrO}_2$  NP have no effects on IFT [166]. In addition to IFT reduction, the adsorption behavior of surfactant was also considered while using NPs within the surfactant flooding. In their study, Zaid et al. [167] added  $\text{ZnO}$  NP and  $\text{Al}_2\text{O}_3$  NP into the sodium dodecyl sulfate (SDS) solution to minimize the adsorption of surfactant onto rock surfaces. In the same way, Zargartalebi et al. [86] used different NPs includes a hydrophilic and slightly hydrophobic

**Table 3**

A summary of previous works on effects of nanoparticles on interfacial tension (IFT).

| NPs                     | NPs size (nm) | NPs Conc.    | Dispersion media   | Porous Media         | IFT (mN/m) |          | Ref.  |
|-------------------------|---------------|--------------|--------------------|----------------------|------------|----------|-------|
|                         |               |              |                    |                      | Clean      | With NPs |       |
| FNP                     | 7–16          | 0.05 wt%     | DIW                | Sandstone cores      | 16.41      | 12.61    | [29]  |
| CNP                     | 8–75          | 0.05 wt%     | DIW                | Sandstone cores      | 16.41      | 12.15    | [29]  |
| HLP                     | N/A           | 0.05 wt%     | Surfactant         | Quartz plate         | 18.4       | 5.4      | [52]  |
| $\text{SiO}_2$          | 7–12          | 1.0 wt%      | SDS                | Sandstone cores      | 20         | 1.87     | [86]  |
| $\text{SiO}_2$          | 20–30         | 5 wt%        | Surfactant         | Sandstone cores      | 35         | 10.9     | [87]  |
| $\text{SiO}_2$          | 40            | 0.05 wt%     | Brine (3 wt% NaCl) | Quartz plates        | 19.2       | 17.5     | [153] |
| $\text{TiO}_2$          | 21            | 0.05 wt%     | Brine (3 wt% NaCl) | Quartz plates        | 19.2       | n.a.     | [153] |
| $\text{Al}_2\text{O}_3$ | 17            | 0.05 wt%     | Brine (3 wt% NaCl) | Quartz plates        | 19.2       | 12.8     | [153] |
| $\text{SiO}_2$          | 10–15         | 10 gr/200 ml | Ethanol            | Glass micromodel     | 37.5       | 22.1     | [159] |
| FSPNs                   | 10–15         | 10 g/200 ml  | Ethanol            | Glass micromodel     | 37.5       | 13       | [159] |
| $\text{Al}_2\text{O}_3$ | 20            | 0.05 wt%     | CTAB               | Carbonate dolomite   | 8.46       | 1.65     | [151] |
| $\text{Al}_2\text{O}_3$ | 20            | 0.05 wt%     | SDS                | Carbonate dolomite   | 9.88       | 2.75     | [151] |
| $\text{Al}_2\text{O}_3$ | 20            | 0.05 wt%     | TX-100             | Carbonate dolomite   | 9.13       | 2.55     | [151] |
| $\text{ZrO}_2$          | 40            | 0.05 wt%     | CTAB               | Carbonate dolomite   | 8.46       | 1.85     | [151] |
| $\text{ZrO}_2$          | 40            | 0.05 wt%     | SDS                | Carbonate dolomite   | 9.88       | 2.78     | [151] |
| $\text{ZrO}_2$          | 40            | 0.05 wt%     | TX-100             | Carbonate dolomite   | 9.13       | 2.64     | [151] |
| $\text{Al}_2\text{O}_3$ | 40            | 50 mg/L      | DIW (26 °C)        | Limestone rocks      | 26.5       | 18       | [154] |
| $\text{TiO}_2$          | 10–30         | 50 mg/L      | DIW (26 °C)        | Limestone rocks      | 26.5       | 17.5     | [154] |
| $\text{SiO}_2$          | 20            | 50 mg/L      | DIW (26 °C)        | Limestone rocks      | 26.5       | 17       | [154] |
| $\text{Al}_2\text{O}_3$ | 40            | 50 mg/L      | DIW (60 °C)        | Limestone rocks      | 21.1       | 13.2     | [154] |
| $\text{TiO}_2$          | 10–30         | 50 mg/L      | DIW (60 °C)        | Limestone rocks      | 21.1       | 12.4     | [154] |
| $\text{SiO}_2$          | 20            | 50 mg/L      | DIW (60 °C)        | Limestone rocks      | 21.1       | 11.2     | [154] |
| HLP                     | 10–40         | 4 g/L        | Ethanol            | Sandstone rocks      | 26.3       | 1.75     | [163] |
| NWP                     | 10–20         | 4 g/L        | Ethanol            | Sandstone rocks      | 26.3       | 2.55     | [163] |
| $\text{Al}_2\text{O}_3$ | ~60           | 0.5–3 g/L    | Propanol           | Sandstone cores      | 38.5       | 2.25     | [164] |
| $\text{Fe}_2\text{O}_3$ | 40–60         | 0.5–3 g/L    | Propanol           | Sandstone cores      | 38.5       | 2.75     | [164] |
| $\text{SiO}_2$          | 10–30         | 0.5–3 g/L    | Propanol           | Sandstone cores      | 38.5       | 1.45     | [164] |
| $\text{SiO}_2$          | 12            | 1–4 g/L      | Brine (5 wt% NaCl) | Sandstone cores      | 26.5       | 1.95     | [169] |
| $\text{ZrO}_2$          | 5–15          | 10–500 mg/L  | Surfactant         | Bidentate carbonates | 48         | 10       | [166] |

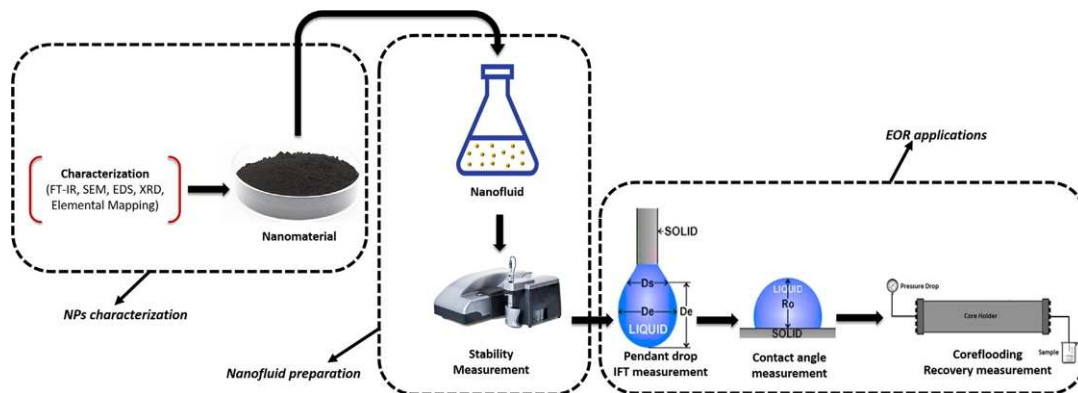


Fig. 6. A schematic diagram shows experimental steps for measuring the IFT, contact angle and recovery factor during the nanofluid injection.

fumed with the SDS surfactant; their results demonstrated that adding of these silica NPs greatly influenced IFT and adsorption of surfactant on the solid surface [86]. In order to improve the suspension stability of NPs, the silica NP was coated by smart surfactant, consequently, the developed surfactant silica-nanofluids were enabled to rearrange the oil-water interface in a better fashion and reduced IFT between oil and water more effectively [168]. A flow-chart illustrates the steps required for studying the effect of nanoparticles on IFT reduction is shown in Fig. 6.

## 5. Conclusions

The world's oil production is still not highly relying on the chemical EOR. However, China is leading the applications of chemical methods for oil recovery. While, there are numerous ongoing projects of surfactant, polymer, SP and ASP processes in Canada and the USA, they are mostly at a pilot scale, despite increasing research interest in chemical based methods to improve oil recoveries in last two decades. Apart from applications in exploration, drilling technology, production, refinery and transportation, recently, application of nanoparticles in EOR has attracted strong research interest and contributed to many experimental investigations. This paper presented a critical review of the most recent research progress in the NPs application for Chemical-EOR. Through this review, the following conclusions were reached: (i) Conventional chemical EOR methods face several challenges and problems, some of them were well solved with introducing nanofluids, (ii) The large surface area, stable dispersion and high transmissibility of NPs are of the main features of nanofluids, (iii) NPs have been dispersed in various aqueous phases (i.e. water, alcohols, surfactant, and polymer) and provided high EOR performance in different formulations nanofluids, nanoemulsions and nanocatalysts, (iv) Various organic and inorganic types of NPs have been applied, silica has been highlighted as the most common and effective NPs which provided an extra oil recovery up to 20% OOIP, (v) NPs have impact on several EOR mechanisms, such as disjoining pressure, wettability alteration, IFT reduction and mobility ratio, (vi) Several parameters including NP size, NP type, NP concentration, temperature, salinity and dispersion media have been identified to affect the nanofluid performance.

## References

- [1] G. Cheraghian, Effects of Nanoparticles on wettability: A review on applications of nanotechnology in the enhanced Oil recovery, *Int. J. Nano Dimen.* 6 (2015) 443–452.
- [2] R. Abhishek, G.S. Kumar, R.K. Sapru, Wettability alteration in carbonate reservoirs using nanofluids, *Petro. Sci. and Tech.* 33 (2015) 794–801.
- [3] G. Cheraghian, L. Hendraningrat, A review on applications of nanotechnology in the enhanced oil recovery part B: effects of Nanoparticles on flooding, *Int. Nano Lett.* 6 (2015) 1–10.
- [4] A. Bera, H. Belhaj, Application of nanotechnology by means of Nanoparticles and nanodispersions in oil recovery - A comprehensive review, *J. Nat. Gas Sci. Eng.* 34 (2016) 1284–1309.
- [5] M. Khalil, B.M. Jan, C.W. Tong, M.A. Berawi, Advanced nanomaterials in oil and gas industry: design, application and challenges, *App. Energy* 191 (2017) 287–310.
- [6] C. Negin, S. Ali, Q. Xie, Application of nanotechnology for enhancing oil recovery - A review, *L. Pet.* 2 (2016) 324–333.
- [7] B. Ju, T. Fan, M. Ma, Enhanced oil recovery by flooding with hydrophilic Nanoparticles, *China Particuol.* 4 (2006) 41–46.
- [8] H.M. Zaid, N. Yahya, N.R.A. Latiff, The effect of nanoparticles crystallite size on the recovery efficiency in dielectric nanofluid flooding, *J. Nano Res.* 21 (2013) 103–108.
- [9] O. Torsater, B. Engeset, L. Hendraningrat, S. Suwarno, Improved oil recovery by Nanofluids flooding: an experimental study, SPE Kuwait international petroleum conference and exhibition, Society of Pet. Eng. (2012) SPE-163335-MS.
- [10] J. Saien, A.M. Gorji, Simultaneous adsorption of CTAB surfactant and magnetite nanoparticles on the interfacial tension of n-hexane-water, *J. Molecule Liq.* (2017), <https://doi.org/10.1016/j.molliq.2017.07.115>.
- [11] S. Al-Anssari, A. Barifcani, S. Wang, L. Maxim, S. Iglauer, Wettability alteration of oil-wet carbonate by silica nanofluid, *J. Colloid Interface Sci.* 461 (2016) 435–442.
- [12] Y. Kazemzadeh, S.E. Eshraghi, S. Sourani, M. Reyhani, An interface-analyzing technique to evaluate the heavy oil swelling in presence of nickel oxide Nanoparticles, *J. Molecular Liq.* 211 (2015) 553–559.
- [13] A. I. El-Diasty, A. M. S. Ragab, Applications of nanotechnology in the oil & gas industry: Latest trends worldwide & future challenges in Egypt, In North Africa Technical Conference and Exhibition: Society of Pet. Eng. (2013) SPE-164716-MS.
- [14] M. Mohammadi, M. Dadvar, B. Dabir, TiO<sub>2</sub>/SiO<sub>2</sub> Nanofluids as novel inhibitors for the stability of asphaltene particles in crude oil: Mechanistic understanding, screening, modeling, and optimization, *J. Mol. Liq.* (2017).
- [15] W. Li, J. Zhu, J. Qi, Application of nano-nickel catalyst in the viscosity reduction of Liaohe heavy oil by aquathermolysis, *J. Fuel Chem. Tech.* 35 (2007) 176–180.
- [16] E.A. Taborda, C.A. Franco, S.H. Lopera, V. Alvarado, F.B. Cortés, Effect of nanoparticles/nanofluids on the rheology of heavy crude oil and its mobility on porous media at reservoir conditions, *Fuel* 184 (2016) 222–232.
- [17] A. Esteban Taborda, A.F. Camilo, A.R. Marco, A. Vladimir, B.C. Farid, Experimental and theoretical study of viscosity reduction in heavy crude oils by addition of Nanoparticles, *Energy Fuels* 31 (2017) 1329–1338.
- [18] H. Ehtesabi, M.M. Ahadian, V. Taghikhani, Enhanced heavy oil recovery using TiO<sub>2</sub> nanoparticles: investigation of deposition during transport in core plug, *Energy Fuels* 29 (2015) 1–8.
- [19] S. Bobbo, L. Fedele, A. Benetti, L. Colla, M. Fabrizio, C. Pagura, S. Barison, Viscosity of water based SWCNH and TiO<sub>2</sub> Nanofluids, *Exp. Thermal Fluid Sci.* 36 (2012) 65–71.
- [20] H. Anganaei, K. Pourabdollah, A. Rostami, Experimental improvement of nano-enhanced oil recovery using nano-emulsions, *Arabian J. Sci. Eng.* 39 (2014).
- [21] R. Hashemi, N.N. Nassar, P.P. Almas, Enhanced heavy oil recovery by in situ prepared ultradispersed multimetallic Nanoparticles: a study of hot fluid flooding for Athabasca bitumen recovery, *Energy Fuels* 27 (2013) 2194–2201.
- [22] C. P.M.O. Mcelfresh, D. Ector, The application of nanoparticle dispersions to remove paraffin and polymer filter cake damage, SPE International Symposium and Exhibition on Formation Damage Control, LA, USA, 2012.

- [23] R.B. Aveyard, J.H. Clint, Emulsions stabilized solely by colloidal particles, *Adv. Colloid Interface Sci.* (2003).
- [24] A. Zamani, B. Maini, P.P. Almas, Flow of nanodispersed catalyst particles through porous media: effect of permeability and temperature, *Can. J. Chem. Eng.* 90 (2012) 304–314.
- [25] P.M. Mcelfresh, C. Olguin, D. Ector, The application of nanoparticle dispersions to remove paraffin and polymer filter cake damage, SPE International Symposium and Exhibition on Formation Damage Control, Lafayette, LA, USA, 2012, SPE-151848-MS.
- [26] E.P. Rodriguez, M. Roberts, H. Yu, C. Huh, S.L. Bryant, Enhanced migration of surface-treated nanoparticles in sedimentary rocks, SPE Ann. Tech. Conf. Exhib. (2009).
- [27] M.Y. Kanj, J.J. Funk, Z. Al-Yousif, Nanofluid Coreflood Experiments in the ARAB-D, SPE Saudi Arabia Section Technical Symposium, 2009.
- [28] S. Li, O. Torsaeter, The Impact of Nanoparticles Adsorption and Transport on Wettability Alteration of Intermediate Wet Berea Sandstone, SPE Middle East Unconventional Resources Conference and Exhibition, 2015.
- [29] K.R. Aurand, G.S. Dahle, O. Torsaeter, Comparison of oil recovery for six nanofluids in Berea Sandstone Cores, SCA A064 (2014) 1–12.
- [30] F.S. Ismailov, E.F. Veliyev, Nanofluid for enhanced oil recovery, JPSE 78 (2011) 431–437.
- [31] T.N. De Castro Dantas, T.T. De Souza, A.A. Dantas Neto, M.C. Moura, E.L. De Barros Neto, Experimental study of nanofluids applied in EOR processes, *J. Surf. Detergents* 20 (2017) 1095–1104.
- [32] M. O. Onyekonwu, N. A. Ogolo, Investigating the Use of Nanoparticles in Enhancing Oil Recovery, Nigeria Annual International Conference and Exhibition, 2010.
- [33] L. Hendraningrat, B. Engeset, S. Suwarno, O. Torsaeter, Improved oil recovery by nanofluids flooding: an experimental study, SPE Kuwait International Petroleum Conference and Exhibition, Kuwait, 2012.
- [34] L. Hendraningrat, S. Li, O. Torsaeter, A Coreflood Investigation of Nanofluid Enhanced Oil Recovery in Low-Medium Permeability Berea Sandstone, SPE International Symposium on Oilfield Chemistry, 2013a.
- [35] L. Hendraningrat, S. Li, O. Torsaeter, Enhancing oil recovery of low-permeability berea sandstone through optimised nanofluids concentration. In: SPE Enhanced Oil Recovery Conference, KL, Malaysia, 2013.
- [36] L. Hendraningrat, S. Li, O. Torsaeter, Effect of Some Parameters Influencing Enhanced Oil Recovery Process using Silica Nanoparticles: An Experimental Investigation, SPE Reservoir Characterization and Simulation Conference and Exhibition (2013b).
- [37] A. Shahrabadi, H. Bagherzadeh, A. Roostaie, H. Golghanddashti, Experimental Investigation of HLP Nanofluid Potential to Enhance Oil Recovery: A Mechanistic Approach. SPE International Oilfield Nanotechnology Conference and Exhibition, 2012.
- [38] M.S. Mohammadi, J. Moghadasi, S. Naseri, An experimental investigation of wettability alteration in carbonate reservoir using  $\gamma\text{-Al}_2\text{O}_3$  nanoparticles, *Iran. J. Oil Gas Sci. Tech.* 2 (2014) 18–26.
- [39] B. Moradi, P. Pourafshary, F. Jalali, M. Mohammadi, M.A. Emadi, Experimental study of water-based nanofluid alternating gas injection as a novel enhanced oil-recovery method in oil-wet carbonate reservoirs, *J. Natural Gas Sci. Eng.* 27 (2015) 64–73.
- [40] M. Tarek, Investigating Nano-Fluid Mixture Effects to Enhance Oil Recovery, SPE Annual Technical Conference and Exhibition, 2015.
- [41] G. Cheraghian, Effects of titanium dioxide Nanoparticles on the efficiency of surfactant flooding of heavy oil in a glass micromodel, *Petro. Sci. Tech.* 34 (2016) 260–267.
- [42] J. Sheng, *Modern Chemical Enhanced Oil Recovery: Theory and Practice*, Gulf Professional, Place of Publication not Identified, 2016.
- [43] N. Ogolo, O. Olafuyi, M. Onyekonwu, Enhanced Oil Recovery Using Nanoparticles. SPE Saudi Arabia Section Technical Symposium and Exhibition, 2012.
- [44] Y. Du, L. Guan, Field-scale Polymer Flooding: Lessons Learnt and Experiences Gained During Past 40 Years, SPE International Petroleum Conference in Mexico, 2004.
- [45] T. Chen, W. Pu, K. Ping, Z. Ye, The rheological behavior of partially hydrolyzed polyacrylamide (HPAM) solutions in reservoir, *J. Southwest Pet Inst.* 2A-3A (19) (1997) 28–34.
- [46] R. A. Mamleev, E. M. Yulbarisov, R. N. Fakhretidinov, L. N. Zagidullina, A. N. Kulikov, Z. R. Kutushev, Composition for pumping into oil stratum—contains specified biopolymer, polydimethylallyl ammonium chloride, water and formaldehyde, SU patent 1 828 161, assigned to Oil Strata Geolog Phys (1997).
- [47] Z.C. Ren, A.P. Shi, S.L. Leng, W.S. Zhang, L.P. Qin, Formulation of crosslinking polyacrylamide solution for EOR, *Oilfield Chem.* 15 (1998) 146–149.
- [48] J. Wang, M. Dong, Optimum effective viscosity of polymer solution for improving heavy oil recovery, *J. Petrol Sci. Eng.* 67 (2009) 155–158.
- [49] D. Wang, J. Cheng, J. Wu, Y. Wang, Producing by polymer flooding more than 300 million barrels of oil what experiences have been learnt, SPE 77872 presented at Asia Pacific oil and Gas Conference and Exhibition, Melbourne, Australia, 2002.
- [50] D.M. Wang, H.F. Xia, Z.C. Liu, Q.Y. Yang, Study on the mechanism of polymer solution with viscous-elastic behavior improving microscopic oil displacement efficiency, *Acta Petrol. Sin.* 22 (2001) 60–65.
- [51] G. Cheraghian, S. KhalilNezhad, S. Bazgir, Improvement of thermal stability of polyacrylamide solution used as a nano-fluid in enhanced oil recovery process by nanoclay, *Int. J. Nanosci. Nanotechnol.* 11 (2015) 201–208.
- [52] A.M. El Shafey, Effect of nanoparticles and polymer nanoparticles implementation on chemical flooding, wettability and interfacial tension for the enhanced oil recovery processes, *Afr. J. Eng. Res.* 5 (2017) 35–53.
- [53] XH. Guo, D. W. Li, J. Tian, YZ. Liu, Pilot test of xanthan gum flooding in Shengli oilfield. In: SPE 57294 Presented at SPE Asia Pacific Improved Oil Recovery Conference, KL, 1999.
- [54] G. Cheraghian, L. Hendraningrat, A review on applications of nanotechnology in the enhanced oil recovery part A: effects of Nanoparticles on interfacial tension, *Int. Nano Lett.* 6 (2016) 129–138.
- [55] Z.B. Ye, G.J. Gou, S.H. Gou, W.C. Jiang, T.Y. Liu, Synthesis and characterization of a water-soluble sulfonates copolymer of acrylamide and N-Allylbenzamide as enhanced oil recovery chemical, *J. Appl. Polym. Sci.* 128 (2013) 2003–2011.
- [56] B.S. Shiran, A. Skauge, Enhanced oil recovery (EOR) by combined low salinity water/polymer flooding, *Energy Fuels* 27 (2013) 1223–1235.
- [57] L. Xue, U.S. Agarwal, P.J. Lemstra, Shear degradation resistance of star polymers during elongational flow, *Macromolecules* 38 (2005) 8825–8832.
- [58] Z. Ye, X. Qin, N. Lai, Q. Peng, X. Li, C. Li, Synthesis and Performance of an Acrylamide Copolymer Containing Nano-SiO<sub>2</sub> as Enhanced Oil Recovery Chemical, *Hindawi Publ. Corp. J. Chem.*, 2013.
- [59] G. Cheraghian, Thermal resistance and application of nanoclay on polymer flooding in heavy oil recovery, *Pet. Sci. Technol.* 33 (2015) 1580–1586.
- [60] I. Lakatos, J. Lakatos-Szabo, Investigation of the sorption phenomena of polyacrylamides in porous media under dynamic conditions, *Acta Chim. Acad. Sci. Hung.* 105 (1980) 57–72.
- [61] L.T. Lee, R. Rahbari, J. Lecoutier, G. Chateveteau, Adsorption of polyacrylamide on the different faces of kaolinites, *J. Colloid Interface Sci.* 147 (1991) 351–357.
- [62] O.A. Magbagbeola, Quantification of the Viscoelastic Behavior of High Molecular Weight Polymers used for Chemical Enhanced Oil Recovery MS Thesis, University of Texas at Austin, 2008.
- [63] H. Moradi, Experimental Investigation of Polymer Flow Through Water- and Oil-wet Porous Media MS Thesis, University of Stavanger, 2011.
- [64] G. Cheraghian, S. Khalili Nezhad, M. Kamari, M. Hemmati, S. Bazgir, Adsorption polymer on reservoir rock and role of the Nanoparticles, clay and SiO<sub>2</sub>. *International. Nano Lett.* 4 (3) (2014) 1–8.
- [65] G. Cheraghian, Effect of nano titanium dioxide on heavy oil recovery during polymer flooding, *Pet. Sci. Tech.* 34 (2016) 633–641.
- [66] S.S. Khalilnezhad, G. Cheraghian, E. Roayaei, H. Tabatabaee, M.S. Karambeigi, Improving heavy oil recovery in the polymer flooding process by utilizing hydrophilic silica Nanoparticles, *Energy Sources Part A Recov Util. Environ. Effects* (2017) 1–10.
- [67] J.B. Yadali, R. Kharrat, F. Ahmadloo, Selection of proper criteria in flow behavior characterization of low tension polymer flooding in heavy oil reservoirs. SPE Kuwait international petroleum conference and exhibition, 2009.
- [68] C. Negin, S. Ali, Q. Xie, Most common surfactants employed in chemical enhanced oil recovery, *J. Petro.* 3 (2017) 197–211.
- [69] B. Yadali Jamaloei, R. Kharrat, Pore-scale description of surfactant-enhanced waterflooding for heavy oil recovery, *J. Petro. Sci. Eng.* 92 (2012) 89–101.
- [70] X. Zhou, M. Han, A. B. Fuseni, A. A. Yousef, Adsorption of an Amphoteric Surfactant onto Permeable Carbonate Rocks. SPE Improved Oil Recovery Symposium, 2012.
- [71] W. Karnanda, M.S. Benzagouta, A. AlQuraishi, M.M. Amro, Effect of temperature, pressure, salinity, and surfactant concentration on IFT for surfactant flooding optimization, *Arab. J. Geosci.* 6 (2013).
- [72] G. Hirasaki, C.A. Miller, M. Puerto, Recent Adv.Surf. EOR (2011).
- [73] A.K. Manshad, M. Rezaei, S. Moradi, I. Nowrouzi, A.H. Mohammadi, Wettability alteration and interfacial tension (IFT) reduction in enhanced oil recovery (EOR) process by ionic liquid flooding, *J. Mol. Liq.* 248 (2017) 153–162.
- [74] S.G. Udeagbara, Effect of Temperature and Impurities on Surface Tension of Crude Oil (reprint), Universal Publishers, 2010.
- [75] A. Bera, K. Ojha, T. Kumar, A. Mandal, Water solubilization capacity, interfacial compositions and thermodynamic parameters of anionic and cationic microemulsions, *Colloids Surfaces A Physicochem. Eng. Aspects* 404 (2012) 70–77.
- [76] M.A. Ahmadi, S.R. Shadizadeh, Adsorption of novel nonionic surfactant and particles mixture in carbonates: enhanced oil recovery implication, *Energy Fuels* 26 (2012) 4655–4663.
- [77] M.A. Ahmadi, S.R. Shadizadeh, Experimental investigation of adsorption of a new nonionic surfactant on carbonate minerals, *Fuel* 104 (2013) 462–467.
- [78] S. Paria, K.C. Khilar, A review on experimental studies of surfactant adsorption at the hydrophilic solid-water interface, *Adv. Colloid Interface Sci.* 110 (2004) 75–95.
- [79] R. Zhang, P. Somasundaran, Advances in adsorption of surfactant and their mixtures at solid/solution interfaces, *Adv. Colloid Interface Sci.* 123 (2006) 213–229.
- [80] E. Ayranci, O. Duman, Removal of anionic surfactants from aqueous solutions by adsorption onto high area activated carbon cloth studied by in situ UV spectroscopy, *J. Hazard. Mater.* 148 (2007) 75–82.
- [81] M.A. Ahmadi, S.R. Shadizadeh, Induced effect of adding nano silica on adsorption of a natural surfactant onto sandstone rock: experimental and theoretical study, *J. Petro. Sci. Eng.* 112 (2013) 239–247.
- [82] M.A. Ahmadi, S.R. Shadizadeh, Nano-surfactant flooding in carbonate reservoirs: A mechanistic study, *Eur. Phys. J. Plus* 132 (2017).

- [83] T. Austad, I. Fjelde, K. Veggeland, Adsorption VI. Non-equilibrium adsorption of ethoxylated sulfonate onto reservoir cores in the presence of Xanthan, *J. Petrol. Sci. Eng.* 12 (1994) 1–8.
- [84] N. Kothari, B. Raina, K. Chandak, V. Iyer, H. Mahajan, Application of ferrofluid for enhanced surfactant flooding in EOR, in: Proceedings of SPE EUROPEC/EAGE Annual Conference and Exhibition, 2010.
- [85] N.Y. Le, D.K. Pham, K.H. Le, P.T. Nguyen, Design and screening of synergistic blends of SiO<sub>2</sub> Nanoparticles and surfactants for enhanced oil recovery in high-temperature reservoirs, *Adv. Nat. Sci. Nanosci. Nanotechnol.* 2 (2011) 035013.
- [86] M. Zargartalebi, N. Barati, R. Kharrat, Influences of hydrophilic and hydrophobic silica Nanoparticles on anionic surfactant properties: Interfacial and adsorption behaviors, *J. Petro. Sci. Eng.* 119 (2014) 36–43.
- [87] S. Emadi, S.R. Shadizadeh, A.K. Manshad, A.M. Rahimi, A.H. Mohammadi, Effect of nano silica particles on Interfacial Tension (IFT) and mobility control of natural surfactant (Cedr Extraction) solution in enhanced oil recovery process by nano – surfactant flooding, *J. Molecular Liq.* 248 (2017) 163–167.
- [88] L.W. Lake, *Enhanced Oil Recovery*, Prentice-Hall, 1989.
- [89] D.W. Green, G.P. Willhite, *Enhanced Oil Recovery*, SPE (1998), 978-1-55563-077-5.
- [90] S. Thomas, *Enhanced oil recovery – an overview*, *Oil Gas Sci. Technol.* 63 (2008) 9–19.
- [91] V. Alvarado, E. Manrique, *Enhanced oil recovery: an update review*, *Energies* 3 (2010) 1529–1575.
- [92] M.F. Nazar, S.S. Shah, M.A. Khosa, Microemulsions in enhanced oil recovery: a review, *Pet. Sci. Technol.* 29 (2011) 1353–1365.
- [93] A.A. Olajire, Review of ASP EOR (alkaline surfactant polymer enhanced oil recovery) technology in the petroleum industry: prospects and challenges, *Energy* 77 (2014) 963–982.
- [94] P. Raffa, D.A.Z. Wever, F. Picchioni, A.A. Broekhuis, Polymeric surfactants: synthesis, properties, and links to applications, *Chem. Rev.* 115 (2005) 8504–8563.
- [95] J. Vargo, J. Turner, B. Vergnani, M. Pitts, K. Wyatt, H. Surkalo, D. Patterson, Alkaline-Surfactant-Polymer flooding of the Cambridge minnelusa field, in: SPE 55633 Presented at SPE Rocky Mountain Regional Meeting held in Gillette, Wyoming, 1999.
- [96] G.A. Pope, Overview of chemical EOR. Presentation: Casper EOR workshop, 2007.
- [97] S. Deng, R. Bai, J.P. Chen, G. Yu, Z. Jiang, F. Zhou, Effects of alkaline/surfactant/polymer on stability of oil droplets in produced water from ASP flooding, *Colloids Surf. A Physicochem. Eng. Asp.* 211 (2002) 275–284.
- [98] J.R. Hou, Z.C. Liu, S.F. Zhang, X.A. Yue, J.Z. Yang, The role of viscoelasticity of alkali/surfactant/polymer solutions in enhanced oil recovery, *J. Petrol. Sci. Eng.* 47 (2005) 219–235.
- [99] D. Wang, P. Han, Z. Shao, J. Chen, R.S. Serigh, Sweep improvement options for Daqing oil field, in: SPE 99441 presented at SPE/DOE symposium on improved oil recovery, Tulsa, Oklahoma, 2006.
- [100] M. A. Bataweel, H. A. Nasr-El-Din, Minimizing scale precipitation in carbonate cores caused by alkalis in ASP flooding in high salinity/high temperature applications, in: SPE 14151 Presented at the SPE International Symposium on Oilfield Chemistry held in The Woodlands, 2011, Texas, USA.
- [101] G. Jing, S. Tang, X. Li, T. Yu, Y. Gai, The scaling conditions for ASP flooding oilfield in the fourth Plant of Daqing oilfield, *J. Petrol. Exp. Prod. Tech.* 3 (2013) 175–178.
- [102] K.A. Elraies, An experimental study on ASP process using a new polymeric surfactant, *J. Petro. Exp. Prod. Tech.* 2 (2012) 223–227.
- [103] C. Maolei, D. Yunhong, Study of interfacial tension between a weakly alkaline three-component flooding system and crude oil, and evaluation of oil displacement efficiency, *Chem. Tech. Fuels Oils* 48 (2012) 33–38.
- [104] Z. Wu, X. Yue, T. Cheng, J. Yu, H. Yang, Effect of viscosity and interfacial tension of surfactant–polymer flooding on oil recovery in high-temperature and high-salinity reservoirs, *J. Petro. Exp. Prod. Tech.* 4 (2014) 9–16.
- [105] B. Yadali Jamaloei, R. Kharrat, K. Asghari, The influence of salinity on the viscous instability in viscous-modified low-interfacial tension flow during surfactant–polymer flooding in heavy oil reservoirs, *Fuel* 97 (2012) 174–185.
- [106] P. Raffan, A.A. Broekhuis, F. Picchioni, Polymeric surfactants for enhanced oil recovery: a review, *JPSE* 145 (2016) 723–733.
- [107] L. Piculell, B. Lindman, Association and segregation in aqueous polymer/polymer, polymer/surfactant, *Adv. Colloid Interf. Sci.* 4 (1992) 149–178.
- [108] B. Lindman, K. Thalberg, E.D. Goddard, K.P. Ananthapadmanabhan, Interactions of Surfactants with Polymers and Proteins, CRC Press, Boca Raton, 1993, pp. 203–276.
- [109] K. Taugbel, T.V. Ly, T. Austad, Chemical flooding of oil reservoirs 3. Dissociative surfactant–polymer interaction with a positive effect on oil recovery, *Colloids Surf. A Physicochem. Eng. Asp.* 10 (1995) 83–90.
- [110] M. Aoudia, M.N. Al-Shibli, L.H. Al-Kasimi, R. Al-Maamari, A. Al-Bemani, Novel surfactants for ultra-low interfacial tension in a wide range of surfactant concentration and temperature, *J. Surf. Deterg.* 9 (2006) 287–293.
- [111] H. Gong, X. Guiying, Y. Zhu, Y. Wang, W. Dan, M. Niu, L. Wang, H. Guo, H. Wang, Influencing factors on the properties of complex systems consisting of hydrolyzedpolyacrylamide/triton x-100/cetyl trimethyl ammonium bromide: viscosity and dynamic interfacial tension studies, *Energy Fuels* 23 (2009) 300–305.
- [112] Z. Cui, X. Du, X. Pei, J. Jiang, F. Wang, Synthesis of didodecylmethylcarboxyl betaine and its application in surfactant. polymer flooding, *J. Sur. Deter.* 15 (2012) 685–694.
- [113] H. Zhang, M. Dong, S. Zhao, Experimental study of the interaction between NaOH, surfactant, and polymer in reducing court heavy oil/brine interfacial tension, *Energy Fuels* 26 (2012) 3644–3650.
- [114] S. Ferdous, M.A. Ioannidis, D.E. Henneke, Effects of temperature, pH, and ionic strength on the adsorption of Nanoparticles at liquid interfaces, *J. NPs. Res.* 14 (2012) 850–855.
- [115] Y. Cao, R. Zhao, L. Zhang, Z. Xu, Z. Jin, L. Luo, L. Zhang, S. Zhao, Effect of electrolyte and temperature on interfacial tensions of alkylbenzene sulfonate solutions, *Energy Fuels* 26 (2012) 2175–2181.
- [116] G. Cheraghian, An experimental study of surfactant polymer for enhanced heavy oil recovery using a glass micromodel by adding nanoclay, *JPST* 33 (2015) 1410–1417.
- [117] G. Cheraghian, L. Hendraningrat, A review on applications of nanotechnology in the enhanced oil recovery part A: effects of Nanoparticles on interfacial tension, *Int. Nano Lett.* (2016).
- [118] T. Sharma, G.S. Kumar, J.S. Sangwai, Comparative effectiveness of production performance of Pickering emulsion stabilized by nanoparticle–surfactant–polymerover surfactant–polymer (SP) flooding for enhanced oil recoveryfor Brownfield reservoir, *J. Petro. Sci. & Eng.* 129 (2015) 221–232.
- [119] M.H. Sedaghat, H. Mohammadi, R. Razmi, Application of SiO<sub>2</sub> and TiO<sub>2</sub> nanoparticles to enhance the efficiency of polymer-surfactant floods, *Energy Sourc. Part A Recov. Util. Environ. Effects* 38 (2015) 22–28.
- [120] T. Sharma, J.S. Sangwai, Silica Nanofluids in polyacrylamide with and without surfactant: Viscosity, surface tension, and interfacial tension with liquid paraffin, *J. Petro. Sci. Eng.* 152 (2017) 575–585.
- [121] G. Cheraghian, Evaluation of clay and fumed silica nanoparticles on adsorption of surfactant polymer during enhanced oil recovery, *J. Japan Petrol. Inst.* 60 (2017) 85–94.
- [122] G.G. Bernard, Effect of floodwater salinity on recovery of oil from cores containing clays, *SPE* (1967), 1725–MS.
- [123] J.A. Ali, K. Stephen, A semi-analytical method for history matching and improving geological models of layered reservoirs: CGM analytical method, *J. Chem. Petro. Eng.* 52 (1) (2018) 69–88.
- [124] G.-Q. Tang, N.R. Morrow, Salinity, temperature, oil composition, and oil recovery by waterflooding, *SPE Res. Eng.* (1997) 269–276.
- [125] N.R. Morrow, G.-Q. Tang, M. Valat, X. Xie, Prospects of improved oil recovery related to wettability and brine composition, *J. Petrol. Sci. Eng.* 20 (1998) 267–276.
- [126] G.-Q. Tang, N.R. Morrow, Influence of brine composition and fines migration on crude oil/brine/rock interactions and oil recovery, *J. Petrol. Sci. Eng.* 24 (1999) 99–111.
- [127] G.-Q. Tang, N.R. Morrow, Oil recovery by waterflooding and imbibition – invading brine cation valency and salinity, *Soc. Core Anal. SCA* 11 (1999).
- [128] K.J. Webb, C.J.J. Black, H. Al-Ajeel, Low salinity oil recovery - log-inject-log, *SPE* 81460 (2003).
- [129] S. Patil, A. Y. Dandekar, S. L. Patil, S. Khataniar, Low salinity brine injection for EOR on Alaska North Slope (ANS), *IPTC12004*, 2008.
- [130] K. Webb, A. Lager, C. Black, Comparison of high/low salinity water/oil relative permeability, *Int. Sym. Soc. Core Analysis SCA* 39 (2008).
- [131] S. Boussour, M. Cissokho, P. Cordier, H. Bertin, G. Hamon, Oil recovery by low salinity brine injection: laboratory results on outcrop and reservoir cores, *SPE* 124277 (2009).
- [132] B.S. Mahmood, J.A. Ali, S.B. Nazhat, D. Devlin, A sensitivity study on low salinity waterflooding, *Modern Environ. Sci. Eng.* 04 (03) (2017) 231–236.
- [133] M. Kumar, A. Fogden, N.R. Morrow, J.S. Buckley, Mechanisms of improved oil recovery from sandstone by low salinity flooding, *Int. Sym. Soc. Core Anal. SCA* 25 (2010).
- [134] P. Gamage, G.D. Thyne, Systematic Investigation of the Effect of Temperature during Aging and Low-Salinity Flooding of Sandstones, in: 16th European Symposium on Improved Oil Recovery, Cambridge, UK, 2011.
- [135] I.R. Collins, Holistic benefits of low salinity waterflooding, in: 16th European Symposium on Improved Oil Recovery, Cambridge, UK, 2011.
- [136] P. Gamage, G. D. Thyne, Comparison of Oil Recovery by Low Salinity Waterflooding in Secondary and Tertiary Recovery Models, *SPE Annual Technical Conference and Exhibition, Colorado, USA*, 2011.
- [137] M. R. Haroun, S. Alhassan, A. A. Ansari, N. A. Al Kindy, N. Abu Sayed, B. A. Abdul Kareem, H. K. Sarma, Smart Nano-EOR Process for Abu Dhabi Carbonate Reservoirs, Abu Dhabi International Petroleum Conference and Exhibition, 2012.
- [138] Y. Assef, D. Arab, P. Pourafshary, Application of nanofluid to control fines migration to improve the performance of low salinity waterflooding and alkaline flooding, *J. Petro. Sci. Eng.* 124 (2014) 331–340.
- [139] T. Huang, J. Han, G. Agrawal, P. A. Sookprasong, Coupling Nanoparticles with Waterflooding to Increase Water Sweep Efficiency for High Fines-Containing Reservoir – Lab and Reservoir Simulation Results, *SPE Annual Technical Conference and Exhibition*, 2015.
- [140] B. Yuan, R. G. Moghanloo, D. Zheng, Enhanced Oil Recovery by Combined Nanofluid and Low Salinity Waterflooding in Multi-Layer Heterogeneous Reservoirs, *SPE Annual Technical Conference and Exhibition*, 2016a.
- [141] B. Yuan, R. G. Moghanloo, D. Zheng, Analytical Modeling of Nanofluid Injection to Improve the Performance of Low Salinity Waterflooding, *Offshore Technology Conference Asia*, 2016b.

- [142] B. Yuan, R.G. Moghanloo, K. Wang, Injectivity improvement by nanofluid preflush during low salinity waterflooding, *Int. Petro. Tech. Con.* (2016).
- [143] M. Zallaghi, R. Kharrat, A. Hashemi, Improving the microscopic sweep efficiency of waterflooding using silica nanoparticles, *J. Petro. Exp. Prod. Tech.* (2017), <https://doi.org/10.1007/s13202-017-0347-x>.
- [144] H.C. Lau, M. Yu, Q.P. Nguyen, Nanotechnology for oilfield applications: challenges and impact, Abu Dhabi Int. Petro. Exhibit. Con. (2016).
- [145] X. Sun, Y. Zhang, G. Chen, Z. Gai, Application of nanoparticles in enhanced oil recovery: a critical review of recent progress, *Energies* 10 (2017) 345.
- [146] A. Chengara, A.D. Nikolov, D.T. Wasan, A. Trokhymchuk, D. Henderson, Spreading of Nanofluids driven by the structural disjoining pressure gradient, *Adv. Colloid Interface Sci.* 280 (2004) 192–201.
- [147] M. Paul, M. Holcomb, D. Lee, E. Daniel, Application of nanofluid technology to improve recovery in oil and gas wells, SPE Int. Oilfield Nanotechnology Conference, Noordwijk, the Netherlands, 2012.
- [148] R. Aveyard, B.P. Binks, J.H. Clint, Emulsions stabilized solely by colloidal particles, *Adv. Colloid Interface Sci.* 100 (2003) 503–546.
- [149] B. Ju, T. Fan, Z. Li, Improving water injectivity and enhancing oil recovery by wettability control using nanopowders, *J. Petro. Sci. Eng.* 86 (2012) 206–216.
- [150] A. Karimi, Z. Fakhroueian, A. Bahramian, N. Pour Khiabani, J.B. Darabad, R. Azin, S. Arya, Wettability alteration in carbonates using zirconium oxide nanofluids: EOR implications, *Energy Fuels* 26 (2012) 1028–1036.
- [151] M.S. Moslan, W.R.W. Sulaiman, A.R. Ismail, M.Z. Jaafar, Applications of aluminium oxide and zirconium oxide nanoparticles in altering dolomite rock wettability using different dispersing medium, *Chemical Eng. Trans.* 65 (2017) 1339–1344.
- [152] J. Giraldo, P. Benjumea, S. Lopera, F.B. Cortés, M.A. Ruiz, Wettability alteration of sandstone cores by alumina-based nanofluids, *Energy Fuels* 27 (2013) 3659–3665.
- [153] L. Hendraningrat, O. Torsæter, Metal oxide-based Nanoparticles: revealing their potential to enhance oil recovery in different wettability systems, *Appl. Nanosci.* 5 (2014) 181–199.
- [154] A. Esfandiyari Bayat, R. Junin, A. Samsuri, A. Piroozian, M. Hokmabadi, Impact of metal oxide nanoparticles on enhanced oil recovery from limestone media at several temperatures, *Energy Fuels* 28 (2014) 6255–6266.
- [155] R. Nazari Moghaddam, A. Bahramian, Z. Fakhroueian, A. Karimi, S. Arya, Comparative study of using nanoparticles for enhanced oil recovery: wettability alteration of carbonate rocks, *Energy Fuels* 29 (2015) 2111–2119.
- [156] A. Maghzi, S. Mohammadi, M.H. Ghazanfari, R. Kharrat, M. Masihi, Monitoring wettability alteration by silica Nanoparticles during waterflooding to heavy oils in five-spot systems: a pore-level investigation, *Experiment. Thermal Fluid Sci.* 40 (2012) 168–176.
- [157] H. Yousefvand, A. Jafari, Enhanced oil recovery using polymer/nanosilica, *Procedia Mater. Sci.* 11 (2015) 565–570.
- [158] L. Hendraningrat, O. Torsæter, A study of water chemistry extends the benefits of using silica-based Nanoparticles on enhanced oil recovery, *Appl. Nanosci.* 6 (2015) 83–95.
- [159] S. Azarshin, J. Moghadasi, Z. Aboosadi, Surface functionalization of silica Nanoparticles to improve the performance of waterflooding in oil wet reservoirs, *Energy Exploration Exploitation* 35 (2017) 685–697.
- [160] S. Li, L. Hendraningrat, O. Torsæter, Improved oil recovery by hydrophilic silica nanoparticles suspension: 2-phase flow experimental studies, *Int. Petro. Tech. Con.* (2013), <https://doi.org/10.2523/16707-MS>.
- [161] S.G. Dahle, The effect of nanoparticles on oil/water interfacial tension. Project thesis, NTNU (2013).
- [162] L. Hendraningrat, S. Li, O. Torsæter, A coreflood investigation of nanofluid enhanced oil recovery, *J. Petrol. Sci. Eng.* 111 (2013) 128–138.
- [163] A. Roustaei, J. Moghadasi, H. Bagherzadeh, A. Shahrabadi, An Experimental Investigation of Polysilicon Nanoparticles' Recovery Efficiencies through Changes in Interfacial Tension and Wettability Alteration, SPE Int. Oilfield Nanotechnology Conference and Exhibition, 2012, Noordwijk, the Netherlands.
- [164] E. Joonaki, S. Ghanaatian, The application of nanofluids for enhanced oil recovery: effects on interfacial tension and coreflooding process, *Petro. Sci. Tech.* 32 (2014) 2599–2607.
- [165] T. Saigal, H. Dong, K. Matyjaszewski, R.D. Tilton, Pickering emulsions stabilized by nanoparticles with thermally responsive grafted polymer brushes, *Langmuir* 26 (2010) 15200–15209.
- [166] P. Esmailzadeh, N. Hosseinpour, A. Bahramian, Z. Fakhroueian, S. Arya, Effect of ZrO<sub>2</sub> Nanoparticles on the interfacial behavior of surfactant solutions at air–water and n-heptane–water interfaces, *Fluid Phase Equil.* 361 (2014) 289–295.
- [167] H.M. Zaid, N.R. Ahmad Latiff, N. Yahya, The effect of zinc oxide and aluminum oxide nanoparticles on interfacial tension and viscosity of nanofluids for enhanced oil recovery, *Adv. Res.* 1024 (2014) 56–59.
- [168] A. Ahmed, I.M. Saaid, A.H. Tunio, R.M. Pilus, L.M. Mumtaz, I. Ahmad, Investigation of dispersion stability and IFT reduction using surface modified nanoparticle: enhanced oil recovery, *J. App. Environ. Bio. Sci.* 7 (4s) (2017) 56–62.
- [169] A. Roustaei, S. Saffarzadeh, M. Mohammadi, An evaluation of modified silica Nanoparticles' efficiency in enhancing oil recovery of light and intermediate oil reservoirs, *Egypt. J. Petro.* 22 (2013) 427–433.
- [170] R.D. Shah, Application of Nanoparticle Saturated Injectant Gases for EOR of Heavy Oils, SPE Annual Technical Conference and Exhibition, 2009. doi:10.2118/129539-stu.
- [171] N. Nassar, M.E. Al-Jabari, M. Husein, Removal of asphaltenes from heavy oil by nickel nano and micro particle adsorbents, in: *Proceeding (615) Nanotechnology and Applications*, Crete, Greece, 2008.
- [172] A.N. Naje, A.S. Norry, A.M. Suhail, Preparation and characterization of SnO<sub>2</sub> nanoparticles, *Int. J. Innov. Res. Sci. Eng. Technol.* 12 (2013) 7068–7072.
- [173] G.E. Patil, D.D. Kajale, V.B. Gaikwad, G.H. Jain, Preparation and characterization of SnO<sub>2</sub> Nanoparticles by hydrothermal route, *Springer Int. Nano Lett.* 2 (2012).
- [174] H. Ehtesabi, M.M. Ahadian, V. Taghikhani, M.H. Ghazanfari, Enhanced heavy oil recovery in sandstone cores using TiO<sub>2</sub> nanofluids, *Energy Fuels* 28 (2013) 423–430.
- [175] N.B. Yahya, M. Kashif, N. Nasir, M.N. Akhtar, N.M. Yusof, Cobalt ferrite nanoparticles: an innovative approach for enhanced oil recovery application, *J. Nano Res.* 17 (2012) 115–126.
- [176] K. Chandran, Multiwall Carbon Nanotubes (MWNT) Fluid in EOR Using Core Flooding Method under the Presence of Electromagnetic Waves, *Petronas University of Technology*, 2013.
- [177] A. Maghzi, R. Kharrat, A. Mohebbi, M.H. Ghazanfari, The impact of silica Nanoparticles on the performance of polymer solution in presence of salts in polymer flooding for heavy oil recovery, *Fuel* 123 (2014) 123–132.
- [178] A. Roustaei, H. Bagherzadeh, Experimental investigation of SiO<sub>2</sub> nanoparticles on enhanced oil recovery of carbonate reservoirs, *J. Petro. Exp. Prod. Technol.* 5 (2014) 27–33.
- [179] T. Zhang, D. Davidson, S.L. Bryant, C. Huh, Nanoparticle-stabilized emulsions for applications in enhanced oil recovery, SPE Improved Oil Recovery Symposium, Tulsa, Oklahoma, USA, 2012.
- [180] P.-T. Nguyen, B.-P.H. Do, D.-K. Pham, Q.-T. Nguyen, D.-Q.P. Dao, H.A. Nguyen, Evaluation on the EOR potential capacity of the synthesized composite silica-core/polymer-shell Nanoparticles blended with surfactant systems for the HPHT offshore reservoir conditions, SPE Int. Oilfield Nanotechnol. Con., The Netherlands, 2012.
- [181] K. Jian-Shu, Y. Cai-li, Zh. Fa-Ai, Effect of silane modified SiO<sub>2</sub> particles on poly (MMA-HEMA) soap-free emulsion polymerization, *Iran. Polymer J.* (2009) 927–935.
- [182] S. Kapusta, L. Balzano, P.M. Te Riele, Nanotechnology applications in oil and gas exploration and production, in: *International Petroleum Technology International Petroleum Technology Conference*, 2012.
- [183] T. Skauge, K. Spildo, A. Skauge, Nano-sized particles for EOR, in: *SPE Improved Oil Recovery*, Society of Petroleum Engineers, Oklahoma, USA, 2010.
- [184] H.L. Chang, X. Sui, L. Xiao, Z. Guo, Y. Yao, Y. Yiao, et al., Successful field pilot of in-depth colloidal dispersion gel (CDG) technology in daqing oilfield, *SPE Reserv. Eval. Eng.* (2006).
- [185] J.P. Rao, K.E. Geckeler, Polymer Nanoparticles: preparation techniques and size-control parameters, *Prog. Polym. Sci.* 36 (7) (2011) 887–913.
- [186] H. Shamsijazeyi, C.A. Miller, M.S. Wong, J.M. Tour, R. Verduzco, Polymer-coated Nanoparticles for enhanced oil recovery, *J. App. Poly. Sci.* 131 (15) (2014), <https://doi.org/10.1002/app.4057>.
- [187] L. Fedele, L. Colla, S. Bobbo, Viscosity and thermal conductivity measurements of water-based nanofluids containing titanium oxide Nanoparticles, *Int. J. Refrigeration* 35 (2012) 1359–1366.
- [188] G. Cheraghian, S.S. Khalili Nezhad, M. Kamari, M. Hemmati, M. Masihi, S. Bazgir, Effect of nanoclay on improved rheology properties of polyacrylamide solutions used in enhanced oil recovery, *J. Petro. Exp. Prod. Technol.* 5 (2) (2014) 189–196.

## Appendix 2

*Potential application of low-salinity polymeric-nanofluid in carbonate oil reservoirs: IFT reduction, wettability alteration, rheology and emulsification characteristics*

**Jagar A. Ali**, Kamal Kolo, Abbas Khaksar Manshad, Karl D. Stephen

Journal of Molecular Liquids 284 (2019) 735–747



Contents lists available at ScienceDirect

Journal of Molecular Liquids

journal homepage: [www.elsevier.com/locate/molliq](http://www.elsevier.com/locate/molliq)

## Potential application of low-salinity polymeric-nanofluid in carbonate oil reservoirs: IFT reduction, wettability alteration, rheology and emulsification characteristics

Jagar A. Ali <sup>a,b,\*</sup>, Kamal Kolo <sup>c</sup>, Abbas Khaksar Manshad <sup>a,d</sup>, Karl D. Stephen <sup>e</sup>

<sup>a</sup> Department of Petroleum Engineering, Faculty of Engineering, Soran University, Kurdistan Region, Iraq

<sup>b</sup> Department of Petroleum Engineering, College of Engineering, Knowledge University, Kurdistan Region, Iraq

<sup>c</sup> Scientific Research Centre, Soran University, Kurdistan Region, Iraq

<sup>d</sup> Department of Petroleum Engineering, Abadan Faculty of Petroleum Engineering, Petroleum University of Technology (PUT), Abadan, Iran

<sup>e</sup> Institute of Petroleum Engineering, Heriot-Watt University, Riccarton, Edinburgh, EH14 4AS, United Kingdom

### ARTICLE INFO

#### Article history:

Received 20 November 2018

Received in revised form 4 March 2019

Accepted 10 April 2019

Available online 11 April 2019

#### Keywords:

Green synthesis

Polymer-coated nanocomposite

Wettability alteration

Low-salinity polymeric-nanofluid

Chemical EOR

### ABSTRACT

Polymer and low-salinity water flooding have been shown, repeatedly, to be effective methods for chemical Enhanced Oil Recovery (cEOR). The benefits are obtained by increasing the viscosity of the injected fluid, minimizing the interfacial tension (IFT) of the crude oil/aqueous phase, and by wettability alteration. Similarly, nanofluids (fluids injected with nanoparticles) have also been demonstrated to induce the same processes. We have analyzed the EOR response of green nanofluids when formulated with a typical natural polymer mixed with low salinity water. For this purpose, a polymer coated ZnO/SiO<sub>2</sub> nanocomposite (NC) has been produced from the pomegranate seed extract using a simple, economical and, importantly, green method. The characterization of the synthesized NC has been investigated using the scanning electron microscopy (SEM), electron dispersive spectroscopy (EDS), and X-ray diffraction (XRD). The polymeric nanofluids were then tested in various experimental studies related to the stability of injected fluids, IFT behavior, wettability alteration, oil/nanofluid emulsification, and EOR flooding dependent on the NC concentration, time and salinity. The low salinity-polymeric nanofluid (LPN), with 2000 ppm NC concentration, enabled higher oil recovery by about 19.28% OOIP due to a significant reduction in IFT, higher viscosity, better emulsion stability, and wettability alteration towards a stronger water-wet system from 137° to 34° contact angle.

© 2019 Elsevier B.V. All rights reserved.

### 1. Introduction

Crude oil and natural gas are non-renewable energy fuels that are in highest demand. On the basis of current trends of world, energy needs along with the obvious depletion of oilfield production, the enhancement of oil recovery from existing resources is necessary considering that only about one-third to two fifths of the original oil in place (OOIP) can be produced using primary and secondary oil recovery strategies [1]. Additionally, the target of Enhanced Oil Recovery (EOR) is generally exceed 40% of OOIP for light oil while the target is much higher for heavy oil reservoirs as shown in Fig. 1 [2,3]. During waterflooding, as a secondary oil recovery technique, the crude oil is displaced towards the production well without leaving any chemical or physical impact on the properties of the rock and fluids. The sweep efficiency and recovery factor of this process is relatively low due to high mobility ratio

leading to viscous fingering [4]. To eliminate this problem, the polymer flooding as an effective chemical EOR method was introduced several decades ago [2]. Adding polymer into the injected water regulates the rheological properties of the solution to boost oil recovery by providing better (reduced) mobility ratio, improved sweep efficiency, stable oil/water emulsion, and minimized water channeling [5]. The performance of polymer flooding is strongly influenced by the reservoir condition, crude oil properties, temperature and salinity [6]. On the other hand, low salinity water flooding (LSWF) was introduced to modify some important reservoir characteristics including the wettability, IFT, capillary pressure, relative permeability and saturation of residual oil [7–10]. Fines migration has been identified as one process that occurs during LSWF [11]. Although a small amount of residual oil might be carried by fines due to separating the oil-coated particles from rock surfaces [12], the permeability is thought to be reduced by partial blocking of the pore space during the fines migration [13,14]. Moreover, there are some other common cEOR techniques, such as surfactant flooding, surfactant-polymer flooding, and alkali-surfactant-polymer flooding which combine various chemicals and behaviors. However, the high

\* Corresponding author at: Department of Petroleum Engineering, Faculty of Engineering, Soran University, Kurdistan Region, Iraq.

E-mail addresses: [jagar.pet@gmail.com](mailto:jagar.pet@gmail.com), [jagar.ali@soran.edu.iq](mailto:jagar.ali@soran.edu.iq) (J.A. Ali).

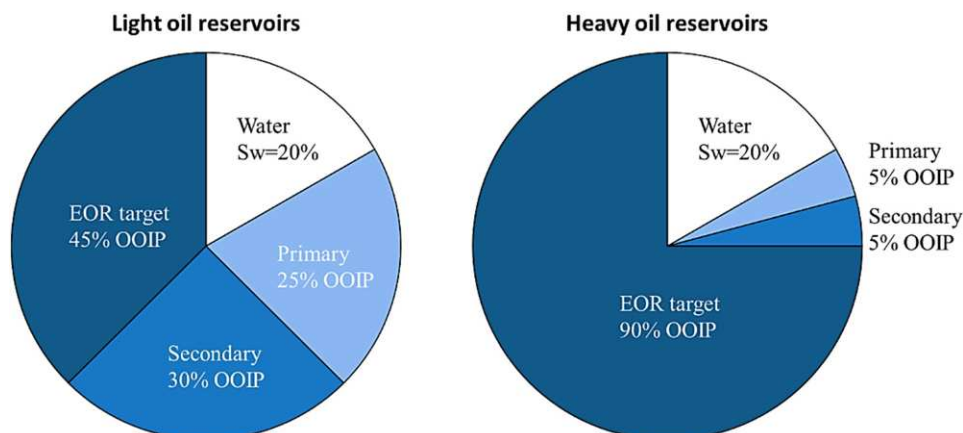


Fig. 1. Primary, secondary and EOR oil recovery targets for light and heavy oils when water saturation is about 20% PV [2].

cost of these chemicals, the possibility that they may damage the reservoir, and the likelihood that they will be ineffective due to adsorption and other losses mean that they are not always suitable for EOR [15,16]. Therefore, a new EOR technology needs to be developed that has low costs, high efficiency, and is eco-friendly. Based on this principle, nanofluids (water with nanoparticles and other chemicals in solution) have been developed and show promise due to their EOR response. They are able to invoke processes such as wettability alteration [17,18] possibly through induction of the structural disjoining pressure [23,24], IFT reduction [19,20], viscosity improvement [21], and control the migration of fines [22].

Nanofluids are usually developed by dispersing the nanoparticles (NPs) into various aqueous phases such as water (fresh, low salinity or sea water), polymeric solutions, glycols, or alcohols. They have received high levels of attention in the oil and gas industry, particularly for EOR applications as shown in Table 1. As a result of dispersing the nanoparticles within the low salinity water, most of the problems related to rock/fluid interactions can be eliminated, by improving attractive forces between fine particles and grain surfaces [22] and preventing formation damage [25]. Kiani et al. [26] obtained 10% OOIP additional oil recovery from injecting low salinity  $\gamma$ -alumina nanofluid into the sandstone core compared to low salinity waterflooding. Simultaneously, adding nanoparticles into polymer solution for EOR purposes

was recently investigated and suggested by some researchers [27–34]. In their attempt to stabilize oil-in-water emulsions during polymer flooding, Saleh et al. [35] were successful in improving the stability of oil/water emulsion using 0.04–0.07 wt% silica nanoparticles coated with a polyelectrolyte. More recently, Alvarez et al. [36] studied the impact of the polymer coated nanoparticles on IFT reduction, and were able to achieve the maximum reduction in IFT and high stability of oil/water emulsion at low grafting density of polymer. The adsorption of water-soluble polymers onto the surface of the carbonate and sandstone rocks was also minimized by adding the nanoparticles into polymer solutions [37–39]. Additionally, the effect of nanoparticles on recovery efficiency of the polymer flooding can be improved due to increasing the viscosity of the solution, reducing the adsorption of the polymer, and improving the breakthrough time; for instance, Cheraghian [38] and Khalilnezhad et al. [39] enabled to produce 3.9–10% OOIP additional oil by injecting  $\text{TiO}_2$  and  $\text{SiO}_2$  polymeric nanofluids compared to conventional polymer flooding.

The ultimate goal of this study is to produce  $\text{ZnO/SiO}_2$ /xanthan nanocomposite from pomegranate seed extract, as an efficient nano-adsorbent substrate, using one-pot biosynthesis method. The surface of the nanoparticles has been modified using a polymer coating technique in order to improve their stability and develop a strong polymeric link between them, as a continued chain. Thus, the low salinity-

Table 1

A summary of previous works on effects of various nanofluid categories on interfacial tension (IFT), contact angle (CA) and oil recovery.

| Category                 | Dispersion phase        | NP                      | NP conc. [wt%] | Rock type | IFT [mN/m] |         | CA [°] |         | EOR recovery [%OOIP] | References                    |
|--------------------------|-------------------------|-------------------------|----------------|-----------|------------|---------|--------|---------|----------------------|-------------------------------|
|                          |                         |                         |                |           | Clean      | With NP | Clean  | With NP |                      |                               |
| Polymer-coated NPs       | Prop-2-enamide          | $\text{SiO}_2$          | 0.6–1.2        | Sandstone | 28         | 7       | 87     | 28      | 21                   | Ju & Fan [40]                 |
|                          | Chitosan                | $\text{Fe}_2\text{O}_4$ | 0.01–0.03      | Sandstone | 30         | 17.3    | 127    | 92      | 10.8                 | Rezvani et al. [33]           |
|                          | Poly2(DMAEA)            | $\text{SiO}_2$          | 0.1            | Sandstone | 27         | 14      | 85     | 62.2    | 9.9                  | Qi et al. [32]                |
|                          | 2-Poly(MPC)             | $\text{SiO}_2$          | 0.1–0.2        | Sandstone | 47         | 35      | –      | –       | 5.2                  | Choi et al. [31]              |
| Polymer-dispersed NPs    | Polyethyl glycol        | $\text{CuO}$            | 0.1–0.2        | Glass     | 47.9       | 1.5     | 9      | 1.8     | 15                   | Lim & Wasan [29]              |
|                          | Ethylene glycol         | $\text{SiO}_2$          | 0.277          | Glass     | 43         | 8.8     | 66     | 25      | 17                   | Zhang et al. [24]             |
|                          | PAM                     | $\text{SiO}_2$          | 1–2            | Sandstone | 27         | 10.2    | –      | –       | 24.7                 | Sharma et al. [1]             |
|                          | Xanthan gum             | $\text{SiO}_2$          | 0.1–0.5        | Sandstone | 17.8       | 6.4     | 86     | 20      | 7.81                 | Saha et al. [5]               |
| Surfactant-dispersed NPs | SDS                     | $\text{ZnO}$            | 0.05           | Carbonate | 2.8        | 3.5     | 22.5   | 72.2    | 0                    | Zaid et al. [41]              |
|                          | SDS                     | $\text{ZnO}$            | 0.05–0.5       | Calcite   | 27.4       | 18.6    | –      | 11.8    | 11                   | Soleimani [42]                |
| Alcohol-dispersed NPs    | Ethanol                 | $\text{SiO}_2$          | 0.4            | Sandstone | 26.3       | 1.7     | 55     | 78      | 23                   | Roustaei et al. [43]          |
|                          | Propanol                | $\text{Al}_2\text{O}_3$ | 0.05–0.3       | Sandstone | 5.7        | 2.3     | 56.6   | 76.8    | 19.4                 | Joonaki & Ghanaatian [44]     |
|                          |                         | $\text{SiO}_2$          |                |           | 5          | 1.5     | 56.6   | 79.1    | 21.6                 |                               |
|                          | $\text{Fe}_2\text{O}_3$ |                         |                | 6.3       | 2.7        | 56.6    | 73.9   | 17.1    |                      |                               |
| Water-dispersed NPs      | Brine                   | $\text{SiO}_2$          | 0.05           | Sandstone | 19.2       | 12.8    | 33     | 26      | 17                   | Hendraningrat & Torsæter [45] |
|                          |                         | $\text{Al}_2\text{O}_3$ | 0.05           | Limestone | 18         | 13.4    | 55.8   | 65.7    | 9.9                  | Bayat et al. [46]             |
|                          | DIW                     | $\text{TiO}_2$          |                |           | 17.5       | 12.5    | 55.3   | 61.9    | 6.6                  |                               |
|                          |                         | $\text{SiO}_2$          |                |           | 16.7       | 11      | 54.8   | 57.7    | 2.9                  |                               |
|                          | Brine                   | $\text{SiO}_2$          | 0.1            | Sandstone | 17.5       | 7       | 12     | 40      | 28                   | Li et al. [47]                |
|                          | Low salinity            | $\text{SiO}_2$          | 0.1            | Sandstone | –          | –       | –      | –       | 7                    | Abhishek et al. [25]          |

polymeric nanofluid that we derived from dispersing the synthesized polymer coated nanocomposite within the diluted seawater were used in EOR applications, which provided a stable emulsion within the crude oil, as schematically illustrated in Fig. 2. Additionally, the effect of NC concentration and salinity on contact angle and oil recovery was investigated.

## 2. Experimental setup

### 2.1. Materials

To prepare nanofluids, seawater was collected from the Persian Gulf and found to contain various ionic concentrations and salt composition as shown in Table 2. The crude oil used for the contact angle, IFT, emulsification and flooding tests, was obtained from the Asmari reservoir (Rag-e-Sefid oilfield, Iran) with the density of 0.89 g/cm<sup>3</sup> (28° API) and viscosity 98.88 cP at 30 °C, which has been filtered using 5 μm mesh. A carbonate core sample (length 6.61 cm and diameter 3.81 cm) was collected from the Upper Qamchoqa Formation outcrop in Bekhma Area in the Kurdistan Region-Iraq (N 36°40'17.00": E044°15'04.4") for the displacement experiment. The porosity and gas permeability of the core sample were measured as 16.8% and 13.2 mD, respectively. Other chemical reagents including salts and solvents of high-purity (about 99.5 mol%) were purchased from Merck and Aldrich chemical companies. Xanthan gum with the purity >98 mol% in powder form was supplied by AGREMA, Germany.

### 2.2. Synthesis and characterization of xanthan coated ZnO/SiO<sub>2</sub> nanocomposite

The experimental steps of fabricating ZnO/SiO<sub>2</sub>/xanthan nanocomposite using pomegranate seed extract are shown in Fig. 3. Pomegranate seeds extract rich is rich in antioxidants, including anthocyanins, flavonoids, phenolic acids, and tannins. Which they are able to produce more uniform nanoparticle shapes and sizes as compared to other plant extracts due to having high biological activity [48,49]. In a 500 mL beaker, 2 g of ZnCl<sub>2</sub> and 5 g of sodium metasilicate (Na<sub>2</sub>SiO<sub>3</sub>) were mixed with 200 mL pomegranate seed extract at 80 °C and stirred at 850 rpm for 2 h until the formation of a light black precipitate was observed. The precipitate was then separated using filtration and heated up to 600 °C using a furnace in order to burn all the remaining plant particles. Then, it was washed with the hot distillate water many times to remove the impurities. The clean precipitate was then dried at room temperature and mixed with 10 g of xanthan powder using mortar and pestle, and

**Table 2**  
Compositional details of seawater used in this study.

| Ion         | Na <sup>+</sup> | Ca <sup>2+</sup> | Mg <sup>2+</sup> | K <sup>+</sup> | Cl <sup>-</sup> | SO <sub>4</sub> <sup>2-</sup> | HCO <sub>3</sub> <sup>-</sup> | T.H. | T.D.S. |
|-------------|-----------------|------------------|------------------|----------------|-----------------|-------------------------------|-------------------------------|------|--------|
| Conc. (ppm) | 7337            | 1920             | 936              | 92             | 11,502          | 6893                          | 106                           | 8700 | 33,194 |

under reflux for 2 h at 80 °C. Finally, the dried and cleaned nanocomposite was characterized to be used for EOR related tests. Current work proposes the mechanism of the electrostatic interaction between zinc oxide/silicon dioxide/xanthan gum as well as their emulsification interaction with the crude oil when dispersed within the low salinity water (Fig. 2). For confirming and identifying the purity, morphology and mineralogy of the synthesized nanocomposite, several analytical methods have been used, with the focus on X-ray diffraction (XRD), scanning electron microscope (SEM) and energy dispersive X-ray spectroscopy (EDS) in the current work.

### 2.3. Preparation of polymeric nanofluids

Polymeric nanofluids (PNs) have been designed using various concentrations of polymer coated ZnO/SiO<sub>2</sub> nanocomposite (500 ppm, 1000 ppm and 2000 ppm). Initially, polymeric nanofluid formulations were tried in seawater (which obviously has high salinity) as a base fluid (Table 3). According to Spildo et al. [50] and Abhishek et al. [25], the salting-out approach was used to lower the salinity of seawater by 10 and 20 times dilutions (1:10 and 1:20) to derive the low salinity-polymeric nanofluid (LPN) (Fig. 4). These nanofluids were prepared using the stirring (LABINCO L81 Stirrer) at 600 rpm for 6 h with keeping the operating temperature below 30 °C to avoid overheating of homogenizer.

### 2.4. Nanofluid characterization

To obtain nanofluids with high dispersion stability of nanocomposite (NC), ultrasonic waves emitted from a VIP 200HD ultrasonic mixer, manufactured by Hielscher in Germany, to mix the fluid solutions for 2 h at 400 W. The dispersion stability of the synthesized NC within the nanofluids was investigated by visual observation, in which the produced nanofluids have been monitored through transparent vessels with time. Additionally, the density, viscosity, conductivity and pH of nanofluids have been measured at ambient temperature and pressure using PAAR density meter, Brookfield DV2T viscometer, Mettler Toledo S230, and WTW™ inoLab™ Cond 7310, respectively.

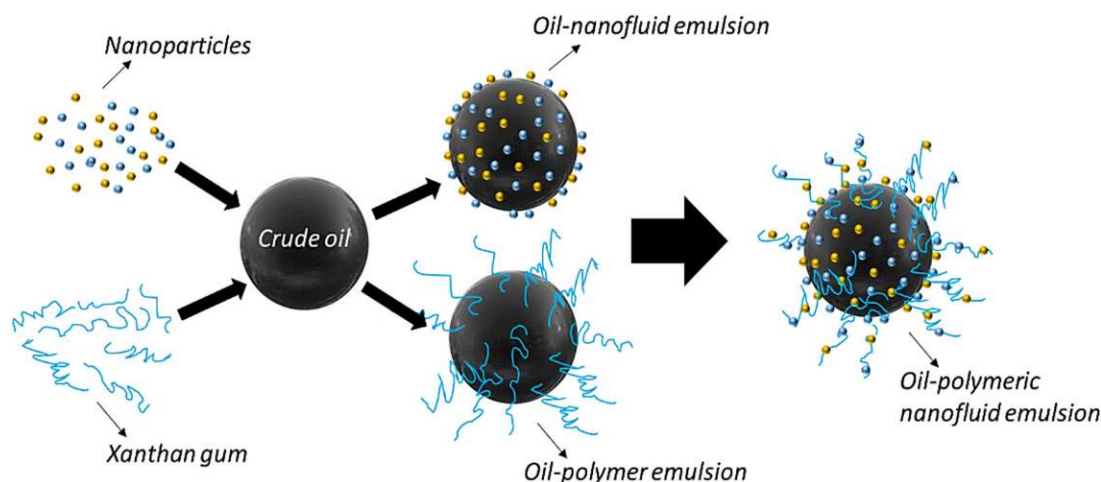


Fig. 2. Schematic diagram illustrates the trapped crude oil and low-salinity polymeric-nanofluid emulsion.

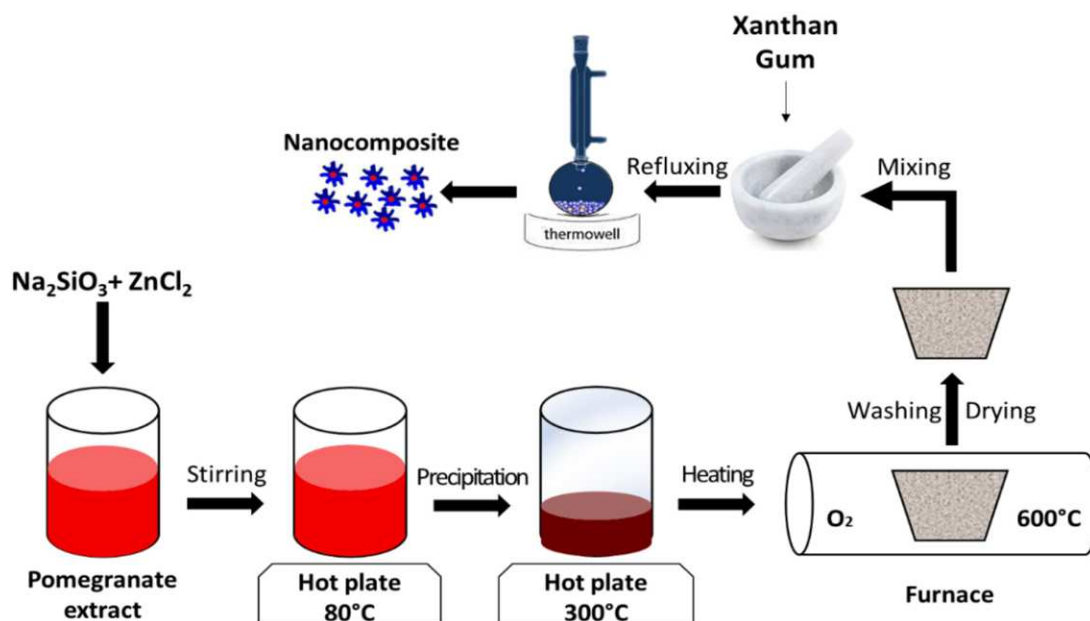


Fig. 3. Schematic diagram illustrates procedural steps of one-pot biosynthesis method used in work [70].

Furthermore, the IFT between oil-aqueous phases were measured with an interfacial tension apparatus (IFT-400) using a pendant drop method from estimating the dimensions of the suspended droplet of liquid. After receiving the image of the droplet from a camera, the software identified the value of IFT based on the formula:

$$\gamma = \frac{\Delta\rho \cdot g \cdot D}{H} \quad (1)$$

where  $\Delta\rho$  is the difference between the density of the drop and bulk fluids ( $\text{g}/\text{cm}^3$ ),  $g$  is the gravitational acceleration of the earth ( $\text{cm}/\text{s}^2$ ),  $D$  is the large diameter of the droplet (cm), and  $H$  is the droplet shape factor.

Initially, oil-seawater and oil-distilled water (DW) IFTs without the presence of nanocomposite have been measured. The same procedure was then applied to measure IFT values between oil-polymeric nanofluids (PN500, PN1000 and PN2000), and oil-low salinity-polymeric nanofluids (LPN500, LPN1000 and LPN 2000).

### 2.5. Contact angle

In this study, the contact angle measurements between crude oil and various polymeric-nanofluids on the surface of the carbonate pellets

**Table 3**  
Formulation of fluid solutions used in this study.

| Sample       | NC conc. [ppm] | Water salinity [dilution level] | Density [ $\text{g}/\text{cm}^3$ ] | Description                      |
|--------------|----------------|---------------------------------|------------------------------------|----------------------------------|
| Seawater     | 0              | High (no dilution)              | 1.03                               | Seawater (high salinity)         |
| PN500        | 500            |                                 | 1.0337                             | Polymeric nanofluid              |
| PN1000       | 1000           |                                 | 1.0342                             |                                  |
| PN2000       | 2000           |                                 | 1.0352                             |                                  |
| Low salinity | 0              | Low (1:20 seawater dilution)    | 1.008                              | Low salinity water               |
| LPN500       | 500            |                                 | 1.0112                             | Low salinity-polymeric nanofluid |
| LPN1000      | 1000           |                                 | 1.0114                             |                                  |
| LPN2000      | 2000           |                                 | 1.0117                             |                                  |

were taken using the sessile drop technique (Fig. 5). For this purpose, thin sections of about 2 mm were trimmed from the carbonate outcrop and polished to become entirely smooth. The prepared thin sections were then cleaned with toluene and distilled water to remove all possible surface impurities, and in accordance with Villard et al. [51] and Manshad et al. [52], they were aged 12 days in the crude oil at a temperature of 70 °C. In order to change the wettability of oil-wet rock slices under static condition, they were submerged in enclosed containers filled with nanofluid solutions (PN and LPN with various NC concentrations) for 3 days. The qualitative assessment of the wettability of the carbonate cores was conducted by estimating the contact angle of the crude oil droplets on the surface of the prepared thin sections at room temperature, before and after the treatment with nanofluids.

### 2.6. Oil displacement and emulsification

The carbonate rock plug used in oil displacement experiments was collected from the Upper Qamchoqa outcrop in Kurdistan Region-Iraq [55]. The plug was cleaned by a Soxhlet extraction using ethanol and toluene at a temperature between 60 and 80 °C for 24 h in order to remove all the presence water, oil and any other residues. The core sample was then dried by placing into an oven at 70 °C for 6 h. Afterwards, core displacement tests were conducted using water and low salinity-polymeric nanofluid (LPN2000) prepared by dispersing 2000 ppm of  $\text{ZnO}/\text{SiO}_2/\text{xanthan}$  NC in 1:20 diluted seawater. LPN2000 has been chosen as the tertiary injection fluid according to the results obtained from the IFT and contact angle tests. Tests were performed at 75 °C and 1350–1380 psi with the injection rate of 0.5  $\text{cm}^3/\text{min}$ ; initially, water about 2 pore volumes (PV) was injected to the core plug under controlled flow rate, in which two pressure transducers were used to record the pressure values at the injection and production points, and 2 PV of LPN2000 injected to the core plug with collecting the displaced volume of crude oil. Furthermore, the emulsification stability analysis has been considered for the crude oil–various nanofluid systems including PN500, PN1000, PN2000, LPN500, LPN1000, and LPN2000. For this purpose, the prepared samples of 3:7 (v/v) emulsions have been maintained in an aqueous phase by shaking for 30 min using an

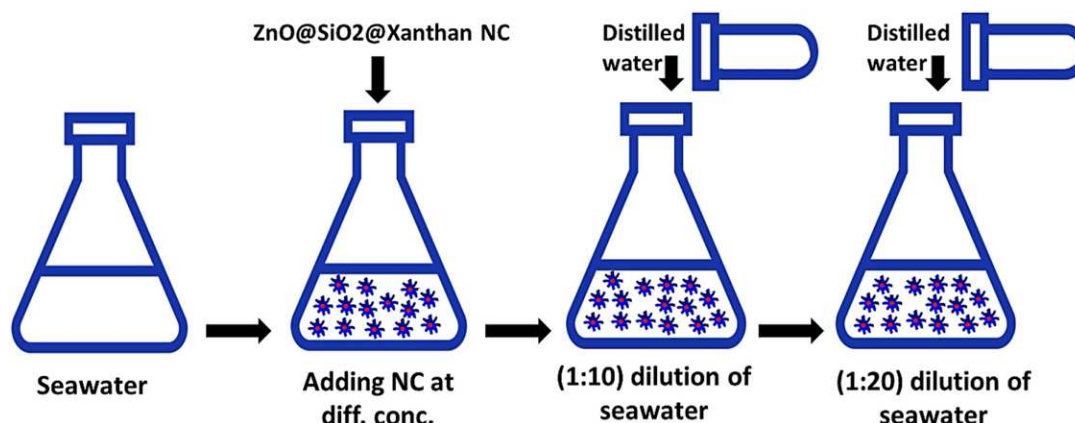


Fig. 4. Schematic illustration of preparing the polymeric and low-salinity polymeric nanofluids.

orbital shaker. The produced samples were then collected in transparent cylinders and observed visually over different time-steps.

### 3. Results and discussions

#### 3.1. Characterization of polymer coated ZnO/SiO<sub>2</sub> nanocomposite

ZnO/SiO<sub>2</sub>/xanthan NC has been prepared using one-pot green synthesis method and characterized using various analytical techniques (see our previous papers [53–55]). After confirming the presence of potent antioxidants inside the plant extract, ZnO/SiO<sub>2</sub>/xanthan NC has been produced. The mechanistic relationship of zinc NPs–silica NPs–xanthan is shown schematically in Fig. 6.

The results of XRD analysis on the synthesized ZnO/SiO<sub>2</sub>/xanthan NC using PANalytical X'Pert are presented in Fig. 7, which contains all the peaks associated with the crystalline planes of pure SiO<sub>2</sub> and ZnO NPs and phase purity of nanoparticles deposited on the surface of the xanthan gum. Three 010, 002 and 012 noticed peaks with the reflections from 31.5 to 36° are similar to the peaks of Zinc and silica NPs observed in the previous studies [56–60].

For further confirmation of the biosynthesis of NC, the morphology and element ratio analyses were performed using SEM and EDS (Quanta 450). The morphology of the green NC is illustrated by SEM micrograph at 40,718 magnifications (Fig. 8a). According to the morphology of the SEM image reported previously [61,62], the shapes of SiO<sub>2</sub> and ZnO NPs on the surface of the polymer were observed with various sizes below 100 nm. Fig. 8b demonstrates the EDS data which strongly

depicted the presence of Si, Zn and Ca elements as elemental composition of the synthesized NC. Meanwhile, the Au peak belongs to the gold used in coating the sample for conducting the SEM analysis. This analysis technique again strongly proves the validity of the method of fabrication of a green nanocomposite.

#### 3.2. Nanofluid characterization

##### 3.2.1. Stability

In this part, we have focused on the dispersion stability of colloidal solid particles within the nanofluid solutions. The key point is that the dispersion should stay in its designed condition under the experimental circumstances or else flocculation is going to happen. According to Yang and Liu [63], Chen and Xie [64], Yu and Xie [65] the synthesized nanocomposite was coated by polymer as a NP surface modifier in order to provide the high stability. After sonicating the low-salinity polymeric–nanofluids with three 500, 1000 and 2000 ppm concentrations of synthesized NC, they were kept in a static state and monitored through transparent vessels for a period of one week. Consequently, an excellent suspension stability of the nanofluids was observed as shown in Fig. 9. In addition, as it has been reported that the pH of a colloidal solution significantly influences the particle aggregation and the stability of the suspension [65–67]. Fig. 10a shows the pH values of the polymeric nanofluids, which varied between 5.8 and 6.8 and indicates a stable consistency between the nanofluids. Meanwhile, the conductivity readings of the polymeric nanofluids formed by dispersing the synthesized NC in seawater are shown in Fig. 10b. As it can be seen that the

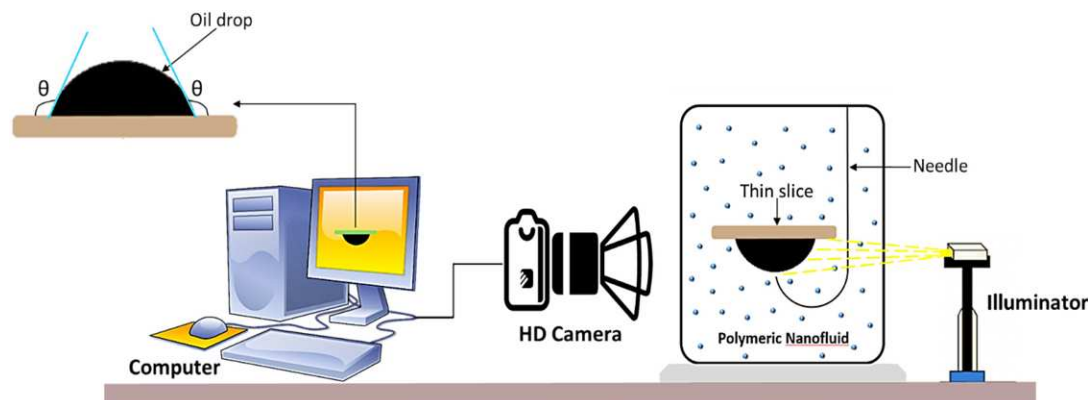


Fig. 5. Schematic illustration of sessile drop method for contact angle measurements.

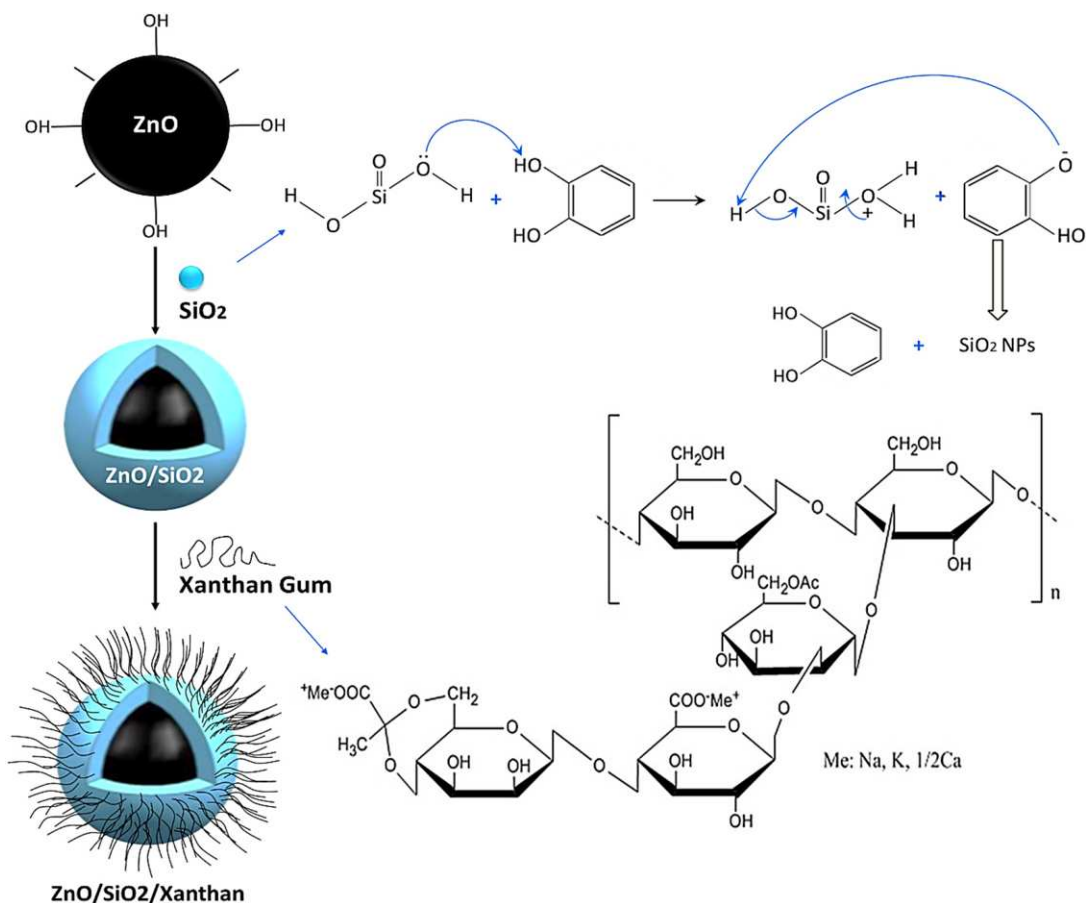


Fig. 6. Schematic view of coating process of ZnO/SiO<sub>2</sub> NPs with xanthan Gum particle chains, which shows the structural mechanisms of Zinc NPs, Silica NPs and xanthan Gum.

conductivity was increased along with salinity and NC concentration, but the effect of salinity on conductivity is higher compared to NC concentration. For instance, the minimum conductivity of 3.26 mS/m was obtained from the low-salinity polymeric-nanofluid at concentration of 2000 ppm of NC; however, at the same NC concentration the seawater polymeric nanofluid provided the maximum value of conductivity about 59.6 mS/m.

### 3.2.2. Viscosity

In addition to the stability of synthesized NC, it is also worth examining the effect of nanocomposite on the viscosity of nanofluids as shown in Fig. 10c. The viscosity of the injected nanofluid is important due to its effect on mobility ratio and sweep efficiency, consequently, the EOR efficiency. The viscosity of displacing fluid was significantly

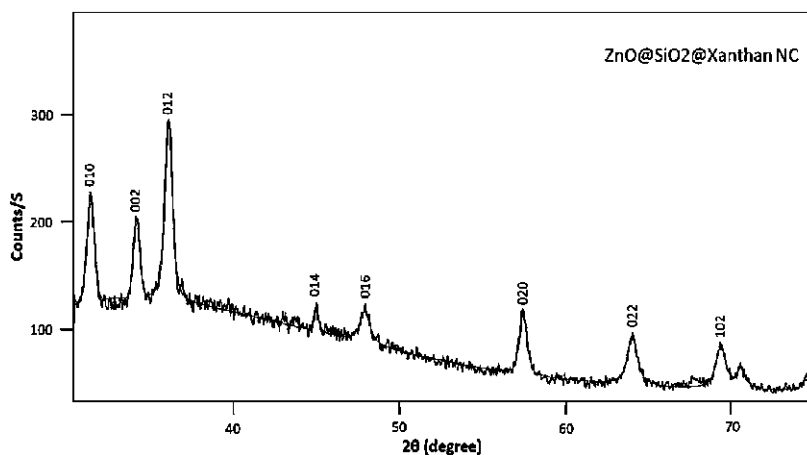


Fig. 7. The XRD pattern of green synthesized ZnO/SiO<sub>2</sub>/xanthan NC [53].

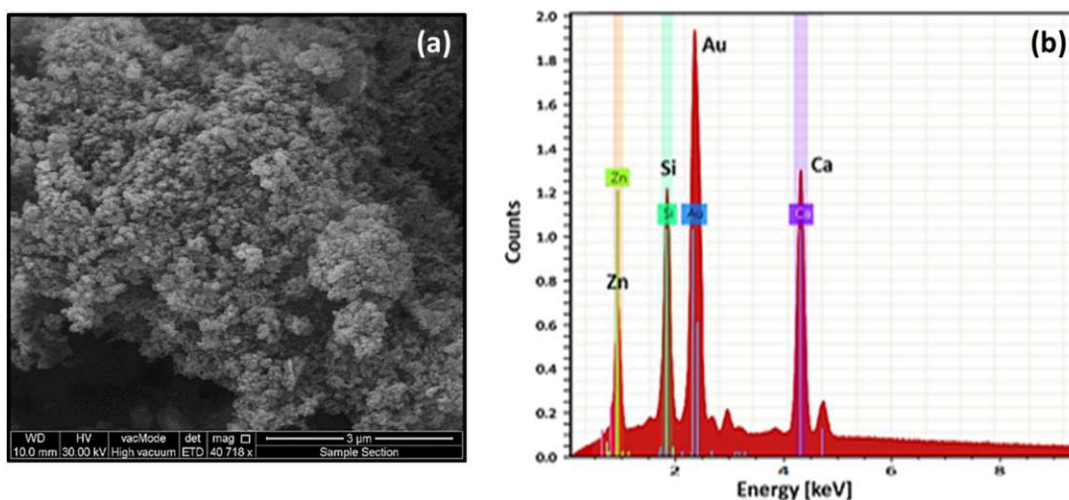


Fig. 8. a) SEM morphology at 3  $\mu\text{m}$ , and b) EDS spectrum of synthesized  $\text{ZnO/SiO}_2/\text{xanthan NC}$  [54].

increased by increasing the concentration of synthesized NC for various salinity ranges; low salinity (6.72 to 16.68 cP), moderate salinity (4.74 to 8.52 cP), and high salinity (7.78 to 7.78 cP) (Fig. 10c). Hence, the impact of the NC concentration on viscosity with the low salinity solution is higher compared to that with the moderate and high salinities. With the aim of minimizing the mobility ratio and improving the sweep efficiency and based on [68], the low-salinity polymeric-nanofluid with 2000 ppm NC concentration (LPN2000) was selected as the best EOR displacing candidate since its viscosity ratio is the highest which ranged 16.68 cP.

### 3.2.3. IFT behavior

IFT measurements were conducted for crude oil against different aqueous phases (seawater, low salinity, PNs, and LPNs) at ambient temperature and pressure condition as shown in Fig. 11. From the figure, it can be seen that the IFT reduced gradually from its original to the lowest

value due to the effect of salinity and NC concentration. The initial IFT values of oil-seawater and oil-low salinity system were measured as 31.8 and 19.68 mN/m, respectively. This reduction, about 38.1%, was achieved by the effect of water salinity on IFT, which is quite consistent with the explanation of Nowrouzi et al. [69] where they described the effect of various concentrations and ionic compounds of the seawater and reported that diluting the seawater reduced the IFT, effectively. Afterwards, the synthesized polymer coated  $\text{ZnO/SiO}_2$  NC was added to the seawater and IFT values between crude oil and polymeric nanofluids (NP500, NP1000 and NP2000) were recorded. These ranged from 9.45 to 16.041 mN/m. The IFT of oil-NP500 was higher than for oil-NP1000 and oil-NP2000 systems. In this section of the experiment, we reduced the IFT by about 52% from 19.68 to 9.45 mN/m by application of the synthesized NC at appropriate concentration. This observation agrees with Choi et al. [31] and Qi et al. [32], where they stated that a layered structure develops by the presence of the nanoparticles at the interface

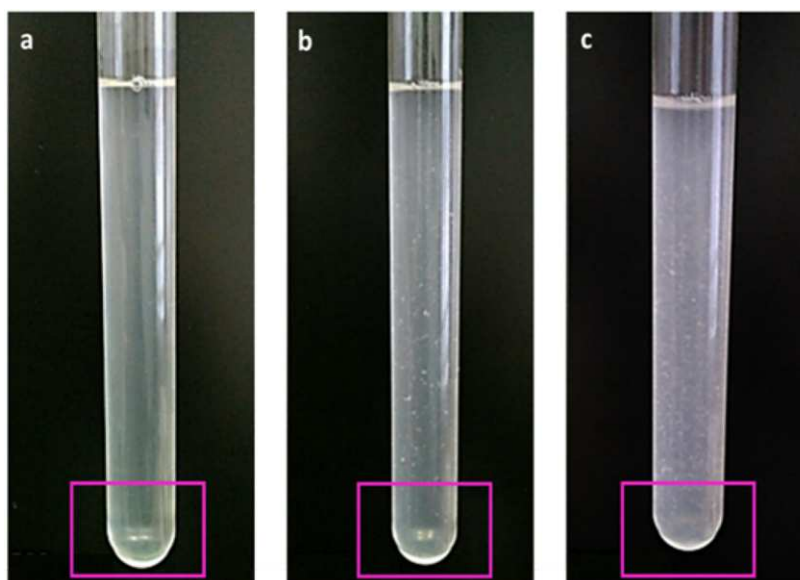


Fig. 9. Dispersion stability of low-salinity polymeric-nanofluids with NC concentrations of (a) 500 ppm, (b) 1000 ppm, and (c) 2000 ppm after 7 days [53].

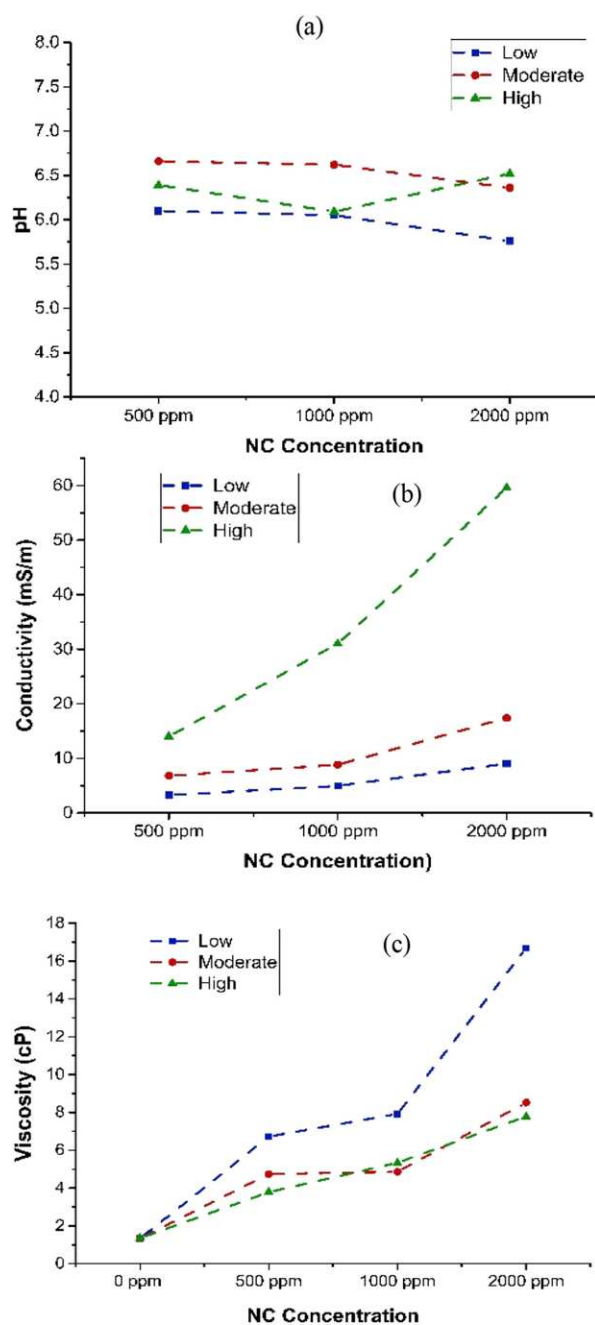


Fig. 10. Characteristics of polymeric nanofluids at 500, 1000 and 2000 ppm NC concentrations and low, moderate and high salinity; (a) pH, (b) conductivity, and (c) viscosity.

between the crude oil and polymeric nanofluids, which reduces the IFT. This mechanism will become more effective and stronger by increasing the concentration of polymer coated nanoparticles. Moreover, the IFT of oil-LPN systems at different NC concentrations were measured after reducing the salinity of seawater by 1:20 dilution; oil-LPN500 (9.45 mN/m), oil-LPN1000 (6.95 mN/m), and oil-LPN2000 (2.215 mN/m). By adding the synthesized NC into low salinity

water, the IFT was reduced by about 88.7% from 19.68 (oil-low salinity system) to 2.215 mN/m. In general, by reducing the salinity of seawater and adding the synthesized polymer coated NC, we significantly reduced the IFT value by about 93% from 31.8 to 2.215 mN/m, which was achieved using the LPN2000 solution (Fig. 11).

### 3.3. Wettability alteration by polymeric nanofluids

As mentioned earlier, the wettability behavior for several aqueous systems was identified by measuring the contact angle of crude oil on the carbonate plates before and after treatment with the synthesized nanocomposite. Fig. 12 illustrates the measured contact angles of crude oil with the presence of various aqueous solutions. The contact angle measurement was initially applied to estimate the wettability behavior of carbonate thin sections in the presence of distilled (DW), sea- and low salinity waters without the presence of nanomaterials. From this, it was identified that DW and seawater induced a very strong oil-wet system ( $132.62^\circ$  contact angle) and a strong oil-wet behavior ( $91.63^\circ$  contact angle), respectively. Meanwhile, reducing the salinity of water by about 1:20 dilutions, altered wetting towards the water-wet due to the reduction in contact angle of carbonate/crude oil/low salinity to about  $63.41^\circ$ . Then, the effect of the synthesized NC was investigated by dispersing into the seawater to develop the polymeric-nanofluids (PNs) with different concentrations ranged between 500 and 2000 ppm. After PNs treatment, the contact angles were significantly reduced depending on the NC concentration (these were 500, 1000 and 2000 ppm). For this type of aqueous phase, the lowest contact angle was achieved for a crude oil treated with the PN2000 which was measured at  $57^\circ$ .

Additionally, to study the wettability condition of the carbonate rock as a result of using polymer, nanoparticles, and changing salinity, the developed polymer coated NC was added into the low salinity water. For this purpose, the carbonate plates were treated with prepared with low salinity-polymeric nanofluid (LPN) solutions at various NC concentrations. After 3 days, the contact angle measurements were obtained for the crude oil on these pellets. As it can be seen in Fig. 12, the measured contact angles between oil/LPN-500, oil/LPN-1000 and oil/LPN-2000 nanofluids were  $54.48^\circ$ ,  $49.33^\circ$ , and  $34.08^\circ$ , respectively. As it is obvious, the maximum reduction of crude oil contact angle on carbonate slice was achieved when it was treated with LPN2000 solution, which was about 74.3% from  $132.62^\circ$  to  $34.08^\circ$ . Thus, according to Giraldo et al. [17], Al-Anssari et al. [18] and Rezvani et al. [33] wettability behavior has been altered from the strong oil-wet to strong water-wet condition from utilizing LPN-2000 aqueous phase containing 2000 ppm of developed polymer coated ZnO/SiO<sub>2</sub> nanocomposite, which it has been selected as an injection fluid in this study.

In order to better understand the influences of the salinity and NC concentration on the wettability alteration, the contact angle of crude oil droplets on several carbonate slices (that were aged in seawater, low salinity water, PNs and LPNs) have been illustrated schematically in Fig. 13. As it can be seen in the figure, the contact angle was reduced by about  $28.2^\circ$  when the salinity of the water was decreased by 20 times without the presence of nanomaterials. In addition, the contact angle variations between PNs and LPNs with 500, 1000, 2000 ppm NC concentrations were  $31.5^\circ$ ,  $29.5^\circ$  and  $23^\circ$ , respectively. The highest reduction in contact angle was achieved between PN500 and LPN500 nanofluids by adding 500 ppm NC, which was about  $31.5^\circ$  (from  $86^\circ$  to  $54.4^\circ$ ). Generally, with the maximum NC concentration (2000 ppm), the contact angle of the rock slice that was aged in the polymeric nanofluid was lowered by about 37.8% (from  $91.63^\circ$  to  $57^\circ$ ). However, we reduced the contact angle by about 62.8% (from  $91.63^\circ$  to  $34^\circ$ ) by decreasing the salinity of seawater. Thus, the contact angle of carbonate rock was

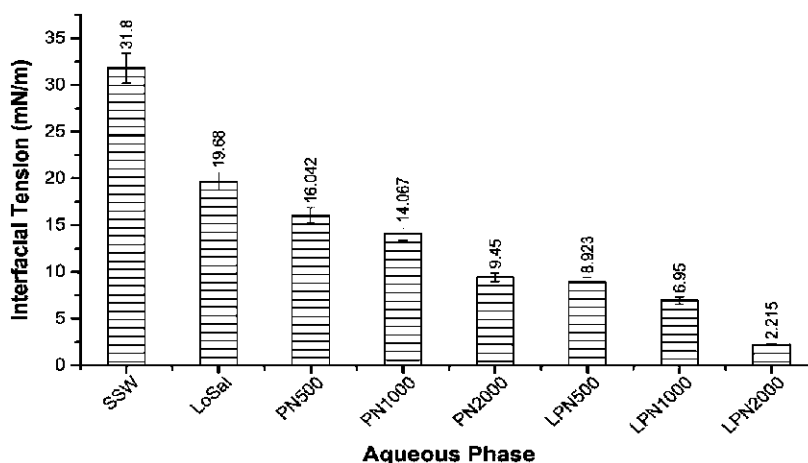


Fig. 11. IFTs measured between oil-various aqueous phases of different salinities and NC concentrations.

significantly influenced by the effect of salinity and synthesized nanocomposite.

#### 3.4. Oil displacement and emulsification

Oil displacement experiments were performed by injecting water as a secondary recovery process and low-salinity polymeric-nanofluid as an EOR technique with a constant injection rate of  $0.5 \text{ cm}^3/\text{min}$  into a carbonate core plug. LPN2000 nanofluid as the best of the low-salinity polymeric- and polymeric-nanofluids was selected according to the IFT, viscosity and contact angle results described above. The nanofluid was prepared from dispersing 2000 ppm of polymer coated  $\text{ZnO}/\text{SiO}_2$  NC in 1:20 diluted seawater. The oil recovery profile across the core plug for both injections is shown in Fig. 14. In accordance with the tendency stated in other studies, the cumulative oil recovery was usually improved steadily as more brine was injected before approaching a plateau at around 2 PV. The waterflooding recovery factor was identified to be 46.96% of original oil in place (OOIP). Then, the cumulative oil production was further increased by about 19.28% OOIP by injecting LPN nanofluid. Again, the 2nd plateau value was arrived at after injecting

roughly 2 PV. At that point the total cumulative oil recovery from both of waterflooding and low salinity-polymeric nanofluid flooding was 66.24% OOIP.

Furthermore, in this section, the emulsification stability analysis was carried out for the crude oil with various nanofluid. The NC concentrations ranged from 500 to 2000 ppm including PN500, PN1000, PN2000, LPN500, LPN1000 and LPN2000. Fig. 15a–e presents the emulsification behavior of all fluid systems at different time steps, over 12 h. On the whole, the stability varied between the time steps and across NC concentrations. As it can be seen, after shaking the emulsions for 30 min, the coalescence of some mixtures was quickly occurred during the first 2 h and increased (Fig. 15b–d). On the other hand, the stable emulsion, with no flocculation and coalescence, for all other fluid systems was observed at 8 h and 12 h after settling (Fig. 15e–f). At lower concentration of polymer coated  $\text{ZnO}/\text{SiO}_2$  NC, higher reduction of the emulsion stability has been observed in both PNs and LPNs reduced. This is true according to the theory of Dickinson et al. [70] in which they stated that oil droplets quickly experience coalescence to develop larger droplets with low polymer concentration which causes the emulsion stability to become decreased. However, with increasing the concentration of

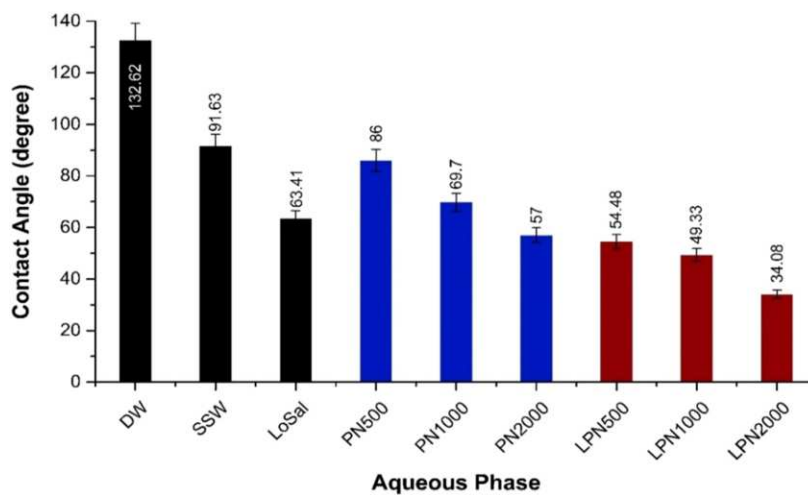
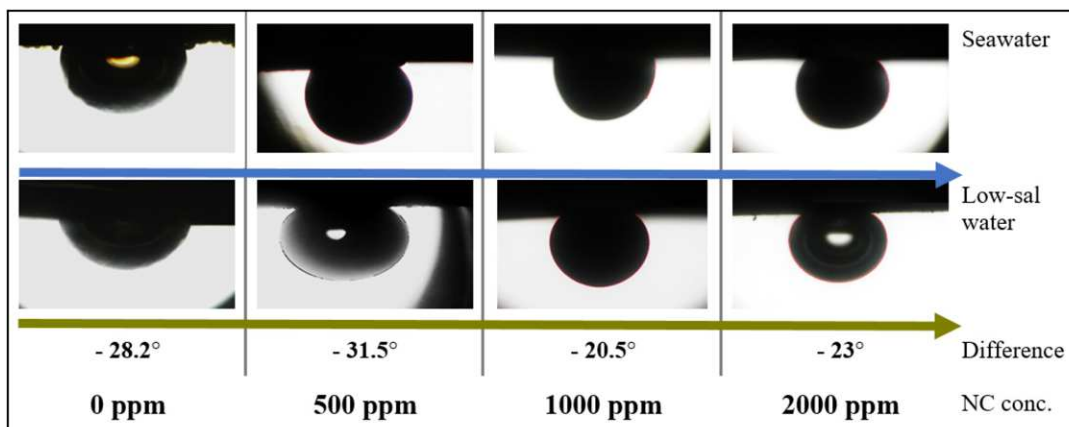


Fig. 12. Measured contact angles between crude oil and various aqueous phases (seawater, low salinity, PNs and LPNs).



**Fig. 13.** Oil droplet images of several carbonate pellets indicate the variations in contact angles between (i) seawater and low-salinity water, (ii) PNs and LPNs with 500, 1000, and 2000 ppm NC concentrations.

the synthesized NC, better emulsion stability was obtained due to the better adsorption of the nanocomposite on oil droplets and occurring isolation between oil droplets [71]. The emulsification stability of the polymeric nanofluids – PNs developed from the high salinity seawater was gradually improved with increasing the NC concentration for all time steps as shown by purple line on Fig. 15. The stability of the PN emulsion formed at 500 ppm NC was reduced very quickly after 1 h of settling, and started to reduce after 4 h with 1000 ppm NC concentration. However, a high stable emulsion of crude oil/PN2000 was observed through the all settling time-steps, which was inferred as an optimal nanofluid [5]. However, there was no steady trend observed with the low salinity-polymeric nanofluids – LPNs with increasing the NC concentration. The stability of oil/LPN emulsion with 500, 1000 and 2000 ppm was started to reduce after 1–2 h of settling. In addition to this, better stability of LPN was identified with 2000 ppm NC concentration compared to 500 and 1000 ppm.

We compared the results achieved by the performance of the low-salinity polymeric-nanofluid used in this study with the findings described in the literature for nanofluid EOR applications in terms of IFT

reduction, wettability alteration and oil recovery improvement on Fig. 16. For instance, Ju and Fan [40] increased oil recovery by about 21% of OOIP using polymer coated-SiO<sub>2</sub> NPs. They also confirmed that the role of wettability alteration was higher than the IFT reduction to produce the residual oil. In addition, Rezvani et al. [33] produced an extra 10.8% OOIP by using Chitosan coated Fe<sub>3</sub>O<sub>4</sub> nanocomposite by modifying the IFT and wettability behavior. According to the percentages of modifications in IFT, wettability and oil recovery from previous studies, current work obtained a huge reduction in IFT (93%), significant alteration in wettability towards a water-wet system (from 132.6 to 34°) and large improvement in oil recovery (19.3%) by creating better interactions between crude oil, polymer, nanoparticles and carbonate rocks.

#### 4. Conclusions

This paper described a new green technology to develop a low-salinity polymeric-nanofluid using a polymer coated ZnO/SiO<sub>2</sub> nanocomposite for the Enhanced Oil Recovery. ZnO/SiO<sub>2</sub>/xanthan NC was synthesized from pomegranate seed extract in a green and economical

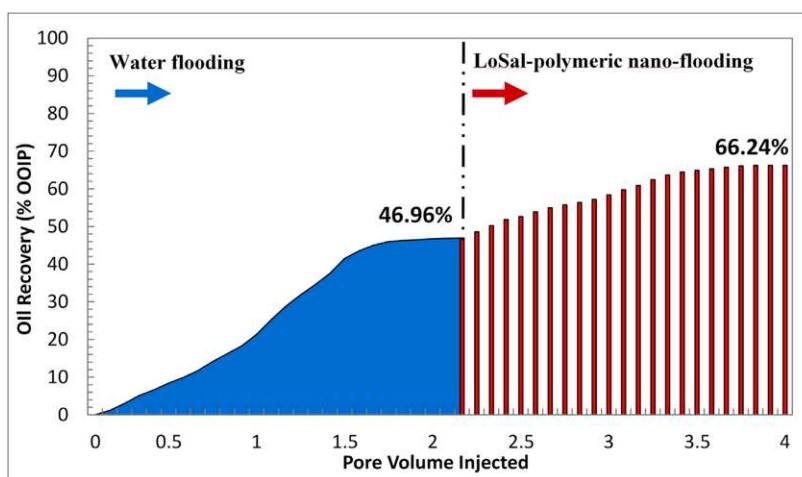


**Fig. 14.** Production profiles of brine and LPN2000 nanofluid flooding as a function of injected PV.



Fig. 15. Emulsification images of oil/polymeric and oil/low salinity-polymeric nanofluids over various time-steps.

way, and characterized using UV–Vis, XRD, FE-SEM and EDS techniques. The prepared nanofluid utilized the properties of several components, as follows: (i) polymer coated ZnO/SiO<sub>2</sub> NC was evenly dispersed in water with high suspension stability for long time, (ii) the low-salinity polymeric-nanofluid (LPN) presented an excellent rheology and interfacial activity due to the effects of synthesized NC and salinity, (iii) the developed LPN nanofluid enabled alteration of wettability of the carbonate

rock from an oil-wet to a strong water-wet system, (iv) LPN flooding improved the cumulative oil recovery by about 19.28% OOIP, and (v) high stable emulsification between crude oil and polymeric nanofluid achieved over various time-steps. This preparation method could be widely applied to acquire low salinity-polymeric nanofluids, which shows great potential for EOR applications in carbonate reservoirs.

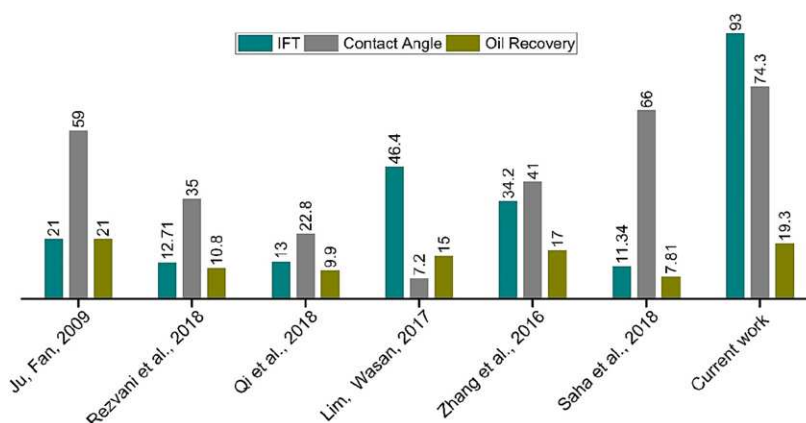


Fig. 16. Clustered column chart demonstrates best results obtained in this work and those reported in the literature in terms of IFT reduction, wettability alteration and oil recovery.

## References

- [1] T. Sharma, S. Iglauer, J.S. Sangwai, Silica nanofluids in an oilfield polymer polyacrylamide: interfacial properties, wettability alteration, and applications for chemical enhanced oil recovery, *Industrial Eng. Chem. Res.* 55 (2016) 12387–12397.
- [2] S. Thomas, Enhanced oil recovery—an overview, *Oil Gas Sci. Tech.* 63 (2008) 9–19 *Revue de l'IEP*.
- [3] M. Almahfood, B. Bai, The synergistic effects of nanoparticle-surfactant nanofluids in EOR applications, *J. Pet. Sci. Eng.* 171 (2018) 196–210.
- [4] T. Sharma, G.S. Kumar, J.S. Sangwai, Comparative effectiveness of production performance of Pickering emulsion stabilized by nanoparticle-surfactant-polymer over surfactant-polymer (SP) flooding for enhanced oil recovery for Brownfield reservoir, *J. Pet. Sci. Eng.* 129 (2015) 221–232.
- [5] R. Saha, R.V. Uppaluri, P. Tiwari, Silica nanoparticle assisted polymer flooding of heavy crude oil: emulsification, rheology, and wettability alteration characteristics, *Industrial Eng. Chem. Res.* 57 (2018) 6364–6376.
- [6] Q. Chen, Y. Wang, Z. Lu, Y. Feng, Thermoviscosifying polymer used for enhanced oil recovery: rheological behaviors and core flooding test, *Polym. Bull.* 70 (2013) 391–401.
- [7] I. Tripathi, K.K. Mohanty, Flow instability associated with wettability alteration, Paper SPE 110202 Presented at SPE Annual Technical Conference and Exhibition, Anaheim CA 2007, pp. 11–14.
- [8] M. Hourshad, G. Jerauld, Mechanistic Modeling of the Benefit of Combining Polymer With Low Salinity Water for Enhanced Oil Recovery, Paper SPE-153161-MS Presented at SPE Improved Oil Recovery Symposium, Tulsa, Oklahoma 2012, pp. 14–18.
- [9] S.S. Behruz, A. Skauge, Enhanced oil recovery (EOR) by combined low salinity water/polymer flooding, *Energy Fuel* 27 (2013) 1223–1235.
- [10] B.S. Mahmood, J.A. Ali, S.B. Nazhat, D. Devlin, A sensitivity study on low salinity waterflooding, *Modern Environ. Sci. Eng.* 04 (2017) 231–236.
- [11] G.Q. Tang, N.R. Morrow, Influence of brine composition and fines migration on crude oil/brine/rock interactions and oil recovery, *J. Petroleum Sci. Eng.* 24 (1999) 99–111.
- [12] H. Aksulu, D. Hamso, S. Strand, et al., The evaluation of low salinity enhanced oil recovery effects in sandstone: effects of temperature and pH gradient, *Energy Fuel* 26 (2012) 3497–3503.
- [13] P. Lemon, A. Zeinijahromi, P. Bedrikovetsky, Effects of injected water chemistry on waterflood sweep efficiency via induced fines migration, *J. Can. Petroleum Technol.* 50 (2011) 82–94.
- [14] A. Zeinijahromi, P. Lemon, P. Bedrikovetsky, Effects of induced fines migration on water cut during water flooding, *J. Petroleum Sci. Eng.* 78 (2011) 609–617.
- [15] A.M. Ahmadi, S. Zendejboudi, A. Shafiei, L. James, Nonionic surfactant for enhanced oil recovery from carbonates: adsorption kinetics and equilibrium, *Industrial Eng. Chem. Res.* 51 (2012) 9894–9905.
- [16] M. Zargartalebi, R. Kharrat, N. Barati, Enhancement of surfactant flooding performance by the use of silica nanoparticles, *Fuel* 143 (2015) 21–27.
- [17] J. Giraldo, P. Benjumea, S. Lopera, F.B. Cortés, M.A. Ruiz, Wettability alteration of sandstone cores by alumina-based nanofluids, *Energy Fuel* 27 (2013) 3659–3665.
- [18] S. Al-Anssari, A. Barifcani, S. Wang, L. Maxim, S. Iglauer, Wettability alteration of oil-wet carbonate by silica nanofluid, *J. Colloid Interface Sci.* 461 (2016) 435–442.
- [19] K. Kondiparty, A.D. Nikolov, D. Wasan, K.L. Liu, Dynamic spreading of nanofluids on solids. Part I: experimental, *Langmuir* 28 (2012) 14618–14623.
- [20] J.A. Ali, K. Kolo, A.K. Manshad, A.H. Mohammadi, Recent advances in application of nanotechnology in chemical enhanced oil recovery: effects of nanoparticles on wettability alteration, interfacial tension reduction, and flooding, *Egyptian J. Petrol.* 27 (2018) 1371–1383, <https://doi.org/10.1016/j.ejpe.2018.09.006>.
- [21] H. Zhang, A. Nikolov, D. Wasan, Enhanced oil recovery (EOR) using nanoparticle dispersions: underlying mechanism and imbibition experiments, *Energy Fuel* 28 (2014) 3002–3009.
- [22] D. Arab, P. Pourafshary, Nanoparticles-assisted surface charge modification of the porous medium to treat colloidal particles migration induced by low salinity water flooding, *Colloids Surfaces A Physicochem. Eng. Aspects* 436 (2013) 803–814.
- [23] K. Liu, K. Kondiparty, A.D. Nikolov, D. Wasan, Dynamic spreading of nanofluids on solids part II: modeling, *Langmuir* 28 (2012) 16274–16284.
- [24] H. Zhang, T.S. Ramakrishnan, A. Nikolov, D. Wasan, Enhanced oil recovery driven by nanofilm structural disjoining pressure: flooding experiments and microvisualization, *Energy Fuel* 30 (2016) 2771–2779.
- [25] R. Abhishek, A.A. Hamouda, I. Murzin, Adsorption of silica nanoparticles and its synergistic effect on fluid/rock interactions during low salinity flooding in sandstones, *Colloids and Surfaces A: Physicochemical Eng. Aspects* 555 (2018) 397–406.
- [26] S. Kiani, M. Zadeh, S. Khodabakhshi, A. Rashidi, J. Moghadasi, Newly prepared Nano gamma alumina and its application in enhanced oil recovery: an approach to low-salinity waterflooding, *Energy Fuel* 30 (2016) 3791–3797.
- [27] H. Shamsi-Jazeyi, C.A. Miller, M.S. Wong, J.M. Tour, R. Verduzco, Polymer-coated nanoparticles for enhanced oil recovery, *J. App. Polymer Sci.* 131 (2014).
- [28] I. Nowrouzi, A.K. Manshad, A.H. Mohammadi, Effects of ions and dissolved carbon dioxide in brine on wettability alteration, contact angle and oil production in smart water and carbonated smart water injection processes in carbonate oil reservoirs, *Fuel* 235 (2019) 1039–1051.
- [29] S. Lim, D. Wasan, Structural disjoining pressure induced solid particle removal from solid substrates using nanofluids, *J. Colloid Interface Sci.* 500 (2016) 96–104.
- [30] T. Sharma, J.S. Sangwai, Silica nanofluids in polyacrylamide with and without surfactant: viscosity, surface tension, and interfacial tension with liquid paraffin, *J. Pet. Sci. Eng.* 152 (2017) 575–585.
- [31] S.K. Choi, H.A. Son, H.T. Kim, J.W. Kim, Nanofluid enhanced oil recovery using hydrophobically associative zwitterionic polymer-coated silica nanoparticles, *Energy Fuel* 31 (2017) 7777–7782.
- [32] L. Qi, C. Song, T. Wang, Q. Li, G.J. Hirasaki, R. Verduzco, Polymer-coated nanoparticles for reversible emulsification and recovery of heavy oil, *Langmuir* 34 (2018) 6522–6528.
- [33] H. Rezvani, M. Riazi, M. Tabaei, Y. Kazemzadeh, M. Sharifi, Experimental investigation of interfacial properties in the EOR mechanisms by the novel synthesized Fe<sub>3</sub>O<sub>4</sub>/Chitosan nanocomposites, *Colloids and Surfaces A: Physicochemical Eng. Aspects* 544 (2018) 15–27.
- [34] A.B. Fossati, M.M. Alho, S.E. Jacobo, Polymer-functionalized nanoparticles for improving oil displacement, *Adv. Natural Sci.: Nanoscience Nanotechnology* 9 (2018), 015–007.
- [35] N. Saleh, T. Sarbu, K. Sirk, G.V. Lowry, K. Matyjaszewski, R.D. Tilton, Oil-in-water emulsions stabilized by highly charged polyelectrolyte-grafted silica nanoparticles, *Langmuir* 21 (2005) 9873–9878.
- [36] N.J. Alvarez, S.L. Anna, T. Saigal, R.D. Tilton, L.M. Walker, Interfacial dynamics and rheology of polymer-grafted nanoparticles at air–water and xylene–water interfaces, *Langmuir* 28 (2015) 8052–8063.
- [37] G.S. Cheraghian, K. Nezhad, M. Kamari, M. Hemmati, S. Bazgir, Adsorption polymer on reservoir rock and role of the nanoparticles, clay and SiO<sub>2</sub>, *Int. Nano Letters* 4 (2014) 1–8.
- [38] G. Cheraghian, Effect of nano titanium dioxide on heavy oil recovery during polymer flooding, *Pet. Sci. Tech.* 34 (2016) 633–641.
- [39] S.S. Khalilnezhad, G. Cheraghian, E. Roayaei, H. Tabatabaee, M.S. Karambeigi, Improving heavy oil recovery in the polymer flooding process by utilizing hydrophilic silica nanoparticles, *Energy Sources, Part A: Recovery, Utilization, and Environmental Effects* (2017) 1–10.
- [40] B. Ju, T. Fan, Experimental study and mathematical model of nanoparticle transport in porous media, *Powder Tech* 192 (2009) 195–202.

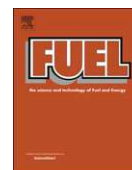
- [41] H.M. Zaid, N.R. Ahmad Latiff, N. Yahya, The effect of zinc oxide and aluminum oxide nanoparticles on interfacial tension and viscosity of nanofluids for enhanced oil recovery, *Adv. Materials Res.* 1024 (2014) 56–59.
- [42] H. Soleimani, M.K. Baig, N. Yahya, L. Khodapanah, M. Sabet, B.M. Demiral, M. Burda, Synthesis of ZnO nanoparticles for oil–water interfacial tension reduction in enhanced oil recovery, *App. Physics A* 124 (2018).
- [43] A. Roustaei, J. Moghadasi, H. Bagherzadeh, A. Shahrabadi, An experimental investigation of polysilicon nanoparticles' recovery efficiencies through changes in interfacial tension and wettability alteration, *SPE Int. Oilfield Nanotechnology Conference Exhibition*, 2012.
- [44] E. Joonaki, S. Ghanaatian, The application of nanofluids for enhanced oil recovery: effects on interfacial tension and coreflooding process, *Petrol. Sci. Tech.* 32 (2014) 2599–2607.
- [45] L. Hendraningrat, O. Torsæter, Metal oxide-based nanoparticles: revealing their potential to enhance oil recovery in different wettability systems, *App. Nanoscience* 5 (2014) 181–199.
- [46] E.A. Bayat, R. Junin, A. Samsuri, A. Piroozian, M. Hokmabadi, Impact of metal oxide nanoparticles on enhanced oil recovery from limestone media at several temperatures, *Energy Fuel* 28 (2014) 6255–6266.
- [47] Y. Li, C. Dai, H. Zhou, X. Wang, W. Lv, M. Zhao, Investigation of spontaneous imbibition by using a surfactant-free active silica water-based nanofluid for enhanced oil recovery, *Energy Fuel* 32 (2017) 287–293.
- [48] M.N. Nadagouda, N. Iyanna, J. Lalley, C. Han, D.D. Dionysiou, R.S. Varma, Synthesis of silver and gold nanoparticles using antioxidants from blackberry, blueberry, pomegranate, and turmeric extracts, *ACS Sustainable Chemistry Eng* 2 (2014) 1717–1723.
- [49] S. Basiri, Evaluation of antioxidant and antiradical properties of Pomegranate (*Punica granatum L.*) seed and defatted seed extracts, *J. Food Sci. Techno.* 52 (2013) 1117–1123.
- [50] K. Spildo, A.M. Johannessen, A. Skauge, Low salinity waterflood at reduced capillarity, *SPE Improved Oil Recovery Symposium*, 2012.
- [51] J.M. Villard, J.S. Buckley, N.R. Morrow, R. Gauchet, *Wetting and Waterflood Oil Recovery of a Moderately Viscous Crude Oil*, SCA1993-23, Society of Core Analysts, 1993.
- [52] A.K. Manshad, M. Rezaei, S. Moradi, I. Nowrouzi, A.H. Mohammadi, Wettability alteration and interfacial tension (IFT) reduction in enhanced oil recovery (EOR) process by ionic liquid flooding, *J. Molecular Liquids* 248 (2017) 153–162.
- [53] J.A. Ali, K. Kolo, A.K. Manshad, K.D. Stephen, A. Keshavarz, Modification of LoSal water performance in reducing interfacial tension using green ZnO/SiO<sub>2</sub> nanocomposite coated by xanthan, *Appl. Nanosci.* (2018), <https://doi.org/10.1007/s13204-018-0923-5>.
- [54] J.A. Ali, S.M. Sajadi, A.K. Manshad, K. Kolo, K.D. Stephen, Green synthesis of ZnO/SiO<sub>2</sub> nanocomposite from pomegranate seed extract: coating by natural xanthan polymer and its characterizations, *Micro Nano Letters* (2019), <https://doi.org/10.1049/mnl.2018.5617>.
- [55] J.A. Ali, K. Kolo, A.K. Manshad, K.D. Stephen, Low-salinity polymeric nanofluid-enhanced oil recovery using green polymer-coated ZnO/SiO<sub>2</sub> nanocomposites in the Upper Qamchuqa Formation in Kurdistan Region, Iraq, *Energy Fuel* 33 (2019) 927–937, <https://doi.org/10.1021/acs.energyfuels.8b03847>.
- [56] C. López, J.E. Rodríguez-Páez, Synthesis and characterization of ZnO nanoparticles: effect of solvent and antifungal capacity of NPs obtained in ethylene glycol, *Appl. Phys. A Mater. Sci. Process.* 123 (2017).
- [57] Y.S. Patil, I.D. Patil, Synthesis and characterization of zinc oxide nanostructures, *Int. J. Sci. Spiritual. Bus. Tech.* 2 (2014) 88–91.
- [58] J. Li, X.L. Wu, D.S. Hu, Y.M. Yang, T. Qiu, J.C. Shen, Splitting of X-ray diffraction peak in (Ge:SiO<sub>2</sub>)/SiO<sub>2</sub> multilayers, *Solid State Commun.* 131 (2014) 21–25.
- [59] C.C. Qiaohong, M. Wang, J. Cai, J. Xu, C. Xia, Facile preparation of highly-dispersed cobalt-silicon mixed oxide nanosphere and its catalytic application in cyclohexane selective oxidation, *Nanoscale Res. Letters* 6 (2011).
- [60] A. Yeganeh-Faal, M. Bordbar, N. Negahdar, M. Nasrollahzadeh, Green synthesis of the Ag/ZnO nanocomposite using *Valeriana officinalis L.* root extract: application as a reusable catalyst for the reduction of organic dyes in a very short time, *IET Nanobiotechnology* 11 (2017) 669–676.
- [61] A.M. El Shafey, Effect of nanoparticles and polymer nanoparticles implementation on chemical flooding, wettability and interfacial tension for the enhanced oil recovery processes, *African J. Eng. Res.* 5 (2017) 35–53.
- [62] S. Azarshin, J. Moghadasi, A.Z. Aboosadi, Surface functionalization of silica nanoparticles to improve the performance of water flooding in oil wet reservoirs, *Energy Exploration Exploitation* 35 (2017) 685–697.
- [63] X. Yang, Z.H. Liu, A kind of nanofluid consisting of surface-functionalized nanoparticles, *Nanoscale Res. Lett.* 5 (2010) 1324–1328.
- [64] L. Chen, H. Xie, Surfactant-free nanofluids containing double- and single-walled carbon nanotubes functionalized by a wet mechanochemical reaction, *Thermochim. Acta* 497 (2010) 67–71.
- [65] W. Yu, H. Xie, A review on nanofluids: preparation, stability mechanisms, and applications, *J. Nanomaterials* (2012) 1–17.
- [66] Y. Fovet, J.Y. Gal, F. Toumelin-Chemla, Influence of pH and fluoride concentration on titanium passivating layer: stability of titanium dioxide, *Talanta* 53 (2001) 1053–1063.
- [67] D. Wen, G. Lin, S. Vafaei, K. Zhang, Review of nanofluids for heat transfer applications, *Particuology* 7 (2009) 141–150.
- [68] Z. Hu, M. Haruna, H. Gao, E. Nourafkan, D. Wen, Rheological properties of partially hydrolyzed polyacrylamide seeded by nanoparticles, *Industrial Eng. Chem. Res.* 56 (2017) 3456–3463.
- [69] I. Nowrouzi, A.K. Manshad, A.H. Mohammadi, Effects of dissolved binary ionic compounds and different densities of brine on interfacial tension (IFT), wettability alteration, and contact angle in smart water and carbonated smart water injection processes in carbonate oil reservoirs, *J. Molecular Liquids* 254 (2018) 83–92.
- [70] E. Dickinson, J.G. Ma, M.J.W. Povey, Creaming of concentrated oil in-water emulsions containing xanthan, *Food Hydrocoll.* 8 (1994) 481–497.
- [71] A.K. Ghosh, P. Bandyopadhyay, Polysaccharide-protein interactions and their relevance in food colloids, *The Complex World of Polysaccharide*; Intech Open Science Open Minds 2012, p. 395–408.

### Appendix 3

*Experimental investigation of the effect of green TiO<sub>2</sub>/Quartz nanocomposite on interfacial tension reduction, wettability alteration, and oil recovery improvement*

Ghasem Zargar, Tooraj Arabpour, Abbas Khaksar Manshad, **Jagar A. Ali**, S.  
Mohammad Sajadi, Alireza Keshavarz, Amir H. Mohammadi

Fuel 263 (2020) 116599



## Full Length Article

## Experimental investigation of the effect of green TiO<sub>2</sub>/Quartz nanocomposite on interfacial tension reduction, wettability alteration, and oil recovery improvement



Ghasem Zargar<sup>a,\*</sup>, Tooraj Arabpour<sup>a</sup>, Abbas Khaksar Manshad<sup>a</sup>, Jagar A. Ali<sup>b,c</sup>, S. Mohammad Sajadi<sup>d,e</sup>, Alireza Keshavarz<sup>f</sup>, Amir H. Mohammadi<sup>g</sup>

<sup>a</sup> Department of Petroleum Engineering, Abadan Faculty of Petroleum Engineering, Petroleum University of Technology (PUT), Abadan, Iran

<sup>b</sup> Department of Petroleum Engineering, Faculty of Engineering, Soran University, Soran, Kurdistan Region, Iraq

<sup>c</sup> Department of Petroleum Engineering, College of Engineering, Knowledge University, Erbil, Kurdistan Region, Iraq

<sup>d</sup> Department of Nutrition, Cihan University-Erbil, Erbil, Iraq

<sup>e</sup> Scientific Research Centre, Soran University, Soran, Iraq

<sup>f</sup> School of Engineering, Edith Cowan University, WA 6027, Australia

<sup>g</sup> Discipline of Chemical Engineering, School of Engineering, University of KwaZulu-Natal, Howard College Campus, King George V Avenue, Durban 4041, South Africa

## ARTICLE INFO

## Keywords:

Green synthesis  
Titanium oxide  
Quartz  
Nanocomposite  
Nanofluid  
Enhanced oil recovery

## ABSTRACT

Nanoparticles (NPs) have shown a promising role in improving oil recovery as potential enhanced oil recovery (EOR) agents. In this study, one-pot green technique was used to synthesize titanium oxide NPs from the *euphoria condylocarpa* extract, and graft it on the surface of quartz to develop a green nanocomposite (NC) for enhanced oil recovery (EOR) applications. The synthesized TiO<sub>2</sub>/Quartz NC was identified using X-ray diffraction (XRD), Fourier-transform infrared spectroscopy (FTIR) and scanning electron microscopy (SEM). In order to prepare the novel nanofluids, the synthesized NC was dispersed in desilted water, seawater and low-salinity water (seawater dilution), which were characterized through analyzing their stability, viscosity, pH, density and conductivity behaviors. The prepared nanofluids were used to minimize the interfacial tension (IFT) and contact angle between crude oil and water on the surface of carbonate rocks. The obtained results show that TiO<sub>2</sub>/Quartz-nanofluid (DWN1000), with 1000 ppm dispersed in distilled water, enables an additional oil recovery of 21% OOIP due to a significant reduction in IFT from 36.4 to 3.5 mN/m, improving the rheology behavior and wettability alteration towards a stronger water-wet system from 103° to 48° contact angle. Thus, the synthesized NC provides high stability solution with a promising potential in EOR applications.

## 1. Introduction

Energy demand across the world increases instantly due to rapid economic improvement. As one of the most important basic energy sources, crude oil is an indispensable strategic resource for national development, which is known as the blood of industry [1]. Generally, primary and secondary recovery techniques can typically extract one-third of the original oil in place (OOIP), and the rest is usually trapped within the rock pore spaces and throats, and can hardly be produced by conventional processes [2]. This low recovery of oil is mainly linked to the displacement efficiency of porous media, which is primarily influenced by two factors, namely wettability and interfacial tension (IFT) [1,2]. The oil-wet system makes the crude oil difficult to isolate from the rock surface due to the high adhesion relation between the crude oil

and the reservoir rock [3,4]. While a high interfacial tension between the crude oil and water makes oil difficult to be transferred [5]. Thus, several methods and materials have been developed to enhance and improve oil recovery, such as chemical processes (polymer, surfactant and alkaline), gas injection (nitrogen and CO<sub>2</sub>), thermal techniques (steam cyclic, in-situ combustion and hot water) and microbial [6]. Although, these EOR agents and methods can improve oil recovery to a limit, however, there are some limitations, for instance, the high cost of chemicals, possible reservoir damage, high consumption, and chemical loss. Therefore, nanomaterials, as novel EOR agents, have highly attracted researchers to be used for overcoming the limitations of conventional methods due to their low cost, high efficiency, and eco-friendly features, as shown in Table 1 [6–8]. Based on this principle, nanofluids are recently the most common solutions because of their

\* Corresponding author.

E-mail address: [gzha.nano113@gmail.com](mailto:gzha.nano113@gmail.com) (G. Zargar).

<https://doi.org/10.1016/j.fuel.2019.116599>

Received 23 February 2019; Received in revised form 26 May 2019; Accepted 5 November 2019

Available online 16 December 2019

0016-2361/© 2019 Elsevier Ltd. All rights reserved.

**Table 1**

A summary of previous works on effects of various nanofluid categories on interfacial tension (IFT), contact angle (CA) and oil recovery.

| Nanomaterial                             | Dispersion media | NP conc. [wt.%] | Rock type | IFT [mN/m] |         | CA [degree] |         | EOR [%OOIP] | References                    |
|--|------------------|-----------------|-----------|------------|---------|-------------|---------|-------------|-------------------------------|
|  |                  |                 |           | clean      | with NP | clean       | with NP |             |                               |
| CuO                                      | Polyethyl glycol | 0.1–0.2         | Glass     | 47.9       | 1.5     | 9           | 1.8     | 15          | Lim & Wasan [25]              |
| SiO <sub>2</sub>                         | Ethylene glycol  | 0.277           | Glass     | 43         | 8.8     | 66          | 25      | 17          | Zhang et al. [16]             |
| SiO <sub>2</sub>                         | PAM              | 1–2             | Sandstone | 27         | 10.2    | –           | –       | 24.7        | Sharma et al. [23]            |
| SiO <sub>2</sub>                         | Xanthan gum      | 0.1–0.5         | Sandstone | 17.8       | 6.4     | 86          | 20      | 7.81        | Saha et al. [24]              |
| ZnO                                      | SDS              | 0.05            | Carbonate | 2.8        | 3.5     | 22.5        | 72.2    | 0           | Zaid et al. [21]              |
| ZnO                                      | SDS              | 0.05–0.5        | Calcite   | 27.4       | 18.6    | –           | 11.8    | 11          | Soleimani [22]                |
| SiO <sub>2</sub>                         | Ethanol          | 0.4             | Sandstone | 26.3       | 1.7     | 55          | 78      | 23          | Roustaei et al. [33]          |
| Al <sub>2</sub> O <sub>3</sub>           | Propanol         | 0.05–0.3        | Sandstone | 5.7        | 2.3     | 56.6        | 76.8    | 19.4        | Joonaki & Ghanaatian [32]     |
| SiO <sub>2</sub>                         |                  |                 |           | 5          | 1.5     | 56.6        | 79.1    | 21.6        |                               |
| Fe <sub>2</sub> O <sub>3</sub>           |                  |                 |           | 6.3        | 2.7     | 56.6        | 73.9    | 17.1        |                               |
| SiO <sub>2</sub>                         | Brine            | 0.05            | Sandstone | 19.2       | 12.8    | 33          | 26      | 17          | Hendraningrat & Torsæter [21] |
| Al <sub>2</sub> O <sub>3</sub>           | DIW              | 0.05            | Limestone | 18         | 13.4    | 55.8        | 65.7    | 9.9         | Bayat et al. [19]             |
| TiO <sub>2</sub>                         |                  |                 |           | 17.5       | 12.5    | 55.3        | 61.9    | 6.6         |                               |
| SiO <sub>2</sub>                         |                  |                 |           | 16.7       | 11      | 54.8        | 57.7    | 2.9         |                               |
| SiO <sub>2</sub>                         | Brine            | 0.1             | Sandstone | 17.5       | 7       | 12          | 40      | 28          | Li et al. [20]                |
| SiO <sub>2</sub>                         | LoSal water      | 0.1             | Sandstone | –          | –       | –           | –       | 7           | Abhishek et al. [17]          |
| SiO <sub>2</sub> /prop-2-enamide         |                  | 0.6–1.2         | Sandstone | 28         | 7       | 87          | 28      | 21          | Ju & Fan [29]                 |
| Fe <sub>3</sub> O <sub>4</sub> /chitosan | Brine            | 0.01–0.03       | Sandstone | 30         | 17.3    | 127         | 92      | 10.8        | Rezvani et al. [28]           |
| SiO <sub>2</sub> /Poly2(DMAEA)           |                  | 0.1             | Sandstone | 27         | 14      | 85          | 62.2    | 9.9         | Qi et al. [27]                |
| SiO <sub>2</sub> /2-Poly(MPC)            |                  | 0.1–0.2         | Sandstone | 47         | 35      | –           | –       | 5.2         | Choi et al. [26]              |
| ZnO/SiO <sub>2</sub> /xanthan            | LoSal water      | 0.05–0.2        | Carbonate | 31.8       | 2.016   | 137         | 34      | 19.3        | Ali et al. [31]               |

**Table 2**

The composition of seawater.

| Ion                           | Concentration (ppm) |
|-------------------------------|---------------------|
| Na <sup>+</sup>               | 7330                |
| Ca <sup>2+</sup>              | 1920                |
| Mg <sup>2+</sup>              | 930                 |
| K <sup>+</sup>                | 90                  |
| Cl <sup>-</sup>               | 11,500              |
| SO <sub>4</sub> <sup>2-</sup> | 6860                |
| HCO <sub>3</sub> <sup>-</sup> | 180                 |
| T.D.S.                        | 33,194              |
| T.H.                          | 8,700               |

**Table 3**

The composition of crude oil.

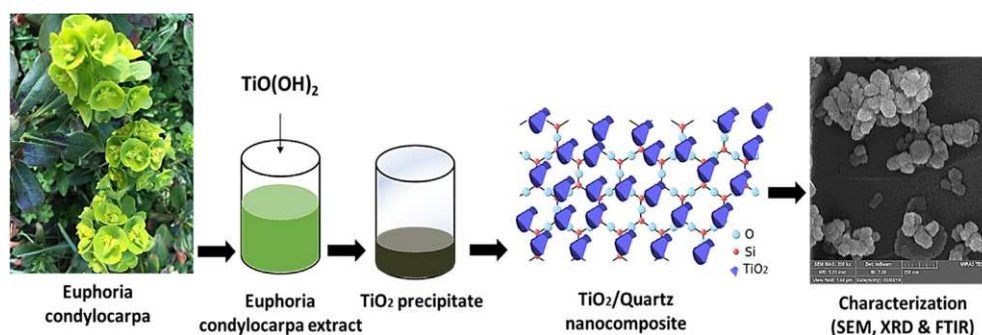
| Component                             | Mole %  |
|---------------------------------------|---------|
| C1                                    | 0.0285  |
| C2                                    | 0.4036  |
| C3                                    | 2.4806  |
| nC4                                   | 3.264   |
| iC4                                   | 0.0864  |
| nC5                                   | 2.7529  |
| iC5                                   | 2.0948  |
| C6                                    | 5.6658  |
| C7                                    | 9.32    |
| C7+ (MW = 269 g/gmol and SG = 0.9149) | 82.3193 |
| H <sub>2</sub> S                      | 0.093   |
| CO <sub>2</sub>                       | 0.0294  |

crucial EOR applications, such as wettability alteration [9,10], IFT reduction [11,12], viscosity improvement [13], controlling the fines migration [14] and inducing the structural disjoining pressure [15,16].

Since the last decade, the roles of several nanoparticles in EOR applications have been widely investigated, such as silicon dioxide (SiO<sub>2</sub>), aluminum oxide (Al<sub>2</sub>O<sub>3</sub>), zinc oxide (ZnO), and titanium dioxide (TiO<sub>2</sub>). These nanoparticles were applied in different manners, such as dispersed in brine [17–20], dispersed in surfactant [21,22], dispersed in polymer [23–25], and polymer-coated nanocomposite [26–30]. Hendraningrat and Torsæter [18] used hydrophilic silica as EOR agent to displace more oil in the porous media, and achieved a wettability alteration of quartz rocks with an increase of oil recovery by about 4.9%. While, Shahrabadi et al. [32] stated that using a nanofluid prepared of

hydrophobic silica dispersed in brine can provide better wettability to the rock surface and improves oil recovery. Joonaki and Ghanaatian [33] reported that Al<sub>2</sub>O<sub>3</sub> and SiO<sub>2</sub> can provide better EOR displacement performance when dispersed within the propanol compared with Fe<sub>2</sub>O<sub>3</sub> due to their ability to reduce IFT and alter wettability. Bayat et al. [19] illustrated the role of TiO<sub>2</sub> deionized water-based nanofluid in increasing the flooding efficiency of EOR in carbonate rocks at different temperatures. Moreover, Saha et al. [24] obtained a significant reduction in IFT up to 66% from dispersing the silica NPs within the xanthan gum polymer in association with improving a cumulative oil recovery about 7.8% OOIP. Furthermore, fabricating composite of nanoparticles or modifying and coating their surfaces for EOR applications have been considered by some researchers. Ju and Fan [29] enabled to increase oil recovery using polymer coated-SiO<sub>2</sub> up to 21% due to the role of wettability alteration more than the effect of IFT reduction on the residual oil. Rezvani et al. [28] stated that using a fabricated Fe<sub>3</sub>O<sub>4</sub>/chitosan nanocomposite was successful in producing an extra 10.8% OOIP due to modifying the IFT and wettability behaviors. In addition, Qi et al. [27] could increase residual oil recovery by about 10% from coating the silica nanoparticles by polymer. They were not able to change the IFT and wettability significantly. However, Lim and Wasan [25] dispersed CuO in polyethylene glycol, and were not successful in producing an extra crude oil compared to the water-based nanofluid flooding. Meanwhile, Zhang et al. [16] dispersed SiO<sub>2</sub> in polyethylene glycol, and they enabled to produce more oil recovery ranged 17% by the combined effect of IFT reduction and wettability alteration. Ali et al. [12,30,31] obtained a huge reduction in IFT (93%), significant alteration in wettability towards a water-wet system and high improvement in oil recovery (19.3%) from using a green-synthesized ZnO/SiO<sub>2</sub>/xanthan nanocomposite due to creating better interactions between crude oil–polymer–nanoparticles–carbonate rocks.

The ultimate goal of this study was to synthesize a TiO<sub>2</sub>/Quartz nanocomposite for increasing EOR displacement performance of carbonate rocks. The surface of titanium nanoparticle was modified using substrate technique in order to improve its stability and to provide long term stability of nanofluids. Thus, the water-based nanofluids with different salinity ranges from dispersing the synthesized nanocomposite was developed for IFT reduction, wettability alteration, and improving oil recovery.


 Fig. 1. Schematic diagram of experimental steps and mechanism of developing  $\text{TiO}_2/\text{Quartz}$  NC.

**Table 4**  
 Formulation of fluid solutions used in this study.

| Sample  | NC conc. [ppm] | Water salinity [dilution level]   | Density [ $\text{gm}/\text{cm}^3$ ] | Description  |
|---------|----------------|-----------------------------------|-------------------------------------|--|
| DW      | 0              | Free                              |                                     | Distilled water  |
| DWN250  | 250            |                                   |                                     | Distilled water-based nanofluid with different NC concentrations         |
| DWN500  | 500            |                                   |                                     |  |
| DWN1000 | 1000           |                                   |                                     |  |
| HiSal   | 0              | High (no dilution)                |                                     |  |
| HSN250  | 250            |                                   |                                     | Seawater-based nanofluid with different NC concentrations                |
| HSN500  | 500            |                                   |                                     |  |
| HSN1000 | 1000           |                                   |                                     |  |
| MoSal   | 0              | Moderate (1:10 seawater dilution) |                                     |  |
| MSN250  | 250            |                                   |                                     | Moderate salinity water-based nanofluid with different NC concentrations |
| MSN500  | 500            |                                   |                                     |  |
| MSN1000 | 1000           |                                   |                                     |  |
| LoSal   | 0              | Low (1:20 seawater dilution)      |                                     |  |
| LSN250  | 250            |                                   |                                     | Low salinity water-based nanofluid with different NC concentrations      |
| LSN500  | 500            |                                   |                                     |  |
| LSN1000 | 1000           |                                   |                                     |  |

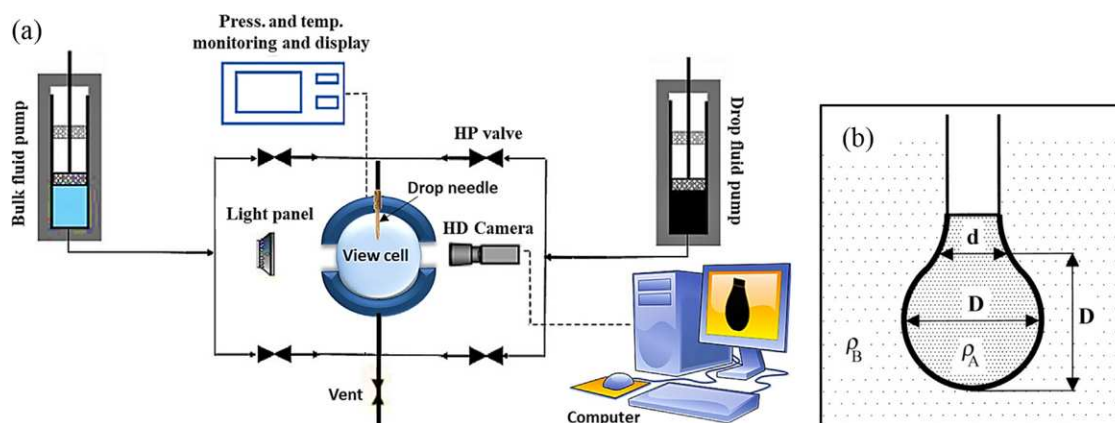


Fig. 2. Schematic presentation interfacial tension measurement; a) HPHT pendant drop IFT-400 apparatus, and b) shape of crude oil droplet [32].

## 2. Experimental section

### 2.1. Materials

Seawater ( $\text{pH} = 7.67$ ) was collected from Persian Gulf which contains various ionic concentrations and salt composition as shown in Table 2. The crude oil with the density of  $0.879 \text{ gm}/\text{cm}^3$  ( $29.5^\circ \text{ API}$ ) and viscosity of  $98.88 \text{ cP}$  was obtained from the Rag-e-Sefid oilfield in Iran for the contact angle, IFT, and flooding experiments (Table 3). The used crude oil was filtered with a  $5 \mu\text{m}$  mesh. A carbonate core sample

(length 8 m and diameter 3.7 cm; 75% dolomite and 25% calcite) was taken from the Asmari Outcrop in southwest of Iran for contact angle and displacement measurement tests. The porosity and permeability of the core sample were 12.8% and 13 mD, respectively. Other chemical reagents including salts and solvents of high-purity (about 99.5 mol%) were purchased from Merck and Aldrich chemical companies.

### 2.2. Synthesis and characterization of $\text{TiO}_2/\text{Quartz}$ nanocomposite

Titanium oxide NPs was synthesized from *euphorbia condylocarpa*

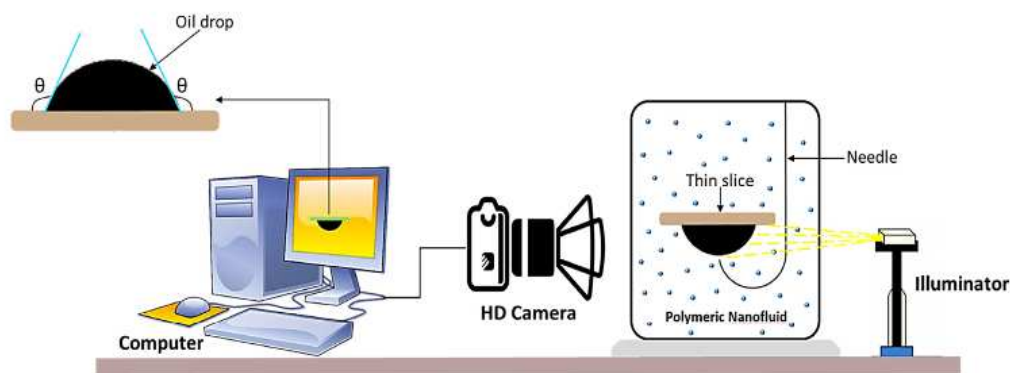


Fig. 3. Schematic illustration of sessile drop method for contact angle measurements [31].

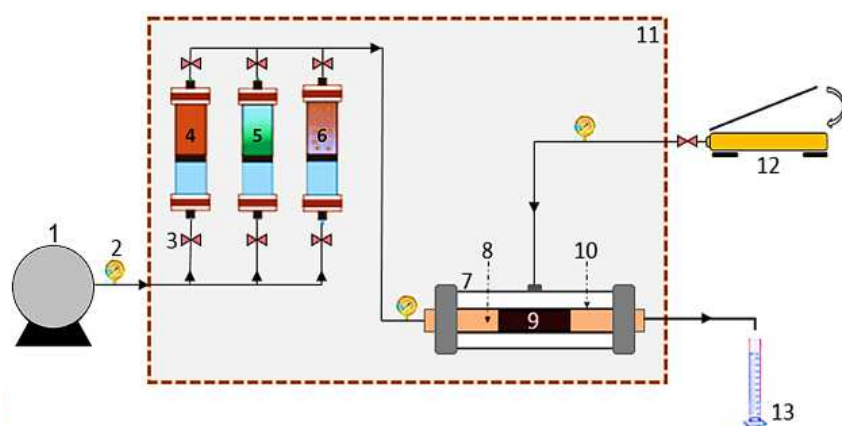


Fig. 4. Schematic illustration of the apparatus for oil displacement tests: (1) HPLC pump, (2) pressure gauges, (3) valves, (4) cylinder containing crude oil, (5) cylinder containing brine, (6) cylinder containing nanofluid, (7) core holder chamber, (8) fluid flow distributor, (9) core, (10) blocking rubber around the core, (11) oven, (12) manual hydraulic pump, and (13) outlet fluid collecting vessel [31].

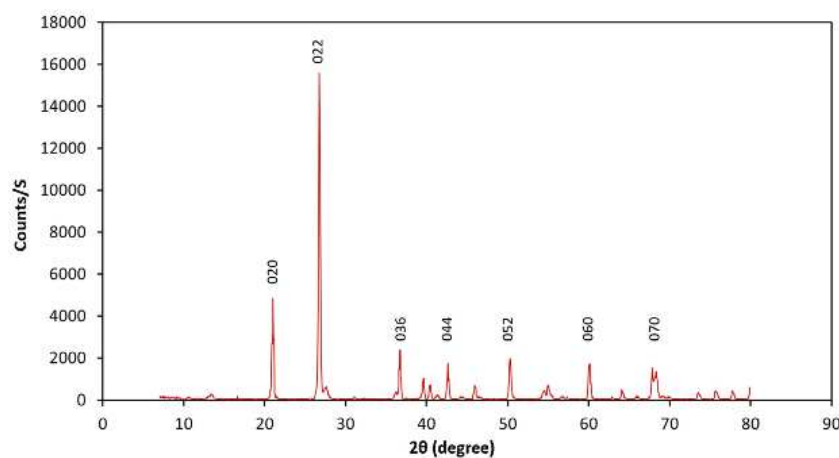


Fig. 5. XRD pattern of synthesized  $\text{TiO}_2$ /Quartz nanocomposite.

extract in a green way then was combined in a composite with the quartz (Fig. 1). First, 400 mL of plant extract was collected in a beaker and 6 g of  $\text{TiO}(\text{OH})_2$  was mixed with it by stirring until a dark brown-greenish formation become precipitated. The precipitate was then filtered from the solution and heated up to 600 °C using a furnace to burn all the remained plant particles. Afterwards, the burned precipitate was washed to remove the impurities and dried at room temperature. The clean obtained  $\text{TiO}_2$  was mixed with 12 g of quartz powder using mortar

and pestle, and under reflux for 3 hr at 80 °C. Finally, the dried and cleaned  $\text{TiO}_2$ /quartz NC was collected and characterized to be used for EOR applications. In order to identify the accuracy of the synthesized nanocomposite, X-ray diffraction (XRD) and Fourier transform infrared spectroscopy (FTIR) analytical approaches were used to study the mineralogical composition of prepared nanomaterial. Moreover, scanning electron microscope (SEM) technique was used to characterize the size and shape of  $\text{TiO}_2$  NPs on quartz as a substrate.

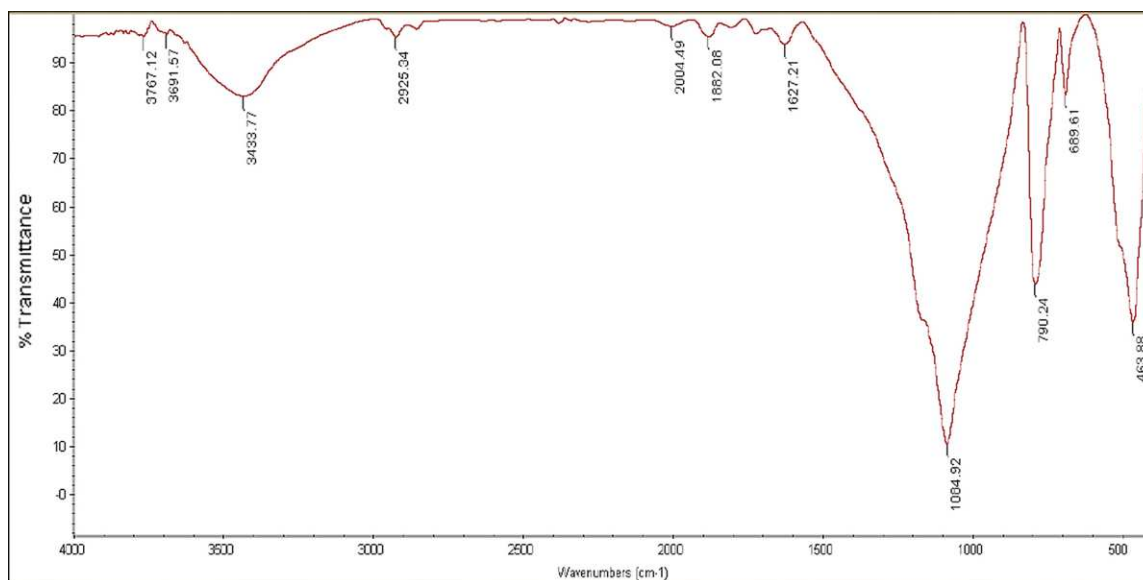


Fig. 6. FTIR spectrum of synthesized  $\text{TiO}_2/\text{Quartz}$  nanocomposite.

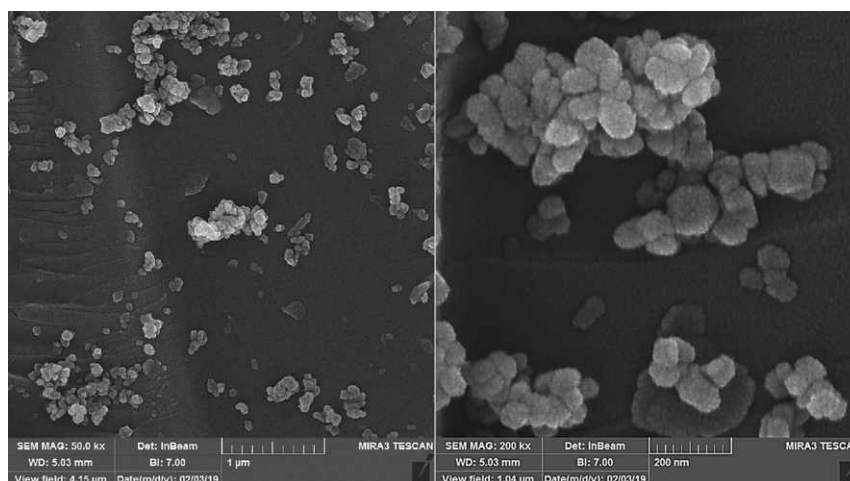


Fig. 7. SEM micrographs of  $\text{TiO}_2/\text{Quartz}$  NC at 1  $\mu\text{m}$  and 200 nm.

### 2.3. Nanofluid preparation and characterization

Novel nanofluids used in the current study were designed using various concentrations of  $\text{TiO}_2/\text{Quartz}$  nanocomposite (250, 500, and 1000 ppm). Initially, nanofluid solutions were prepared using seawater (high salinity) and distilled water (DW) as base fluids (Table 4). On the basis of salting-out approach, the salinity of seawater was lowered by 10 and 20 times dilutions (1:10 and 1:20) for developing the low salinity water-based nanofluid (LSN) [17,35]. For each dilution, we added 100 mL of distilled water into a liter of seawater. A magnetic stirrer (LABINCO L81) at 600 rpm for 6 h was used to prepare nanofluids with keeping the operating temperature below 30 °C.

Nanofluids used in this study were mixed using ultrasonic mixer (VIP 200HD) waves for 2 h at 400 W to obtain high dispersion stability of  $\text{TiO}_2/\text{Quartz}$  nanocomposite (NC). First, the visual observation was considered for checking the stability of the NC dispersed in different

water solutions, wherein the developed nanofluids were monitored through transparent vessels during various time periods. In addition, the density, viscosity, conductivity and pH behaviors of the prepared nanofluids were measured at ambient temperature and pressure using PAAR density meter, Brookfield DV2T viscometer, Mettler Toledo S230, and WTW™ inoLab™ Cond 7310, respectively.

### 2.4. Interfacial tension measurement

Interfacial tension of the crude oil-nanofluid system was measured using the interfacial tension apparatus (IFT-400) on the basis of the pendant drop procedure (Fig. 2a). In this way, the image and volume of suspended droplet of crude oil within the nanofluid can be estimated (Fig. 2b). The actual value of IFT for a liquid–liquid system can be measured from the droplet image received in computer using a typical software dependent on the below equation [51]:

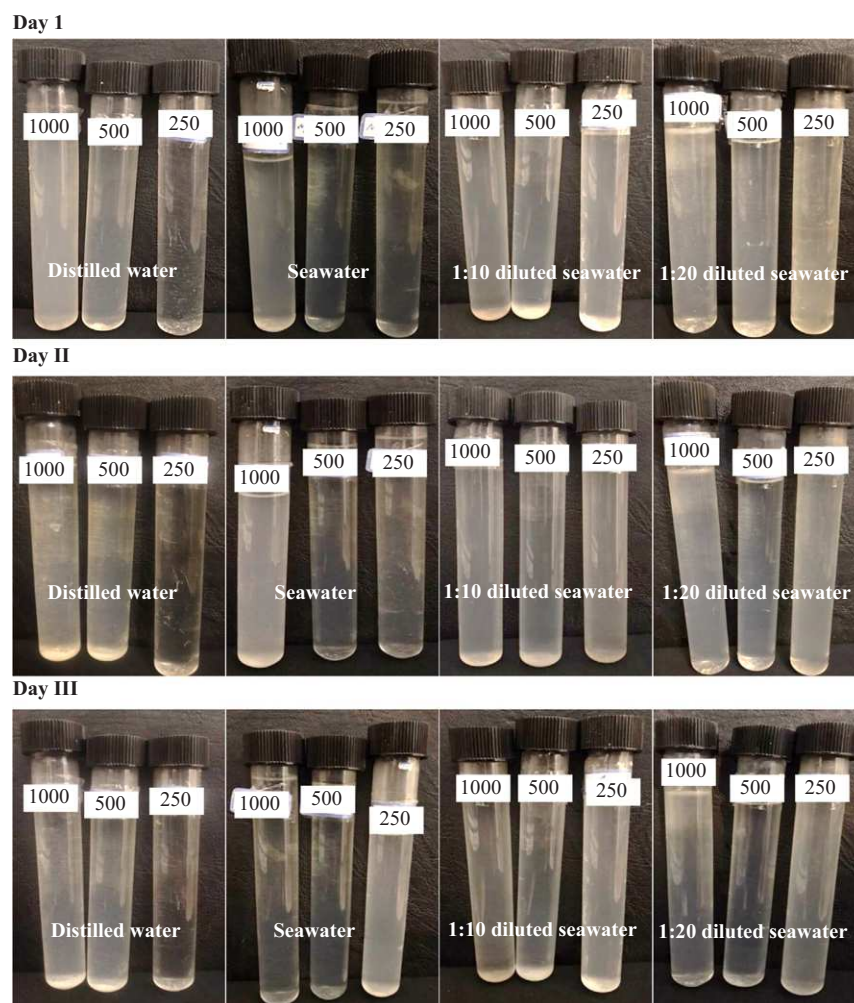


Fig. 8. Dispersion stability of prepared nanofluids at different NC concentrations (250, 500 and 1000 ppm) and different salinity level of water (seawater, 1:10 diluted seawater, and 1:20 diluted seawater) after three days.

$$\gamma = \frac{\Delta\rho \cdot g \cdot D}{H} \quad (1)$$

where  $\Delta\rho$  is the difference between the density of the drop and bulk fluids ( $\text{gm}/\text{cm}^3$ ),  $g$  is the gravitational acceleration of the earth ( $\text{cm}/\text{sec}^2$ ),  $D$  is the large diameter of the droplet (cm), and  $H$  is the droplet shape factor.

Initially, IFT of crude oil and various water solutions with different salinity ranges without the presence of nanomaterial was measured. Then, the same procedure was applied to measure the IFT between crude oil and various nanofluid solutions with different salinity ranges and NC concentrations. All the IFT measurements of different liquid-liquid systems were carried out at different conditions of temperature (30, 50 and 70 °C) and pressure (500, 1000 and 1500 psi).

### 2.5. Contact angle measurement

In this study, the sessile drop technique was used to measure the contact angle between crude oil and various water-based nanofluids with different NC concentrations and salinity ranges on the surface of the carbonate rocks (Fig. 3). Smooth pellets of carbonate rock were

prepared from cutting the rock plugs into thin sections in 2 mm, and carefully polished and cleaned by distilled water and toluene to remove all the possible surface impurities. In addition, the trimmed carbonate pellets were aged by immersing and leaving inside the crude oil at temperature of 70 °C for 12 days. The contact angle of the crude oil droplet on carbonate rocks was estimated under the static condition submerging the prepared rock slices in enclosed containers filled with nanofluid solutions for 3 days.

### 2.6. Oil displacement experimental set-up and procedure

Core flooding set-up consists mainly fluids, a core holder, pumps, and output collector as shown schematically in Fig. 4. The selected fluid from the cylinder can be pumped into the core holder chamber using a HPLC pump, wherein injects the hydraulic fluid to the piston rears of cylinders. In this work, crude oil, brine, and nanofluid were stored in the three cylinders which are placed inside an oven along with a core holder. The core holder chamber itself consists of two parts of the fluid flow (inlet and outlet), and a special rubber to block the fluid flow around 1.5" plug, which is operated by a hydraulic fluid pump manually. The outlet fluid is usually stored in a special fluid collection vessel

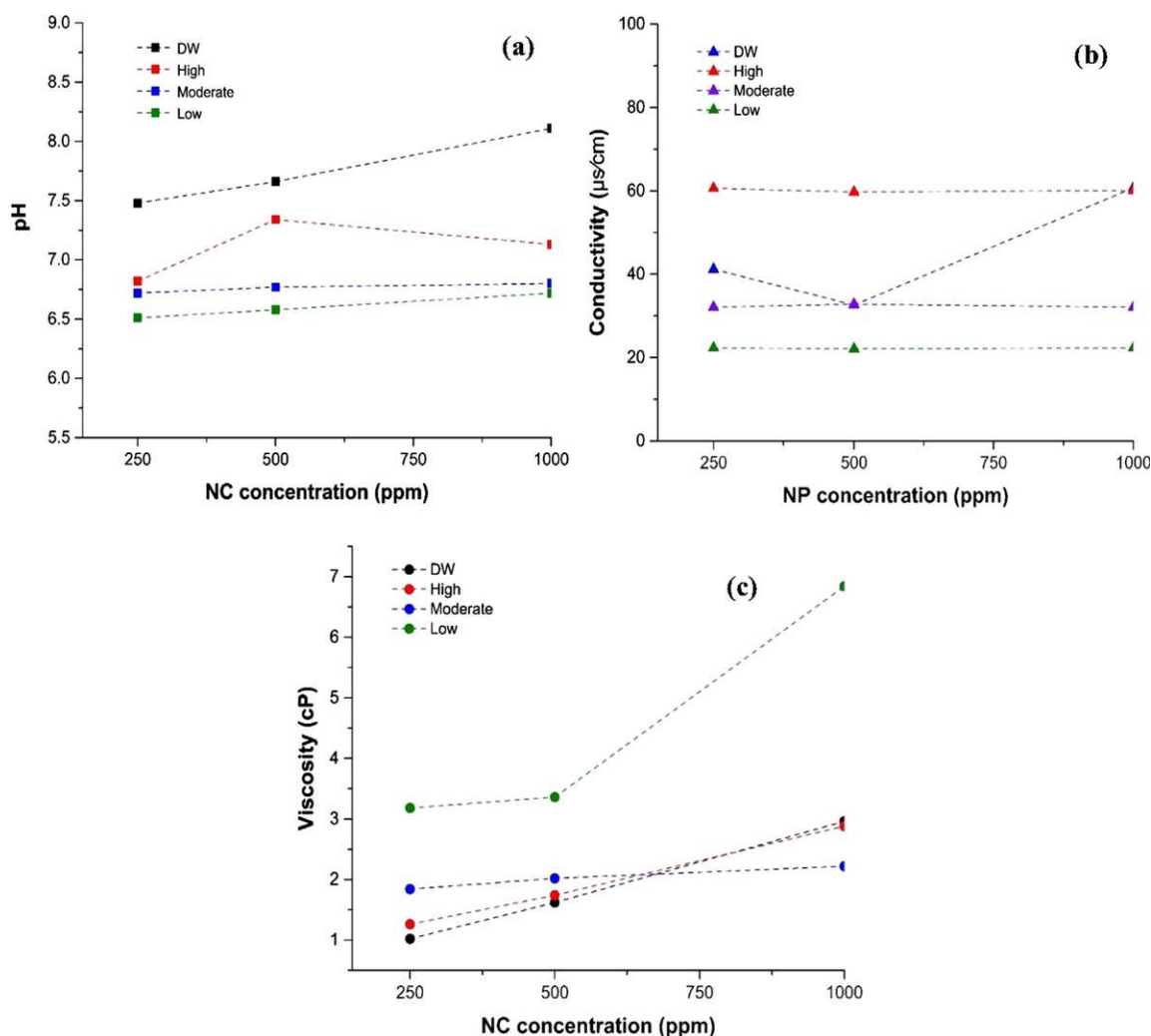


Fig. 9. Characteristics of polymeric nanofluids at 250, 500, and 1000 ppm NC concentrations and free, low, moderate and high salinities; (a) pH, (b) conductivity, and (c) viscosity.

from the camper output line. Composition of carbonate rock plugs used in oil displacement tests were collected from the Asmari Formation outcrop in Iran. All the presence water, oil and other residues were removed from the collected plugs by ethanol and toluene using a Soxhlet extraction at temperature between 60 and 80 °C for 24 h. The core samples were then placed into an oven at 70 °C for 6 h in order to be dried. Afterward, core displacement tests were conducted using brine as a secondary recovery, and DWN1000, HSN1000, MSN1000 and LSN1000 nanofluids as tertiary recovery prepared by dispersing 1000 ppm of  $\text{TiO}_2$ @Quartz NC within distilled water and seawater with dilutions. Tests were performed at 75 °C and 1400 psi with the injection rate of 0.5  $\text{cm}^3/\text{min}$ ; initially, water about 1.5 pore volumes (PV) was injected into the core plugs under controlled flow rate, in which two pressure transducers were used to record the pressure values at the injection and production points, and 1.5 PV of nanofluids injected to the core plugs with collecting the displaced volume of crude oil.

## 2.7. Emulsification behavior

In this section, according to Ali et al. [31] and Ghosh and Bandyopadhyay [57], the emulsification stability analysis was considered for the crude oil–various nanofluid systems prepared by dispersing 250, 500 and 1000 ppm NCs within distilled water, seawater and low-salinity water. For this purpose, the prepared samples of 3:7 (v/v) emulsions were maintained in an aqueous phase by shaking for 30 min using an orbital shaker. The produced samples were then collected in transparent cylinders and observed visually over different time-steps.

## 3. Results and discussion

### 3.1. Characterization of $\text{TiO}_2$ /Quartz nanocomposite

In order to identify the synthesized nanocomposite, XRD, FTIR and SEM analyses were conducted. The pattern of XRD analysis on  $\text{TiO}_2$ /Quartz NC indicate the main peaks associated with the crystalline planes of pure  $\text{TiO}_2$  and phase purity of nanoparticles deposited on the

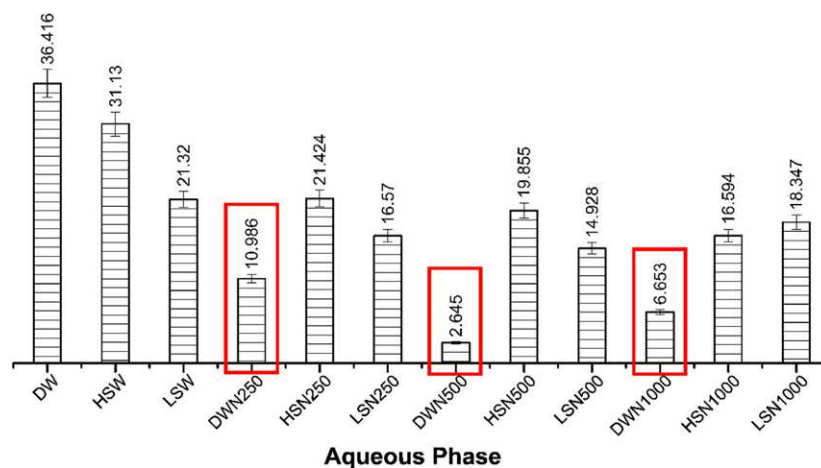


Fig. 10. IFT of oil-various aqueous phase systems with different salinities and NC concentrations measured at both LTLF and HTHP conditions of reservoirs.

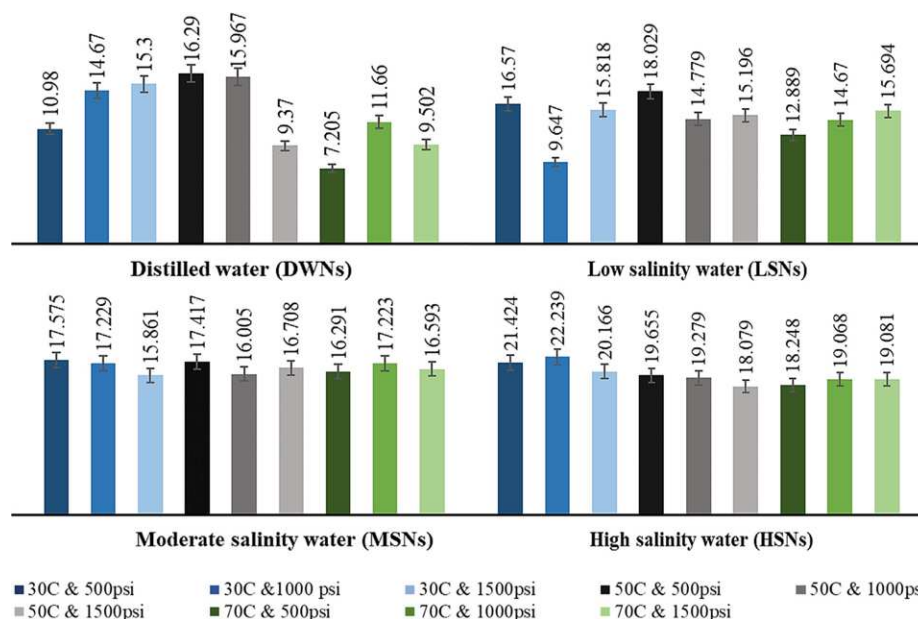


Fig. 11. The effects of pressure and temperature on IFT reduction at 250 ppm  $\text{TiO}_2/\text{Quartz}$  NC concentration for different nanofluids solutions prepared by distilled water, low salinity water (1:20 seawater dilution), moderate salinity water (1:10 seawater dilution) and high salinity water.

surface of the quartz (Fig. 5). The noticed peaks (020, 022, 036, 044, 052, 060 and 070) with the reflections vary between 20 and 70° are in standard with the peaks of  $\text{TiO}_2$  and quartz reported in the literature [36–40]. In addition, Fig. 6 illustrates the FTIR spectrum of  $\text{TiO}_2/\text{Quartz}$  nanocomposite, which contains a broad band between 1084.9 and 3433.8  $\text{cm}^{-1}$  to represent the O–H stretching vibration of incomplete salt groups (Ti–OH) with the consideration of the remaining absorbed water. However, the vibration's peaks between 463.9 and 1084.9  $\text{cm}^{-1}$  belonged to the nanocomposite stretching modes. These results provide an evidence of a successful synthesis process of nanocomposite [40–43].

For further confirmation of the green synthesis of  $\text{TiO}_2/\text{Quartz}$  NC, the morphology analysis was carried out using SEM. Fig. 7 presents the SEM morphology of the synthesized NC at 1  $\mu\text{m}$  and 200 nm. According to the SEM micrographs of  $\text{TiO}_2$  and quartz reported by Ze et al. [37],

Selli and Tunali [45], and Mahalingam et al. [44], the morphology of the synthesized NC with the various sizes below 100 nm were observed. In the figure, the particles were prepared with the formation of clusters with a random distribution of the  $\text{TiO}_2$  on the surface of quartz.

### 3.2. Nanofluid characterization

Stability of the dispersed nanomaterial within the nanofluid solution is one of the important characteristics of the injection nanofluid. First, the dispersion stability of  $\text{TiO}_2/\text{Quartz}$  NC was observed by monitoring the papered nanofluids through transparent cylinders for three days. During this period, no sedimentation of the nanocomposite in the bottom of cylinders can be seen. Hence, in accordance to Chen and Xie [46], Yu and Xie [47], it can be stated that the high stability was achieved for all nanofluids (DWN250, DWN500, DWN1000,

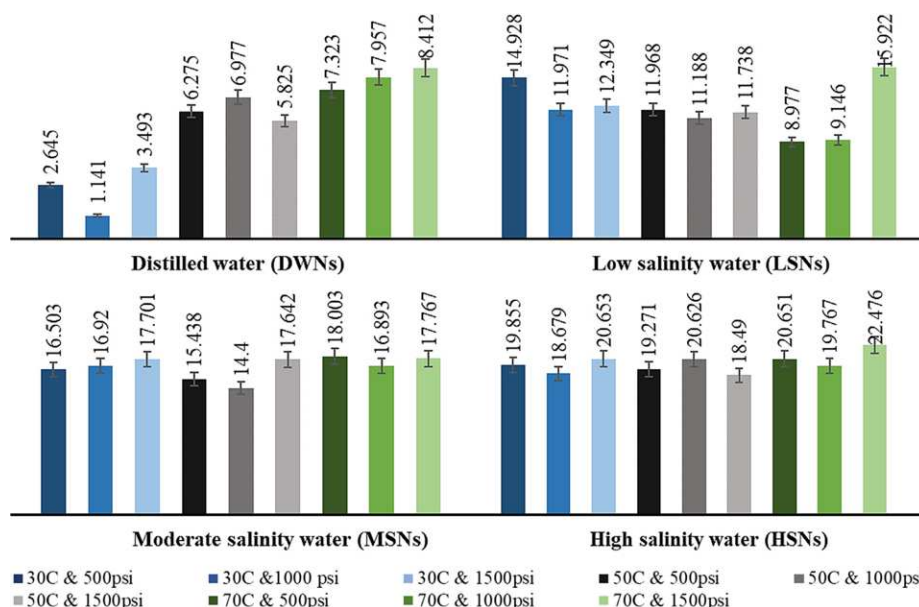


Fig. 12. The effects of pressure and temperature on IFT reduction at 500 ppm TiO<sub>2</sub>/Quartz NC concentration for different nanofluids solutions prepared by distilled water, low salinity water (1:20 seawater dilution), moderate salinity water (1:10 seawater dilution) and high salinity water.

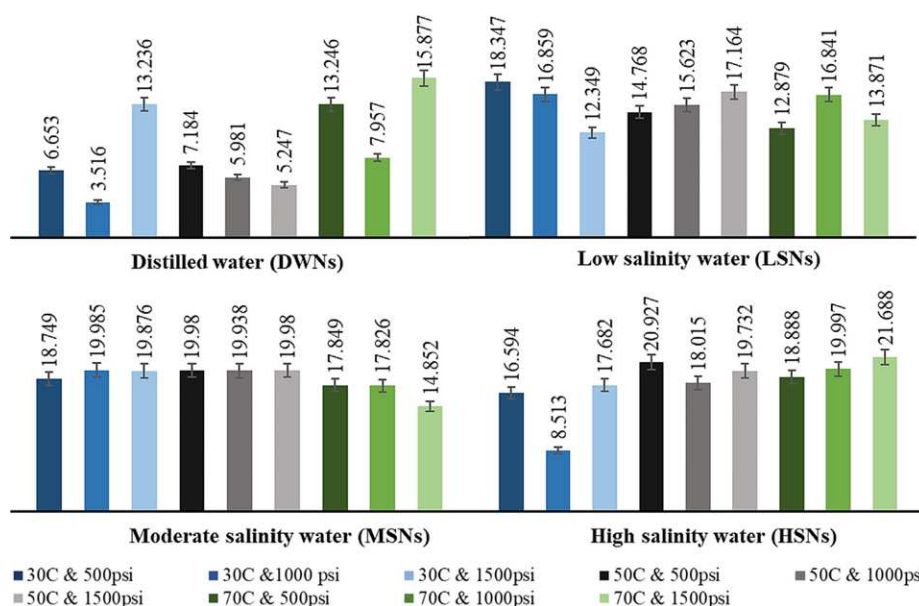


Fig. 13. The effects of pressure and temperature on IFT reduction at 1000 ppm TiO<sub>2</sub>/Quartz NC concentration for different nanofluids solutions prepared by distilled water, low salinity water (1:20 seawater dilution), moderate salinity water (1:10 seawater dilution) and high salinity water.

HSN250, HSN500, HSN1000, MSN250, MSN500, MSN1000, LSN250, LSN500 and LSN1000) at different concentrations of nanocomposite (250, 500 and 1000 ppm) and different salinity level of water (seawater, 1:10 diluted seawater, and 1:20 diluted seawater) as shown in Fig. 8.

In addition, as it is clear that the pH of a colloidal solution significantly influences the particle aggregation and the suspension stability [49,50]. Fig. 9a shows the pH values of the nanofluids used in this study, wherein pH varied from 6.5 to 8 which indicates a stable

consistency between the nanofluids, except for distilled water. Meanwhile, the conductivity readings of the prepared nanofluids are shown in Fig. 9b. As it can be seen, the conductivity was basically increased with increasing the salinity of the solutions and not affected by NC concentration. Conductivities of LSN, MSN and HSN were about 20, 32 and 60 μS/cm and were not changed with increasing the NC concentration, respectively. However, the conductivity for DWN was changed depending on the NC concentration from 40 to 60 μS/cm. Furthermore, since its crucial for controlling the mobility ratio, sweep

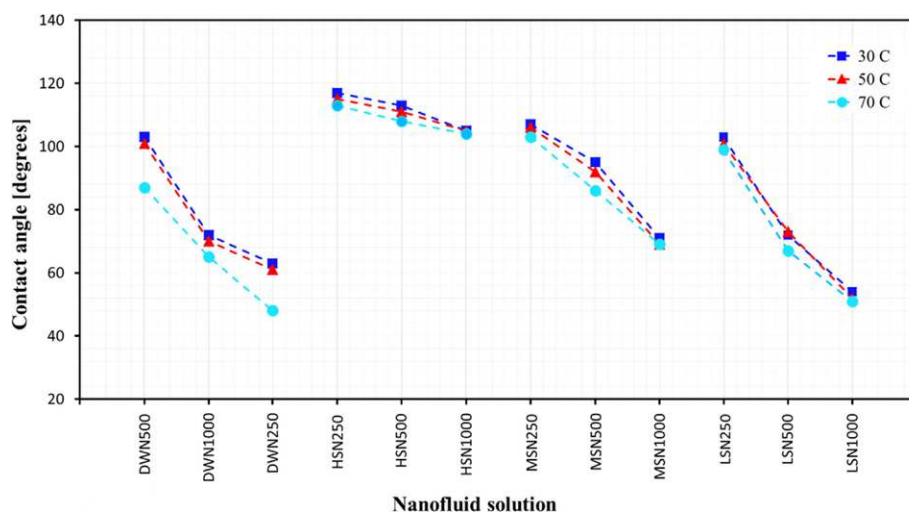


Fig. 14. Measured contact angles between crude oil and various aqueous phases (SSW, LoSal, PNs and LPNs).

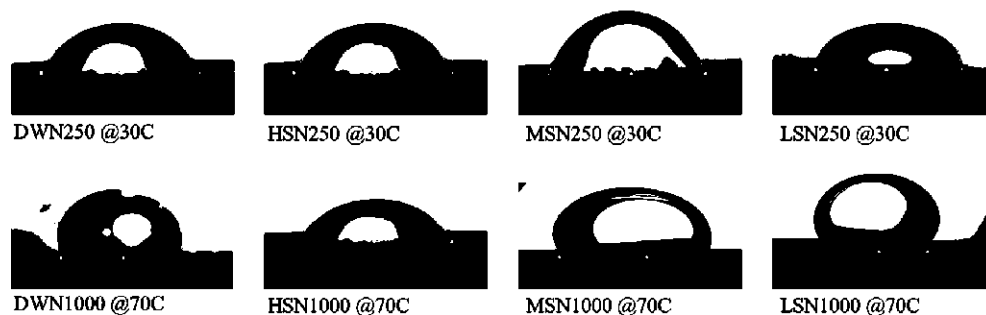


Fig. 15. Oil droplet images on several carbonate pellets present variations in contact angles between (i) SSW and LoSal water, (ii) PNs and LPNs with 500, 1000, and 2000 ppm NC concentrations.

**Table 5**  
Summary of the oil displacement tests.

| Core   | Porosity[%] | Perm. [mD] | PV [cm <sup>3</sup> ] | S <sub>wi</sub> [%] | Nanofluid | Oil recovery [%OOIP] |          | Total oil recovery [%OOIP] |
|--------|-------------|------------|-----------------------|---------------------|-----------|----------------------|----------|----------------------------|
|        |             |            |                       |                     |           | Secondary            | Tertiary |                            |
| Plug#1 | 14.1        | 7.71       | 11.18                 | 27                  | DWN1000   | 37                   | 21       | 58                         |
| Plug#2 | 12.2        | 6.4        | 10.25                 | 25.3                | HSN1000   |                      | 10       | 47                         |
| Plug#3 | 12.14       | 7.1        | 10.38                 | 26                  | MSN1000   |                      | 12       | 49                         |
| Plug#4 | 13          | 8.3        | 10.93                 | 27.4                | LSN1000   |                      | 17       | 54                         |

efficiency and EOR efficiency, the viscosity of nanofluids has been also measured. Fig. 9c shows the effect of the TiO<sub>2</sub>/Quartz NC on the viscosity of the injection fluids. The viscosity of displacing fluid was increased with increasing the concentration of synthesized NC for various salinity ranges; distilled water, low salinity, moderate salinity and high salinity. As it can be seen that the effect of NC concentration on the nanofluid viscosity was significantly higher compared with other nanofluids, which was increased from 3.2 to 7 Cp. This improvement in nanofluid viscosity was crucial for minimizing the mobility ratio and improving the sweep efficiency. On the basis on this with the support of [51], the LoSal nanofluid with 1000 ppm NC concentration (LSN1000) can be selected as the best EOR displacing candidate.

### 3.3. IFT reduction

IFT values of different crude oil–water and crude oil–nanofluid systems have been measured at ambient temperature and pressure as shown in Fig. 10. Several aqueous phases were used based on the salinity and nanocomposite concentration. From the figure, it can be seen that the initial IFT values measured for distilled water (DW), seawater (HSW) and low salinity water (LSW) were about 36.416, 31.13 and 21.32 mN/m, respectively. It is clear that the IFT of oil–seawater was highly reduced by reducing the seawater salinity by 20 times dilution, which is quite consistent with the explanation of Nowrouzi et al. [51,52,53] and Manshad et al. [54,55,56] where they described the effect of different densities and ionic compounds of the seawater on the IFT reduction and reported that diluting the seawater

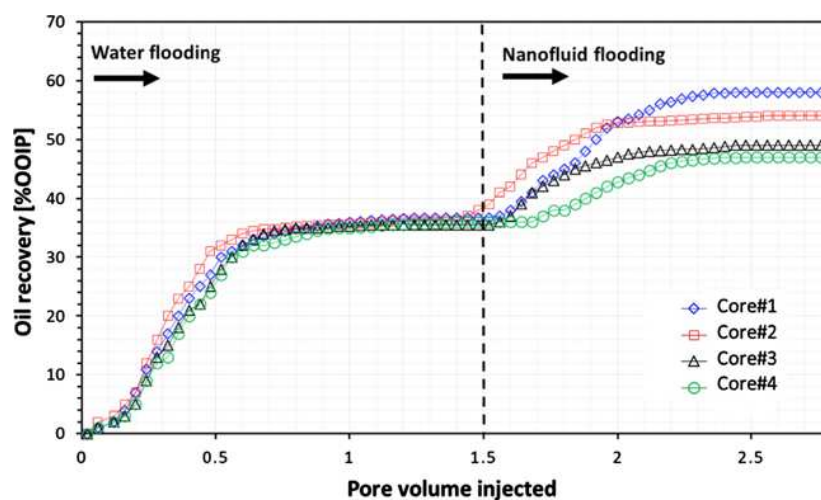


Fig. 16. Production profiles of water and LoSal-polymeric nanofluid flooding as a function of injected PV.

reduces the IFT, effectively. Afterward, the synthesized  $\text{TiO}_2/\text{Quartz}$  NC with 250, 500 and 1000 ppm concentrations have been added to the distilled water and seawater with various salinity ranges, and the IFT between crude oil and nanofluids (DWN, HSN and LSN) was measured, which was ranged between 2.645 and 21.424 mN/m. In this section of the experiment, we enabled to minimize the IFT by about 92.7% from 36.416 to 2.645 mN/m by the effect of synthesized NC and its concentration. This observation agrees with Choi et al. [26] and Qi et al. [27], which they stated that a layered structure develops by the presence of the nanoparticles at the interface between the crude oil and polymeric nanofluids, which reduces the IFT. This mechanism will become more effective and stronger by increasing the concentration of polymer coated nanoparticles. In this work,  $\text{TiO}_2/\text{Quartz}$  was more effective the distilled water compared to the seawater-based nanofluids for all the three different nanocomposite concentrations, and the minimum value IFT has been obtained for between crude oil and distilled water with 500 ppm NC concentration. According to Al-Ansari et al. [10], the selected percentage error of IFT measurement was  $\pm 5\%$ .

Figs. 11–13 illustrate the effects of pressure and temperature on IFT reduction at different NC concentrations and water salinity ranges. In this work, the experiments were performed at 30, 50 and 70 °C and 500, 1000 and 1500 psi. The impact of temperature on IFT reduction is stronger compared with the effect of pressure. When adding 250 ppm of  $\text{TiO}_2/\text{Quartz}$  NC into the distilled water, its IFT was significantly reduced by about 69.8% from 36.14 to 19.986 mN/m, however, this value was changed with increasing the temperature and pressure (Fig. 11). Generally, IFT was increased with increasing pressure, and less reduction in its value achieved under the effect of nanocomposite. While, the temperature had a stronger impact on IFT compared with the pressure, and it resulted more reduction in the IFT value, for example from increasing the temperature from 30 to 70 °C, IFT between oil-DWN250 was reduced from 10.98 to 7.205 mN/m and increased again to 9.502 mN/m when subjected to higher pressure (1500 psi). Additionally, for all three other kinds of nanofluids (LSNs, MSNs and HSNs) the IFT value was rarely reduced by adding 250 ppm of NC, and remained almost constant under the effect of pressure and temperature except for the low salinity water-based nanofluid.

Fig. 12 shows the IFT values measured between crude oil and different nanofluids with the 500 ppm nanocomposite concentration under the effects of temperature and pressure. As it is obvious, the lowest IFT about 2.645 mN/m was achieved when the crude oil was immersed in the DWN500 solution under the ambient temperature and pressure

condition, which was more reduced to 1.14 mN/m with increasing the pressure to 1000 psi. However, it was again increased with increasing temperature and pressure up to 8.412 mN/m. For the crude oil and LSNs systems, the IFT was also reduced but gradually and not effectively when NC concentration was increased to 500 ppm; even the effect of temperature and pressure was also very low. Particularly, for both MSNs and HSNs, IFT value almost remained the same when increasing the NC concentration to 500 ppm with no changes due to the impacts of pressure and temperature.

Lastly, with dispersing 1000 ppm of  $\text{TiO}_2/\text{Quartz}$  within the different saline waters, only a desirable reduction of IFT was obtained with the distilled water-based nanofluid (DWN1000), but still lower than the minimum value achieved with the DWN500 (Fig. 13). IFT value was also influenced by the impact of the temperature and pressure. Unlike, the similar trends of IFT reduction were achieved for LSN1000, MSN1000 and HSN1000 nanofluids as with 250 and 500 ppm in previous cases.

### 3.4. Wettability alteration

The contact angle of the several aqueous systems was measured to describe the wettability behavior of the carbonate thin sections with and without the presence of the synthesized nanocomposites. In this section, the effect of  $\text{TiO}_2/\text{Quartz}$  on the value of the contact angle while using distilled water, seawater, and diluted seawater (1:10 times and 1:20 times) has been discussed in details. Fig. 14 illustrates values of contact angles measured under the effect of nanocomposite, salinity and temperature. Basically, the initial contact angle measurements showed a strong oil-wet system on the carbonate pellets for all different solutions with 250 ppm NC concentration. The maximum contact angle was measured when the aged thin section was submerged into the seawater-based nanofluid with 250 ppm NC (HSN250), which was about 117°. Generally, the effect of  $\text{TiO}_2/\text{Quartz}$  on the wettability alteration was very weak while using seawater, and the contact angle was only reduced by about 10.25% from 117° to 105° with increasing the NC concentration from 250 to 1000 ppm. However, an effective reduction in contact angle was noticed when diluting seawater by 10 and 20 times. Under the same experimental condition and NC concentration, contact angle was reduced by about 33.6% with 1:10 dilutions and 47.5% with 1:20 dilutions of seawater. From the obtained results in accordance to Sharma et al. [23], the synthesized nanocomposite was more effective with low salinity water compared with high salinity waters and enabled to alter the wettability of the carbonate rock from

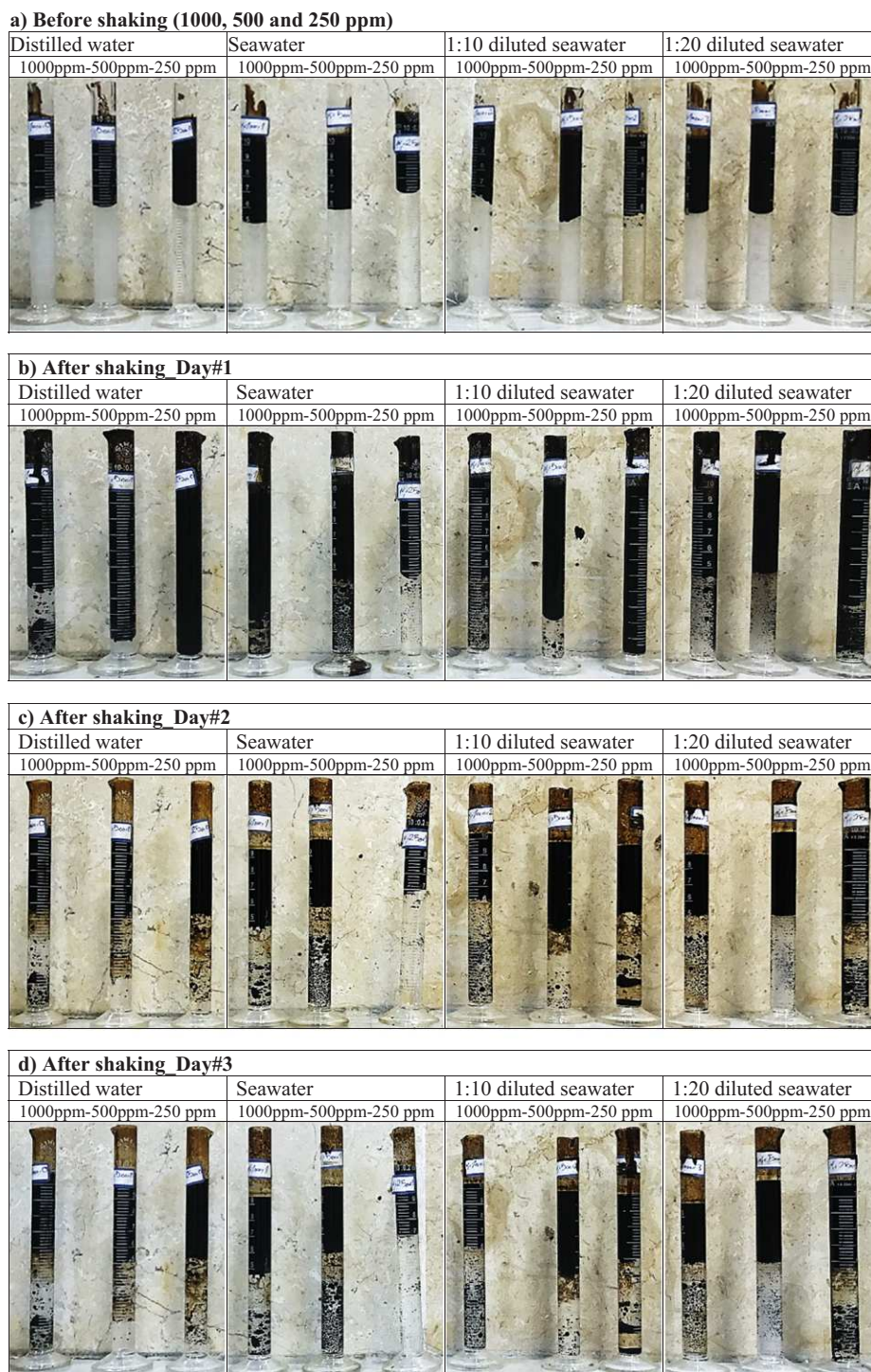


Fig. 17. Emulsification behaviour of crude oil-nanofluid systemes with various salinity ranges (distilled water; low-salinity water; moderate-salinity water; high-salinity water), and NC concentrations (250, 500 and 1000 ppm).

the oil-wet to water-wet system. Additionally, to study the wettability condition of the carbonate rock under the consequence of TiO<sub>2</sub>/Quartz NC without the presence of the salinity effect, the developed NC has been added into the distilled water (DW) in different concentrations of 250, 500 and 1000 ppm. For this purpose, the carbonate pellets were treated with prepared DW based-nanofluid (DWN250, DWN500 and DWN1000), and after 3 days the contact angle measurements for the crude oil on these pellets were performed. As it can be seen in Fig. 14, determined values of contact angles between oil/DWN250, oil/DWN500 and oil/DWN1000 nanofluids were about 103°, 72°, and 63° under 30 °C, respectively.

Furthermore, in order to identify the effect of the synthesized NC on wettability alteration under the high temperature condition, contact angle measurements have been conducted at 30, 50 and 70 °C temperatures (Fig. 14). With increasing the temperature, the reduction in contact angle was increased for all the nanofluid solutions. While, the impact of NC on the contact angle reduction for the DW-based nanofluid was higher compared with other water-based nanofluids under high temperature condition. Wherein, the minimum value of contact was achieved for crude oil/DWN1000 system ranged about 48°. Thus, according to Al-Ansari et al. [10] and Rezvani et al. [28], the wettability behavior was altered from the oil-wet to water-wet system from utilizing DWN-1000 nanofluid containing 1000 ppm of developed TiO<sub>2</sub>/Quartz nanocomposite. In order to better understand the influences of the salinity, NC concentration and temperature on the wettability alteration, contact angles of crude oil droplet on several carbonate slices aged in DWNs, HSNs, MSNs and LSNs have been illustrated schematically in Fig. 15. As it can be seen in the figure, oil droplets were strongly adsorbed by the carbonate surface with adding 250 ppm of NC into the DW, HSW, MSW and LSW at 30 °C. However, more-free oil can be seen on the carbonate slices when the concentration of NC was increased to 1000 ppm and temperature to 70 °C.

### 3.5. Oil displacement and emulsification

Oil displacement experiments were performed from injecting water as a secondary recovery process and nanofluid as tertiary recovery technique with a constant injection rate of 0.5 cm<sup>3</sup>/min to several carbonate core plugs (Table 5). For this purpose, four plugs with the porosity about 12–14% and permeability ranges between 6 and 8.5 mD have been used. Initially, brine was injected into the four prepared plugs separately, which enabled to extract crude oil about 37% OOIP.

The injection theme and oil recovery across core plugs is shown in Fig. 16. HSN1000 nanofluid composed of 1000 ppm NC dispersed in seawater was then injected into core#2 in order to improve the oil recovery factor, and an additional 10% OOIP has been produced. A nanofluid prepared from dispersing 1000 ppm NC within 1:10 diluted seawater has been pumped into core#3 and increased oil recovery up to 49% OOIP. In order to observe the impact of TiO<sub>2</sub>/Quartz NC with low salinity water, LSN1000 nanofluid prepared from mixing 1000 ppm NC within 1:20 diluted seawater and injected into core#4. From low-salinity nanofluid flooding, better improvement in oil recovery was achieved ranged about 54%. According to the high performance of synthesized NC achieved with distilled water in reducing IFT and altering the wettability, the distilled water based-nanofluid was also suggested to be applied in enhancing oil recovery. We thus pumped LSN1000 nanofluid to core#1, which was successfully enabled to increase oil recovery up to 58% OOIP. As it can be seen the maximum oil recovery factor was achieved with injecting distilled water based-nanofluid with 1000 ppm TiO<sub>2</sub>/Quartz nanocomposite.

### 3.6. Emulsification behavior

Furthermore, the emulsification visibility between crude oil and different nanofluids has been studied. Fig. 17 illustrates oil-nanofluid emulsification behavior for distilled water, seawater and its dilutions

with 250, 500 and 1000 ppm NC concentrations at different time steps during 3 days. Basically, various emulsification stability limits have been achieved dependent on the NC concentration and nanofluid salinity. As it can be seen, after shaking the emulsions for 30 min, the stability of some systems was quickly reduced to a certain level during the first day, for instance SWN250 nanofluid of 250 ppm NC dispersed in seawater (Fig. 17b). At the same time, a strong emulsion of oil-nanofluid system was observed with the DWN250, MSN250 and LSN250 solutions. During time, the emulsification was reduced and more separation of phases was noticed, especially, for SWN250 nanofluid and other water based nanofluids with 1000 ppm NC concentration (Fig. 17c and d). Thus, for distilled, moderate-salinity and low-salinity waters, better separation of phases was achieved with increasing the NC concentration. This is true in accordance with Ghosh and Bandyopadhyay [57], wherein they stated that with increasing the concentration of the synthesized NC, emulsion stability improved due to the better adsorption of the nanocomposite on oil droplets and occurring isolation between oil droplets. However, for seawater, a complete phase separation was identified with low NC concentration and high emulsification with 1000 ppm NC.

## 4. Conclusions

This work described a new green technology to develop a novel nanofluid using TiO<sub>2</sub>/Quartz nanocomposite for enhanced oil recovery applications. TiO<sub>2</sub>/Quartz NC was synthesized from *euphoria condylocarpa* extract in a green and economical way, and characterized using XRD, FTIR and SEM analytical techniques. The following major conclusions can be drawn on the basis of the results obtained from this study:

- High suspension stability of SiO<sub>2</sub>/Quartz NC in water at different salinity ranges was achieved for the long time.
- DWN and LSN nanofluids presented an excellent rheology and interfacial activity due to the effects of synthesized NC and salinity.
- Developed DWNs and LSNs enabled to alter the wettability of the carbonate rock from oil-wet system to a strong water-wet system.
- DWN1000 and LSN1000 injections improved the cumulative oil recovery by about 21 and 17% OOIP, respectively.
- This preparation method could be widely applied to acquire novel nanofluids, which shows great potential for EOR applications in carbonate reservoirs.

## References

- [1] Cheng Y, Zhao M, Zheng C, Guo S, Li X, Zhang Z. Water-dispersible reactive nanosilica and poly(2-acrylamido-2-methyl-1-propanesulfonic acid sodium) nanohybrid as potential oil displacement agent for enhanced oil recovery. *Energy Fuels* 2017;31:6345–51.
- [2] Jha N, Iglauer S, Barifcani A, Sarmadivaleh M, Sangwai JS. Low-salinity surfactant nanofluid formulations for wettability alteration of sandstone: role of the SiO<sub>2</sub> nanoparticle concentration and divalent cation/SO<sub>4</sub><sup>2-</sup> Ratio. *Energy Fuels* 2019;33:739–46.
- [3] Naik S, You Z, Bedrikovetsky P. Productivity index enhancement by wettability alteration in two-phase compressible flows. *J Natural Gas Sci Eng* 2015;26:1573–84.
- [4] Naik S, You Z, Bedrikovetsky P. Rate enhancement in unconventional gas reservoirs by wettability alteration. *J Natural Gas Sci Eng* 2017;50:101–14.
- [5] Youssif MI, El-Maghraby RM, Saleh SM, Elgibaly AA. Sol-gel tailored synthesized nanosilica for enhanced oil recovery in water-wet and oil-wet Benthemier Sandstone. *Energy Fuels* 2018;32:12373–82.
- [6] Sun X, Zhang Y, Chen G, Gai Z. Application of nanoparticles in enhanced oil recovery: a critical review of recent progress. *Energies* 2017;10:345.
- [7] Betancur S, Carrasco-Marín F, Franco CA, Cortés BF. Development of composite materials based on the interaction between nanoparticles and surfactants for application in chemical enhanced oil recovery. *Indus Eng Chem Res* 2018;57:12367–77.
- [8] Ali JA, Kolo K, Manshad AK, Mohammadi AH. Recent advances in application of nanotechnology in chemical enhanced oil recovery: effects of nanoparticles on wettability alteration, interfacial tension reduction, and flooding. *Egyptian J Petrol* 2018. <https://doi.org/10.1016/j.ejpe.2018.09.006>.
- [9] Giraldo J, Benjumea P, Lopera S, Cortés Ruiz AM. Wettability alteration of sandstone cores by alumina-based nanofluids. *Energy Fuels* 2013;27:3659–65.

- [10] Al-Anssari S, Barifcani A, Wang S, Maxim L, Iglauer S. Wettability alteration of oil-wet carbonate by silica nanofluid. *J. Colloid Interface Sci.* 2016;461:435–42.
- [11] Kondiparty K, Nikolov AD, Wasan D, Liu KL. Dynamic Spreading of Nanofluids on Solids. Part I *Exp Langmuir* 2012;28:4618–23.
- [12] Ali JA, Kolo K, Manshad AK, Stephen KD, Keshavarz A. Modification of LoSal water performance in reducing interfacial tension using green ZnO/SiO<sub>2</sub> nanocomposite coated by xanthan. *Appl Nanosci* 2018. <https://doi.org/10.1007/s13204-018-0923-5>.
- [13] Zhang H, Nikolov A, Wasan D. Enhanced oil recovery (EOR) using nanoparticle dispersions: underlying mechanism and imbibition experiments. *Energy Fuels* 2014;28:3002–9.
- [14] Arab D, Pourafshary P. Nanoparticles-assisted surface charge modification of the porous medium to treat colloidal particles migration induced by low salinity water flooding. *Coll Surf A Physicochem Eng Aspects* 2013;436:803–14.
- [15] Liu K, Kondiparty K, Nikolov AD, Wasan D. Dynamic spreading of nanofluids on solids part II: modeling. *Langmuir* 2012;28:16274–84.
- [16] Zhang H, Ramakrishnan TS, Nikolov A, Wasan D. Enhanced oil recovery driven by nanofilm structural disjoining pressure: flooding experiments and microvisualization. *Energy Fuels* 2016;30:2771–9.
- [17] Abhishek R, Hamouda AA, Murzin I. Adsorption of silica nanoparticles and its synergistic effect on fluid/rock interactions during low salinity flooding in sandstones. *Coll Surf A Physicochem Eng Aspects* 2018;555:397–406.
- [18] Hendraningrat L, Torsæter O. Metal oxide-based nanoparticles: revealing their potential to enhance oil recovery in different wettability systems. *Appl Nanosci* 2014;5:181–99.
- [19] Bayat EA, Junin R, Samsuri A, Piroozian A, Hokmabadi M. Impact of metal oxide nanoparticles on enhanced oil recovery from limestone media at several temperatures. *Energy Fuels* 2014;28:6255–66.
- [20] Li Y, Dai C, Zhou H, Wang X, Lv W, Zhao M. Investigation of spontaneous imbibition by using a surfactant-free active silica water-based nanofluid for enhanced oil recovery. *Energy Fuels* 2017;32:287–93.
- [21] Zaid HZ, Ahmad Latiff NR, Yahya N. The effect of zinc oxide and aluminum oxide nanoparticles on interfacial tension and viscosity of nanofluids for enhanced oil recovery. *Adv Mater Res* 2014;1024:56–9.
- [22] Soleimani H, Baig MK, Yahya Y, Khodapanah L, Sabet M, Demiral BM, et al. Synthesis of ZnO nanoparticles for oil–water interfacial tension reduction in enhanced oil recovery. *Appl Phys A* 2018. 124.
- [23] Sharma T, Iglauer S, Sangwai JS. Silica nanofluids in an oilfield polymer polyacrylamide: interfacial properties, wettability alteration, and applications for chemical enhanced oil recovery. *Industrial Eng Chem Res* 2016;55:12387–97.
- [24] Saha R, Uppaluri RV, Tiwari P. Silica nanoparticle assisted polymer flooding of heavy crude oil: emulsification, rheology, and wettability alteration characteristics. *Industrial Eng Chem Res* 2018;57:6364–76.
- [25] Lim S, Wasan D. Structural disjoining pressure induced solid particle removal from solid substrates using nanofluids. *J Colloid Interface Sci* 2016;500:96–104.
- [26] Choi SK, Son HA, Kim HT, Kim JW. Nanofluid enhanced oil recovery using hydrophobically associative zwitterionic polymer-coated silica nanoparticles. *Energy Fuels* 2017;31:7777–82.
- [27] Qi L, Song C, Wang T, Li Q, Hirasaki GJ, Verduzco R. Polymer-coated nanoparticles for reversible emulsification and recovery of heavy oil. *Langmuir* 2018;34:6522–8.
- [28] Rezvani H, Riazi M, Tabaei M, Kazemzadeh Y, Sharifi M. Experimental investigation of interfacial properties in the EOR mechanisms by the novel synthesized Fe<sub>3</sub>O<sub>4</sub>@Chitosan nanocomposites. *Coll Surf A Physicochem Eng Aspec* 2018;544:15–27.
- [29] Ju B, Fan T. Experimental study and mathematical model of nanoparticle transport in porous media. *Powder Tech* 2009;192:195–202.
- [30] Ali JA, Kolo K, Manshad AK, Stephen KD. Low-salinity polymeric nanofluid-enhanced oil recovery using green polymer-coated ZnO/SiO<sub>2</sub> nanocomposites in the upper qamchuqa formation in Kurdistan region, Iraq. *Energy Fuels* 2019;33:927–37.
- [31] Ali JA, Kolo K, Manshad AK, Stephen KD. Potential application of low-salinity polymeric-nanofluid in carbonate oil reservoirs: IFT reduction, wettability alteration, rheology and emulsification characteristics. *J Mol Liquids* 2019;284:735–47.
- [32] Shahrabadi A, Bagherzadeh H, Roustaei A. Experimental Investigation of HLP Nanofluid Potential to Enhance Oil Recovery: A Mechanistic Approach, Society for Petroleum Engineers (SPE) Conference Paper SPE-156642-MS 2012. DOI: 10.2118/156642-MS.
- [33] Joonaki E, Ghanaatian S. The application of nanofluids for enhanced oil recovery: effects on interfacial tension and coreflooding process. *Petrol Sci Tech* 2014;32:2599–607.
- [34] Spildo K, Johannessen AM, Low Skauge A. Salinity Waterflood at Reduced Capillarity. *SPE Improv Oil Recovery Sympos* 2012.
- [35] Sugimoto T, Zhou X, Muramatsu A. Synthesis of uniform anatase TiO<sub>2</sub> nanoparticles by gel-sol method. *J Colloid Interface Sci* 2002;252:339–46.
- [36] Ze Y, Sheng L, Zhao X, Hong J, Ze X, Yu X, et al. TiO<sub>2</sub> Nanoparticles Induced Hippocampal Neuroinflammation in Mice. *PLoS ONE* 2014;9:922–30.
- [37] Ali JA, Kolo K, Sajadi SM, Manshad AK, Stephen KD. Green synthesis of ZnO/SiO<sub>2</sub> nanocomposite from pomegranate seed extract: coating by natural xanthan polymer and its characterisations. *Micro Nano Lett* 2019;14(6):638–41. <https://doi.org/10.1049/mnl.2018.5617>.
- [38] Wang W, Cong J, Deng J, Weng X, Lin Y, Huang Y, et al. Developing effective separation of feldspar and Quartz while recycling tailwater by HF pretreatment. *Minerals* 2018;8:149.
- [39] Adamczyk A, Długoń E. The FTIR studies of gels and thin films of Al<sub>2</sub>O<sub>3</sub>–TiO<sub>2</sub> and Al<sub>2</sub>O<sub>3</sub>–TiO<sub>2</sub>–SiO<sub>2</sub> systems. *Spectrochim Acta Part A Mol Biomol Spectrosc* 2012;89:11–7.
- [40] Su L, Lu Z. Spectroelectrochemical study of TiO<sub>2</sub> particulate films. *Spectrochim Acta Part A Mol Biomol Spectrosc* 1997;53:1719–22.
- [41] Kronenberg AK, Hasnan HF, Holyoke III CW, Law RD, Liu Z, Thomas JB. Synchrotron FTIR imaging of OH in quartz mylonites. *Solid Earth Discuss* 2017:1–72.
- [42] Kim B, Lee J, Choi B. Comparison of analytical methods for α-quartz by FTIR and XRD. *Korean J Environ Health Sci* 2009;35:130–42. <https://doi.org/10.5668/jehs.2009.35.2.130>.
- [43] Mahalingam T, Selvakumar C, Kumar ER, Venkatachalam T. Structural, optical, morphological and thermal properties of TiO<sub>2</sub>–Al and TiO<sub>2</sub>–Al<sub>2</sub>O<sub>3</sub> composite powders by ball milling. *Phys Lett A* 2017;381:1815–9.
- [44] Selli N, Tunali A. Role of the Quartz particles on stain resistance of the polished porcelain tiles. *Acta Phys Pol A* 2014;125:506–8.
- [45] Chen L, Xie H. Surfactant-free nanofluids containing double- and single-walled carbon nanotubes functionalized by a wet mechanochemical reaction. *Thermochim Acta* 2010;497:67–71.
- [46] Yu W, Xie H. A review on nanofluids: preparation, stability mechanisms, and applications. *J Nanomater* 2012:1–17.
- [47] Wen D, Lin G, Vafaei S, Zhang Z. Review of nanofluids for heat transfer applications. *Particuology* 2009;7:141–50.
- [48] Hu Z, Haruna M, Gao H, Nourafkan E, Wen D. Rheological properties of partially hydrolyzed polyacrylamide seeded by nanoparticles. *Industrial Eng Chem Res* 2017;56:3456–63.
- [49] Nowrouzi I, Manshad AK, Mohammadi AH. Effects of dissolved binary ionic compounds and different densities of brine on interfacial tension (IFT), wettability alteration, and contact angle in smart water and carbonated smart water injection processes in carbonate oil reservoirs. *J Mol Liq* 2018;254:83–92.
- [50] Nowrouzi I, Manshad AK, Mohammadi AH. Effects of ions and dissolved carbon dioxide in brine on wettability alteration, contact angle and oil production in smart water and carbonated smart water injection processes in carbonate oil reservoirs. *Fuel* 2019;2019(235):1039–51.
- [51] Nowrouzi I, Manshad AK, Mohammadi AH. Effects of dissolved carbon dioxide and ions in water on the dynamic interfacial tension of water and oil in the process of carbonated smart water injection into oil reservoirs. *Fuel* 2019;243:569–78.
- [52] Manshad AK, Olad M, Taghipour SA, Nowrouzi I, Mohammadi AH. Effects of water soluble ions on interfacial tension (IFT) between oil and brine in smart and carbonated smart water injection process in oil reservoirs. *J Mol Liquids* 2016;223:987–93.
- [53] Manshad AK, Nowrouzi I, Mohammadi AH. Effects of water soluble ions on wettability alteration and contact angle in smart and carbonated smart water injection process in oil reservoirs. *J Mol Liquids* 2017;244:440–52.
- [54] Manshad AK, Rezaei M, Moradi S, Nowrouzi I, Mohammadi AH. Wettability alteration and interfacial tension (IFT) reduction in enhanced oil recovery (EOR) process by ionic liquid flooding. *J Mol Liquids* 2017;248:53–162.
- [55] Ghosh AK, Bandyopadhyay P. Polysaccharide-protein interactions and their relevance in food colloids. In *The complex world of polysaccharide*; Intech open science open minds 2012; 395 – 408.

## Appendix 4

*Impact of a novel biosynthesized nanocomposite (SiO<sub>2</sub>@Montmorilant@Xanthan) on wettability shift and interfacial tension: Applications for enhanced oil recovery*

Mohammad Javad Nazarahari, Abbas Khaksar Manshad, Muhammad Ali, **Jagar A Ali**, Ali Shafiei, S. Mohammad Sajadi, Siyamak Moradi, Stefan Iglauer, Alireza Keshavarz

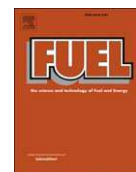
Fuel 298 (2021) 120773

Fuel 298 (2021) 120773



Contents lists available at ScienceDirect

Fuel

journal homepage: [www.elsevier.com/locate/fuel](http://www.elsevier.com/locate/fuel)

Full Length Article

## Impact of a novel biosynthesized nanocomposite (SiO<sub>2</sub>@Montmorilant@Xanthan) on wettability shift and interfacial tension: Applications for enhanced oil recovery

Mohammad Javad Nazarahari<sup>a</sup>, Abbas Khaksar Manshad<sup>a,\*</sup>, Muhammad Ali<sup>b</sup>, Jagar A Ali<sup>c</sup>, Ali Shafiei<sup>d</sup>, S. Mohammad Sajadi<sup>e</sup>, Siyamak Moradi<sup>a</sup>, Stefan Iglauer<sup>f</sup>, Alireza Keshavarz<sup>f,\*</sup>

<sup>a</sup> Department of Petroleum Engineering, Abadan Faculty of Petroleum Engineering, Petroleum University of Technology (PUT), Abadan, Iran

<sup>b</sup> Western Australia School of Mines, Minerals, Energy and Chemical Engineering, Curtin University, 26 Dick Perry Avenue, Kensington 6151, WA, Australia

<sup>c</sup> Department of Petroleum Engineering, Faculty of Engineering, Soran University, Kurdistan Regional Government, Soran 44008, Iraq

<sup>d</sup> Petroleum Engineering Program, School of Mining & Geosciences, Nazarbayev University, Nur-Sultan, Astana 010000, Kazakhstan

<sup>e</sup> Department of Nutrition, Cihan University-Erbil, Kurdistan Region, Iraq

<sup>f</sup> Petroleum Engineering Discipline, School of Engineering, Edith Cowan University, 270 Joondalup Dr, Joondalup 6027, WA, Australia



## ARTICLE INFO

## Keywords:

SiO<sub>2</sub>@Montmorilant@Xanthan

Nanocomposites

Wettability

Interfacial tension

Enhanced oil recovery

## ABSTRACT

Nanoparticles are used in various nano-energy applications such as wettability shift of hydrophobic surfaces to hydrophilic surfaces in oil-brine-mineral systems and interfacial tension (IFT) reduction for enhanced oil recovery. This is possible due to their small size (1–100 nm) and chemical and physical properties. Mechanistically, they can interact with a fluid in the pore space and provide favourable conditions for wettability shift, IFT and oil viscosity reduction, and thus improve oil recovery. However, literature is scarce in terms of providing comprehensive information about the behaviour of nanocomposites (NCs) and associated formulations.

In this paper, we present biosynthesis, characterization, and application of a novel nanocomposite (SiO<sub>2</sub>@-Montmorilant@Xanthan) which is used with various concentrations (100, 250, 500, 1000, 1500, and 2000 ppm) as dispersing agents in porous media. The NC was characterized using X-Ray Diffraction (XRD), Scanning Electron Microscopy (SEM), Thermogravimetric Analysis (TGA), Fourier Transform Infrared Spectroscopy (FTIR), and Energy Dispersive Spectroscopy (EDS). The effects of different concentrations of the nano-suspensions on zeta potential, pH, conductivity, IFT, and wettability are investigated. Core flooding tests were done on sandstone and carbonate reservoir rocks to measure the secondary and tertiary recovery potential by injecting seawater and optimum NC concentrations, respectively.

Zeta potential and conductivity experiments demonstrated that 250 ppm NCs can optimally reduce the IFT from 36 mN/m to 15.42 mN/m (56% reduction). The similar optimum concentration has shifted the wettability of examined carbonate rocks from 150° to 33° leading to an 11.72% increase in tertiary oil recovery. Whereas, the optimum concentration of NCs for sandstone rocks was 1000 ppm; which, has optimally altered the wettability from 140° to 34°, and has increased the tertiary oil recovery by 15.79%. This reduction in IFT, the reversal of wettability, and an increase in tertiary oil recovery can improve significantly the design of effective enhanced oil recovery schemes for petroleum reservoirs.

## 1. Introduction

With the steady increase in demand for consumption of hydrocarbon energy resources, enhanced production from conventional and unconventional petroleum reservoirs is inevitable [1–4]. Because of world population growth in the decades to come and an increasing demand for

energy resources in developing economies and the fact that production from the current petroleum reservoirs is declining rapidly, the new discoveries are unable to close the gap between production and consumption [5]. Hence, new technologies are needed to optimize and enhance production from the current reserves to address this issue [6–8].

\* Corresponding authors.

E-mail addresses: [Khaksar@put.ac.ir](mailto:Khaksar@put.ac.ir) (A.K. Manshad), [A.keshavarz@ecu.edu.au](mailto:A.keshavarz@ecu.edu.au) (A. Keshavarz).

<https://doi.org/10.1016/j.fuel.2021.120773>

Received 26 January 2021; Received in revised form 26 March 2021; Accepted 28 March 2021

Available online 16 April 2021

0016-2361/© 2021 Elsevier Ltd. All rights reserved.

After the primary phase of oil production, a significant part of the oil in place cannot be produced due to natural depletion and this huge amount of petroleum is residually trapped in rock matrix [9,10]. After the primary pressure decline phase, usually water and gas are injected into the reservoirs to extract residual oil and maintain the reservoir pressure [11,12]. However, these methods are viable to some extent and can produce between 10 and 20% of the residual oil in place. Hence, enhancing oil production with tertiary recovery methods such as chemical flooding, nano-suspension flooding, miscible and immiscible CO<sub>2</sub> flooding, fracturing, and in-situ thermal recovery can be a solution [13–16].

Considering all these tertiary methods, nanoparticles (NPs) are drawing more attention due to their small sizes which can avoid problems of clogging in oil reservoirs and greater ability to disperse with injection fluids such as brine, polymers, and surfactants to achieve higher recoveries [13,17,18]. Nano-suspensions are currently used in various applications of reservoir operations such as enhanced oil recovery [13,17], low salinity water flooding [19], chemical flooding [6,20,21], drilling [22–24], IFT reduction, and wettability alteration [25,26].

These minute particles are categorized into four different groups: inorganic, magnetic, natural, and metal oxides and can be used as nano-emulsions, nano-suspensions, and nano-catalysts in EOR techniques [27,28]. Typically, oil reservoirs are oil-wet and the efficient EOR method requires high water to oil viscosity ratio, maximum decrease in the oil–water interfacial tension, and change in wettability from oil-wet to water-wet [29–33]. However, typical reservoir situations are reductive and may contain the presence of organic acids which can significantly alter the wettability [34–38]. In this context, nano-suspensions can be a pertinent factor to reverse the wettability from hydrophobicity to hydrophilicity and improved the oil recovery [17]. The properties and type of chemicals used in formulation of nano-suspension are dependent on the specific applications, conditions, and type of the targeted oil reservoirs [39,40]. For instance, water flooding was initially replaced by polymer flooding as a chemical EOR method in reservoirs containing heavy oil [41,42]. Whereas, various factors such as, increased temperature, heterogeneity, and high salinity can substantially reduce the viability of polymer flooding [43,44], which can be avoided by using nanoparticles in the base fluid (polymer in this case) [45].

Several studies have suggested the use of different chemicals such as surfactants [46], polymers [17,47], and traditional nanoparticles for shifting hydrophobic wettability and reducing IFT for CO<sub>2</sub> geo-storage applications and EOR processes [48–52]. However, injection of these chemical agents into oil wells can be toxic for shallow water zones at onshore locations [53–56] and marine environment at offshore locations [22,57–59], due to the risk of oil spills and injection fluid spills. Hence, it is pertinent to acquaint with green nanocomposites that are feasible for improving oil recovery and remain non-harmful in shallow water zones and marine environments. We have thus biosynthesized a green novel nanocomposite including silica (SiO<sub>2</sub>, an abundant mineral in subsurface formation), nano-clay (montmorillonite), *Adinandra dumosa* plant extract (an antioxidant as stabilizing and reducing agent), and xanthan (viscosifier and stabilizing agent). This nanocomposite is non-toxic to the marine environment and shallow water zones and it also results in higher oil recovery. To the best of our knowledge, this nanocomposite is not previously used in EOR techniques.

This research work is organized in three sections. Initially, we report biosynthesis and characterization of a green novel nanocomposite (SiO<sub>2</sub>@Montmorilant@Xanthan) using state of the art laboratory facilities such as XRD, SEM, TGA, FTIR, and EDS. Then, various concentrations (100, 250, 500, 1000, 1500, and 2000 ppm) of the NCs were used as dispersing agents for measuring zeta potential, pH, conductivity, IFT, and wettability for quantification of optimal concentration as efficient EOR agent in petroleum reservoirs. Afterward, core flooding tests were conducted on sandstone and carbonate rock samples with their respective optimum nanofluid concentrations to measure the enhanced oil

recovery potential. Table 1 depicts a summary of some related studies of nanoparticles in nano-energy applications.

## 2. Experimental

### 2.1. Materials

Silica, nano-clay (montmorilant), *Adinandra dumosa* leaf extract (Tiup-Tiup tree) from the family of Thecae (stabilizing and reducing agent), and Xanthan (stabilizing agent) were used to biosynthesize a green novel nanocomposite (SiO<sub>2</sub>@Montmorilant@Xanthan) with a size of 31–50 nm. The synthesized nanocomposite was then mixed with deionized water (Ultrapure, from David Gray, electrical conductivity =

**Table 1**  
A summary of related studies of nanoparticles for efficient EOR process.

| Author & year               | Type of NPs & NCs   | Subject of study                 | Outcomes   |
|-----------------------------|---|----------------------------------|--|
| Wu, W et al. (2008)         | Fe <sub>2</sub> O <sub>3</sub> /Fe <sub>3</sub> O <sub>4</sub>    | Oil recovery                     | RF was increased by 82.5% at laboratory scale by using Iron Oxide [60]   |
| N.B. Yahya et al. (2012)    | CoFe <sub>2</sub> O <sub>4</sub>                                  | Oil recovery                     | Residual oil recovery factor was increased by 22.8% [61]   |
| K. Chandran et al. (2013)   | CNTs  | EOR agent in HPHT                | The suggested NCs were impressive in reducing the viscosity [62]   |
| E.A. Bayat et al. (2014)    | SiO <sub>2</sub> + DIW  | Wettability & IFT modification   | Reduced the IFT and altered the wettability from hydrophobic to hydrophilic [63]   |
| Joonaki, E et al. (2014)    | Al <sub>2</sub> O <sub>3</sub>                                    | Wettability & IFT modification   | Reduced the IFT (38.5 to 2.25) and altered the wettability from oil-wet to water-wet (altered the contact angle from 131 to 92) [64]                 |
| Ragab et al. (2015)         | Al <sub>2</sub> O <sub>3</sub> and SiO <sub>2</sub> and nanofluid | IFT modification & Oil recovery  | The nanofluids reduced the IFT and oil production was more by using SiO <sub>2</sub> compare to Al <sub>2</sub> O <sub>3</sub> [65]                  |
| Assef et al. (2016)         | MgO on LoSal water flooding                                       | Fines migration                  | These nanoparticles were non-effective on oil recovery but have enhanced the fine migration [66]   |
| Kapusta et al. (2016)       | SiO <sub>2</sub>  | Wettability alteration           | SiO <sub>2</sub> has demonstrated irreversible NP adsorption and has shifted the wettability towards a more water-wet system in calcite samples [67] |
| Y. Kazemzadeh et al. (2018) | Fe <sub>2</sub> O <sub>3</sub> /SiO <sub>2</sub>                  | Wettability & IFT modification   | The nanofluids used in this study have reduced the IFT form 39 to 17.5 mN/m and altered the contact angle from 138 to 52 [68]                        |
| J.A. Ali et al. (2019)      | SiO <sub>2</sub> /TiO <sub>2</sub> /xanthan                       | Wettability & IFT & Oil recovery | IFT reduction and wettability shift was noted with improved oil recovery factor by 19.3% [69]  |
| K.P. Dahkaee et al. (2019)  | NiO/SiO <sub>2</sub>  | Wettability & IFT modification   | The nanofluids used in this study have reduced the IFT form 28 to 1.84 mN/m and altered the contact angle from 154 to 32 [70]                        |
| Bahraminejad et al. (2019)  | CuO/TiO <sub>2</sub> /PAM   | Wettability & IFT modification   | The nanofluids used in this study have altered the contact angle from 151 to 14.7 [71]   |
| Nowrouzi et al. (2020)      | TiO <sub>2</sub> , MgO, -Al <sub>2</sub> O <sub>3</sub>           | Wettability & Oil recovery       | The wettability shift was noted with an improved oil recovery factor by 75.93% [72]  |

0.02 mS/cm) of different concentrations (100, 250, 500, 1000, 1500, and 2000 ppm) to formulate nano-suspensions using a magnetic stirrer.

Distilled water (density = 1.068 g/cm<sup>3</sup> and viscosity = 1.42 cP at 25 °C) was used to formulate aqueous Adinandra dumosa plant extract. Ethanol (from Chem supply, purity > 99.9 mol%) was used for mixing SiO<sub>2</sub>@montmorillonite precipitate and Xanthan (further described in section 2.2). Kerosene (from Chem supply, purity > 99.9 mol%) was used as a cleaning agent for thin sections of rock surfaces to remove possible contaminations. Toluene (from Rowe scientific, purity > 99 mol %) was used as a calibration liquid for IFT and contact angle measurements.

The crude oil used for the purpose of this study was collected from Gachsaran oilfield in the south of Iran. The crude oil properties are presented in Table 2a. Carbonate samples (95% CaCO<sub>3</sub>) were acquired from Asmari carbonate formation and sandstone samples (63% SiO<sub>2</sub> and 37% CaCO<sub>3</sub>) were acquired from Aghajari sandstone formation located in southwestern Iran. Table 2b shows the physical properties of the core plugs. NaCl (from Chem supply, purity > 99.9%) was used to formulate 2 wt% brine solutions for ionizing the rock thin sections. Ultra-pure nitrogen (purity = 99.999 wt%, from BOC, gas code-234) was used to clean the rock thin sections after ionization and crude oil ageing process.

## 2.2. Biosynthesis of (SiO<sub>2</sub>@Montmorilant@Xanthan) nanocomposite

First, 100 g of Adinandra Dumosa plant leaves extract was mixed with 500 ml of distilled water at 80 °C for 30 min under reflex conditions. Then, the prepared aqueous extract was filtered and stored at 4 °C for further application. Further, 1 g of sodium metasilicate (Na<sub>2</sub>SiO<sub>3</sub>) and 4 g of montmorillonite were mixed with 100 ml of Adinandra dumosa plant extract by maintaining the pH = 9 (adjusted by 0.1 mol/L, Na<sub>2</sub>CO<sub>3</sub>) while stirring at 80 °C for 5 h. This mixing process was continued until SiO<sub>2</sub>@montmorillonite precipitate was formed followed by the drying process (SiO<sub>2</sub>@montmorillonite precipitate was dried at 80 °C for 24 h). Thereafter, SiO<sub>2</sub>@montmorillonite precipitate was mixed with 10 g of Xanthan in presence of 100 ml ethanol at 80 °C for 3 h to form (SiO<sub>2</sub>@Montmorilant@Xanthan) nanocomposite precipitate followed by filtration and drying process. The SiO<sub>2</sub>@Montmorilant@Xanthan NC precipitate was dried at 80 °C for 24 h. The biosynthesis of (SiO<sub>2</sub>@Montmorilant@Xanthan) is described in Scheme 1.

The biosynthesis of (SiO<sub>2</sub>@Montmorilant@Xanthan) nanocomposite is dependent on the precipitation of water-consisting solution. Initially, Adinandra Dumosa plant leaves were mixed with distilled water for producing the plant extract, which acts as a stabilizing medium providing perfect conditions for successful reaction and at the same time works as a reducing agent for the synthesis process. Thereafter, sodium metasilicate and montmorillonite were mixed with the Adinandra Dumosa plant extract. In this mixing reaction, sodium metasilicate acts as a primary precursor of the SiO<sub>2</sub> nanoparticles by dissolution of sodium in aqueous phase (distilled water) causing precipitation of metasilicate anions that will instantly bond with hydrogen atoms due to the presence of reducing agent, forming hydrogen metasilicate. This reducing property of Adinandra Dumosa plant extract causes the loss of electrons during the synthesis process for providing feasible conditions in order to achieve successful redox reaction by the oxidation of metasilicate. Thus, hydroxide ions are released into the aqueous solution forming SiO<sub>2</sub>. The silica particles are one of the stable compounds which

does not dissolve in any aqueous phase. However, presence of hydroxyl groups in the sheets of montmorillonite clay and hydroxyl groups in silica particles will create a strong chemical reaction, thus, covalently chemically binding them together [26]. Thereafter, refluxing of xanthan will provide coating of pre-synthesized material resulting in SiO<sub>2</sub>/Montmorillonite/Xanthan nanocomposite.

## 2.3. Preparation of Nano-suspensions

Nano-suspensions with different concentrations (100, 250, 500, 1000, 1500, and 2000 ppm) of SiO<sub>2</sub>@Montmirilliant@Xanthan NCs were formulated and prepared for quantifying their effects on IFT reduction and wettability reversal in nano-oil-rock systems. The pre-determined weight of SiO<sub>2</sub>@Montmirilliant@Xanthan NCs for different concentrations was added to the pre-determined weight of deionized water followed by mixing them with an ultrasonic homogenizer (from Hielscher Company, UP200 model, frequency 20 kHz) for one hour. It should be noted here that magnetic stirring is not suitable for preparation of homogeneous nano-suspensions [73]. A micro-tip of 9.5 mm diameter was used with energy of 9000 Joules and sonication amplitude of 35% to conduct this process.

### 2.3.1. Characterization of physical properties and electrical stability of (SiO<sub>2</sub>@Montmirilliant@Xanthan) nanocomposite

It is pertinent to measure the physical properties (viscosity, density, and pH) and electrical stability (conductivity and zeta-potential) of nano-suspensions for quantifying the optimum nano-concentration for IFT reduction and wettability reversal in nano-oil-rock systems (Table 3 and Figs. 1 and 2) [74]. Density and viscosity (from KEM company, model DA-640 KEN) measurements have shown an increase in physical properties of nano-suspensions with the increase of nano-concentration. Whereas, pH (pH meter from Mettler Toledo, resolution 0.1 pH) remained neutral at all nano-concentrations tested.

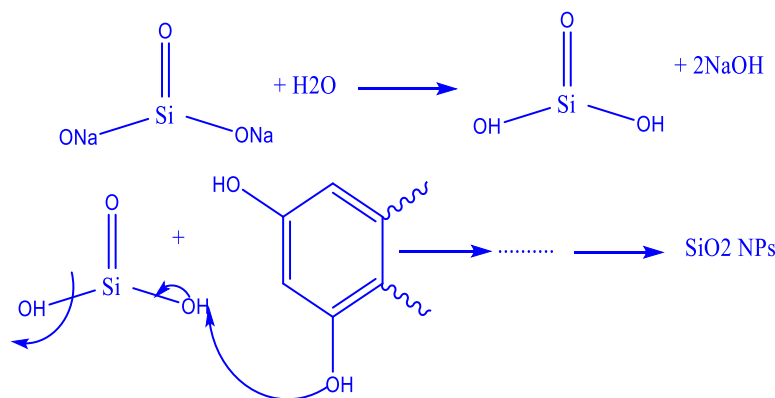
However, electrical stability measurements (zeta-potential from Malvern Zetasizer, model nano ZS90, and conductivity from Jenway, model 4510) have shown mixed behaviour with the increasing nano-concentrations as shown in Figs. 1 and 2. It is reported in the literature that lower zeta-potential (+10 to -10 mV) values of the nano-suspensions are not electrically stable and are likely to coagulate faster than as compared to higher values (i.e., absolute zeta potential > ± 35 mV) [14,75]. Moreover, the repulsive forces (negatively or positively charged) are considerably reduced, creating a quicker accelerated aggregation process of nanoparticles that contain sedimentation in the existence of the electrolyte. Anionic and cationic surfactants can provide electrical stability by covering the nanoparticle's outer layer with their respective ion heads, thus causing supercharged particles [14,76]. It is clear from Figs. 1 and 2 that at 250 ppm concentration of nano-composite, conductivity and zeta-potential values suddenly increase which is due to the release of the ions into the environment. Thus, the layered structure of clay minerals in nanoparticles creates a strong negative electrical field which increases the adsorption of positive ions in dispersion medium causing greater stability and increased electrical conductivity. This phenomenon also represents the critical missile concentration (CMC) point for determining the optimum concentration for IFT reduction and wettability reversal [6].

**Table 2a**  
Properties of the crude oil used in this study.

| Component  | C <sub>1</sub> | C <sub>2</sub> | C <sub>3</sub> | iC <sub>4</sub> | nC <sub>4</sub> | iC <sub>5</sub> | nC <sub>5</sub> | C <sub>6</sub>                    | C <sub>7</sub> | C <sub>8</sub> | C <sub>9</sub> | C <sub>10</sub> | C <sub>11</sub> | C <sub>12</sub> <sup>+</sup> | Total |               |
|--|----------------|----------------|----------------|-----------------|-----------------|-----------------|-----------------|-----------------------------------|----------------|----------------|----------------|-----------------|-----------------|------------------------------|-------|---------------|
| Molar percent  | 0.00           | 0.08           | 0.73           | 0.72            | 2.22            | 1.10            | 1.10            | 8.66                              | 9.32           | 6.60           | 7.14           | 5.36            | 5.01            | 51.96                        | 100.0 |               |
| Molecular weight(MW) = 247   |                |                |                |                 |                 |                 |                 | SARA analysis of crude oil sample |                |                |                |                 |                 |                              |       |               |
| Molecular weight of C <sub>12</sub> <sup>+</sup> = 380               |                |                |                |                 |                 |                 |                 | Saturates (%)                     |                |                |                | Aromatics (%)   |                 | Resins(%)                    |       | Asphaltene(%) |
| Specific gravity of C <sub>12</sub> <sup>+</sup> @ 15.55 °C = 0.9369 |                |                |                |                 |                 |                 |                 | 45                                |                |                |                | 32              |                 | 5                            |       | 8             |
| Saturation pressure of reservoir fluid @ 60.6 °C = 14.04 MPa         |                |                |                |                 |                 |                 |                 |                                   |                |                |                |                 |                 |                              |       |               |

**Table 2b**  
 Properties of the core plugs used in this study.

| Core Sample | Diameter (cm) | Length (cm) | Bulk Volume (cm <sup>3</sup> ) | Dry weight (g) | Saturated weight (by de-ionized water) (g) | Pore Volume (cm <sup>3</sup> ) | Porosity (%) | Permeability (mD) |
|-------------|---------------|-------------|--------------------------------|----------------|--|--------------------------------|--------------|-------------------|
| Sandstone   | 3.7           | 6.32        | 67.91                          | 149.04         | 159.41                                     | 10.41                          | 15.32        | 30                |
| Carbonate   | 3.7           | 7           | 75.22                          | 174.48         | 184.13                                     | 9.65                           | 12.82        | 8.23              |


**Scheme 1.** Biosynthesis of green novel (SiO<sub>2</sub>@Montmorilant@Xanthan) nanocomposite.

**Table 3**  
 Physical properties of the prepared nano-suspensions.

| NC. Concentration (ppm) | Parameter | Density(g/cm <sup>3</sup> ) | Viscosity (cP) | pH (pKa) |
|-------------------------|-----------|-----------------------------|----------------|----------|
| 100                     |           | 0.9990                      | 1.49           | 7.06     |
| 250                     |           | 0.9990                      | 1.17           | 7.01     |
| 500                     |           | 0.9992                      | 5.57           | 6.88     |
| 1000                    |           | 0.9994                      | 8.40           | 6.92     |
| 1500                    |           | 0.9996                      | 29             | 7.04     |
| 2000                    |           | 1.0002                      | 35             | 7.15     |

## 2.4. Surface ageing procedure of sedimentary rocks

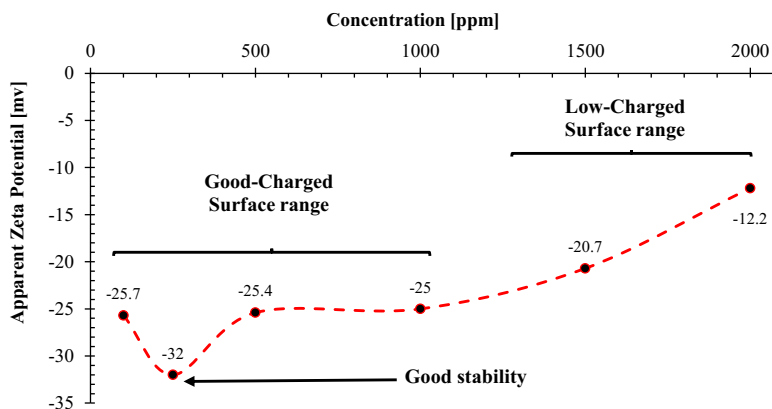
### 2.4.1. Initial cleaning procedure

It is crucially important to clean the rock surfaces when they are received from the outcrop. As they may contain impurities that can cause errors in the contact angle measurements. Hence, acetone and deionized water was used on thin sections acquired from carbonate and

sandstone outcrops to eradicate any organic and inorganic contaminations. Then, an ultra-pure nitrogen blow was used on thin sections followed by drying them at 90 °C for 3 h in a vacuum oven to remove any fluid after the initial cleaning. Further, air plasma (Diemer Yocto instrument) treatment was carried out on thin sections for 30 min to eradicate remaining contaminations after drying procedure [77].

### 2.4.2. Thin sections ageing with crude oil and Nano-suspensions

Hydrocarbon reservoirs have anoxic characteristics that comprehend organic contaminations dissolved in crude oil. These organic molecules are responsible for changing the wettability from intermediate-wet to oil-wet [36,78,79]. Thus, it is crucial to mimic the reservoir conditions at laboratory scale for completely understanding the subsurface physiognomies for wettability measurements [80,81]. There is lack of information in the literature on quantifying the effects of real crude oil on the wetness of hydrocarbon reservoirs. Previously, many studies have shown that silanes can be utilized for changing the wettability of intermediate-wet rock surfaces [82]. However, typical hydrocarbon reservoirs have reductive conditions which does not contain silanes due


**Fig. 1.** Zeta-potential of the SiO<sub>2</sub>@Montmorilant@Xanthan nanocomposite.

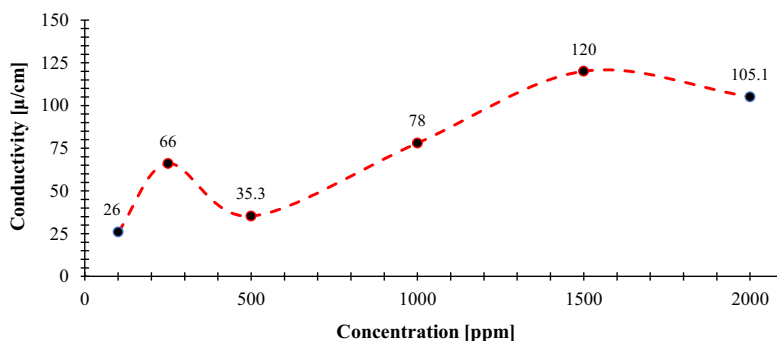


Fig. 2. Conductivity of the  $\text{SiO}_2@\text{Montmorilant}@\text{Xanthan}$  nanocomposite.

to their high reactivity. Hence, altering the intermediate-wet rock surfaces to oil-wet by using real crude oil samples would be more realistic. Further, nano-suspensions have a substantial impact on quantifying the reversal of wettability from oil-wet to intermediate-wet [13,26,83]. This is due to the strong chemical reaction between hydroxyl groups of oil-wet rock surfaces with hydroxyl group of nano-formulations causing an irreversible adsorption of nanoparticles on rock surfaces. Hence, we utilized the following procedures [80,81,84,85].

After the initial cleaning procedure, sandstone and carbonate rock thin sections were submerged into 2 wt% NaCl brine solution, where drops of aqueous hydrochloric acid were used to sustain the pH at 4 pKa for 30 min. This procedure is used to ionize the thin sections to speed up the adsorption rate of crude oil to simulate the real reservoir conditions for a longer depositional period (e.g., millions of years) [25,34–36,86]. Afterward, the thin sections were blown with ultra-pure nitrogen to remove brine solution followed by placing them into crude oil (acquired from Gachsaran oilfield in the south of Iran) for seven days (Fig. 3).

Thereafter, initial contact angle measurements were conducted. To quantify the effects of nano-suspensions, crude oil aged rock thin sections were rinsed with kerosene and were submerged into different nano-formulations for 5 h. The Nano-ageing process was done by placing the rock thin sections vertically to avoid the gravitational deposition of

nanoparticles. Afterward, final contact angle measurements were done to specify the optimum nano-concentration. This phenomenon comprises the chemical bond between hydroxyl groups of rock surfaces and hydroxyl groups of organics dissolved into the crude oil in a condensation reaction scheme (altering the wettability to oil-wet) [25,35,36] and nano-suspension ageing with oil-wet rock surfaces in an irreversible adsorption phenomena (reversing the wettability to water-wet) [13].

#### 2.5. Interfacial tension and contact angle measurement system

Interfacial Tension (IFT) measurement is a procedure to acquire tension between two fluids and contact angle measurement is a method that is used to comprehend the wettability characteristics of a given rock and fluid system [13,29,36,87]. Both methods can be conducted at real reservoir or ambient conditions. In this research work, VIT 6000 contact angle apparatus (manufactured by Fars, accuracy 99%) was used to investigate IFT behaviour and wetting characteristics of rock thin sections. The IFT and contact angle setup is shown in Fig. 4. In this procedure, initially, a drop of crude oil (average drop size was  $5.0 \mu\text{L} \pm 0.70 \mu\text{L}$ ) is suspended from the needle in the presence of different nano-formulations (filled in the main chamber) to measure the IFT between two liquids. The drop of crude oil was controlled by ISCO (Teledyne

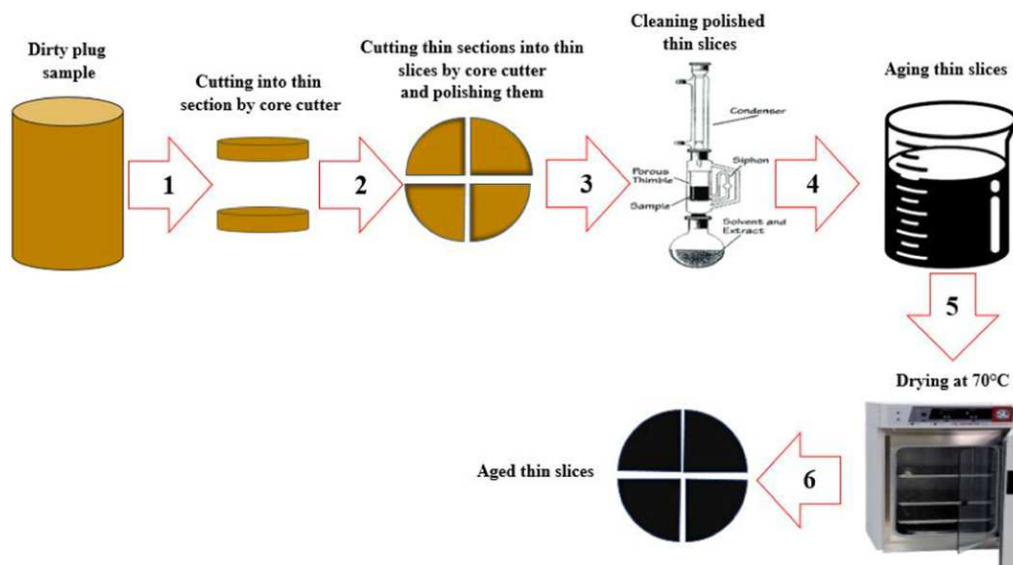


Fig. 3. Ageing procedure of thin sections.

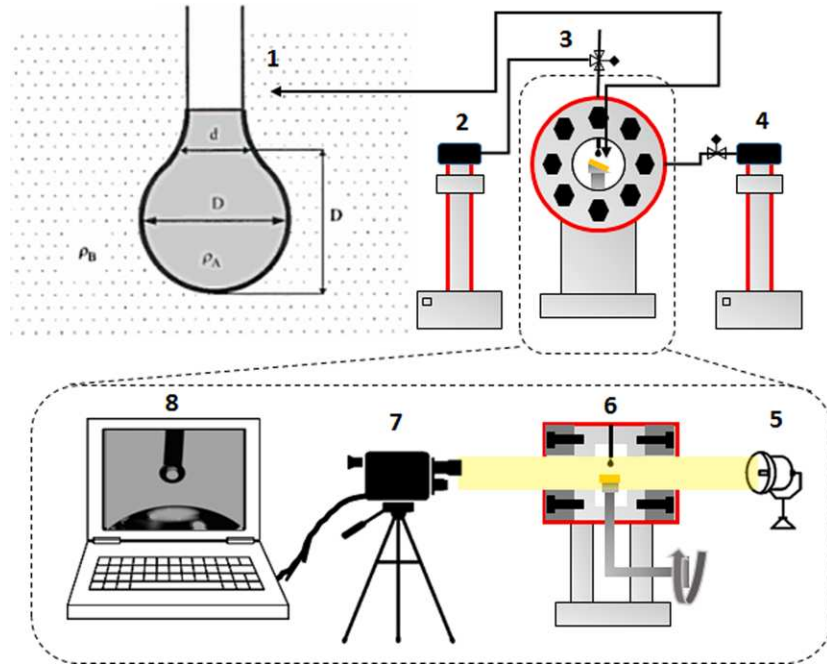


Fig. 4. Illustration of IFT and contact angle measurement setup, (1) Illustration of digital drop of liquid shape (crude oil in this case), (2) ISCO pump for controlling crude oil droplet, (3) Main chamber for the IFT and contact angle measurement, front view, (4) ISCO pump for filling the main chamber with nanofluid, (5) Light projection, (6) Main chamber, side view, (7) Video camera for recording, (8) computer software for interpretation.

ISCO, Model D-500, pressure accuracy of 0.1%) pump for the right accuracy and control, and this procedure is video recorded. Then, images are extracted from the video at the point where the drop is leaving the needle making a spherical shape. This phenomenon comprises due to the relationship between gravity and surface tension of two liquids, as represented in Eq. (1) and Fig. 4.

$$\gamma = \frac{\Delta\rho g D^2}{H} \quad (1)$$

where “ $\Delta\rho$ ” is the density difference between two liquids, “ $g$ ” is the gravity force, “ $D$ ” is diameter of the liquid drop (crude oil in this case) at maximum length and “ $H$ ” is the coefficient of the drop shape.

Similarly, contact angle measurements were conducted using the same experimental setup. To do that, initially thin sections were loaded and different nano-suspensions were injected into the main chamber for each measurement. Initially, a droplet of crude oil (average drop size was  $5.0 \mu\text{L} \pm 0.70 \mu\text{L}$ ) was dispensed on crude oil aged rock thin sections to comprehend the initial wetting characteristics in presence of de-ionized water. Then, a similar process was conducted on rock thin sections aged in nano-suspensions at different concentrations to comprehend their effects on wettability reversal. This process was also videotaped and images were then extracted where drop touches the thin section. Further, Image software was used to analyse the drop shape and its associated tangent angle.

## 2.6. Core flooding experimental setup

To measure porosity, permeability, original oil in place (OOIP), irreducible water saturation ( $S_{w,i}$ ), secondary oil recovery (by seawater), and tertiary oil recovery (by optimum nanofluid concentration), core flooding experiments were conducted. Sandstone and carbonate rock sample’s dimensions were measured to obtain bulk volume and then, dry and saturated weight (by de-ionized water) of each core sample was

measured followed by measuring viscosity and density of the de-ionized water to obtain pore volume, porosity, and permeability.

At the start of core flooding experiments, rock samples (sandstone and carbonate) were saturated with de-ionized water in the core holder. To do that, rock samples were loaded in the core holder and de-ionized water was injected from the inlet end at a constant flow rate (HPLC pump were used at the inlet end to control the flow rate) of 0.2 cc/min until stable flow rate was acquired at inlet and outlet ends. Outlet pressure was set to 2000 Psi (back pressure regulators operated by nitrogen gas were used at outlet end to maintain the reservoir pressure) and overburden pressure was set to 2500 psi, 500 psi greater than outlet pressure to make sure that injection of liquid passes through the core samples. When stable flow and pressure difference at inlet and outlet were recorded, rock samples were flooded with 5 pore volume (PV) of the de-ionized water to completely saturate the core samples. Afterward, the flow of injection fluid was stopped and the pressure was kept constant at 2000 psi (note that this process will allow injection fluid to completely pass through the rock matrix) to fully saturate the rock samples.

After the saturation process, de-ionized water was injected at 3 different flow rates (0.5, 0.3, and 0.1 cc/min) in rock samples, when pressure difference was constant, absolute permeability was calculated. Then, crude oil (from Gachsaran oilfield in the south of Iran) was injected at a constant flow rate of 0.2 cc/min and outlet pressure was kept at 2000 psi (note that reservoir formations examined in this article have a pressure range between 1800 and 2200 psi and a temperature range between 50 and 70 °C) and the temperature was maintained at 60 °C (temperature of core holder was controlled by heating tape and controller, Model No. HTC101-002 from Omega Company) to simulate the real reservoir conditions. Crude oil injection was monitored until no more water was produced to obtain original oil in place (OOIP), and irreducible water saturation ( $S_{w,i}$ ). For measuring enhanced oil recovery potential, initially, seawater was injected at a constant flow rate of 0.2

cc/min and constant outlet pressure of 2000 psi, until no more oil was produced to obtain secondary oil recovery factor. To assess the effectiveness of the biosynthesized smart nanofluid, optimum nanofluid concentrations (250 ppm for carbonate rock sample and 1000 ppm for sandstone rock sample) were selected for injection (based on electrical stability and wettability shift data) in their respective rock samples at a constant flow rate of 0.2 cc/min and constant outlet pressure of 2000 psi until no more oil was produced to obtain tertiary oil recovery factor. The schematic of the core flooding experimental setup is shown in Fig. 5.

### 3. Results and discussion

#### 3.1. Analytical characterization of (SiO<sub>2</sub>@Montmorilliant@Xanthan) NC

In this research work, a new green novel nanocomposite (SiO<sub>2</sub>@Montmorilant@Xanthan NCs) is biosynthesized for quantifying its usage for enhanced oil recovery. Hence, it is important to characterize the nanoscale properties such as surface morphology, crystalline phases, and functional groups. Thus, different characterization techniques like XRD, SEM, TGA, FTIR, and EDS were used.

##### 3.1.1. X-Ray Diffraction characterization test (XRD)

XRD (from Malvern Panalytical, Model Empyrean Nano Edition) is a technique used to characterize the bulk mineralogy of solid-phase [88]. To synthesize and identify the bulk mineralogy and crystalline phase of the SiO<sub>2</sub>@Montmorilant@Xanthan nanocomposite, we conducted an XRD test on the powder nanoparticle sample. The measured XRD spectra has shown that SiO<sub>2</sub> is the predominant phase in the bulk mineralogy of a nanocomposite powder at angles of 19.94°, 20.93°, 26.71°, 27.76°, 36.61°, 62.03°, respectively, which are related to SiO<sub>2</sub> crystallography planes of a cubic fluorite structure of silica particles. Whereas, Montmorilant crystallography peaks were depicted as the second predominant phase in the nanocomposite powder at angles of 6.13°, 19.94°, 20.93°, 26.71°, 27.76°, respectively, as shown in Fig. 6. The abundance of these minerals in nanocomposite is responsible for reversing the hydrophobic rock surfaces to hydrophilic [26].

##### 3.1.2. Fourier-Transform Infrared Spectroscopy characterization test (FTIR)

FTIR (from Perkin Elmer, Model FTIR Spectrum Two) is a technique that is used to characterize the chemical bonding and functional groups on solid surfaces [35]. Hence, biosynthesized (SiO<sub>2</sub>@Montmorilant@Xanthan) nanocomposite powder was exposed to 64 scans in the spectral range of 400 – 4000 cm<sup>-1</sup>. The FTIR spectra as shown in Fig. 7 for nanocomposite powder determine crystalline clay material.

The FTIR spectrum and broad peaks at 468.3 cm<sup>-1</sup>, 795.13 cm<sup>-1</sup>, and 1038.08 cm<sup>-1</sup> shows (Si – O) bending which represents siloxane bonds (Si – O – Si). Whereas, double peaks at 532.39 cm<sup>-1</sup> and 696.26 cm<sup>-1</sup> shows (Al – O – Si) deformation and (Al – OH) bonding. Further, a small peak at 1416.92 cm<sup>-1</sup> shows (CH<sub>3</sub>) bending, a peak at 1632.48 cm<sup>-1</sup> depicts (OH) deformation of the water and a peak at 1726.4 cm<sup>-1</sup> depicts (C = O) stretching. The peak at 2924.7 cm<sup>-1</sup> shows hydrogen bonding (C – H), the peak at 3431.69 cm<sup>-1</sup> depicts hydroxyl bonding (C – OH) [89,90], and the peak at 3620.51 cm<sup>-1</sup> represents (Al/Mg – OH) stretching. All these peaks represent the hydrous nature characteristics of clay material [91–93].

##### 3.1.3. Field emission Scanning Electron Microscopy (FESEM) and energy Dispersive Spectroscopy (EDS) characterization test

FESEM (from Oxford Instruments) can be used to characterize surface morphology of the biosynthesized nanocomposite. EDS is a technique to determine surface elemental composition (in wt%) of the solid or powder samples. To do that, SEM micrographs were taken on thin sections before and after ageing with nanoparticles. It is clear from Fig. 8 that nanoparticles were irreversibly adsorbed on the thin section, note that this irreversible adsorption is responsible for the wettability reversal, and their sizes range from 31 to 50 nm.

Further, the surface elemental analysis was conducted via the EDS technique, which has shown the presence of O, C, and Si elements in the nanocomposite structure. The weight % and atomic % of the different elements are shown in Table 4. A higher percentage of Si element is responsible for the predomination of quartz structure in the biosynthesized nanocomposite.

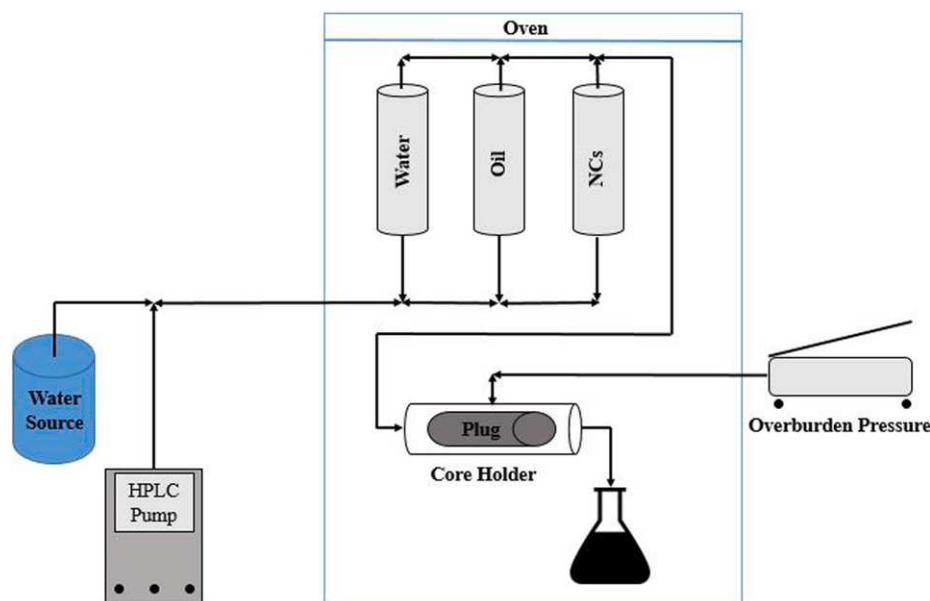


Fig. 5. Schematic of core flood experimental setup.

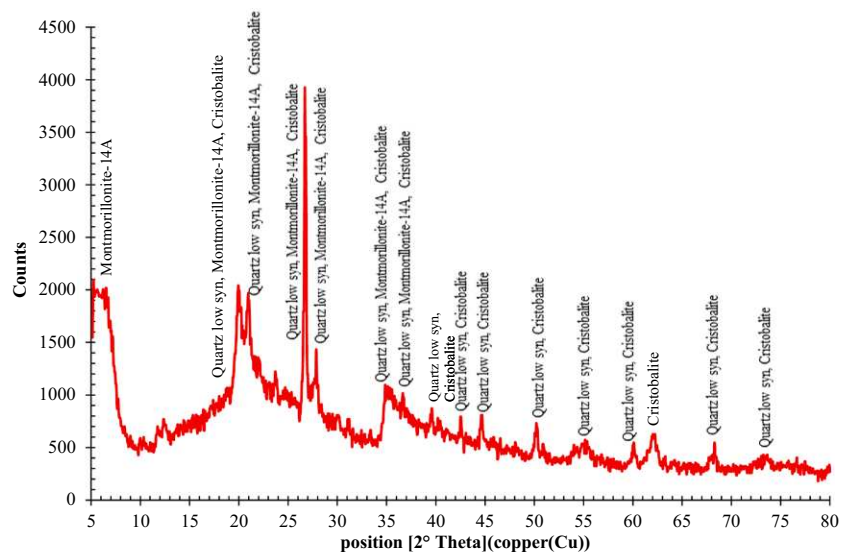


Fig. 6. XRD Spectra of the SiO<sub>2</sub>@Montmorilant@Xanthan nanocomposite.

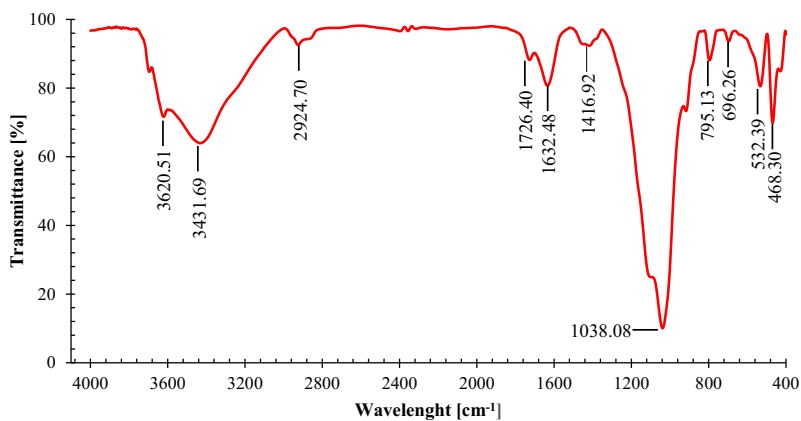


Fig. 7. FTIR Spectra of the SiO<sub>2</sub>@Montmorilant@Xanthan nanocomposite.

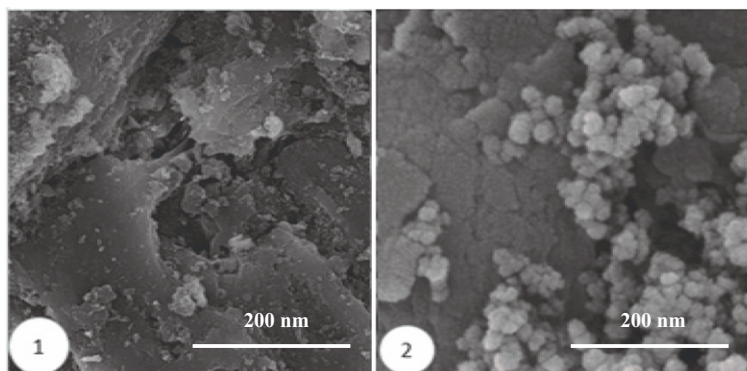


Fig. 8. SEM micrographs, (1) rock thin section before nanoparticle ageing, (2) rock thin section after nanocomposite ageing.

**Table 4**  
Mineral composition of the SiO<sub>2</sub>@Montmorilant@Xanthan nanocomposite.

| Element | Atomic Number | Weight (wt) % | Atom % |
|---------|---------------|---------------|--------|
| Carbon  | 6             | 10.82         | 15.88  |
| Oxygen  | 8             | 59.23         | 65.30  |
| Silicon | 14            | 29.96         | 18.82  |

### 3.1.4. Thermogravimetric analysis (TGA) characterization test

TGA (from Perkin Elmer, Model TGA 8000) is a technique that determines the material's thermal stability and the presence of volatile components associated with nanocomposites and polymer composites as a function of predetermined temperature conditions [94]. To do that, we have exposed 3.72 mg of biosynthesized nanocomposite in presence of argon. The temperature increase rate was set at 10 °C/min.

It is clear from Fig. 9 that this nanocomposite has experienced several stages of weight loss with increasing temperature. The initial part of the weight loss relates to lower temperatures that are less than 200 °C that specifies vaporization and separation of surface water dependent on structure of the material. The second part of weight loss relates to temperatures between 200 and 400 °C, which indicates the separation of water between material structure and dihydroxylation of organic long material. The final stage of weight loss relates to temperatures above 400 °C, which indicates burning structural water (i.e., organic chain) and converting water to Carbon monoxide (CO). As per our results, this nanocomposite depicts the weight loss of 0.91 mg (24.44%) at 1000 °C. Further, this nanocomposite shows low weight loss and high stability at 90 °C, which is similar to the reservoir conditions [95,96].

### 3.2. Effect of (SiO<sub>2</sub>@Montmorilant@Xanthan) nanocomposite on IFT

IFT between two liquids, crude oil and nano-suspensions, at various concentrations of the SiO<sub>2</sub>@Montmorilant@Xanthan nano-formulations were measured at ambient conditions to fully comprehend the IFT reduction behaviour with nanofluids. The selected concentrations for these experiments were 100, 250, 500, 1000, 1500, and 2000 ppm. As shown in Fig. 10, the IFT of crude oil droplet has decreased in presence of various nano-suspensions. However, 250 ppm nanofluid concentration has showed an optimum effectiveness for reducing the IFT at maximum. For instance, the IFT of crude oil droplet in the presence of de-ionized water was reported 35 mN/m; whereas, at 250 ppm nanofluid concentration it has decreased to 15.42 mN/m (56% decrease). This decrease in IFT is due to the contact between nano-suspension and crude oil; where, nanofluids make a thin layer as a result of regular coalescence of nanoparticles. This phenomenon increases the entropy, mobility, and absorbance of nanoparticles on the surface of crude oil, causing a pressure profile (disjoining pressure) that reduces the surface tension between two liquids. The strength of this pressure profile is

controlled by temperature, particle size, and the amount of ionic strength [97].

### 3.3. Effect of (SiO<sub>2</sub>@Montmorilant@Xanthan) nanocomposite on wettability

Wettability is a very important factor governing adherence of a fluid into pore spaces [98] and determines the recovery potential for any hydrocarbon reservoirs [99]. However, wettability of any given rock-fluid system is dependent on salinity, pressure, type of formation, and temperature [29,100]. Nanoparticles are getting high importance due to their ability to shift the hydrophobic wettability into hydrophilic [26,74]. Hence, it is convenient to assess nano-suspensions to determine optimum nanofluid concentration for the reversal of wettability at maximum. Higher nanofluid concentration is also efficient to reduce contact angle [25,101,102], but may cause clogging and thus reducing reservoir permeability [103]. It is also found from the literature that higher nanoparticle concentrations are prone to reduced nanofluids stability [104,105], despite the exposure of surfactants [106], which can reduce its required potential. Thus, it is very important to find optimum effective nano-suspension from a commercial viewpoint [30]. To do that, we have aged oil-wet sandstone and carbonate rock thin sections in various nanofluid concentrations (100, 250, 500, 1000, 1500, and 2000 ppm) to determine their optimum ability for reversing the wettability of sandstone and carbonate rock thin sections at ambient conditions in the presence of crude oil.

Initially, a drop of crude oil was suspended on crude oil aged rock thin section of both reservoir formations to measure the initial contact angle in the presence of de-ionized water, which was measure 150° for the carbonate sample and 140° for the sandstone sample. Then, rock thin sections were aged in various nanofluid concentrations followed by contact angle measurements via dispensing a droplet of crude oil to quantify nanoparticles effect. It is clear from our results (Table 5) that, outer tangent angles of sandstone and carbonate rock thin sections have reduced due to the irreversible adsorption of nanoparticles, but the degree of change depends on the type of formation and nanofluid concentration. For example, the outer contact angle of the carbonate rock thin section aged in 250 ppm nanofluid concentration has been reduced to 33°, whereas, at similar nanofluid concentrations in the sandstone rock thin section, the outer contact angle has reduced to 117°. Similarly, the outer contact angle of the sandstone rock thin section aged in 1000 ppm nanofluid concentration has been reduced to 34°, whereas, at similar nanofluid concentrations in the carbonate rock thin section, the outer contact angle has reduced to 85°. It can be concluded here that 250 ppm nanofluid concentration is the optimum concentration for reversing the wettability of oil-wet carbonate rock thin sections and 1000 ppm nanofluid concentration is the optimum concentration for reversing the wettability of oil-wet sandstone rock thin sections, respectively.

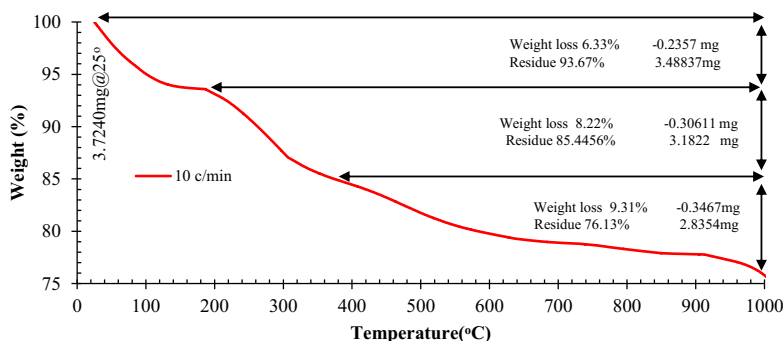


**Fig. 9.** Thermal stability (TGA) curve of the SiO<sub>2</sub>@Montmorilant@Xanthan nanocomposite.

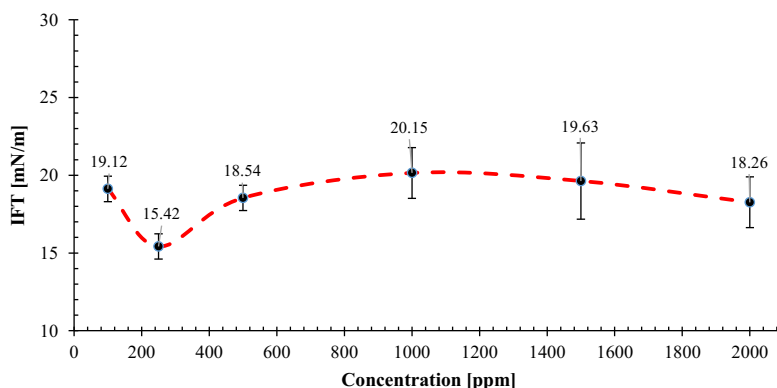
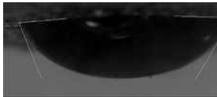


Fig. 10. The IFT values measured for the crude oil in the presence of the SiO<sub>2</sub>@Montmorilant@Xanthan nanocomposite.

Table 5  
Contact angle profile of the SiO<sub>2</sub>@Montmorilant@Xanthan nanocomposite.

| No. | Nanofluid Concentration | Initial Contact Angle                | Final Contact Angle of Carbonate after Ageing with Nanofluid                                | Final Contact Angle of Sandstone after Ageing with Nanofluid                                 |
|-----|-------------------------|--------------------------------------|---|--|
| 1   | 100 (ppm)               | Carbonate = 150°<br>Sandstone = 140° | <br>109°   | <br>77°   |
| 2   | 250 (ppm)               | Carbonate = 150°<br>Sandstone = 140° | <br>33°   | <br>117° |
| 3   | 500 (ppm)               | Carbonate = 150°<br>Sandstone = 140° | <br>50°  | <br>78° |
| 4   | 1000 (ppm)              | Carbonate = 150°<br>Sandstone = 140° | <br>85°  | <br>34° |
| 5   | 1500 (ppm)              | Carbonate = 150°<br>Sandstone = 140° | <br>134° | <br>39° |
| 6   | 2000 (ppm)              | Carbonate = 150°<br>Sandstone = 140° | <br>145° | <br>61° |

3.4. Effect of (SiO<sub>2</sub>@Montmorilant@Xanthan) nanocomposite on oil recovery

In this research work, we conducted core flooding experiments on sandstone and carbonate rock samples with their respective optimum nanofluid concentrations to quantify the effect of biosynthesized nanocomposite. To do this, core flooding experiments were divided into three phases: (1) saturation of rock samples with de-ionized water (for measuring absolute permeability) followed by crude oil injection for measuring OOIP, and Sw<sub>r</sub> (2) injection of seawater to quantify the

secondary recovery potential and (3) injection of respective optimum biosynthesized smart nanofluid concentrations in their respective rock samples for quantifying the effect of tertiary recovery potential. All of the core flooding experiments were conducted at a constant flow rate of 0.2 cc/min and a constant pressure of 2000 psi at 60 °C; which, was high enough to overcome the capillary end effect and results were reasonably close to the real fluid velocity in porous media. The detailed summary of core flooding tests including secondary and tertiary flooding data using carbonate and sandstone core plugs is presented in Table 6.

**Table 6**  
Summary of the core flooding tests.

| Core plug                       | 1 (sandstone)         | 2 (carbonate)         |
|---------------------------------|-----------------------|-----------------------|
| Characteristic                  |                       |                       |
| Porosity (%)                    | 15.32                 | 12.82                 |
| Permeability (mD)               | 30                    | 8.23                  |
| Pore volume (cm <sup>3</sup> )  | 10.41                 | 9.65                  |
| Initial oil saturation (%)      | 61                    | 68.92                 |
| Secondary recovery              |                       |                       |
| Injected fluid                  | Seawater              | Seawater              |
| Oil recovery (%)                | 51.05                 | 40.20                 |
| Oil saturation (%)              | 29.85                 | 41.21                 |
| Capillary number, dimensionless | $0.27 \times 10^{-5}$ | $0.43 \times 10^{-5}$ |
| Mobility ratio, dimensionless   | 28.2                  | 29.1                  |
| Tertiary recovery               |                       |                       |
| Injected fluid                  | 1000 ppm -NCs         | 250 ppm -NCs          |
| Oil recovery (%)                | 15.79                 | 11.72                 |
| Oil saturation (%)              | 25.14                 | 36.38                 |
| Capillary number, dimensionless | $0.58 \times 10^{-5}$ | $0.83 \times 10^{-5}$ |
| Mobility ratio, dimensionless   | 18.2                  | 22.5                  |
| Total oil recovery (%OOIP)      | <b>66.85</b>          | <b>51.92</b>          |

**3.4.1. Nanofluid (1000 ppm) injection in sandstone core sample**

The results of the secondary and tertiary recovery tests on core plug 1 (sandstone) for the 1000 ppm nanofluid injection are presented in Fig. 11. It is clear from our results that biosynthesized smart nanofluid injection was very effective in enhancing oil recovery in sandstone rock samples after seawater injection (secondary recovery potential). After the initial crude oil injection in the fully saturated (by de-ionized water) sandstone sample, the amount of OOIP was 5.7 cc (61%) and the irreducible water saturation was 39%. Then, seawater injection (secondary recovery) produced 51.05% of the OOIP. Afterward, 1000 ppm of biosynthesized smart nanofluid was injected which has resulted in a further 15.79% increase in oil recovery from residually trapped oil in the sandstone pore matrix. The breakthrough point for tertiary oil recovery, where two-phase flow started (crude oil and 1000 ppm nanofluid in this case) has happened in about 1.27 pore volume of 1000 ppm nanofluid injection.

Fig. 12 shows water and oil relative permeability curves plotted via Johnson, Bossler, and Nauman (JBN) method for both secondary and tertiary recoveries in the sandstone core plug. This method requires effluent phase ratio vs time during two-phase displacement and overall pressure drop to calculate relative permeability curves. As shown in Fig. 12, the intersection point (at 57%) of water and oil permeability curves in the secondary recovery stage (located on the left side) indicates that the core is weakly water-wet [107]. In the tertiary recovery stage, the intersection point (at 65%) of water and oil permeability curves moves toward the right side, which confirms that after 1000 ppm NCs

injection the sandstone core plug became strongly water-wet. This shifting in wettability phase towards hydrophilic conditions is responsible for the decrease in residual oil saturation ( $S_{or}$ ) and increase in  $S_{wr}$ , hence resulting in enhancement of oil recovery.

**3.4.2. Nanofluid (250 ppm) injection in carbonate core sample**

Fig. 13 depicts the results of the secondary and tertiary recovery tests on core plug 2 (carbonate) for the 250 ppm nanofluid injection. It is clear from our results that biosynthesized smart nanofluid injection was also very effective in enhancing residual oil recovery in carbonate rock samples after seawater injection (secondary recovery potential). After the initial crude oil injection in a fully saturated (by de-ionized water) carbonate sample, the amount of OOIP was 6.9 cc (68.92%) and the irreducible water saturation was 31.08%. Thereafter, seawater injection (secondary recovery) produced 40.2% of the OOIP. Afterward, 250 ppm biosynthesized smart nanofluid was injected which has resulted in a further 11.72% increase in oil recovery from residually trapped oil in the carbonate pore matrix. The breakthrough point, where two-phase flow started (crude oil and 250 ppm nanofluid in this case) for tertiary oil recovery has happened in about 1.52 pore volume of 250 ppm nanofluid injection.

The water and oil relative permeability curves (Fig. 14) via Johnson, Bossler, and Nauman (JBN) method for both secondary and tertiary recoveries in the carbonate core plug have shown the same phenomena as of sandstone core plug, but the degree of change was different. As shown in Fig. 14, the intersection point (at 53%) of water and oil permeability curves in the secondary recovery stage (located on the left side) indicates that the core is weakly water-wet. In the tertiary recovery stage, the intersection point (at 67%) of water and oil permeability curves moves toward the right side, which confirms that after 250 ppm NCs injection the carbonate core plug became strongly water-wet. This increase in  $S_{wr}$  and decrease in  $S_{or}$  is caused by the shifting of wettability state from weakly water-wet to strongly water-wet (note that the wettability shift in carbonate core plug was 14% compared to 8% in sandstone core plug). In a nutshell, enhanced oil recovery methods require new materials such as our biosynthesized nanofluid which can play an integral part in enhancing the oil recovery and meeting the demand of the overgrowing population from the existing sedimentary reservoirs.

**4. Summary and conclusions**

Nanofluids or nano-suspensions of various nanocomposites suspended in surfactants, brine solutions, or de-ionized water have provided a way to deal with different nano-energy applications in subsurface formations including drilling [22–24], CO<sub>2</sub> storage [32,108],

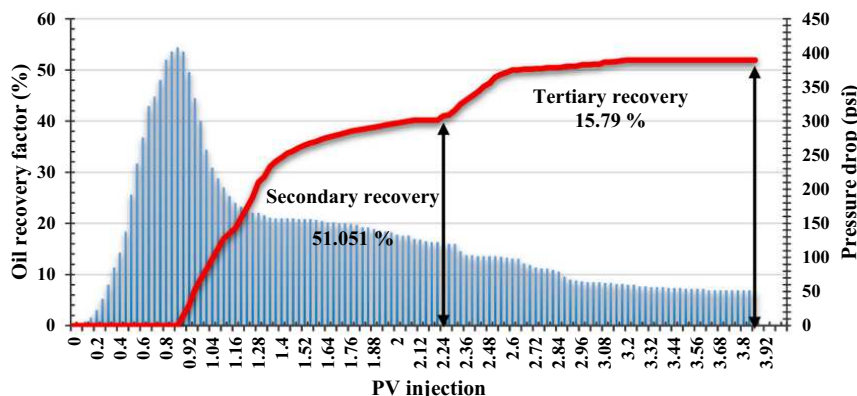


Fig. 11. Oil recovery factor VS pore volume of 1000 ppm, NCs injection.

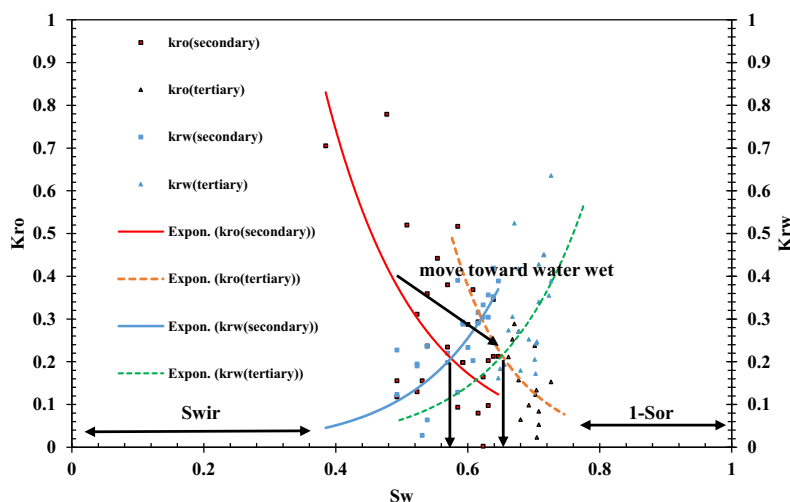


Fig. 12. Relative permeability curves of water and oil for the water-wet sandstone rock during the seawater injection and NCs (1000 ppm) flooding (Plotted using the JBN method).

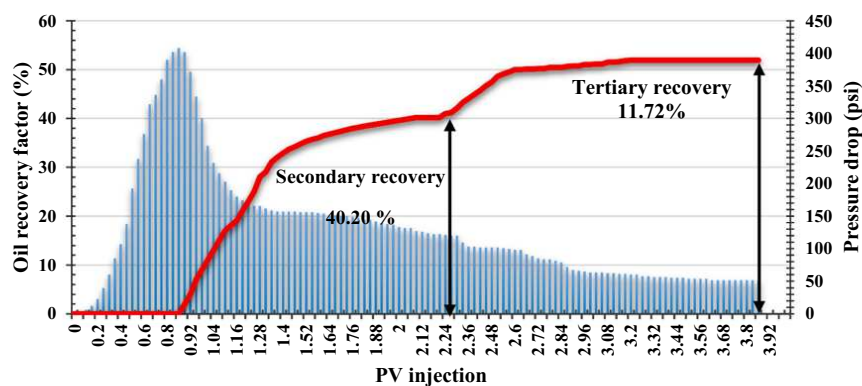


Fig. 13. Oil recovery factor VS pore volume of 250 ppm, NCs injection.

and enhanced oil recovery [13,19,60]. In this article, a green novel ( $\text{SiO}_2$ @Montmorilant@Xanthan) nanocomposite was biosynthesized using silica, montmorilant, xanthan, and Adinandra dumosa plant extract to comprehend its effects for IFT reduction and wettability shift for the applications of EOR. This study was divided into three parts, (1) analytical characterization of biosynthesized nanocomposite using, XRD, FTIR, TGA, SEM, and EDS techniques, (2) formulating different concentrations (100, 250, 500, 1000, 1500, and 2000 ppm) of nanofluid to comprehend its effects on IFT reduction and wettability reversal, (3) optimum concentrations were acquired for EOR applications in sandstone and carbonate formations. The important outcomes of this article are outlined below:

1. XRD analysis showed that silica/quartz is the predominant phase present in the nanocomposite followed by Montmorillonite. FTIR measurements have shown siloxane bonds (Si–O–Si), (Al – OH) bonding, hydrogen bonding (C–H), and hydroxyl bonding (C–OH). TGA measurements have revealed that this nanocomposite exhibits low weight loss (0.91 mg, 24.44% at 1000 °C) and high thermal stability. FESEM micrographs have depicted irreversible adsorption of nanocomposite with the particle size of 31 to 50 nm and EDS measurements have shown that the Si element is responsible for the

predominance of the quartz structure in the biosynthesized nanocomposite.

2. IFT measurements between crude oil and nano-formulations have revealed a 56% reduction from 35 mN/m to 15.42 mN/m at an optimum nano-concentration of 250 ppm. A similar effect was noted in wettability reversal. The initial contact angle of the oil-wet carbonate sample was 150° which has reduced to 33° at an optimum nano-concentration of 250 ppm. The initial contact angle of the oil-wet sandstone sample was 140° which has reduced to 34° at an optimum nano-concentration of 1000 ppm.
3. The total oil recovery in sandstone rock sample was 66.85% after nanofluid injection with the NCs concentration of 1000 ppm, in which secondary recovery was 51.05% by seawater injection and tertiary recovery was 15.8% by 1000 ppm nanofluid injection. However, the core flooding test in a carbonate rock sample resulted in the total oil recovery of 51.92% after nanofluid injection with the NCs concentration of 250 ppm, in which the secondary recovery was 40.20% by seawater injection and tertiary recovery was 11.72% by 250 ppm nanofluid injection.

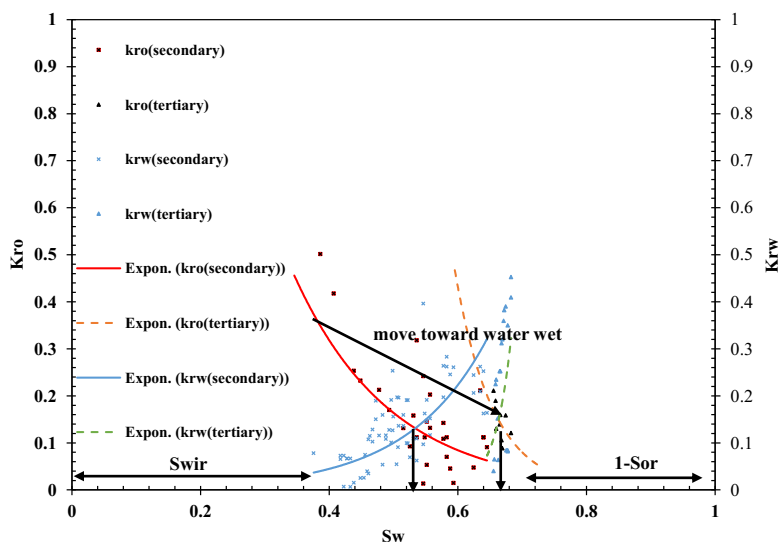


Fig. 14. Relative permeability curves of water and oil for the oil-wet carbonate rock during the seawater injection and NCs (250 ppm) flooding (Plotted using the JBN method).

#### CRediT authorship contribution statement

**Mohammad Javad Nazarahari:** Writing - original draft, Methodology, Formal analysis, Investigation, Data curation. **Abbas Khaksar Manshad:** Conceptualization, Methodology, Resources, Writing - review & editing, Supervision. **Muhammad Ali:** Writing - original draft, Writing - review & editing, Validation, Methodology. **Jagar A Ali:** Data curation, Visualization. **Ali Shafiei:** Software, Formal analysis, Investigation. **S. Mohammad Sajadi:** Formal analysis, Validation. **Siyamak Moradi:** Visualization, Software, Formal analysis. **Stefan Iglauer:** Writing - review & editing, Supervision, Resources. **Alireza Keshavarz:** Writing - review & editing, Supervision, Project administration, Resources.

#### Declaration of Competing Interest

The authors declare that they have no known competing financial interests or personal relationships that could have appeared to influence the work reported in this paper.

#### References

- [1] Mahesar AA, Shar AM, Ali M, Tunio AH, Uqaili MA, Mohanty US, et al. Morphological and petro physical estimation of eocene tight carbonate formation cracking by cryogenic liquid nitrogen; a case study of Lower Indus basin, Pakistan. *J Petrol Sci Eng* 2020;107318.
- [2] Dudley B. BP statistical review of world energy 2016, London, UK, (2015).
- [3] Mahesar AA, Ali M, Shar AM, Memon KR, Mohanty US, Akhondzadeh H, et al. Effect of Cryogenic Liquid Nitrogen on the Morphological and Petrophysical Characteristics of Tight Gas Sandstone Rocks from Kirthar Fold Belt, Indus Basin, Pakistan. *Energy & Fuels*; 2020.
- [4] Memon KR, Mahesar AA, Ali M, Tunio AH, Mohanty US, Akhondzadeh H, et al. Influence of Cryogenic Liquid Nitrogen on Petro-Physical Characteristics of Mancos Shale: An Experimental Investigation. *Energy Fuels* 2020;34:2160–8.
- [5] IEA, *World Energy Outlook*, International Energy Agency (IEA), Paris, (2019).
- [6] Haghghi OM, Zargar G, Khaksar Manshad A, Ali M, Takassi MA, Ali JA, et al. Effect of Environment-Friendly Non-Ionic Surfactant on Interfacial Tension Reduction and Wettability Alteration; Implications for Enhanced Oil Recovery. *Energies* 2020;13:3988.
- [7] Nowrouzi I, Manshad AK, Mohammadi AH. Effects of dissolved binary ionic compounds and different densities of brine on interfacial tension (IFT), wettability alteration, and contact angle in smart water and carbonated smart water injection processes in carbonate oil reservoirs. *J Mol Liq* 2018;254:83–92.
- [8] Nowrouzi I, Manshad AK, Mohammadi AH. Effects of TiO<sub>2</sub>, MgO and  $\gamma$ -Al<sub>2</sub>O<sub>3</sub> nano-particles on wettability alteration and oil production under carbonated nano-fluid imbibition in carbonate oil reservoirs. *Fuel* 2020;259:116110.
- [9] Ali M, Al-Ansari S, Shakeel M, Arif M, Dahraj NU, Iglauer S. Influence of Miscible CO<sub>2</sub> Flooding on Wettability and Asphaltene Precipitation in Indiana Lime Stone, in: SPE/IATMI Asia Pacific Oil & Gas Conference and Exhibition, Society of Petroleum Engineers, 2017.
- [10] Ali M, Dahraj NU, Haider SA. Study of Asphaltene Precipitation during CO<sub>2</sub> Injection in Light Oil Reservoirs, in: SPE/PAPG Pakistan section Annual Technical Conference, Society of Petroleum Engineers, 2015.
- [11] Sheng JJ, Chen K. Evaluation of the EOR potential of gas and water injection in shale oil reservoirs. *J Unconv Oil Gas Resour* 2014;5:1–9.
- [12] Shahverdi H, Sohrabi M. Relative permeability characterization for water-alternating-gas injection in oil reservoirs. *SPE J* 2016;21:799–808.
- [13] Al-Ansari S, Arain Z-U-A, Barifciani A, Keshavarz A, Ali M, Iglauer S. Influence of Pressure and Temperature on CO<sub>2</sub>-Nanofluid Interfacial Tension: Implication for Enhanced Oil Recovery and Carbon Geosequestration, in: Abu Dhabi International Petroleum Exhibition & Conference, Society of Petroleum Engineers, 2018.
- [14] Awan FUR, Keshavarz A, Akhondzadeh H, Al-Ansari S, Al-Yaseri A, Nosrati A, et al. Stable Dispersion of Coal Fines during Hydraulic Fracturing Flowback in Coal Seam Gas Reservoirs—An Experimental Study. *Energy Fuels* 2020;34:5566–77.
- [15] Dahraj NU, Ali M, Khan MN. End of Linear Flow Time Picking in Long Transient Hydraulically Fractured Wells to Correctly Estimate the Permeability, Fracture Half-Length and Original Gas in Place in Liquid Rich Shales. *PAPG/SPE Pakistan Section Annual Technical Conference and Exhibition, Society of Petroleum Engineers* 2016.
- [16] Al-Rubaye A, Al-Yaseri A, Ali M, Mahmud HB. Characterization and analysis of naturally fractured gas reservoirs based on stimulated reservoir volume and petro-physical parameters. *J Pet Explor Prod Technol* 2021;1–11.
- [17] Al-Ansari S, Ali M, Alajmi M, Akhondzadeh H, Khaksar Manshad A, Kalantariasl A, et al. Synergistic Effect of Nanoparticles and Polymers on the Rheological Properties of Injection Fluids: Implications for Enhanced Oil Recovery. *Energy Fuels* 2021.
- [18] Awan FUR, Keshavarz A, Azhar MR, Akhondzadeh H, Ali M, Al-Yaseri A, et al. Adsorption of nanoparticles on glass bead surface for enhancing proppant performance: A systematic experimental study. *J Mol Liq* 2021;115398.
- [19] Jha NK, Iglauer S, Barifciani A, Sarmadivaleh M, Sangwai JS. Low-salinity surfactant nanofluid formulations for wettability alteration of sandstone: role of the SiO<sub>2</sub> nanoparticle concentration and divalent cation/SO<sub>4</sub><sup>2-</sup>-ratio. *Energy Fuels* 2019;33:739–46.
- [20] Ali JA, Kolo K, Khaksar Manshad A, Stephen KD. Low-salinity polymeric nanofluid-enhanced oil recovery using green polymer-coated ZnO/SiO<sub>2</sub> nanocomposites in the Upper Qamchuqa Formation in Kurdistan Region. *Iraq, Energy & fuels* 2019;33:927–37.
- [21] Ali JA, Kolo K, Manshad AK, Mohammadi AH. Recent advances in application of nanotechnology in chemical enhanced oil recovery: Effects of nanoparticles on wettability alteration, interfacial tension reduction, and flooding. *Egypt J Pet* 2018;27:1371–83.

- [22] Ali M, Jarni HH, Aftab A, Ismail AR, Saady NMC, Sahito MF, et al. Nanomaterial-based drilling fluids for exploitation of unconventional reservoirs: A review. *Energies* 2020;13:3417.
- [23] Aftab A, Ali M, Arif M, Panhwar S, Saady NMC, Al-Khdheawi EA, et al. Influence of tailor-made TiO<sub>2</sub>/API bentonite nanocomposite on drilling mud performance: Towards enhanced drilling operations. *Appl Clay Sci* 2020;199:105862.
- [24] Aftab A, Ali M, Sahito MF, Mohanty US, Jha NK, Akhondzadeh H, et al. Environmental Friendliness and High Performance of Multifunctional Tween 80/ZnO-Nanoparticles-Added Water-Based Drilling Fluid: An Experimental Approach. *ACS Sustainable Chem Eng* 2020;8:11224–43.
- [25] Al-Anssari S, Barifcani A, Wang S, Maxim L, Iglauer S. Wettability alteration of oil-wet carbonate by silica nanofluid. *J Colloid Interface Sci* 2016;461:435–42.
- [26] Ali M, Aftab A, Awan FUR, Akhondzadeh H, Keshavarz A, Saeedi A, et al. CO<sub>2</sub>-wettability reversal of cap-rock by alumina nanofluid: Implications for CO<sub>2</sub> geostorage. *Fuel Process Technol* 2021;214:106722.
- [27] Negin C, Ali S, Xie Q. Application of nanotechnology for enhancing oil recovery—A review. *Petroleum* 2016;2:324–33.
- [28] Bera A, Belhaj H. Application of nanotechnology by means of nanoparticles and nanodispersions in oil recovery—A comprehensive review. *J Nat Gas Sci Eng* 2016;34:1284–309.
- [29] Iglauer S. CO<sub>2</sub>–water–rock wettability: variability, influencing factors, and implications for CO<sub>2</sub> geostorage. *Acc Chem Res* 2017;50:1134–42.
- [30] Iglauer S, Wu Y, Shuler P, Tang Y, Goddard III WA. New surfactant classes for enhanced oil recovery and their tertiary oil recovery potential. *J Petrol Sci Eng* 2010;71:23–9.
- [31] Sarmadivaleh M, Al-Yaseri AZ, Iglauer S. Influence of temperature and pressure on quartz–water–CO<sub>2</sub> contact angle and CO<sub>2</sub>–water interfacial tension. *J Colloid Interface Sci* 2015;441:59–64.
- [32] Al-Anssari S, Barifcani A, Keshavarz A, Iglauer S. Impact of nanoparticles on the CO<sub>2</sub>-brine interfacial tension at high pressure and temperature. *J Colloid Interface Sci* 2018;532:136–42.
- [33] Al-Anssari S, Araïn Z-U-A, Shanshool HA, Ali M, Keshavarz A, Iglauer S, et al. Effect of Nanoparticles on the Interfacial Tension of CO-Oil System at High Pressure and Temperature: An Experimental Approach, in: *SPE Asia Pacific Oil & Gas Conference and Exhibition, Society of Petroleum Engineers* 2020.
- [34] Ali M. Effect of Organic Surface Concentration on CO<sub>2</sub>-Wettability of Reservoir Rock, in: *Curtin University*; 2018.
- [35] Ali M, Aftab A, Araïn ZU, Al-Yaseri A, Roshan H, Saeedi A, et al. Influence of Organic Acid Concentration on Wettability Alteration of Cap-Rock: Implications for CO<sub>2</sub> Trapping/Storage. *ACS Appl Mater Interfaces* 2020;12:39850–8.
- [36] Ali M, Arif M, Sahito MF, Al-Anssari S, Keshavarz A, Barifcani A, et al. CO<sub>2</sub>-wettability of sandstones exposed to traces of organic acids: Implications for CO<sub>2</sub> geo-storage. *Int J Greenhouse Gas Control* 2019;83:61–8.
- [37] Iglauer S, Ali M, Keshavarz A. Hydrogen Wettability of Sandstone Reservoirs: Implications for Hydrogen Geo-Storage. *Geophys Res Lett* 2020.
- [38] Ali M, Awan FUR, Ali M, Al-Yaseri A, Arif M, Sánchez-Román M, et al. Effect of humic acid on CO<sub>2</sub>-wettability in sandstone formation. *J Colloid Interface Sci* 2021;588:315–25.
- [39] Li Q, Wei B, Lu L, Li Y, Wen Y, Pu W, et al. Investigation of physical properties and displacement mechanisms of surface-grafted nano-cellulose fluids for enhanced oil recovery. *Fuel* 2017;207:352–64.
- [40] Kamal MS, Hussein IA, Sultan AS. Review on surfactant flooding: phase behavior, retention, IFT, and field applications. *Energy & Fuels* 2017;31:7701–20.
- [41] Zhong H, Zang Q, Yin H, Xia H. Experimental study on medium viscosity oil displacement using viscoelastic polymer. *Geofluids* 2018;2018.
- [42] Abidin A, Puspasari T, Nugroho W. Polymers for enhanced oil recovery technology. *Procedia Chem* 2012;4:11–6.
- [43] Rellegadla S, Prajapat G, Agrawal A. Polymers for enhanced oil recovery: fundamentals and selection criteria. *Appl Microbiol Biotechnol* 2017;101:4387–402.
- [44] Seright R. Use of polymers to recover viscous oil from unconventional reservoirs, in: *New Mexico Institute of Mining And Technology* 2011.
- [45] Yousefvand H, Jafari A. Enhanced oil recovery using polymer/nanosilica. *Procedia Mater Sci* 2015;11:565–70.
- [46] Pal N, Saxena N, Laxmi KD, Mandal A. Interfacial behaviour, wettability alteration and emulsification characteristics of a novel surfactant: Implications for enhanced oil recovery. *Chem Eng Sci* 2018;187:200–12.
- [47] Maurya NK, Kushwaha P, Mandal A. Studies on interfacial and rheological properties of water soluble polymer grafted nanoparticle for application in enhanced oil recovery. *J Taiwan Inst Chem Eng* 2017;70:319–30.
- [48] Maurya NK, Mandal A. Studies on behavior of suspension of silica nanoparticle in aqueous polyacrylamide solution for application in enhanced oil recovery. *Pet Sci Technol* 2016;34:429–36.
- [49] Pal N, Kumar N, Mandal A. Stabilization of dispersed oil droplets in nanoemulsions by synergistic effects of the gemini surfactant. PHPA polymer, and silica nanoparticle. *Langmuir* 2019;35:2655–67.
- [50] Pal N, Kumar N, Saw RK, Mandal A. Gemini surfactant/polymer/silica stabilized oil-in-water nanoemulsions: Design and physicochemical characterization for enhanced oil recovery. *J Petrol Sci Eng* 2019;183:106464.
- [51] Abramov A, Keshavarz A, Iglauer S. Wettability of Fully Hydroxylated and Alkylated (001)  $\alpha$ -Quartz Surface in Carbon Dioxide Atmosphere. *The Journal of Physical Chemistry C* 2019;123:9027–40.
- [52] Asl HF, Zargar G, Manshad AK, Takassi MA, Ali JA, Keshavarz A. Experimental investigation into I-Arg and L-Cys eco-friendly surfactants in enhanced oil recovery by considering IFT reduction and wettability alteration. *Pet Sci* 2020;17:105–17.
- [53] Rebello S, Asok AK, Mundayoor S, Jisha M. Surfactants: toxicity, remediation and green surfactants. *Environ Chem Lett* 2014;12:275–87.
- [54] Olajire AA. Review of ASP EOR (alkaline surfactant polymer enhanced oil recovery) technology in the petroleum industry: Prospects and challenges. *Energy* 2014;77:963–82.
- [55] Vryzas Z, Kelessidis VC. Nano-based drilling fluids: A review. *Energies* 2017;10:540.
- [56] Epelle EI, Gerogiorgis DI. A multiparametric CFD analysis of multiphase annular flows for oil and gas drilling applications. *Comput Chem Eng* 2017;106:645–61.
- [57] Giger W, Brunner PH, Schaffner C. 4-Nonylphenol in sewage sludge: accumulation of toxic metabolites from nonionic surfactants. *Science* 1984;225:623–5.
- [58] KvESTAK R, Ahel M. Occurrence of toxic metabolites from nonionic surfactants in the Krka river estuary. *Ecotoxicol Environ Saf* 1994;28:25–34.
- [59] Lechuga M, Fernández-Serrano M, Jurado E, Núñez-Olea J, Ríos F. Acute toxicity of anionic and non-ionic surfactants to aquatic organisms. *Ecotoxicol Environ Saf* 2016;125:1–8.
- [60] O.A. Alomair, K.M. Matar, Y.H. Alsaedi, Nanofluids application for heavy oil recovery, in: *SPE Asia Pacific oil & gas conference and exhibition, Society of Petroleum Engineers*, 2014.
- [61] W. Wu, Q. He, C.J.N.r.l. Jiang, Magnetic iron oxide nanoparticles: synthesis and surface functionalization strategies, 3 (2008) 397.
- [62] R.D. Shah, Application of nanoparticle saturated injectant gases for EOR of heavy oils, in: *SPE annual technical conference and exhibition, Society of Petroleum Engineers*, 2009.
- [63] Yuan B, Moghanloo RG, Zheng D. Enhanced oil recovery by combined nanofluid and low salinity water flooding in multi-layer heterogeneous reservoirs. *SPE annual technical conference and exhibition. Society of Petroleum Engineers*; 2016.
- [64] H. Karimi-Maleh, P. Biparva, M.J.B. Hatami, Bioelectronics, A novel modified carbon paste electrode based on NiO/CNTs nanocomposite and (9, 10-dihydro-9, 10-ethanoanthracene-11, 12-dicarboximido)-4-ethylbenzene-1, 2-diol as a mediator for simultaneous determination of cysteamine, nicotinamide adenine dinucleotide and folic acid, 48 (2013) 270-275.
- [65] Roustaei A, Moghadasi J, Bagherzadeh H, Shahrabadi A. An experimental investigation of polysilicon nanoparticles' recovery efficiencies through changes in interfacial tension and wettability alteration. *SPE international oilfield nanotechnology conference and exhibition. Society of Petroleum Engineers*; 2012.
- [66] Hendraningrat L, Torsæter OJAN. Metal oxide-based nanoparticles: revealing their potential to enhance oil recovery in different wettability systems 2015;5: 181–99.
- [67] M. Seid Mohammadi, J. Moghadasi, S.J.L.J.o.O. Naseri, G. Science, Technology, An experimental investigation of wettability alteration in carbonate reservoir using  $\gamma$ -Al<sub>2</sub>O<sub>3</sub> nanoparticles, 3 (2014) 18-26.
- [68] Salem Ragab AM, Hannora AE. A Comparative investigation of nano particle effects for improved oil recovery—experimental work. *SPE Kuwait oil and gas show and conference. Society of Petroleum Engineers*; 2015.
- [69] Maghzi A, Kharrat R, Mohebbi A, Ghazanfari MHJF. The impact of silica nanoparticles on the performance of polymer solution in presence of salts in polymer flooding for heavy oil recovery 2014;123:123–32.
- [70] Kapusta S, Balzano L, Te Riele PM. Nanotechnology applications in oil and gas exploration and production, in: *International Petroleum Technology Conference, International Petroleum Technology Conference* 2011.
- [71] Y. Assef, D. Arab, P.J.J.o.P.S. Pourafshary, Engineering, Application of nanofluid to control fines migration to improve the performance of low salinity water flooding and alkaline flooding, 124 (2014) 331-340.
- [72] Kamal MS, Adewunmi AA, Sultan AS, Al-Hamad MF, Mehmood U. Recent advances in nanoparticles enhanced oil recovery: rheology, interfacial tension, oil recovery, and wettability alteration. *Journal of Nanomaterials* 2017;2017.
- [73] Mahdi Jafari S, He Y, Bhandari B. Nano-emulsion production by sonication and microfluidization—a comparison. *Int J Food Prop* 2006;9:475–85.
- [74] Al-Anssari S, Arif M, Wang S, Barifcani A, Lebedev M, Iglauer S. Wettability of nanofluid-modified oil-wet calcite at reservoir conditions. *Fuel* 2018;211:405–14.
- [75] El-sayed GM, Kamel M, Morsy N, Taher F. Encapsulation of nano Disperse Red 60 via modified miniemulsion polymerization. I. Preparation and characterization. *J Appl Polym Sci* 2012;125:1318–29.
- [76] Ahualli S, Iglesias G, Wachter W, Dulle M, Minami D, Glatter O. Adsorption of anionic and cationic surfactants on anionic colloids: supercharging and destabilization. *Langmuir* 2011;27:9182–92.
- [77] Iglauer S, Salamah A, Sarmadivaleh M, Liu K, Phan C. Contamination of silica surfaces: Impact on water–CO<sub>2</sub>–quartz and glass contact angle measurements. *Int J Greenhouse Gas Control* 2014;22:325–8.
- [78] Gomari KR, Hamouda A. Effect of fatty acids, water composition and pH on the wettability alteration of calcite surface. *J Petrol Sci Eng* 2006;50:140–50.
- [79] Hamouda AA, Rezaei Gomari KA. Influence of temperature on wettability alteration of carbonate reservoirs, in: *SPE/DOE Symposium on Improved Oil Recovery, Society of Petroleum Engineers* 2006.
- [80] Davis JA. Adsorption of natural dissolved organic matter at the oxide/water interface. *Geochim Cosmochim Acta* 1982;46:2381–93.
- [81] M. Kleber, K. Eusterhues, M. Keilueit, C. Mikutta, R. Mikutta, P.S. Nico, Mineral-organic associations: formation, properties, and relevance in soil environments, in: *Advances in agronomy, Elsevier*, 2015, pp. 1-140.
- [82] Grate JW, Dehoff KJ, Warner MG, Pittman JW, Wietsma TW, Zhang C, et al. Correlation of oil–water and air–water contact angles of diverse silanized surfaces and relationship to fluid interfacial tensions. *Langmuir* 2012;28:7182–8.

- [83] Ali M, Sahito MF, Jha NK, Arain ZU, Memon S, Keshavarz A, et al. Effect of nanofluid on CO<sub>2</sub>-wettability reversal of sandstone formation; implications for CO<sub>2</sub> geo-storage. *J Colloid Interface Sci* 2020;559:304–12.
- [84] Zullig JJ, Morse JW. Interaction of organic acids with carbonate mineral surfaces in seawater and related solutions: I. Fatty acid adsorption, *Geochimica et Cosmochimica Acta* 1988;52:1667–78.
- [85] Madsen L, Ida L. Adsorption of carboxylic acids on reservoir minerals from organic and aqueous phase. *SPE Reservoir Eval Eng* 1998;1:47–51.
- [86] Jardine P, McCarthy J, Weber N. Mechanisms of dissolved organic carbon adsorption on soil. *Soil Sci Soc Am J* 1989;53:1378–85.
- [87] Arif M, Abu-Khamsin SA, Zhang Y, Iglauer S. Experimental investigation of carbonate wettability as a function of mineralogical and thermo-physical conditions. *Fuel* 2020;264:116846.
- [88] Eskelinen P. X-ray diffraction study of TiO<sub>2</sub> thin films on mica. *J Solid State Chem* 1992;100:356–62.
- [89] Swapna K, Mahamuda S, Rao AS, Shakya S, Sasikala T, Haranath D, et al. Optical studies of Sm<sup>3+</sup> ions doped zinc alumino bismuth borate glasses. *Spectrochim Acta Part A Mol Biomol Spectrosc* 2014;125:53–60.
- [90] Mahamuda S, Swapna K, Venkateswarlu M, Rao AS, Shakya S, Prakash GV. Spectral characterisation of Sm<sup>3+</sup> ions doped Oxy-fluoroborate glasses for visible orange luminescent applications. *J Lumin* 2014;154:410–24.
- [91] Maina E, Wanyika H, Gacanja AJCMR. Instrumental characterization of montmorillonite Clay by FT-IR and XRD from JKUAT farm. the Republic of Kenya 2015;7:43–9.
- [92] Shokri B, Firouzjah MA, Hosseini S. FTIR analysis of silicon dioxide thin film deposited by metal organic-based PECVD, in: Proceedings of 19th international symposium on plasma chemistry society. 2009.
- [93] S. Musić, N. Filipović-Vinceković, L.J.B.j.o.c.e. Sekovanić, Precipitation of amorphous SiO<sub>2</sub> particles and their properties, 28 (2011) 89-94.
- [94] Coats A, Redfern J. Thermogravimetric analysis. A review, *Analyst* 1963;88: 906–24.
- [95] Deshmukh P, Peshwe D, Pathak S. FTIR and TGA analysis in relation with the% crystallinity of the SiO<sub>2</sub> obtained by burning rice husk at various temperatures, in. *Advanced Materials Research, Trans Tech Publ* 2012:77–81.
- [96] Vieillard P, Tajeddine L, Gailhanou H, Blanc P, Lassin AJPAA. Thermo-Analytical Techniques on MX-80 Montmorillonite: A Way to Know the Behavior of Water and its Thermodynamic Properties during Hydration-Dehydration Processes 2016;7:462.
- [97] I. Nowrouzi, A.K. Manshad, A.H.J.J.o.P.S. Mohammadi, Engineering, Effects of concentration and size of TiO<sub>2</sub> nano-particles on the performance of smart water in wettability alteration and oil production under spontaneous imbibition, 183 (2019) 106357.
- [98] Arif M, Abu-Khamsin SA, Iglauer S. Wettability of rock/CO<sub>2</sub>/brine and rock/oil/CO<sub>2</sub>-enriched-brine systems: Critical parametric analysis and future outlook. *Adv Colloid Interface Sci* 2019;268:91–113.
- [99] Abdullelah H, Al-Yaseri A, Ali M, Giwelli A, Negash BM, Sarmadivaleh M. CO<sub>2</sub>/Basalt's Interfacial Tension and Wettability Directly from Gas Density: Implications for Carbon Geo-Sequestration. *J Petrol Sci Eng* 2021;108683.
- [100] Arif M, Al-Yaseri AZ, Barifciani A, Lebedev M, Iglauer S. Impact of pressure and temperature on CO<sub>2</sub>-brine-mica contact angles and CO<sub>2</sub>-brine interfacial tension: implications for carbon geo-sequestration. *J Colloid Interface Sci* 2016; 462:208–15.
- [101] Nwidee L, Al-Anssari S, Barifciani A, Sarmadivaleh M, Iglauer S. Nanofluids for enhanced oil recovery processes: wettability alteration using zirconium oxide, in. *Offshore Technology Conference Asia, Offshore Technology Conference* 2016.
- [102] Roustaei A, Bagherzadeh H. Experimental investigation of SiO<sub>2</sub> nanoparticles on enhanced oil recovery of carbonate reservoirs. *J Pet Explor Prod Technol* 2015;5: 27–33.
- [103] ShamsiJazeyi H, Miller CA, Wong MS, Tour JM, Verduzco R. Polymer-coated nanoparticles for enhanced oil recovery. *J Appl Polym Sci* 2014;131.
- [104] Tantra R, Schulze P, Quincey P. Effect of nanoparticle concentration on zeta-potential measurement results and reproducibility. *Particuology* 2010;8:279–85.
- [105] Metin CO, Lake LW, Miranda CR, Nguyen QP. Stability of aqueous silica nanoparticle dispersions. *J Nanopart Res* 2011;13:839–50.
- [106] Sharma T, Kumar GS, Sangwai JS. Comparative effectiveness of production performance of Pickering emulsion stabilized by nanoparticle-surfactant-polymerover surfactant-polymer (SP) flooding for enhanced oil recoveryfor Brownfield reservoir. *J Petrol Sci Eng* 2015;129:221–32.
- [107] Alizadeh AH, Keshavarz A, Haghghi M. Flow rate effect on two-phase relative permeability in Iranian carbonate rocks. *SPE Middle East oil and gas show and conference. Society of Petroleum Engineers*; 2007.
- [108] Al-Khdheawi EA, Mahdi DS, Ali M, Fauziah CA, Barifciani A. Impact of Caprock Type on Geochemical Reactivity and Mineral Trapping Efficiency of CO<sub>2</sub>, in. *Offshore Technology Conference Asia, Offshore Technology Conference* 2020.

## **Appendix 5**

Low-Salinity Polymeric Nanofluid-Enhanced Oil Recovery Using Green Polymer-Coated ZnO/SiO<sub>2</sub> Nanocomposites in the Upper Qamchuqa Formation in Kurdistan Region, Iraq

**Jagar A. Ali**, Kamal Kolo, Abbas Khaksar Manshad, and Karl D. Stephen

Energy & Fuels 2019 33 (2), 927-937

# Low-Salinity Polymeric Nanofluid-Enhanced Oil Recovery Using Green Polymer-Coated ZnO/SiO<sub>2</sub> Nanocomposites in the Upper Qamchuqa Formation in Kurdistan Region, Iraq

Jagar A. Ali,<sup>\*,†</sup> Kamal Kolo,<sup>‡</sup> Abbas Khaksar Manshad,<sup>§</sup> and Karl D. Stephen<sup>||</sup>

<sup>†</sup>Department of Petroleum Engineering, Faculty of Engineering and <sup>‡</sup>Scientific Research Centre, Soran University, Kurdistan Region, Soran, Iraq

<sup>§</sup>Department of Petroleum Engineering, Abadan Faculty of Petroleum Engineering, Petroleum University of Technology (PUT), Abadan, Iran

<sup>||</sup>Institute of Petroleum Engineering, Heriot-Watt University, Riccarton, Edinburgh EH14 4AS, U.K.

## Supporting Information

**ABSTRACT:** Many carbonate oil fields are known to be oil-wet, which makes production more difficult. Enhanced oil recovery methods have been developed in the past to reduce interfacial tension (IFT) and improve displacement efficiency by injecting higher viscosity solutions. This work focused on the production of ZnO/SiO<sub>2</sub> nanocomposite (NC) that is designed to reduce IFT during water-flooding of an oil-wet rock sample from the Upper Qamchuqa carbonate formation. A natural polymer was used as a mobility modifying agent to increase oil recovery. In addition, the effects of water salinity, NC concentration, temperature, and pressure have been analyzed to determine potential improvement on the performance of the stated chemical additives to the injected fluids. ZnO/SiO<sub>2</sub>/xanthan NC was prepared in a simple, economical, and importantly, green way using the pomegranate seed extract and characterized with scanning electron microscopy, transmission electron microscopy, and X-ray diffraction. The potential effect of the polymeric ZnO/SiO<sub>2</sub> nanofluid on IFT reduction was studied. Core-flooding was carried out to investigate the effects of this IFT reduction on relative permeability curves. The results show that the nanofluid with 2000 ppm NC concentration at high temperature and high pressure significantly reduced the IFT, by about 93.6%, from 31.8 to 2.016 mN/m compared with seawater injection, also increasing the oil recovery by about 19.28% from 46.96 to 66.24%, with high shifting of the relative permeability curve to the right. The derived NC is very promising as a chemical for enhanced oil recovery.

## 1. INTRODUCTION

Oil production from existing oil fields is declining, and new fields are harder to find; hence, difficult to produce oil reservoirs and enhanced oil recovery (EOR) approaches are the focus of research in and around the industry.<sup>1</sup> Conventional EOR techniques (microbial, gas injection, and thermal approaches) can experience significant difficulties, such as earlier breakthrough of injected fluids at production wells, and still leave a large amount of oil unrecovered.<sup>2</sup> Chemical EOR methods were introduced several decades ago and include alkaline, surfactant and polymer flooding, sometimes all together. They were applied to boost the oil recovery due to the modification of interfacial tension (IFT), wettability, and the mobility ratio. The high cost of chemicals, possible reservoir damage, high consumption, and chemical loss are the main challenges of these techniques.<sup>3,4</sup> Therefore, a new EOR technology with low cost, high efficiency, and environmental friendliness needs to be developed. To meet these requirements, nanofluids are highly recommended due to their significant EOR functions. The main EOR mechanisms of nanofluid flooding highlighted in the literature are wettability alteration, IFT reduction, and structural disjoining pressure.<sup>5–12</sup> Nanofluids are receiving much attention in the oil and gas industry, currently (Table 1). To exploit their specific features, these unique fluids are usually developed as a solution of nanoparticles (NPs).<sup>13–15</sup> A large surface area and

high surface energy of the nanostructures provide special thermal, electrical, optical, rheological, and interfacial performance.<sup>16–18</sup> During flooding through a porous medium, nanoparticles tend to form a layer in the interface between water and crude oil.<sup>19</sup> According to Hendraningrat and Li,<sup>20</sup> this layer reduces the IFT between immiscible phases dependent on the type, size, and concentration of the nanoparticles. In addition, the pH ratio,<sup>21</sup> salinity level,<sup>22</sup> and solvent type<sup>21</sup> have also been found to be crucial in reducing the IFT and improving oil recovery.

Furthermore, low-salinity (LoSal) water-flooding (LSWF) has been recognized as an effective EOR process in several research studies and field applications by Tripathi and Mohanty,<sup>29</sup> Hourshad and Jerauld,<sup>30</sup> and Shiran and Skauge.<sup>31</sup> In the last two decades, various mechanisms of LSWF have been identified, including the wettability alteration toward a more water-wet system, IFT reduction, and minimizing the residual oil.<sup>32–34</sup> In addition, fines migration has been identified to be induced during LSWF.<sup>35</sup> It is thought that a small amount of residual oil may be carried by migrating fine-grained material because of separation of the oil-coated particles from rock

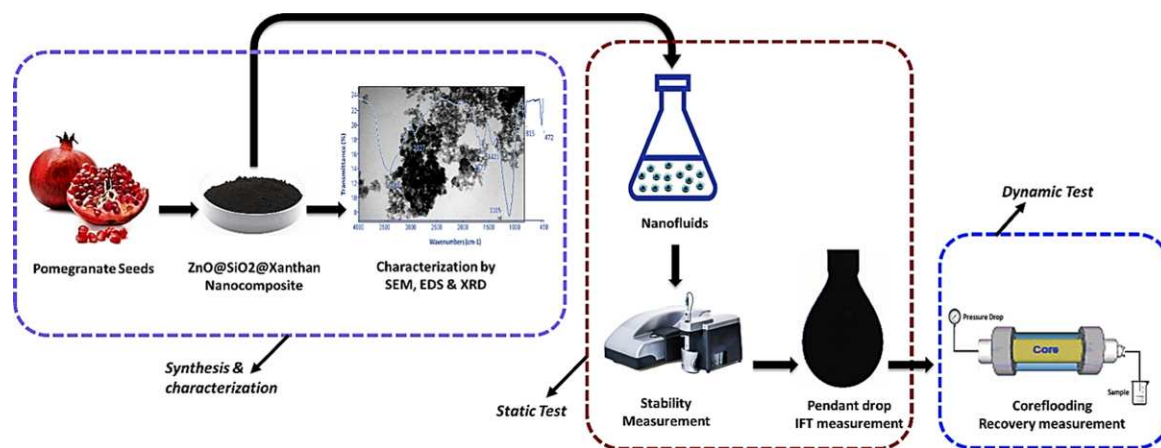
Received: November 5, 2018

Revised: December 24, 2018

Published: January 14, 2019

Table 1. Summary of the Effect of NPs on IFT Reduction and Oil Recovery Reported in the Literature

| references                               | NP                             | NP size (nm) | NP conc.  | dispersion media | porous media | IFT (mN/m) |         | RF (OOIP%) |         |
|--|--------------------------------|--------------|-----------|------------------|--------------|------------|---------|------------|---------|
|  |                                |              |           |                  |              | clean      | with NP | clean      | with NP |
| Roustaei et al. <sup>23</sup>            | SiO <sub>2</sub>               | 10–40        | 4 g/1 L   | ethanol          | sandstone    | 26.3       | 1.75    | 55         | 78      |
| Joonaki and Ghanaatian <sup>24</sup>     | Al <sub>2</sub> O <sub>3</sub> | ~60          | 0.5–3 g/L | propanol         | sandstone    | 5.7        | 2.25    | 56.6       | 76.8    |
| Bayat et al. <sup>25</sup>               | SiO <sub>2</sub>               | 10–35        |           |                  |              | 5          | 1.45    | 56.6       | 79.1    |
|  | Fe <sub>2</sub> O <sub>3</sub> | 40–60        |           |                  |              | 6.3        | 2.75    | 56.6       | 73.9    |
|  | Al <sub>2</sub> O <sub>3</sub> | 40           | 50 mg/L   | DIW              | limestone    | 18         | 13.4    | 55.8       | 65.7    |
|  | TiO <sub>2</sub>               | 10–30        |           |                  |              | 17.5       | 12.5    | 55.3       | 61.9    |
|  | SiO <sub>2</sub>               | 20           |           |                  |              | 16.7       | 11      | 54.8       | 57.7    |
| Zaid et al. <sup>26</sup>                | ZnO                            | 45.93        | 0.05 wt % | SDS              | carbonate    | 2.84       | 3.5     | 22.5       | 72.26   |
|  | Al <sub>2</sub> O <sub>3</sub> | 38.25        |           |                  |              | 2.84       | 4.1     | 22.5       | 53.53   |
| Hendraningrat and Torsæter <sup>27</sup> | Al <sub>2</sub> O <sub>3</sub> | 17           | 0.05 wt % | brine            | sandstone    | 19.2       | 12.8    | 52.22      | 60      |
|  | SiO <sub>2</sub>               | 40           |           |                  |              | 19.2       | 17.5    | 53.4       | 55.4    |
|  | TiO <sub>2</sub>               | 21           |           |                  |              | n.a.       |         | 56.7       | 67.8    |
|  | SiO <sub>2</sub>               | 10–20        | 1.0 g/L   | brine            | sandstone    | 17.5       | 7       | 12         | 40      |
| Li et al. <sup>21</sup>                  | SiO <sub>2</sub>               | 10–20        | 1.0 g/L   | brine            | sandstone    | 17.5       | 7       | 12         | 40      |
| Soleimani <sup>28</sup>                  | ZnO                            | 60           | 0.05–0.5% | SDS              | calcite      | 27.43      | 18.65   | n.a.       | 11.82   |

Figure 1. Schematic illustration of the experimental procedure of synthesizing ZnO/SiO<sub>2</sub>/xanthan NC and its application.

surfaces.<sup>36</sup> An additional effect is that permeability might be reduced as pores are partially blocked by fines migration.<sup>37,38</sup> Arab and Pourafshary<sup>39</sup> stated that attractive forces between mobilized fine-grained particles and static grain surfaces can be strengthened using nanoparticles because of changes to the surface zeta potentials. Amongst various possibilities, silica and zinc nanoparticles have been widely used in EOR applications during surfactant flooding,<sup>40–43</sup> polymer flooding,<sup>2,44</sup> and LSWF.<sup>21,45,46</sup> These nanoparticles are excellent candidates for EOR applications because of having a strong adsorption ability, high-temperature resistance, high surface area, and strong chemical stability. Fabrication of NPs from plant extracts in green procedures has been reported by many researchers wherein they have successfully obtained highly stable nanostructures.<sup>47,48</sup> The extract of pomegranate seeds is one of the most commonly used for producing green nanoparticles, polymer-coated nanoparticles, and nanocomposites (NCs) because they contain a considerable amount of antioxidants and bioactive phytochemicals, such as proanthocyanidins, phenolics, ascorbic acid, and flavonoids, which provide nanomaterials with large surface area.<sup>49,43,50</sup> In this work, we set out to combine the functions of LSWF, surfactant flooding, and polymer flooding together in a novel nanofluid (called low-salinity polymeric nanofluid) that has been designed from

mixing a polymer-coated nanocomposite with low-salinity water. We thus prepared a xanthan-coated ZnO/SiO<sub>2</sub> nanocomposite in an eco-friendly procedure by using the extract of pomegranate seeds to be able to reduce IFT, change the relative permeability curve, and improve oil recovery. We demonstrate this in core-flooding of samples taken from the Upper Qamchoqa carbonate formation in Kurdistan Region, Iraq.

## 2. EXPERIMENTAL SECTION

The experimental work of the current investigation was divided into three parts, as illustrated schematically in Figure 1, which includes the following: (i) synthesis and characterization of polymer-coated ZnO/SiO<sub>2</sub> nanocomposite; (ii) the static experimental part includes the preparation and stability observation of polymeric nanofluids and their effects on IFT reduction; and (iii) the dynamic experimental section covers the oil displacement by low salinity polymeric nanofluid flooding.

**2.1. Materials and Characterization.** For synthesizing the nanocomposite (NC), high-purity (99.5%) chemical reagents, including salts and solvents, were purchased from Merck and Aldrich companies. Xanthan gum with 98% purity in powder form was supplied by AGREMA, Germany. For the reacted plant extract with chemical solution, the UV-visible measurement was performed at room temperature by a PerkinElmer 550ES from 200 to 600 nm, with a resolution of 1 nm. The size and shape of the synthesized NC was

Table 2. Compositional Details of Used Fluids

| (a) seawater  |                 |                  |                  |                 |                 |                               |                               |                |                |                 |                 |                  |
|---------------|-----------------|------------------|------------------|-----------------|-----------------|-------------------------------|-------------------------------|----------------|----------------|-----------------|-----------------|------------------|
| ion           | Na <sup>+</sup> | Ca <sup>2+</sup> | Mg <sup>2+</sup> | K <sup>+</sup>  | Cl <sup>-</sup> | SO <sub>4</sub> <sup>2-</sup> | HCO <sub>3</sub> <sup>-</sup> | T.H.           | T.D.S.         |                 |                 |                  |
| conc. (ppm)   | 7337            | 1920             | 936              | 92              | 11 502          | 6893                          | 106                           | 8700           | 33 194         |                 |                 |                  |
| (b) crude oil |                 |                  |                  |                 |                 |                               |                               |                |                |                 |                 |                  |
| component     | C <sub>1</sub>  | C <sub>2</sub>   | C <sub>3</sub>   | iC <sub>4</sub> | nC <sub>4</sub> | iC <sub>5</sub>               | nC <sub>5</sub>               | C <sub>6</sub> | C <sub>7</sub> | C <sub>7+</sub> | CO <sub>2</sub> | H <sub>2</sub> S |
| mol %         | 0.028           | 0.40             | 2.48             | 0.086           | 3.27            | 2.09                          | 2.75                          | 5.66           | 9.32           | 82.32           | 0.029           | 0.093            |

identified using transmission electron microscopy (TEM) and scanning electron microscopy (SEM) with a CamScan MV2300. Energy-dispersive X-ray (EDS) spectroscopy (S3700N) was utilized for chemical analysis of prepared nanostructures with a scanning rate of 2°/min in the 2θ range from 10 to 90°. The mineralogical composition of the prepared nanomaterial was investigated using X-ray diffraction (XRD, Goniometer-Cu Kα = 1.5406 Å) and Fourier-transform infrared (FTIR) spectroscopy analyses.

Seawater (SSW) was collected from the Persian Gulf, which presented different ionic concentrations and salt compositions, as shown in Table 2a. For IFT measurements and core-flooding, a crude oil with a density of 0.879 g/mL (29.5° API) was used in this work. The composition and SARA details of crude oil are shown in Table 2b and Figure 2, respectively. A carbonate core sample (length 6.61 cm and

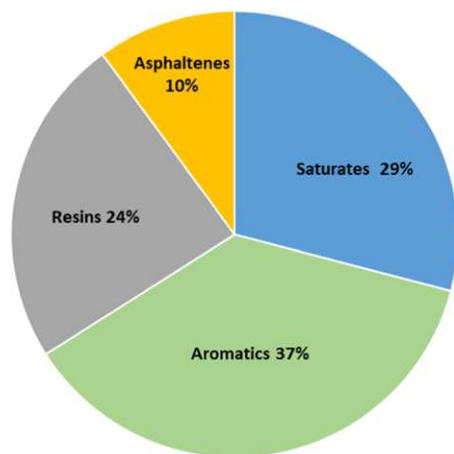


Figure 2. SARA details of the crude oil used in this study.

diameter 3.81 cm) from the Upper Qamchoqa formation outcrop in Bekhma area (36°40'17.00"N; 044°15'04.4"E) in Kurdistan region, Iraq was collected for the core-flooding test. The porosity and gas permeability of the core sample were 16.85% and 13.15 mD, respectively.

**2.2. Green Synthesis of Xanthan-Coated ZnO/SiO<sub>2</sub> Nanocomposite.** The synthesis steps for preparing the nanocomposite are shown in Figure 3. Initially, the extract of the pomegranate seed was collected and filtered using a filter paper. Then, 2 g of ZnCl<sub>2</sub> and 5 g of sodium metasilicate (Na<sub>2</sub>SiO<sub>3</sub>) were added to 200 mL of the filtered extract in a 500 mL beaker and mixed at 80 °C and 850 rpm while stirring for 2 h until a light black precipitate was formed at the bottom of the beaker. After separating the precipitate by filtration, it was heated up to 600 °C in a furnace to burn all the plant particles within the nanomaterials. Afterward, the hot distillate water was used to clean the collected nanomaterials from the plant-burned impurities. Furthermore, the cleaned nanomaterial was dried at room temperature and mixed with 10 g of xanthan gum by mortar and pestle, under reflux for 2 h at 80 °C. Finally, the dried and cleaned nanocomposite was collected and characterized using various analytical techniques.

**2.3. Preparation of Nanofluids.** In this study, varying concentrations of the polymer-coated ZnO/SiO<sub>2</sub> nanocomposite

(500, 1000, and 2000 ppm) were utilized to prepare the polymeric nanofluid. Initially, polymeric nanofluids formulations were first tried in distilled water (DW) and seawater (with high salinity (HiSal)) as base fluids. Then, LoSal-polymeric nanofluids were developed by reducing the salinity of the seawater (SSW) by 10 and 20 times dilutions based on the salting-out approach described by Spildo et al.<sup>51</sup> (Table 3). Thus, a liter of seawater was usually diluted by adding 100 mL of distilled water. Nanofluids were prepared by stirring (LABINCO L81 Stirrer) at 600 rpm for 6 h, keeping the operating temperature below 30 °C to avoid overheating of the homogenizer. Furthermore, to produce nanofluids with high dispersion stability, ultrasonic waves emitted from the VIP 200HD ultrasonic mixer, manufactured by Hielscher in Germany, were used for mixing the fluid solutions for 2 h at 400 W. The dispersion stability of the synthesized nanocomposite within the nanofluids was investigated by visual observation, which has been monitored through transparent vessels with time. Finally, the PAAR density meter was used to measure the density of the polymeric nanofluids at room temperature.

**2.4. Interfacial Tension (IFT) Measurements.** Interfacial tension (IFT) is developed by co-presence of two immiscible fluids, including crude oil and water, in porous media. IFT is the energy that forces the molecule toward the solid surface from the bulk phase per unit area to produce an interface between two immiscible liquids, and it is usually measured in dynes/cm (milli-newtons/meter).<sup>38</sup> Generally, several techniques are available to measure the value of IFT, such as a Wilhelmy plate, spinning drop, sessile drop, Du Noüy ring, maximum bubble pressure, capillary rise, and pendant drop.<sup>39</sup> In this study, we used the pendant drop method (Figures 4 and S1) to measure the IFT by estimating the dimensions of the suspended oil droplet. Then, according to the following formula, the software will start to approximate the IFT on receiving the image of the crude oil droplet from the camera.

$$\gamma = \frac{\Delta\rho \cdot g \cdot D}{H} \quad (1)$$

where  $\Delta\rho$  is the difference between the density of the drop and bulk fluids (g/cm<sup>3</sup>),  $g$  is the gravitational acceleration of the earth (cm/s<sup>2</sup>),  $D$  is the large diameter of the droplet (cm), and  $H$  is the droplet shape factor.

The initial IFT measurements using the pendant drop technique have been taken between oil and different saline water solutions without the presence of nanomaterials. The same procedure was applied for measuring the IFT between oil and polymeric nanofluids containing polymer-coated ZnO/SiO<sub>2</sub> NC at zero-, high-, medium-, and low-salinity levels. Finally, to check the effects of temperature and pressure on the IFT values for all different solutions, the IFT tests were performed under 30, 50, and 70 °C temperature and 500, 1000, and 1500 psi pressure.

**2.5. Oil Displacement Experimental Setup and Procedure.** Core-flooding experimental setups are illustrated schematically in Figure 5. The setup mainly consists of tanks containing the fluids, pumps, a core holder, and a fraction collector. The high-performance liquid chromatography (HPLC) pump injects the hydraulic fluid automatically to the rear of the pistons in three cylinders on the basis of the fluid selection, which needs to be pumped into the core-holder chamber and injected into the core with the rate or input pressure chosen by the user. Cylinders containing crude oil, water, and nanofluid solution are located along with a core holder inside an oven to apply the temperature to the system. The output line of the core-holder chamber is removed from the oven, and the outlet fluid is stored in a special fluid

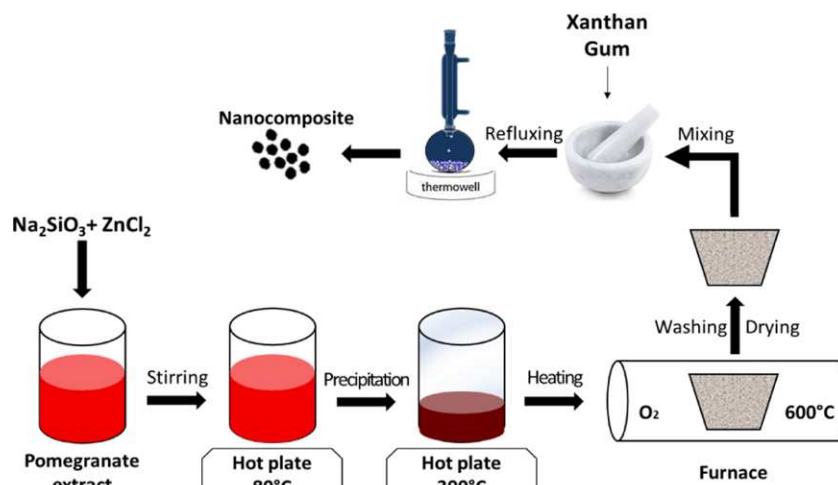


Figure 3. Schematic diagram of a green process to synthesize the ZnO/SiO<sub>2</sub>/xanthan nanocomposite.<sup>46</sup>

Table 3. Formulation of Fluid Solutions Used in This Study

| sample | NC conc. (ppm) | dispersion media  | salinity         | density (g/cm <sup>3</sup> ) | description                     |
|--------|----------------|-------------------|------------------|------------------------------|---------------------------------|
| S0     | 0              | DW                | zero             | 1                            | distilled water                 |
| S0H    |                | SSW               | high             | 1.03                         | high-salinity water             |
| S0M    |                | 1:10 SSW dilution | moderate         | 1.014                        | moderate-salinity (MoSal) water |
| S0L    |                | 1:20 SSW dilution | low              | 1.08                         | low-salinity water              |
| S1     | 500            | DW                | zero             | 1.0004                       | polymeric nanofluid             |
| S1H    |                | SSW               | high (HiSal)     | 1.0337                       | HiSal-polymeric nanofluid       |
| S1M    |                | 1:10 SSW dilution | moderate (MoSal) | 1.0168                       | MoSal-polymeric nanofluid       |
| S1L    |                | 1:20 SSW dilution | low (LoSal)      | 1.0112                       | LoSal-polymeric nanofluid       |
| S2     | 1000           | DW                | zero             | 1.0009                       | polymeric nanofluid             |
| S2H    |                | SSW               | high (HiSal)     | 1.0342                       | HiSal-polymeric nanofluid       |
| S2M    |                | 1:10 SSW dilution | moderate (MoSal) | 1.0171                       | MoSal-polymeric nanofluid       |
| S2L    |                | 1:20 SSW dilution | low (LoSal)      | 1.0114                       | LoSal-polymeric nanofluid       |
| S3     | 2000           | DW                | zero             | 1.0019                       | polymeric nanofluid             |
| S3H    |                | SSW               | high (HiSal)     | 1.0352                       | HiSal-polymeric nanofluid       |
| S3M    |                | 1:10 SSW dilution | moderate (MoSal) | 1.0176                       | MoSal-polymeric nanofluid       |
| S3L    |                | 1:20 SSW dilution | low (LoSal)      | 1.0117                       | LoSal-polymeric nanofluid       |

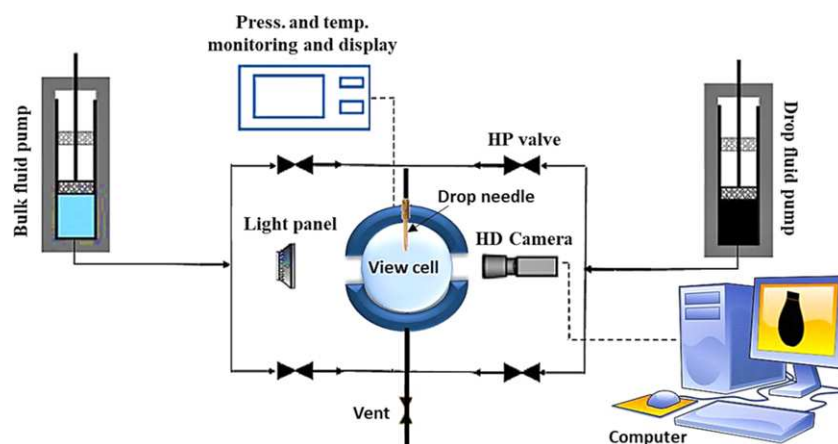
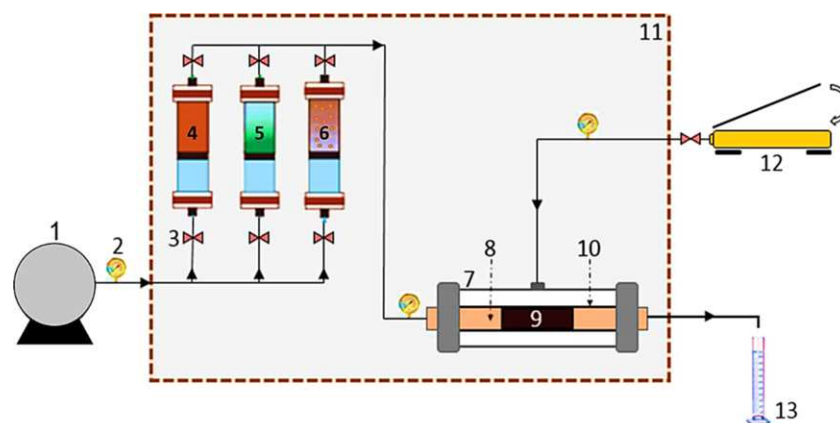


Figure 4. Schematic presentation of high-pressure (HP)–high-temperature (HT) pendant drop IFT400 interfacial tension-measuring apparatus.

collection vessel. The core-holder chamber itself consists of two parts of the fluid flow (inlet and outlet) and a special rubber to block the fluid

flow around a 1.5 in. plug, which is operated by a hydraulic fluid pump manually.



**Figure 5.** Schematic illustration of the apparatus for oil displacement tests: (1) HPLC pump, (2) pressure gauges, (3) valves, (4) cylinder containing crude oil, (5) cylinder containing brine, (6) cylinder containing nanofluid, (7) core-holder chamber, (8) fluid flow distributor, (9) core, (10) blocking rubber around the core, (11) oven, (12) manual hydraulic pump, and (13) outlet fluid-collecting vessel.

To carry out displacement tests, a carbonate core plug was selected from the Upper Qamchuqa outcrop in the Kurdistan region, Iraq. The selected plug was cleaned by soxhlet extraction using ethanol and toluene at a temperature between 60–80 °C for 24 h to remove all of the present water, oil, and any other residues. Afterward, before core-flooding, the sample was dried by placing into an oven at 70 °C for 6 h. Core displacement tests were conducted using a water and LoSal-polymeric nanofluid mixture prepared by dispersing 2000 ppm of ZnO/SiO<sub>2</sub>/xanthan NC in low-salinity water. Tests were performed at 75 °C and 1350–1380 psi, with an injection rate of 0.5 cm<sup>3</sup>/min.

The following five-step procedure was performed for evaluating the effectiveness of the injected LoSal-polymeric nanofluid to determine the improvements on oil recovery: (1) the optimum nanofluid was identified from conducting the IFT test measurements based on NC concentration and water salinity. (2) Water, about 2 pore volume (PV), was injected into the core plug under a controlled flow rate (0.5 cm<sup>3</sup>/min), and two pressure transducers were used to record the pressure values at the injection and production points. (3) The relative permeability curve was constructed after injecting 2 PV water (i.e., before nanofluid flooding). The oil and water effective permeabilities were measured as water replaced oil within the core, and new oil and water saturations were obtained. Then, the effective permeability to water and oil at residual oil saturation and irreducible water saturation ( $K_{rw}$  at  $S_{or}$  and  $K_{ro}$  at  $S_{wir}$ ) was measured using the Johnson, Bossler, and Naumann (JBN) method as shown in Section 1, Supporting Information. (4) Two pore volume of LoSal-polymeric nanofluid was injected into the core plug, and the displaced volume of water in the porous media was measured. (5) Relative permeability curve was constructed after nanofluid treatment.

### 3. RESULTS AND DISCUSSION

In this section, first, characterization details of the synthesized green nanocomposite have been presented, followed by the discussion on IFT reduction by various fluid solutions (S0, SOH, SOM, SOL, S1, S1H, S1M, S1L, S2, S2H, S2M, S2L, S3, S2H, S3M, and S3L) under various temperature and pressure conditions. Subsequently, results show that the NC concentration, temperature, pressure, and salinity were directly influenced by the IFT reduction. Finally, the results of core-flooding from injecting water and nanofluid were presented and discussed, in detail.

Generally, the performance of the synthesized NC in this work was compared with the efficiency of the commercial and synthesized nanoparticles used in the literature, as shown in

**Figure 6.** Comparisons of the IFT reductions and oil recovery improvements are shown. In 2012, Roustaei et al.<sup>23</sup> obtained a

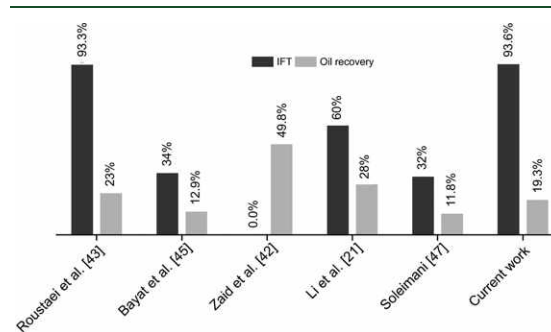


**Figure 6.** Clustered column chart demonstrates the best results obtained in this work and those reported in the literature in terms of IFT reduction and oil recovery.

great reduction in IFT and increased oil recovery by about 92 and 23%, respectively, by adding silica NPs into brine, whereas Bayat et al.<sup>25</sup> applied Al<sub>2</sub>O<sub>3</sub> with the deionized water (DIW), which caused the IFT to be reduced by about 34% and oil recovery increased by about 13%. In addition, Zaid et al.<sup>26</sup> stated that using ZnO and Al<sub>2</sub>O<sub>3</sub> surfactant nanoemulsions, oil recovery can be increased by about 50% with no reduction in IFT. More recently, Soleimani et al.<sup>28</sup> used a synthesized ZnO with the sodium dodecyl sulfate (SDS) surfactant, which reduced IFT and improved oil recovery by about 32 and 17%, respectively. According to these studies, a great reduction in IFT (93.6%) was achieved in this work from using LoSal-polymeric nanofluid, and oil recovery was increased by about 19.3%.

**3.1. Characterization of Polymer-Coated ZnO/SiO<sub>2</sub> Nanocomposite.** The production and characterization of the same ZnO/SiO<sub>2</sub>/xanthan NC were presented and discussed in detail in our previous paper (Ali et al.<sup>46</sup>). The nanomaterial was prepared after verifying the presence of potent antioxidants inside the pomegranate extract by using the UV-vis spectrum (Figure S2), with the support of the results obtained by previous research.<sup>52</sup> Additionally, the crystallinity and phase purity of nanomaterials deposited on the surface of xanthan polymer,

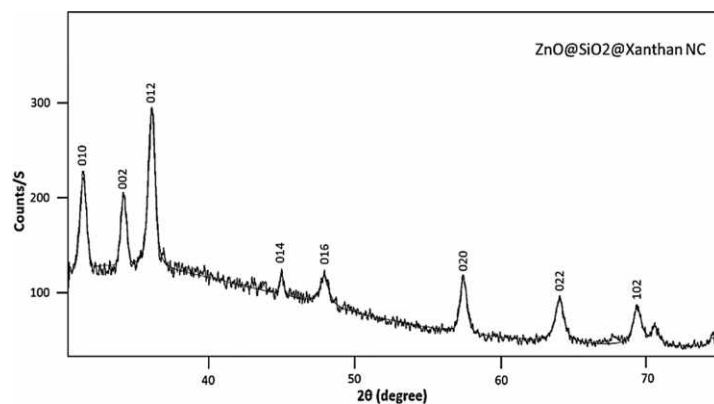


Figure 7. XRD diffractogram of the green synthesized  $\text{SiO}_2/\text{ZnO}/\text{Xanthan NC}$ .<sup>46</sup>

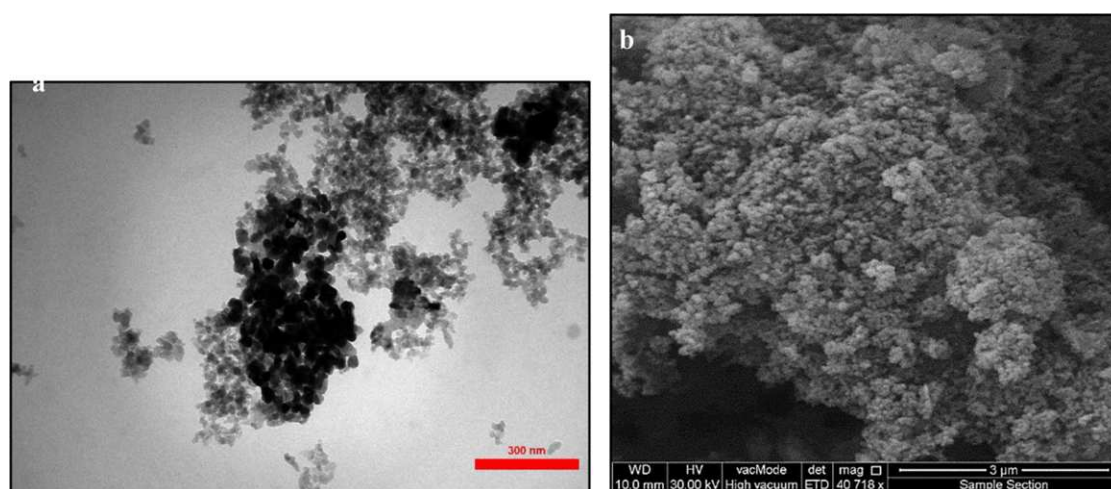


Figure 8. Morphology, shape, size, and distribution of the nanomaterials of the synthesized NC; (a) 300 nm TEM image and (b) 3  $\mu\text{m}$  SEM image.<sup>46</sup>

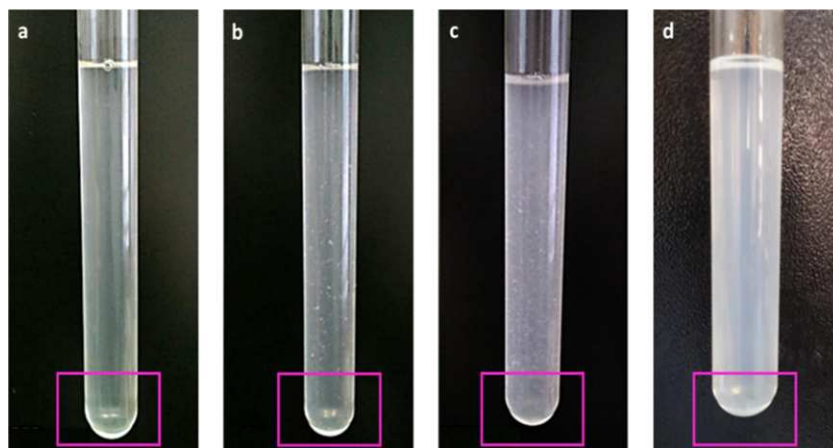


Figure 9. Dispersion stability of nanocomposites within LoSal-polymeric nanofluids after resting for a week with concentrations of (a) 500, (b) 1000, and (c) 2000 ppm used for IFT tests and (d) with 2000 ppm as concentration of an optimum nanofluid for core-flooding.

within the synthesized NC, were identified by the XRD peaks containing all associated crystalline planes of pure silica and zinc

NPs (Figure 7).<sup>53–55</sup> As it can be seen, the three observed peaks (010, 002, and 012) with the reflections from 31.5 to 36° are

**Table 4.** Measured Values of IFT between Crude Oil and Various Aqueous Phases under the Effects of NC Concentration, Water Salinity, Pressure, and Temperature

| press. (psi) | temp. (°C) | interfacial tension (IFT) (mN/m) |       |       |       |       |       |       |      |      |       |       |      |      |      |      |       |
|--------------|------------|----------------------------------|-------|-------|-------|-------|-------|-------|------|------|-------|-------|------|------|------|------|-------|
|              |            | S0                               | S0H   | S0M   | S0L   | S1    | S1H   | S1M   | S1L  | S2   | S2H   | S2M   | S2L  | S3   | S3H  | S3M  | S3L   |
| 500          | 30         | 28.31                            | 31.24 | 24.76 | 19.68 | 12.96 | 16.04 | 12.77 | 8.92 | 8.01 | 14.06 | 11.41 | 6.95 | 3.00 | 9.45 | 8.51 | 2.21  |
|              | 50         | 25.4                             | 30.3  | 21.5  | 17.3  | 10.39 | 16.32 | 10.85 | 7.32 | 6.63 | 12.62 | 10.43 | 5.01 | 2.76 | 9.77 | 7.94 | 2.29  |
|              | 70         | 26.84                            | 29.65 | 20.02 | 16.02 | 9.765 | 16.27 | 10.39 | 6.21 | 5.12 | 10.65 | 9.173 | 3.59 | 2.09 | 8.94 | 6.63 | 2.41  |
| 1000         | 30         | 29.0                             | 32.76 | 25.1  | 19.13 | 13.41 | 18.86 | 12.89 | 8.16 | 7.64 | 16.14 | 10.74 | 6.71 | 3.81 | 10.3 | 8.72 | 3.16  |
|              | 50         | 24.89                            | 29.21 | 29.6  | 18.84 | 9.972 | 14.51 | 11.54 | 8.19 | 6.29 | 11.29 | 10.96 | 4.57 | 3.51 | 9.29 | 7.50 | 2.73  |
|              | 70         | 24.62                            | 28.96 | 19.05 | 18.3  | 9.541 | 13.68 | 10.68 | 6.83 | 4.70 | 9.014 | 8.820 | 3.77 | 2.65 | 8.75 | 5.92 | 2.14  |
| 1500         | 30         | 27.56                            | 31.97 | 24.38 | 20.03 | 12.76 | 16.65 | 12.73 | 9.01 | 8.75 | 16.50 | 12.86 | 6.30 | 3.01 | 10.1 | 7.86 | 3.71  |
|              | 50         | 23.54                            | 31.7  | 20.9  | 16.61 | 11.42 | 16.49 | 11.60 | 7.92 | 5.81 | 13.17 | 10.07 | 4.36 | 2.61 | 9.43 | 8.49 | 2.91  |
|              | 70         | 20.56                            | 25.2  | 17.96 | 14.78 | 10.67 | 13.29 | 10.84 | 7.56 | 5.97 | 11.52 | 10.13 | 3.92 | 2.54 | 9.53 | 5.64 | 2.016 |

similar to the peaks of zinc and silica NPs reported in the literature.<sup>56</sup>

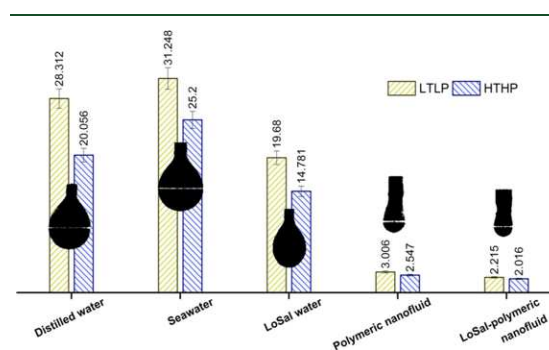
The morphology of the synthesized NC at different magnifications by SEM and TEM images is illustrated in Figure 8. The appearance, size, and distribution of silica and zinc NPs were observed clearly on the reported TEM and SEM images.<sup>57–59</sup> For further confirmation concerning the biosynthesis of NC, EDS and FTIR spectra analyses were also conducted, as shown in (Figures S3 and S4). Results of both analyses clearly confirm the presence of SiO<sub>2</sub> and ZnO in the elemental composition of the nanocomposites.

**3.2. Nanocomposite Suspension Stability.** The stability of the distribution of the nanocomposite colloidal particles within the nanofluid solutions is very important. The dispersion should remain homogenous under the experimental circumstances, else flocculation is going to happen, in which case, the desired effects will no longer take place. The excellent stability of LoSal-polymeric nanofluids for both IFT tests and core-flooding is illustrated in Figure 9. Three of the nanofluids were prepared for the IFT tests, with 500, 1000, and 2000 ppm NC concentrations within LoSal water (Figure 9a–c). Also, the LoSal-polymeric nanofluid that was identified as optimal by its NC concentration is shown in Figure 9d. Before conducting the IFT and core-flooding experiments, the nanofluids were kept in a static state for a duration of 1 week. The precipitation of nanomaterials in the bottom of the tubes was prevented by stabilizing the fluids using ultrasonic waves, and no sedimentation was observed, as shown by lavender boxes. Additionally, from the left to the right of the figure, the presence of the NC within the LoSal water can be seen as the cloudiness increases with NC concentration.

**3.3. IFT Measurements of Fluid Systems.** IFT between immiscible liquids in the reservoir has an important role in improving the production of oil, depending on the type of rock and present fluids.<sup>60</sup> IFT for different immiscible liquid systems was measured, such as oil/water, oil/polymeric nanofluid, and oil/LoSal-polymeric nanofluid systems. The measured values of IFT for fluids under various NC concentrations (0, 500, 1000, and 2000 ppm), salinities (zero, low, moderate, and high), temperatures (30, 50, and 70 °C) and pressures (500, 1000, and 1500 psi) are summarized in Table 4. The minimum value of IFT of 2.016 mN/m was achieved between oil and LoSal-polymeric nanofluid (S3L) at 70 °C and 1500 psi for the polymer-coated nanocomposite with a concentration of 2000 ppm.

The initial IFT values between oil/SSW and oil/DW were measured at low temperature low pressure (LTLP) and high-

temperature high-pressure (HTHP) conditions (Figure 10). When the salinity of seawater has been reduced, by a 20 time

**Figure 10.** IFT values and droplet shapes of crude oil with the presence of various aqueous phases at LTLP and HTHP conditions.

dilution, on the basis of the salting-out approach, the IFT between oil and LoSal water at LTLP condition was decreased by about 38% from 31.8 to 19.68 mN/m. However, it was greatly reduced under the HTHP condition by about 53.5% from 31.8 to 14.781 mN/m. Further, by adding polymer-coated ZnO/SiO<sub>2</sub> NC into the DW and LoSal water, the IFT was further decreased to its lowest values in both reservoir conditions. The IFT values measured between the oil/polymeric nanofluid and oil/LoSal-polymeric nanofluid were about 3.006 and 2.215 mN/m, respectively, at LTLP condition and 2.547 and 2.016 mN/m, respectively, at HTHP condition. As can be seen, it is clear that the IFT was considerably reduced when changing from seawater to low-salinity polymeric nanofluid by about 93.6% at higher temperature and pressure. The variations of IFT between the various immiscible liquids can be clearly seen in assessing the oil droplets, with the presence of different aqueous phases, shown in Figure 10.

Figure 11 shows the measured IFT values for the various conditions that were considered. We first examined the effect of water salinity on IFT reduction, without adding NC. In this way, the IFT between crude oil and distilled, high salinity (seawater), moderate salinity, and LoSal waters has been measured and only a small reduction in IFT was observed, as shown in region I on Figure 11. As it is clear, this reduction of the IFT was achieved due to the salinity effect of water. By decreasing the salinity of seawater by 10 and 20 time dilutions, a further reduction to the IFT was observed. This is quite consistent with the outputs of Nowrouzi et al.<sup>43</sup> wherein they described the effect of various

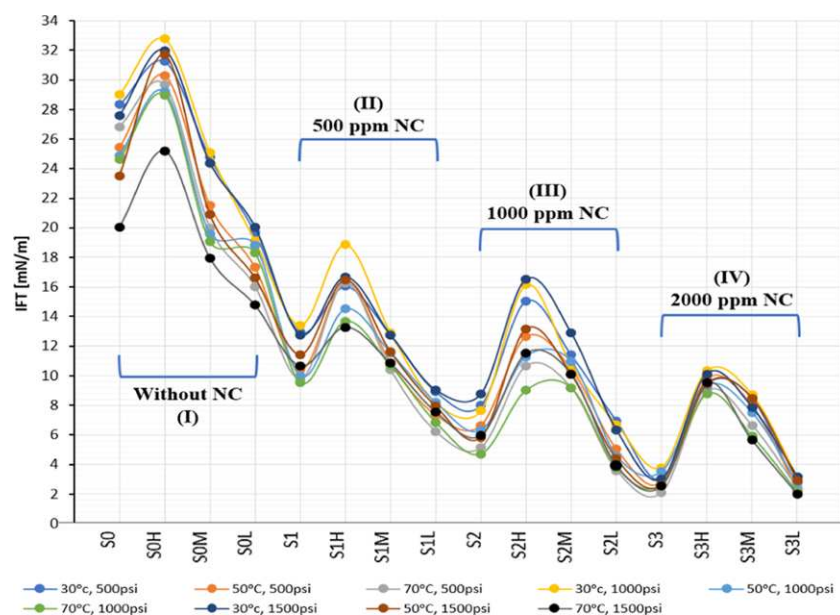


Figure 11. Effects of the NC concentration, water salinity, temperature, and pressure on IFT reduction.

Table 5. Summary of the Oil Displacement Tests

| core      | nanofluid                 | NC conc. (ppm) | injected rate (cc/s) | $S_{or}$ (%) | water-flooding |                       | nanofluid flooding |                       | total oil recovery (% OOIP) |
|-----------|---------------------------|----------------|----------------------|--------------|----------------|-----------------------|--------------------|-----------------------|-----------------------------|
|           |                           |                |                      |              | $S_{or}$ (%)   | oil recovery (% OOIP) | $S_{or}$ (%)       | oil recovery (% OOIP) |                             |
| carbonate | LoSal-polymeric nanofluid | 2000           | 0.5                  | 77           | 53             | 46.96                 | 33.76              | 19.28                 | 66.24                       |

densities and ionic compounds of the seawater on IFT reduction. In the same region, the effect of pressure and temperature on the IFT reduction was strong; by increasing the temperature and pressure from 30 °C and 500 psi to 70 °C and 1500 psi, the IFT of oil/S0, oil/SOH, oil/SOM, and oil/SOL were reduced from 28.4 to 20, 31.8 to 26, 24.6 to 18, and 19.8 to 14.8 mN/m, respectively. Generally, the water salinity, temperature, and pressure were the only factors behind the reduction of IFT in this region; the impact of the salinity was about 37% and that of temperature and pressure effects was 27.8%.

However, even further IFT reduction was observed in the other regions II–IV shown in Figure 11 by adding the polymer-coated NC into different water-based solutions.<sup>61</sup> Basically, the effect of the synthesized NC within the distilled and LoSal waters was higher than within the high-salinity waters. This is supported by Li et al.<sup>19</sup> and Dahle et al.<sup>62</sup> studies, where they reported that adding nanoparticles into the smart and LoSal waters greatly reduced the IFT due to the development of a layered structure of the nanoparticles at the interface between crude oil and nanofluids. In region II, the IFT for all salinity cases was reduced significantly by adding only 500 ppm NC. Typically, between oil and LoSal-polymeric nanofluid, the IFT value was reduced by about 55% from 19.8 mN/m (oil/SOL) to 8.923 mN/m (oil/S1L) whereas the effect of pressure and temperature on IFT reduction was about 16.3% in this region, which was smaller than the effect of pressure and temperature in region I. Furthermore, by increasing the concentration of nanocomposites to 1000 ppm in region III, little variations in IFT values were observed for both moderate and high-salinity

polymeric nanofluids; this is where the NC concentration was very active with the DW and LoSal-polymeric nanofluids. The IFT between oil/S2L was reduced by about 56% from 8.923 to 3.935 mN/m at HTHP condition.

In region IV, by increasing the concentration of NC to 2000 ppm, the relative IFT for all types of nanofluids reduced gradually except that for the high-salinity water, which reduced further in some cases. Similarly, Standal et al.<sup>63</sup> reported that IFT of the oil/aqueous phases would be reduced on increasing the salinity due to developing the component with higher concentration in the oil phase. On the other hand, Lashkarbolooki et al.<sup>64</sup> claimed that the IFT value of the oil/nanofluid system would be always lower than the IFT between oil and smart nanofluid with a sufficient concentration of nanoparticles and it would be kept down to its minimum value at the lowest salinity. In this region, the IFT of oil/S3L (LoSal-polymeric nanofluid) system was reduced by about 68% from 6.950 to 2.215 mN/m due to the effect of NC concentration and it was further reduced to 2.016 mN/m (9%) by increasing the temperature (from 30 to 70 °C) and pressure (from 500 to 1500 psi).

**3.4. Oil Displacement Experiments.** In this section, oil displacement experiments were performed to mimic water-flooding and LoSal-polymeric nanofluid flooding processes with varied injected PV to a carbonate core plug. According to the IFT results, the LoSal-polymeric nanofluid was selected as the most effective nanofluid, which is composed of the LoSal water (1:20 SSW dilution) and a 2000 ppm polymer-coated ZnO/SiO<sub>2</sub> nanocomposite. Plots of the evolution of the cumulative oil

production factor with the injected pore volume and the relative permeability curves for both water and nanofluid injections are presented and discussed below. Table 5 summarizes the results collected from these experiments.

Figure 12 shows the oil recovery and differential pressure ( $\Delta P$ ) across the core plug as a function of pore volume injected

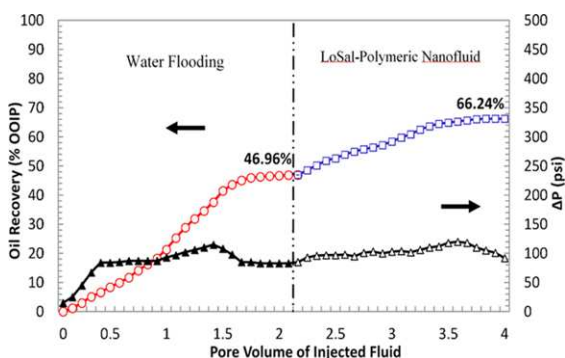


Figure 12. Production profiles of water and LoSal-polymeric nanofluid flooding as a function of injected PV.

into the two stages of the core-flooding. As observed in other studies, the cumulative oil recovery is improved steadily with the volume of injected brine before approaching a plateau at around 2 PV. The water-flooding oil recovery factor was identified to be about 46.96% of the original oil in place (OOIP). The injection of a LoSal-polymeric nanofluid, as shown in Figure 12, was capable of further increasing the cumulative oil recovery by about 19.28% OOIP over the water-flooding process. Again, the second plateau was reached after injecting roughly 2 PV of nanofluid solution. By this point, the total cumulative oil recovery from both water-flooding and LoSal-polymeric nanofluid flooding increased to about 66.24% OOIP. It was also found that the differential pressures ( $\Delta P$ ) across the model for these both experiments generated by brine and nanofluid injections were relatively similar and low. This smooth behavior of the  $\Delta P$  curves between both floods indicates the high dispersion stability of nanostructures within the nanofluids, as discussed above.<sup>65</sup>

Figure 13 represents the relative permeability curves of a carbonate core sample before and after the treatment with the LoSal-polymeric nanofluid. Both curves were determined from running the oil displacement data in CYDAR software by applying the JBN approach.<sup>66</sup> Comparing the relative permeability values before and after the nanofluid flooding, it can be observed that there were appreciable variations in the irreducible water saturation ( $S_{wir}$ ), the point where the water and oil relative permeabilities are equal (crossover point), and the relative permeability curves. The values of the irreducible water saturation, before ( $S_{wir} = 0.23$ ) and after treatment ( $S_{wir} = 0.47$ ), indicate that, according to Craig's rules of thumb,<sup>67</sup> the wettability of the carbonate plug was changed from the oil-wet system to a strongly water-wet system. The most likely explanation for this considerable change in relative permeability curves is the adsorption of ZnO/SiO<sub>2</sub>/xanthan NC on the surface of the carbonate. The oil relative permeability curve was considerably shifted to the right due to the effect of nanofluid flooding, which suggests that the oil effective permeability at a particular water saturation point improved as the wettability

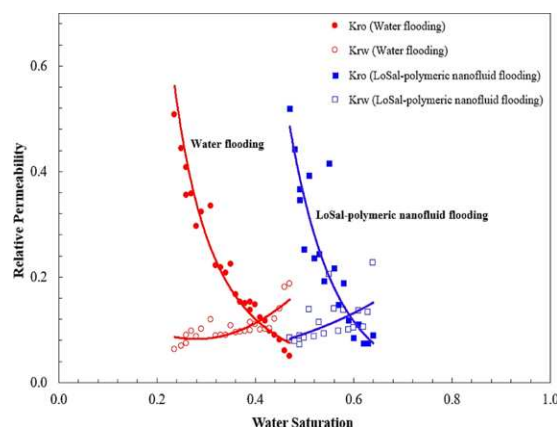


Figure 13. Relative permeability curves before and after nanofluid treatment from the experimental data using JBN method.

system was changed to a stronger water-wet condition. Similar to the oil relative permeability curve, the crossover point was also moved to the right. After injecting the nanofluid, the water saturation at which the water and oil relative permeabilities become equal was changed from 0.4 to 0.6. According to Craig's rules of thumb,<sup>67</sup> this value is typical of strongly water-wet cores.

#### 4. CONCLUSIONS

This paper described a new green technology to develop a Low-salinity polymeric nanofluid using a polymer-coated ZnO/SiO<sub>2</sub> nanocomposite for the enhanced oil recovery. ZnO/SiO<sub>2</sub>/xanthan NC was synthesized from pomegranate seed extract in a green and economical way and characterized using UV-vis, XRD, TEM, SEM, FTIR, and EDS techniques. The following major conclusions can be drawn on the basis of the results obtained from this study:

- Polymer-coated ZnO/SiO<sub>2</sub> NC was highly dispersed in water and maintained a high suspension stability for a long time.
- LoSal-polymeric nanofluid was shown to control the interfacial tension due to the effects of the synthesized NC, salinity, temperature, and pressure.
- The nanofluid helped to improve the oil displacement efficiency from a carbonate core by about 19.3% of the original oil in place.
- The LoSal-polymeric nanofluid altered the relative permeability curves, displacing them to the right in a fashion consistent with wettability alteration.
- The method used to prepare the low-salinity polymeric nanofluid could be widely applied to improve oil recovery from carbonate reservoirs.

#### ■ ASSOCIATED CONTENT

##### Supporting Information

The Supporting Information is available free of charge on the ACS Publications website at DOI: 10.1021/acs.energyfuels.8b03847.

Procedure of JBN relative permeability method (Section 1); IFT400 apparatus (Figure S1); UV-vis spectrum of pomegranate seed extract (Figure S2); EDS spectrum of green synthesized NC (Figure S3); FTIR spectra of green synthesized ZnO/SiO<sub>2</sub>/xanthan NC (Figure S4) (PDF).

## AUTHOR INFORMATION

### Corresponding Author

\*E-mail: jagar.pet@gmail.com. Tel: +964-750-481-0567.

### ORCID

Jagar A. Ali: 0000-0002-7327-4243

### Notes

The authors declare no competing financial interest.

## REFERENCES

- (1) Liu, P.; Zhang, X.; Wu, Y.; Li, X. Enhanced oil recovery by air-foam flooding system in tight oil reservoirs: Study on the profile-controlling mechanisms. *J. Pet. Sci. Eng.* **2017**, *150*, 208–216.
- (2) Sharma, T.; Kumar, G. S.; Sangwai, J. S. Comparative effectiveness of production performance of Pickering emulsion stabilized by nanoparticle–surfactant–polymer over surfactant–polymer (SP) flooding for enhanced oil recovery for Brownfield reservoir. *J. Pet. Sci. Eng.* **2015**, *129*, 221–232.
- (3) Zargartalebi, M.; Kharat, R.; Barati, N. Enhancement of surfactant flooding performance by the use of silica nanoparticles. *Fuel* **2015**, *143*, 21–27.
- (4) Ahmadi, M. A.; Zendejboudi, S.; Shafiei, A.; James, L. Nonionic Surfactant for Enhanced Oil Recovery from Carbonates: Adsorption Kinetics and Equilibrium. *Ind. Eng. Chem. Res.* **2012**, *51*, 9894–9905.
- (5) Al-Ansari, S.; Barifcani, A.; Wang, S.; Maxim, L.; Iglauer, S. Wettability alteration of oil-wet carbonate by silica nanofluid. *J. Colloid Interface Sci.* **2016**, *461*, 435–442.
- (6) Ali, J. A.; Kolo, K.; Manshad, A. K.; Mohammadi, A. H. Recent advances in application of nanotechnology in chemical enhanced oil recovery: Effects of nanoparticles on wettability alteration, interfacial tension reduction, and flooding. *Egypt. J. Pet.* **2018**, 1371.
- (7) Wei, B.; Li, Q.; Jin, F.; Li, H.; Wang, C. The Potential of a Novel Nanofluid in Enhancing Oil Recovery. *Energy Fuels* **2016**, *30*, 2882–2891.
- (8) Nowrouzi, I.; Manshad, A. K.; Mohammadi, A. H. Effects of ions and dissolved carbon dioxide in brine on wettability alteration, contact angle and oil production in smart water and carbonated smart water injection processes in carbonate oil reservoirs. *Fuel* **2019**, *235*, 1039–1051.
- (9) Liu, K. L.; Kondiparty, K.; Nikolov, A. D.; Wasan, D. Dynamic Spreading of Nanofluids on Solids Part II: Modeling. *Langmuir* **2012**, *28*, 16274–16284.
- (10) Zhang, H.; Nikolov, A.; Wasan, D. Enhanced Oil Recovery (EOR) Using Nanoparticle Dispersions: Underlying Mechanism and Imbibition Experiments. *Energy Fuels* **2014**, *28*, 3002–3009.
- (11) Zhang, H.; Ramakrishnan, T. S.; Nikolov, A.; Wasan, D. Enhanced Oil Recovery Driven by Nanofilm Structural Disjoining Pressure: Flooding Experiments and Microvisualization. *Energy Fuels* **2016**, *30*, 2771–2779.
- (12) Sharma, T.; Iglauer, S.; Sangwai, J. S. Silica Nanofluids in an Oilfield Polymer Polyacrylamide: Interfacial Properties, Wettability Alteration, and Applications for Chemical Enhanced Oil Recovery. *Ind. Eng. Chem. Res.* **2016**, *55*, 12387–12397.
- (13) Hashemi, R.; Nassar, N. N.; Almas, P. P. Nanoparticle technology for heavy oil in-situ upgrading and recovery enhancement: Opportunities and challenges. *Appl. Energy* **2014**, *133*, 374–387.
- (14) Luo, D.; Wang, F.; Zhu, J.; Cao, F.; Liu, Y.; Li, X.; Willson, R. C.; Yang, Z.; Chu, C.; Ren, Z. Nanofluid of graphene-based amphiphilic Janus nanosheets for tertiary or enhanced oil recovery: High performance at low concentration. *Proc. Natl. Acad. Sci. U.S.A.* **2016**, *113*, 7711–7716.
- (15) Khalil, M.; Jan, B. M.; Tong, C. W.; Berawi, M. A. Advanced nanomaterials in oil and gas industry: Design, application and challenges. *Appl. Energy* **2017**, *191*, 287–310.
- (16) Li, Y.; Zhou, J.; Tung, S.; Schneider, E.; Xi, S. A review on development of nanofluid preparation and characterization. *Powder Technol.* **2009**, *196*, 89–101.
- (17) Zheng, C.; Cheng, Y.; Wei, Q.; Li, X.; Zhang, Z. Suspension of surface-modified nano-SiO<sub>2</sub> in partially hydrolyzed aqueous solution of polyacrylamide for enhanced oil recovery. *Colloids Surf., A* **2017**, *524*, 169–177.
- (18) Cheraghian, G.; Kiani, S.; Nassar, N. N.; Alexander, S.; Barron, A. R. Silica Nanoparticle Enhancement in the Efficiency of Surfactant Flooding of Heavy Oil in a Glass Micromodel. *Ind. Eng. Chem. Res.* **2017**, *56*, 8528–8534.
- (19) Li, S.; Hendraningrat, L.; Torsæter, O. In *Improved Oil Recovery by Hydrophilic Silica Nanoparticles Suspension: 2-Phase Flow Experimental Studies*, International Petroleum Technology Conference; Society of Petroleum Engineers, 2013.
- (20) Hendraningrat, L.; Li, S.; Torsæter, O. A coreflood investigation of nanofluid enhanced oil recovery. *J. Pet. Sci. Eng.* **2013**, *111*, 128–138.
- (21) Li, Y.; Dai, C.; Zhou, H.; Wang, X.; Lv, W.; Zhao, W. Investigation of Spontaneous Imbibition by Using a Surfactant-Free Active Silica Water-Based Nanofluid for Enhanced Oil Recovery. *Energy Fuels* **2018**, *32*, 287–293.
- (22) Yuan, B.; Moghanloo, R. G. Nanofluid pre-treatment, an effective strategy to improve the performance of low-salinity waterflooding. *J. Pet. Sci. Eng.* **2018**, *165*, 978–991.
- (23) Roustaei, A.; Moghadasi, J.; Bagherzadeh, H.; Shahrbadi, A. In *An Experimental Investigation of Polysilicon Nanoparticles' Recovery Efficiencies through Changes in Interfacial Tension and Wettability Alteration*, SPE International Oilfield Nanotechnology Conference and Exhibition; Society of Petroleum Engineers, 2012.
- (24) Joonaki, E.; Ghanaatian, S. The Application of Nanofluids for Enhanced Oil Recovery: Effects on Interfacial Tension and Coreflooding Process. *Pet. Sci. Technol.* **2014**, *32*, 2599–2607.
- (25) Bayat, A. E.; Junin, R.; Samsuri, A.; Piroozian, A.; Hokmabadi, M. Impact of Metal Oxide Nanoparticles on Enhanced Oil Recovery from Limestone Media at Several Temperatures. *Energy Fuels* **2014**, *28*, 6255–6266.
- (26) Zaid, H. M.; Ahmad-Latiff, N. R.; Yahya, N. The Effect of Zinc Oxide and Aluminum Oxide Nanoparticles on Interfacial Tension and Viscosity of Nanofluids for Enhanced Oil Recovery. *Adv. Mater. Res.* **2014**, *1024*, 56–59.
- (27) Hendraningrat, L.; Torsæter, O. Metal oxide-based nanoparticles: revealing their potential to enhance oil recovery in different wettability systems. *Appl. Nanosci.* **2015**, *5*, 181–199.
- (28) Soleimani, H.; Baig, M. K.; Yahya, N.; Khodapanah, L.; Sabet, M.; Demiral, N. M.; Burda, M. Synthesis of ZnO nanoparticles for oil–water interfacial tension reduction in enhanced oil recovery. *Appl. Phys. A* **2018**, *124*, 128.
- (29) Tripathi, I.; Mohanty, K. K. In *Flow Instability Associated with Wettability Alteration*, Presented at SPE Annual Technical Conference and Exhibition; Society of Petroleum Engineers: Anaheim, CA, 2007.
- (30) Hourshad, M.; Jerauld, G. In *Mechanistic Modeling of the Benefit of Combining Polymer with low Salinity Water for Enhanced Oil Recovery*, Paper SPE-153161-MS presented at SPE Improved Oil Recovery Symposium; Society of Petroleum Engineers: Tulsa, Oklahoma, 2012.
- (31) Shiran, B. S.; Skauge, A. Enhanced oil recovery (EOR) by combined low salinity water/polymer flooding. *Energy Fuels* **2013**, *27*, 1223–1235.
- (32) Alagic, E.; Skauge, A. Combined low salinity brine injection and surfactant flooding in mixed-wet sandstone cores. *Energy Fuels* **2010**, *24*, 3551–3559.
- (33) Mahmood, B. S.; Ali, J.; Nazhat, S. B.; Devlin, D. A. Sensitivity Study on Low Salinity Waterflooding. *Mod. Environ. Sci. Eng.* **2017**, *04*, 231–236.
- (34) Sorbie, K. S.; Collins, I. R. In *A Proposed Pore-Scale Mechanism for How Low Salinity Water Flooding Works*, Paper SPE 129833 Presented at SPE Improved Oil Recovery Symposium; Society of Petroleum Engineers: Tulsa, 2010.
- (35) Tang, G. Q.; Morrow, N. R. Influence of brine composition and fines migration on crude oil/brine/rock interactions and oil recovery. *J. Pet. Sci. Eng.* **1999**, *24*, 99–111.

- (36) Aksulu, H. H.; Strand, S. D.; et al. The evaluation of low salinity enhanced oil recovery effects in sandstone: effects of temperature and pH gradient. *Energy Fuels* **2012**, *26*, 3497–3503.
- (37) Lemon, P.; Zeinijahromi, A.; Bedrikovetsky, P.; Shahin, I. Effects of injected water chemistry on waterflood sweep efficiency via induced fines migration. *J. Can. Pet. Technol.* **2011**, *50*, 82–94.
- (38) Zeinijahromi, A.; Lemon, P.; Bedrikovetsky, P. Effects of induced fines migration on water cut during water flooding. *J. Pet. Sci. Eng.* **2011**, *78*, 609–617.
- (39) Arab, D.; Pourafshary, P. Nanoparticles-assisted surface charge modification of the porous medium to treat colloidal particles migration induced by low salinity water flooding. *Colloids Surf., A* **2013**, *436*, 803–814.
- (40) Ahmadi, M. A.; Shadzadeh, S. R. Induced effect of adding nano silica on adsorption of a natural surfactant onto sandstone rock: Experimental and theoretical study. *J. Pet. Sci. Eng.* **2013**, *112*, 239–247.
- (41) Ahmadi, M. A.; Sheng, J. Performance improvement of ionic surfactant flooding in carbonate rock samples by use of nanoparticles. *Pet. Sci.* **2016**, *13*, 725–736.
- (42) Ahmadi, M.; Ahmad, Z.; Phung, L. T.; Kashiwao, T.; Bahadori, A. Experimental investigation the effect of nanoparticles on micellization behavior of a surfactant: Application to EOR. *Pet. Sci. Technol.* **2016**, *34*, 1055–1061.
- (43) Chidambara Murthy, K. N.; Jayaprakasha, G. K.; et al. Studies on Antioxidant Activity of Pomegranate (*Punica granatum*) Peel Extract Using in Vivo Model. *J. Agric. Food Chem.* **2002**, *50*, 4791–4795.
- (44) Chaturvedi, K. R.; Kumar, R.; Trivedi, J.; Sheng, J. J.; Sharma, T. Stable Silica Nanofluids of an Oilfield Polymer for Enhanced CO<sub>2</sub> Absorption for Oilfield Applications. *Energy Fuels* **2018**, 12730.
- (45) Abhishek, R.; Hamouda, A. A.; Murzin, I. Adsorption of silica nanoparticles and its synergistic effect on fluid/rock interactions during low salinity flooding in sandstones. *Colloids Surf., A* **2018**, *555*, 397–406.
- (46) Ali, J. A.; Kolo, K.; Khaksar Manshad, A.; Stephen, K.; Keshavarz, A. Modification of LoSal water performance in reducing interfacial tension using green ZnO/SiO<sub>2</sub> nanocomposite coated by xanthan. *Appl. Nanosci.* **2018**, 1–13.
- (47) Fawaz, J.; Mittal, V. Synthesis of Polymer Nanocomposites: Review of Various Techniques. *Synth. Tech. Polym. Nanocompos.* **2014**, 1–30.
- (48) Sajadi, S. M.; Kolo, K.; Pirouei, M.; Mahmud, S. A.; Ali, J. A.; Hamad, S. Natural iron ore as a novel substrate for the biosynthesis of bioactive-stable ZnO@CuO@iron ore NCs: a magnetically recyclable and reusable superior nanocatalyst for the degradation of organic dyes, reduction of Cr(vi) and adsorption of crude oil aromatic compounds, including PAHs. *RSC Adv.* **2018**, *8*, 35557–35570.
- (49) Basiri, S. Evaluation of antioxidant and antiradical properties of Pomegranate (*Punica granatum* L.) seed and defatted seed extracts. *J. Food Sci. Technol.* **2015**, *52*, 1117–1123.
- (50) Zak, A. K.; Razali, R.; Abd-Majid, W. H. B.; Darroudi, M. Synthesis and characterization of a narrow size distribution of zinc oxide nanoparticles. *Int. J. Nanomed.* **2011**, 1399–1403.
- (51) Spildo, K.; Johannessen, A. M.; Skauge, A. In *Low Salinity Waterflood at Reduced Capillarity*, SPE Improved Oil Recovery Symposium, 2012.
- (52) Tsujimoto, T.; Uyama, H.; Kobayashi, S.; Oikawa, S.; Yamahiro, M. Green Nanocomposites from Renewable Plant Oils and Polyhedral Oligomeric Silsesquioxanes. *Metals* **2015**, *5*, 1136–1147.
- (53) López, C.; Rodríguez-Páez, J. E. Synthesis and characterization of ZnO nanoparticles: effect of solvent and antifungal capacity of NPs obtained in ethylene glycol. *Appl. Phys. A.* **2017**, *123*, 748.
- (54) Patil, Y. S.; Patil, I. D. Synthesis and characterization of zinc oxide nanostructures. *Int. J. Sci. Spiritual. Bus. Technol.* **2014**, *2*, 88–91.
- (55) Li, J.; Wu, X. L.; Hu, D. S.; Yang, Y. M.; Qiu, T.; Shen, J. C. Splitting of X-ray diffraction peak in (Ge:SiO<sub>2</sub>)/SiO<sub>2</sub> multilayers. *Solid State Commun.* **2004**, *131*, 21–25.
- (56) Zhang, Q.; Chen, C.; Wang, M.; Cai, J.; Xu, J.; Xia, C. Facile preparation of highly-dispersed cobalt-silicon mixed oxide nanosphere and its catalytic application in cyclohexane selective oxidation. *Nanoscale Res. Lett.* **2011**, *6*, 586.
- (57) Yeganeh-Faal, A.; Bordbar, M.; Negahdar, N.; Nasrollahzadeh, M. Green synthesis of the Ag/ZnO nanocomposite using *Valeriana officinalis* L. root extract: application as a reusable catalyst for the reduction of organic dyes in a very short time. *IET Nanobiotechnol.* **2017**, *11*, 669–676.
- (58) El Shafey, A. M. Effect of nanoparticles and polymer nanoparticles implementation on chemical flooding, wettability and interfacial tension for the enhanced oil recovery processes. *Afr. J. Eng. Res.* **2017**, *5*, 35–53.
- (59) Azarshin, S.; Moghadasi, J.; Aboosadi, Z. Surface functionalization of silica nanoparticles to improve the performance of water flooding in oil wet reservoirs. *Energy Explor. Exploit.* **2017**, *35*, 685–697.
- (60) Manshad, A. K.; Rezaei, M.; Moradi, S.; Nowrouzi, I.; Mohammadi, A. H. Wettability alteration and interfacial tension (IFT) reduction in enhanced oil recovery (EOR) process by ionic liquid flooding. *J. Mol. Liq.* **2017**, *248*, 153–162.
- (61) Nowrouzi, I.; Manshad, A. K.; Mohammadi, A. H. Effects of dissolved binary ionic compounds and different densities of brine on interfacial tension (IFT), wettability alteration, and contact angle in smart water and carbonated smart water injection processes in carbonate oil reservoirs. *J. Mol. Liq.* **2018**, *254*, 83–92.
- (62) Dahle, G. S. The Effect of Nanoparticles on Oil/Water Interfacial Tension. Project thesis, NTNU, 2013.
- (63) Standal, S. H.; Blokhus, A. M.; Haavik, J.; Skauge, A.; Barth, T. Partition Coefficient and Interfacial Activity for Polar Components in Oil/Water Model Systems. *J. Colloid Interface Sci.* **1999**, *212*, 33–41.
- (64) Lashkarbolooki, M.; Ayatollahi, S.; Riazi, M. The Impacts of Aqueous Ions on Interfacial Tension and Wettability of an Asphaltic-Acidic Crude Oil Reservoir during Smart Water Injection. *J. Chem. Eng. Data* **2014**, *59*, 3624–3634.
- (65) Wei, B.; Li, Q.; Ning, J.; Wang, Y.; Sun, L.; Pu, W. Macro- and micro-scale observations of a surface-functionalized nanocellulose based aqueous nanofluids in chemical enhanced oil recovery (C-EOR). *Fuel* **2019**, *236*, 1321–1333.
- (66) Johnson, E. F.; Bossler, D. P.; Naumann, V. O. Calculation of relative permeability from displacement experiments. *Pet. Trans., AIME* **1959**, *216*, 370–372.
- (67) Anderson, G. W. Wettability literature survey. Part 5: The effects of wettability on relative permeability. *J. Pet. Technol.* **1987**, *39*, 1453–1468.

## Appendix 6

*Emerging applications of TiO<sub>2</sub>/SiO<sub>2</sub>/poly(acrylamide) nanocomposites within the engineered water EOR in carbonate reservoirs*

**Jagar A. Ali**, Kamal Kolo, Abbas Khaksar Manshad, Karl D. Stephen

Journal of Molecular Liquids 322 (2021) 114943



## Emerging applications of TiO<sub>2</sub>/SiO<sub>2</sub>/poly(acrylamide) nanocomposites within the engineered water EOR in carbonate reservoirs

Jagar A. Ali <sup>a,b,\*</sup>, Kamal Kolo <sup>c</sup>, Abbas Khaksar Manshad <sup>d</sup>, Karl D. Stephen <sup>e</sup>

<sup>a</sup> Department of Petroleum Engineering, Faculty of Engineering, Soran University, Kurdistan Region, Iraq

<sup>b</sup> Department of Petroleum Engineering, College of Engineering, The American University of Kurdistan, Duhok, Kurdistan Region, Iraq

<sup>c</sup> Scientific Research Centre, Soran University, Kurdistan Region, Iraq

<sup>d</sup> Department of Petroleum Engineering, Abadan Faculty of Petroleum Engineering, Petroleum University of Technology (PUT), Abadan, Iran

<sup>e</sup> Institute of Petroleum Engineering, Heriot-Watt University, Riccarton, Edinburgh EH14, United Kingdom



### ARTICLE INFO

#### Article history:

Received 25 August 2020

Received in revised form 11 November 2020

Accepted 2 December 2020

Available online 4 December 2020

#### Keywords:

Green synthesis

Smart water

Nanocomposites

Pomegranate seed extract

Silicon dioxide

Titanium dioxide

### ABSTRACT

In this study, TiO<sub>2</sub>/SiO<sub>2</sub>/poly(acrylamide) nanocomposites (NCs) as a newly-developed-nano enhanced oil recovery (EOR) agent is proposed using a simple, green and economic method from the extract of pomegranate seeds. The ultraviolet-visible spectroscopy (UV-Vis), X-ray diffraction (XRD), Fourier-transform infrared spectroscopy (FT-IR), scanning electron microscopy (FE-SEM), transmission electron microscopy (TEM) and energy-dispersive X-ray spectroscopy (EDS) are applied to analyze the characterization of NCs. Nano-smart solutions are prepared from the dispersion of NCs within the smart water at three different concentrations (500, 1000 and 1500 ppm). The used smart water solutions are formulated from mixing the single and binary systems of the monovalent and divalent salts (NaCl, KCl, MgCl<sub>2</sub>, CaCl<sub>2</sub>, Na<sub>2</sub>SO<sub>4</sub>, MgSO<sub>4</sub>, K<sub>2</sub>SO<sub>4</sub> and CaSO<sub>4</sub>) at different concentrations of 2500, 5000 and 10,000 ppm within the distilled water. In order to identify the effect of the prepared NCs in smart EOR applications, the interfacial tension (IFT) of crude-oil/smart-water and crude-oil/smart-nanofluid systems is measured using the pendant drop technique, the wettability behavior of carbonate rock is studied using the contact angle (CA) measurement, and recovery efficiency is determined by performing the coreflooding test for eight core plugs. According to the obtained experimental results of IFT and CA, KCl-5000, K<sub>2</sub>SO<sub>4</sub>-5000, CaSO<sub>4</sub> + CaCl<sub>2</sub> (5000 + 5000) and K<sub>2</sub>SO<sub>4</sub> + CaCl<sub>2</sub> (2500 + 2500) are selected as the optimal smart solutions. Furthermore, the performance of the selected smart water solutions is influenced by 65% in IFT reduction, 32% in wettability alteration and 10.5% in oil recovery when the prepared NCs is added to the solutions. Nano-OSS3-5000 smart-nanofluid developed from mixing 1500 ppm of TiO<sub>2</sub>/SiO<sub>2</sub>/poly(acrylamide) NCs with 5000 ppm of CaSO<sub>4</sub> and CaCl<sub>2</sub> ions demonstrated the highest performance in increasing oil recovery from 36.0 to 46.53% original oil in place (OOIP).

© 2020 Elsevier B.V. All rights reserved.

### 1. Introduction

Oil is an important source of energy with the demand expected to increase up to 2040. Oil production from mature reservoirs is declining and discovering new oilfields are becoming difficult [2,3]. Currently, the petroleum industry is focusing on improving the oil recovery factor from mature fields given the challenge of replacing resources with new fields [82]. Primary processes of oil recovery, which rely on natural pressure drive, can produce between 5 and 25% of the original oil in place (OOIP) with the larger figure applying to lighter oils [11,12,14]. Waterflooding, as a common secondary recovery process, is usually applied to maintain the internal forces and drive mechanisms of oil

reservoirs after the depletion phase as well as helping to displace fluids, where an incremental recovery by this approach varies between 5 and 30% OOIP [13]. However, some serious challenges are encountered regularly when injecting water. For instance, oil is bypassed as thin films in oil wet reservoirs and can become trapped due to strong capillary pressures in water wet fields. The interfacial tension (IFT) between oil and water has a strong impact on this behavior and reduces displacement efficiency as well as resulting in more oil left behind [6]. Thus, the goal of enhanced oil recovery (EOR) is to increase the recovery factor up to extra 15% OOIP, depending on the type of reservoir and hydrocarbon. For this purpose, the type and concentration of the dissolved ions within water can be managed in a way that would be able to activate the related mechanisms of EOR to displace the oil left in the porous rock by adjusting oil/water/rock interactions, this is called smart water or low-salinity water [84]. The strength of the interaction between the dissolved ions and the carbonate rocks is dependent on the type and

\* Corresponding author at: Department of Petroleum Engineering, Faculty of Engineering, Soran University, Kurdistan Region, Iraq.  
E-mail address: [jagar.pet@gmail.com](mailto:jagar.pet@gmail.com) (J.A. Ali).

concentration of ions. For instance,  $\text{SO}_4^{2-}$  and  $\text{Ca}^{2+}$  are the most effective ions in altering the wettability of the reservoir rock towards the medium and hydrophilic state [19,66].

According to British Petroleum [27] reports, the injection of the smart water, as a cost and environment friendly EOR technique, into the porous media increases oil recovery due to the improvement of reservoir parameters including wetting behavior, relative permeability, fluid flow and capillary forces. Austad et al. [18] and Fathi et al. [38] stated that the smart water can alter the wettability of the reservoir

rocks under different temperature conditions; accordingly, water imbibition capillary forces and sweep efficiency would be improved. The mechanism of the wettability alteration of carbonate rocks by smart water is reported by Strand et al. [85], Zhang et al. [94], Puntervold et al. [66]; wherein, the wettability of the carbonate surfaces can be altered by changing the surface charge of water-wet spots when covered by effective dissolved ions, such as calcium,  $\text{Ca}^{2+}$ , magnesium,  $\text{Mg}^{2+}$  and sulfate,  $\text{SO}_4^{2-}$ . During injecting the smart water, the sulfate ion would be absorbed onto the surface of the carbonate rock and the

**Table 1**  
Summary of experimental studies on the effect of  $\text{TiO}_2$ , and  $\text{SiO}_2$ , and modified  $\text{TiO}_2$  and  $\text{SiO}_2$  in EOR.

| Nanoparticles                 | Base phase or substrate                      | NP conc. [wt%] | Rock type | IFT [mN/m] |         | CA [degree] |         | EOR recovery [%OOIP] | References                    |
|-------------------------------|--|----------------|-----------|------------|---------|-------------|---------|----------------------|-------------------------------|
|                               |  |                |           | Clean      | with NP | Clean       | with NP |                      |                               |
| $\text{SiO}_2$                | Ethanol                                      | 0.4            | Sandstone | 26.3       | 1.7     | 55          | 78      | 23                   | Roustaei et al. [74]          |
|                               | PAM  | 1–2            | Sandstone | 27         | 10.2    | –           | –       | 24.7                 | Sharma et al. [78]            |
|                               | Xanthan gum                                  | 0.1–0.5        | Sandstone | 17.8       | 6.4     | 86          | 20      | 7.81                 | Saha et al. [77]              |
|                               | DIW  | 0.05           | Limestone | 16.7       | 11      | 54.8        | 57.7    | 2.9                  | Bayat et al. [24]             |
|                               | Low-salinity water                           | 0.02–0.1       | Sand pack | 21         | 20.3    | 51          | 30.5    | 10.1                 | Abhishek et al. [11]          |
| $\text{TiO}_2$                | Brine  | 0.1            | Sandstone | 17.5       | 7       | 12          | 40      | 28                   | Li et al. [52]                |
|                               | DIW  | 0.05           | Limestone | 17.5       | 12.5    | 55.3        | 61.9    | 6.6                  | Bayat et al. [24]             |
|                               | Water  | 0.05           | Sandstone | –          | –       | 56          | 21.64   | 6                    | Hendraningrat & Torsæter [42] |
|                               | Water  | 1.0            | Sandstone | –          | –       | 125         | 90      | 31                   | Ehtesabi et al. [34]          |
|                               | Polymer                                      | 2.3            | Sandstone | –          | –       | –           | –       | 41                   | Cheraghian [29,30]            |
| Functionalized $\text{SiO}_2$ | Prop-2-enamide                               | 0.6–1.2        | Sandstone | 28         | 7       | 87          | 28      | 21                   | Ju & Fan [46]                 |
|                               | Poly2(DMAEA)                                 | 0.1            | Sandstone | 27         | 14      | 85          | 62.2    | 9.9                  | Qi et al. [69]                |
|                               | 2-Poly(MPC)                                  | 0.1–0.2        | Sandstone | 47         | 35      | –           | –       | 5.2                  | Choi et al. [31]              |
|                               | $\text{Fe}_2\text{O}_3/\text{SiO}_2$ NC      | 0.1 g          | Carbonate | 39         | 17.5    | 138         | 52      | 31                   | Kazemzadeh et al. [48]        |
|                               | $\text{NiO}/\text{SiO}_2$ NCs                | 0.1            | Carbonate | 28         | 1.84    | 174         | 32      | –                    | Dahkaee et al. [32]           |
| Functionalized $\text{TiO}_2$ | $\text{ZnO}/\text{SiO}_2/\text{xanthan}$ NCs | 2000 ppm       | Carbonate | 31         | 2.017   | –           | –       | 19.3                 | Ali et al. [8–10]             |
|                               | $\text{TiO}_2/\text{SiO}_2$ NCs              | 0.1 g          | Carbonate | 39         | 13.2    | 138         | 48      | 26                   | Kazemzadeh et al. [48]        |
|                               | $\text{SiO}_2/\text{TiO}_2$                  | 0.1            | Sandstone | –          | –       | 154         | 23      | –                    | Sun et al. [83]               |
|                               | $\text{Al}_2\text{O}_3/\text{TiO}_2$         | 0.1            | Sandstone | –          | –       | 154         | 24      | –                    |                               |

**Table 2**  
Properties of dissolved ions used in this study.

| Salt               | Symbol                   | Molecular weight [gm/mol] | Density [gm/cm <sup>3</sup> ] | Water solubility [gm/L] | Assay [%] |
|--------------------|--------------------------|---------------------------|-------------------------------|-------------------------|-----------|
| Sodium chloride    | NaCl                     | 58.44                     | 2.17                          | 359                     | >99.5     |
| Potassium chloride | KCl                      | 74.55                     | 1.98                          | 347                     | >99       |
| Magnesium chloride | $\text{MgCl}_2$          | 95.22                     | 2.32                          | 542                     | >98       |
| Calcium chloride   | $\text{CaCl}_2$          | 110.98                    | 2.15                          | 740                     | >96       |
| Calcium sulfate    | $\text{CaSO}_4$          | 172.17                    | 2.32                          | 2                       | >99       |
| Sodium sulfate     | $\text{Na}_2\text{SO}_4$ | 142.04                    | 2.70                          | 200                     | >99       |
| Magnesium sulfate  | $\text{MgSO}_4$          | 246.48                    | 1.68                          | 710                     | >99.5     |
| Potassium sulfate  | $\text{K}_2\text{SO}_4$  | 174.26                    | 2.66                          | 111                     | >99       |

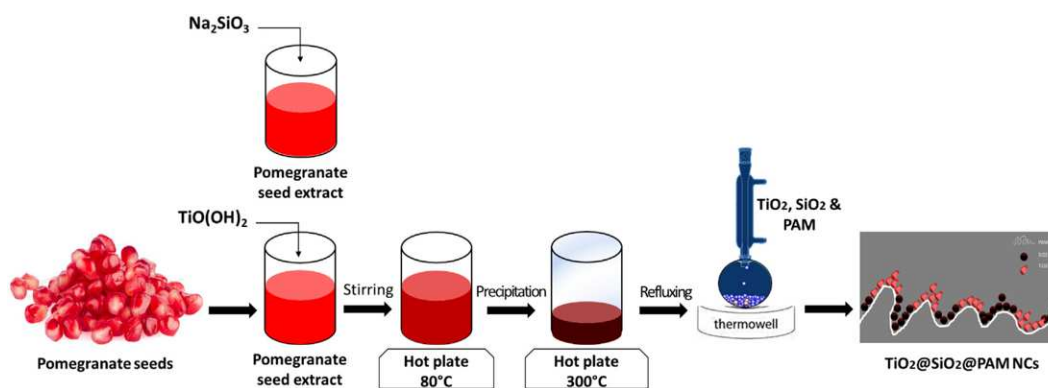


Fig. 1. Schematic diagram of the multi-pots green process to synthesis the  $\text{TiO}_2/\text{SiO}_2/\text{PAM}$  nanocomposites.



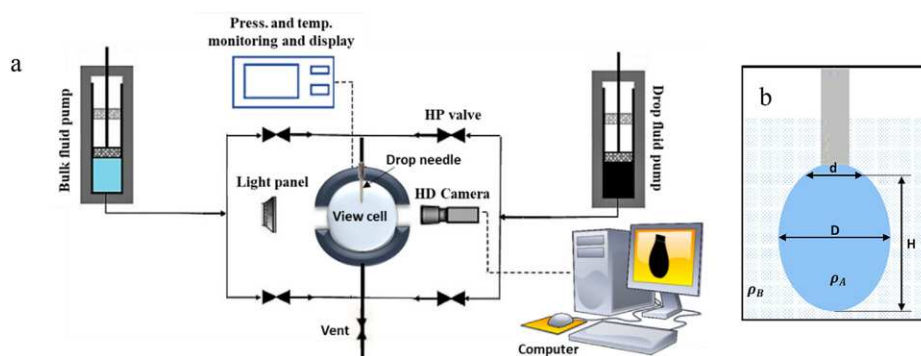


Fig. 2. Schematic presentation of high-pressure (HP) and high-temperature (HT) IFT measuring test; a) pendant drop IFT400 apparatus, and b) crude oil droplet [7].

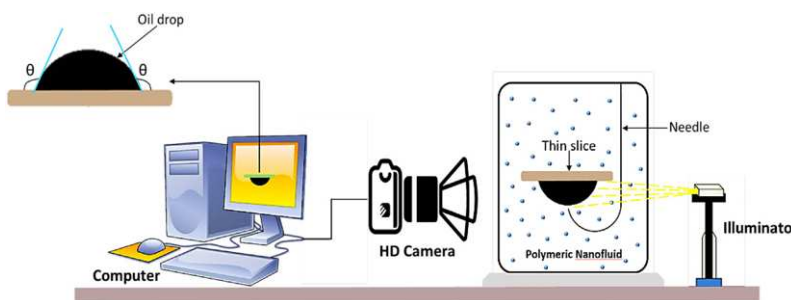


Fig. 3. Schematic illustration of sessile drop method for contact angle measurements [9].

SiO<sub>2</sub> nanocomposites on IFT reduction, wettability alteration and viscosity improvement during EOR application. Their results showed that TiO<sub>2</sub>/SiO<sub>2</sub> and Fe<sub>3</sub>O<sub>4</sub>/SiO<sub>2</sub> nanocomposites helped to improve oil recovery by 23% and 24% OOIP, respectively. More recently, Giraldo et al. [41] investigated the effect of NiO/SiO<sub>2</sub> Janus nanocomposites on IFT reduction and contact angle, and their results showed a significant increase in the capillary number and an effective reduction in IFT at 100 mg/L concentration. Bila et al. [25] evaluated the capability of polymer-coated silica NPs within seawater to improve oil recovery at ambient conditions. Their results showed an improvement in oil recovery by 2.6% to 5.2% OOIP with IFT reduced from 10.6 to between 2.5 and 6.8 mN/m. In our previous work [7,8–10], we synthesized a single-pot green method to

prepare ZnO/SiO<sub>2</sub>/xanthan NCs for EOR applications. We extracted an additional 19.28% OOIP due to the high reduction in the value of IFT from 31.8 to 2.016 mN/m and contact angle from 137° to 34°. Shirazi et al. [80] studied the impact of TiO<sub>2</sub> NPs on the behavior several smart-waters by measuring the CA, IFT reduction, and oil recovery during the spontaneous imbibition process, and they enabled to increase the performance of all types of smart waters drastically under the influence of the used NPs. In 2020, the performance of the engineered (smart) under the effect of several NPs (SiO<sub>2</sub>, CaCO<sub>3</sub>, TiO<sub>2</sub>, and gamma Al<sub>2</sub>O<sub>3</sub>) as hybrid injection EOR solutions is investigated by researchers [56,71,43,68]. All published research works stated that the performance of the smart water is improving under the influence of the nanomaterials.

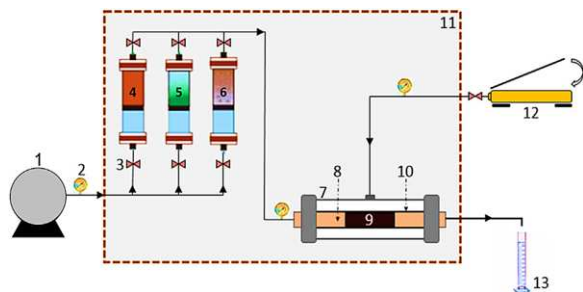


Fig. 4. Schematic illustration of the apparatus for oil displacement tests: (1) HPLC pump, (2) pressure gauges, (3) valves, (4) cylinder containing crude oil, (5) cylinder containing brine, (6) cylinder containing nanofluid, (7) core holder chamber, (8) fluid flow distributor, (9) core, (10) blocking rubber around the core, (11) oven, (12) manual hydraulic pump, and (13) outlet fluid collecting vessel [8].

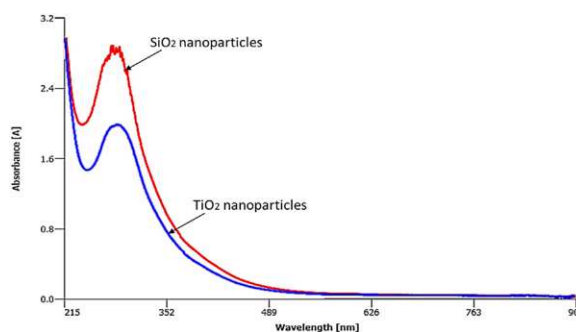
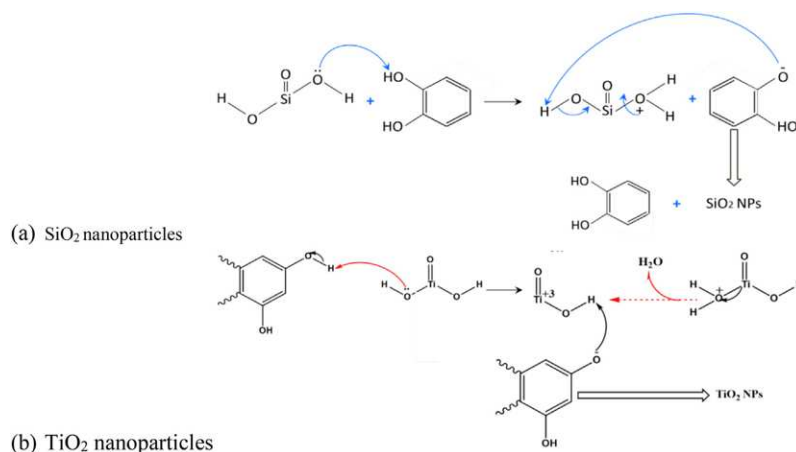


Fig. 5. The Uv-Vis spectroscopy of pomegranate seed extract used for preparing TiO<sub>2</sub> and SiO<sub>2</sub> nanoparticles.



**Fig. 6.** Mechanistic relationship of the synthesized  $\text{TiO}_2$  and  $\text{SiO}_2$  nanoparticles; (a) reaction of  $\text{Na}_2\text{SiO}_3$  with the antioxidants in pomegranate seed extract, and (b) reaction of  $\text{TiO}(\text{OH})_2$  with the antioxidants in pomegranate seed extract.

The ultimate goal of this study is to investigate the effect of a composite nanomaterial that combines NPs with polymer chains on the role of the smart water in reducing IFT and altering the wettability. Silica and titanium NPs are synthesized from the extract of pomegranate seeds using the multi-pots method. Polyacrylamide (PAM) as a well-known EOR polymer is used as a substrate for the nanocomposites. Instead of having NPs dispersed in the polymer solution, we prepared smart-polymeric-nanofluids by dispersing the synthesized  $\text{TiO}_2/\text{SiO}_2/\text{PAM}$  NCs in smart water with various types and concentrations of dissolved ions. The developed smart-polymeric-nanofluids are then applied to reduce the interfacial tension

force and alter the wettability of carbonate rocks with the aim of improving the recovery factor of an oil field.

## 2. Materials and methods

### 2.1. Materials

High-purity chemical reagents including sodium silicate ( $\text{NaSiO}_3$ ), metatitanic acid ( $\text{TiO}(\text{OH})_2$ ), sodium hydroxide ( $\text{NaOH}$ ), ethanol, propanol, polyacrylamide (PAM) and different salts are ordered from

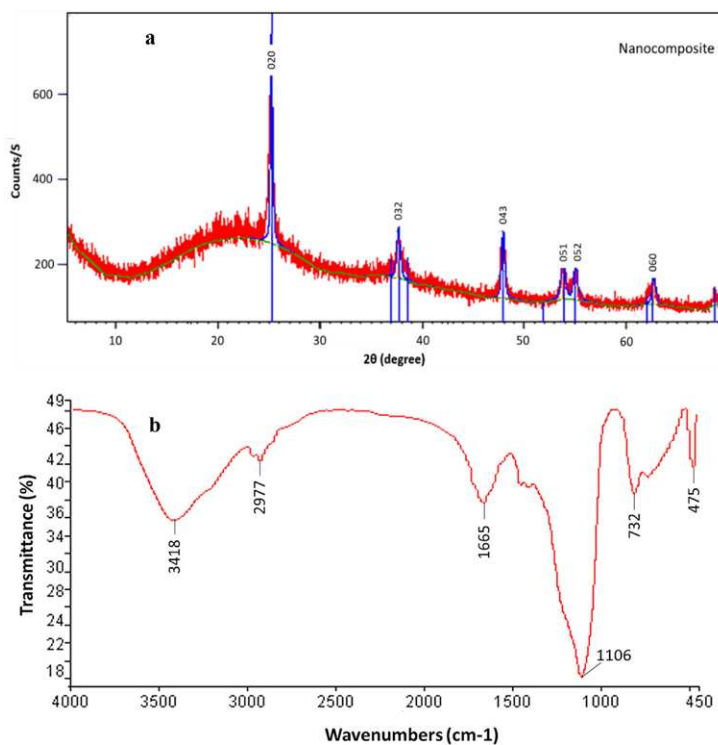


**Fig. 7.** Elemental analysis of a green synthesized  $\text{TiO}_2/\text{SiO}_2/\text{PAM}$  NCs; a) XRD pattern and b) FTIR spectra.

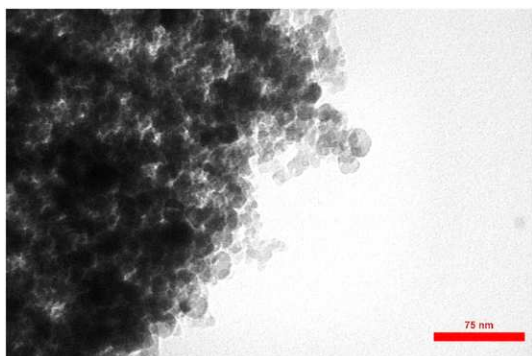


Fig. 8. TEM morphology of  $\text{TiO}_2/\text{SiO}_2/\text{PAM}$  NCs at 75 nm.

the Merck company with a purity higher than 99 mol%. The properties of used salts including molecular weight, density and the solubility are shown in Table 2. The synthetic seawater, as the formation water, with the NaCl concentration of 100,000 ppm is used for waterflooding of secondary recovery. A sample of the dead crude oil of 0.879  $\text{g}/\text{cm}^3$  density (29.5° API) from the Asmari reservoir of the rag-e-sefid oilfield

in Iran is used in this study. In addition, the rock samples are collected from the Asmari Formation outcrop in Khuzestan in Iran for the wettability measurement and coreflooding tests.

## 2.2. Synthesis and characterization of $\text{TiO}_2/\text{SiO}_2/\text{PAM}$ nanocomposites

In this study, we used multi-pots approach to synthesize  $\text{TiO}_2/\text{SiO}_2/\text{PAM}$  NCs in an eco-friendly manner using the pomegranate seed extract as shown schematically in Fig. 1. Polyacrylamide is used as a substrate for the NPs. This plant has a rich makeup of phytochemicals which are the source of a large number of biologically active compounds such as phenolics, aromatic esters, steroids, terpenoids, essential oils and other bioactive constituents used in various applications [61,44,76]. Following the methodology of Nasrollahzadeh et al. [61] and Sajadi et al. [76], the pomegranate juice is collected and filtered into two beakers of 500 mL size. In one beaker, 6 g of  $\text{Na}_2\text{SiO}_3$  is added while 3 g of  $\text{TiO}(\text{OH})_2$  is added to the other. Both are mixed with 200 mL of the filtered extract at 80 °C and 850 rpm and stirred until a dark greenish-brown formation is precipitated. The precipitates for both nanoparticles are filtered, heated up to 600 °C and washed to remove impurities. The obtained NPs are then mixed with 12 g of polyacrylamide (PAM) powder under the refluxing condition with ethanol solvent for 2 h at 80 °C. Finally, the dried and cleaned  $\text{TiO}_2/$

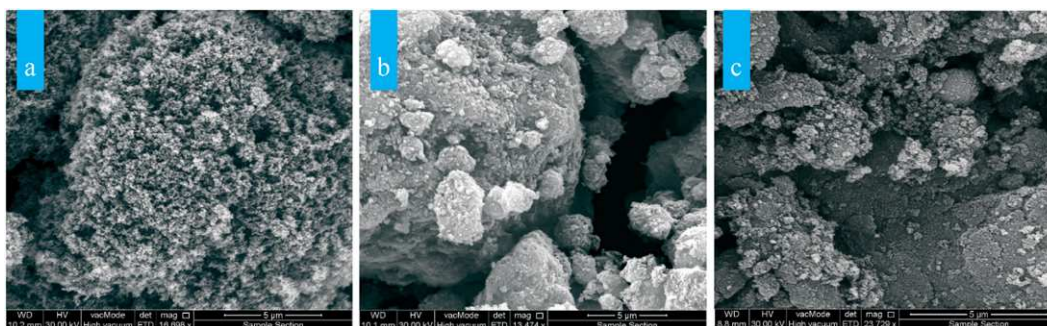


Fig. 9. SEM morphologies of a) Silica NPs, b) Titanium NPs, and c)  $\text{TiO}_2/\text{SiO}_2/\text{PAM}$  NCs at 5 µm.

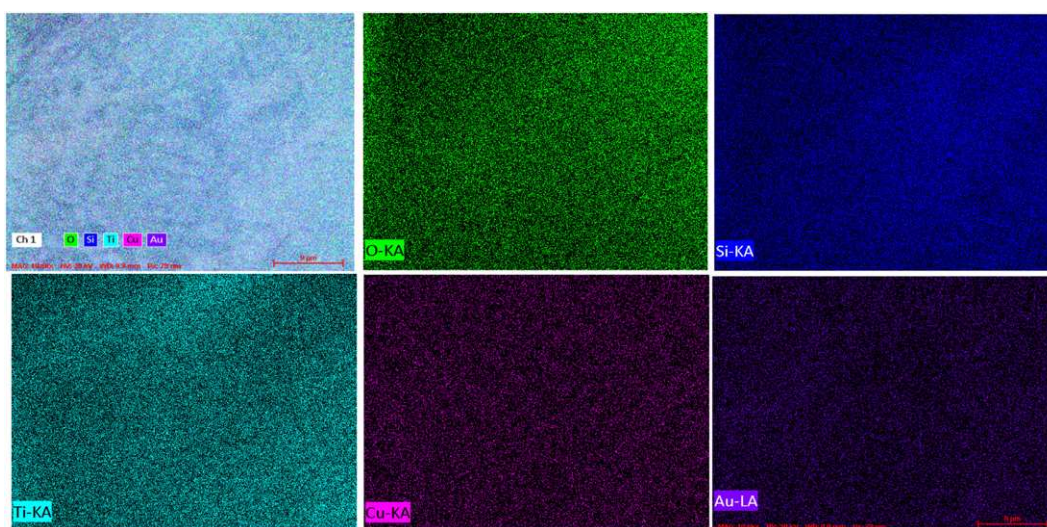


Fig. 10. Elemental mapping analysis of  $\text{TiO}_2/\text{SiO}_2/\text{poly}(\text{acrylamide})$  nanocomposites.

SiO<sub>2</sub>/PAM NCs is collected and characterized as ready to be used for EOR applications.

UV-Vis Spectrophotometer is used to identify the ultraviolet-visible (UV-Vis) spectroscopic characterization of the obtained titanium and silica NPs before drying with the scan range of 200 to 900 nm. Scanning electron microscope (SEM) and transmission electron microscopy (TEM) techniques are used to characterize the size and shape of TiO<sub>2</sub> NPs, SiO<sub>2</sub> NPs, and TiO<sub>2</sub>/SiO<sub>2</sub>/PAM NCs. Additionally, X-ray diffraction (XRD), energy-dispersive X-ray spectroscopy (EDS) and Fourier transform infrared spectroscopy (FTIR) analytical approaches are used to study the mineralogical composition of prepared nanomaterial.

### 2.3. Preparation and characterization of smart-water and smart-polymeric-nanofluids solutions

The experiment work is started by preparing the single and binary ion-based smart water solutions from mixing the selected ions with the distilled water at different concentrations of 2500, 5000 and 10,000 ppm using the magnet stirrer (Table 3a,b). The density of the prepared smart solutions is measured using PAAR density meter. From the IFT and contact angle measurements (as shown in Section 3.4), the optimal smart solutions (OSS) are identified, which are KCl (5000 ppm), K<sub>2</sub>SO<sub>4</sub> (5000), CaSO<sub>4</sub> + CaCl<sub>2</sub> (5000 + 5000) and

K<sub>2</sub>SO<sub>4</sub> + CaCl<sub>2</sub> (2500 + 2500). The smart-polymeric-nanofluids are prepared from dispersing 500, 1000 and 1500 ppm TiO<sub>2</sub>/SiO<sub>2</sub>/PAM NCs within the identified OSS solutions using the LABINCO L81 Stirrer at 600 rpm for 6 h at temperature below 30 °C (Table 3c).

In order to keep the dispersed nanocomposites in smart water stable, the prepared smart nanofluids are mixed by ultrasonic waves emitted from the UP200 ultrasonic mixer, manufactured by Hielscher in Germany, for 2 h. The stability of the nanofluids is one of the most important parameters in EOR. The visual observation approach is used to investigate the stability of TiO<sub>2</sub>/SiO<sub>2</sub>/PAM NCs dispersed in seawater, wherein the developed nanofluids are monitored through transparent vessels over time. Additionally, other characteristics of polymeric nanofluids including density, viscosity, conductivity and pH at ambient temperature and pressure are measured using PAAR density meter, Brookfield DV2T viscometer, Mettler Toledo S230, and WTW™ inoLab™ Cond 7310, respectively.

### 2.4. Interfacial tension measurement

The pendant drop method is used to measure interfacial tension of the liquid-liquid system using the IFT-400 apparatus by estimating the dimensions of the suspended crude oil droplet (Fig. 2). After receiving the droplet image in the computer from a camera, the software derives the value of IFT using the equation:

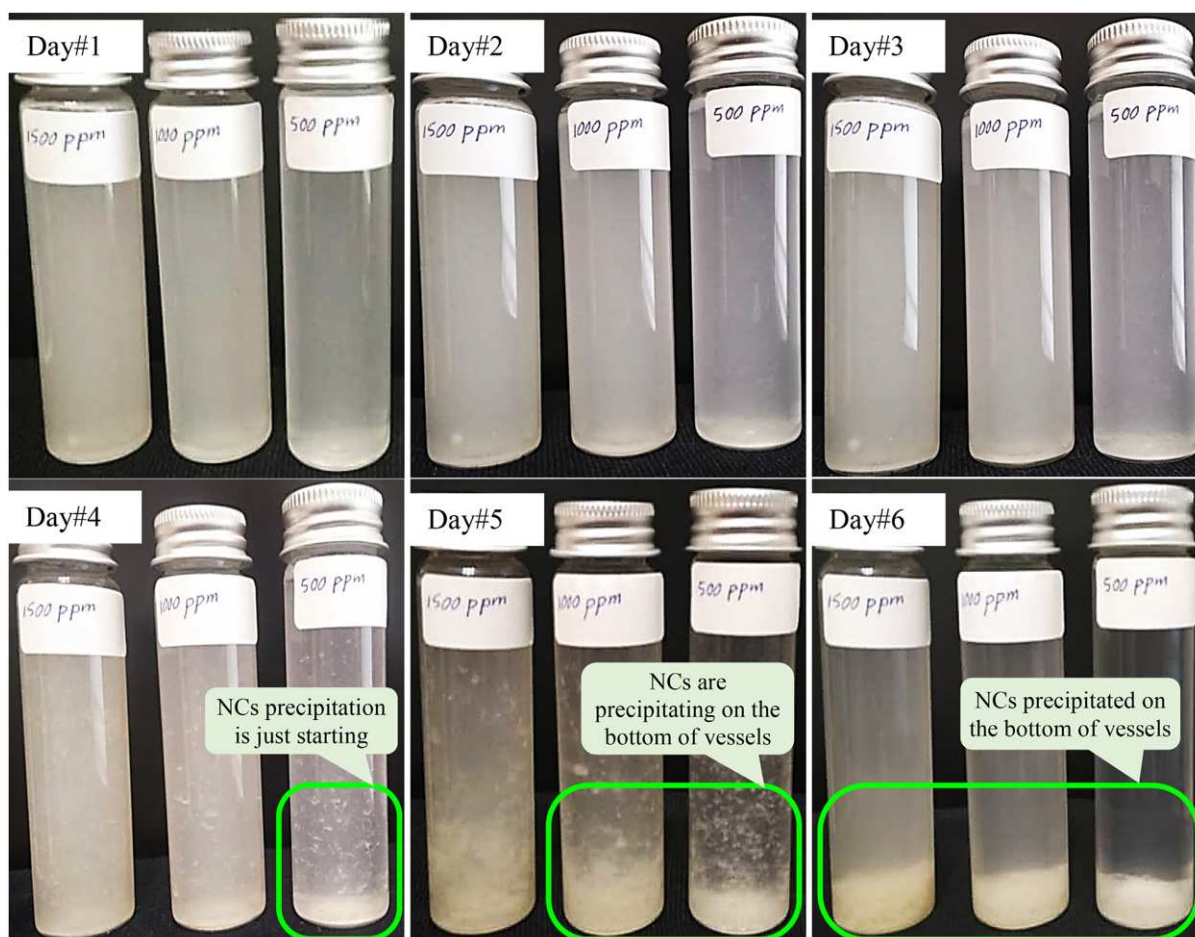


Fig. 11. Visual stability observation of OSS1-nanofluid with NCs concentrations of 500, 1000 and 1500 ppm during 6 days.

$$\gamma = \frac{\Delta\rho \cdot g \cdot D}{H} \quad (1)$$

where  $\Delta\rho$  is the difference between the density of the drop and bulk fluids ( $\text{gm}/\text{cm}^3$ ),  $g$  is the gravitational acceleration of the earth ( $\text{cm}/\text{s}^2$ ),  $D$  is the large diameter of the droplet (cm), and  $H$  is the droplet shape factor.

Initially, the IFT between crude oil and smart water prepared from mixing the singular and binary ion-based systems with the distilled water at different concentrations is measured without the presence of the synthesized NCs. Afterwards, the IFT of the oil/smart-polymeric-nanofluids (nano-OSS1, nano-OSS2, nano-OSS3 and nano-OSS4) at different concentrations of the  $\text{TiO}_2/\text{SiO}_2/\text{PAM}$  nanocomposites is estimated.

### 2.5. Contact angle measurement

The sessile drop technique presented schematically in Fig. 3 is used to measure the contact angle of the crude oil on the surface of carbonate rocks with the presence of smart water and smart-polymeric-nanofluids. This is started with preparing the rock pellets of 2 mm from the carbonate outcrop samples. After obtaining the smooth pellets, they are cleaned using the toluene and distilled water. The smooth and cleaned sections are then submerged into the crude oil for 12 days under  $70^\circ\text{C}$  to achieve the oil-wet state. Afterwards, the aged rock slices are dropped into the enclosed containers filled with smart-water and smart-polymeric-nanofluids solutions under the static condition for 3 days to study the wettability alteration. Finally, the contact angle of the crude oil droplets on the surface of all

aged slices is measured under the influences of dissolved ions and the synthesized nanocomposites.

### 2.6. Oil displacement set-up and procedure

The coreflooding experimental set-up illustrated schematically in Fig. 4 is used to conduct the oil displacement tests. The apparatus is mainly composed of 3 cylinders containing the injected fluids (dead crude oil, brine and smart solution) that can be pumped into a core holder chamber using the hydraulic pump. In order to carry out the test under the desirable temperature, the fluid containing cylinders and core holder are placed in an oven. There are also pressure and temperature gauges and valves placed on the different locations of the apparatus to monitor and control the flow behavior.

Eight carbonate core plugs with the porosity of 7.75–9.65% and permeability of 3.2–4.2 mD are collected from the Asmari carbonate outcrop in Iran. The prepared plugs are kept in the Soxhlet extraction under  $60\text{--}80^\circ\text{C}$  for 24 h and cleaned using the ethanol and toluene. The cleaned plugs are dried in an oven under  $70^\circ\text{C}$  for 6 h. In order to establish the saturation profiles inside the prepared cores, initially, each core sample is placed inside the core holder and the brine accumulator is connected to the core holder, then a confining pressure of 1000 psi greater than the injection pressure is applied. After connecting the coreflooding system, the brine is injected with  $0.25\text{ cm}^3/\text{min}$  rate by fluid injection pump. The saturation of the cores is achieved when the core produce brine and injection is stooped. Afterwards, oil accumulator is connected to the core holder instead of the brine accumulator and the confining pressure is applied to the core. Then, crude oil is injected into the core samples at different rates from  $0.1$  to  $0.5\text{ cm}^3/\text{min}$  and the produced water is measured in a graduated flask. After occurring the breakthrough, extra 2 pore volumes (PVs) of crude oil are injected

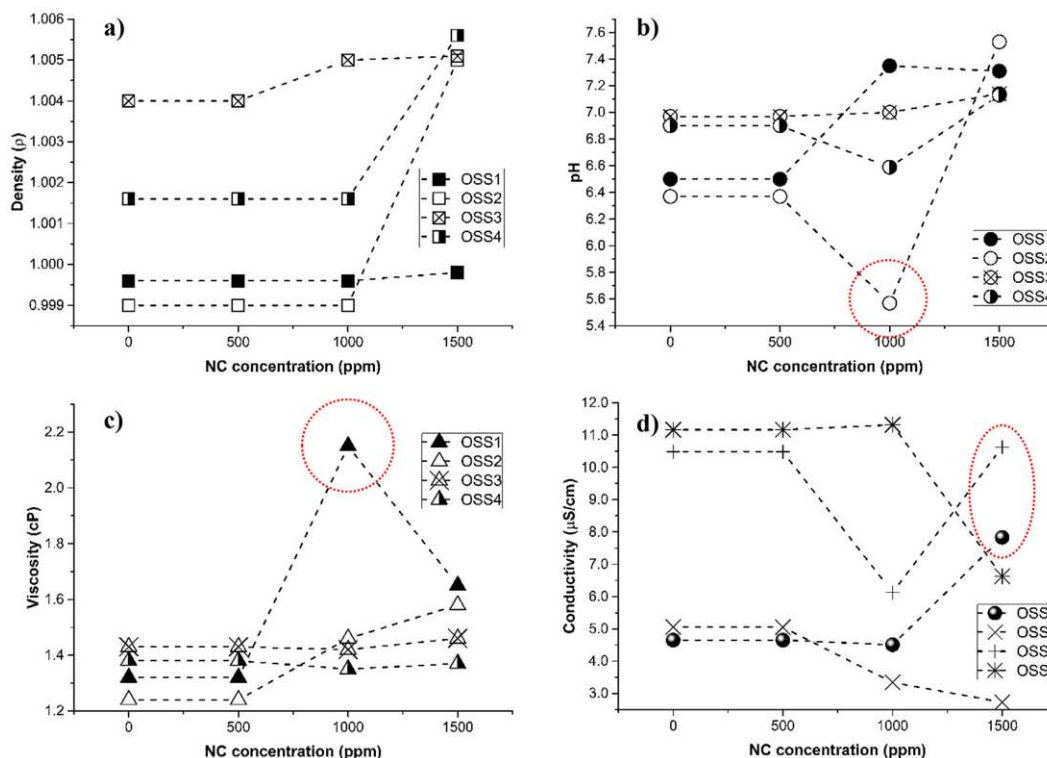


Fig. 12. Characteristics of smart-polymeric-nanofluids with 500, 1000 and 1500 ppm NCs concentrations a) density, b) pH, c) viscosity, and d) conductivity.

to complete the saturation process. From the collected water in the graduated flask, the initial water saturation ( $S_{wi}$ ) is measured. Then, the saturated cores are kept for one week to achieve the complete and stable oil-wet state.

Generally, the coreflooding tests are carried out under 75 °C temperature and 1350–1500 psi pressure with the injection rate of 0.5 cm<sup>3</sup>/min. The procedural steps of the coreflooding used in the current work consists of injecting the formation water into the all core plugs, separately, as the secondary recovery method. Then, the enhanced oil recovery is performed in two phases; first, four identified optimal smart water solutions (OSS1: KCl-5000, OSS2: K<sub>2</sub>SO<sub>4</sub>, OSS3: CaSO<sub>4</sub> + CaCl<sub>2</sub>, OSS4: K<sub>2</sub>SO<sub>4</sub> + CaCl<sub>2</sub>) are injected into core plugs 1, 3, 5 and 7. Secondly, the most effective smart-polymeric-nanofluids (nano-OSS1-1000, nano-OSS2-1500, nano-OSS3-1500, nano-OSS4-500) are injected into the remaining core plugs (2, 4, 6 and 8). The volume of the oil displaced is collected in a vessel from the outlet of core holder. The pressure, temperature and pore volume injected into cores are recorded throughout the tests. In addition, relative permeabilities of core plug#6 to water and oil before and after the smart nanofluid flooding are estimated from the obtained data of the coreflooding using the Johnson, Bossler, and Naumann (JBN) method [8].

### 3. Results and discussions

#### 3.1. Identification of the plant extract

The extract of the pomegranate seeds is prepared and filtered for preparing silica and titanium nanoparticles. In order to determine the possibility of synthesizing nanoparticles from the related salt reactions with the plant extract, Uv-Vis analysis is carried out for the dark red

solutions. From Uv-Vis results, two bonds of phenolics around 300 nm wavelength with the absorbance of 1.9 and 2.8 are observed for TiO<sub>2</sub> and SiO<sub>2</sub>, respectively (see Fig. 5). Titanium and silica NPs bonds provide strong proof of the presence of potent antioxidants inside the pomegranate seed extract in accordance with the results reported in the literature [22,40,64,65].

#### 3.2. Characterization of TiO<sub>2</sub>/SiO<sub>2</sub>/PAM nanocomposites

After confirming the synthesis of TiO<sub>2</sub> and SiO<sub>2</sub> NPs using Uv-Vis spectroscopy, they are mixed with the polyacrylamide (PAM) polymer to produce TiO<sub>2</sub>/SiO<sub>2</sub>/PAM. The mechanistic relationships of salt reactions to the antioxidants of the pomegranate extract are shown schematically in Fig. 6a,b. Generally, TiO<sub>2</sub> and SiO<sub>2</sub> NPs are distributed on the surface (chains) of the polyacrylamide as a substrate. In this embodiment, a continuous chain is formed between the synthesized NPs which is likely to make the nanofluid flow with an even displacement front in porous media. Thus, the inter-fingering of normal water that is expected within the oil phase may be prevented and better displacement efficiency can be achieved.

As additional analysis, X-ray diffraction (XRD) and Fourier transform infrared spectroscopy (FTIR) are carried out to identify the mineralogical composition of the synthesized NCs. A typical XRD pattern and FTIR spectrum for TiO<sub>2</sub>/SiO<sub>2</sub>/PAM NCs are shown in Fig. 7. Fig. 7a contains all the peaks associated with the crystalline planes of pure TiO<sub>2</sub> and SiO<sub>2</sub> nanoparticles deposited on the surface of polyacrylamide. Three major ("023", "032" and "043") and three minor ("051", "052" and "060") peaks are observed with the reflections about 25, 38 and 48°, and 54, 55 and 63°, respectively. Three mentioned major peaks represent the crystalline plane of TiO<sub>2</sub>. While,

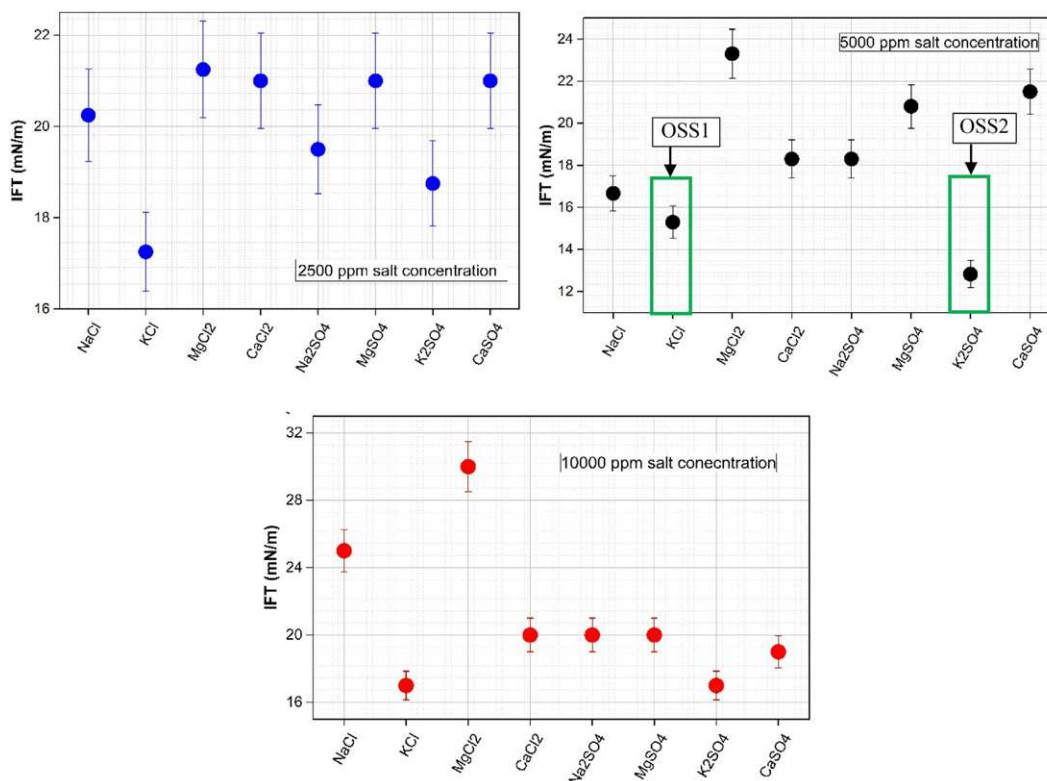


Fig. 13. IFT values measured between crude oil and smart water solutions prepared from mixing different dissolved ions within the distilled water at 2500, 5000 and 10,000 ppm concentrations.

the minor peaks are mainly belonged to  $\text{SiO}_2$ . Additionally, Fig. 7b illustrates the FTIR spectrum of the synthesized NCs, which contains a broad band from 1665 and 3418  $\text{cm}^{-1}$  and represents the O-H stretching vibration of incomplete salt groups (Ti-OH and Si-OH) with the consideration of the remaining absorbed water. However, the vibration peaks from 475 and 1106  $\text{cm}^{-1}$  belonged to the NCs stretching modes. These results provide evidence of a successful synthesis process of nanocomposites [53,70,81,91,93].

The morphology of the synthesized NCs is illustrated by SEM and TEM micrographs in Figs. 8 and 9, respectively. TEM results of the synthesized NCs on Fig. 8 show nanomaterials of size less than 10 nm. This has been also confirmed by SEM in accordance with the observed shapes of nanomaterials, which are very similar to shapes of  $\text{TiO}_2$  and  $\text{SiO}_2$  reported in the literature [55,35,21]. As can be seen, the particles are clustered together with random distribution of the silica and titanium NPs on the surface of the polyacrylamide. It is clear that the similar morphologies of  $\text{TiO}_2$  and  $\text{SiO}_2$  NPs have been achieved separately and in combination on the PAM surface (Fig. 9). Fig. 10 illustrates the elemental mapping of the green synthesized NCs. The figure is strongly depicted the presence of Si, Ti, O and Cu elements as elemental composition of the prepared nanocomposites. Au stands for the gold element that used for coating the nanocomposites. As is clear, Si and Ti elements are widely distributed in the map that confirms the validity of  $\text{TiO}_2/\text{SiO}_2/\text{poly}(\text{acrylamide})$  NCs.

### 3.3. Characterization of smart nanofluids

In this section, some main characteristics of the derived nanofluids are presented and discussed, such as dispersion stability, pH, conductivity, viscosity and density. The dispersion stability of nanomaterials

within the smart nanofluid solutions over long period of time is one of the important requirements of the injection fluid. The main observation is that either dispersion is maintained in the desired status under the experimental circumstances or flocculation will occur. After sonicating the dispersed nanocomposites within the optimal smart water solutions at 500, 1000 and 1500 ppm concentrations, they are stored in transparent vessels at the static state and monitored over 6 days (see Fig. 11 as an example). Consequently, an excellent suspension stability of the nano-KCl-5000 (OSS1) nanofluids is observed in first four days as shown in Fig. 11. This high stability might be due to the presence of PAM as a substrate in the synthesized NCs [28,88,90]. However, the sedimentation of the dispersed NCs started to happen in day 5, and the NCs at the concentrations of 500 ppm are completely precipitated at the bottom of the vessels at the end of day 6. While, the NCs of 1000 and 1500 ppm are partially precipitated at the bottom of the vessels.

The main properties of the developed smart nanofluids including the density, pH, viscosity and conductivity as function of the NCs concentration are shown in Fig. 12. The density of all optimal smart solutions is varied between 0.999 and 1.0006  $\text{g}/\text{cm}^3$  by adding NCs at 500, 1000 and 1500 ppm concentrations. It is clear that the density is slightly increased with increasing the NCs concentration which proves the low presence of NCs inside the solutions. However, the density measured for the binary-ion based smart nanofluids (OSS3 and OSS4) is higher compared with the single-ion based smart nanofluids (OSS1 and OSS2). Among the binary systems, the OSS3 solution showed the highest density at three NCs concentrations because it is made-up of 5000 ppm of both  $\text{CaSO}_4$  and  $\text{CaCl}_2$ . As is obvious, pH of a colloidal solution significantly influences the particle aggregation and the stability of the suspension of the NPs [39,87]. In general, the

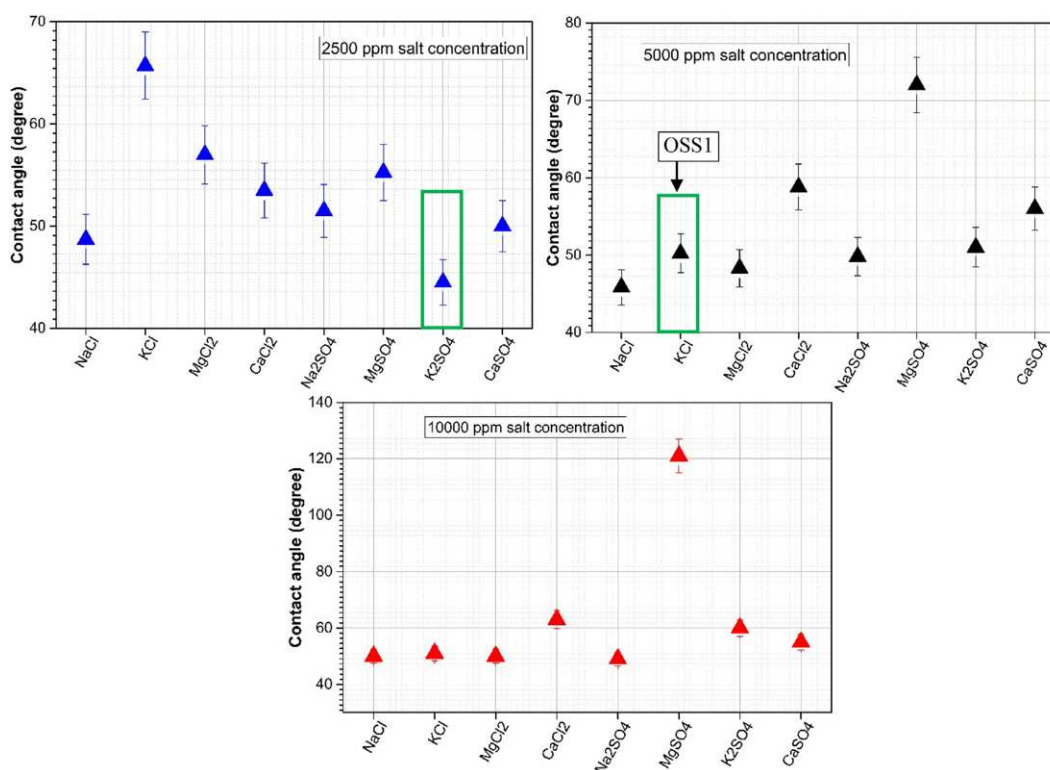


Fig. 14. Contact angles measured for the crude oil droplet on the carbonate surface with the presence of smart water solutions prepared from mixing different singular dissolved ions within the distilled water at 2500, 5000 and 10,000 ppm concentrations.

value of pH is varied from 6.3 to 7.5 depends on the type of the dissolved ion and the NCs concentration. For this property, binary-ion based nanofluids showed the higher trends similar with what observed with the density. pH of four optimal smart solutions is increased with increasing the NCs concentration, except the OSS2 solution at 1000 ppm NCs concentration which expressed a significant reduction in the pH value to 5.5 (see the dash-lined circle on Fig. 12b). Since it is very far from the trend of pH of all other solutions, this point can be considered as an error and neglected. This high changes and irregularities in the trends of the solutions is might be due to the influences of some materials at once including TiO<sub>2</sub> NPs, SiO<sub>2</sub> NPs, K<sub>2</sub>SO<sub>4</sub> and polyacrylamide. The used salts and nanomaterials might have various influences on the performance of the water which leads to have irregular distribution of the values of fluid properties. Thus, irregular points of density, pH, viscosity and conductivity can be seen on Fig. 12. Moreover, the viscosity of the smart-nanofluids is remained low between 1.2 and 1.7 cP but it is increased with increasing the concentration of the NCs. Here also a rapid change in the viscosity value is obtained when 1000 ppm NCs mixed with OSS2 solution. Meanwhile, the conductivity readings of the smart nanofluids formed by dispersing the synthesized NCs in the optimal smart solutions are also shown on Fig. 12d. The conductivity of the binary-ion based nanofluids (about 11  $\mu$ S/cm) is higher compared with the single-ion based nanofluids (about 5  $\mu$ S/cm), and remained constant for all solutions at 500 ppm concentration of NCs. After this NCs concentration, the conductivity of OSS2 and OSS4 started to decline with increasing NCs concentration. Two irregular points for OSS1 and OSS3 at 1500 ppm NCs are identified, which are opposite to the main trend of the curves and showed a high raise in the value of conductivity.

### 3.4. IFT and contact angle

#### 3.4.1. Smart water with the single dissolved ion

Interfacial tension (IFT) is one of the most important mechanisms of EOR, which is directly related to the capillary number. According to Kamal et al. [47], increasing the capillary number from around  $10^{-7}$  or  $10^{-6}$  to about  $10^{-3}$  or  $10^{-2}$  will reduce the oil saturation by 90% or to zero. To reach such saturations, the IFT between oil and water must be reduced to its minimum value, which can be achieved by injecting chemicals or nanofluids. Thus, we measured the value of IFT between crude oil and different aqueous phases of smart-water and smart-nanofluids. The improved efficiency in oil displacement, simplicity of injection, availability and low cost compared to other EOR techniques make smart water injection attractive for EOR [30]. According to Norouzi et al. [62,63] and Manshad et al. [57,58] the IFT is measured between oil and smart water. Fig. 13 illustrates the value of IFT measured between crude oil and different smart-waters prepared from mixing different dissolved ions (NaCl, KCl, MgCl<sub>2</sub>, CaCl<sub>2</sub>, Na<sub>2</sub>SO<sub>4</sub>, MgSO<sub>4</sub>, K<sub>2</sub>SO<sub>4</sub>, CaSO<sub>4</sub>) within the distilled water at 2500, 5000 and 10,000 ppm concentrations. As can be seen, the value of IFT measured for each smart solution is varied from each to another and dependent on the salt concentration. By considering 2500 ppm concentration of dissolved ions, a smart water prepared from KCl showed the lowest value of IFT which is about 17.25 mN/m. However, the maximum IFT of 21.25 mN/m is recorded for the MgCl<sub>2</sub> smart water. Although, the IFT of KCl smart water is reduced to 15.3 mN/m by increasing its concentration to 5000 ppm, but the minimum IFT of 12.83 mN/m is obtained with 5000 ppm K<sub>2</sub>SO<sub>4</sub> smart water. IFTs of all smart solutions are increased by increasing the concentration of ions to 10,000 ppm. From the single-ion based smart waters, both KCl and K<sub>2</sub>SO<sub>4</sub> dissolved

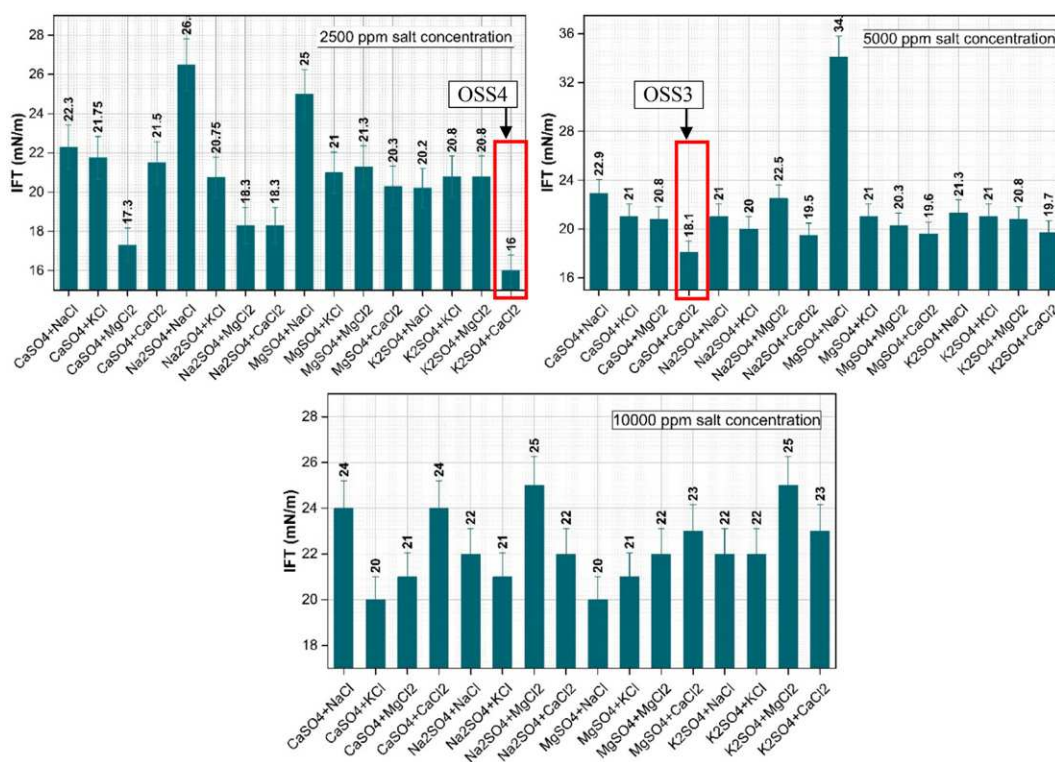


Fig. 15. IFT values measured between crude oil and smart water solutions prepared from mixing binary ionic compound within the distilled water at 2500 + 2500, 5000 + 5000 and 10,000 + 10,000 ppm concentrations.

ions with the concentration of 5000 ppm are selected as the optimal smart solutions (OSS1 and OSS2).

In addition, the role of the dissolved ion as smart water on the contact angle and wettability alteration of the carbonate rocks is analyzed. Fig. 14 demonstrates the measured values of contact angle for each above mentioned single-ion based smart water at different concentrations. In general, the contact angle measured for all smart water solutions at all different concentrations is varied between 44 and 72°. Smart waters prepared with 2500 ppm dissolved ions showed the minimum average range of contact angle of about 53°, and this average value of contact angle for all smart water solutions is increased to 54° and 62° by increasing the NCs concentration to 5000 and 10,000 ppm, respectively. RezaeiDoust et al. [73] stated that  $\text{SO}_4^{2-}$ ,  $\text{Mg}^{2+}$ , and  $\text{Ca}^{2+}$  are the most effect ions in altering the wettability of carbonate rocks. By considering each group of smart waters based on the concentration of the dissolved ion, the lowest contact angles of 44.5°, 45.84° and 49° are obtained from the smart waters prepared with the 2500 ppm  $\text{K}_2\text{SO}_4$ , 5000 ppm NaCl, and 10,000 ppm  $\text{Na}_2\text{SO}_4$ . However, the highest contact angle of 121 is recorded for a smart water contains 10,000 ppm of  $\text{MgCl}_2$ .

### 3.4.2. Smart water with the binary ion compounds

In this section, the results of the IFT and contact angle measured between crude oil/rock/smart water prepared from dissolving the pairs of NaCl, KCl,  $\text{MgCl}_2$ ,  $\text{CaCl}_2$ ,  $\text{Na}_2\text{SO}_4$ ,  $\text{MgSO}_4$ ,  $\text{K}_2\text{SO}_4$ ,  $\text{CaSO}_4$  ions with equal concentration ratios of (2500 + 2500, 5000 + 5000, 10,000 + 10,000) ppm in the distilled water are discussed. Fig. 15 demonstrates the measured IFT values for all ionic compounds at different concentrations. As is obvious, the IFT varied between 16 mN/m and its highest value of 34 mN/m depending on the type and concentration of the dissolved ions [62].

The lowest IFT is obtained for the oil/ $\text{K}_2\text{SO}_4$  +  $\text{CaCl}_2$  solution with the concentration of (2500 + 2500 ppm). There are some other values of IFTs obtained by some ionic compounds, such as  $\text{CaSO}_4$  + KCl,  $\text{Na}_2\text{SO}_4$  +  $\text{MgCl}_2$  and  $\text{Na}_2\text{SO}_4$  +  $\text{CaCl}_2$  with concentrations of (2500 + 2500),  $\text{CaSO}_4$  +  $\text{CaCl}_2$ ,  $\text{Na}_2\text{SO}_4$  +  $\text{CaCl}_2$ ,  $\text{MgSO}_4$  +  $\text{CaCl}_2$  and  $\text{K}_2\text{SO}_4$  +  $\text{CaCl}_2$  with the concentration of (5000 + 5000) ppm. While, the values of all IFTs measured for all ionic compound solutions at (10,000 + 10,000) ppm are equal to or higher than 20 mN/m. Generally, 5000 + 5000 ppm showed a better performance compared with the other two selected concentrations. According to the achieved results, the smart waters prepared from 2500 + 2500 ppm of  $\text{K}_2\text{SO}_4$  +  $\text{CaCl}_2$  and 5000 + 5000 ppm of  $\text{CaSO}_4$  +  $\text{CaCl}_2$  are identified as two optimal smart solutions (OSS3 and OSS4) from the binary-ion compound solutions.

Furthermore, the values of the measured contact angles for the dissolved binary-ions are shown in Fig. 16. The prepared smart waters demonstrated various performance in reducing the contact angle and different values are measured between 45° to 95.7°. This is quite consistent with the observations and explanation of Nowrouzi et al. [62]. The minimum contact angle of 45° is obtained with the pair of dissolved ions of  $\text{CaSO}_4$  +  $\text{MgCl}_2$  at (10,000 + 10,000) ppm concentration. Meanwhile, the smart waters composed of 2500 + 2500 ppm ( $\text{K}_2\text{SO}_4$  +  $\text{CaCl}_2$ ) and 5000 + 5000 ppm ( $\text{CaSO}_4$  +  $\text{CaCl}_2$ ) provided 47.5° and 49.5°, respectively, as two others minimum IFTs below 50 mN/m. However,  $\text{Na}_2\text{SO}_4$  +  $\text{CaCl}_2$  at different concentrations established the high contact angle up to 90°, and  $\text{K}_2\text{SO}_4$  + KCl at concentration of (5000 + 5000 ppm) provided the highest contact angle of 95.7°.

### 3.4.3. Optimal smart water with nanocomposites

From carrying out all the IFT and contact angle measurements under the effect of smart water with the presence of the single dissolved-ion

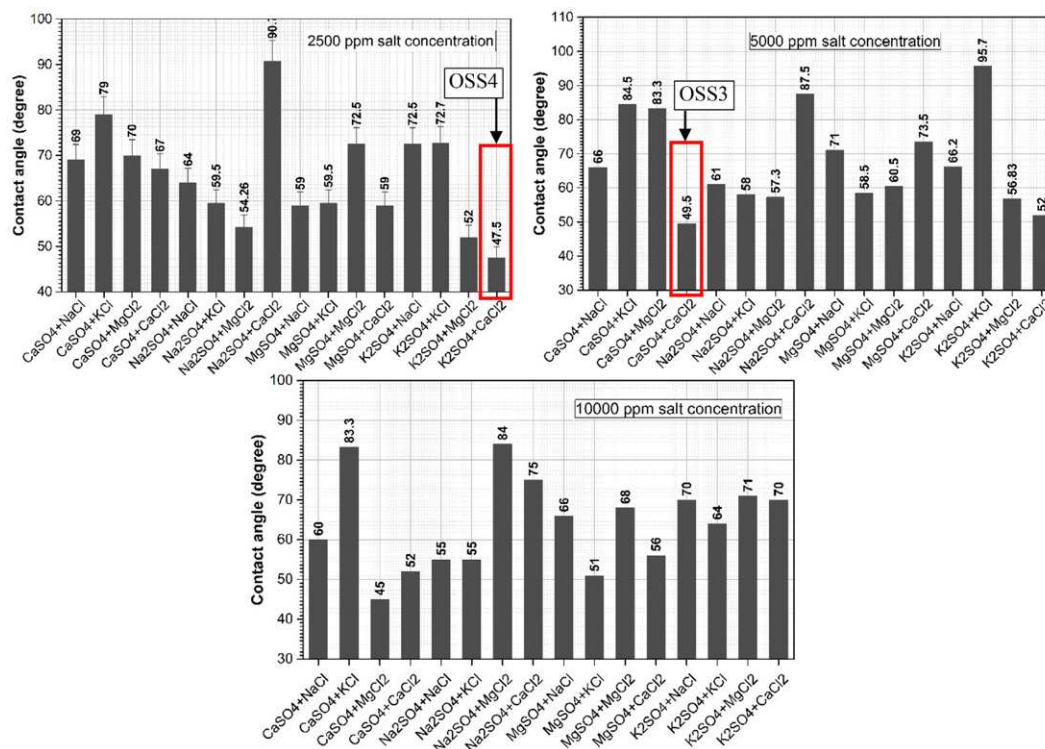


Fig. 16. Contact angles measured for the crude oil droplet on the carbonate surface with the presence of smart water solutions prepared from mixing binary ionic compounds within the distilled water at 2500 + 2500, 5000 + 5000 and 10,000 + 10,000 ppm concentrations.

and binary dissolved ions, four optimal smart solutions are selected; OSS1 consist of 5000 ppm KCl, OSS2 made-up of 5000 ppm  $K_2SO_4$  dissolved in water, 5000 + 5000 ppm  $CaSO_4 + CaCl_2$  is identified as the first optimal smart solution (OSS3) of binary-ion system, and the last optimal smart solution (OSS4) is with 2500 + 2500 ppm of  $K_2SO_4 + CaCl_2$ . In order to study its effect on the IFT reduction and wettability alteration, smart nanofluids are prepared by adding  $TiO_2/SiO_2/PAM$  NCs to the optimal solutions at 500, 1000 and 1500 ppm concentrations. Fig. 17 presents the results of the IFT measured under the influences of the smart nanofluids. As can be seen, the minimum IFT is achieved with the nano-KCl-5000 smart nanofluid prepared from dispersing 500 NCs within the OSS1. With this smart nanofluid, the IFT is reduced by 60.7% from 15.3 to 6 mN/m. This drop in IFT could be due to the accumulation of nanoparticles as a single-layer at the interface between two immiscible phases in the porous media, which provide a weak IFT similar to the surfactants [52,33]. Additionally, Hendraningrat and Torsaeter [42] stated that this force can be justified by managing the concentration of nanoparticles. For example, with the same smart water (OSS1) the value of IFT increased by increasing the NCs concentration from 500 to 1000 and 1500 ppm, which is quite consistent with the results reported by Bahraminejad et al. [23]. Similarly, when the NCs added to other optimal smart solutions (OSS2, OSS3 and OSS4) at different concentrations, different IFTs with the small variation are obtained from the smart nanofluids. The variation in the IFT value for all the studied nanofluids prepared from OSS2, OSS3 and OSS4 is ranged

between 8 and 12 mN/m. Hence, we mostly focused on the CA results to select the optimum concentration of NCs.

Fig. 18 illustrates the CAs measured for the oil droplets on the carbonate surface under the influences of the optimal smart solutions with and without the presence of  $TiO_2/SiO_2/PAM$  NCs. Different values of CAs are achieved depending on the dissolved ions and NCs concentrations, but entirely the variation is between 49 and 109°. This variation in the measured CAs dependent on the NCs concentrations is quite normal based on the reports of Azarshin et al. [21] and Saha et al. [77]. As is shown in Fig. 18, the reduction trend of CA curves is also random and not straight. The similar curve trend is reported by Bahraminejad et al. [23]. For instance, the CA curve of the OSS1 (KCl-5000) is firstly increased 65.7 to 70° by adding 500 ppm NCs, then reduced to 59° by increasing NCs concentration to 1000 ppm and raised again to 90° at 1500 ppm. The minimum CA of 48.3° is measured with the presence of the OSS2 ( $K_2SO_4$ -5000) at 1500 ppm NCs, which is reduced by 45% from 89°. Moreover, the lowest CAs measured with OSS3 and OSS4 are 62° and 57° at 1500 ppm concentrations of NCs, respectively. Generally, the OSS2 consists of  $SO_4^{2-}$  divalent ion and OSS3 solution contains the divalent ions ( $Ca^{2+}$  and  $SO_4^{2-}$ ) together represented the best performance in proving a good water-wet state.

Furthermore, the pictures of the oil droplets captured on the carbonate surfaces during the contact angle measurement tests are shown in Fig. 19. From each picture, both right and left sides angles of the crude oil droplet with the pellet surface can be seen. The contact angle from

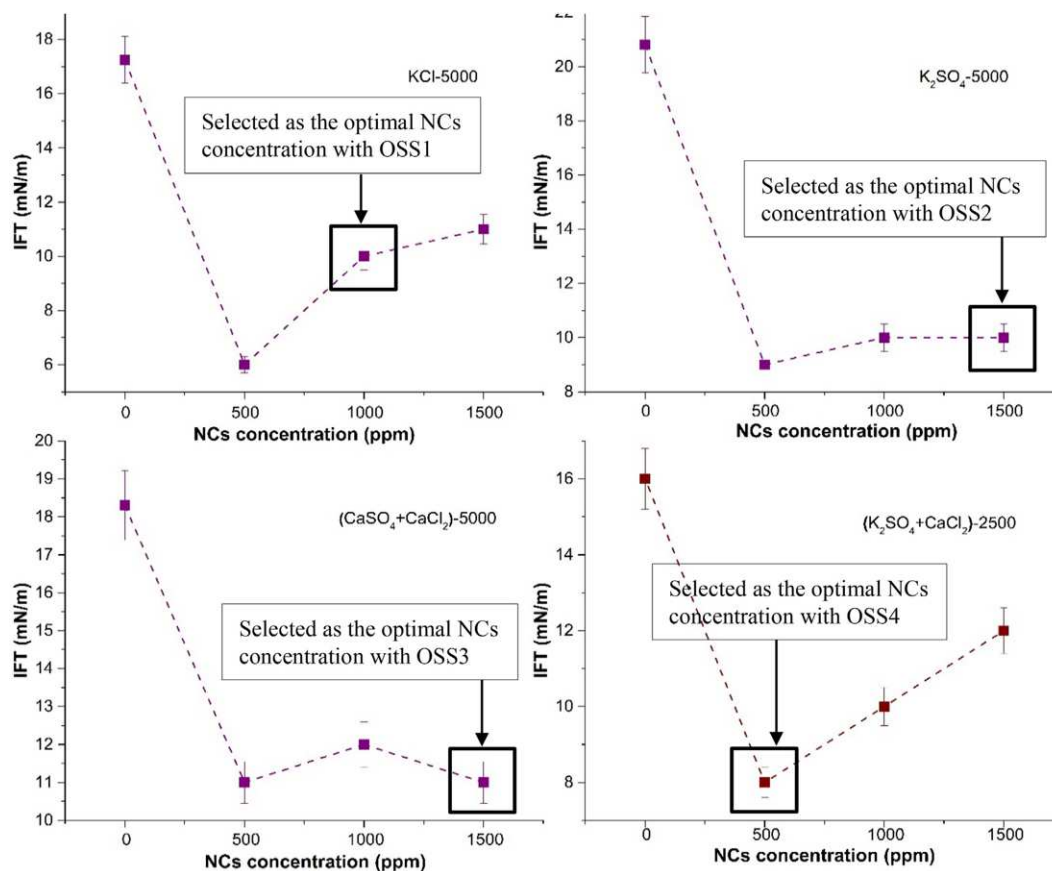


Fig. 17. IFTs measured between crude oil and smart nanofluids prepared from mixing  $TiO_2/SiO_2/PAM$  NCs with the optimal smart solutions (KCl-5000,  $K_2SO_4$ -5000,  $(CaSO_4 + CaCl_2)$  - (2500 + 2500), and  $K_2SO_4 + CaCl_2$  - (25,000 + 25,000) at 500, 1000 and 1500 ppm NCs concentration.

both right and left sides of the droplet is varied somehow depending on the interaction available between the immiscible phases with the rock.

### 3.5. Oil recovery

Coreflooding is conducted for eight core plugs prepared from the Asmari carbonate outcrop to evaluate the role of smart waters and smart-nanofluids in improving oil recovery factor. For this purpose, four optimal smart solutions (OSSs) are selected dependents on the IFT and CA results, such as OSS1 (KCl-5000), OSS2 ( $K_2SO_4$ -5000), OSS3 ( $(CaSO_4 + CaCl_2)$ -5000), and OSS4 ( $(K_2SO_4 + CaCl_2)$ -2500). On the other hand, among the smart-nanofluids prepared from mixing  $TiO_2/SiO_2$ /PAM NCs within the selected optimal smart water solutions at different concentrations, nano-OSS1-1000, nano-OSS2-1500, nano-OSS3-1500 and nano-OSS4-500 are chosen. Before injecting any smart water and smart-nanofluid solutions, the synthesized seawater (brine) is injected into each core plug with the rate of  $0.5 \text{ cm}^3/\text{min}$  up to 1.5 pore volumes (PVs). Then, the chemical EOR flooding is performed to displace the remained hydrocarbons inside the core plugs. The optimal smart solutions (OSSs) including OSS1 (KCl-5000), OSS2 ( $K_2SO_4$ -5000), OSS3 ( $(CaSO_4 + CaCl_2)$ -5000), and OSS4 ( $(K_2SO_4 + CaCl_2)$ -2500) are injected into the core plugs 1, 3, 5 and 7, respectively. Meanwhile, the optimal smart nano-fluids including nano-OSS1 1000, nano-OSS2 1500, nano-OSS3 1500 and nano-OSS4 500 are injected into the core plugs 2, 4, 6 and 8, respectively. The porosity of the plugs is ranged between 7.75 and 9.65% and permeability is varied from 3.2 to 4.2 mD. The pore volume (PV) and the initial oil saturation ( $S_{oi}$ ) of the plugs are also varied between  $5.3$  and  $6.6 \text{ cm}^3$  and 54.7–69%, respectively (Table 4).

Table 5 illustrates the status of the coreflooding tests during the secondary recovery process. Although, the used core plugs used in this work have different values of permeability, pore volume, porosity and initial water saturation, but the differences are too small. As can be seen different values of recovery factors are obtained from the various core plugs which basically ranged between 36 and 42.18% OOIP. The highest oil recovery factor of 42.18% OOIP during this phase of injection is achieved from the core Plug#4 that has the highest permeability value compared with the other plug samples. This is could be due to the availability of the better-quality reservoir properties such as porosity of 8.04% and permeability of 4.10 mD [31,41,92]. Oil saturation in this core plug is reduced by 42% from its initial value of 57.8 to 33.4%. However, the core plug#6 enabled the injected water to displace the minimum percentage of crude oil compared with the other core samples which is 36% OOIP, and it is oil saturation is reduced to 35%. Moreover, the initial oil saturation of plug#5 is the maximum which is 69% and its permeability is 3.8 mD but the oil recovery factor of 36.8% OOIP is obtained from the waterflooding.

The tertiary recovery is started by injecting the selected optimal smart solutions (OSSs) into four core plugs, known as plug#1, plug#3, plug#5 and plug#7. While, the smart nanofluids are injected into other four core plugs. Table 6 demonstrates the outcomes of the coreflooding tests of used core plugs. During this phase of the flooding, the maximum oil recovery factor of 10.5% OOIP is achieved from the core plug#6 by injecting nano-OSS3-1500 solution prepared from mixing 1500 ppm NCs with 5000 ppm of each  $CaSO_4$  and  $CaCl_2$  dissolved ions. Oil saturation of this core plug is reduced from the residual saturation of 35% established by waterflooding to 29.2%. However, the minimum oil recovery factor of 5.3% OOIP is obtained during the tertiary

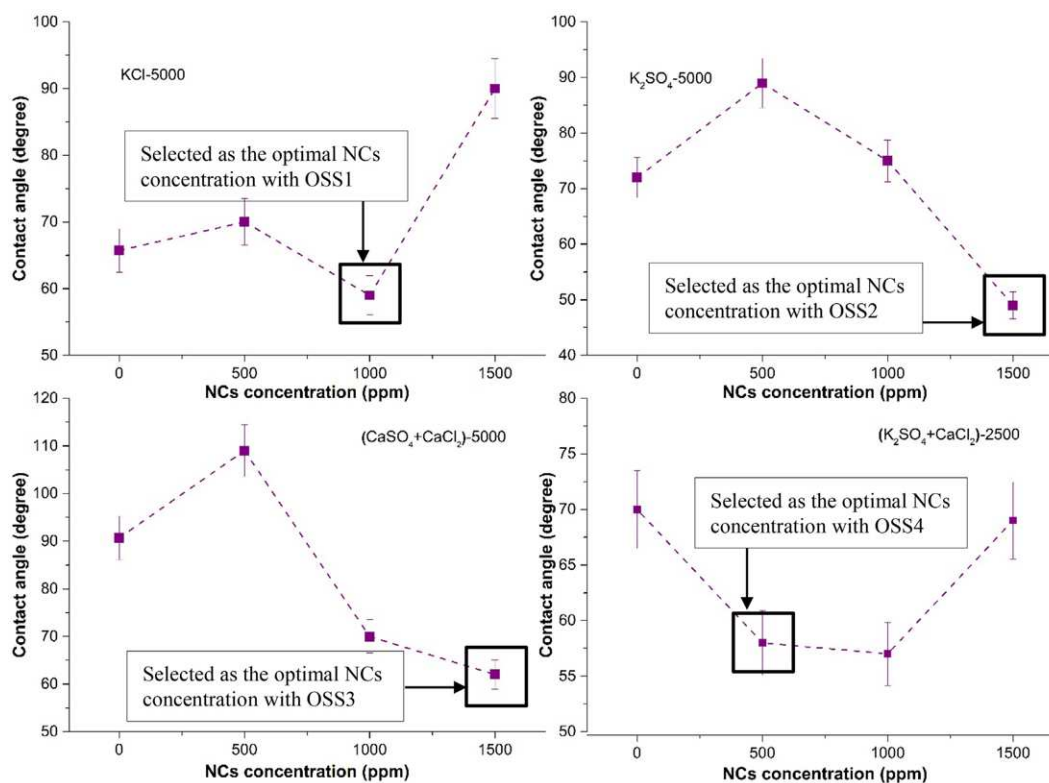


Fig. 18. Contact angles measured between crude oil and smart nanofluids prepared from mixing  $TiO_2/SiO_2$ /PAM NCs with the optimal smart solutions (KCl-5000,  $K_2SO_4$ -5000,  $(CaSO_4 + CaCl_2)$ -2500 + 2500) and  $(K_2SO_4 + CaCl_2)$ -25,000 + 25,000) at 500, 1000 and 1500 ppm NCs concentration.

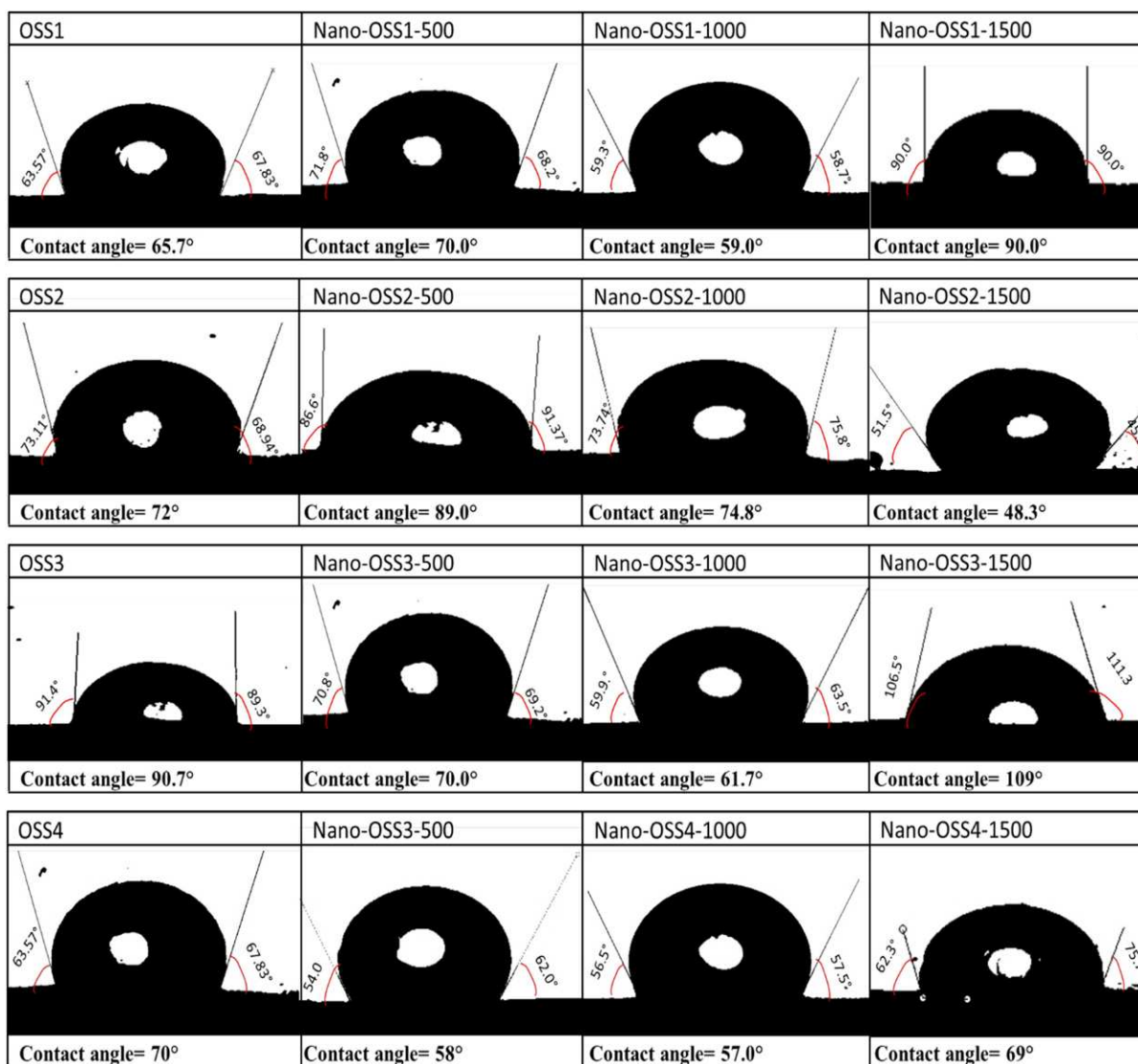


Fig. 19. Shapes of crude oil droplets on the carbonate surface under the influence of the optimal smart solutions (OSS1, OSS2, OSS3 and OSS4) and smart nanofluids (nano-OSS1, nano-OSS2, nano-OSS3 and nano-OSS4) at different concentrations of TiO<sub>2</sub>/SiO<sub>2</sub>/PAM NCs.

phase when OSS3 smart water contains 5000 ppm of each CaSO<sub>4</sub> and CaCl<sub>2</sub> ions is injected into plug#5.

Fig. 20 depicts the recovery factor of oil production from eight used core plugs during the secondary and tertiary phases. In general, the waterflooding showed better performance in displacing the

hydrocarbon through the core plugs#1–4 compared with the plugs#5–8. While, smart nanofluids (see red color of plug 2,4,6 and 8 on Fig. 20) showed better performance compared with the smart water solutions (see red color of plug 1,3,5 and 7 on Fig. 20) during the tertiary recovery process. According to the results illustrated on

Table 4  
Petrophysical properties of core plugs used in coreflooding tests.

| Core plug                                   | Plug#1 | Plug#2 | Plug#3 | Plug#4 | Plug#5 | Plug#6 | Plug#7 | Plug#8 |
|---|--------|--------|--------|--------|--------|--------|--------|--------|
| Porosity, $\phi$ (%)                        | 8.00   | 9.65   | 7.75   | 8.04   | 8.63   | 7.75   | 8.92   | 8.04   |
| Permeability, K (mD)                        | 3.20   | 3.60   | 3.40   | 4.10   | 3.80   | 3.70   | 3.50   | 4.20   |
| Pore volume, PV (cm <sup>3</sup> )          | 5.50   | 6.60   | 5.30   | 5.50   | 5.90   | 5.30   | 6.10   | 5.50   |
| Initial oil saturation, So <sub>i</sub> (%) | 66.0   | 61.8   | 62.7   | 57.8   | 69.0   | 69.0   | 67.2   | 58.5   |

**Table 5**  
Detailed summary of the waterflooding tests performed in eight core plugs.

| Secondary recovery    |                     |          |        |        |        |        |        |        |        |
|-----------------------|---------------------|----------|--------|--------|--------|--------|--------|--------|--------|
| Injected fluid        |                     | Seawater |        |        |        |        |        |        |        |
| Core plug             |                     | Plug#1   | Plug#2 | Plug#3 | Plug#4 | Plug#5 | Plug#6 | Plug#7 | Plug#8 |
| Oil recovery (% OOIP) |                     | 40.0     | 41.1   | 40.5   | 42.18  | 36.8   | 36.0   | 39.0   | 36.8   |
| Oil saturation (%)    | Initial, Soi        | 66.0     | 61.8   | 62.7   | 57.8   | 69.0   | 69.0   | 67.2   | 58.5   |
|                       | Waterflooding, Sor2 | 39.6     | 36.4   | 37.3   | 33.4   | 53.6   | 54.3   | 41.0   | 37.0   |

**Table 6**  
Detailed summary of the EOR flooding tests including smart water and smart-nanofluid injections performed in eight core plugs.

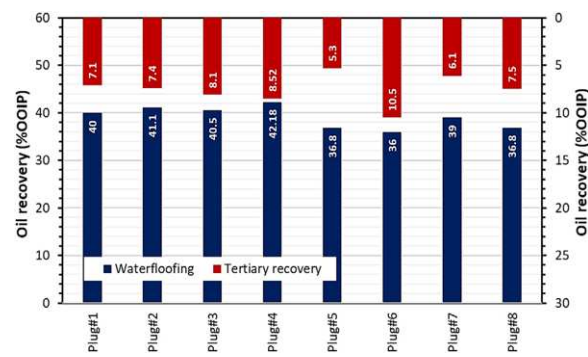
| Tertiary recovery          |                      |        |                |        |                |        |                |        |               |
|----------------------------|----------------------|--------|----------------|--------|----------------|--------|----------------|--------|---------------|
| Core plug                  |                      | Plug#1 | Plug#2         | Plug#3 | Plug#4         | Plug#5 | Plug#6         | Plug#7 | Plug#8        |
| Injected fluid             |                      | OSS1   | Nano-OSS1-1000 | OSS2   | Nano-OSS2-1500 | OSS3   | Nano-OSS3-1500 | OSS4   | Nano-OSS4-500 |
| Oil recovery (% OOIP)      |                      | 7.1    | 7.4            | 8.1    | 8.52           | 5.3    | 10.5           | 6.1    | 7.5           |
| Oil saturation (%)         | Initial (Soi)        | 66.0   | 61.8           | 62.7   | 57.8           | 69.0   | 69.0           | 67.2   | 58.5          |
|                            | Waterflooding (Sor1) | 39.6   | 36.4           | 37.3   | 33.4           | 53.6   | 54.3           | 41.0   | 37.0          |
|                            | EOR (Sor2)           | 34.9   | 31.8           | 32.2   | 24.8           | 39.9   | 40.2           | 36.8   | 32.5          |
| Total oil recovery (%OOIP) |                      | 47.14  | 48.53          | 48.64  | 50.70          | 42.10  | 46.53          | 45.15  | 44.31         |

Fig. 20, core plugs expressed various capabilities in permitting oil displacement and extraction during the secondary and tertiary phases. For example, plug#4 provided a favorable ability in permitting the injected fluids to displace a high amount of hydrocarbon during both phases of recovery; the maximum recovery factor of 42.18% OOIP by waterflooding, and extra 8.52% OOIP is extracted by injecting the OSS2-1500. This is could be due the role of existing  $K_2$  and  $SO_4$  ions together and their influences on breaking a strong bond available between the rock surface and hydrocarbon. As is clear, these dissolved ions are active in enhancing the disjoining pressure [19,38]. However, the performance of both waterflooding and smart water is low in displacing the hydrocarbon through the core plug#5. Meanwhile, the porosity and permeability of the mentioned plug are in the average range with others plugs. This is could be due to the strong interaction presents between the rock and fluids inside the core plugs or the bad performance of the injected smart water which contains 5000 ppm of  $CaSO_4$  and 5000 ppm of  $CaCl_2$ . However, the same smart water showed the maximum performance in improving oil recovery when 1500 ppm of  $TiO_2/SiO_2/PAM$  NCs added into  $CaSO_4-CaCl_2$  smart water solution and injected into plug#6. This is happened when plug#6 demonstrated the lowest recovery factor of 36% during the secondary recovery stage. As can be seen, when the synthesized seawater is changed to the hybrid EOR solution by adding both  $CaSO_4$  and  $CaCl_2$  salt ions and the prepared nanocomposites, the recovery factor of oil is highly increased from 36 to 46.5% OOIP. This amount of enhancement in oil recovery factor is due to the improvement in the main EOR mechanism, such IFT reduction, wettability alteration, even flow of the fluid within the core plug [56]. By combining the nanomaterials with the smart solutions, their functions and usages can be emerged for example the engineered water has the role in changing the wettability state of the rock [66,84] and nanomaterials have impact on the IFT reduction [49]. In addition, nanocomposites have role in improving the fluid flow behavior of the injected fluid in the porous media [32].

Fig. 21 demonstrates the flooding profiles of plug#6 that provided the highest oil recovery factor compared with the other core plugs used in this study. The oil recovery factor and pressure distribution through the core plug versus the pore volume injected are illustrated on the figure. In this core plug, 1.6 PVs of water and 2.4 PVs of nano-OSS3-1500 are injected into the core. Nano-OSS3-1500 solution as the smart nanofluid contains 5000 ppm  $CaSO_4$ , 5000 ppm  $CaCl_2$  and 1500 ppm  $TiO_2/SiO_2/PAM$  NCs. This enhancement of oil recovery is

could be due to the role of the synthesized NCs in a smart solution contains  $CaSO_4$  and  $CaCl_2$  because the same core plug showed a low performance during waterflooding, and nano-OSS3-1500 showed the low recovery performance when injected into core plug#5 without the presence of the NCs.

Furthermore, the relative permeability curves of the core plug#6 before and after the treatment with nano-OSS3-1500 smart nanofluid are shown in Fig. 22. The curves mentioned in this figure are estimated from the coreflooding outcomes by applying the JBN method in CYDAR software [45]. As can be on the figure, a clear comparison between both curves in terms of saturation distribution and relative permeability values is observed before and after the smart nanofluid flooding [16]. A considerable variation in the value of the irreducible water saturation ( $S_{wir}$ ) can be seen from its initial value of 69% to 54%. According to Anderson [17], this change in the value of the irreducible water saturation indicates that the wettability of the displaced core plug is altered from the oil-wet to a strongly water-wet. In addition, the crossover point where the water and oil relative permeabilities are equal is shifted towards the right side of the graph due to the effect of the smart nanofluid. The most suited description for this substantial variation in relative permeability curves is due to the increasing the disjoining force in the interface between the liquid phases and the surface of the rock under the influences of the synthesized NCs and dissolved ions.



**Fig. 20.** A clustered column shows the recovery factors of crude oil obtained from the water-flooding, smart-water flooding and smart-nanofluid flooding through 8 core plugs.

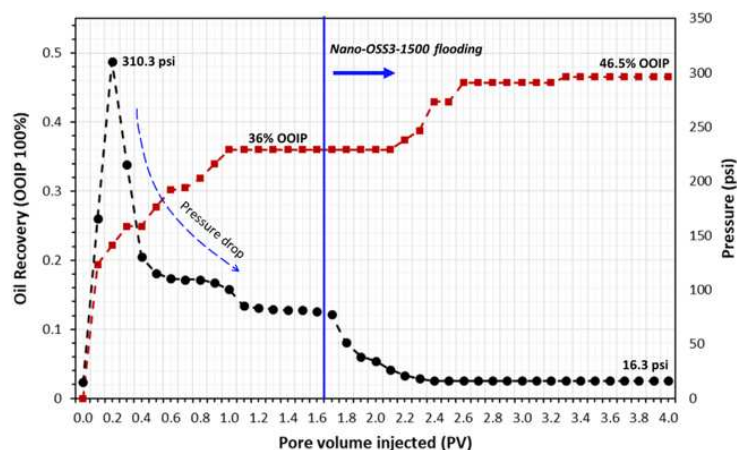


Fig. 21. Recovery profile of core plug#6 when water and nano-OSS3-1500 are injected; black color line expresses the pressure curve through the injection process, and red color curve shows the oil recovery factor versus the pore volume injected.

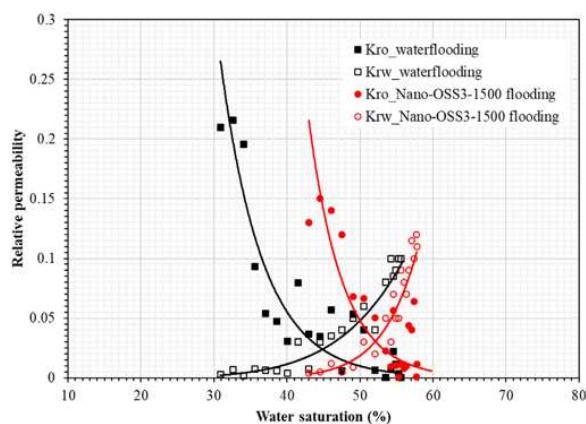


Fig. 22. Relative permeability curves of core plug#6 when water and nano-OSS3-1500 are injected; black color line expresses the pressure curve through the injection process, and red color curve shows the oil recovery factor versus the pore volume injected.

#### 4. Economic feasibility of $\text{TiO}_2/\text{SiO}_2/\text{poly}(\text{acrylamide})$ nanocomposites

Enhanced oil recovery is usually implemented to increase the cumulative production rate of the oilfield, and consequently, the total profit and revenue must be increased. In order to utilize a successful chemical EOR approach, all project steps including design, economic viability, implementation way and material fabrication must be well studied. The primary target of the chemical EOR flooding is providing and improving the IFT reduction and wettability alteration. In this work,  $\text{TiO}_2/\text{SiO}_2/\text{poly}(\text{acrylamide})$  nanocomposites is fabricated in a green and economic way from the pomegranate juice and used with the smart water as a hybrid chemical EOR approach. The synthesized NCs is effectively decreased the IFT and CA from 30 mN/m and  $95.7^\circ$  to 6 mN/m and  $48^\circ$ , respectively. This confirms the wettability alteration from oil-wet to water-wet, which led to improve oil recovery factor by 10.5% OOIP. In the initial phases of nanomaterial preparation including the design, investigation and evaluation, the cost is not considerable. However, the cost of the nanomaterial fabrication has a significant impact in the later steps of the field implementation. The most applicable advantage

of the nanomaterial is that a good improvement in oil recovery factor can be achieved using very low concentrations. Thus, the total cost of the nanomaterial implementation in the field scale would be reduced.

#### 5. Conclusions

A novel nano-EOR agent named  $\text{TiO}_2/\text{SiO}_2/\text{PAM}$  nanocomposites is synthesized from the extract of the pomegranate seeds in a green and economical way, which consists of the titanium NPs, silica NPs and polyacrylamide. The results of several analyses including UV-Vis, XRD, FT-IR, TEM, EDS and SEM techniques confirmed the validity of the synthesized NCs. From the prepared single and binary smart systems, KCl and  $\text{K}_2\text{SO}_4$  ions at concentration of 5000 ppm and  $\text{CaSO}_4 + \text{CaCl}_2$  (5000 + 5000 ppm) and  $\text{K}_2\text{SO}_4 + \text{CaCl}_2$  (2500 + 2500 ppm) are selected as the optimal smart solution dependent on the IFT and CA results. The minimum value of IFT between crude-oil/smart-water system is achieved when 5000 ppm  $\text{K}_2\text{SO}_4$  are used, which is 12.83 mN/m. At the same time, the contact angle of  $44.5^\circ$  of the oil droplets on the surface of the carbonate rock is obtained as the minimum value with the presence of 5000 ppm  $\text{K}_2\text{SO}_4$ . However, the minimum values of IFT and CA of the crude-oil/smart-nanofluid are obtained by nano-OSS1 (5000 ppm KCl + 500 ppm NCs) and nano-OSS2-1500 (5000 ppm  $\text{K}_2\text{SO}_4$ ) which are 6.1 mN/m and  $49^\circ$ , respectively. In addition, nano-OSS3-1500 provided the highest oil recovery factor of 10.5% OOIP compared with all other smart-nanofluid solutions. Thus, oil and water relative permeability curves are shifted to the right side under the influence of the most effective smart-nanofluid solution.

#### Credit author statement

**Jagar A. Ali:** Data curation; Formal analysis; Investigation; Methodology; Writing - original draft; Resources; Software. **Kamal Kolo:** Project administration; Writing - review & editing; Supervision. **Abbas Khaksar Manshad:** Conceptualization; Writing - review & editing; Data curation; Supervision. **Karl D. Stephen:** Writing - review & editing; Supervision.

#### Declaration of Competing Interest

None.

## References

- [1] R. Abhishek, A.A. Hamouda, I. Murzin, Adsorption of silica nanoparticles and its synergistic effect on fluid/rock interactions during low salinity flooding in sandstones, *Colloids Surf. A Physicochem. Eng. Asp.* 555 (2018) 397–406.
- [2] R.O. Afolabi, E.O. Yusuf, Nanotechnology and global energy demand: challenges and prospects for a paradigm shift in the oil and gas industry, *J. Petrol. Exp. Prod. Technol.* (2018) <https://doi.org/10.1007/s13202-018-0538-0>.
- [3] M. Agista, K. Guo, Z. Yu, A state-of-the-art review of nanoparticles application in petroleum with a focus on enhanced oil recovery, *Appl. Sci.* 8 (6) (2018) 871.
- [4] H. Aksulu, D. Håmsø, S. Strand, T. Puntervold, T. Austad, Evaluation of low salinity EOR-effects in sandstone: effects of temperature and pH gradient, *Energy Fuel* 26 (6) (2012) 3497–3503, <https://doi.org/10.1021/ef300162n>.
- [5] E. Alagic, K. Spildo, A. Skauge, J. Solbakken, Effect of crude oil ageing on low salinity and low salinity surfactant flooding, *J. Pet. Sci. Eng.* 78 (2) (2011) 220–227.
- [6] J.A. Ali, K. Kolo, A.K. Manshad, A.H. Mohammadi, Recent advances in application of nanotechnology in chemical enhanced oil recovery: effects of nanoparticles on wettability alteration, interfacial tension reduction, and flooding, *Egypt. J. Pet.* 27 (4) (2018) 1371–1383.
- [7] J.A. Ali, K. Kolo, A.K. Manshad, K.D. Stephen, A. Keshavarz, Modification of LoSal water performance in reducing interfacial tension using green ZnO/SiO<sub>2</sub> nanocomposite coated by xanthan, *Appl. Nanosci.* 9 (3) (2018) 397–409, <https://doi.org/10.1007/s13204-018-0923-5>.
- [8] J.A. Ali, K. Kolo, A.K. Manshad, K.D. Stephen, Low-salinity polymeric nanofluid-enhanced oil recovery using green polymer-coated ZnO/SiO<sub>2</sub> nanocomposites in the upper Qamchuqa formation in Kurdistan region, Iraq, *Energy Fuel* 33 (2) (2019) 927–937, <https://doi.org/10.1021/acs.energyfuels.8b03847>.
- [9] J.A. Ali, K. Kamal, A.K. Manshad, K.D. Stephen, Potential application of low-salinity polymeric-nanofluid in carbonate oil reservoirs: IFT reduction, wettability alteration, rheology and emulsification characteristics, *J. Mol. Liq.* 284 (2019) 735–747, <https://doi.org/10.1016/j.molliq.2019.04.053>.
- [10] J. Ali, S. Sajadi, K. Kamal, A.K. Manshad, K.D. Stephen, Green synthesis of ZnO/SiO<sub>2</sub> nanocomposite from pomegranate seed extract: coating by natural xanthan polymer and its characterizations, *Micro Nano Lett.* 14 (6) (2019) 638–641, <https://doi.org/10.1049/mnl.2018.5617>.
- [11] J.A. Ali, A.M. Kalthury, A.N. Sabir, R.N. Ahmed, N.H. Ali, A.D. Abdullah, A state-of-the-art review of the application of nanotechnology in the oil and gas industry with a focus on drilling engineering, *J. Pet. Sci. Eng.* 191 (2020) 107–118, <https://doi.org/10.1016/j.petrol.2020.107118>.
- [12] J. Ali, A.K. Manshad, I. Imani, S.M. Sajadi, A. Keshavarz, Greenly synthesized magnetite@SiO<sub>2</sub>@xanthan nanocomposites and its application in enhanced oil recovery: IFT reduction and wettability alteration, *Arab. J. Sci. Eng.* 45 (9) (2020) 7751–7761, <https://doi.org/10.1007/s13369-020-04377-x>.
- [13] M. Almahfood, B. Bai, The synergistic effects of nanoparticle-surfactant nanofluids in EOR applications, *J. Pet. Sci. Eng.* 171 (2018) 196–210.
- [14] E.W. Al-Shalabi, K. Sepehrmoori, G.A. Pope, Mysteries behind the low salinity water injection technique, *J. Petrol. Eng.* 11 (2014).
- [15] S. Al-Anssari, Z. Arain, A. Barifcani, A. Keshavarz, M. Ali, S. Iglauer, Influence of pressure and temperature on CO<sub>2</sub>-nanofluid interfacial tension: implication for enhanced oil recovery and carbon geosequestration, *Abu Dhabi Int. Petrol. Exhib. Conf.* 2018.
- [16] A.H. Alizadeh, A. Keshavarz, M. Haghighi, Flow rate effect on two-phase relative permeability in Iranian carbonate rocks, *Soc. Petrol. Eng.* (2007) <https://doi.org/10.2118/104828-MS>.
- [17] G.W. Anderson, Wettability literature survey. Part 5: the effects of wettability on relative permeability, *J. Pet. Technol.* 39 (11) (1987) 1453–1468.
- [18] T. Austad, S. Strand, M. Madland, T. Puntervold, R. Korsnes, Sea water in chalk: an EOR and compaction fluid, *J. SPE Res. Eval. Eng.* (2008) 648–654.
- [19] T. Austad, A. Rezaeidoust, T. Puntervold, Chemical mechanism of low salinity water flooding in sandstone reservoirs, *Proceedings of the SPE Improved Oil Recovery Symposium*, SPE-129767-MS, Tulsa, Okla, USA, 2010, April 2010.
- [20] F.U. Awan, A. Keshavarz, H. Akhondzadeh, S. Al-Anssari, S. Iglauer, A novel approach for using silica nanoparticles in a proppant pack to fixate coal fines, *APPEA J.* 60 (1) (2020) 88.
- [21] S. Azarshin, J. Moghadasi, Z. Aboosadi, Surface functionalization of silica nanoparticles to improve the performance of water flooding in oil wet reservoirs, *Energy Explor. Exploit.* 35 (6) (2017) 685–697.
- [22] R.H. Babu, P. Yugandhar, N. Savithramma, Synthesis, characterization and antimicrobial studies of bio silica nanoparticles prepared from *Cynodon dactylon* L.: a green approach, *Bull. Mater. Sci.* (3) (2018) 41, <https://doi.org/10.1007/s12034-018-1584-4>.
- [23] H. Bahraminejad, A.K. Manshad, M. Riazi, J.A. Ali, S.M. Sajadi, A. Keshavarz, CuO/TiO<sub>2</sub>/PAM as a novel introduced hybrid agent for water–oil interfacial tension and wettability optimization in chemical enhanced oil recovery, *Energy Fuel* (2019) <https://doi.org/10.1021/acs.energyfuels.9b02109>.
- [24] E.A. Bayat, R. Junin, A. Samsuri, A. Piroozian, M. Hokmabadi, Impact of metal oxide nanoparticles on enhanced oil recovery from limestone media at several temperatures, *Energy Fuel* 28 (10) (2014) 6255–6266.
- [25] A. Bila, A.J. Stensen, O. Torsæter, Experimental investigation of polymer-coated silica nanoparticles for enhanced oil recovery, *Nanomaterials* 9 (6) (2019) 822, <https://doi.org/10.3390/nano9060822>.
- [26] A.B.H. Belhaji, Application of nanotechnology by means of nanoparticles and nanodispersions in oil recovery—a comprehensive review, *J. Nat. Gas Sci. Eng.* 34 (2016) 1284–1309.
- [27] BP, Enhanced Oil Recovery, Technology Now Retrieved Access Date, 2016, from <http://www.bp.com/en/global/corporate/technology/technology-now/enhanced-oilrecovery.html> 2016.
- [28] L. Chen, H. Xie, Surfactant-free nanofluids containing double- and single-walled carbon nanotubes functionalized by a wet mechanochemical reaction, *Thermochim. Acta* 497 (2010) 67–71.
- [29] G. Cheraghian, Effects of titanium dioxide nanoparticles on the efficiency of surfactant flooding of heavy oil in a glass micromodel, *Pet. Sci. Technol.* 34 (2016) 260–267.
- [30] G. Cheraghian, Effect of nano titanium dioxide on heavy oil recovery during polymer flooding, *Pet. Sci. Technol.* 34 (7) (2016) 633–641.
- [31] S.K. Choi, H.A. Son, H.T. Kim, J.W. Kim, Nanofluid enhanced oil recovery using hydrophobically associative zwitterionic polymer-coated silica nanoparticles, *Energy Fuel* 31 (2017) 7777–7782.
- [32] K.P. Dahkaee, M.T. Sadeghi, Z. Fakhroueian, P. Esmailzadeh, Effect of NiO/SiO<sub>2</sub> nanofluids on the ultra-interfacial tension reduction between heavy oil and aqueous solution and their use for wettability alteration of carbonate rocks, *J. Pet. Sci. Eng.* 176 (2017) 11–26.
- [33] G.S. Dahle, The effect of nanoparticles on oil/water interfacial tension, 2013 Project thesis, NTNU.
- [34] H. Ehtesabi, M.M. Ahadian, V. Taghikhani, M.H. Ghazanfari, Enhanced heavy oil recovery in sandstone cores using TiO<sub>2</sub> nanofluids, *Energy Fuel* 28 (1) (2013) 423–430.
- [35] A.M. El Shafey, Effect of nanoparticles and polymer nanoparticles implementation on chemical flooding, wettability and interfacial tension for the enhanced oil recovery processes, *African J. Eng. Res.* 5 (3) (2017) 35–53.
- [36] A.I. El-Diasty, The potential of nanoparticles to improve oil recovery in bahariya formation, Egypt: an experimental study, *Proceedings of the SPE Asia Pacific enhanced oil recovery conference*, Kuala Lumpur, Malaysia, 11–13 August 2015, 2015.
- [37] M. Eslahati, P. Mehrabianfar, A.A. Isari, H. Bahraminejad, A.K. Manshad, A. Keshavarz, Experimental investigation of alfalfa natural surfactant and synergistic effects of Ca<sup>2+</sup>, Mg<sup>2+</sup>, and SO<sub>4</sub><sup>2-</sup> ions for EOR applications: interfacial tension optimization, wettability alteration and imbibition studies, *J. Mol. Liq.* 310 (2020) 113–123, <https://doi.org/10.1016/j.molliq.2020.113123>.
- [38] S.J. Fathi, T. Austas, S. Strand, Smart water as a wettability modifier in chalk: the effect of salinity and ionic composition, *Energy Fuel* 24 (2010) 2514–2519.
- [39] Y. Fovet, J.Y. Gal, F. Toumelin-Chema, Influence of pH and fluoride concentration on titanium passivating layer: stability of titanium dioxide, *Talanta* 53 (2001) 1053–1063.
- [40] W. Ghann, H. Kang, T. Sheikh, S. Yadav, T. Chavez-Gil, F. Nesbitt, J. Uddin, Fabrication, optimization and characterization of natural dye sensitized solar cell, *Sci. Rep.* 7 (1) (2017) <https://doi.org/10.1038/srep41470>.
- [41] L.J. Giraldo, J. Gallego, J.P. Villegas, C.A. Franco, F.B. Cortés, Enhanced waterflooding with NiO/SiO<sub>2</sub> 0-D Janus nanoparticles at low concentration, *J. Pet. Sci. Eng.* 174 (2019) 40–48.
- [42] L. Hendraningrat, O. Torsæter, Metal oxide-based nanoparticles: revealing their potential to enhance oil recovery in different wettability systems, *Appl. Nanosci.* 5 (2) (2014) 181–199.
- [43] S.U. Ilyas, S. Ridha, F.A. Abdul Kareem, Dispersion stability and surface tension of SDS-stabilized saline nanofluids with graphene nanoplatelets, *Colloids Surf. A Physicochem. Eng. Asp.* 592 (2020) 1245–1284, <https://doi.org/10.1016/j.colsurfa.2020.124584>.
- [44] N.U. Islam, I. Khan, A. Rauf, N. Muhammad, M. Shahid, M.R. Shah, Antinociceptive, muscle relaxant and sedative activities of gold nanoparticles generated by methanolic extract of *Euphorbia milii*, *BMC Complement. Altern. Med.* 15 (1) (2015).
- [45] E.F. Johnson, D.P. Bossler, V.O. Naumann, Calculation of relative permeability from displacement experiments, *Petroleum transactions*, AIME 216 (1959) 370–372.
- [46] B. Ju, T. Fan, Experimental study and mathematical model of nanoparticle transport in porous media, *Powder Technol.* 192 (2009) 195–202.
- [47] M.S. Kamal, I.A. Hussein, A.S. Sultan, Review on surfactant flooding: phase behavior, retention, IFT, and field applications, *Energy Fuel* 31 (8) (2017) 7701–7720.
- [48] Y. Kazemzadeh, M. Sharifi, M. Riazi, H. Rezvani, M. Tabaei, Potential effects of metal oxide/SiO<sub>2</sub> nanocomposites in EOR processes at different pressures, *Colloids Surf. A Physicochem. Eng. Asp.* 559 (2018) 372–384.
- [49] L. Kewen, D. Wang, S. Jiang, Review on enhanced oil recovery by nanofluids, *Oil Gas Sci. Technol.—Revue d'IFP Energies nouvelles* 73 (2018) 37, <https://doi.org/10.2516/ogst/2018025>.
- [50] M. Lashkarbolooki, S. Ayatollahi, M. Riazi, The impacts of aqueous ions on interfacial tension and wettability of an Asphaltene—acidic crude oil reservoir during smart water injection, *J. Chem. Eng. Data* 59 (2014) 3624–3634.
- [51] M. Lashkarbolooki, S. Ayatollahi, M. Riazi, Mechanical study of effect of ions in smart water injection into carbonate oil reservoir, *Process. Saf. Environ. Prot.* 105 (2017) 361–372, <https://doi.org/10.1016/j.psep.2016.11.022>.
- [52] Y. Li, C. Dai, H. Zhou, X. Wang, M. Zhao, Investigation of spontaneous imbibition by using a surfactant-free active silica water-based nanofluid for enhanced oil recovery, *Energy Fuel* 32 (2017) 287–293.
- [53] J. Li, X.L. Wu, D.S. Hu, Y.M. Yang, T. Qiu, J.C. Shen, Splitting of X-ray diffraction peak in (Ge:SiO<sub>2</sub>)/SiO<sub>2</sub> multilayers, *Solid State Commun.* 31 (1) (2004) 21–25.
- [54] S. Llanos, L.J. Giraldo, O. Santamaria, C.A. Franco, F.B. Cortés, Effect of sodium oleate surfactant concentration grafted onto SiO<sub>2</sub> nanoparticles in polymer flooding processes, *ACS Omega* 3 (12) (2018) 18673–18684.
- [55] T. Mahalingam, C. Selvakumar, R.E. Kumar, T. Venkatchalam, Structural, optical, morphological and thermal properties of TiO<sub>2</sub>–Al and TiO<sub>2</sub>–Al<sub>2</sub>O<sub>3</sub> composite powders by ball milling, *Phys. Lett. A* 381 (21) (2017) 1815–1819.
- [56] M. Mahmoudpour, P. Pourafshary, Investigation of the effect of engineered water/nanofluid hybrid injection on enhanced oil recovery mechanisms in carbonate

- reservoirs, *J. Pet. Sci. Eng.* 196 (2021) 107662, <https://doi.org/10.1016/j.petrol.2020.107662>.
- [57] A.K. Manshad, M. Olad, S.A. Taghipour, I. Nowrouzi, A.H. Mohammadi, Effects of water soluble ions on interfacial tension (IFT) between oil and brine in smart and carbonated smart water injection process in oil reservoirs, *J. Mol. Liq.* 223 (2016) 987–993.
- [58] A.K. Manshad, I. Nowrouzi, A.H. Mohammadi, Effects of water soluble ions on wettability alteration and contact angle in smart and carbonated smart water injection process in oil reservoirs, *J. Mol. Liq.* 244 (2017) 440–452.
- [59] A.K. Manshad, J.A. Ali, I. Imani, S.M. Sajadi, N.A. Tayeb Ubaid, A. Keshavarz, Green synthesis of CuO@Fe<sub>3</sub>O<sub>4</sub>@Xantane nanocomposites and its application in enhanced oil recovery by considering IFT and wettability behaviours, *Micro Nano Lett.* 15 (8) (2020) 550–555, <https://doi.org/10.1049/mnl.2019.0431>.
- [60] C.R. Miranda, L.S.D. Lara, B.C. Tonetto, Stability and mobility of functionalized silica nanoparticles for enhanced oil recovery applications, Proceedings of the SPE International Oilfield Nanotechnology Conference and Exhibition, Noordwijk, The Netherlands, 12–14 June 2012, Society of Petroleum Engineers, Richardson, TX, USA, 2012.
- [61] M. Nasrollahzadeh, M. Sajjadi, M. Maham, S.M. Sajadi, A.A. Barzinjy, Biosynthesis of the palladium/sodium borosilicate nanocomposite using Euphorbia mili extract and evaluation of its catalytic activity in the reduction of chromium(VI), nitro compounds and organic dyes, *Mater. Res. Bull.* 102 (2018) 24–35.
- [62] I. Nowrouzi, A.K. Manshad, A.H. Mohammadi, Effects of dissolved binary ionic compounds and different densities of brine on interfacial tension (IFT), wettability alteration, and contact angle in smart water and carbonated smart water injection processes in oil reservoirs, *J. Mol. Liq.* 254 (2018) 83–92.
- [63] I. Nowrouzi, A.K. Manshad, A.H. Mohammadi, Effects of concentration and size of TiO<sub>2</sub> nano-particles on the performance of smart water in wettability alteration and oil production under spontaneous imbibition, *J. Pet. Sci. Eng.* 183 (2019) 106357, <https://doi.org/10.1016/j.petrol.2019.106357>.
- [64] J. Panda, U.P. Singh, R. Sahu, Synthesis, characterization of TiO<sub>2</sub> nano particles for enhancement of electron transport application in DSSC with Cu-BPCA dye, *IOP Conf. Ser. Mater. Sci. Eng.* 410 (2018) 012008, <https://doi.org/10.1088/1757-899x/410/1/012008>.
- [65] Patil NB, Sharanagouda H, Doddagoudar S, Ramachandra C, Ramappa K (2018) Bio-synthesis and characterization of silica nanoparticles from rice (*Oryza sativa* L.) husk. *Int. J. Curr. Microbiol. App. Sci.* 7(12), 2298–2306. [DOI:10.20546/ijcmas.2018.712.261](https://doi.org/10.20546/ijcmas.2018.712.261).
- [66] T. Puntervold, S. Strand, R. Ellouz, T. Austad, Modified seawater as a smart EOR fluid in chalk, *J. Pet. Sci. Eng.* 133 (2015) 440–443, <https://doi.org/10.1016/j.petrol.2015.06.034>.
- [67] N. Ogolo, O. Olafuyi, M. Onyekonwu, Enhanced oil recovery using nanoparticles, Proceedings of the SPE Saudi Arabia Section Technical Symposium and Exhibition, Al-Khobar, Saudi Arabia, 8–11 April 2012, 2012.
- [68] A. Omid, A.K. Manshad, S. Moradi, J.A. Ali, S. Sajadi, A. Keshavarz, Smart- and nano-hybrid chemical EOR flooding using Fe<sub>3</sub>O<sub>4</sub>/eggshell nanocomposites, *J. Mol. Liq.* 316 (2020) 113880, <https://doi.org/10.1016/j.molliq.2020.113880>.
- [69] L. Qi, C. Song, T. Wang, Q. Li, G.J. Hirasaki, R. Verduzco, Polymer-coated nanoparticles for reversible emulsification and recovery of heavy oil, *Langmuir* 34 (2018) 6522–6528.
- [70] C.C. Qiaohong, M. Wang, J. Cai, J. Xu, C. Xia, Facile preparation of highly-dispersed cobalt-silicon mixed oxide nanosphere and its catalytic application in cyclohexane selective oxidation, *Nanoscale Res. Lett.* 6 (1) (2011).
- [71] A. Rafiei, E. Khamehchi, Design of smart water composition based on scale minimization and its effect on wettability alteration in the presence of nanoparticles and mineral scales, *J. Pet. Sci. Eng.* 196 (2021) 107832, <https://doi.org/10.1016/j.petrol.2020.107832>.
- [72] M. Rashidi, A. Kalantariasl, R. Saboori, A. Haghani, A. Keshavarz, Performance of environmental friendly water-based calcium carbonate nanofluid as enhanced recovery agent for sandstone oil reservoirs, *J. Pet. Sci. Eng.* 196 (2021) 107644, <https://doi.org/10.1016/j.petrol.2020.107644>.
- [73] A. RezaeiDoust, T. Puntervold, S. Strand, T. Austad, Smart water as wettability modifier in carbonate and sandstone: a discussion of similarities/differences in the chemical mechanisms, *Energy Fuel* 23 (9) (2009) 4479–4485, <https://doi.org/10.1021/ef900185q>.
- [74] A. Roustaei, J. Moghadasi, H. Bagherzadeh, A. Shahrabadi, An experimental investigation of polysilicon nanoparticles' recovery efficiencies through changes in interfacial tension and wettability alteration, *SPE Intern. Oilfield Nanotechnol. Conf. Exhibit.* (2012) <https://doi.org/10.2118/156976-ms>.
- [75] E. Sadatshojaei, M. Jamialahmadi, F. Esmailzadeh, M.H. Ghazanfari, Effects of low-salinity water coupled with silica nanoparticles on wettability alteration of dolomite at reservoir temperature, *Pet. Sci. Technol.* 34 (15) (2016) 1345–1351.
- [76] S.M. Sajadi, K. Kolo, S.M. Hamad, S.A. Mahmud, A.A. Barzinjy, S.M. Hussein, Green synthesis of the Ag/bentonite nanocomposite using Euphorbia larica extract: a reusable catalyst for efficient reduction of nitro compounds and organic dyes, *ChemistrySelect* 3 (43) (2018) 12274–12280.
- [77] R. Saha, R.V. Uppaluri, P. Tiwari, Silica nanoparticle assisted polymer flooding of heavy crude oil: emulsification, rheology, and wettability alteration characteristics, *Ind. Eng. Chem. Res.* 57 (2018) 6364–6376.
- [78] T. Sharma, J.S. Sangwai, Silica nanofluids in polyacrylamide with and without surfactant: viscosity, surface tension, and interfacial tension with liquid paraffin, *J. Pet. Sci. Eng.* 152 (2017) 575–585.
- [79] S.B. Shiran, A. Skauge, Enhanced oil recovery (EOR) by combined low salinity water/polymer flooding, *Energy Fuel* 27 (3) (2013) 1223–1235.
- [80] M. Shirazi, S. Kord, Y. Tamsilian, Novel smart water-based Titania nanofluid for enhanced oil recovery, *J. Mol. Liq.* 296 (2019) 112064, <https://doi.org/10.1016/j.molliq.2019.112064>.
- [81] L. Su, Z. Lu, Spectroelectrochemical study of TiO<sub>2</sub> particulate films, *Spectrochim. Acta A Mol. Biomol. Spectrosc.* 53 (11) (1997) 1719–1722.
- [82] X. Sun, Y. Zhang, G. Chen, Z. Gai, Application of nanoparticles in enhanced oil recovery: a critical review of recent progress, *Energies* 10 (3) (2017) 345.
- [83] X. Sun, Y. Zhang, G. Chen, T. Liu, D. Ren, J. Ma, S. Karwani, Wettability of hybrid nanofluid-treated sandstone/heavy oil/brine systems: implications for enhanced heavy oil recovery potential, *Energy Fuel* 32 (11) (2018) 11118–11135.
- [84] S. Strand, S.C. Henningsen, T. Puntervold, T. Austad, Favorable temperature gradient for maximum low-salinity enhanced oil recovery effects in carbonates, *Energy Fuel* 31 (5) (2017) 4687–4693.
- [85] S. Strand, E.J. Hognose, T. Austad, Wettability alteration of carbonates-effects of potential determining ions (Ca<sup>2+</sup> and SO<sub>4</sub><sup>2-</sup>) and temperature, *Colloids Surf. A: Physicochem. Eng. Asp.* 275 (2006) 1–10.
- [86] T.W. Teklu, W. Alameri, H. Kazemi, R.M. Graves, A.M. AlSumaiti, Low salinity water-surfactant-CO<sub>2</sub> EOR, *Petroleum* 3 (3) (2017) 309–320.
- [87] D. Wen, G. Lin, S. Vafaei, K. Zhang, Review of nanofluids for heat transfer applications, *Particology* 7 (2009) 141–150.
- [88] X. Yang, Z.H. Liu, A kind of nanofluid consisting of surface-functionalized nanoparticles, *Nanoscale Res. Lett.* 5 (2010) 1324–1328.
- [89] F. Yu, Y. Chen, X. Liang, J. Xu, C. Lee, Q. Liang, P. Tao, T. Deng, Dispersion stability of thermal nanofluids, *Prog. Nat. Sci. Mater. Int.* 27 (2017) 531–542.
- [90] W. Yu, H. Xie, A review on nanofluids: preparation, stability mechanisms, and applications, *J. Nanomater.* (2012) 1–17.
- [91] P. Zaumseil, High-resolution characterization of the forbidden Si 200 and Si 222 reflections, *J. App. Crystallogr.* 48 (2) (2015) 528–532.
- [92] G. Zargar, T. Arabpour, A. Khaksar Manshad, J.A. Ali, S. Mohammad Sajadi, A. Keshavarz, A.H. Mohammadi, Experimental investigation of the effect of green TiO<sub>2</sub>/quartz nanocomposite on interfacial tension reduction, wettability alteration, and oil recovery improvement, *Fuel* 263 (2020) 116599, <https://doi.org/10.1016/j.fuel.2019.116599>.
- [93] Y. Ze, L. Sheng, X. Zhao, J. Hong, X. Ze, X. Yu, F. Hong, TiO<sub>2</sub> nanoparticles induced hippocampal neuroinflammation in mice, *PLoS One* 9 (3) (2014) 922–930.
- [94] P. Zhang, M.T. Tweheyo, T. Austad, Wettability alteration and improved oil recovery by spontaneous imbibition of sea water into chalk: impact of the potential determining ions Ca<sup>2+</sup>, Mg<sup>2+</sup> and SO<sub>4</sub><sup>2-</sup>, *Colloids. Surf. A: Physicochem. Eng. Asp.* 301 (2007) 199–208.
- [95] A. Roustaei, H. Bagherzadeh, Experimental investigation of SiO<sub>2</sub> nanoparticles on enhanced oil recovery of carbonate reservoirs, *J. Petro. Exp. Prod. Technol.* 5 (2014) 27–33.

## Appendix 7

*Oil recovery aspects of ZnO/SiO<sub>2</sub> nano-clay in carbonate reservoir*

Abbas Khaksar Manshad, **Jagar A. Ali**, Omid Mosalman Haghghi, S. Mohammad Sajadi, Alireza Keshavarz

Fuel 307 (2022) 121927



Contents lists available at ScienceDirect

Fuel

journal homepage: [www.elsevier.com/locate/fuel](http://www.elsevier.com/locate/fuel)

Full Length Article

Oil recovery aspects of ZnO/SiO<sub>2</sub> nano-clay in carbonate reservoir

Abbas Khaksar Manshad<sup>a,\*</sup>, Jagar A. Ali<sup>b,c,\*</sup>, Omid Mosalman Haghghi<sup>a</sup>,  
S. Mohammad Sajadi<sup>d,e</sup>, Alireza Keshavarz<sup>f</sup>

<sup>a</sup> Department of Petroleum Engineering, Abadan Faculty of Petroleum Engineering, Petroleum University of Technology (PUT), Abadan, Iran

<sup>b</sup> Department of Petroleum Engineering, Faculty of Engineering, Soran University, Soran, Kurdistan Region, Iraq

<sup>c</sup> Department of Geology, Palacký University, 17. Listopadu 12, Olomouc 77146, Czech Republic

<sup>d</sup> Department of Nutrition, Cihan University-Erbil, Kurdistan Region, Iraq

<sup>e</sup> Department of Phytochemistry, SRC, Soran University, KRG, Iraq

<sup>f</sup> School of Engineering, Edith Cowan University, WA 6027, Australia

## ARTICLE INFO

## Keywords:

Green synthesis  
Polymer-coated nanocomposite  
Wettability alteration  
Low-salinity polymeric-nanofluid  
Chemical EOR

## ABSTRACT

Several chemical solutions have been used to improve oil recovery as enhanced oil recovery (EOR) effective agents. However, the conventional chemical EOR solutions face some difficulties and challenges in the mobilizing and displacing the crude oil in the porous media. Nowadays, nanofluids (a mixture of nanoparticles and fluid) are used for EOR applications. In this study, a composite containing zinc and silica nanoparticles and bentonite, as a natural clay, is prepared using a simple, economic and green way from the extract of the *Cordyline fruticosa* plant. The validity of the synthesized nanocomposites (NCs) is analyzed using X-ray diffraction (XRD), Fourier-transform infrared spectroscopy (FTIR) and scanning electron microscopy (SEM). Since the salinity has an influence on the performance of the injected fluids in the porous media, we decided to evaluate the impact of the prepared NCs dispersed within water at different salinity levels, such as distilled water (DW), seawater (SW, HiSal), 10-times seawater dilution (MoSal) and 20-times seawater dilution (LoSal). The prepared nanofluids with 250, 500, 1000 and 2000 ppm NCs passed through several experimental tests, such as pH, viscosity, density, conductivity, interfacial tension (IFT), contact angle (CA) and core flooding under different temperature conditions. The obtained results show that the prepared nanofluids have a good stability, and the IFT and contact angle are decreased with increasing the NCs concentration, but they have an inverse relationship with the water salinity. The minimum IFT is achieved for the oil/nanofluid system prepared from mixing 2000 ppm NCs within the distilled water, meanwhile, the same nanofluid showed the best performance in reducing the contact angle, which is 65.5°. Nanofluids prepared from 2000 ppm NCs and water at its four different levels of salinity are injected into core plugs as secondary and tertiary recovery phases. DW-based nanofluid enabled to extract 62.14 % original oil in place (OOIP) during the secondary recovery, however, it is improved the oil recovery from 44 to 65.41 %OOIP when it is used as the tertiary recovery process.

## 1. Introduction

Hydrocarbon is continuing and expected to remain as the dominant source of energy in the world for the daily live consumption of human and industry. Accordingly, with the growth of the renewable energy, the globe needs for hydrocarbon is expected to rise by 50% in the next 20 years [1]. However, oil production from the conventional oil reservoirs is declining in a way that the era of "easy oil" is near end due to losing the internal supportive forces [6]. Thus, the future supply of

hydrocarbons will come from unconventional and matured reservoirs. For instance, the cumulative proven of unconventional oil reserves in China is estimated at 14.1 billion tons (70% of national oil resources). With the current capacity, EOR methods enable to extract 20 to 40% OOIP (original oil in place) as the average oil recovery rate [31]. Currently, companies and researchers, with a huge effort, are trying to maximize oil recovery from the mature oilfields by implementing new techniques in the enhanced oil recovery (EOR).

In the conventional EOR processes, some chemicals and materials are

\* Corresponding authors at: Department of Petroleum Engineering, Abadan Faculty of Petroleum Engineering, Petroleum University of Technology (PUT), Abadan, Iran and Department of Petroleum Engineering, Faculty of Engineering, Soran University, Soran, Kurdistan Region, Iraq.  
E-mail addresses: [akmanshad113@gmail.com](mailto:akmanshad113@gmail.com) (A.K. Manshad), [jagar.pet@gmail.com](mailto:jagar.pet@gmail.com) (J.A. Ali).

<https://doi.org/10.1016/j.fuel.2021.121927>

Received 24 April 2021; Received in revised form 12 August 2021; Accepted 4 September 2021

Available online 11 September 2021

0016-2361/© 2021 Elsevier Ltd. All rights reserved.

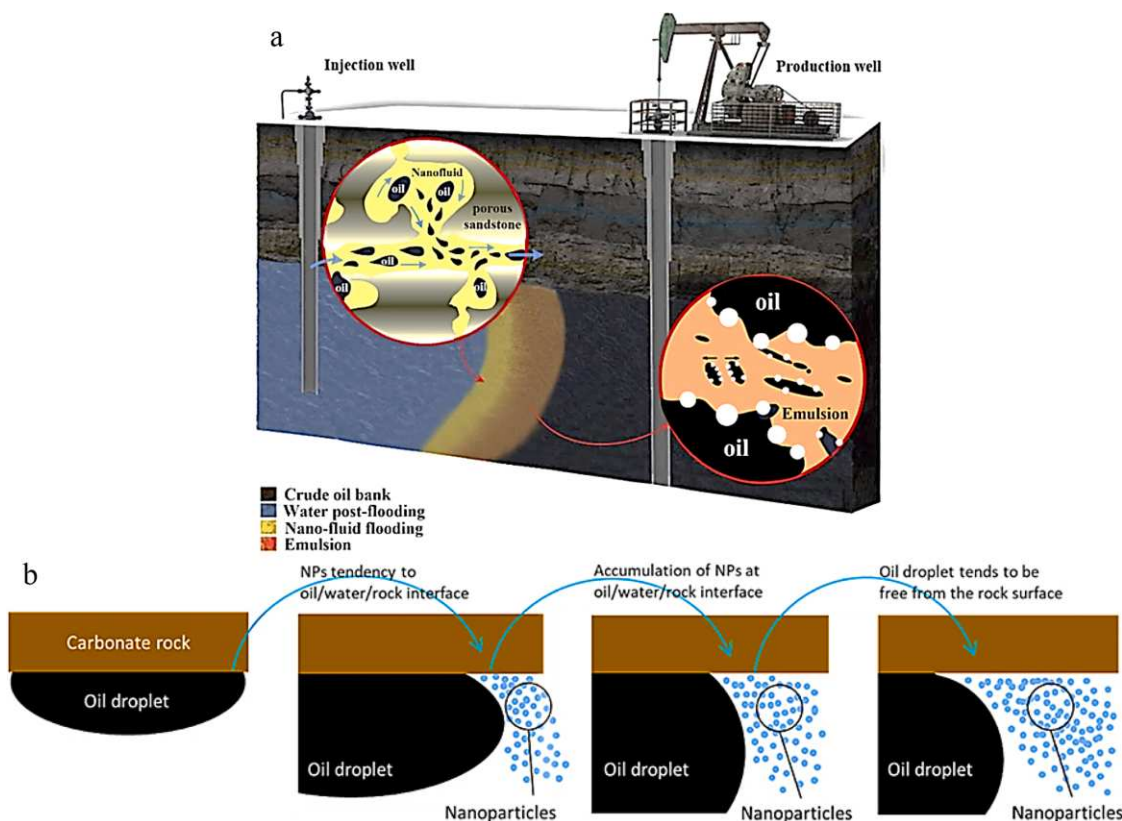


Fig. 1. EOR mechanisms of nanofluid flooding in porous media; a) the red circle on the right shows the capability of NPs creating effective emulsions, while, the red circle in the left illustrates that how NPs enable to displace hydrocarbons [51], and b) development of disjoining pressure at the oil droplet-nanofluid interface [42]. (For interpretation of the references to colour in this figure legend, the reader is referred to the web version of this article.)



Fig. 2. Images of the *Cordyline fruticosa* plant.

injected to alter the physical interaction of the reservoir rock and fluids (injected and existing). Hence, this leads more hydrocarbon be extracted from the mature reservoirs. For example, waterflooding, as one of the oldest and most common method, is used to maintain and boost the pressure after the depletion of the internal driving forces of the reservoir [8,42]. Nevertheless, this process leads high amount of hydrocarbon be trapped and remained immobile due to its poor sweep efficiency, adverse mobility ratio, small capillary number ( $N_c$ ) and decreased

microscopic displacement efficiency. Chemical EOR methods involve the injection of surfactants, polymer and alkaline solutions into the reservoir to improve the viscosity and capillary number (IFT reduction), and minimize the residual oil saturation [43,14]. In the contrast, the performance of these EOR agents is limited in the reservoir under harsh conditions of temperature and salinity. In addition, the adsorption of these chemicals on the rock surfaces is another limitation of these chemicals [29]. Nowadays, more attention and focus are attracted

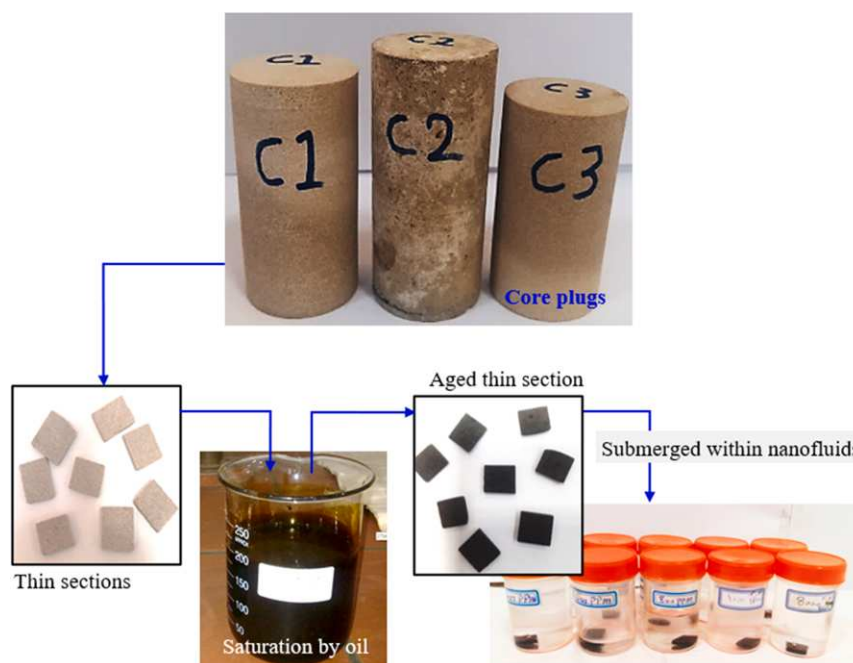


Fig. 3. Schematic diagram illustrates rock plugs and slices preparation.

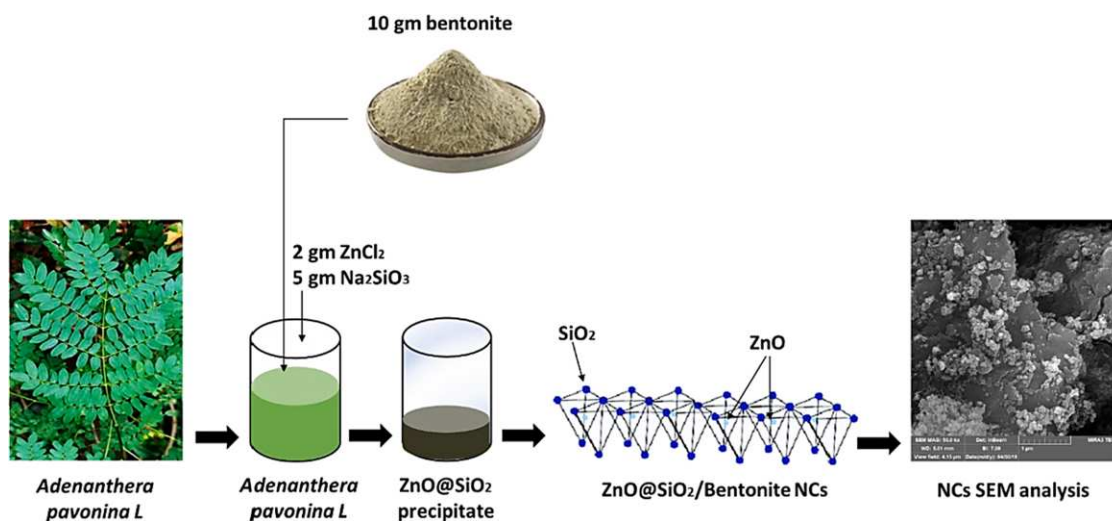


Fig. 4. Schematic diagram illustrates procedural steps of one-pot biosynthesis method used in work.

towards the application of nanotechnology in EOR applications. In nano-EOR technology, nanofluids (nanoparticle containing fluids) are used to provide the better performance in the normal and harsh conditions of the reservoir as shown in Fig. 1. Nanoparticles (NPs), with the size of 100 nm or less, can be dispersed with various types of fluids including water, surfactant, alcohol and polymer to develop EOR nanofluids [24]. These NPs are added to the EOR chemical solution to improve the rock-fluid interaction that leads to wettability alteration and oil recovery enhancement due to their small particle size, thermally stable, highly reactive, high surface area, and dispersibility [37,7]. Moreover, the surfaces of NPs can be modified to form more complex stable

nanomaterials including nanocomposites, polymer-coated NPs and functionalized NPs that performs well in the porous media. Fig. 1b illustrates the distribution of nanoparticles in the porous media. As can be seen the oil droplet is in contact with the rock surface strongly with a strong oil-wet state. However, when nanofluids is injected into the porous media, the dispersed nanoparticles try to entire the interface exists between oil and water phases. Thus, the disjoining pressure would be increased and cause oil droplets be released.

Several researchers confirmed the validity of NPs in the EOR applications by utilizing several flow mechanisms at optimum sizes, types and concentrations. Underlying EOR mechanisms for nanofluids reported in

**Table 1**  
Formulation of fluid solutions used in this study.

| Sample     | NC conc. [ppm] | Density [gm/cm <sup>3</sup> ] | Water salinity [dilution level]                 |
|------------|----------------|-------------------------------|---|
| HiSal      | 0              | 1.0120                        | no dilution; seawater; high salinity water      |
| HiSal-250  | 250            | 1.0282                        |   |
| HiSal-500  | 500            | 1.0283                        |   |
| HiSal-1000 | 1000           | 1.0283                        |   |
| HiSal-2000 | 2000           | 1.0286                        |   |
| MoSal      | 0              | 1.0010                        | 1:10 seawater dilution; moderate salinity water |
| MoSal-250  | 250            | 1.0020                        |   |
| MoSal-500  | 500            | 1.0030                        |   |
| MoSal-1000 | 1000           | 1.0060                        |   |
| MoSal-2000 | 2000           | 1.0100                        |   |
| LoSal      | 0              | 0.9983                        | 1:20 seawater dilution; low salinity water      |
| LoSal-250  | 250            | 0.9989                        |   |
| LoSal-500  | 500            | 0.9993                        |   |
| LoSal-1000 | 1000           | 0.9998                        |   |
| LoSal-2000 | 2000           | 1.0010                        |   |
| DW         | 0              | 0.9960                        | No salinity; distilled water                    |
| DW-250     | 250            | 0.9961                        |   |
| DW-500     | 500            | 0.9963                        |   |
| DW-1000    | 1000           | 0.9981                        |   |
| DW-2000    | 2000           | 0.9992                        |   |

the literature include asphaltene inhibition [33], structural disjoining pressure [55], viscosity reduction [15], IFT reduction [25], wettability alteration [47,27]. In recent years, different types of hydrophilic NPs used in EOR applications including IFT reduction and wettability alteration by Hendraningrat and co-authors [20–23]. Their obtained results showed a high reduction in the value of IFT between water and oil using hydrophilic NPs. Roustaei et al. [45] performed an experimental work on the effect of the hydrophobic, lipophilic and neutrally wet polysilicon NPs on the IFT reduction and wettability alteration, and reported that all used NPs are effective. This has been proved to be due to the formation a wedge-like structure of nanoparticles on the oil–water interface that releases oil droplets from the rock surface [54]. Chengara et al. [11] stated that NPs form a thin film in well-ordered layers on the solid surface under the influence of the injection pressure. Thus, the impact of the disjoining pressure would be higher in the interface between oil and water. The developed film of NPs on the surface of rocks has the ability to separate and release the reservoir hydrocarbon and

change the wetting system towards the water wet [35]. Lim et al. [30] investigated the IFT reduction and wettability alteration under the impact of silica-based nanofluid at different concentration. They identified the simultaneous modification in the IFT and wettability behaviour with NPs concentration. The wettability state of ZrO<sub>2</sub> based nanofluid has also been studied on the surface of limestone rocks in the porous media, where they expressed a great potential in oil recovery enhancement [41]. The role of silica NPs as significant EOR agents is verified in altering the wettability of carbonate rock towards the water-wet phase [46]. Ehtesabi et al. [15] demonstrated that titanium NPs has an effective role in improving the recovery of heavy oil from the sandstone cores due to altering the wettability from the strongly oil wet towards water-wet. Therefore, the wettability alteration and IFT reduction are two dominant governor mechanisms of the nanofluid oil displacement in the porous media. More recently, an attempt to modify the dispersibility and migration of nanoparticles in the porous media is made using surface modified NPs, thus, better and more EOR mechanisms can be achieved [2–5,9,16,39,38,34,42,56]. In 2014, Shamsijazeyi et al. synthesized and used the polymer coated silica NPs to improve oil recovery [48]. Choi et al. [12] studied the impact of polymer-coated NPs in EOR and reported 5% OOIP increase in oil recovery due to the IFT reduction and wettability alteration. In their experimental study regarding rheology, IFT, adsorption and wettability behaviours of polymer flooding, Llanos et al. [32] reported that the functionalized silica NPs greatly improved oil recovery but have not shown any desirable change in viscosity. Additionally, Kazemzadeh et al. [28] reported that TiO<sub>2</sub>/SiO<sub>2</sub> and Fe<sub>3</sub>O<sub>4</sub>/SiO<sub>2</sub> nanocomposites extracted additional 20–25% OOIP compared with the conventional recovery strategy due to the IFT reduction, wettability alteration and viscosity improvement. A significant increase in the capillary number and an effective reduction in IFT were obtained under the influence of NiO/SiO<sub>2</sub> Janus nanocomposites [18].

The ultimate goal of this study is the fabrication of a newly multi-functional nanocomposite for EOR applications. This nanomaterial was prepared from two most effective metallic nanoparticles in a combination with the natural clay, as a substrate. Accordingly, ZnO<sub>2</sub>/SiO<sub>2</sub>/bentonite nanocomposite is synthesized from the extract of *Cordyline fruticosa* plant in a green way. The prepared NCs is used to prepare EOR nanofluids at different salinity levels of seawater. The prepared smart nanofluids can have an influence on the crude oil displacement, rock/oil/water interactions and oil recovery; low salinity water is effective in altering the wettability, nanoparticles can highly reduce the IFT and natural clay can carry the nanoparticles in chain and improve the displacement efficiency. Several EOR experiments are performed to measure viscosity, IFT, contact angle and oil recovery factor under the influence of the synthesized NCs. Moreover, the stability and

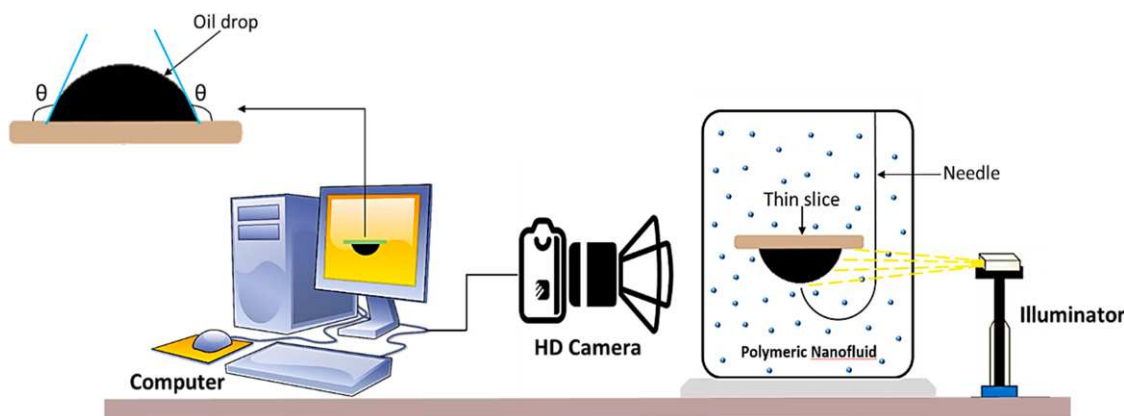


Fig. 5. Schematic illustration of sessile drop method for contact angle measurements [55].

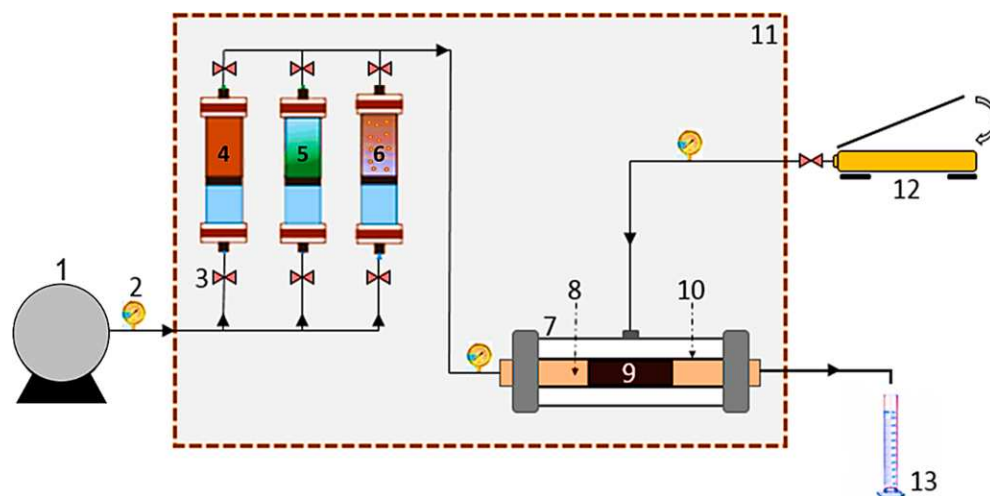


Fig. 6. Schematic illustration of the apparatus for oil displacement tests: (1) HPLC pump, (2) pressure gauges, (3) valves, (4) cylinder containing crude oil, (5) cylinder containing nanofluid, (6) cylinder containing brine, (7) core holder chamber, (8) fluid flow distributor, (9) core, (10) blocking rubber around the core, (11) oven, (12) manual hydraulic pump, and (13) outlet fluid collecting vessel [55].

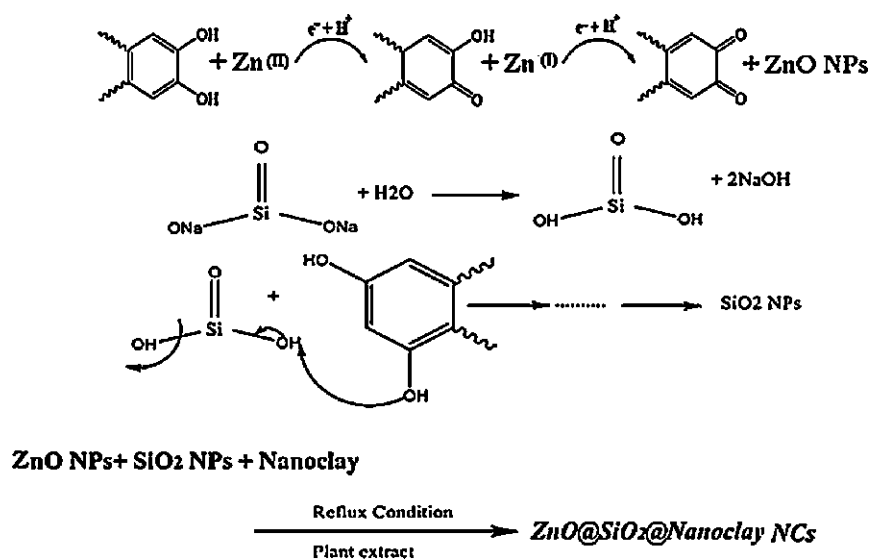


Fig. 7. Schematic view of coating process of ZnO/SiO<sub>2</sub> NPs with bentonite particle chains, which shows the structural mechanisms of the prepared ZnO/SiO<sub>2</sub>/bentonite NCs.

emulsification behaviors of the prepared nanofluids are investigated. The genus *Cordyline* distributed in Southern hemisphere is among the greatest diversity concentrated in Australia and New Zealand. *Cordyline fruticosa* from the family of Asparagaceae is a woody plant traditionally its different parts are used for various diseases such as treatment of haemostatic, toothache, laryngitis, bloody cough, dysentery, fever, headache, inflammation of the digestive tract, kidney diseases and bloody urine (Fig. 2). Reported researches about the plant demonstrated a rich phytochemical content mainly including flavonoids, glycosides, alkaloids, saponines, phenolics and tannins. The water extract of the plant is exclusively containing flavonoids and phenolic glycosides with a considerable antioxidant power [19,13,52]. Through this research the antioxidant extract of the plant was used as a bioreducing source for green synthesis of nanoparticles.

## 2. Experimental setup

### 2.1. Materials

Seawater with the total dissolved solids of 33,194 TDS was collected from the Persian Gulf in the Southwest of Abadan (30.3473°N latitudes and 48.2934°E longitudes). Crude oil with the density of 0.878 gm/cm<sup>3</sup> (32.6° API) and viscosity 13.32 cP at 30 °C was collected from Ahwaz oilfield in Iran. All the other chemical reagents including salts and solvents of high-purity (about 99.5 mol%) were purchased from Merck and Aldrich chemical companies. Different core samples for oil displacement tests and slices for contact angle measurements were prepared from the taken carbonate rocks as shown in Fig. 3. Seven carbonate core plugs were prepared and cleaned by toluene using the Soxhlet extraction at 80

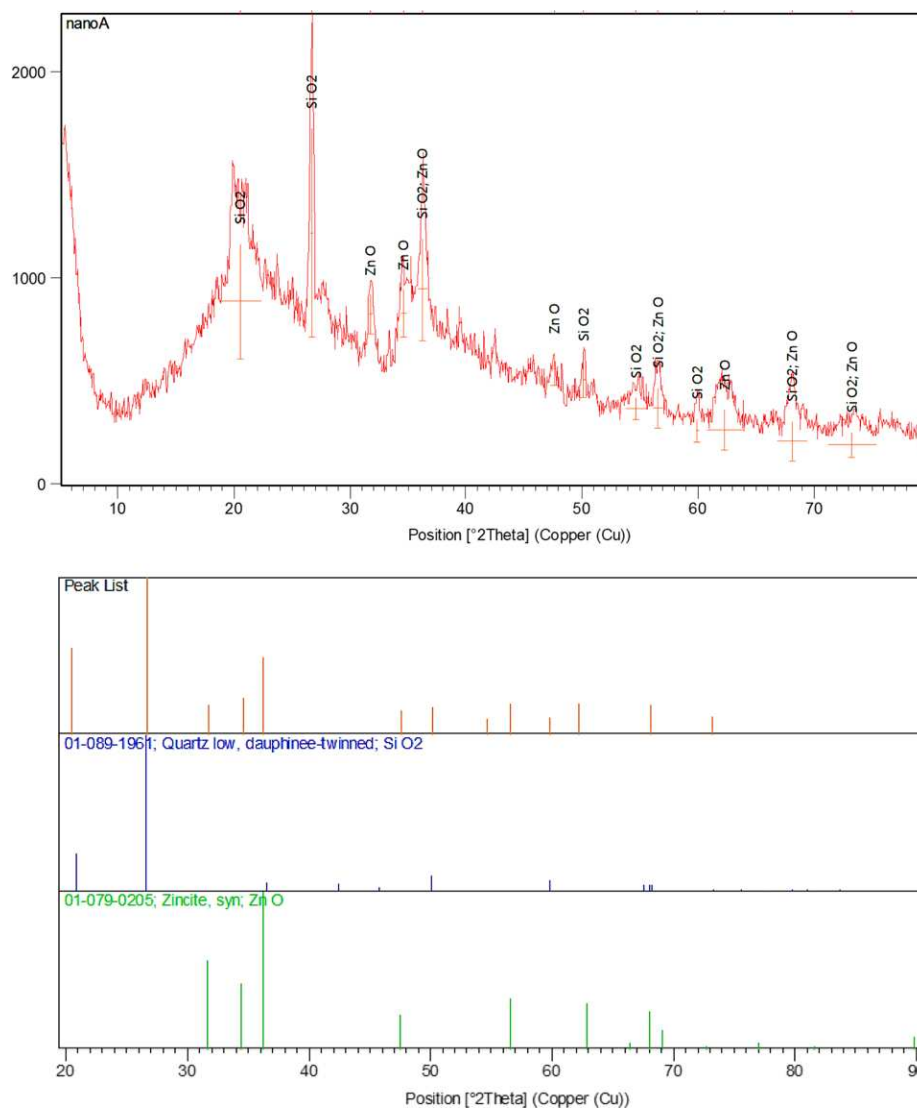


Fig. 8. XRD pattern and ICDD card of ZnO/SiO<sub>2</sub>/bentonite NCs.

°C for 24 hrs. Additionally, other prepared core plugs were trimmed into the small pellets (rock slices) of 2 mm size. The surface of the pellets was smoothed well and cleaned by the distilled water and toluene to remove all the possible impurities available. The cleaned pellet samples were submerged into crude oil at 70 °C for twelve days to be aged well. Then, the aged carbonate slices were submerged in enclosed containers contain water and nanofluids solutions for three days in order to alter the wetting status of the slices under the static condition (see Fig. 3).

## 2.2. Synthesis and characterization of ZnO/SiO<sub>2</sub>/bentonite nanocomposites

Fig. 4 illustrates the procedural steps of synthesizing ZnO/SiO<sub>2</sub>/bentonite nanocomposites schematically. To create the extract of the plant, 50 gm of the dried powder of *Cordyline fruticosa* leaves mixed with 500 mL distilled water at 80 °C under continues stirring at 600 rpm for 30 min. Later, in a 250 mL flask, 2 gm ZnCl<sub>2</sub>, 5 gm Na<sub>2</sub>SiO<sub>3</sub> and 10 gm

bentonite were mixed with 100 mL *Cordyline fruticosa* leaves extract under reflux condition at 9 pH (adjusted by 0.1 mg Na<sub>2</sub>CO<sub>3</sub>) and kept under the stirring at 60 °C for 24 hr until absolutely formation of NPs and their deposition on the surface of bentonite. The reason of adding clay is due to its cheap cost. In addition, it behaves as polymer chains in order to create a better distribution of nanoparticles rather than agglomeration. The mixture then filtered and obtained precipitate was dried and kept to identification and application processes. For confirming and identifying the purity, morphology and mineralogy of the synthesized nanocomposite, several analytical methods have been used, with the focus on X-ray diffraction (XRD), Fourier-transform infrared spectroscopy (FTIR) and scanning electron microscopy (SEM) in the current work.

## 2.3. Preparation and characterization of nanofluids

The collected seawater was used to prepare nanofluids using the

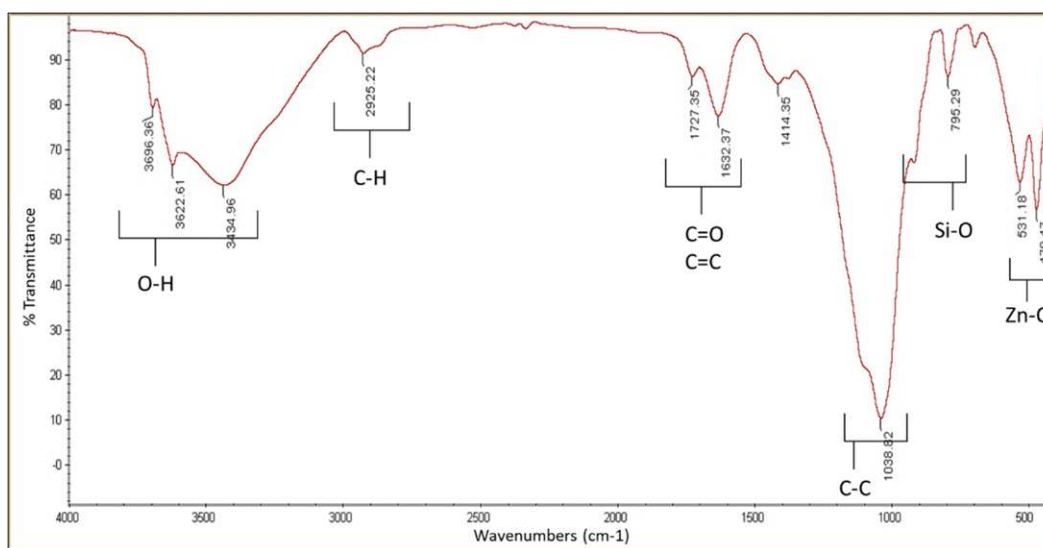


Fig. 9. FTIR spectrum of ZnO/SiO<sub>2</sub>/bentonite NCs.

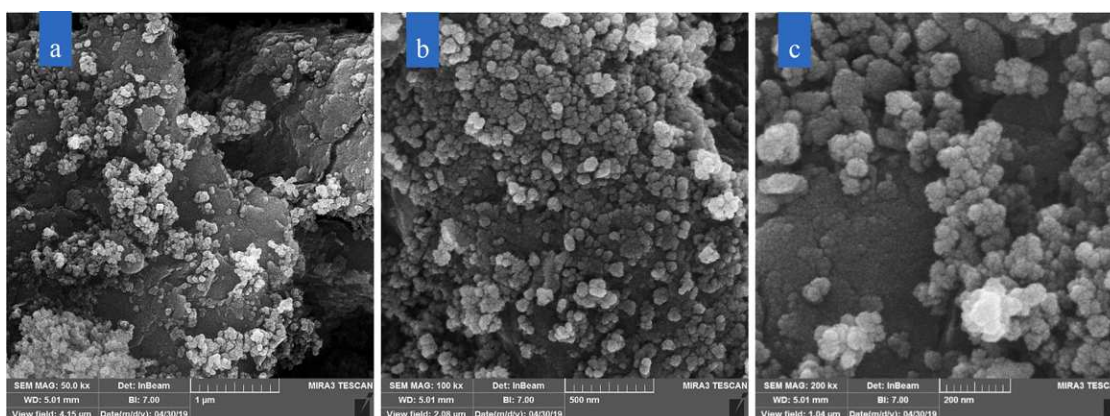


Fig. 10. SEM morphology of ZnO/SiO<sub>2</sub>/bentonite NCs at a) 1 μm, and b) at 500 nm, and c) 200 nm.

synthesized NCs at different concentrations (see Table 1). The dispersion media for the nanocomposites is prepared from seawater that is divided into four phases of salinity; seawater (high salinity), 10-times diluted seawater (moderate salinity), 20-times diluted seawater (low salinity), and distilled water (no salinity) ([50]; Abhishek et al., 2018). The synthesized NCs at different concentrations of 250, 500, 1000 and 2000 ppm are mixed with all designed water solutions. These nanofluids were prepared using the stirring (LABINCO L81 Stirrer) at 600 rpm for 6 h with keeping the operating temperature below 30 °C to avoid overheating of homogenizer. Afterwards, nanofluids were mixed for 2 h by ultrasonic waves emitted from a VIP 200HD ultrasonic mixer to obtain high stability. Thus, the stability the prepared nanofluids was monitored and investigated visually through transparent vessels during a certain time. Furthermore, the density, viscosity, conductivity and pH of nanofluids were measured at ambient temperature and pressure using PAAR density meter, Brookfield DV2T viscometer, Mettler Toledo S230, and WTW™ inoLab™ Cond 7310, respectively.

#### 2.4. Interfacial tension (IFT) and contact angle (CA) measurements

The principle of a pendant drop that estimates the dimensions of the suspended droplet of the crude oil with the presence of an immiscible phase was used to measure the interfacial tension oil-aqueous phase systems using IFT-400 apparatus (see Fig. 5). Accordingly, the taken image of the crude oil droplet that transferred from the IFT-400 device to the computer was used for the IFT calculation using the following formula:

$$\gamma = \frac{\Delta\rho \cdot g \cdot D}{H} \quad (1)$$

where  $\Delta\rho$  is the difference between the density of the drop and bulk fluids ( $\text{gm/cm}^3$ ),  $g$  is the gravitational acceleration of the earth ( $\text{cm/sec}^2$ ),  $D$  is the large diameter of the droplet (cm), and  $H$  is the droplet shape factor. Initially, IFTs of oil-HiSal, oil-MoSal, oil-LowSal and oil-DW systems without the presence of the prepared NCs were measured at different temperatures. Afterwards, the same procedure was then applied to measure IFTs of all the mentioned systems under the influence



Fig. 11. Dispersion stability of HiSal, LowSal and DW nanofluids w/ NCs concentrations of (a) 250 ppm, (b) 500 ppm, and (c) 1000 ppm after four days.

of the prepared NCs at different concentrations (250, 500, 1000 and 2000 ppm) under different temperature conditions of 20, 40 and 80 °C.

In addition, the sessile drop technique was used to measure the contact angle of the crude oil drop on the surface of the prepared carbonate pellets using IFT-400 apparatus (see Fig. 5). Firstly, the contact

angle of the oil drops on the surface of the prepared slices was measured with the presence of water solutions of various salinities without NCs. Later, the oil contact angle was measured with the presence of all prepared solutions of HiSal, MoSal, LowSal and DW based nanofluids different temperature conditions of 20, 40 and 80 °C.

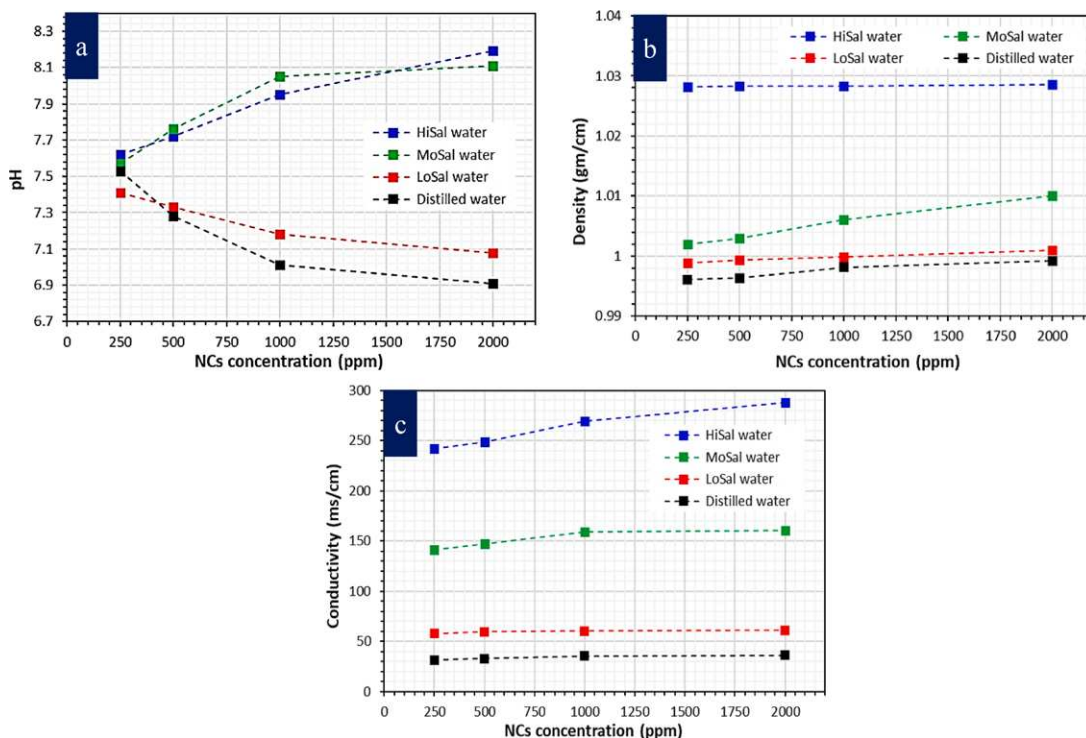


Fig. 12. Characteristics of nanofluids prepared from mixing 250, 500, 1000 and 2000 ppm ZnO/SiO<sub>2</sub>/bentonite NCs within HiSal, MoSal, LoSal and DW water.

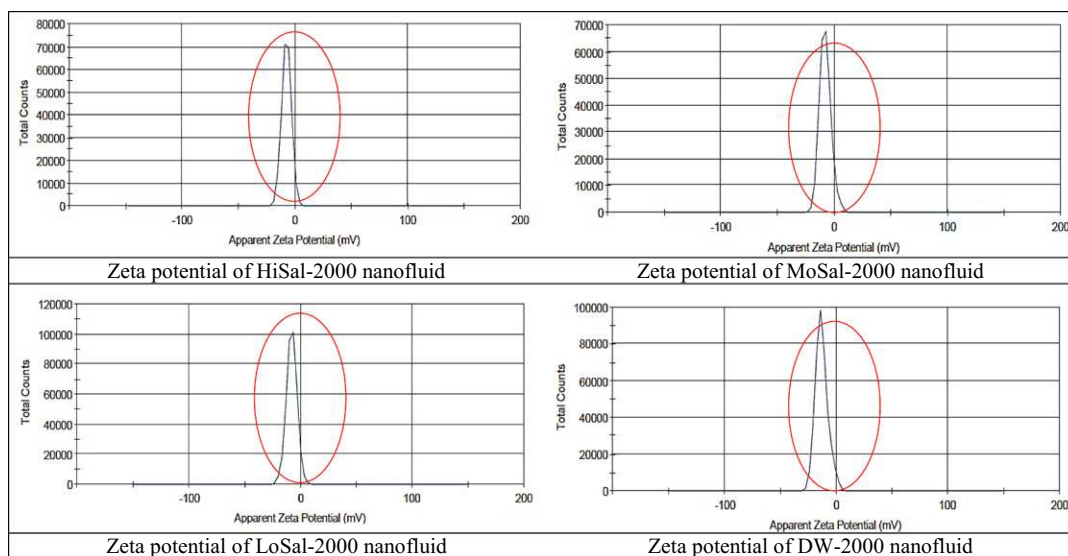


Fig. 13. Zeta potential of ZnO/SiO<sub>2</sub>/bentonite NCs within four selected dispersion medias including seawater (HiSal), 10-times diluted seawater (MoSal), 20-times diluted seawater (LoSal) and distilled water (DW) at 2000 ppm concentration.

### 2.5. Oil displacement

Oil displacement tests were carried out using a coreflooding setup shown schematically in Fig. 6, which consists of fluid chambers, a core holder, pumps, and output collector. Fluids stored inside chambers can

be pumped into the core plug using the high-performance liquid chromatography (HPLC) pump. In this study, three main liquid including crude oil, brine and nanofluids were stored in three cylinders that pumped into the prepared core plugs; crude oil was used for establishing the initial water saturation, brine used for secondary recovery and

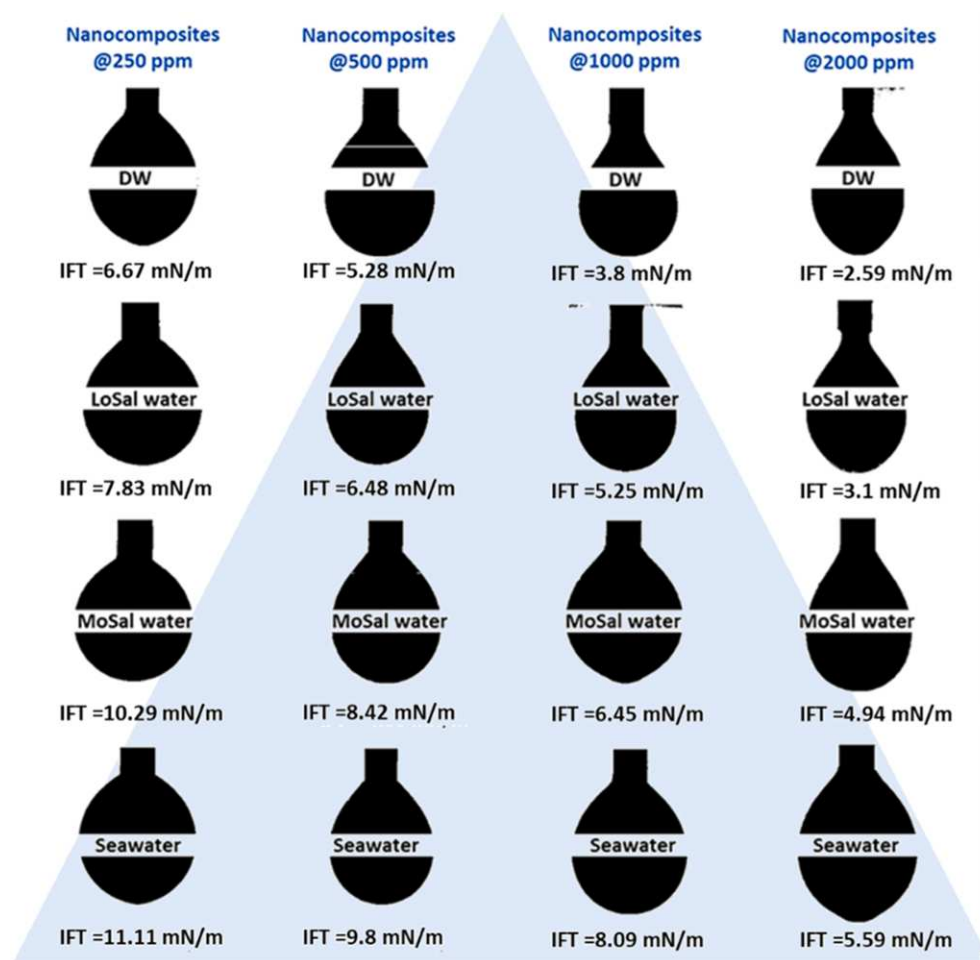


Fig. 14. Captured droplets of crude oil with the presence of nanofluids prepared from dispersing ZnO/SiO<sub>2</sub>/bentonite NCs within water at different salinity levels at 80 °C.

nanofluids used for oil recovery in both secondary and tertiary phases. Oil was displaced in six prepared core plugs at 75 °C and 1400 psi with the injection rate of 0.5 cm<sup>3</sup>/min, as follows: firstly, 2.1 pore volumes (PVs) of brine, HiSal-2000 nanofluid, LoSal-2000 nanofluid and DW-2000 nanofluid were injected separately into four first core plugs as secondary recovery phase. While, two other core plugs were used for the tertiary recovery phase where 1.5 PVs of LoSal-2000 and DW-2000 nanofluids were injected after injecting 2.1 PVs brine (waterflooding).

### 3. Results and discussions

#### 3.1. Characterization of ZnO/SiO<sub>2</sub>/bentonite nanocomposites

During the interactions of metal salts to plant extract, firstly, the metal salts are dissolved in the aqueous media of the extract to generate the Zn<sup>+2</sup> and SiO<sub>2</sub><sup>-2</sup> ions (see Fig. 7). Then after their temporary reaction to hydronium and hydroxyl ions of the water media activated to influenced by *Cordyline fruticosa* plant bioreducing agents and then through an electron transfer it converted to correspondence NPs. Finally, according the concentrations of the salts, the biosynthesized NPs coated on together and nanoclay as natural substrate which was used to increasing the synergistic effects, reducing the agglomeration side effect and also

increasing the surface area of the nanocomposite to its more efficiency.

According the XRD shown in Fig. 8, it clearly reveals the presence of SiO<sub>2</sub>, ZnO and some other peaks concerning the nanoclay minerals. Of course, it should be considered that the SiO<sub>2</sub> in its nature is an amorphous system but in the mentioned nanocomposite, the ZnO NPs were coated on their surface thus we can see the silicon oxide nanoparticles as a crystalline system. In addition, the XRD diffractogram confidently demonstrates the fabrication of ZnO@SiO<sub>2</sub>@bentonite NCs in a crystallinity pure and nanosized form. Moreover, the ICDD card of the synthesized nanocomposites is shown in Fig. 9.

In addition, the FT-IR spectrum of ZnO@SiO<sub>2</sub>@bentonite NCs shown in Fig. 9 presents some main signals concerning the OH, C = O, C = C and C–C functional groups probably belonging to the antioxidant phenolics of the plant extract and the natural clay used ([10]; Tapondjou et al., 2013). Additionally, the main peaks of Zn-O and Si-O are also shown according to Kang et al. [26] and Singh et al. [49]. These signals confirm the adsorption of plant phytochemicals on the surface of nanocomposite which beside showing the green synthesis of the system, they increase the stability of nano-surface against environmental decomposition and deformation side processes. Moreover, Fig. 10 shows the SEM micrographs of ZnO@SiO<sub>2</sub>@bentonite NCs at various magnifications. According the SEM images, nanocomposites was green

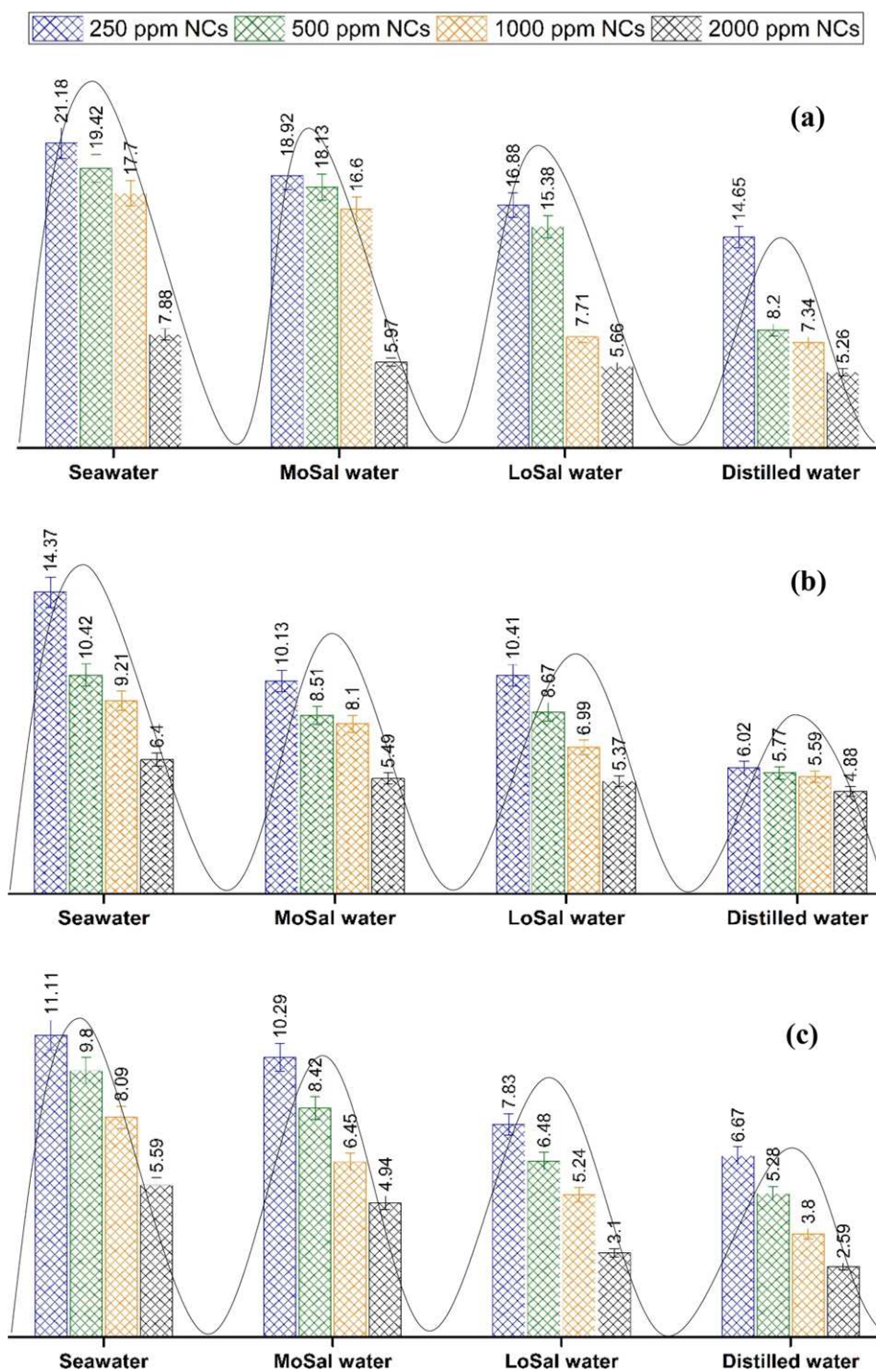


Fig. 15. IFTs of crude oil/nanofluid systems measured at ambient temperature and pressure including HiSal, MoSal, LoSal and DW based nanofluids at 250, 500, 1000 and 2000 ppm, at; a) 20 °C (ambient) temperature, b) 40 °C temperature, and c) 80 °C temperature.

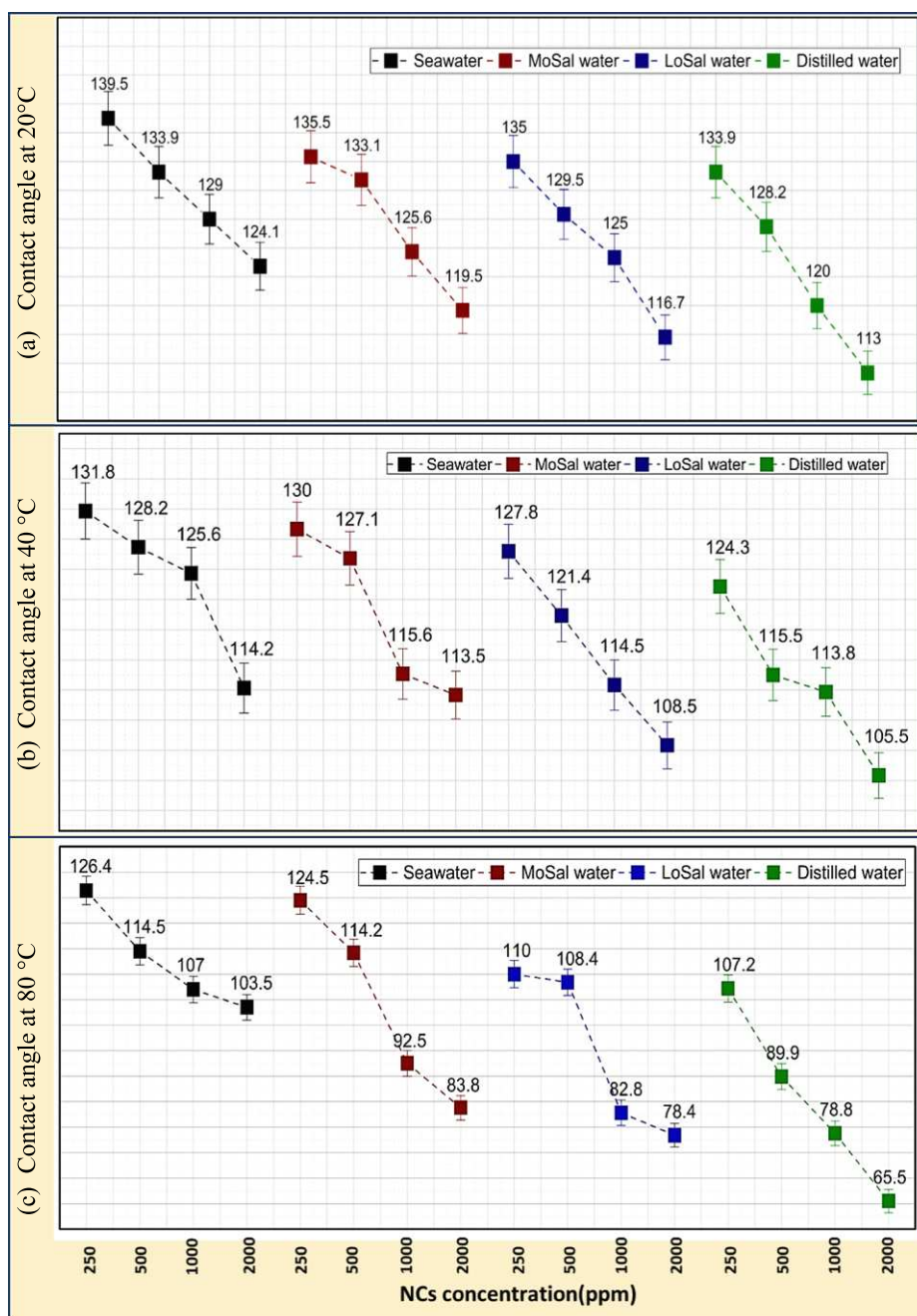


Fig. 16. Measured contact angles of oil drops on the surface of the carbonate slices with the presence of the HiSal, MoSal, LoSal and DW nanofluids at 250, 500, 1000 and 2000 ppm ZnO/SiO<sub>2</sub>/bentonite NCs and different temperature conditions of; a) 20 °C, b) 40 °C, and 80 °C.

synthesized in a nanosized form ranging 35 to 55 nm and in a spherical shape and homogeneous morphology. This technique is also strongly confirming the fabrication of NCs.

### 3.2. Nanofluid characterization

The dispersion stability of the prepared NCs within the dispersion

media is crucial to identify the role of NCs accurately. In this part, the dispersion stability of colloidal solid particles within the prepared nanofluids by measuring and observing pH, density, conductivity, zeta potential and appearance features of nanofluids. After the preparation, nanofluids at different concentrations of NCs were well sonicated. Nanofluids were stored in the transparent vessels kept at the static condition to be monitored during four weeks as shown in Fig. 11. In the

**Table 2**  
Detailed test summary of secondary and tertiary flooding through six used core plugs of used carbonate rocks.

| Core name | Porosity (%) | K (md) | PV (cc) | Soi (%) | Inj. fluid |            | Oil recovery [%OOIP] |          |       |
|-----------|--------------|--------|---------|---------|------------|------------|----------------------|----------|-------|
|           |              |        |         |         | Secondary  | Tertiary   | Secondary            | Tertiary | Total |
| Plug#1    | 14.32        | 7.36   | 11.32   | 59.03   | Brine      |            | 44.2                 |          |       |
| Plug#2    | 16.3         | 7.55   | 13.07   | 63.0    | LoSal-2000 |            | 55                   |          |       |
| Plug#3    | 15.2         | 6.93   | 11.61   | 55.2    | HiSal-2000 |            | 49.6                 |          |       |
| Plug#4    | 15.0         | 8.13   | 11.7    | 54.7    | DW-2000    |            | 62.14                |          |       |
| Plug#5    | 16.0         | 7.7    | 14.0    | 57.5    | Brine      | LoSal-2000 | 41.2                 | 18.2     | 59.4  |
| Plug#6    | 15.52        | 7.93   | 12.5    | 58.4    | Brine      | DW-2000    | 44                   | 21.41    | 65.41 |

\* K is the permeability of the rock sample.

\*\* PV is the pore volume of the used core plugs.

\*\*\* Soi is the initial oil saturation of the core plugs.

\*\*\*\* OOIP is the original oil in place.

figure solutions of HiSal, LowSal and DW nanofluids at 250, 500 and 1000 ppm of ZnO/SiO<sub>2</sub>/bentonite NCs are shown during four days. As can be seen, high stability of the dispersed nanoparticles within nanofluids were achieved with observing the concentration variation between solutions.

Fig. 12 illustrates the measured physiochemical properties of nanofluids dependents on the NCs concentration and salinity of the dispersion media. As is obvious, pH has the direct influence on the aggregation and the suspension stability of nanoparticles within the colloidal solution [17,57]. The measured pH of all prepared nanofluids at different salinity level and NCs concentrations are shown in Fig. 12a. As can be seen, the value of pH is in the range of 6.9 to 8.1 where a stable aqueous phase can be obtained. The pH is changed with changing the salinity and increasing the concentration of NCs; when the salinity of the aqueous phase is high, pH is increased with increasing the NCs concentration, however, the pH of the nanofluids is decreased with increasing the NCs concentration when the salinity is too low. Meanwhile, more stable trends of the conductivity and density of nanofluids were achieved (see Fig. 12b,c). These two properties were more influenced by the effect of salinity compared with concentration of ZnO/SiO<sub>2</sub>/bentonite NCs. Generally, the density of the nanofluid was slightly increased from 0.995 to 1.028 gm/cm<sup>3</sup> which is belonged to the HiSal nanofluids. Nevertheless, the conductivity was highly changed from 30 mS/m to 284 mS/m under the impact of water salinity rather than NCs concentration.

Moreover, the zeta potential curves of HiSal, MoSal, LoSal and DW nanofluids at 2000 ppm NCs concentration are shown in Fig. 13. Generally, the same trends of the zeta potential were achieved for all tests nanofluids with a little variation in the range -27 to 6 mV, which shows a high dispersion stability of ZnO/SiO<sub>2</sub>/bentonite NCs within all kinds of waters. However, the peaks of nanofluids were measured at different counts in two groups; the measured peaks of HiSal-2000 and MoSal-2000 nanofluids were counted at about 7000 total counts, and the peaks of LoSal-2000 and DW-2000 nanofluids are up to 10,000 total counts.

### 3.3. Interfacial tension

Interfacial tension of crude oil and prepared nanofluids was measured at different temperatures and ambient pressure. Figs. 14 and 15 illustrate the results of the IFT measured for the selected liquid/liquid systems. The captured images of the crude oil droplet with the presence of the prepared nanofluids at different NCs concentrations and 80 °C are shown in Fig. 14, in which different sizes of droplets can be seen dependents on the salinity with almost the same shape. As is obvious, the highest values of IFTs were achieved when the HiSal-based nanofluids were used, and reduced gradually with reducing the salinity of water from the base of the drawn triangle to the pyramid. Consequently, the minimum IFTs of 6.67, 5.28, 3.8 and 2.59 mN/m were obtained when 250, 500, 1000 and 2000 synthesized NCs dispersed within the distilled water, respectively.

The measured values of IFTs under the influences of the NCs

concentration (250, 500, 1000 and 2000 ppm), salinity level (HiSal, MoSal, LoSal and DW) and experimental condition (20, 40 and 80 °C) are shown in Fig. 15. As can be seen, the maximum IFT of 21.18 mN/m was measured when HiSal-250 nanofluid used at ambient temperature; while, DW nanofluid-2000 established the minimum IFT of 2.59 mN/m at 80 °C. Generally, the IFT was reduced with increasing the concentration of ZnO/SiO<sub>2</sub>/bentonite NCs, increasing the temperature and reducing water salinity. At ambient condition shown in Fig. 15a, IFT was reduced from 21.18 to 6.36 mN/m with increasing NCs concentration from 250 to 2000 ppm, when seawater (HiSal water) was the dispersion phase [12,44,40], and it was dropped to 5.26 mN/m when the salinity of water decreased to DW. Hence, the synthesized NCs was more effect with the low salinity water at the same experimental condition [40]. Additionally, the performance of ZnO/SiO<sub>2</sub>/bentonite NCs in reducing IFT was enhanced when the temperature of the experiment was increased to 40 and 80 °C (see Fig. 15b,c). The impact of the synthesized NCs on the IFT reduction was 62.7% in the high salinity environment and at ambient temperature. While, the NCs effect on the IFT reduction increased to 73.2% when the impact of water salinity was combined. Similarly, the performance of the NCs was significantly improved up to 87.7% in the harsh condition of temperature.

### 3.4. Wettability alteration

Wettability behavior of the several aqueous systems was identified by measuring the contact angle of crude oil on the surface of carbonate slices before and after treatment with ZnO/SiO<sub>2</sub>/bentonite nanocomposites (see Fig. 16a-d). The performance of the synthesized NCs was investigated under the impact of water salinity and experimental temperature. Basically, the strongest oil-wet state of 139.5° CA was identified with the presence of HiSal-250 nanofluid made from mixing 250 ppm NCs within seawater at 20 °C (see Fig. 16a). However, a favorable wettability behavior on the carbonate rock was obtained with utilizing DW-2000 nanofluid at 80 °C, which was indicted by 65.5° contact angle (see Fig. 16d).

Fig. 16a shows the contact angles measured using different nanofluid solutions considering different NCs concentrations and salinity levels, but under ambient temperature condition of 20 °C. As is clear, the synthesized NCs have not shown an effective favorable impact in decreasing the contact angle that made wettability to stay at oil-wet phase for all used experimental test trials. The minimum CA was obtained with the presence of DW-2000 nanofluid which is 113° but is still above 90° and represents oil-wet system dependent on Teklu et al. [53] and Naik et al. [36]. When the temperature of the experiment was increased to 40 °C, different values of CAs were measured for the same used nanofluids. Fig. 16b demonstrates measured CAs of the four prepared types of nanofluids at different salinities and NC concentrations. As can be seen the oil droplet CA measured with the presence of nanofluids was reduced up to 10% compared with the values measured at room temperature. Moreover, better performance of the prepared nanofluids with different salinities was obtained when the temperature

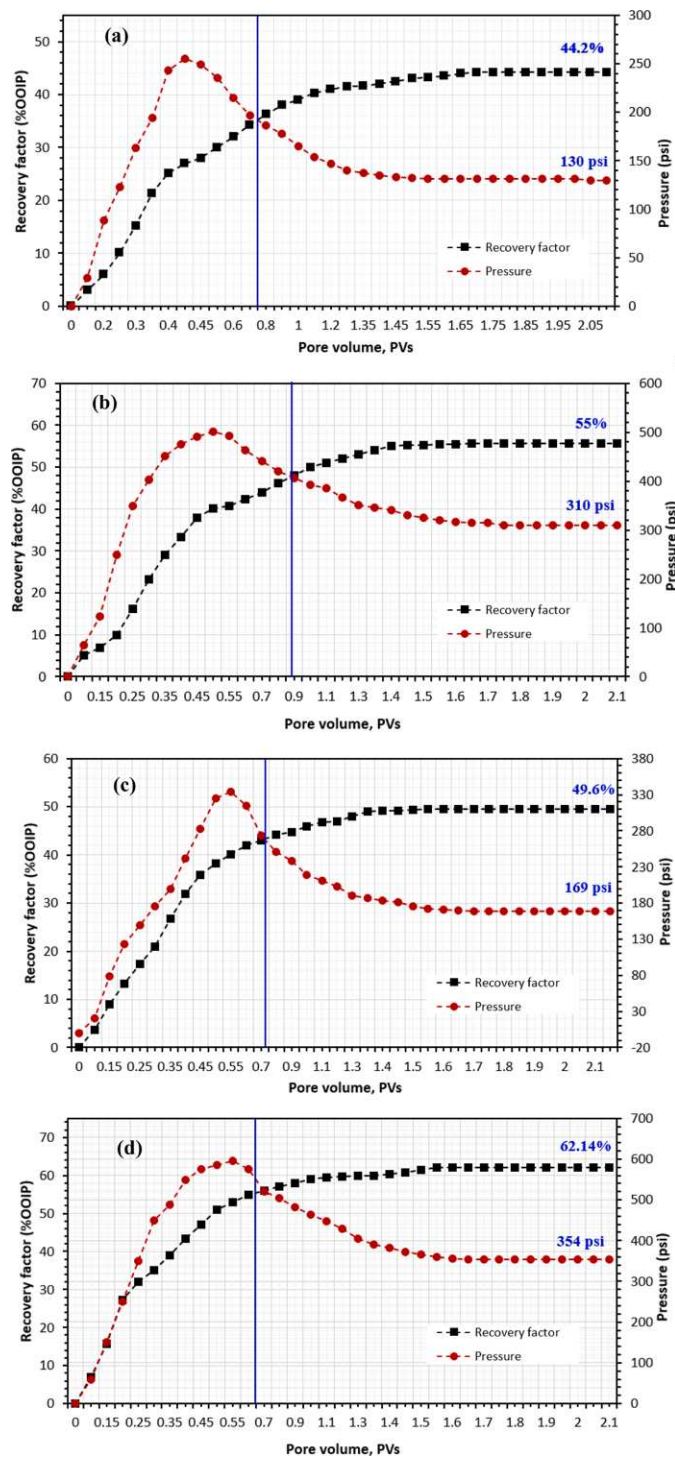


Fig. 17. Secondary recovery profiles of oil recovery factor and pressure curve obtained from core plugs 1 to 4 by injecting; a) brine (seawater), and b) LoSal-2000 nanofluid, c) HiSal-2000 nanofluid, and d) DW-2000 nanofluid.

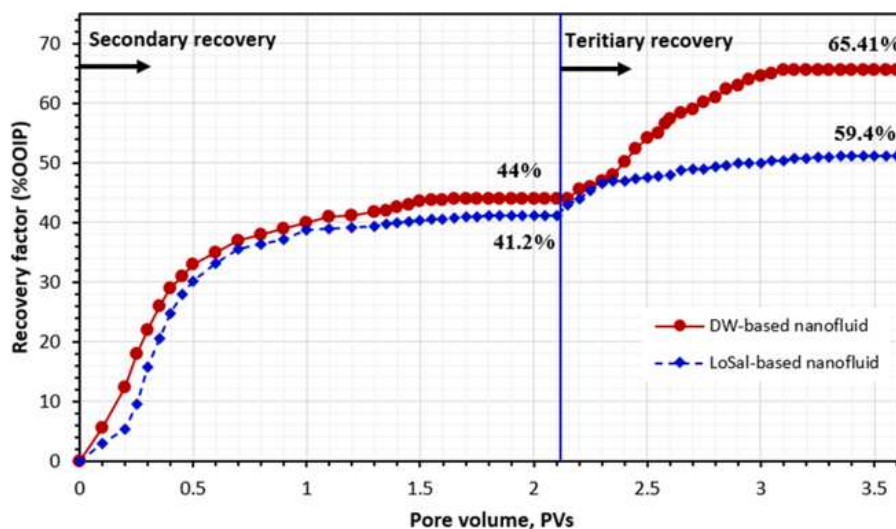


Fig. 18. Production profiles of displacing core plugs 5 and 6; sweater was injected into both plugs as secondary recovery method, and LoSal-2000 and DW-2000 nanofluids injected into plug 5 and 6, respectively as tertiary recovery.

of tests doubled to 80 °C. Thus, nanofluids enabled to reduce the CA up to 38% and 42% compared with what achieved in both experiment conditions of 20 °C and 40°, respectively. In this experimental condition, DW-2000 nanofluid prepared from mixing 2000 ppm NCs within the distilled water enabled to reduce the CA of oil droplet on the surface of the used carbonate rock by 53% from 139.5° to 65.5°. Hence, it can be reported that the wettability of the carbonate rock was altered to a moderate water-wet system which is favorable for the extra oil production as EOR recovery [18].

### 3.5. Oil displacement

Oil displacement experiments were carried out in two phases; in the first phase, seawater, LoSal-2000 nanofluid, HiSal-2000 nanofluid and DW-2000 nanofluid were injected into core plugs 1 to 4, respectively. These displacements of crude oil were handled as a secondary recovery directly after the achieving the favourable aging of plugs. Additionally, in the second phase oil from core plugs 5 and 6 was displaced in two steps, <sup>(1)</sup> by water as secondary recovery method, and <sup>(2)</sup> by LoSal-2000 and DW-2000 nanofluids as tertiary recovery. The oil displacement in all core plugs was carried out under the same experimental condition of temperature, pressure and injection rate. However, the petrophysical properties of the used core plugs are not exactly same but with little variation and from the same outcrop (see Table 2). The porosity of the used plugs varies from 14.32 to 16.3% and permeability is ranged between 6.93 and 8.13 mD.

The recovery and pressure profiles of the oil displacement from core plugs 1 to 4 are illustrated in Fig. 17. As a secondary recovery, the maximum oil recovery of 62.14% OOIP was achieved from displacing core plug 4 by DW-2000 nanofluid prepared from dispersing 2000 ppm of ZnO<sub>2</sub>/SiO<sub>2</sub>/bentonite NCs within the distilled water. The water saturation in this core plug was reduced from its initial value of 0.547 to 0.245 (see Fig. 17d). The interaction of the pressure curve with the recovery curve can be seen after injecting 0.7–0.9 PVs of fluids into core plugs as shown in Fig. 17. Waterflooding was enabled to produce only 44.2% OOIP, wherein, more hydrocarbon was produced from injecting the nanofluids. LoSal-2000 nanofluid produced 55% OOIP and HiSal-2000 nanofluid displaced 49.6% of oil. As is obvious, the recovery efficiency of the core plug was improved with reducing the salinity of water and adding the synthesized NCs.

Furthermore, Fig. 18 illustrates the production profile of the oil displacement from core plugs 5 and 6. Waterflooding enabled to extract 41.2% OOIP from plug#5, and was increased to 59.4% OOIP by injecting LoSal-2000 nanofluid. However, core plug 6 showed the better recovery efficiency in both phases of recovery. Sweater displaced 44% OOIP as secondary recovery, and 21.41% OOIP extra oil was extracted when DW-2000 nanofluid was injected into plug#6 after waterflooding. Generally, the highest recovery factor of oil was achieved from core plug 6 when DW-2000 nanofluid was injected as a tertiary recovery method, which 65.41% OOIP.

## 4. Conclusions

This study reported the impact of the newly developed nanocomposites, called ZnO<sub>2</sub>/SiO<sub>2</sub>/bentonite, on the oil recovery, IFT reduction and wettability alteration during secondary and tertiary recovery methods at different experimental conditions. In this study, several points were raised as summarized below:

- The minimum IFT of crude oil droplet was achieved with the presence of DW-2000 nanofluid prepared from mixing 2000 ppm ZnO<sub>2</sub>/SiO<sub>2</sub>/bentonite NCs within the distilled water at 80 °C, which is 2.59 mN/m.
- Additionally, the same nanofluid enabled to alter the wettability from the strong oil-wet to a moderate water-wet.
- The NC concentration and experiment temperature showed a strong impact on the reduction of both IFT and CA.
- The salinity had an inverse influence on the IFT and CA. Thus, the minimum values of both EOR parameters were achieved when the salinity is near to zero and NC concentration and temperature were the highest.
- The best recovery efficiency was obtained when the DW-2000 nanofluid was injected into a core plug as the chemical EOR flooding at 75 °C and 1400 psi with the injection rate of 0.5 cm<sup>3</sup>/min, which is 65.41% OOIP.

### CRedit authorship contribution statement

Abbas Khaksar Manshad: . : Supervision, Writing – review & editing. Jagar A. Ali: Writing – original draft. Omid Mosalman

**Haghighi:** Data curation, Formal analysis, Methodology, Project administration. **S. Mohammad Sajadi:** Supervision. **Alireza Keshavarz:** Writing – review & editing.

### Declaration of Competing Interest

The authors declare that they have no known competing financial interests or personal relationships that could have appeared to influence the work reported in this paper.

### References

- Ali JA, Kolo K, Manshad AK, Mohammadi AH. Recent advances in application of nanotechnology in chemical enhanced oil recovery: effects of nanoparticles on wettability alteration, interfacial tension reduction, and flooding, Egypt. *J Petrol* 2018;27(4):1371–83. <https://doi.org/10.1016/j.ejpe.2018.09.006>.
- Ali JA, Kolo K, Khaksar Manshad A, Stephen K, Keshavarz A. Modification of LoSal water performance in reducing interfacial tension using green ZnO/SiO<sub>2</sub> nanocomposite coated by xanthan. *Appl Nanosci* 2018;9(3):397–409. <https://doi.org/10.1007/s13204-018-0923-5>.
- Ali JA, Kolo K, Manshad AK, Stephen KD. Potential application of low-salinity polymeric-nanofluid in carbonate oil reservoirs: IFT reduction, wettability alteration, rheology and emulsification characteristics. *J Mol Liq* 2019;284: 735–47. <https://doi.org/10.1016/j.molliq.2019.04.053>.
- Ali JA, Kolo K, Sajadi SM, Hamad KH, Salman R, Wanli M, et al. Modification of rheological and filtration characteristics of water-based mud for drilling oil and gas wells using green SiO<sub>2</sub>@ZnO@Xanthan nanocomposite. *IET Nanobiotechnol* 2019; 13(7):748–55. <https://doi.org/10.1049/nbt.2.v13.710.1049/iet-nbt.2018.5205>.
- Ali JA, Kolo K, Khaksar Manshad A, Stephen KD. Low-salinity polymeric nanofluid-enhanced oil recovery using green polymer-coated ZnO/SiO<sub>2</sub> Nanocomposites in the upper Qamchuqa formation in Kurdistan region, Iraq. *Energy Fuels* 2019;33(2): 927–37.
- Ali JA, Kalhury AM, Sabir AN, Ahmed RN, Ali NH, Abdullah AD. A state-of-the-art review of the application of nanotechnology in the oil and gas industry with a focus on drilling engineering. *J Petrol Sci Eng* 2020;191:107118. <https://doi.org/10.1016/j.petrol.2020.107118>.
- Ali JA, Kolo K, Manshad AK, Stephen KD. Emerging applications of TiO<sub>2</sub>/SiO<sub>2</sub>/poly(acrylamide) nanocomposites within the engineered water EOR in carbonate reservoirs. *J Mol Liq* 2021;322:114943. <https://doi.org/10.1016/j.molliq.2020.114943>.
- Almahfood M, Bai B. The synergistic effects of nanoparticle-surfactant nanofluids in EOR applications. *J Petrol Sci Eng* 2018;171:196–210.
- Bahraminejad H, Khaksar Manshad A, Riazi M, Ali JA, Sajadi SM, Keshavarz A. CuO/TiO<sub>2</sub>/PAM as a novel introduced hybrid agent for water—oil interfacial tension and wettability optimization in chemical enhanced oil recovery. *Energy Fuels* 2019;33(11):10547–60. <https://doi.org/10.1021/acs.energyfuels.9b02109>.
- Banik N, Jahan SA, Mostofa S, Kabir H, Sharmin N, Rahman M, et al. Synthesis and characterization of organoclay modified with cetylpyridinium chloride. *Bangladesh J Scientific Ind Res* 2015;50(1):65–70.
- Chengara A, Nikolov AD, Wasan DT, Trokhymchuk A, Henderson D. Spreading of nanofluids driven by the structural disjoining pressure gradient. *Adv Colloid Interface Sci* 2004;280(1):192–201.
- Choi SK, Son HA, Kim HT, Kim JW. Nanofluid enhanced oil recovery using hydrophobically associative zwitterionic polymer-coated silica nanoparticles. *Energy Fuels* 2017;31(8):7777–82.
- Dahlia AA, Ahmad AR, Milhawati W. Extraction of the color pigment and determination of the flavonoid content of leaves and long leaves (Cordyline Fruticosa) source Makassar City. *J Biol Scientific Opinion* 2013;1(4):294–6. <https://doi.org/10.7897/2321328.01401>.
- Du D-J, Pu W-F, Chen B-W, Varfolomeev MA, Liu R. Experimental study on EOR potential of water-in-oil emulsion via CO<sub>2</sub>/N<sub>2</sub> triggered wormlike micelle solution. *Fuel* 2021;288:119639. <https://doi.org/10.1016/j.fuel.2020.119639>.
- Ehtesabi H, Ahadian MM, Taghikhani V, Ghazanfari MH. Enhanced heavy oil recovery in sandstone cores using TiO<sub>2</sub> nanofluids. *Energy Fuels* 2014;28(1): 423–30.
- Eslahati M, Mehrabianfar P, Isari AA, Bahraminejad H, Manshad AK, Keshavarz A. Experimental investigation of alfalfa natural surfactant and synergistic effects of Ca<sup>2+</sup>, Mg<sup>2+</sup>, and SO<sub>4</sub><sup>2-</sup> ions for EOR applications: Interfacial tension optimization, wettability alteration and imbibition studies. *J Mol Liq* 2020;310: 113123. <https://doi.org/10.1016/j.molliq.2020.113123>.
- Fovet Y, Gal JY, Toumelin-Chemla F. Influence of pH and fluoride concentration on titanium passivating layer: stability of titanium dioxide. *Talanta* 2001;53:1053–63.
- Giraldo LJ, Gallego J, Villegas JP, Franco CA, Cortés FB. Enhanced waterflooding with NiO/SiO<sub>2</sub> 0-D Janus nanoparticles at low concentration. *J Petrol Sci Eng* 2019;174:40–8. <https://doi.org/10.1016/j.petrol.2018.11.007>.
- Han, S.T. 1998. Medicinal plants in south pacific, World health organization, WHO regional publication, western pacific series 19; 62-63.
- Hendraningrat L, Li S, Torsæter O. A glass micromodel experimental study of hydrophilic nanoparticles retention for EOR project. *Society of Petroleum Engineers* 2012. <https://doi.org/10.2118/159161-MS>.
- Hendraningrat L, Li S, Torsæter O. A coreflood investigation of nanofluid enhanced oil recovery. *J Petrol Sci Eng* 2013;111:128–38.
- Hendraningrat L, Torsæter O. Effects of the initial rock wettability on silica-based nanofluid-enhanced oil recovery processes at reservoir temperatures. *Energy Fuel* 2014;28(10):6228–41.
- Hendraningrat L, Torsæter O. Metal oxide-based nanoparticles: revealing their potential to enhance oil recovery in different wettability systems. *Appl Nanosci* 2015;5(2):181–99.
- Jia H, Dai J, Miao L, Wei X, Tang H, Huang P, et al. Potential application of novel amphiphilic Janus-sio2 nanoparticles stabilized o/W/O emulsion for enhanced oil recovery. *Colloids Surf A* 2021;622:126658. <https://doi.org/10.1016/j.colsurfa.2021.126658>.
- Joonaki E, Ghanaatian S. The application of nanofluids for enhanced oil recovery: effects on interfacial tension and coreflooding process. *Pet Sci Technol* 2014;32(21):2599–607.
- Kang S, Park Y, Yang J, Shin Y, Yun J. Fourier transform infrared studies of the aluminum chemical vapor deposition using aluminum boro-hydride trimethylamine. *Thin Solid Films* 2010;518(8):2228–33. <https://doi.org/10.1016/j.tsf.2009.07.159>.
- Karimi A, Fakhroueian Z, Bahramian A, Pour Khiabani N, Darabad JB, Azin R, et al. Wettability alteration in carbonates using zirconium oxide nanofluids: EOR implications. *Energy Fuels* 2012;26(2):1028–36.
- Kazemzadeh Y, Sharifi M, Riazi M, Rezvani H, Tabaei M. Potential effects of metal oxide/SiO<sub>2</sub> nanocomposites in EOR processes at different pressures. *Colloids Surf A* 2018;559:372–84. <https://doi.org/10.1016/j.colsurfa.2018.09.068>.
- Liang T, Zhao X, Yuan S, Zhu J, Liang X, Li X, et al. Surfactant-EOR in tight oil reservoirs: current status and a systematic surfactant screening method with field experiments. *J Petrol Sci Eng* 2021;196:108097. <https://doi.org/10.1016/j.petrol.2020.108097>.
- Limf S, Horiuchi H, Nikolov AD, Wasan D. Nanofluids alter the surface wettability of solids. *Langmuir* 2015;31(2):5827–35.
- Liu Qi, Qu H, Liu S, Zhang Y, Zhang S, Liu J, et al. Modified Fe<sub>3</sub>O<sub>4</sub> nanoparticle used for stabilizing foam flooding for enhanced oil recovery. *Colloids Surf A* 2020; 605:125383. <https://doi.org/10.1016/j.colsurfa.2020.125383>.
- Llanos S, Giraldo LJ, Santamaria O, Franco CA, Cortés FB. Effect of sodium oleate surfactant concentration grafted onto SiO<sub>2</sub> nanoparticles in polymer flooding processes. *ACS Omega* 2018;3(12):18673–84. <https://doi.org/10.1021/acsomega.8b02944>.
- Mohammadi M, Akbari M, Fakhroueian Z, Bahramian A, Azin R, Arya S. Inhibition of asphaltene precipitation by TiO<sub>2</sub>, SiO<sub>2</sub>, and ZrO<sub>2</sub> nanofluids. *Energy Fuels* 2011;25(7):3150–6.
- Manshad AK, Ali JA, Imani I, Sajadi SM, Tayeb Ubaid NA, Keshavarz A. Green synthesis of CuO/Fe<sub>3</sub>O<sub>4</sub>@Xanthan nanocomposites and its application in enhanced oil recovery by considering IFT and wettability behaviours. *Micro Nano Lett* 2020;15(8):550–5. <https://doi.org/10.1049/mna.2.v15.810.1049/mnl.2019.0431>.
- Mcelfresh PM, Olguin C, Ector D. 2012. The application of nanoparticle dispersions to remove paraffin and polymer filter cake damage, SPE International Symposium and Exhibition on Formation Damage Control, Lafayette, LA, USA, SPE-151848-MS.
- Naik S, You Z, Bedrikovetsky B. Productivity index enhancement by wettability alteration in two-phase compressible flows. *J Nat Gas Sci Eng* 2018;50:101–14.
- Javad Nazarahari M, Khaksar Manshad A, Moradi S, Shafiei A, Abdulazez Ali J, Sajadi S, et al. Synthesis, characterization, and assessment of a CeO<sub>2</sub>@Nanoclay Nanocomposite for enhanced oil recovery. *Nanomaterials* 2020;10(11):2280. <https://doi.org/10.3390/nano10112280>.
- Nowrouzi I, Khaksar Manshad A, Mohammadi AH. Effects of TiO<sub>2</sub>, MgO and γ-al<sub>2</sub>O<sub>3</sub> nano-particles on wettability alteration and oil production under carbonated nano-fluid imbibition in carbonate oil reservoirs. *Fuel* 2020;259: 116110. <https://doi.org/10.1016/j.fuel.2019.116110>.
- Nowrouzi I, Manshad AK, Mohammadi AH. Effects of concentration and size of TiO<sub>2</sub> nano-particles on the performance of smart water in wettability alteration and oil production under spontaneous imbibition. *J Petrol Sci Eng* 2019;183: 106357. <https://doi.org/10.1016/j.petrol.2019.106357>.
- Nowrouzi I, Manshad AK, Mohammadi AH. Effects of dissolved binary ionic compounds and different densities of brine on interfacial tension (IFT), wettability alteration, and contact angle in smart water and carbonated smart water injection processes in carbonate oil reservoirs. *J Mol Liq* 2018;254:83–92.
- Nwidae LN, Al-Ansari S, Barifcani A, Sarmadivaleh M, Iglauer S. 2016. Nanofluids for enhanced oil recovery processes: Wettability alteration using zirconium oxide. Day 1 Tue, March 22, 2016. doi:10.4043/26573-ms.
- Omid A, Manshad AK, Moradi S, Ali JA, Sajadi SM, Keshavarz A. Smart- and nano-hybrid chemical EOR flooding using Fe<sub>3</sub>O<sub>4</sub>/eggshell nanocomposites. *J Mol Liq* 2020;316:113880. <https://doi.org/10.1016/j.molliq.2020.113880>.
- Panchal H, Patel H, Patel J, Shah M. A systematic review on nanotechnology in enhanced oil recovery. *Petrol Res* 2021. <https://doi.org/10.1016/j.ptlr.2021.03.003>.
- Qi L, Song C, Wang T, Li Q, Hirasaki GJ, Verduzco R. Polymer-Coated Nanoparticles for Reversible Emulsification and Recovery of Heavy Oil. *Langmuir* 2018;34(22):6522–8.
- Roustaei A, Moghadasi J, Bagherzadeh H, Shahrabadi A. 2012. An Experimental Investigation of Polysilicon Nanoparticles' Recovery Efficiencies through Changes in Interfacial Tension and Wettability Alteration, SPE Int. Oilfield Nanotechnology Conference and Exhibition, Noordwijk, the Netherlands.
- Roustaei A, Bagherzadeh H. Experimental investigation of SiO<sub>2</sub> nanoparticles on enhanced oil recovery of carbonate reservoirs. *J Petrol Explor Prod Technol* 2015;5(1):27–33.

- [47] Sagala F, Montoya T, Hethnawi A, Vitale G, Nassar NN. Nanopyroxene-based Nanofluids for Enhanced Oil Recovery in Sandstone Cores. *Energy Fuels* 2019.
- [48] ShamsiJazeyi H, Miller CA, Wong MS, Tour JM, Verduzco R. Polymer-coated nanoparticles for enhanced oil recovery. *J Appl Polym Sci* 2014;131(15):n/a--.
- [49] Singh J, Kaur S, Kaur G, Basu S, Rawat M. Biogenic ZnO nanoparticles: A study of blueshift of optical band gap and photocatalytic degradation of reactive yellow 186 dye under direct sunlight. *Green Process Synth*, 2019;8(1):272-80. <https://doi.org/10.1515/gps-2018-008>.
- [50] Spildo, k., Johannessen, A.M., Skauge, A., 2012. Low Salinity Waterflood at Reduced Capillarity, SPE Improved Oil Recovery Symposium.
- [51] Sun Y, Yang D, Shi L, Wu H, Cao Y, He Y, Xie T, et al. Properties of Nanofluids and their applications in enhanced oil recovery: a comprehensive review. *Energy Fuels* 2020;34(2):1202-18. <https://doi.org/10.1021/acs.energyfuels.9b03501>.
- [52] Tapondjou LA, Fouedjou RT, Nguелеfack EP, Ponou BK, Nguелеfack TB, Barboni L. 2016. Antioxidant activities and chemical constituents of extracts from cordyline fruticosa (L.) A. Chev. (Agavaceae) and Eriobotrya japonica (Thunb) Lindl, (Rosaceae). *Pharmacologia* 7(2);103-113.
- [53] Teklu TW, Alamer W, Kazem H, Graves RM, 2015. Contact angle measurements on conventional and unconventional reservoir cores. In: Proceedings of the Unconventional Resources Technology Conference, San Antonio, TX, USA, 20-22 July (2015).
- [54] Wasan DT, Nikolov AD. Spreading of nanofluids on solids. *Nature* 2003;423(6936): 156-9. <https://doi.org/10.1038/nature01591>.
- [55] Wasan D, Nikolov A, Kondiparty K. The wetting and spreading of nanofluids on solids: role of the structural disjoining pressure. *Curr Opin Colloid Interface Sci* 2011;16(4):344-9.
- [56] Yang Y, Cheng T, Wu H, You Z, Shang D, Hou J. Enhanced oil recovery using oleic acid-modified titania nanofluids: underlying mechanisms and oil-displacement performance. *Energy and Fuel* 2020;34(5):5813-22.
- [57] Yu W, Xie H. A review on nanofluids: preparation, stability mechanisms, and applications. *J. Nanomater.* 2012;2012:1-17.

## Appendix 8

*Synergistic Efficiency of Zinc Oxide/Montmorillonite Nanocomposites and a New Derived Saponin in Liquid/Liquid/Solid Interface-Included Systems: Application in Nanotechnology- Assisted Enhanced Oil Recovery*

Ahmad Nourinia, Abbas Khaksar Manshad, Seyed Reza Shadizadeh, **Jagar A. Ali**, Stefan Iglauer, Alireza Keshavarz, Amir H. Mohammadi,\* and Muhammad Ali

ACS Omega 2022, 7, 24951–24972

# Synergistic Efficiency of Zinc Oxide/Montmorillonite Nanocomposites and a New Derived Saponin in Liquid/Liquid/Solid Interface-Included Systems: Application in Nanotechnology-Assisted Enhanced Oil Recovery

Ahmad Nourinia, Abbas Khaksar Manshad,\* Seyed Reza Shadizadeh, Jagar A. Ali, Stefan Iglauer, Alireza Keshavarz, Amir H. Mohammadi,\* and Muhammad Ali



Cite This: *ACS Omega* 2022, 7, 24951–24972



Read Online

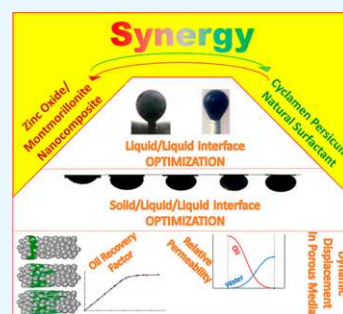
ACCESS |

 Metrics & More

 Article Recommendations

 Supporting Information

**ABSTRACT:** Oil production faces challenges such as limited oil production from carbonate reservoirs, high oil production costs, and environmental issues. Chemical flooding as an enhanced oil recovery (EOR) method (CEOR) can increase oil production by the use of chemical additives such as surfactants into the reservoirs. Surfactants can increase oil recovery by interfacial tension (IFT) reduction and alteration of the rock wettability from oil-wet to water-wet. The synthesis of chemicals such as synthetic surfactants is usually costly and harmful to the environment. To solve these problems, many researchers have oriented on the use of natural surfactants instead of synthetic ones within the CEOR process. A new approach to increase the efficiency of CEOR is the synergizing of the chemical additives with nanoparticles as a hybrid fluid, which is known as the nanotechnology-assisted EOR method. In this research, a natural surfactant derived from *Cyclamen persicum* (CP) plant was extracted, and its performance was optimized with the zinc oxide/montmorillonite (ZnO/MMT) nanocomposite in a synergistic usage. At the optimum concentration of the surfactant, the measurements of the IFT and the contact angle show 57.78 and 61.58% optimizations, respectively. Also, in the presence of NaCl, the performance of CP is improved. IFT and contact angle measurements were also conducted for ZnO/MMT nanofluids and CP-ZnO/MMT as hybrid nanofluids. Results indicate that ZnO/MMT nanocomposites can alter the wettability of the carbonate rock to the water-wet state. Also, the CP-ZnO/MMT hybrid nanofluid shows a good potential in both IFT reduction and altering wettability from oil-wet to water-wet. Finally, to investigate the effects of solutions on increasing oil recovery factor (RF), the optimum concentrations of the surfactant, nanocomposite, and hybrid solutions were selected for dynamic core flooding experiments, and improvements showed oil RF increases of 8.2, 6, and 13%, respectively.



## 1. INTRODUCTION

Due to declining oil reserves, oil extraction methods are constantly being improved. One of the enhanced oil recovery (EOR) methods is chemical injection defined as chemical enhanced oil recovery (CEOR), which includes injecting chemical additives such as surfactants, polymers, alkalis, and the combination of them into the reservoir.

The main mechanism of surfactants to increase oil production is interfacial tension (IFT) reduction.<sup>1</sup> In some cases, the surfactants have shown their ability to alter the wettability of reservoir rock.<sup>2</sup> In terms of surfactant types, they are typically divided into two categories: synthetic and natural surfactants.<sup>3</sup>

The use of synthetic surfactants in the petroleum industry faces challenges. The high production cost of synthetic surfactants can make the EOR process economically impossible. On the other hand, environmental and human hazards due to the use of chemical surfactants are unavoidable. Corrosion of equipment and toxicity of the environment as a

result of the use of the ionic surfactants are examples of these hazards.<sup>4</sup> One of the solutions to overcome these challenges is the use of natural surfactants, which has been considered by many researchers in recent years. Due to the saponin content of natural surfactants, they are known as nonionic surfactants.<sup>5</sup> Table S1 shows examples of the natural surfactants and their plant sources. Unfortunately, natural surfactants do not work well compared to synthetics. One of the reasons for the poor performances of natural surfactants could be mentioned as the presence of impurities in elementary laboratory plant extracts.

Nanoparticles can be used in the CEOR methods as a hybrid agent to improve the performances of the additives, which is

Received: December 20, 2021

Accepted: June 23, 2022

Published: July 15, 2022



known as the nanotechnology-assisted enhanced oil recovery (NEOR) method.<sup>6</sup> The target of using new additives in CEOR is satisfaction with the mechanisms applied in enhancing the recovery of oil that could mainly be mentioned as mobility control improvement, IFT reduction, and wettability alteration. Used chemicals in CEOR have to sustain the harsh conditions of hydrocarbon reservoirs; therefore, the properties of certain additives should not be altered by the changes in conditions. Nanotechnology acts here as an intensifier in enhancing the properties and will make a synergistic effect with used additives. Recently, many studies have been conducted on the use of nanotechnology as a synergy with surfactants to improve their performances. The use of nanoparticles with surfactants as a hybrid fluid improves the performances of some surfactants for EOR applications.<sup>7</sup> Nanoparticles, for example, can overcome the weakness of surfactants in wettability alteration and cause a higher oil recovery factor (RF).<sup>8–10</sup> However, the mechanisms of nanosurfactant hybrids are not yet entirely understood, and complementary studies are continuing.

Chhetri et al. introduced a natural surfactant prepared from the *Sapindus mukurossi* fruit, and this surfactant can reduce IFT.<sup>11</sup> Pordel Shahri et al. investigated the effect of the *Ziziphus spina-christi* (ZSC) leaf extract on IFT. This surfactant decreases the IFT value from 48 to 9 mN/m.<sup>12</sup> Deymeh et al. investigated the effect of the *Seidlitzia rosmarinus* extract on IFT reduction. The extract decreases the IFT from an initial value of 32 to 9 mN/m at critical micelle concentration (CMC).<sup>13</sup> Ahmadi et al. investigated the effect of the *mulberry* leaf extract on IFT reduction and oil recovery. The recorded data indicate that the extract reduces the IFT from 44 to 17.9 mN/m. Based on the core flooding experiment results, the natural surfactant can increase the oil recovery from 49 to 66.8%.<sup>14</sup> Rahmati et al. compared the effect of the *mulberry* leaf extract with a natural surfactant named *henna* on IFT and wettability alteration. Based on the obtained results, the *henna* extract shows a better performance to reduce the IFT and contact angle of the oil with a sandstone rock.<sup>15</sup> Emadi et al. investigated the effects of ZSC and silica nanoparticles on the IFT and RF. The results of IFT measurement show that the ZSC can reduce the IFT, and adding silica nanoparticles to the CMC of ZSC reduces the IFT more. Also, by adding nanosilica to ZSC, the RF increases from 53 to 74% of the ordinary oil in place (OOIP).<sup>16</sup> Xu et al., Cheraghian et al., Haeri et al., Songolzadeh and Moghadasi, Zhao et al., and Zhong et al. have shown that the combinations of silica nanoparticles with different surfactants have a good potential to alter wettability from oil-wet to water-wet.<sup>17–22</sup> Suleimanov et al. showed that nonferrous metal NPs can reduce IFT/surface tension.<sup>23</sup> Mohajeri et al., by combining ZrO<sub>2</sub> NPs with sodium dodecyl sulfate and CTAB, showed that the nanofluids optimize IFT/surface tension and alter wettability.<sup>24</sup> Table S2 summarizes the studies on the synergistic effects of nanosurfactants.<sup>17–29</sup>

There is not enough information in the field of studying the mechanisms of IFT reduction, wettability alteration, and oil displacement of natural surfactants and their synergy effects in the presence of nanoparticles. Therefore, in the present study, after extracting a natural surfactant solution from a saponin-containing plant, its synergistic effects were studied together with a green nanocomposite. Both the natural surfactant and synthesized nanocomposite are novel and have not yet been studied in the field of EOR.

In this study, the researchers intended to investigate the effect of the *Cyclamen persicum* (CP) plant extract as a natural surfactant on the increasing oil recovery. Thermogravimetric (TGA) and Fourier transform infrared spectroscopy (FT-IR) analyses were applied to characterize the extracted solution. To obtain the CMC of the extracted surfactant, electrical conductivity, pH, IFT, and wettability alteration methods were used. Pendant drop and contact angle methods were used to investigate the IFT and wettability alteration, respectively. The ZnO/montmorillonite (ZnO/MMT) nanocomposite that was synthesized in a green manner was analyzed as an EOR agent by the pendant drop and contact angle methods too. FTIR, X-ray diffraction (XRD), and field emission scanning electron microscopy (FE-SEM) analyzes were accomplished to characterize the synthesized matter as a nanocomposite. Then, the nanocomposite combined with the surfactant as a hybrid agent. To study the synergistic effects of the nanocomposite and surfactant, different concentrations of the nanocomposite were mixed with CMC of surfactant solution as the base fluid. Finally, proper concentrations of the surfactant, nanocomposite, and hybrid solutions were selected to study the additional oil recovery by core flooding experiment.

## 2. MATERIALS AND METHODS

**2.1. Materials.** **2.1.1. Aqueous Phase.** Double-deionized water (DDW) with ultralow electrical conductivity was used to prepare aqueous solution for the natural surfactant and nanofluid solutions with different concentrations of CP and ZnO/MMT, respectively. Seawater from the Persian Gulf with a pH of 7.67 was used in this study as brine solution in the dynamic fluid flooding process. The composition of prepared seawater is illustrated in Table S3. The used salt of sodium chloride for ion engineering analysis of aqueous solutions was purchased from Merck with 99% purity.

**2.1.2. Oil Phase.** The crude oil used in this study was prepared from Iranian oil fields and used in the aging process of rock core plugs and rock pellets, IFT measurements, wettability alteration tests, and dynamic oil injections into the core plug. The oil density is 0.89 and 0.771 gr/cm<sup>3</sup> under ambient and reservoir conditions, respectively. Table S4 presents the composition of the used crude oil. The obtained crude oil was filtered by a 5 μm mesh before applying wettability alteration, IFT, and core flooding experiments for the prevention of any undesirable plugging.

**2.1.3. Natural Surfactant.** CP is a rich saponin plant, in which the tuber part contains saponin.<sup>30</sup> Figure S1 shows the structure of the CP extract.<sup>31</sup> After preparing the CP plants, their tubers were separated from the plants, cleaned and cut into small pieces, and dried under ambient conditions. The prepared tubers (100 g) with 350 ml of DDW were placed in the Soxhlet extractor apparatus for 15 h until a saponin-rich solution was obtained in the chamber of the Soxhlet extractor. After that, to remove solids, the obtained solution was filtered with a laboratory steel cone sieve. The vacuum rotary evaporation method with the water bath set at 50 °C was used to remove water from the filtrate blend. Vacuum conditions cause evaporation to occur at much lower temperatures than the boiling temperature under normal conditions and prevent the degradation of the molecules of the surfactant. The evaporation process continued until 80% volumetric percent of the solution was produced. This volumetric ratio was considered in the manufacture of natural surfactant solutions with various concentrations of the extract.

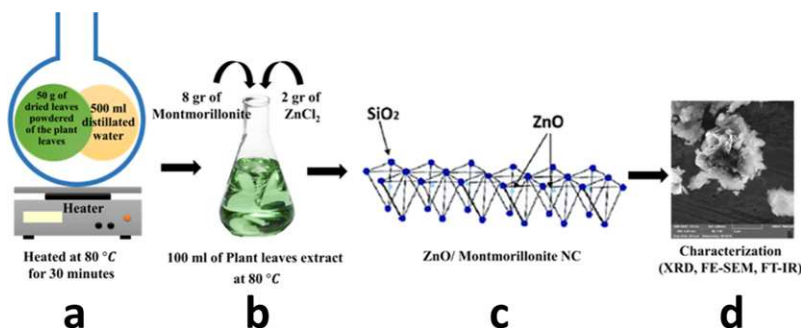


Figure 1. Biosynthesis process of ZnO/MMT nanocomposites (a–d show the steps of the procedure).

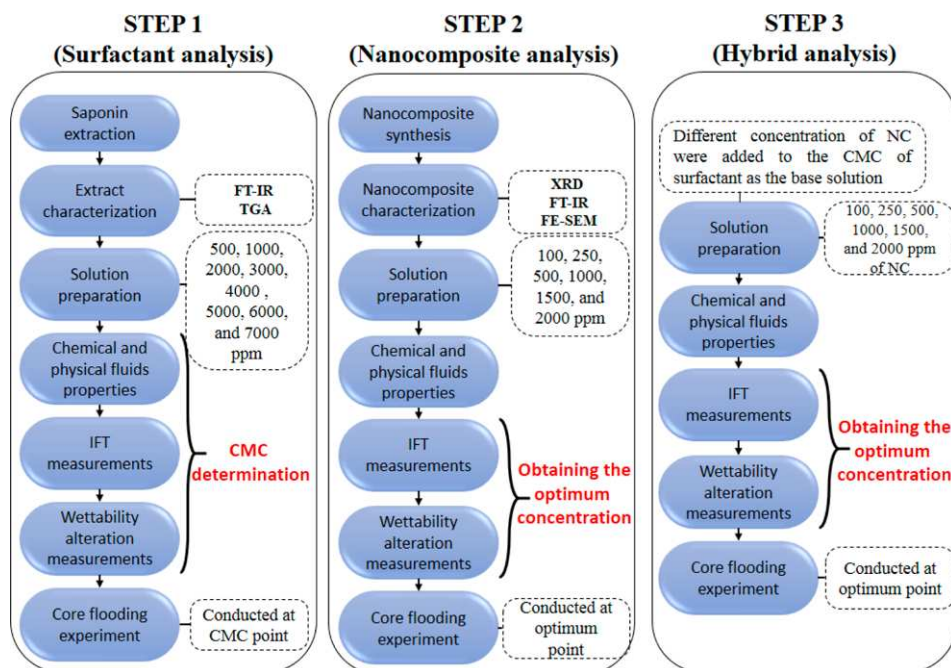


Figure 2. General road map of the present study with details of each step.

**2.1.3.1. Characterization of the Natural Surfactant.** Even though the literature in medicinal subjects introduces the CP plant extract as a saponin-rich mixture,<sup>32,33</sup> there is no study on the use of this extract in EOR. Therefore, further characterizations were required to approve the presence of saponin and to confirm the successful extraction. FTIR spectroscopy (Bruker Tensor II), in the 400–4000  $\text{cm}^{-1}$  wavenumber range, was used to identify the functional group of the extract. TGA was conducted to show the thermal degradation of the natural used extract for a temperature range of 25 to 300 °C. The thermal degradation durability and value of degradation of the extracted material within 25 to 90 °C could also be considered as the thermal stability of the surfactant under general reservoir conditions.

**2.1.4. Nanocomposite.** In this study, the ZnO/MMT nanocomposite was synthesized as the nanofluid and hybrid agent. From the literature, ZnO nanoparticles can increase the adsorption of MMT on interfaces, and the performance of the

MMT is improved in altering the wettability in comparison to MMT individually at solid/liquid/liquid interfaces. The improvement in adsorption can be related to additional active sites that are created by ZnO nanoparticles between the MMT layers. Another reason for improving MMT adsorption phenomena is the increase in the surface area by sited ZnO nanoparticles.<sup>34</sup> Due to the economics and cheapness of MMT, it was decided to use this substance in large quantities and the amount of ZnO by less than half of the whole material.

**2.1.4.1. Preparation of the Plant Extract as the Eco-friendly Reducing–Stabilizing Agent.** *Ageratum conyzoides* L, a plant of Asteraceae plant family, was used as the eco-friendly agent to provide the reducing media and stabilize the synthesized environment. The potent antioxidant content of the plant strongly confirms the application of its extract as a stabilizing and bioreducing agent for the green synthesis of ZnO/MMT nanostructures.<sup>35,36</sup>

Dried powder (50 g) of the plant leaves was mixed with 500 mL of DDW at 80 °C for 30 min under reflux conditions. The gained extract was monitored using a UV–vis spectrophotometer during the different time intervals to study its stabilization and resistance against decomposition and deformation processes.

**2.1.4.2. Synthesis of ZnO/MMT Nanocomposites When Applied in an Environmentally Friendly Manner.** The prepared *A. conyzoides* L plant extract (100 mL) was placed within a beaker of 250 cm<sup>3</sup> volume to provide the stabilized reducing medium of synthesis. Chemical powders of zinc chloride and microscopic crystals of MMT phyllosilicates were then added to the reducing environment for 2 and 8 g, in turn. To increase the chemical reaction rate on surfaces, the solution was continuously stirred; also, to increase the reaction rate, the temperature increased to 80 °C and was kept constant. The used synthesized method was the precipitation method; therefore, the stirring process continued until a white precipitate was formed within the system. The precipitated materials were then screened from the synthesized environment through the filtration process. The product went under a 100 °C heating process and washing with DDW for any elimination of purity inclusions. Figure 1 illustrates the biosynthesis process of ZnO/MMT nanocomposites.

**2.1.5. Carbonate Core Sample.** The carbonate rock sections were obtained from an *Asmari* outcrop located in the south of Iran. The sections were cut into both the cylindrical core plug and circular pellet state of use for dynamic fluid displacement in porous media and wettability alteration experiments, respectively. Circular pellets were polished and divided into four sections to be applicable in the wettability experimental device because of the limitation of visual cell dimensions and use of the contact angle measurement method. Obtained core plugs and circular pellets were then rinsed through a cyclic hydrophilic–lipophilic washing procedure of DDW–acetone–toluene–acetone–DDW to eliminate any probability of dust, precipitated salts, available oleic matters, and other impurities. These unwanted inclusions (if the washing procedure was not applied to the samples) could affect the process as new materials when liquid/liquid and solid/liquid interfacial phenomena were happening and induce errors in measurements.

Induced wettability alterations caused by the presence of different solvents in the samples were not affected during the experiments because the aging processes for gaining a strong oil wetting state were conducted on all the samples.

XRD was conducted on the used sample to determine the composition of the rock. Results of the XRD analysis shows that the used rock type is approximately pure carbonate and contains a high percentage of calcite. Figure S2 shows the result of the XRD test for the prepared rock.

**2.2. Methods.** Figure 2 illustrates all the steps of the present study. In the first step, it is necessary to characterize the prepared materials to ensure the correct saponin extraction. To evaluate the thermal stability and also to determine functional groups of the natural surfactant, TGA and FT-IR tests were applied on the extracted material, respectively. Surfactant solutions were prepared with 500 to 7000 ppm concentrations of the extract. Electrical conductivity, pH, IFT, and contact angle measurements were used to obtain the CMC of the surfactant. After determining the CMC, the performance of the surfactant at CMC was evaluated in the presence of NaCl. At the end of the first step, the core flooding experiment

was applied with the most appropriate concentration of the surfactant and salinity. In the second step, the synthesized nanocomposite is characterized by FT-IR, XRD, and FE-SEM tests to determine functional groups, nanocomposite components, and morphology, respectively. Then, solutions with concentrations of 100, 250, 500, 1000, 1500, and 2000 ppm of the nanocomposite were prepared. After measuring the physical and chemical properties of the prepared solutions, IFT and wettability alteration tests were performed. Finally, the core flooding experiment was conducted at the optimal concentration of nanocomposites, which was obtained from the IFT and wettability alteration tests. In the third step, surfactant solution at CMC was used as the base solution and different concentrations of the nanocomposite were added to it. As in the previous two steps, after measuring the solution properties, the IFT and wettability alteration tests were performed. Finally, the optimal concentrations of hybrid solutions, which were obtained from the IFT and wettability alteration tests, were used as the selected EOR solution in the core flooding experiments.

**2.2.1. IFT Measurements.** In this study, the pendant drop method was used to calculate the IFT between oil and investigated solutions. The reason for using this method is its accuracy and simplicity.<sup>36,37</sup> In this method, a camera takes pictures from pendant oil droplets and calculates the IFT/surface tension using the below-mentioned equation<sup>36,37</sup>

$$\gamma = \frac{\Delta\rho \cdot g \cdot D}{H}$$

where  $\gamma$  is the IFT (mN/m<sup>2</sup>),  $\Delta\rho$  is the difference between the density of the drop and bulk phase (g/cm<sup>3</sup>),  $g$  is the earth gravitational acceleration (cm/s<sup>2</sup>),  $D$  is the largest diameter of the droplet (cm), and  $H$  is the shape factor of the droplet. The VIT 6000 apparatus designed by *Fars EOR technologies* was used for both IFT and contact angle measurements. The schematic of the apparatus used in this study is shown in Figure S3. All measurements of IFT were performed under ambient conditions and different concentrations of CP (500 to 7000 ppm) as the basis of hybrid solution and different concentrations of nanocomposites (100, 250, 1000, 1500, and 2000 ppm) used as the hybrid agent.

**2.2.2. Wettability Tests.** The sessile drop method was utilized to study the wettability alteration of the carbonate rock. Yang's relation for an oil droplet in equilibrium with the rock surface is given below<sup>38</sup>

$$\sigma_{so} = \sigma_{sw} + \sigma_{ow} \cos \theta_{ow}$$

where  $\sigma_{so}$  is the tension between the oil and solid rock surface,  $\sigma_{sw}$  is the tension between the water and solid rock surface,  $\sigma_{ow}$  is the tension between oil and water surfaces, and  $\theta_{ow}$  represents the contact angle of the droplet that is attached to the rock surface. Given this relation, if the contact angle is less than 90°, the tension between the rock and the oil is low, so the rock is water-wet. If the contact angle is 90°, the water and oil stresses are equal, and the wettability is mediate. Also, if the contact angle is above 90°, the tension between the rock and oil is high and it is an oil-wetted state.<sup>39</sup>

The VIT6000 was also used to calculate the contact angle between the oil droplets and carbonate surface by the sessile drop method in the presence of CP and hybrid solutions as the medium. Figure S3 shows the schematic of the utilized apparatus. The carbonate rocks are not oil-wet generally; therefore, to achieve the oil-wet system and study the effects of

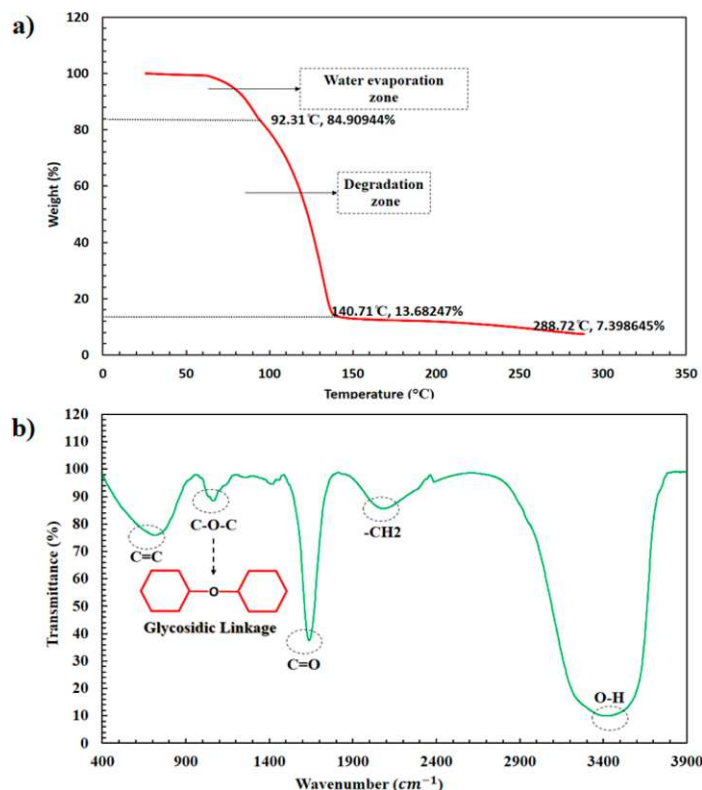


**Figure 3.** Characterizations of the CP: (a) TGA analysis and (b) FT-IR analysis.

CP and hybrid solutions on wettability alteration, the smooth pellet was immersed in crude oil at 70 °C for 15 days to be aged with oil-wetting agents of the crude oil. During this aging time, the polar components of crude oil adhere onto the surface of the carbonate rock, and they designate a lipophilic or hydrophobic layer on the surface. This prepared lipophilic layer causes a strong oil-wetting state for the surface of the carbonate rock and mimics the original condition of a reservoir oil-wet rock.

In the sessile drop method, the sessile drop is released and placed on the surface, and causes a competition between the oil phase and aqueous phase to adhere on the solid surface. Therefore, the equilibrium of this system requires a minimum time to reach this. Regarding the literature, different times are reported as the equilibrium time which ranged from minutes to hours; therefore, we choose the maximum time of the reported equilibrium to reach it. Consequently, then, each oil-wet pellet was immersed in the selected concentrations of CP and hybrid solutions for 24 h to observe their effects on the wettability alteration in an equilibrium reached state with the sessile drop method of measurement.

**2.2.3. Core Flooding Procedure.** The core flooding experiments were applied to measure the increase in oil RF by the CP and ZnO/MMT-CP as hybrid solutions at nominated optimal concentrations. A core-flood device made by Fars EOR Technologies Company located in the Abadan Faculty of Petroleum was used to perform the dynamic core flooding tests. In addition to calculating the increase in oil recovery, the porosity and pore volume (PV) of the cores are

measured by this device. All the flooding experiments were performed with a flow rate of 0.2 cm<sup>3</sup>/min. First, the core was saturated with seawater. Then, by subtraction the dry weight of the cores from the weight of saturated cores, the PV is obtained using the below equation

$$\text{pore volume (CC)} = \frac{\text{saturated weight} - \text{dry weight}}{\text{fluid density}}$$

After obtaining the amount of PV, the oil was then injected into the core to obtain irreducible water saturation (Swirr). To achieve Swirr, the oil injection continued until water production from the core was stopped. The cumulative amount of extracted water from the core was considered as the OOIP, and the below equation was used to calculate irreducible water saturation

$$\text{Swirr (\%)} = \frac{\text{PV} - \text{total extracted water}}{\text{PV}}$$

After reaching the Swirr, the first recovery phase begins with the injection of seawater to the core. This recovery phase is designed to be conducted on the oil-saturated rock plug with including irreducible water saturation and resembles the situation of real secondary oil flooding and acts as a basis for comparison of proposed EOR methods. During the injection of seawater into the core, the differential pressure and accumulative PV injection information were recorded through a differential-pressure transmitter and a hydraulic pump, in turn. The injection of seawater was continued until there was

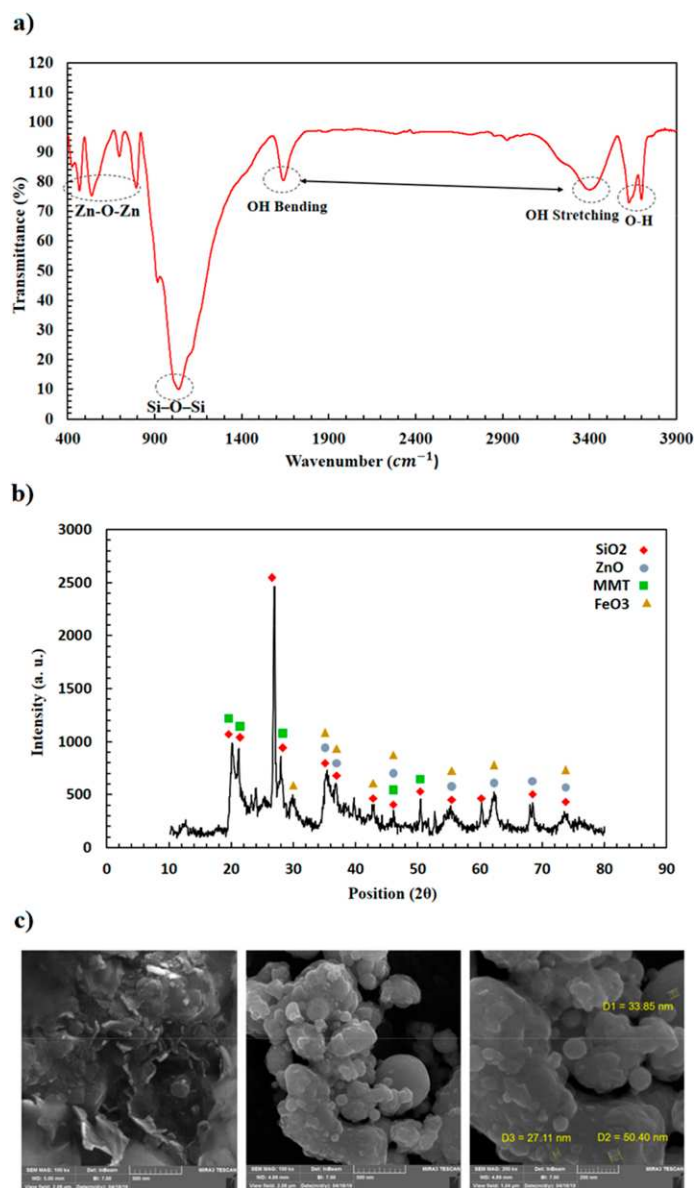


**Figure 4.** Characterizations of the nanocomposite: (a) FT-IR analysis, (b) XRD test, and (c) FE-SEM analysis.

no more oil production. Finally, the following equation was used to calculate the oil recovery of the first recovery phase

$$\text{RF seawater injection (\% OOIP)} = \frac{\text{oil production in seawater injection}}{\text{original oil in place}}$$

To investigate the effectiveness and impacts of both IFT reduction and wettability alteration toward water wetness by surfactant and hybrid solutions and the ion engineering process, two dynamic displacement experiments were designed to be applied under the same conditions. The first flooding scenario is to observe the effectiveness of ion engineering to

the optimum state of the surfactant (CMC), and the second flooding scenario is to investigate the effect of the hybrid state of use of ZnO/MMT with the optimum state of the surfactant (CMC). It should be noted that two designed scenarios were conducted on two similar rock plugs with the same saturation and primary productions.

Just like the first recovery phase, in the second recovery phase, the injections were applied and the pressures and PV injections were recorded. Finally, the increase in oil RF was calculated using the following equation

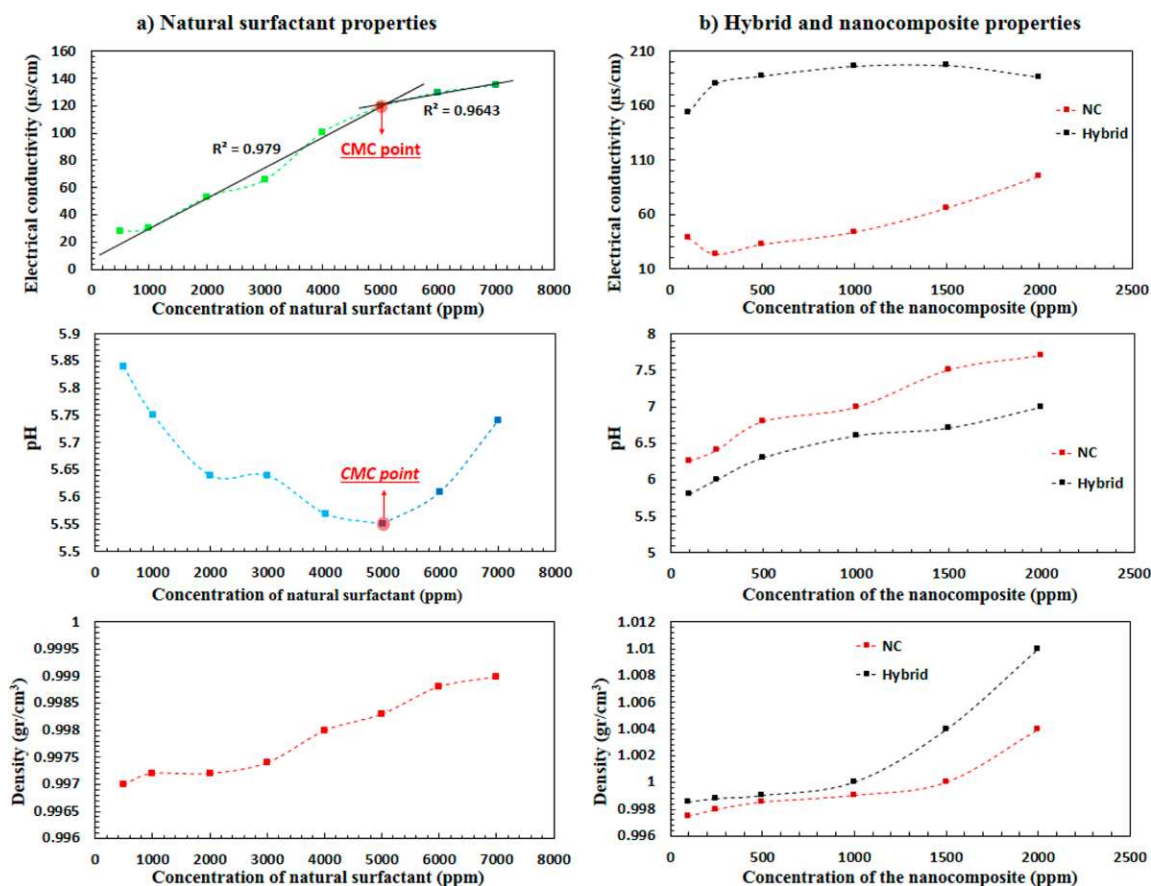


Figure 5. Properties of the solutions: (a) natural surfactant solution and (b) hybrid and nanocomposite solutions.

$$\text{RF surfactant/hybrid injection (\% OOIP)} = \frac{\text{oil production in surfactant/hybrid injection injection}}{\text{original oil in place}}$$

Figure S4 shows the scheme of the dynamic core flooding device made by Fars EOR Technologies. The required force for precise injection of fluids into the porous medium is governed by a hydraulic pump with high accuracy in injection rates. Accumulators are based on the accumulation and injection of different fluids with different scenarios at different times; also, they act as transfer vessels to inject fluids into the core holder to be injected to the porous medium.

A core holder of the Hassler type is applied with a system of the overburden pressure simulator to mimic a semirealized condition. During the conduction of the dynamic displacement test, the differential pressure transmitter records the difference of injection and production pressures to govern the breakthrough and other information. Simultaneous measurement of effluent fluid volumes, displaced volumes, and differential pressures shows the efficiency of each scenario, and the comparison between different scenarios and injection steps is available.

### 3. RESULTS AND DISCUSSION

**3.1. Characterization of the CP Extract.** Figure 3a illustrates the TGA test results for CP. In this test, the weight loss of the material was calculated versus temperature. In the presented results, three weight loss zones are observed. The first zone that occurred at ambient to 96.5 °C is related to water evaporation with an 18.22% weight loss. The second degradation zone from 96.5 to 139 °C illustrates 66.6% weight loss which is related to the decomposition of chemical compounds. Increasing temperature from 139 to 300 °C caused an 8% weight loss which can be attributed to the decomposition of more stable chemical components. According to the results obtained from the TGA test, it is concluded that the extracted natural surfactant is stable under the thermal conditions of the reservoir.

The FTIR transmittance spectrum of the CP was obtained in the range of 400–4000  $\text{cm}^{-1}$ . Figure 3b illustrates the FTIR test results for CP. The hydroxyl group (O–H) and carbon-hydrogen (–CH<sub>2</sub>) absorbance are observed at 3416.39  $\text{cm}^{-1}$  and 2084.89  $\text{cm}^{-1}$ , respectively. A sharp peak at 1639.36  $\text{cm}^{-1}$  indicates the existence of the amide group (C=O). Another peak at 1064.2  $\text{cm}^{-1}$  is attributed to glycosidic linkage (C–O–C), and the C=C is observed at 712.92  $\text{cm}^{-1}$ . According to the compounds approved in this FTIR test and compared to

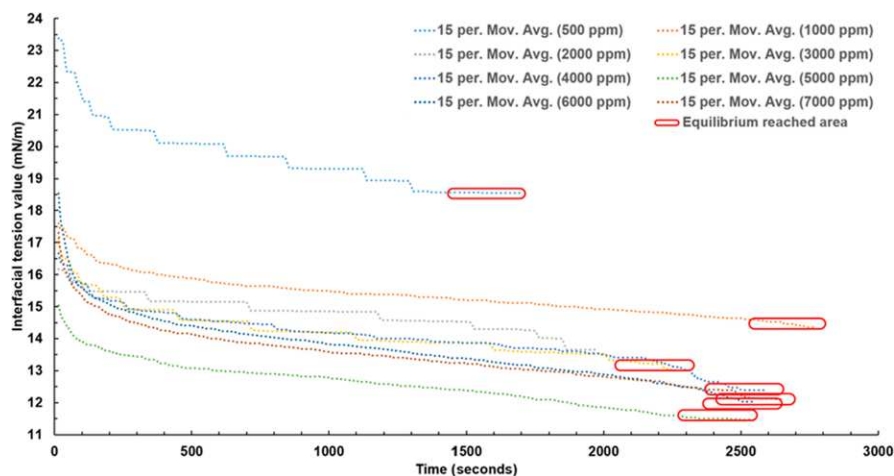


**Figure 6.** Dynamic measured IFT values of CP at different concentrations in DDW (different surfactant solutions) with crude oil under ambient temperature and pressure conditions.

the pure saponin spectrum, it is confirmed that the extracted solution contains saponin.<sup>40–42</sup>

### 3.2. Characterization of ZnO/MMT Nanocomposites.

The FT-IR spectra of ZnO/MMT nanocomposites are shown in Figure 4a. The 3627.61 and 3698.09  $\text{cm}^{-1}$  peaks correspond to the hydroxyl group (O–H). The bands at 3401.91 and 1639.66  $\text{cm}^{-1}$  represent stretching and bending vibration of water, respectively. The sharp peak at 1036.39  $\text{cm}^{-1}$  has been resulted in Si–O–Si groups of the tetrahedral sheets of MMT. The peaks at 793.46, 536, and 467.73  $\text{cm}^{-1}$  represent the bending and stretching vibration of the Zn–O–Zn.<sup>43–45</sup> Based on the results obtained from the FTIR test applied to the synthesized nanocomposite, the correctness of the synthesis and the presence of ZnO and MMT compounds are confirmed.

Figure 4b presents the XRD spectra of the synthesized ZnO/MMT nanocomposite. Xpert High Score Plus software was used to analyze the results of the XRD test. Figure S5 shows the identified compounds of the synthesized nanocomposite. The XRD diffraction patterns show that the synthesized nanocomposite contains  $\text{SiO}_2$ ,  $\text{Fe}_3\text{O}_4$ , ZnO, and MMT nanoparticles by peaks at  $2\theta$  values of 20.143, 21.13, 23.85, 25.32, 26.91, 27.983, 29.9, 35.34, 36.75, 42.7, 46, 50.392, 55.26, 60.223, 61.18, 68.3, and 73.65.

The morphology of the ZnO/MMT nanocomposite by the FE-SEM technique is illustrated in Figure 4c. Figure 4c shows the size, shape, homogeneity, and morphology of the synthesized nanocomposite at 500 nm–100kx and 200 nm–200kx magnification. According to the FE-SEM pictures, the size range of the synthesized nanocomposite is between 25 and 50. Therefore, the nanoscaled sizes of the synthesized green nanocomposite are confirmed.

**3.3. Solution Properties.** Figure 5 illustrates the electrical conductivity, pH, and density values of solutions at different concentrations. Column a corresponds to the CP solution, and column b corresponds to the nanofluid and hybrid solutions. Measurements of electrical conductivity and pH are common methods of obtaining the CMC point.<sup>46,47</sup> From Figure 5a, it can be seen that with increasing CP concentration, the electrical conductivity of the solution increases. It should be

noted that from the concentration of 5000 ppm onward, the slope of the graph decreases and is not as sharp as the lower concentrations. Due to the change in the slope of the graph at 5000 ppm, this concentration is considered as the CMC point. Another method for obtaining the CMC is calculating the pH at different concentrations. In this research, by calculating the pH of different concentrations of the CP solutions, the CMC was obtained, and the result is presented in Figure 5a. From 500 to 5000 ppm, the pH value has a downward trend, but at concentrations above 5000 ppm, an upward trend is observed. According to the pH values and trend change at this point, like the electrical conductivity results, it is concluded that the CMC point is 5000 ppm. Figure 5 also shows the density values of the surfactant at different concentrations. It is clear that the density increases with increasing the CP concentration. Figure 5b illustrates the fluid properties of nanocomposites and hybrid solutions. From the electrical conductivity data of the nanocomposite shown in Figure 5b, it is clear that the conductivity has increased from 250 ppm, which is due to the release of ZnO electrons. It is also known that the conductivity of a hybrid solution is higher than that of a solution without a surfactant. In justification of the increase in electrical conductivity by the use of the CP extract, it could be mentioned that the CP extract includes different saponins that are categorized as nonionic surface-active agents, and also, an electric field of sufficient strength can generate electric conductivity. This phenomenon as explained by Onsager could be described by the break-up of “ion pairs” into separate free ions at high field strength.<sup>48</sup>

From the pH values of the nanocomposite and hybrid solutions in Figure 5b, it can be seen that the pH increases with increasing the concentration of the nanocomposite. The presence of different acidic components in the CP extracted reduces the pH in the hybrid solution compared to the nanofluid without the CP. The pH of the aqueous solution of the CP extract could be placed within 5.55 to 5.85 ranges that could act as a pH-reducing material. In hybrid solutions, the available materials within the extract could induce this property to the hybrid colloidal nanofluid and to the nanosized particles and decrease the total pH to a lower value if compared with

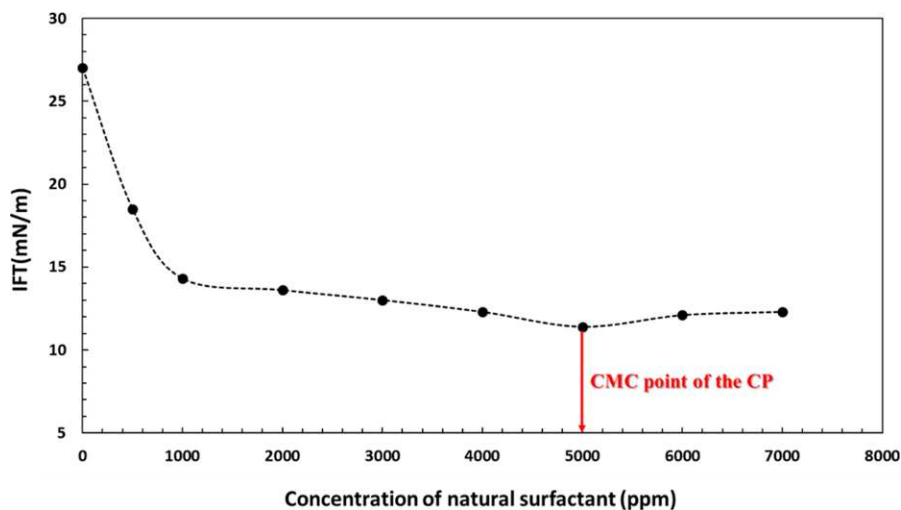


Figure 7. IFT values between water and oil in the presence of different concentrations of CP.

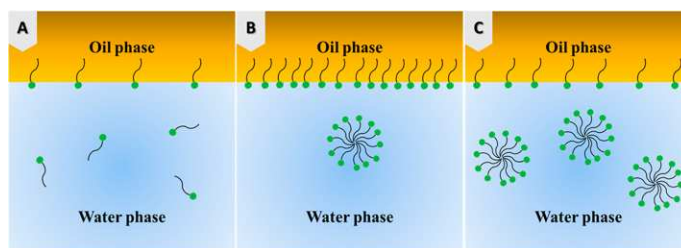


Figure 8. Mechanism of IFT alteration at various concentrations of the surfactant: (A) Below CMC. (B) At CMC. (C) Above CMC.

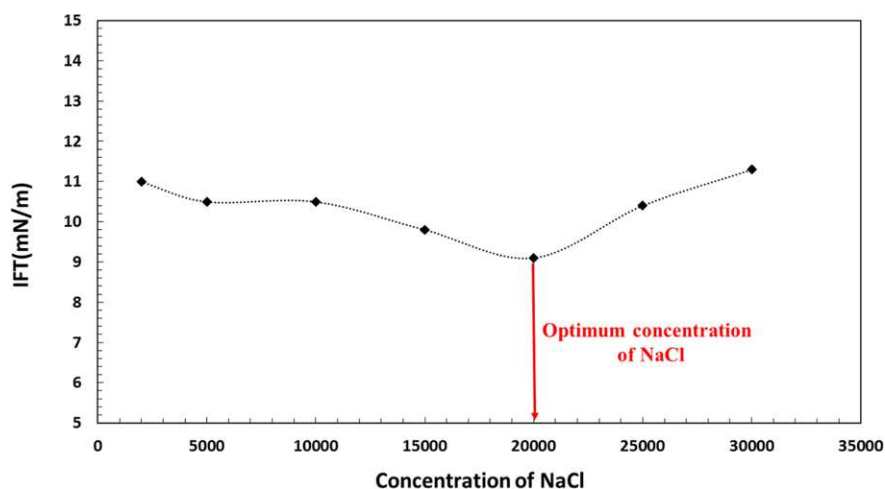


Figure 9. IFT values between water and oil in the presence of CP at CMC and different concentrations of NaCl.

approximate pH neutral colloidal nanofluids. The density data in Figure 5b show that the increase in ZnO/MMT concentration of the hybrid and nanocomposite solution increases the density.

**3.4. IFT and Wettability Tests.** **3.4.1. Natural Surfactant.** Various concentrations of the surfactant were applied to

calculate the IFT between crude oil and DDW. CP concentrations of 500 to 7000 ppm were used to measure the IFT under ambient conditions. Figure 6 illustrates the dynamic IFT between the various concentrations of CP and crude oil. The vertical axis is the instantaneous measured IFT value reported through the applied software, and the dotted-

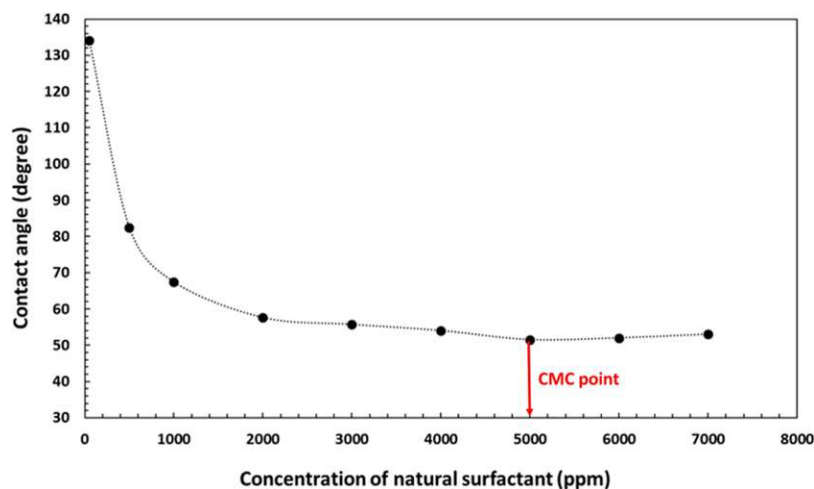


Figure 10. Contact angle values of the oil droplets on the surface of the carbonate pellets in the presence of different concentrations of CP.

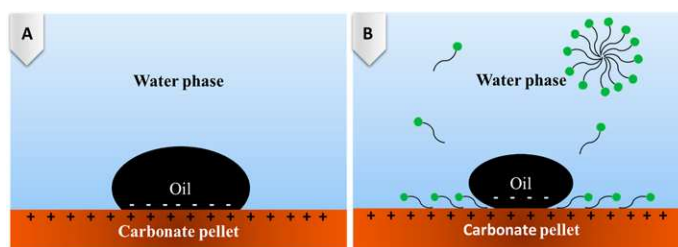


Figure 11. Mechanism of wettability alteration of an oil-wet carbonate rock in the presence of a nonionic surfactant. (A) Attach the oil droplet to oil-wet carbonate rock. (B) Wettability alteration of carbonate rock by the natural surfactant.

colored series are the 15 pointed moving averaged governed trend lines of the oscillating real IFT curves. Figure 7 shows the equilibrium values of the IFTs. The initial IFT value of DDW/crude oil was 27 mN/m, which decreased to 18.5, 14.3, 13.59, 13, 12.3, 11.4, 12.1, and 12.3 mN/m at 500, 1000, 2000, 3000, 4000, 5000, 6000, and 7000 ppm, respectively. As can be seen in Figure 7, the IFT decreases with increasing CP concentration up to 5000 ppm. The CMC point was detected at 5000 ppm, which indicates an 87.5% decrease. The CMC obtained from IFT measurements is consistent with the CMC obtained from the electrical conductivity and pH results. At concentrations above 5000 ppm, the IFT did not decrease.

CP as a surfactant tends to occupy the interface between two immiscible fluids, which alters the physical and chemical properties of the interface. The arrangement of the surfactant in a solution is such that the hydrophilic head is in the lipid part and the hydrophobic tail is in the water phase. Such a placement of surfactants reduces the IFT between the two immiscible fluids. The optimal concentration of the surfactant to reduce IFT is the micelle formation concentration. At higher concentrations of CMC, the IFT increases because more surfactants participate in the formation of micelles, and their numbers decrease at the oil–water interface (Figure 8).<sup>49</sup>

After identifying the CMC point of the CP, IFT values at 2000, 5000, 10 000, 15 000, 20 000, 25 000, and 30 000 ppm concentrations of NaCl were investigated at the CMC point of CP. As can be seen in Figure 9, the CP surfactant shows better

performance in the presence of NaCl. The NaCl reduces the IFT value of crude oil/DDW from 11.4 to 9.1 mN/m at the 20 000 ppm concentration of NaCl as the optimum concentration.

When the ions of salts are joined into reactions, the variation of IFT values could be affected by the positioning of ions at the interface and adsorption of ions on this intermediate phase boundary: The origination of positioning of ions from aqueous solution at the interface in the positioning of oil polar components such as available asphaltene at the interface from the other phase. At low concentrations, the salt-in effect occurs and causes a decrease in IFT at this interface. In this state, the organic particles tend to be dissolved in the aqueous solution, while in pure water, the aquatic molecules create a strong structure on one side of the water–organic matter interface and do not allow any disorder in their interfacial arranged structure and any entrance of organic molecules to the water phase. Therefore, any interface disturbance is low, and reduction of the IFT value is not achieved. In a low saline solution, positively charged sodium ions surround the oil droplet due to negative charges and adhere to it. This phenomenon causes the water molecules to adhere to the oil droplet. This behavior causes an IFT reduction between water and oil up to a certain salt concentration, and after that, the IFT increases. The reason for this increase is that with the increase in salt concentration, sodium ions in the environment

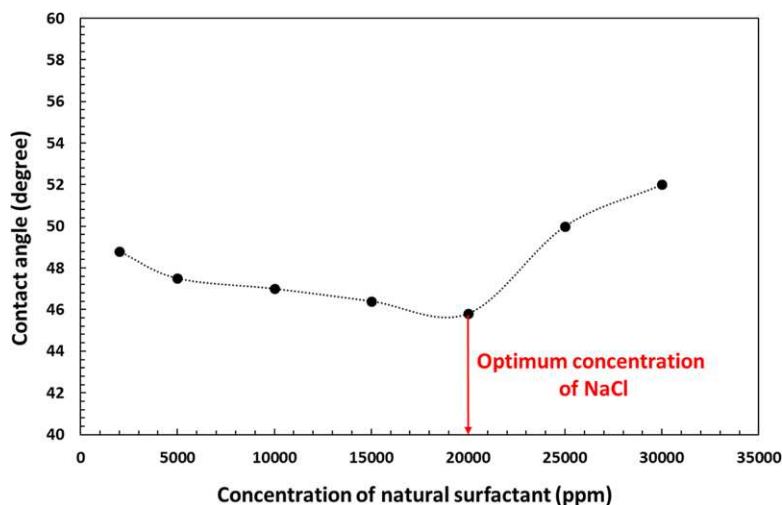


**Figure 12.** Contact angle values of the oil droplets on the surface of the carbonate pellets in the presence of CP at CMC and different concentrations of NaCl.

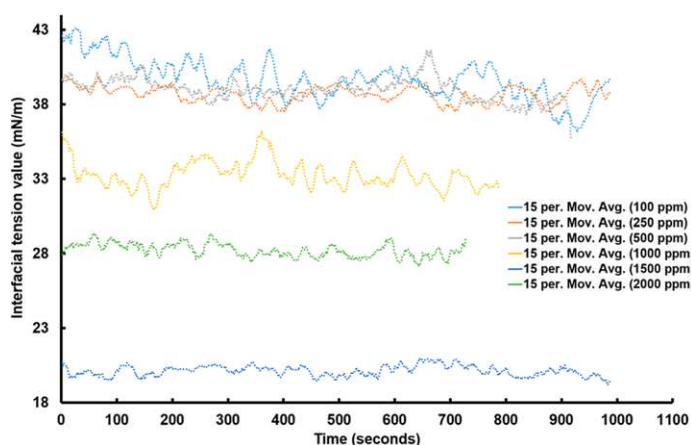


**Figure 13.** Measured dynamic IFT values at different concentrations of the synthesized nanocomposite in DDW (different nanofluid concentrations) with crude oil under ambient conditions.

increase and water molecules become involved in sodium ions in the environment and fewer water molecules attach to oil.<sup>50</sup>

In this study, the contact angle method was used to study the wettability alteration of carbonate rock. Figure 10 shows the changes in the contact angle of oil droplets on the carbonate rock surface versus different concentrations of CP under ambient conditions. The initial value of the contact angle of the oil drop on the oil-wet carbonate surface was  $134^\circ$ , which decreased to 82.5, 67.4, 57.6, 55.7, 54, 51.5, 52, and  $53^\circ$  at 500, 1000, 2000, 3000, 4000, 5000, 6000, and 7000 ppm of CP, respectively. The trend of contact angles has been decreased from 0 to 5000 ppm and then increased, and the lowest value of the contact angle was obtained at a concentration of 5000 ppm, which was identified as the CMC point.

The reason for the oil droplets sticking to the surface of the carbonate rock is the negative charge of oil composition such as stearic acid ( $\text{R-COO}^-$ ), which is adsorbed by the positive

charge ( $-\text{Ca}^+$ ) of the carbonate rock, and this is an electrostatic interaction.<sup>51</sup> CP as a nonionic surfactant contains benzene rings in its hydrophobic tail, which are the source of electrons. The tail of the saponin adheres onto the positive surface of the carbonate rock and forms a thin layer that alters the wettability from oil-wet to water-wet.<sup>52</sup> Figure 11 shows the wettability alteration mechanism by a nonionic surfactant.

After determining the CMC point of CP from the contact angle measurements, the wettability alteration of carbonate rock was performed in the presence of different concentrations of NaCl and CMC of the surfactant as the base solution. 2000, 5000, 10000, 15 000, 20 000, 25 000, and 30 000 ppm of NaCl were added to the CMC solution of CP, and the wettability alteration of carbonate rock at these concentrations was investigated. As can be seen in Figure 12, NaCl shows a synergy effect with CP to reduce the contact angle. From 2000 to 20 000 ppm of NaCl, the contact angle trend was decreasing, but at concentrations above 20 000 ppm, the

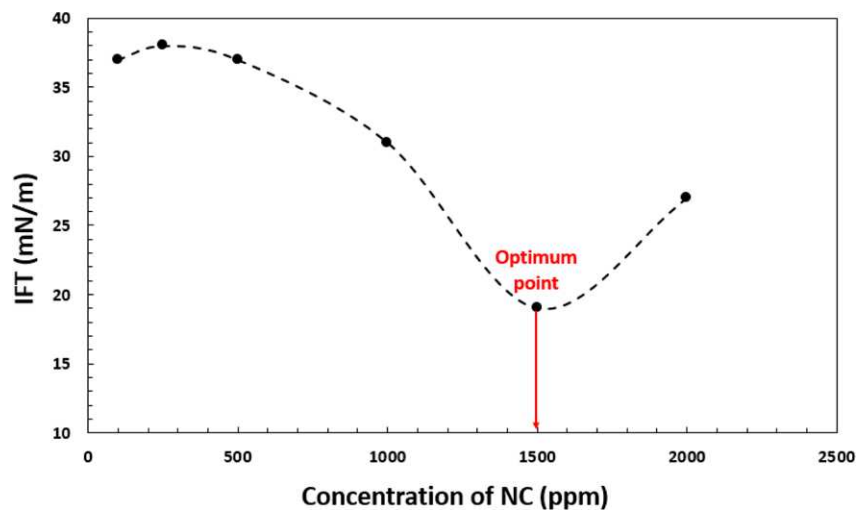


Figure 14. IFT value between water and oil in the presence of nanocomposite solutions.

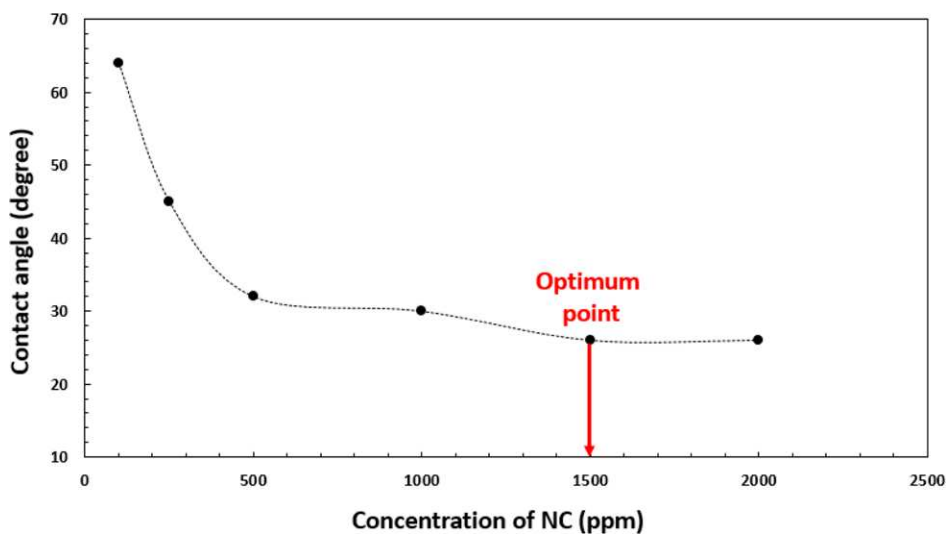
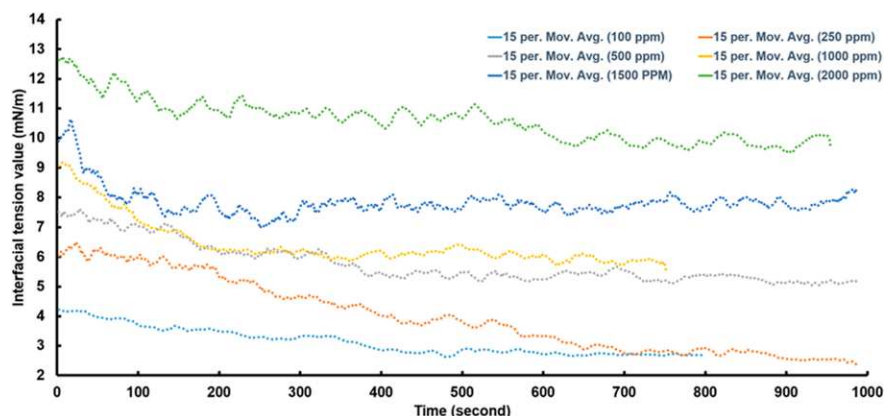


Figure 15. Contact angle of oil droplets to the carbonate pellets in the presence of nanocomposite solutions.

contact angle trend was increasing. As a result, 20 000 ppm of NaCl was identified as the optimal concentration, which represents 60% optimization compared to the initial value. The same procedure of the salting-in effect like its impact on IFT change applies here in alteration of the wettability state. This salinity effect causes a reduction release of active polar components adhered previously to the rock surface. Sodium ions allow oil droplets to easily separate from the rock surface. For this reason, the surface wettability of carbonate rock in the surfactant and salt solution is more hydrophilic than surfactant solution and DDW solution.

**3.4.2. Nanocomposite Solution (ZnO/MMT).** IFT experiments were conducted at different concentrations of the synthesized ZnO/MMT nanocomposite under the ambient condition. Figure 13 shows the dynamic IFT values of different concentrations of nanocomposite solutions during the time.

The vertical axis is the instantaneous measured IFT value reported through the applied software, and the dotted-colored series are the 15 pointed moving averaged governed trend lines of the oscillating real IFT curves. Figure 14 illustrates the IFT values of the nanocomposite solutions as the equilibrium IFT values, which were obtained from the dynamic IFT measurements. As shown in this figure, ZnO/MMT nanocomposites initially increases the IFT at a concentration of 100 to 250, but after increasing the concentration, the IFT decreases. There was an abnormality for the nanofluid at a concentration of 250 ppm of nanocomposites for both electrical conductivity and IFT measurements. At concentrations of 100 and 250 ppm of the nanocomposite, MMT reduces the electrical conductivity of the solution. At higher concentrations than 250 ppm, the concentration of ZnO increases, and the conductivity of



**Figure 16.** Measured dynamic IFT values of different concentrations of the synthesized nanocomposite in CMC solutions of the surfactant (different hybrid concentrations).

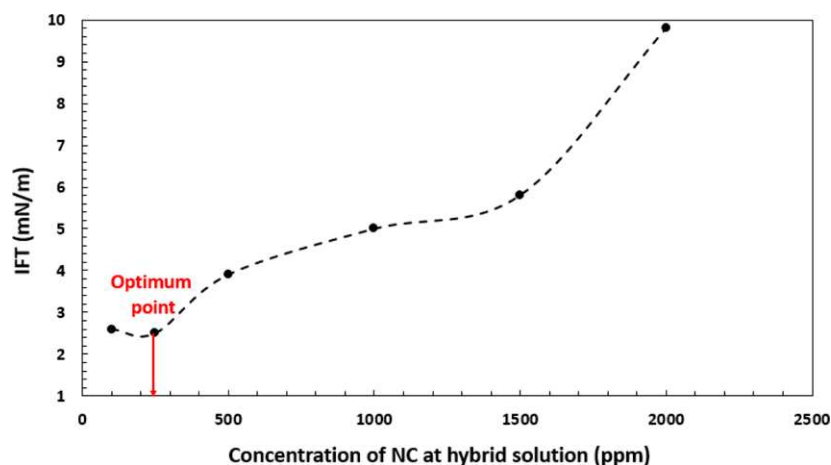


**Figure 17.** IFT values between water and oil in the presence of the CP–ZnO/MMT hybrid solutions vs different concentrations of ZnO/MMT nanocomposites.

nanocomposites also increases due to the generation of free electrons.<sup>53</sup>

At the selected concentration of 1500 ppm, the lowest IFT 19 mN/m was obtained and considered as the optimum concentration. Although this nanocomposite was not very successful in reducing the IFT, the main purpose of the nanocomposites is not to reduce IFT. Therefore, other mechanisms such as wettability alteration should be investigated.

Wettability alteration is one of the most important effective parameters of nanofluids in increasing the oil recovery from the reservoirs. Hence, the contact angle measurements were conducted in the presence of different concentrations of ZnO/MMT under ambient conditions.

Figure 15 shows the contact angle values of the oil droplets with carbonate pellets at different concentrations of the nanofluid. According to the contact angle measurement results, the ZnO/MMT nanocomposite was able to alter the wettability of the carbonate rock from oil-wet to water-wet. As can be seen from Figure 15, until 1500 ppm, with increasing concentration of NC, the contact angles have decreased. The

concentrations of 100, 250, 500, 1000, 1500, and 2000 ppm result in contact angles of 63.94, 45, 32, 30, 26, and 26°, respectively. Although higher concentrations of nanofluids are usually more effective in altering wettability, they may reduce the permeability of the reservoir rock.<sup>54</sup>

The concepts of nanofluids and resulting wettability alteration should be discussed in a procedure that causes nanofluids to affect the surface wettability of rocks. Nanofluids are fluids that include dispersed nanoparticles with a diameter of 1–100 nm.<sup>55,56</sup> Nanofluids generate a thin film on the surface of the solid, according to Chengara, Nikolov, Wasan, Trokhymchuk, and Henderson (2004), and the consequent restrictions of the positioning of the nanomaterials inside of this film force the nanomaterials to emerge in regular layers.<sup>57</sup> The entropy of the whole system grows as a result of the increased space available for the nanomaterials' twisted movement, and as a result, a tremendous pressure value is induced on the system's restricted volume. The configuration and size of nanoparticles can affect the generated pressure profile.<sup>58</sup> According to McElfresh, Olguin, Ector, and others (2012), a thin film diffused over the rock's surface can separate

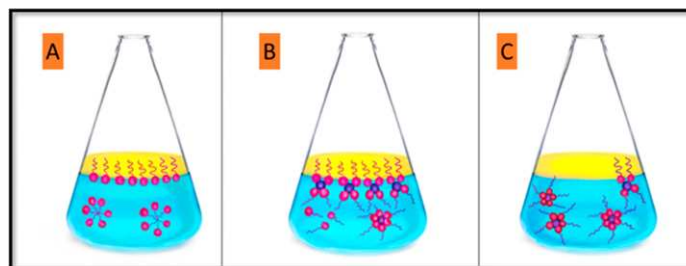


**Figure 18.** Mechanism of a hybrid solution to change IFT: (A) surfactant solution at CMC concentration. (B) Hybrid solution at the optimum concentration of nanocomposites. (C) Decreasing nanosurfactants at the interface of oil–water by increasing the nanocomposite concentration.

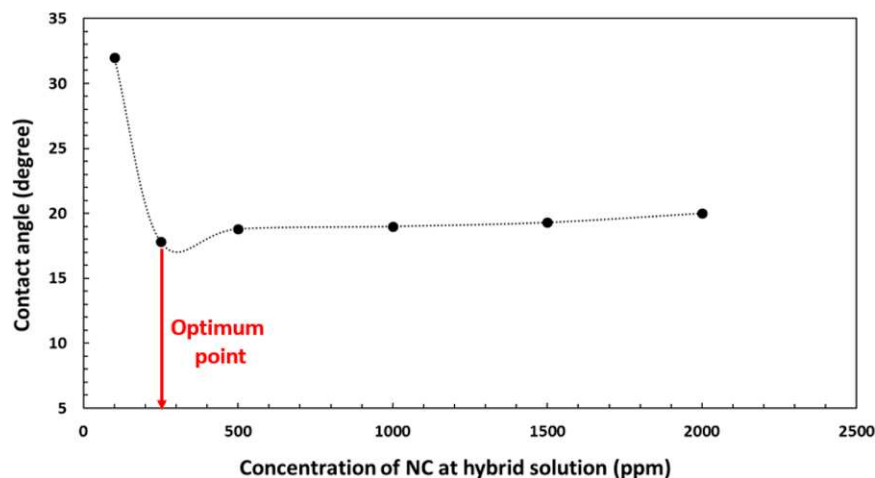


**Figure 19.** Contact angle values of the oil droplets on the surface of the carbonate pellets in the presence of hybrid solutions versus different concentrations of the nanocomposite.

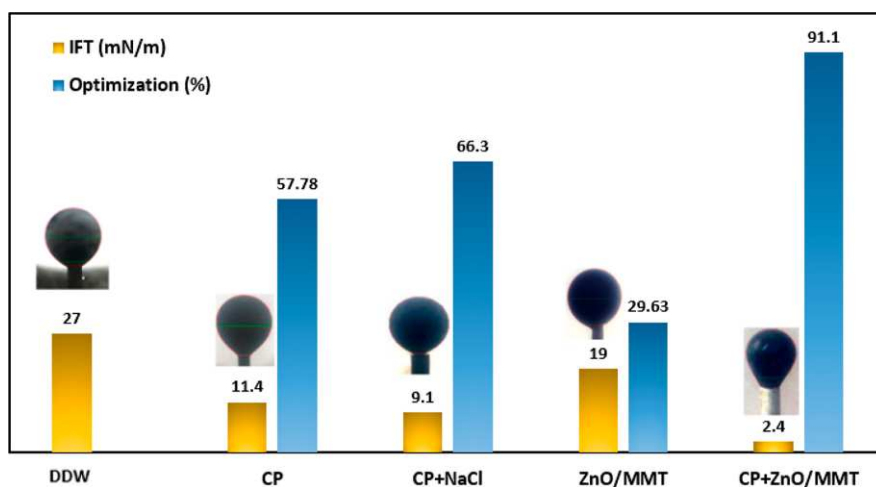
adherent oil, paraffin, and gas from the rock surface.<sup>59</sup> The separation of these components, which causes the rock to be oil-wetting, ends in a water-wetting situation. When compared to the fluid and reservoir rock, the intensity of this phenomenon is mostly determined by the characteristics of the nanofluid and dispersed nanoparticles. The effects of altering the wettability of nanosized materials lead the film to form. The development of pressure in the system also results in the formation of a wedge-like film, which is referred to as structural disjoint pressure.<sup>59</sup> It is caused by Brownian motion (random movements of suspended nanoparticles in a fluid) and repulsive electrostatic interactions between nanoparticles.<sup>60,61</sup> According to Aveyard, Binks, and Clint, the properties of the rock surface, the temperature of the base fluid, salt content, and, in particular, the quantity and size of nanoparticles all impact the nanofilm's progression. An elevated level of nanoparticle particle numbers leads to an amplification of disjoint overpressure in the system and a consequent decrease in the contact angle if no other mechanism—such as the attraction of nanocomposites on the surface of solid rock—disputes with the nanofilm. Increasing concentrations leads to larger disjointed pressure values, resulting in a reduction of contact angle values.<sup>62</sup>

**3.4.3. Hybrid Solution (CP–ZnO/MMT).** In this step, the IFT between oil and different concentrations of ZnO/MMT as a solute in the hybrid solution was measured. To make the

hybrid solution, the CP at the CMC which was obtained earlier from electrical conductivity, pH, IFT, and contact angle methods was used as the dispersing agent, and the ZnO/MMT nanocomposite with different concentrations was used as the dispersed agent. 100, 250, 500, 1000, 1500, and 2000 ppm of ZnO/MMT nanocomposites were used to make hybrid solutions and then used in the IFT and contact angle measurements. Figure 16 illustrates the dynamic IFTs in the presence of different concentrations of nanocomposites in the hybrid solution. The vertical axis is the instantaneous measured IFT value reported through the applied software, and the dotted-colored series are the 15 pointed moving averaged governed trend lines of the oscillating real IFT curves. Figure 17 presents the equilibrium values of the IFTs in the presence of different concentrations of the nanocomposite. 2.6, 2.4, 5, 5.8, 7.7, and 9.8 mN/m were obtained at concentrations of 100, 250, 500, 1000, 1500, and 2000 ppm of nanocomposites in the hybrid solution, respectively. Compared to the CP, the hybrid solution significantly reduces the IFT. The optimal concentration of the nanocomposite at the hybrid solution was observed at 250 ppm which shows an 80% reduction in IFT. The reason for this significant reduction in IFT is due to the stability created in the new solution (Figure 18B). At concentrations higher than 250 ppm, the IFT increases because the surfactants become more involved with the

**Table 1. Results of IFT and Contact Angle Measurements in the Presence of Different Solutions**

| material                | concentration (ppm)   | IFT (mN/m)  | contact angle ( $\theta$ ) | base solution                      |
|-------------------------|-----------------------|-------------|----------------------------|------------------------------------|
| CP (surfactant)         | 0                     | 27          | 134                        | DDW                                |
|                         | 500                   | 18.5        | 82.5                       |                                    |
|                         | 1000                  | 14.3        | 67.4                       |                                    |
|                         | 2000                  | 13.59       | 57.6                       |                                    |
|                         | 3000                  | 13          | 55.7                       |                                    |
|                         | 4000                  | 12.3        | 54                         |                                    |
|                         | <b>5000</b>           | <b>11.4</b> | <b>51.5</b>                |                                    |
|                         | 6000                  | 12.1        | 52                         |                                    |
| CP + NaCl               | CMC+ 0                | 11.4        | 51.5                       | CMC of surfactant (5000 ppm of CP) |
|                         | CMC+2000              | 11          | 48.8                       |                                    |
|                         | CMC+5000              | 10.5        | 47.5                       |                                    |
|                         | CMC+10 000            | 10.5        | 47                         |                                    |
|                         | CMC+15 000            | 9.8         | 46.4                       |                                    |
|                         | <b>CMC + 20 000</b>   | <b>9.1</b>  | <b>45.8</b>                |                                    |
|                         | CMC + 25 000          | 10.4        | 50                         |                                    |
|                         | CMC + 30 000          | 11.3        | 52                         |                                    |
| ZnO/MMT (nanocomposite) | 0                     | 27          | 134                        | DDW                                |
|                         | 100                   | 37          | 63.94                      |                                    |
|                         | 250                   | 38          | 45                         |                                    |
|                         | 500                   | 37          | 32                         |                                    |
|                         | 1000                  | 31          | 30                         |                                    |
|                         | <b>1500</b>           | <b>19</b>   | <b>26</b>                  |                                    |
|                         | 2000                  | 27          | 26                         |                                    |
|                         | CP + ZnO/MMT (hybrid) | CMC + 0     | 11.4                       |                                    |
| CMC + 100               |                       | 2.6         | 32                         |                                    |
| <b>CMC + 250</b>        |                       | <b>2.4</b>  | <b>17.8</b>                |                                    |
| CMC + 500               |                       | 5           | 18.8                       |                                    |
| CMC + 1000              |                       | 5.8         | 19                         |                                    |
| CMC + 1500              |                       | 7.7         | 19.3                       |                                    |
| CMC + 2000              |                       | 9.8         | 20                         |                                    |

**Figure 20.** Optimization percentages of IFT measurements in the presence of different solutions.

nanocomposite, and their amount at the oil–water interface decreases (Figure 18C).

Figure 19 illustrates the results of contact angle measurements of CP-ZnO/MMT solutions which were measured at concentrations of 100 to 2000 ppm of ZnO/MMT nanocomposites. As the results show, 32, 17.82, 18.8, 19, 19.3, and

20° were obtained at concentrations of 100, 250, 500, 1000, 1500, and 2000 ppm of the nanocomposite, respectively. The lowest contact angle was obtained at 250 ppm which reduced the contact angle from the initial value of 134 to 17.82° which shows 86.7% optimization. This hybrid fluid has altered the wettability from oil-wet to strong water-wet.

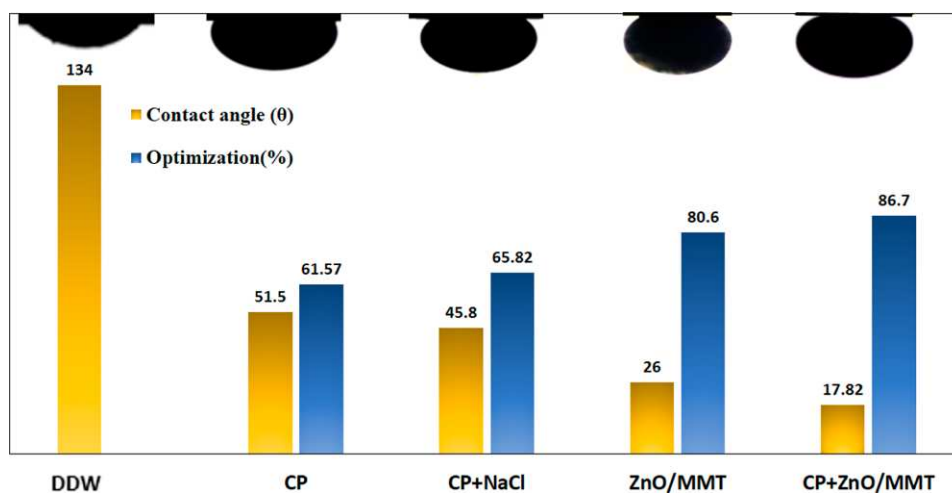


Figure 21. Optimization percentages of wettability alteration tests in the presence of different solutions.

Table 2. Specifications of Carbonate Cores

| core number | diameter (cm) | length (cm) | bulk volume (cm <sup>3</sup> ) | dry core weight (gr) | saturated core weight (gr) | PV (cm <sup>3</sup> ) | porosity (%) | permeability (MD) | S <sub>wirr</sub> (%) | OOIP (%) |
|-------------|---------------|-------------|--------------------------------|----------------------|----------------------------|-----------------------|--------------|-------------------|-----------------------|----------|
| no. 1       | 3.74          | 6.5         | 71.37                          | 164.35               | 178                        | 8.4                   | 11.76        | 3.5               | 36.54                 | 63.46    |
| no. 2       | 3.74          | 6.79        | 74.55                          | 178.038              | 187.038                    | 9.612                 | 12.89        | 3.6               | 38.4                  | 61.6     |
| no. 3       | 3.74          | 5.65        | 62.04                          | 148.8                | 155.3                      | 6.5                   | 10.48        | 3.9               | 38.46                 | 61.54    |

### 3.5. Comparison of IFT and Wettability Alteration Test Results.

All the results of the IFT and wettability alteration tests in the presence of CP, CP + NaCl, ZnO/MMT, and CP + ZnO/MMT as hybrid solutions are reported in Table 1. As mentioned in the previous sections, all of the tests were performed under ambient conditions. According to the results obtained from IFT measurements in different solutions, it has been observed that the CP is able to reduce the IFT from the initial value of 27 to 11.4 mN/m at 5000 ppm as CMC. Also, by adding NaCl to the CMC of CP, its performance is improved and the IFT is reduced to 9.1 mN/m at 20 000 ppm of NaCl. The nanofluid increases the IFT between oil and water at low concentrations. At 1500 ppm of the nanocomposite as the optimum concentration of the ZnO/MMT nanofluid, the IFT decreases from an initial value of 27 to 19 mN/m, which indicates 29% optimization. By measuring the IFT of oil–water in the presence of the hybrid solution of CP and ZnO/MMT, 2.4 mN/m is obtained as the optimum value at 250 ppm of the ZnO/MMT nanocomposite. In other words, the obtained optimization percentages for CP, CP + NaCl, and the CP + ZnO/MMT nanofluid are 57.78, 66.3, and 91.1%, respectively (Figure 20).

The wettability alteration of carbonate rocks in the presence of different solutions was investigated, and the results at the optimal concentration for each solution are presented in Figure 21. At the CMC of CP, the contact angle decreases from 134 to 51.5°. In other words, this surfactant alters the wettability from oil-wet to water-wet. By adding NaCl to the surfactant, the contact angle is reduced more until a contact angle value of 45.8° is obtained at 20000 ppm of NaCl and the CMC of the surfactant. Then, the wettability alteration of carbonate rock in the presence of the ZnO/MMT nanocomposite was studied. The ZnO/MMT nanocomposite is able to alter the wettability

from oil-wet to water-wet. At an optimum concentration of 1500 ppm of ZnO/MMT, the contact angle decreases from the initial value of 134° to 26°. The best results of wettability alteration tests were obtained in the presence of the nanocomposite-surfactant hybrid solution. In other words, the hybrid solution is able to reduce the contact angle of the oil droplet to 17.82°, which indicates strong water-wet wettability. As can be seen in Figure 21, the optimization percentages for CP, CP + NaCl, ZnO/MMT nanofluid, and hybrid solutions to wettability alteration are 61.57, 65.82, 80.59, and 86.70%, respectively.

**3.6. Core Flooding and Reservoir Properties.** To evaluate the potential of the natural surfactant, nanocomposite, and hybrid solutions, three flooding experiments at the optimum concentrations of CP + NaCl (CMC + 20 000 ppm of NaCl), nanocomposite (1500 ppm), and hybrid (CMC + 250 ppm of nanocomposite) solutions under ambient conditions were performed. In this study, three carbonate cores were used to perform core flooding tests. The specifications of each core can be seen in Table 2. First, the cores were saturated with seawater, and the saturated core weight was measured. By subtracting the saturated weight from the dry weight of the core, the PV of each core was obtained. Also, by dividing the obtained PVs by the density of seawater, the volume of water in the cores was obtained. In the next step, oil was injected into the cores until no more water was produced from the cores. By reducing the volume of produced water from the total amount of water in the pores, the irreducible water of each core was obtained. As can be seen in Table 4, the irreducible water was 36.54, 38.4, and 38.46% for cores number 1, 2, and 3, respectively.

After saturating the cores with crude oil and achieving irreducible water saturation, seawater was injected into the

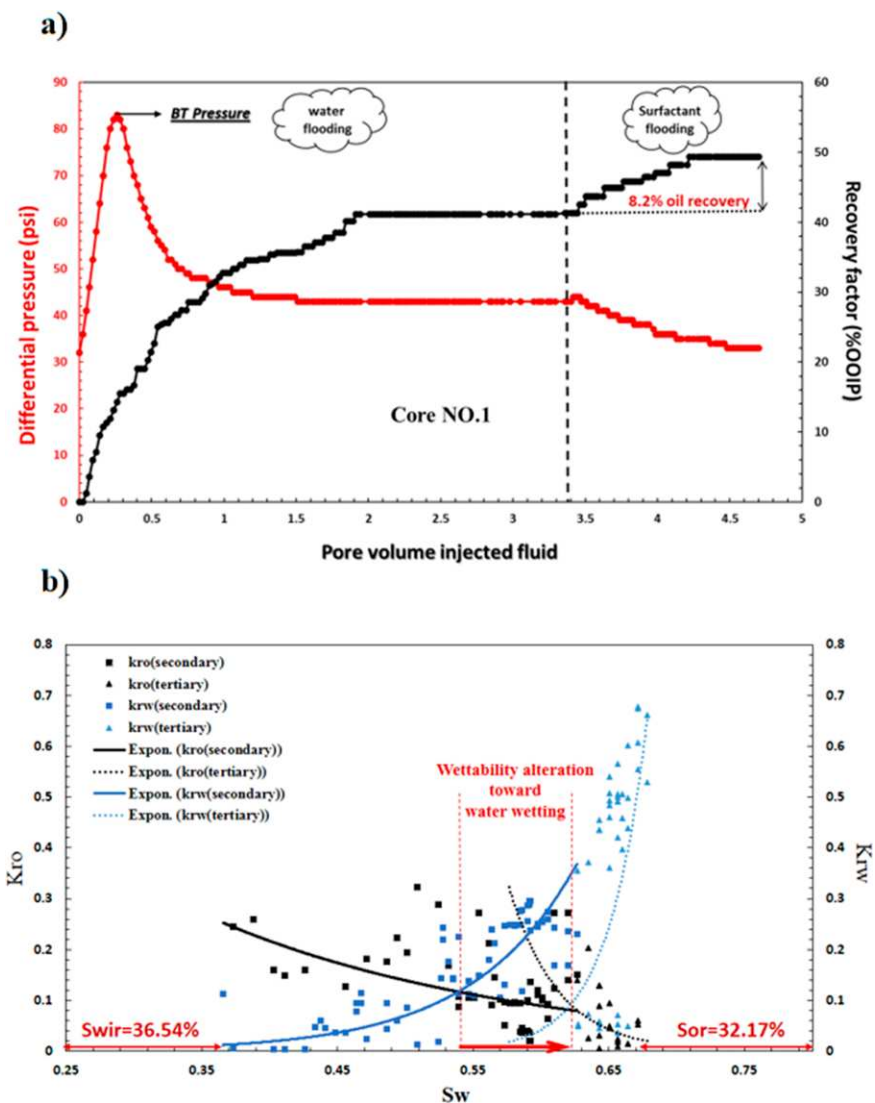


**Figure 22.** Dynamic core flooding results: (a) oil recovery by water and CP flooding and (b) relative permeability curve of water and the surfactant by the JBN method.

cores at 0.2 cm<sup>3</sup>/min rates to produce oil from the cores as secondary production. The oil recovery, pressure, and PV of injection into cores 1, 2, and 3 are illustrated in Figures 22, 23, and 24, respectively. The secondary production is 41.12, 43.16, and 42.5% for core nos. 1, 2, and 3, respectively. Also, according to the pressure diagram, the breakthrough points for core nos. 1, 2, and 3 occur at 0.28, 0.27, and 0.24 PV, respectively.

CMC of CP solution (5000 ppm) at the optimum concentration of NaCl (20000 ppm) was injected into the core no. 1 to investigate the effect of the natural surfactant on increasing oil recovery. Figure 22 illustrates the results of water and surfactant flooding. After 3.4 PV water flooding, the CP solution was injected into the core no. 1. As can be seen in Figure 22a, the flooding process at this step continued until 4.8

PV, in which the oil production was not increased more. By injecting surfactant solution after water flooding, the RF increased from 41.12 to 49.3%, which indicates an 8.2% additional oil recovery. Figure 22b shows the relative permeability curve of water and surfactant flooding by the JBN method.

To investigate the effect of nanocomposites on increasing oil recovery, a solution with a concentration of 1500 ppm of the ZnO/MMT nanocomposite was injected into core no. 2 as the secondary recovery step. As shown in the Figure 23a, the nanofluid has increased oil production from 43.16 to 49.2%. The nanocomposite has the ability of 6% additional oil recovery. Figure 23b presents the relative permeability curve of nanocomposite flooding obtained from the JBN method.

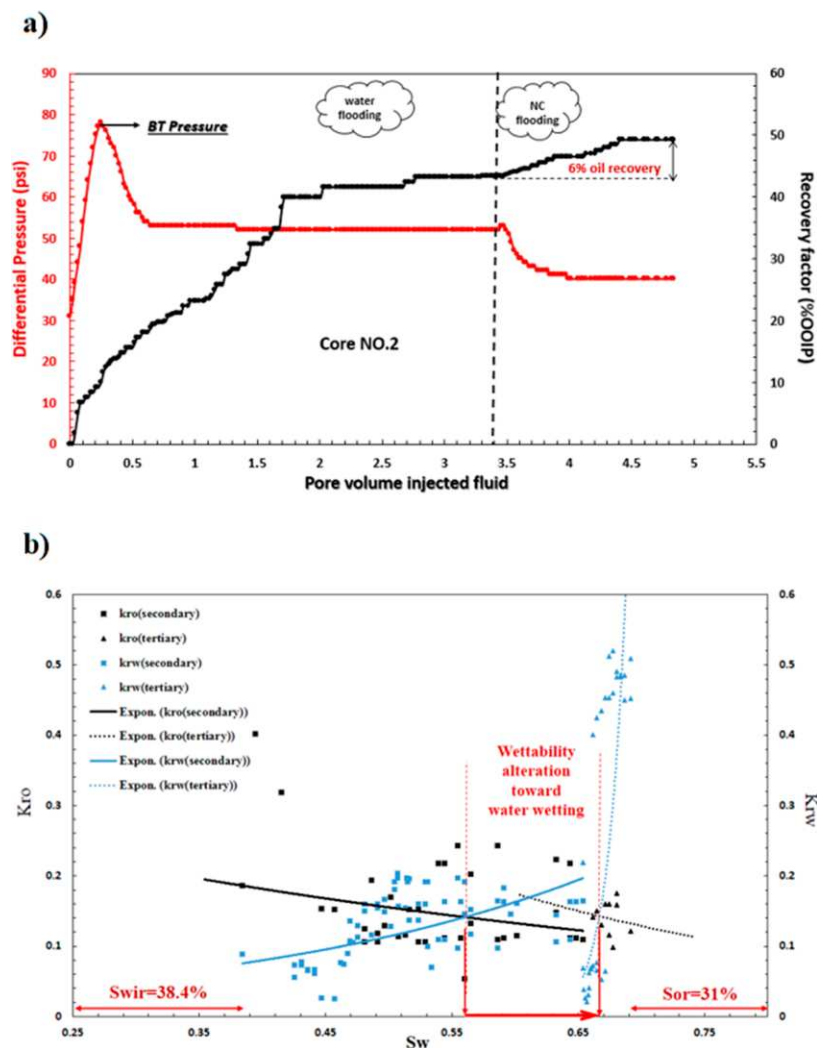


**Figure 23.** Dynamic core flooding results: (a) oil recovery by water and nanofluid flooding and (b) relative permeability curve of water and the nanofluid by the JBN method.

Adding nanocomposites to the surfactant as a hybrid agent can improve the performance of the surfactant, and the results obtained from the pendant drop and contact angle tests confirm this statement. According to the results obtained from the previous tests, the optimum concentration of the CP-ZnO/MMT nanocomposite solutions was identified at concentrations of 5000 ppm of CP as CMC and 250 ppm of the ZnO/MMT nanocomposite. Like the surfactant flooding, the nanofluid was injected into the core after the water flooding. The oil recovery was fixed after 4.6 PV injection. The oil recovery of water flooding of core no. 3 was 42.5% which increased to 55.5% after nanofluid flooding. In other words, 13% additional oil recovery was obtained by nanofluid flooding (Figure 24a). Figure 24b shows the relative permeability curve of water and nanocomposite-surfactant flooding by the JBN method.

The optimized values for contact angle modifications in CP + NaCl, ZnO/MMT, and CP + ZnO/MMT systems are 65.82,

80.6, and 86.7% in turn, while analysis of relative permeability curves shows different values for the same systems. By governing optimized values for analysis of the wettability alteration in carbonate and sandstone systems, intersection points could be analyzed and their shifts to higher water saturations are inferred as a more water-wet state. Therefore, by measurement of these intersection points, optimized values of 15.7, 19.64, and 4.6% are gained for CP + NaCl, ZnO/MMT, and CP + ZnO/MMT systems, respectively. These optimized values are different from each other for even the same systems because of the effects of different parameters in each system. In contact angle measurement experiments, all rock pellets were polished to eliminate the surface roughness effect, while in the porous medium, the parameter of surface roughness is included within the wettability shifting system. Another reason could be the lithological heterogeneities that are included in the porous medium, while their impacts were eliminated in contact angle measurement experiments. The

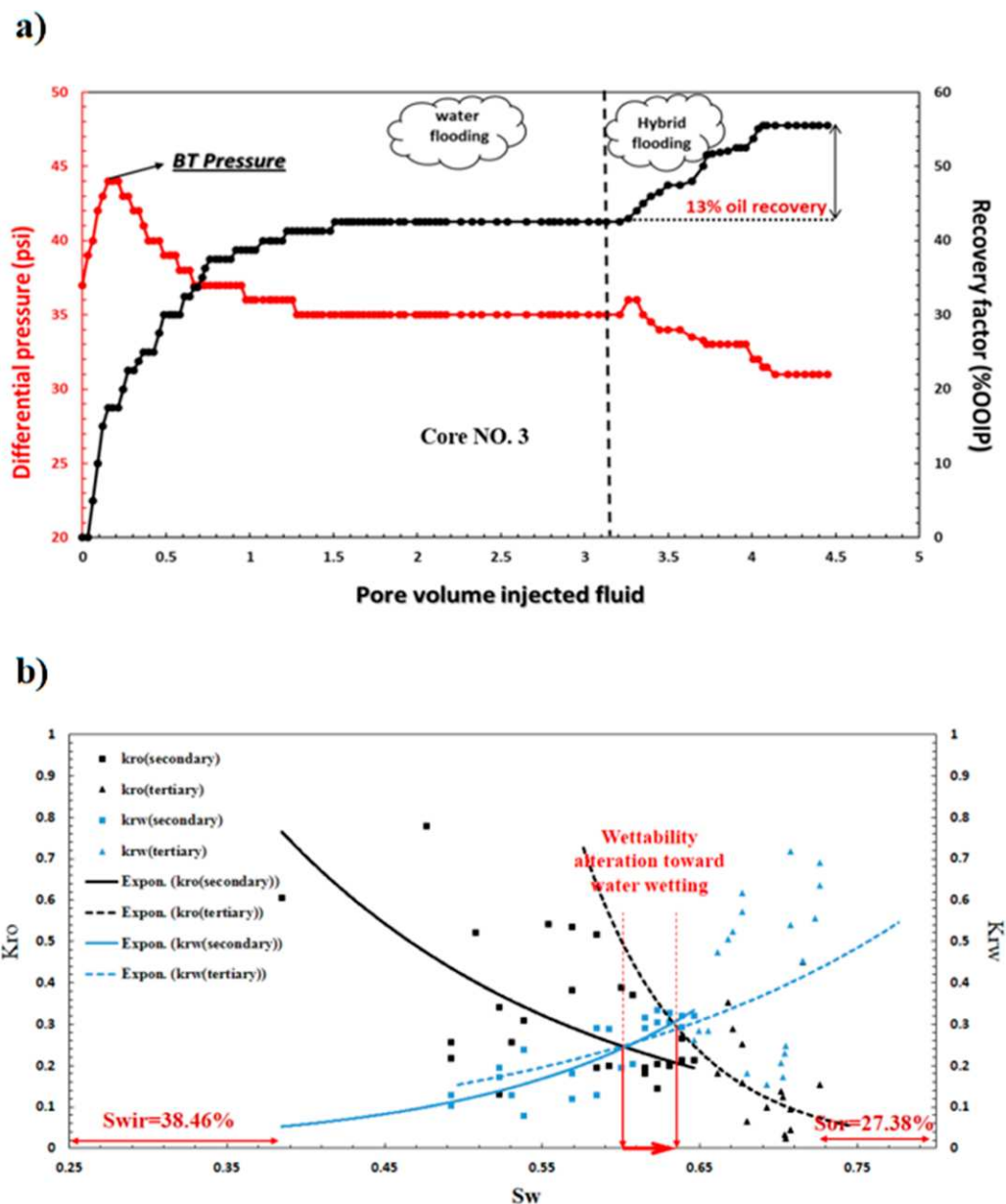


Figure 24. Dynamic core flooding results: (a) oil recovery by water and hybrid solution flooding and (b) relative permeability curve of water and hybrid solution by the JBN method.

time of fluid/solid contact is also different in contact angle measurement experiments and dynamic core flooding experiments that gain different results in this comparison. The observation of wettability alteration in each dynamic core flooding system is a difference of the wettability state induced by both seawater and EOR fluid, while in contact angle measurement experiments, EOR fluids were analyzed with the initial oil-wetted state.

The following equations were used to calculate the mobility ratio and capillary number<sup>63,64</sup>

$$M = \frac{(k/\mu)_{\text{water}}}{(k/\mu)_{\text{oil}}}$$

where  $M$ ,  $k$ , and  $\mu$  are the mobility ratio, relative permeability, velocity, and viscosity, respectively.

$$C_a = \frac{\mu V}{\gamma}$$

where  $C_a$  is the capillary number,  $\mu$  represents the viscosity,  $V$  stands for the velocity, and  $\gamma$  shows water–oil IFT.

According to the calculated relative permeability of oil and water for secondary water injection and viscosity values, mobility ratios of 27.64, 28.2, and 29.4 were obtained for core nos. 1, 2, and 3, respectively. Based on the IFT values of IFT of 27 mN/m during water flooding as secondary flooding, capillary numbers of  $3.7 \times 10^{-7}$ ,  $2.5 \times 10^{-7}$ , and  $2.8 \times 10^{-7}$  were obtained for core nos. 1, 2, and 3, respectively. Like the secondary flooding step, the mobility ratio was calculated for tertiary steps, and the 10.65, 8.3, and 10.15 values were obtained for the surfactant, nanocomposite, and hybrid flooding, respectively. The capillary numbers  $7.3 \times 10^{-6}$ ,  $9.1 \times 10^{-6}$ , and  $6.7 \times 10^{-6}$  were obtained for the surfactant, nanocomposite, and hybrid flooding, respectively.

#### 4. CONCLUSIONS

CP plant was introduced as a new natural surfactant source, and the performance of the natural surfactant was investigated in the presence of the ZnO/MMT nanocomposite as a hybrid solution on the EOR. The following results were obtained:

- (1) The IFT measurements show that the CP at CMC has the potential to reduce IFT of the oil–water from 27 to 11.4 mN/m. Also, by adding NaCl to the CMC of CP, this amount is reduced to 9.1 mN/m.
- (2) Although the ZnO/MMT nanocomposite solution does not perform well in reducing the IFT between oil and water, in combination with the extracted surfactant as a hybrid agent, it is able to reduce the IFT well and reduce its value from 27 to 2.5 mN/m.
- (3) The results of wettability alteration tests demonstrate that the CP surfactant alters the surface of carbonate rock to the weakly water-wet. When the various concentrations of NaCl are combined with the CP surfactant at CMC, the wettability becomes more water-wet.
- (4) Nanofluids have a better performance than the extracted surfactant in altering the wettability, which alters the wettability from oil-wet to strong water-wet.
- (5) Core flooding experiment results show 8.2, 6, and 13% additional oil recovery for the surfactant at optimum salinity, nanocomposite, and hybrid solution at the optimum concentrations of the nanocomposite, respectively.

#### ■ ASSOCIATED CONTENT

##### Supporting Information

The Supporting Information is available free of charge at <https://pubs.acs.org/doi/10.1021/acsomega.1c07182>.

Summary of the effects of utilized natural surfactants in the field of EOR, summary of the effects of nano-surfactant solutions in the field of EOR, composition of the seawater, compositional properties of the used crude oil, structure of the CP extract, XRD of the carbonate rock sample, schematic of the used pendant and sessile drop apparatus designed by authors, schematic of the utilized core flood apparatus, and peak list of synthesized nanocomposites and identified compounds (PDF)

#### ■ AUTHOR INFORMATION

##### Corresponding Authors

Abbas Khaksar Manshad – Department of Petroleum Engineering, Abadan Faculty of Petroleum, Petroleum

University of Technology (PUT), Abadan 6318714331, Iran; Email: [khaksar@put.ac.ir](mailto:khaksar@put.ac.ir)

Amir H. Mohammadi – Discipline of Chemical Engineering, School of Engineering, University of KwaZulu-Natal, Durban 4041, South Africa; [orcid.org/0000-0002-2947-1135](https://orcid.org/0000-0002-2947-1135); Email: [amir\\_h\\_mohammadi@yahoo.com](mailto:amir_h_mohammadi@yahoo.com)

#### Authors

Ahmad Nourinia – Department of Petroleum Engineering, Abadan Faculty of Petroleum, Petroleum University of Technology (PUT), Abadan 6318714331, Iran

Seyed Reza Shadizadeh – Department of Petroleum Engineering, Abadan Faculty of Petroleum, Petroleum University of Technology (PUT), Abadan 6318714331, Iran

Jagar A. Ali – Department of Petroleum Engineering, Faculty of Engineering, Soran University, Kurdistan Region 44008, Iraq; [orcid.org/0000-0002-7327-4243](https://orcid.org/0000-0002-7327-4243)

Stefan Iglauer – Discipline of Petroleum Engineering, School of Engineering, Edith Cowan University, Joondalup 6027 WA, Australia; [orcid.org/0000-0002-8080-1590](https://orcid.org/0000-0002-8080-1590)

Alireza Keshavarz – Discipline of Petroleum Engineering, School of Engineering, Edith Cowan University, Joondalup 6027 WA, Australia; [orcid.org/0000-0002-8091-961X](https://orcid.org/0000-0002-8091-961X)

Muhammad Ali – Discipline of Petroleum Engineering, School of Engineering, Edith Cowan University, Joondalup 6027 WA, Australia; [orcid.org/0000-0002-2446-3072](https://orcid.org/0000-0002-2446-3072)

Complete contact information is available at: <https://pubs.acs.org/10.1021/acsomega.1c07182>

#### Notes

The authors declare no competing financial interest.

#### ■ ACKNOWLEDGMENTS

The authors would like to acknowledge the Petroleum University of Technology (P.U.T) for its support and funding this study through the research grant. The authors also would like to appreciate the Shahriari laboratory center located in Abadan Institute of Technology for providing access to the required laboratory equipment.

#### ■ NOMENCLATURE

|        |   |
|--------|---|
| EOR    | enhanced oil recovery                         |
| CEOR   | chemical enhanced oil recovery                |
| NEOR   | nanotechnology-assisted enhanced oil recovery |
| RF     | recovery factor                               |
| IFT    | interfacial tension                           |
| CMC    | critical micelle concentration                |
| CP     | Cyclamen persicum                             |
| MMT    | montmorillonite                               |
| ZSC    | Ziziphus spina-christi                        |
| DDW    | double-deionized water                        |
| TGA    | thermogravimetric analysis                    |
| FT-IR  | Fourier transform infrared spectroscopy       |
| XRD    | X-ray diffraction analysis                    |
| FE-SEM | field-emission scanning electron microscopy   |
| PV     | pore volume                                   |

#### ■ REFERENCES

- (1) Saira, S.; Yin, H.; Le-Hussain, F. Effect of Alcohol-Treated CO<sub>2</sub> On Interfacial Tension Between CO<sub>2</sub> and Oil, And Oil Swelling. *Adv. Geo-Energy Res.* **2021**, *6069*, 5, 407–421.
- (2) Bahraminejad, H.; Manshad, A. K.; Keshavarz, A. Characterization, micellization behavior, and performance of a novel surfactant

- derived from *Gundelia tournefortii* plant during chemical enhanced oil recovery. *Energy Fuels* **2021**, *35*, 1259–1272.
- (3) Saira, S.; Janna, F.; Le-Hussain, F. Effectiveness of modified CO<sub>2</sub> injection at improving oil recovery and CO<sub>2</sub> storage-Review and simulations. *Energy Rep.* **2020**, *6*, 1922–1941.
- (4) Saira, S.; Ajoma, E.; Le-Hussain, F. A Laboratory Investigation of the Effect of Ethanol-Treated Carbon Dioxide Injection On Oil Recovery and Carbon Dioxide Storage. *SPE J.* **2021**, *26*, 3119–3135.
- (5) Nowrouzi, I.; Mohammadi, A. H.; Manshad, A. K. Characterization and Evaluation of a Natural Surfactant Extracted from Soapwort Plant for Alkali-Surfactant-Polymer (ASP) Slug Injection into Sandstone Oil Reservoirs. *J. Mol. Liq.* **2020**, *318*, 114369.
- (6) Bahraminejad, H.; Manshad, A. K.; Iglauer, S.; Keshavarz, A. NEOR Mechanisms and Performance Analysis in Carbonate/Sandstone Rock Coated Microfluidic Systems. *Fuel* **2022**, *309*, 122327.
- (7) He, Y.; Liao, K.; Bai, J.; Fu, L.; Ma, Q.; Zhang, X.; Ren, Z.; Wang, W. Study on a nonionic surfactant/nanoparticle composite flooding system for enhanced oil recovery. *ACS Omega* **2021**, *6*, 11068–11076.
- (8) Almahfood, M.; Bai, B. The Synergistic Effects of Nanoparticle-Surfactant Nanofluids in EOR Applications. *J. Pet. Sci. Eng.* **2018**, *171*, 196–210.
- (9) Asl, H. F.; Zargar, G.; Manshad, A. K.; Takassi, M. A.; Ali, J. A.; Keshavarz, A. Effect of SiO<sub>2</sub> Nanoparticles On the Performance of L-Arg and L-Cys Surfactants for Enhanced Oil Recovery in Carbonate Porous Media. *J. Mol. Liq.* **2020**, *300*, 112290.
- (10) Sun, X.; Zhang, Y.; Chen, G.; Gai, Z. Application of Nanoparticles in Enhanced Oil Recovery: A Critical Review of Recent Progress. *Energies* **2017**, *10*, 345.
- (11) Chhetri, A. B.; Watts, K. C.; Rahman, M. S.; Islam, M. R. Soapnut Extract as A Natural Surfactant for Enhanced Oil Recovery. *Energy Sources, Part A* **2009**, *31*, 1893–1903.
- (12) Pordel Shahri, M.; Shadizadeh, S. R.; Jamialahmadi, M. A New Type of Surfactant for Enhanced Oil Recovery. *Pet. Sci. Technol.* **2012**, *30*, 585–593.
- (13) Deymeh, H.; Shadizadeh, S. R.; Motafakkerfard, R. Experimental investigation of *Seidlitzia rosmarinus* effect on oil-water interfacial tension: Usable for chemical enhanced oil recovery. *Sci. Iran.* **2012**, *19*, 1661–1664.
- (14) Ahmadi, M. A.; Arabsahebi, Y.; Shadizadeh, S. R.; Shokrollahzadeh Behbahani, S. Preliminary Evaluation of Mulberry Leaf-Derived Surfactant On Interfacial Tension in an Oil-Aqueous System: EOR Application. *Fuel* **2014**, *117*, 749–755.
- (15) Rahmati, M.; Mashayekhi, M.; Songolzadeh, R.; Daryasafar, A. Effect of Natural Leaf-Derived Surfactants On Wettability Alteration and Interfacial Tension Reduction in Water-Oil System: EOR Application. *J. Jpn. Pet. Inst.* **2015**, *58*, 245–251.
- (16) Emadi, S.; Shadizadeh, S. R.; Manshad, A. K.; Rahimi, A. M.; Mohammadi, A. H. Effect of Nano Silica Particles On Interfacial Tension (IFT) And Mobility Control of Natural Surfactant (Cedr Extraction) Solution in Enhanced Oil Recovery Process by Nano - Surfactant Flooding. *J. Mol. Liq.* **2017**, *248*, 163–167.
- (17) Xu, D.; Kang, W.; Zhang, L.; Jiang, J.; Li, Z.; Lu, Y.; Zhang, P.; Wu, H. Ultra-Low Interfacial Tension of a Surfactant Under a Wide Range of Temperature and Salinity Conditions for Chemical Enhanced Oil Recovery. *Tenside, Surfactants, Deterg.* **2018**, *55*, 252–257.
- (18) Cheraghian, G.; Kiani, S.; Nassar, N. N.; Alexander, S.; Barron, A. R. Silica Nanoparticle Enhancement in The Efficiency of Surfactant Flooding of Heavy Oil in A Glass Micromodel. *Ind. Eng. Chem. Res.* **2017**, *56*, 8528–8534.
- (19) Haeri, F.; Rao, D. N. Precise Wettability Characterization of Carbonate Rocks to Evaluate Oil Recovery Using Surfactant-Based Nanofluids. *Energy Fuels* **2019**, *33*, 8289–8301.
- (20) Songolzadeh, R.; Moghadasi, J. Stabilizing Silica Nanoparticles in High Saline Water by Using Ionic Surfactants for Wettability Alteration Application. *Colloid Polym. Sci.* **2016**, *295*, 145–155.
- (21) Zhao, M.; Lv, W.; Li, Y.; Dai, C.; Wang, X.; Zhou, H.; Zou, C.; Gao, M.; Zhang, Y.; Wu, Y. Study On the Synergy Between Silica Nanoparticles and Surfactants for Enhanced Oil Recovery During Spontaneous Imbibition. *J. Mol. Liq.* **2018**, *261*, 373–378.
- (22) Zhong, X.; Li, C.; Li, Y.; Pu, H.; Zhou, Y.; Zhao, J. X. Enhanced Oil Recovery in High Salinity and Elevated Temperature Conditions with A Zwitterionic Surfactant and Silica Nanoparticles Acting in Synergy. *Energy Fuels* **2020**, *34*, 2893–2902.
- (23) Suleimanov, B. A.; Ismailov, F. S.; Veliyev, E. F. Nanofluid for Enhanced Oil Recovery. *J. Pet. Sci. Eng.* **2011**, *78*, 431–437.
- (24) Mohajeri, M.; Hemmati, M.; Shekarabi, A. S. An experimental study on using a nanosurfactant in an EOR process of heavy oil in a fractured micromodel. *J. Pet. Sci. Eng.* **2015**, *126*, 162–173.
- (25) Shadizadeh, S. S.; Kharat, R. Experimental Investigation of *Matricaria chamomilla* Extract Effect on Oil-Water Interfacial Tension: Usable for Chemical Enhanced Oil Recovery. *Pet. Sci. Technol.* **2015**, *33*, 901–907.
- (26) Daghlian Sofla, S. J.; Sharifi, M.; Hemmati Sarapardeh, A. Toward Mechanistic Understanding of Natural Surfactant Flooding in Enhanced Oil Recovery Processes: The Role of Salinity, Surfactant Concentration and Rock Type. *J. Mol. Liq.* **2016**, *222*, 632–639.
- (27) Betancur, S.; Carrasco-Marín, F.; Pérez-Cadenas, A. F.; Franco, C. A.; Jiménez, J.; Manrique, E. J.; Quintero, H.; Cortés, F. B. Effect of Magnetic Iron Core-Carbon Shell Nanoparticles in Chemical Enhanced Oil Recovery for Ultralow Interfacial Tension Region. *Energy Fuels* **2019**, *33*, 4158–4168.
- (28) Betancur, S.; Giraldo, L. J.; Carrasco-Marín, F.; Riazi, M.; Manrique, E. J.; Quintero, H.; García, H. A.; Franco-Ariza, C. A.; Cortés, F. B. Importance of the Nanofluid Preparation for Ultra-Low Interfacial Tension in Enhanced Oil Recovery Based on Surfactant-Nanoparticle-Brine System Interaction. *ACS Omega* **2019**, *4*, 16171–16180.
- (29) Nwideo, L. N.; Lebedev, M.; Barifcani, A.; Sarmadivaleh, M.; Iglauer, S. Wettability Alteration of Oil-Wet Limestone Using Surfactant-Nanoparticle Formulation. *J. Colloid Interface Sci.* **2017**, *504*, 334–345.
- (30) Al-zuabe, M. a.; Ismail, Y.; Hasan, D.; Alhrou, H.; Al-Zeidaneen, S.; Albawarshi, Y.; Abu-Hamra, E. Antimicrobial Effect of Cyclamen Persicum Tuber Extracts Against Bacteria and Candida Species. *J. Pure Appl. Microbiol.* **2019**, *13*, 107–116.
- (31) Hussien, F. M. A. Activated carbon from Cyclamen Persicum Tubers for Diclofenac removal from aqueous solution. Master's dissertation, An-Najah National University, Nablus, Palestine, 2013.
- (32) Jodeh, S.; Abdelwahab, F.; Jaradat, N.; Warad, I.; Jodeh, W. Adsorption of diclofenac from aqueous solution using *Cyclamen persicum* tubers based activated carbon (CTAC). *Journal of the Association of Arab Universities for Basic and Applied Sciences* **2016**, *20*, 32–38.
- (33) Jaradat, N. A.; Abualhasan, M.; Ali, I. Comparison of Anti-Oxidant Activities and Exhaustive Extraction Yields Between Wild and Cultivated *Cyclamen Persicum*, *Malva Sylvestris* and *Urtica Pilulifera* Leaves. *J. Appl. Pharmaceut. Sci.* **2015**, *5*, 101–106.
- (34) Sani, H. A.; Ahmad, M. B.; Hussein, M. Z.; Ibrahim, N. A.; Musa, A.; Saleh, T. A. Nanocomposite Of ZnO With Montmorillonite For Removal Of Lead And Copper Ions From Aqueous Solutions. *Process Saf. Environ. Prot.* **2017**, *109*, 97–105.
- (35) Maham, M.; Nasrollahzadeh, M.; Mohammad Sajadi, S. Facile Synthesis of Ag/ZrO<sub>2</sub> Nanocomposite as A Recyclable Catalyst for The Treatment of Environmental Pollutants. *Compos. B Eng.* **2020**, *185*, 107783.
- (36) Arashiro, E. Y.; Demarquette, N. R. Use of The Pendant Drop Method to Measure Interfacial Tension Between Molten Polymers. *Mater. Res.* **1999**, *2*, 23–32.
- (37) Shahrabadi, A.; Bagherzadeh, H.; Roustaei, A.; Golghanddashti, H. *Experimental Investigation of HLP Nanofluid Potential to Enhance Oil Recovery: A Mechanistic Approach. All Days; OnePetro*, 2012.
- (38) Mousavi Moghadam, A.; Baghban Salehi, M. Enhancing Hydrocarbon Productivity Via Wettability Alteration: A Review On the Application of Nanoparticles. *Rev. Chem. Eng.* **2018**, *35*, 531–563.

- (39) Talal, J. H.; Mohammed, D. B.; Jawad, K. H. Fabrication of Hydrophobic Nanocomposites Coating Using Electrospinning Technique for Various Substrate. *J. Phys. Conf.* **2018**, *1032*, 012033.
- (40) Samal, K.; Das, C.; Mohanty, K. Eco-Friendly Biosurfactant Saponin for The Solubilization of Cationic and Anionic Dyes in Aqueous System. *Dyes Pigm.* **2017**, *140*, 100–108.
- (41) Almutairi, M. S.; Ali, M. Direct Detection of Saponins in Crude Extracts of Soapnuts by FTIR. *Nat. Prod. Res.* **2014**, *29*, 1271–1275.
- (42) Li, R.; Wu, Z. L.; Wang, Y. J.; Li, L. L. Separation of Total Saponins from The Pericarp of Sapindus Mukorossi Gaerten. By Foam Fractionation. *Ind. Crops Prod.* **2013**, *51*, 163–170.
- (43) Tehrani, M. M.; Molahasani, N.; Aghabeygi, S. Sonosynthesis and characterization of nano ZnO/Montmorillonite nano clay composite via Sol-Gel method. *Int. J. Bio-Inorg. Hybr. Nanomater.* **2016**, *5*, 167–172.
- (44) Chakraborty, T.; Chakraborty, A.; Shukla, M.; Chattopadhyay, T. ZnO-Bentonite nanocomposite: an efficient catalyst for discharge of dyes, phenol and Cr(VI) from water. *J. Coord. Chem.* **2019**, *72*, 53–68.
- (45) Xiong, G.; Pal, U.; Serrano, J. G.; Ucer, K. B.; Williams, R. T. Photoluminescence and FTIR Study of ZnO Nanoparticles: The Impurity and Defect Perspective. *Phys. Status Solidi C* **2006**, *3*, 3577–3581.
- (46) Ravi, S. G.; Shadizadeh, S. R.; Moghaddasi, J. Core Flooding Tests to Investigate the Effects of IFT Reduction and Wettability Alteration On Oil Recovery: Using Mulberry Leaf Extract. *Pet. Sci. Technol.* **2015**, *33*, 257–264.
- (47) Pal, N.; Saxena, N.; Divya Laxmi, K. V.; Mandal, A. Interfacial Behaviour, Wettability Alteration and Emulsification Characteristics of a Novel Surfactant: Implications for Enhanced Oil Recovery. *Chem. Eng. Sci.* **2018**, *187*, 200–212.
- (48) Onsager, L. Deviations from Ohm's Law in Weak Electrolytes. *J. Chem. Phys.* **1934**, *2*, 599–615.
- (49) Kumar, A.; Mandal, A. Synthesis and Physicochemical Characterization of Zwitterionic Surfactant for Application in Enhanced Oil Recovery. *J. Mol. Liq.* **2017**, *243*, 61–71.
- (50) Nowrouzi, I.; Mohammadi, A. H.; Manshad, A. K. Water-Oil Interfacial Tension (IFT) Reduction and Wettability Alteration in Surfactant Flooding Process Using Extracted Saponin from Anabasis Setifera Plant. *J. Pet. Sci. Eng.* **2020**, *189*, 106901.
- (51) Buckley, J. S.; Liu, Y.; Monsterleet, S. Mechanisms of Wetting Alteration by Crude Oils. *SPE J.* **1998**, *3*, 54–61.
- (52) Jarrahian, K.; Seiedi, O.; Sheykhan, M.; Sefti, M. V.; Ayatollahi, S. Wettability Alteration of Carbonate Rocks by Surfactants: A Mechanistic Study. *Colloids Surf., A* **2012**, *410*, 1–10.
- (53) Benabid, F.; Kharchi, N.; Zouai, F.; Mourad, A.-H. I.; Benachour, D. Impact of Co-Mixing Technique and Surface Modification of ZnO Nanoparticles Using Stearic Acid On Their Dispersion into HDPE to Produce HDPE/ZnO Nanocomposites. *Polym. Polym. Compos.* **2019**, *27*, 389–399.
- (54) Nazarahari, M. J.; Manshad, A. K.; Ali, M.; Ali, J. A.; Shafiei, A.; Sajadi, S. M.; Moradi, S.; Iglauer, S.; Keshavarz, A. Impact of A Novel Biosynthesized Nanocomposite (SiO<sub>2</sub>@Montmorillonite@Xanthan) On Wettability Shift and Interfacial Tension: Applications for Enhanced Oil Recovery. *Fuel* **2021**, *298*, 120773.
- (55) Lau, H. C.; Yu, M.; Nguyen, Q. P. Nanotechnology for Oilfield Applications: Challenges and Impact. *J. Pet. Sci. Eng.* **2017**, *157*, 1160–1169.
- (56) Dolai, J.; Mandal, K.; Jana, N. R. Nanoparticle Size Effects in Biomedical Applications. *ACS Appl. Nano Mater.* **2021**, *4*, 6471–6496.
- (57) Chengara, A.; Nikolov, A. D.; Wasan, D. T.; Trokhymchuk, A.; Henderson, D. Spreading of Nanofluids Driven by The Structural Disjoining Pressure Gradient. *J. Colloid Interface Sci.* **2004**, *280*, 192–201.
- (58) Manshad, A. K.; Ali, J. A.; Haghighi, O. M.; Mohammad Sajadi, S.; Keshavarz, A. Oil Recovery Aspects Of ZnO/SiO<sub>2</sub> Nano-Clay In Carbonate Reservoir. *Fuel* **2022**, *307*, 121927.
- (59) Mcelfresh, P.; Olguin, C.; Ector, D. *The Application of Nanoparticle Dispersions to Remove Paraffin and Polymer Filter Cake Damage. All Days*; OnePetro, 2012.
- (60) Bahraminejad, H.; Khaksar Manshad, A.; Riazi, M.; Ali, J. A.; Sajadi, S. M.; Keshavarz, A. CuO/TiO<sub>2</sub>/PAM as a Novel Introduced Hybrid Agent for Water-Oil Interfacial Tension and Wettability Optimization in Chemical Enhanced Oil Recovery. *Energy Fuels* **2019**, *33*, 10547–10560.
- (61) Meng, X. W.; Li, Y.; Shen, L.; Yang, X. Q. Reinforcing A Water Bridge in A Disjoint Nanochannel. *Europhys. Lett.* **2020**, *131*, 20003.
- (62) Horozov, T. S.; Aveyard, R.; Clint, J. H.; Binks, B. P. Order-Disorder Transition in Monolayers of Modified Monodisperse Silica Particles at the Octane–Water Interface. *Langmuir* **2003**, *19*, 2822–2829.
- (63) Conn, C. A.; Ma, K.; Hirasaki, G. J.; Biswal, S. L. Visualizing Oil Displacement with Foam in A Microfluidic Device with Permeability Contrast. *Lab Chip* **2014**, *14*, 3968–3977.
- (64) Majidaie, S.; Muhammad, M.; Tan, I.; Demiral, B. Green Surfactant for Enhanced Oil Recovery. *2011 National Postgraduate Conference*, 2011.

## Recommended by ACS

### Synergistic Effect of Low Salinity Surfactant Nanofluid on the Interfacial Tension of Oil–Water Systems, Wettability Alteration, and Surfactant Adsorption on the Quartz Surface

Devakumar N. P., Jitendra S. Sangwai, et al.

MAY 05, 2023  
ENERGY & FUELS

READ 

### Experimental Investigation of the Synergistic Effect of Two Nonionic Surfactants on Interfacial Properties and Their Application in Enhanced Oil Recovery

Rohit Kumar Saw, Ajay Mandal, et al.

MARCH 24, 2023  
ACS OMEGA

READ 

### Experimental Investigation on Spontaneous Imbibition of Surfactant Mixtures in Low Permeability Reservoirs

Huan Wang, Mingwei Gao, et al.

APRIL 04, 2023  
ACS OMEGA

READ 

### Investigation of Hybrid Nanoparticle–Acid Fluids (HNAFs): Influence of Wettability and Interfacial Tension Mechanisms in Harsh Carbonate Reservoirs for Improved Oil Recovery

Mohamed Haroun, Soham Punjabi, et al.

NOVEMBER 04, 2022  
ACS OMEGA

READ 

Get More Suggestions >

## **Appendix 9**

*Effect of Fe<sub>3</sub>O<sub>4</sub>/Mineral–Soil Nanocomposites on Wettability Alteration and Oil Production Under the Spontaneous Imbibition Process*

**Jagar A. Ali**

Arabian Journal for Science and Engineering (2023) 48:9259–9268



## Effect of Fe<sub>3</sub>O<sub>4</sub>/Mineral–Soil Nanocomposites on Wettability Alteration and Oil Production Under the Spontaneous Imbibition Process

Jagar A. Ali<sup>1,2</sup> Received: 17 June 2022 / Accepted: 21 September 2022 / Published online: 29 September 2022  
© King Fahd University of Petroleum & Minerals 2022

### Abstract

Nanoparticles as novel EOR agents are used to enhance the production of crude oil. This improvement is due to the improved surface activity at the crude oil–brine–rock interface and disjoining pressure. The aim of this study was to examine the role of the greenly synthesized nanocomposites (NCs) in EOR applications. For this purpose, Fe<sub>3</sub>O<sub>4</sub>/mineral–soil NCs were synthesized from the extract of *Euodia hortensis* plant and characterized using several analytical techniques. Nanofluids were prepared from dispersing the synthesized NCs in distilled water at different ranges of concentrations from 250 to 1000 ppm. The role of the developed nanofluids on the IFT reduction, wettability alteration and oil recovery was experimentally examined. Different IFT values of crude oil with the presence of nanofluids were estimated, and the minimum IFT of 3.69 mN/m was obtained with NF1000 solution formulated from mixing 1000 ppm within the distilled water, while the wettability was highly altered toward the strong water-wet system from 99.15 to 22° contact angle when dispersing 1000 ppm of NCs in water. In addition, NF1000 solution was enabled to improve oil recovery by 11.28% original oil recovery (OOIP) under the spontaneous imbibition process.

**Keywords** Green synthesis · Nanocomposites · Nanofluid · Interfacial tension · Wettability · Spontaneous imbibition

### 1 Introduction

Water injection is commonly used worldwide to maintain the reservoir pressure and increase oil recovery, which is able to produce around 40% of crude oil [1, 2]. The remaining 60% of the original oil in place (OOIP) in the reservoir is bypassed and/or trapped because of the poor sweep and displacement efficiencies of the injected water [3, 4]. The trapped hydrocarbons are usually extracted from the reservoirs due to the change in rock/fluid/fluid interactions using several chemical EOR methods, such as surfactant, polymer, low salinity water and alkaline [5, 6]. Chemical methods are dominant in some mechanisms; surfactants are active the IFT reduction [7, 8], low salinity can alter the wettability of rock surfaces, and the mobility ratio is controlled by polymers [9].

Nowadays, nanoscale materials are dispersed in water or other solvents to prepare nanofluids with improved physico-chemical properties, which are used in different applications in the oil and gas industry [10–13]. In 2012, Roustaiei et al. used hydrophobic and lipophilic polysilicon (HLP) and neutrally wet polysilicon (NWP) NPs to improve the IFT reduction and oil recovery [14]. Authors reported that three used types of NPs had a positive impact on oil recovery, but HLP reduced IFT more greatly compared with others. The influences of Fe<sub>2</sub>O<sub>3</sub>, Al<sub>2</sub>O<sub>3</sub> and SiO<sub>2</sub> NPs on the EOR performance were studied by Joonaki and Ghanaatian [15]. Since the high reduction in the value of IFT and strong alteration in the wettability are obtained, Al<sub>2</sub>O<sub>3</sub> and SiO<sub>2</sub> enabled to improve oil recovery more efficiently compared with Fe<sub>2</sub>O<sub>3</sub>. Bayat et al. [16] developed deionized water nanofluids using Al<sub>2</sub>O<sub>3</sub> and TiO<sub>2</sub> NPs and demonstrated improved recovery in a carbonate system at different temperatures. Their experimental results showed that the impact of TiO<sub>2</sub> in IFT reduction and recovery improvement is less compared with Al<sub>2</sub>O<sub>3</sub>. Furthermore, improving the surface of the NPs can improve their activity and role in improving oil recovery due to providing more EOR mechanisms. In this way, Ju and Fan [17] reported improved oil recovery up to 21% by

✉ Jagar A. Ali  
jagar.ali@soran.edu.iq

<sup>1</sup> Department of Petroleum Engineering, Faculty of Engineering, Soran University, Soran, Kurdistan Region, Iraq

<sup>2</sup> Department of Geology, Palacký University, 17. Listopadu 12, 77146 Olomouc, Czech Republic



preparing and applying the polymer-coated SiO<sub>2</sub> nanomaterial in IFT reduction and wettability alteration. Synthesizing Fe<sub>3</sub>O<sub>4</sub>/chitosan nanocomposites was successful in extracting 10.8% OOIP additional crude oil due to reducing the IFT forces between oil and aqueous phases, altering the wettability behavior of carbonate rock [18]. In addition, Qi et al. [19] coated the surface of SiO<sub>2</sub> NPs with polymer and studied its effect on the IFT and wettability behaviors. They are successful in improving oil recovery by extra 10% OOIP, while Lim and Wasan [20] were not successful in producing an extra crude oil from carbonate rocks by dispersing copper NPs within the polyethylene glycol. Meanwhile, Zhang et al. [21] produced additional 17% OOIP by mixing the silica NPs in polyethylene glycol. In addition, Nowrouzi et al. [22] studied the impact of titanium oxide nanoparticles on oil recovery factor by spontaneous imbibition. They reported that TiO<sub>2</sub> at 1000 ppm concentration enabled to produce 70% OOIP by spontaneous imbibition process. The role of TiO<sub>2</sub> induced by xanthan gum in EOR was investigated by Keykhosravi et al. [23]. Their obtained results showed that extra 25% OOIP was extracted by injecting the polymer nanofluid solution. Nourinia et al. [24] investigated the role of the ZnO/Montmorillonite nanocomposites in EOR applications. The used NCs was capable in reducing IFT by 46%, alter the wettability toward the water-wet and improve oil recovery by 7.8% OOIP.

The ultimate goal of this study was to synthesize the objective-oriented nanocomposites in eco-friendly and green way from the extract of the *Euodia hortensis* plant to be used in EOR applications. The validity of the synthesized NCs was confirmed using different analytical techniques including SEM, XRD and FTIR. The change in the values of IFT and contact angle was investigated under the influence of the synthesized NCs.

## 2 Materials and Methods

### 2.1 Materials

In this study, several chemicals with the high purity of 99% were purchased from Merck Company for the synthesis of nanomaterials (sodium carbonate, Na<sub>2</sub>CO<sub>3</sub>; iron(III) chloride hexahydrate, FeCl<sub>3</sub>·6H<sub>2</sub>O; n-hexane) and cleaning the rock samples (methanol and ethanol). For aging rock pellets, saturation of core plugs and performing the experimental measurements of IFT, CA and coreflooding, a sample of the crude oil with the density of 0.879 gm/cc (29.5° API) and viscosity of 1.37 cP was used. In addition, the rock samples were taken from the carbonate outcrops for coreflooding and contact angle measurements. For synthesizing the nanocomposites in a green way, *Euodia hortensis leaves* were used. *Euodia hortensis* is from the family of Rutaceae

that is a shrub to small tree and mostly distributed in the South Pacific. The plant has some medicinal effects such as treating yellow eyes and urine and neurological diseases. The phytochemical content of the plant is mainly included in essential oils, menthofuran, evodone, hortensol, berberine, furoquinoline, alkaloids, phenolics and flavonoids in which the last three constituents are major components of the plant extract. Meanwhile, the presence of the considerable amount antioxidants within the *Euodia hortensis* plant was confirmed [25–29].

### 2.2 Synthesis and Characterization of Fe<sub>3</sub>O<sub>4</sub>/Mineral–Soil Nanocomposites

The synthesis of Fe<sub>3</sub>O<sub>4</sub>/mineral–soil NCs was carried out in several steps; (1) Preparation of the plant extract, (2) Synthesis of Fe<sub>3</sub>O<sub>4</sub> nanoparticles, (3) Development of nanocomposites, and (4) Characterization of the synthesized NCs as shown in Fig. 1. The *Euodia hortensis* leaf was dried at ambient temperature and powdered. In 500-mL flask, 50 gm of the dried powder was mixed within the distilled water using magnetic hot plat stirrer at 70 °C for 2 h. The achieved extract was then filtered using the centrifugation at 7000 rpm. Afterward, 5 gm of FeCl<sub>3</sub>·6H<sub>2</sub>O and a certain amount of Na<sub>2</sub>CO<sub>3</sub> to keep pH above 10 were mixed with 100 mL of the filtered extract in 250-mL flask. The mixture was well mixed until the dark color was obtained and filtered using the centrifuge to separate the precipitate. The collected precipitate was burned in an oven and then washed using ethanol to achieve the green iron oxide NPs. Lastly, the synthesized NPs were mixed with 12 gm of natural mineral soil using a refluxing system at 70 °C and 700 rpm for 12 h to obtain Fe<sub>3</sub>O<sub>4</sub>/mineral–soil NCs. The validity of synthesized NCs was confirmed by conducting several analytical techniques of scanning electron microscope (SEM), X-ray diffraction (XRD and Fourier transform infrared spectroscopy (FTIR).

### 2.3 Preparation and Characterization of Nanofluids

Nanofluid, as EOR injection solutions, was formulated from mixing the nanomaterials within the aqueous phase; water was selected in this study. Nanofluids are those fluids that carry the nanomaterials in the porous media [30]. In this study, the synthesized green NCs were mixed with water at different concentrations of 250, 500, 750 and 1000 ppm to formulate NF250, NF500, NF750 and NF1000 EOR injection solutions using the magnetic stirrer hot plat for 2–3 h at ambient temperature and 600 rpm. In order to obtain the better dispersion stability of the nanofluids, they were mixed using the ultrasonic homogenizer for 30 min. Afterward, the main characteristics (pH and conductivity) of the formulated nanofluids were measured.

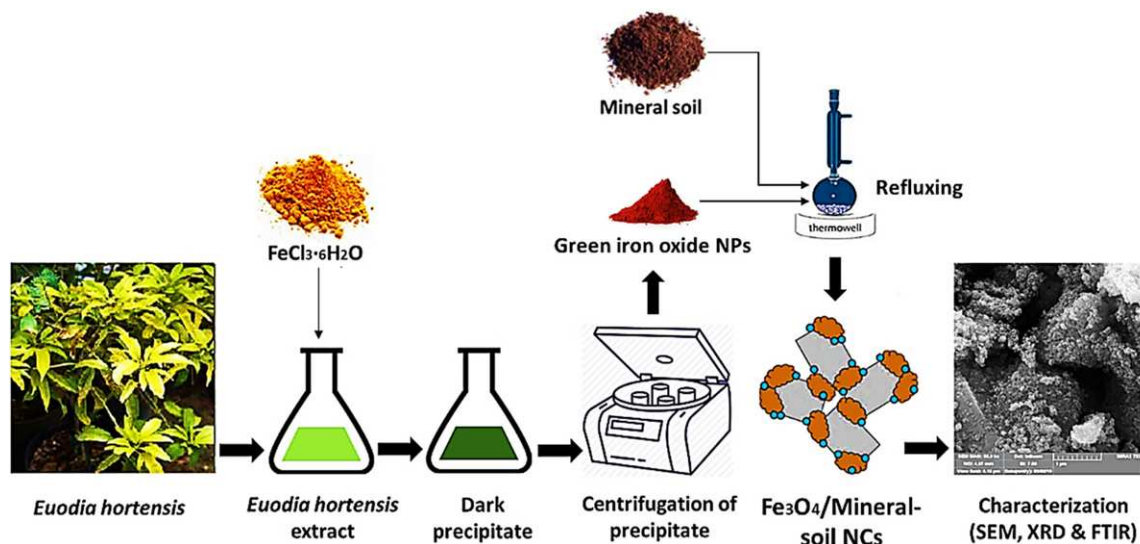


Fig. 1 Schematic illustration of the green synthesis of  $\text{Fe}_3\text{O}_4$ /mineral–soil NCs from the extract of *Euodia hortensis* plant

## 2.4 IFT and Contact Angle Measurements

The schematic illustration of the setup used in measuring the IFT and contact angle of the oil droplet with the presence of the nanofluids is shown in Fig. 2. As can be seen, the used setup consists of the HD camera, pumps, projection light, chambers and computer. To measure the IFT, the high-resolution camera was used to take the image of the crude oil droplet and transferred to the computer to measure its dimensions (see Fig. 2i). In addition, the wettability of the used carbonate rock was determined using the contact angle measured for the crude oil droplet on the surface of the prepared rock slices using the theory shown in Fig. 2. As can be seen, the state can be defined as the oil-wet when the contact angle is higher  $90^\circ$  (see Fig. 2iv), neutral wet when the contact angle equals to  $90^\circ$  (see Fig. 2iii) or water-wet at the contact angle less than  $90^\circ$  (see Fig. 2ii) [31, 32]. The contact angle of the crude oil droplet was measured using the setup shown in Fig. 2v with the presence of  $\text{Fe}_3\text{O}_4$ /mineral–soil NCs at different concentrations. From the collected rock samples, the smooth slices about 2 mm were prepared. The prepared thin slices were carefully polished and cleaned by distilled water and toluene. The cleaned and dried rock pellets were then immersed and left within the crude oil for 1 week to obtain the aging. Then, the aged thin slices were put into the formulated nanofluids for 2 days to evaluate the performance of the synthesized NCs at different concentrations.

## 2.5 Spontaneous Imbibition

The experimental setup of the spontaneous imbibition (SI) test used in this study to evaluate the performance of the synthesized NCs in improving oil recovery is shown in Fig. 3. The setup consists of an Amott cell installed in an oven, a piston, a manual pump,  $\text{CO}_2$  cylinder, gauges and valves [22]. Two core plugs shown in Table 1 were used for the spontaneous imbibition tests. The porosity and permeability of the core plugs are ranged between 17 and 18% and about 7.5 mD, respectively. The initial water saturation of core plugs 1 and 2 is 21 and 23.4%, respectively. After conducting the rock properties measurements, the prepared core plugs were saturated with the crude oil for two weeks. The saturated plugs were placed within the Amott cells and filled with water using the burette to the specific level (see Fig. 3). The experimental test was monitored to determine the amount of the oil expelled from the core plugs and recorded as % of original oil in place (%OOIP) versus for 28 days at  $50^\circ\text{C}$ . In this study, the aqueous phase of water and nanofluid is prepared from mixing 1000 ppm of the prepared  $\text{Fe}_3\text{O}_4$ /mineral–soil NCs within water.

**Fig. 2** Schematic illustration of IFT and CA measurement setup for fluid/fluid and fluid/fluid/rock systems exist in this study: i) IFT measurement, and v) contact angle measurement (CA)

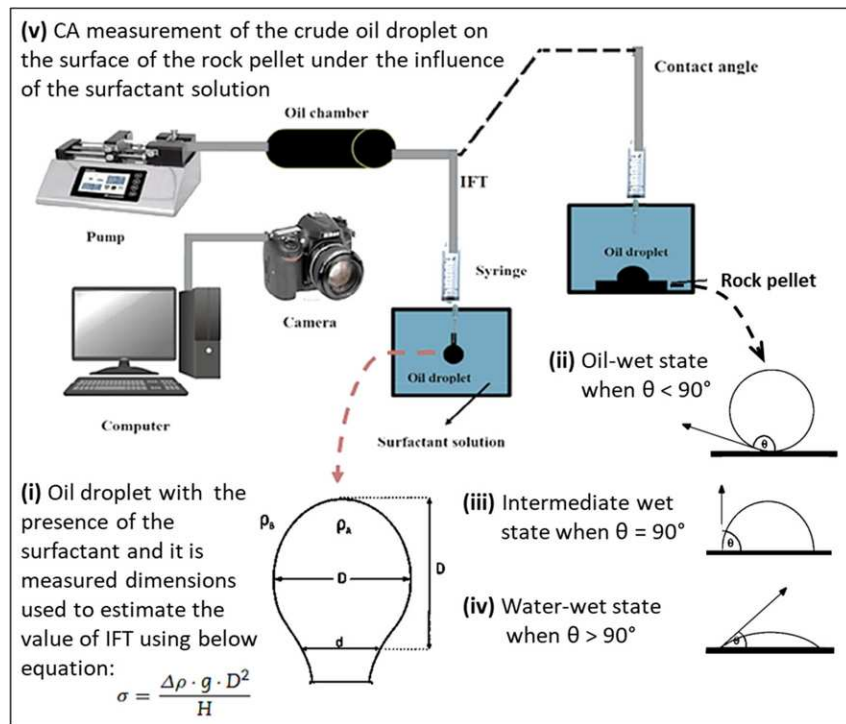


**Fig. 3** Schematic illustration of the spontaneous imbibition setup

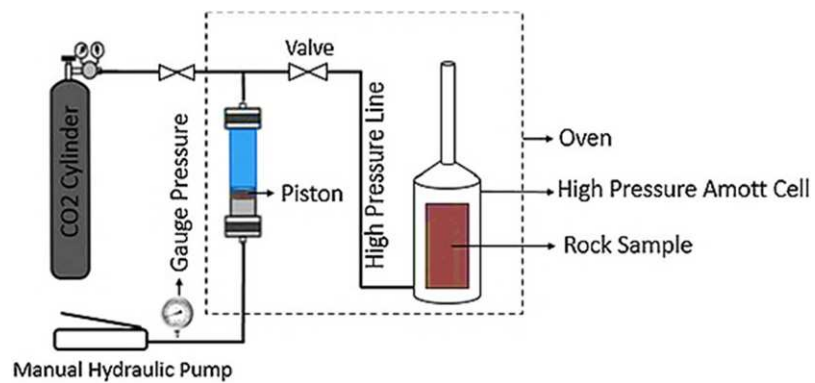


**Table 1** Main features of the carbonate core plugs used in the study

| Core plug | L (cm) | D (cm) | Porosity (%) | K (mD) | PV (cc) | OOIP (cc) | Swi (%) | Sor (%) |
|-----------|--------|--------|--------------|--------|---------|-----------|---------|---------|
| Plug#1    | 8.5    | 3.7    | 17.23        | 7.36   | 9.31    | 7.35      | 21.0    | 79.0    |
| Plug#2    | 8.4    | 3.7    | 18.41        | 7.55   | 10.17   | 7.79      | 23.4    | 76.6    |

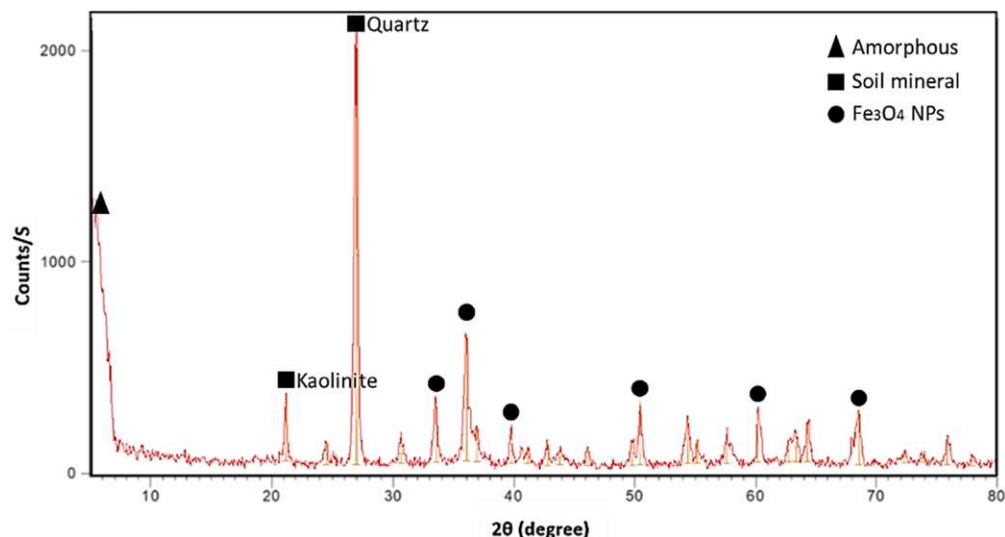
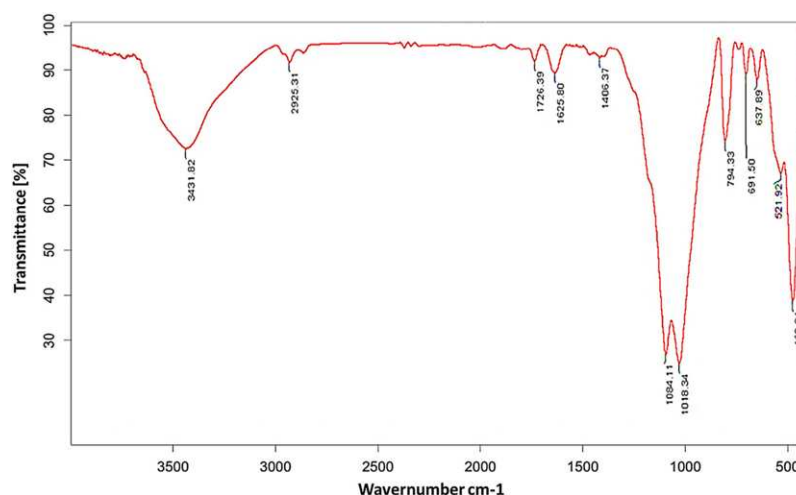


Fig. 4 XRD pattern of green synthesized  $\text{Fe}_3\text{O}_4$ /mineral-soil NCs

Fig. 5 FTIR spectra of green synthesized  $\text{Fe}_3\text{O}_4$ /mineral-soil nanocomposites



### 3 Results and Discussions

#### 3.1 Characterization of $\text{Fe}_3\text{O}_4$ /Mineral-Soil NCs

XRD spectrum of the synthesized NCs is shown in Fig. 4. As can be seen, the XRD spectrum of  $\text{Fe}_3\text{O}_4$ /mineral-soil NCs contains all the peaks associated with the crystalline planes of magnetite NPs along with the mineral soil. The peak with the highest intensity at the diffraction angle of  $27^\circ$  is related to the magnetite nanoparticles. Other existing peaks in the diffractogram suggest the availability of the polymer chain which is the mineral soil. In addition, Fig. 5 presents the FTIR analysis of the  $\text{Fe}_3\text{O}_4$ /mineral-soil NCs at the wavenumber ranged

from 450 to  $4000\text{ cm}^{-1}$  and ambient temperature. The existing main peaks at  $462.94$ ,  $1018.34$ ,  $1084.11$ ,  $3431.82\text{ cm}^{-1}$  confirm the deposition of the phytochemicals on the surface of the nanostructure available in the synthesized of  $\text{Fe}_3\text{O}_4$  and mineral soil. The bending peak of S–O group can be seen at the wavenumber of  $462\text{ cm}^{-1}$ , and the stretching vibration of S=O group is observed at  $1018\text{ cm}^{-1}$ . However, a very broad trough of O–H stretch is recognized at the wavenumber of  $3431\text{ cm}^{-1}$ . Figure 6 illustrates the SEM images of  $\text{Fe}_3\text{O}_4$ /mineral-soil NCs. The size, shape, morphology and the distribution of the particles within the synthesized NCs are verified. As can be seen, the nanoparticles on the surface of the mineral-soil have the quasi-spherical shape with a size

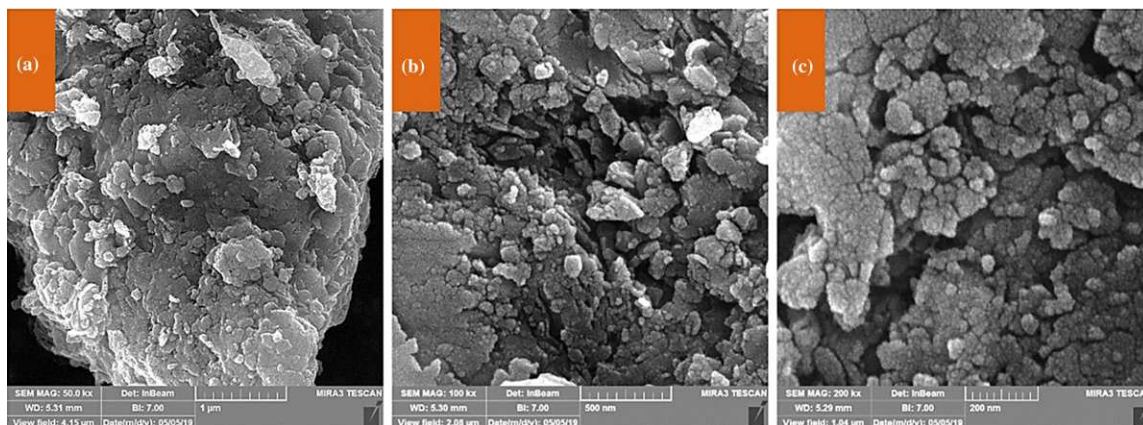


**Fig. 6** SEM morphologies of the  $\text{Fe}_3\text{O}_4/\text{mineral-soil}$  NCs; **a** 1  $\mu\text{m}$ , **b** 500 nm, and **c** 200 nm

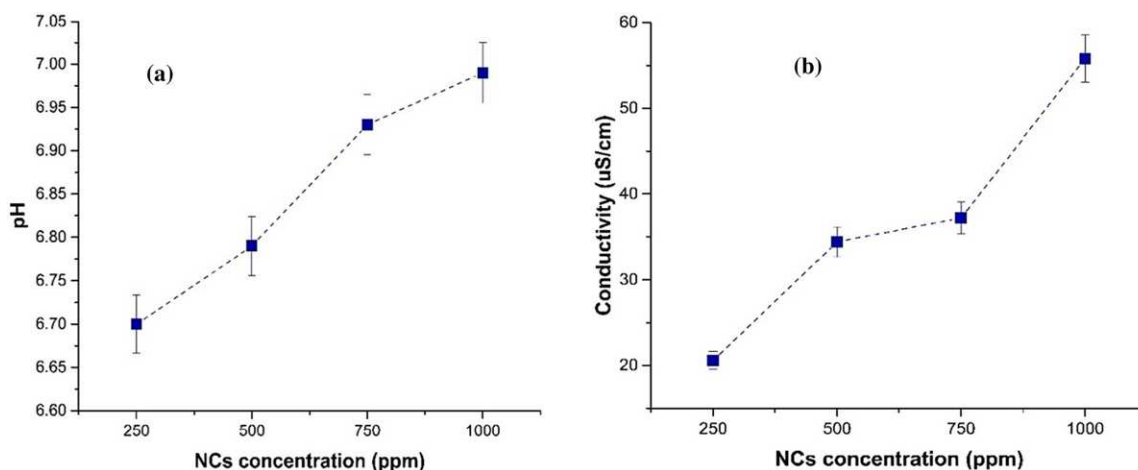


**Fig. 7** Properties of the formulated nanofluids at different concentrations; **a** pH, and **b** conductivity

ranged between 10 and 50 nm [33]. These analyses confirmed the synthesis of the green  $\text{Fe}_3\text{O}_4/\text{mineral-soil}$  NCs.

### 3.2 Characterization of Nanofluids

The prepared nanofluids from  $\text{Fe}_3\text{O}_4/\text{mineral-soil}$  NCs at different concentrations were characterized using pH and conductivity. The particle aggregation and the suspension stability of the nanomaterials are significantly influenced by pH as stated by Fovet and Gal [34] and Wen et al. [35]. They reported that a solution with the pH value ranged between 6 and 7 could have a high suspension stability. The pH values measured of the developed nanofluids are shown in Fig. 7a. As can be seen, a minimum pH of 6.7 was measured from the nanofluid containing 250 ppm of  $\text{Fe}_3\text{O}_4/\text{mineral-soil}$  NCs. The pH was gradually increased by increasing the concentration of the synthesized NCs from 250 to 1000 ppm. Even

though the variation is not high and a weak impact of the NCs concentration was identified, the change happened in the value of pH was favorable as gives a high stability [34, 35]. The maximum pH value obtained at 1000 ppm of NCs is 7, while Fig. 7b shows the conductivity of the prepared nanofluids. As is obvious, the value of conductivity is varied between 20 and 55  $\mu\text{S}/\text{cm}$ . The minimum conductivity of 20  $\mu\text{S}/\text{cm}$  was measured at nanofluid prepared from concentration of 250 ppm, and the maximum conductivity of 55  $\mu\text{S}/\text{cm}$  was recorded at the concentration of 1000 ppm of  $\text{Fe}_3\text{O}_4/\text{mineral-soil}$  NCs.

### 3.3 IFT Reduction

The reduction in the IFT value is crucial in improving oil recovery that was achieved with the influence of  $\text{Fe}_3\text{O}_4/\text{mineral-soil}$  NCs. The maximum value of IFT was

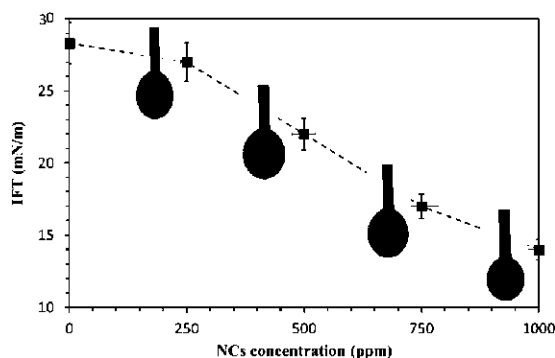


**Fig. 8** IFTs of crude oil/nanofluid systems at different concentration from 250 to 1000 ppm

recorded for the crude–oil/water system when no nanomaterials were existed which is 28.3 mN/m. The IFT started to be reduced directly after adding a small percentage of the synthesized NCs of 250 ppm into water. At this stage, the decline was 5% from 28.3 to 27 mN/m as demonstrated schematically by the shape of the crude oil in Fig. 8. The IFT was continuously reduced by 19% when the concentration of the  $\text{Fe}_3\text{O}_4/\text{mineral}$ –soil NCs was doubled to 500 ppm. In addition, a better reduction in the value of IFT can be seen when the concentration of the synthesized NCs was increased to 750 ppm. With increasing the concentration of the  $\text{Fe}_3\text{O}_4/\text{mineral}$ –soil NCs within water, a higher percentage of the reduction in the value of IFT was noticed. Thus, with having a nanofluid prepared from dispersing 750 ppm within water a reduction of 23% was achieved. The IFT of the oil droplet was continued in reduction to its minimum value of 14 mN/m with the presence of NF1000. Overall, the IFT was dropped by 50.5% under the influence of the prepared nanocomposites from 28.3 to 14 mN/m (see Fig. 8).

### 3.4 Wettability Alteration

The wettability alteration has a significant role in improving oil recovery when the oil-wet alters to water-wet in the porous media. This happens by reducing the disjoining pressure exists in the interference between the aqueous phases exit on the surface of the rock. In this study, the wettability alteration was estimated based on the values of the contact angles (CAs) measured for the crude oil droplets on the surface of the rock slices with and without the presence of the nanofluids, as shown in Fig. 9. As can be seen, a strong oil-wet state with the contact angle of  $134^\circ$  was recorded before adding the synthesized NCs into water. Meanwhile, the wettability was changed to oil-wet by reducing the contact angle to  $99.15^\circ$  with the presence of NF250 solution at 250 ppm of  $\text{Fe}_3\text{O}_4/\text{mineral}$ –soil NCs. The value of the contact angle is

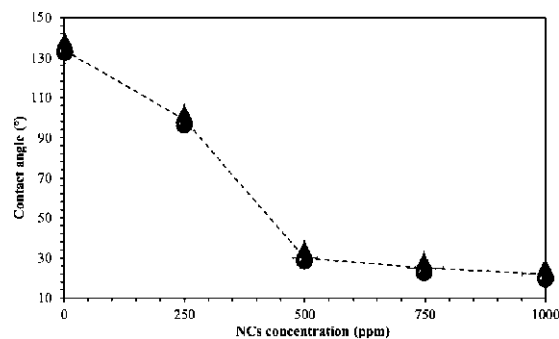


**Fig. 9** Contact angles the crude oil droplets on carbonate slices under the impact of  $\text{Fe}_3\text{O}_4/\text{mineral}$ –soil NCs

then decreased with increase in the concentration of the synthesized NCs. A sharp decline ranged of 77.5% in the value of the contact angle was observed when the concentration of the green NCs was doubled to 500 ppm. The reduction in the value of the contact was continued to  $24.8^\circ$  and  $22^\circ$  by adding 750 and 1000 ppm of  $\text{Fe}_3\text{O}_4/\text{mineral}$ –soil NCs. In addition, the mechanism of the wettability alteration along with the distribution of the crude oil on the carbonate slices with existing the nanofluids (NF250, NF500 and NF1000) is shown in Fig. 10. As is obvious, the minimum contact angle was achieved with NF1000 solution which is  $22^\circ$  when the crude oil is almost free. This proves a significant alteration of the wettability from the oil-wet to the strong water-wet system which leads the hydrocarbon to move easily toward the production well.

### 3.5 Spontaneous Imbibition

The spontaneous imbibition test was carried out to evaluate the role of the synthesized NCs on oil recovery. Two core samples from the carbonate rock were used to conduct this test (plugs#1 and #2). Both used core plugs have the porosity around 17–18% and permeability around 7.5 mD. The used core plugs were saturated by crude oil ( $S_{or}$ ) when the connate water saturation ( $S_{wi}$ ) exists as shown in Table 1. Figure 11 illustrates the oil recovery performance of the used core plugs versus time for 28 days. From imbibing water into the core plug#1, the oil recovery of 47.7% OOIP was obtained after 28 days of the experiment, while the NF1000 solution prepared from mixing 1000 ppm of  $\text{Fe}_3\text{O}_4/\text{mineral}$ –soil NCs within water was imbibed into the core plug#2; the total accumulated oil recovery factor from was 58.98% OOIP. Thus, the NF1000 solution enabled to displace extra 11.28% OOIP compared with water imbibition. The results obtained from spontaneous imbibition are consistent with what are presented by Nowrouzi et al. [22].

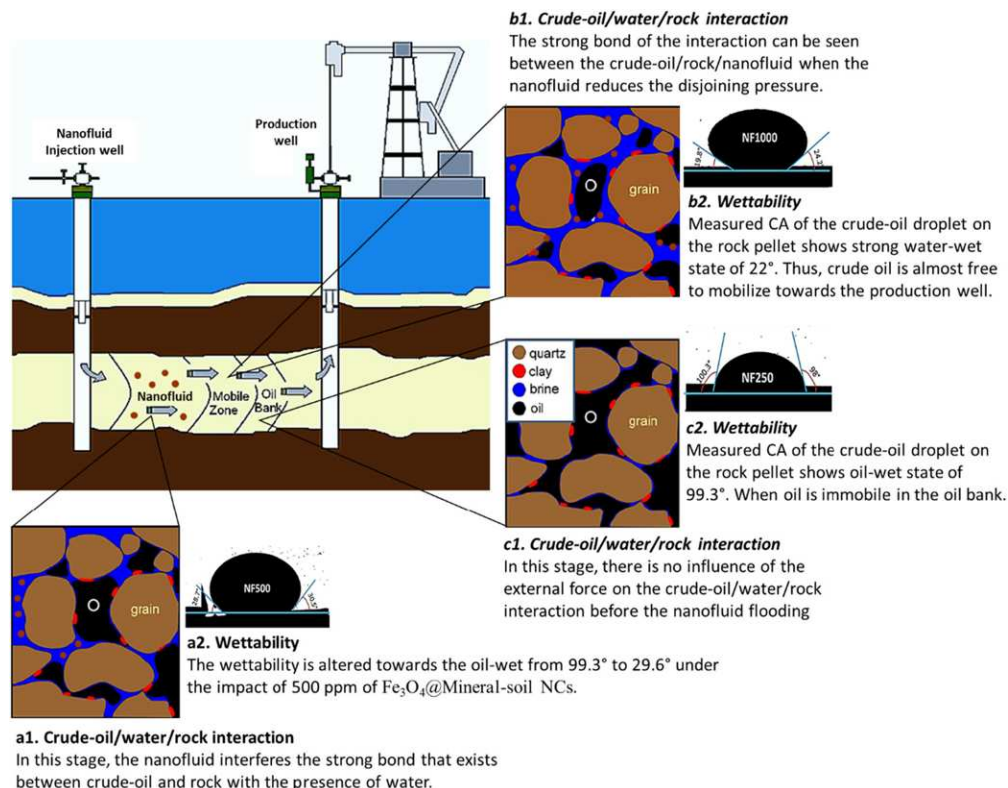


**Fig. 10** Mechanism of altering the wettability of the carbonate rock under the influence of Fe<sub>3</sub>O<sub>4</sub>/mineral–soil NCs depends on the contact angle measurements at different stages: **a** early stage of the

wettability alteration, **b** late stage of wettability alteration toward the strong water-wet, and **c** the strong oil-wet exists in the porous media without any alteration

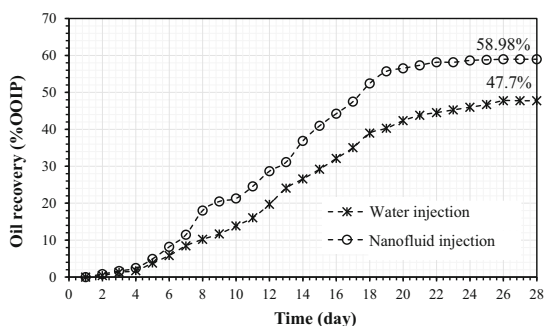


**Fig. 11** Oil recovery profile of water and nanofluid imbibition test during 28 days

spontaneous imbibition process. The green NCs were synthesized from the extract of *Euodia hortensis* plant in a green and economical way that combines the magnetite and mineral soil. The analytical results from the XRD pattern, FTIR spectrum and SEM size and shape confirmed the validity of the synthesized NCs. 1000 ppm of Fe<sub>3</sub>O<sub>4</sub>/mineral–soil NCs was capable of reducing the IFT from 28.3 to 3.69 mN/m. The wettability of the carbonate rock was strongly altered from strong oil-wet of 134° contact angle to water-wet of 22° contact angle using NF1000 solution. The NF1000 solution prepared from mixing 1000 ppm Fe<sub>3</sub>O<sub>4</sub>/mineral–soil NCs within water enabled in displacing extra 11.28% OOIP compared with water imbibition.

**Declarations**

**Conflicts of interests** The author declares that he has no known competing financial interests or personal relationships that could have appeared to influence the work reported in this paper.

**4 Conclusions**

Green Fe<sub>3</sub>O<sub>4</sub>/mineral–soil nanocomposites were synthesized for an objective-oriented purpose which is enhancement of oil recovery from the carbonate reservoirs under the

## References

- Ahmadi, M.A.; Galedarzadeh, M.; Shadzadeh, S.R.: Wettability alteration in carbonate rocks by implementing new derived natural surfactant: Enhanced oil recovery applications. *Transp. Porous Media* **106**(3), 645–667 (2015). <https://doi.org/10.1007/s11242-014-0418-0>
- Ali, J.A.; Kolo, K.; Manshad, A.K.; Mohammadi, A.H.: Recent advances in application of nanotechnology in chemical enhanced oil recovery: Effects of nanoparticles on wettability alteration, interfacial tension reduction, and flooding. *Egyptian J Petrol.* **27**(4), 1371–1383 (2018). <https://doi.org/10.1016/j.ejpe.2018.09.006>
- Ali, J.A.; Kahlury, A.M.; Sabir, A.N.; Ahmed, R.N.; Ali, N.H.; Abdullah, A.D.: A state-of-the-art review of the application of nanotechnology in the oil and gas industry with a focus on drilling engineering. *J. Petrol. Sci. Eng.* **191**, 107118 (2020)
- Udoh, T.H.: Improved insight on the application of nanoparticles in enhanced oil recovery process. *Scientific African* **13**, e00873 (2021)
- Nandwani, S.K.; Malek, N.I.; Lad, V.N.; Chakraborty, M.; Gupta, S.: Study on interfacial properties of Imidazolium ionic liquids as surfactant and their application in enhanced oil recovery. *Colloids Sur. A Physicochem. Eng. Asp.* **516**, 383–393 (2017). <https://doi.org/10.1016/j.colsurfa.2016.12.037>
- Ding, B.; Xiong, C.; Geng, X.; Guan, B.; Pan, J.; Xu, J.; Dong, J.; Zhang, C.: Characteristics and EOR mechanisms of nanofluids permeation flooding for tight oil. *Pet. Explor. Dev.* **47**(4), 810–819 (2020)
- Saborian-Jooybari H, Dejam M, Chen Z.: Half-century of heavy oil polymer flooding from laboratory core floods to pilot tests and field applications. In: Paper SPE 174402, 2015 SPE Canada Heavy Oil Technical Conference, Calgary, Alberta, Canada, 9–11, (2015) <https://doi.org/10.2118/174402-ms>
- Kumar, A.; Mandal, A.: Characterization of rock-fluid and fluid-fluid interactions in presence of a family of synthesized zwitterionic surfactants for application in enhanced oil recovery. *J. Petrol. Sci. Technol.* **549**, 1–12 (2018). <https://doi.org/10.1016/j.colsurfa.2018.04.001>
- Rostami, A.; Hashemi, A.; Takassi, M.A.; Zadehnazari, A.: Experimental assessment of a lysine derivative surfactant for enhanced oil recovery in carbonate rocks: Mechanistic and core displacement analysis. *J. Mol. Liq.* **232**, 310–318 (2017). <https://doi.org/10.1016/j.molliq.2017.01.042>
- Yang, X.; Liu, Z.H.: A kind of nanofluid consisting of surface - functionalized nanoparticles. *Nanoscale Res. Lett.* **5**, 1324–1328 (2010)
- Yu, W.; Xie, H.: A Review on nanofluids: preparation, stability mechanisms, and applications. *J. Nanomaterials* (2012). <https://doi.org/10.1155/2012/435873>
- Negi, G.; Anirbid, S.; Sivakumar, P.: Applications of silica and titanium dioxide nanoparticles in enhanced oil recovery: Promises and challenges. *Petroleum Research* **6**(3), 224–246 (2021)
- Afifi, H.R.; Mohammadi, S.; Mirzaei Derazi, A.; Mahmoudi, A.F.: Enhancement of smart water-based foam characteristics by SiO<sub>2</sub> nanoparticles for EOR applications. *Colloids Surf., A* **627**, 127143 (2021)
- Roustaei A, Moghadasi J, Bagherzadeh H, Shahrabadi A.: An experimental investigation of polysilicon nanoparticles' recovery efficiencies through changes in interfacial tension and wettability alteration. In: SPE Int. Oilfield Nanotechnology Conference Exhibition. (2012) <https://doi.org/10.2118/156976-ms>
- Joonaki, E.; Ghanaatian, S.: The application of nanofluids for enhanced oil recovery: effects on interfacial tension and coreflooding process. *Petro. Sci. Technol.* **32**(21), 2599–2607 (2014)
- Bayat, E.A.; Junin, R.; Samsuri, A.; Piroozian, A.; Hokmabadi, M.: Impact of metal oxide nanoparticles on enhanced oil recovery from limestone media at several temperatures. *Energy Fuels* **28**(10), 6255–6266 (2014)
- Ju, B.; Fan, T.: Experimental study and mathematical model of nanoparticle transport in porous media. *Powder Tech.* **192**, 195–202 (2009)
- Rezvani, H.; Riazi, M.; Tabaei, M.; Kazemzadeh, Y.; Sharifi, M.: Experimental investigation of interfacial properties in the EOR mechanisms by the novel synthesized Fe<sub>3</sub>O<sub>4</sub>@Chitosan nanocomposites. *Colloid Surf A: Physicochem Eng. Aspects* **544**, 15–27 (2018)
- Qi, L.; Song, C.; Wang, T.; Li, Q.; Hirasaki, G.J.; Verduzco, R.: Polymer-coated nanoparticles for reversible emulsification and recovery of heavy oil. *Langmuir* **34**, 6522–6528 (2018)
- Lim, S.; Wasan, D.: Structural disjoining pressure induced solid particle removal from solid substrates using nanofluids. *J. Colloid Interface Sci.* **500**, 96–104 (2016)
- Zhang, H.; Ramakrishnan, T.S.; Nikolov, A.; Wasan, D.: Enhanced oil recovery driven by nanofilm structural disjoining pressure: Flooding experiments and microvisualization. *Energy Fuels* **30**, 2771–2779 (2016)
- Nowrouzi, I.; Manshad, A.K.; Mohammadi, A.H.: Effects of concentration and size of TiO<sub>2</sub> nano-particles on the performance of smart water in wettability alteration and oil production under spontaneous imbibition. *J. Petrol. Sci. Eng.* **183**, 106357 (2019)
- Keykhosravi, A.; Vanani, M.B.; Aghayari, C.: TiO<sub>2</sub> nanoparticle-induced xanthan gum polymer for EOR: Assessing the underlying mechanisms in oil-wet carbonates. *J. Petrol. Sci. Eng.* **204**, 108756 (2021)
- Nourinia, A.; Manshad, A.K.; Shadzadeh, S.R.; Ali, J.A.; Iglauer, S.; Keshavarz, A.; Mohammadi, A.; Ali, M.: Synergistic efficiency of zinc oxide/Montmorillonite Nanocomposites and a new derived saponin in liquid/Liquid/Solid interface-included systems: Application in nanotechnology-assisted enhanced oil recovery. *ACS Omega* **7**(29), 24951–24972 (2022)
- Han, S.T.: Medicinal plants in south pacific World health organization, WHO regional publication. *Western Pacific Series* **19**, 9–10 (1998)
- Bagdy, G.; Kecskemeti, V.; Riba, P.; Jakus, R.: Serotonin and epilepsy. *J. Neurochem.* **100**(4), 857–873 (2007). <https://doi.org/10.1111/j.1471-4159.2006.04277>
- Dalith, M.D.; Bhanu, K.P.: Evaluation of anti-epileptic effect of methanolic extracts of euodia hortensis forster. *Inter. J. Pharmacother.* **1**, 20–24 (2011)
- Dixit, P.K.; Mittal, S.; Chauhan, B.: Screening models used for anti-epileptic activity and various herbal sources beneficial in epilepsy: a review. *Eur. J. Pharm. Med. Res.* **2**, 843–855 (2015)
- Ak, R.; Dalith, D.: Evaluation of antioxidant properties of euodia hortensis forster extracts on brain enzymes level in rats. *Inter. J. Phytother.* **1**, 11–15 (2011)
- Jafarbeigi, E.; Salimi, F.; Kamari, E.; Mansouri, M.: Effects of modified graphene oxide (GO) nanofluid on wettability and IFT changes: Experimental study for EOR applications. *Pet. Sci.* (2021). <https://doi.org/10.1016/j.petsci.2021.12.022>
- Omidi, A.; Manshad, A.K.; Moradi, S.; Ali, J.A.; Sajadi, S.; Keshavarz, A.: Smart- and nano-hybrid chemical EOR flooding using Fe<sub>3</sub>O<sub>4</sub>/eggshell nanocomposites. *J. Mol. Liq.* **316**, 113880 (2020)
- Nazarahari, M.J.; Manshad, A.K.; Ali, M.; Ali, J.A.; Shafiei, A.; Sajadi, S.M.; Moradi, S.; Iglauer, S.; Keshavarz, A.: Impact of a novel biosynthesized nanocomposite (SiO<sub>2</sub>@Montmorilant@Xanthan) on wettability shift and interfacial tension: Applications for enhanced oil recovery. *Fuel* **298**, 120773 (2021)



33. Mohammadi, A.; Barikani, M.: Synthesis and characterization of superparamagnetic Fe<sub>3</sub>O<sub>4</sub> nanoparticles coated with thiodiglycol. *Mater. Charact.* **90**, 88–93 (2014)
34. Fovet, Y.; Gal, J.Y.; Toumelin-Chemla, F.: Influence of pH and fluoride concentration on titanium passivating layer: Stability of titanium dioxide. *Talanta* **53**, 1053–1063 (2001)
35. Wen, D.; Lin, G.; Vafaei, S.; Zhang, K.: Review of nanofluids for heat transfer applications. *Particuology* **7**, 141–150 (2009)

Springer Nature or its licensor holds exclusive rights to this article under a publishing agreement with the author(s) or other rightsholder(s); author self-archiving of the accepted manuscript version of this article is solely governed by the terms of such publishing agreement and applicable law.

## Appendix 10

*Interfacial tension reduction of hybrid crude-oil/mutual-solvent systems under the influence of water salinity, temperature and green SiO<sub>2</sub>/KCl/ Xanthan nanocomposites*

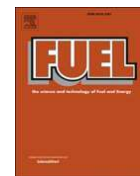
Fatemeh Motraghi, Abbas Khaksar Manshad, Majid Akbari, **Jagar A. Ali**, S. Mohammad Sajadi, Stefan Iglauer, Alireza Keshavarz

Fuel 340 (2023) 127464



Contents lists available at ScienceDirect

Fuel

journal homepage: [www.elsevier.com/locate/fuel](http://www.elsevier.com/locate/fuel)

Full Length Article

## Interfacial tension reduction of hybrid crude-oil/mutual-solvent systems under the influence of water salinity, temperature and green SiO<sub>2</sub>/KCl/Xanthan nanocomposites

Fatemeh Motraghi<sup>a</sup>, Abbas Khaksar Manshad<sup>a,\*</sup>, Majid Akbari<sup>a</sup>, Jagar A. Ali<sup>b,c</sup>, S. Mohammad Sajadi<sup>d</sup>, Stefan Iglauer<sup>e,f</sup>, Alireza Keshavarz<sup>e,f</sup>

<sup>a</sup> Department of Petroleum Engineering, Abadan Faculty of Petroleum Engineering, Petroleum University of Technology (PUT), Abadan, Iran

<sup>b</sup> Department of Geology, Palacký University, 17. Listopadu 12, Olomouc 77146, Czech Republic

<sup>c</sup> Department of Petroleum Engineering, Faculty of Engineering, Soran University, Kurdistan Regional Government, Soran 44008, Iraq

<sup>d</sup> Department of Nutrition, Cihan University-Erbil, Kurdistan Region, Iraq

<sup>e</sup> School of Engineering, Edith Cowan University, Joondalup, WA 6027, Australia

<sup>f</sup> Centre for Sustainable Energy and Resources, Edith Cowan University, 270 Joondalup Dr, Joondalup 6027, WA, Australia



## ARTICLE INFO

## Keywords:

Smart water  
Interfacial tension (IFT)  
Mutual solvents  
Ethanol  
Methyl ethyl ketone  
Nanocomposites

## ABSTRACT

In order to maximize oil recovery, combined enhanced oil recovery (EOR) methods can be used, which benefit from several mechanisms simultaneously. The application of nanotechnology and mutual solvents were studied separately in recent years. Mutual solvents have the ability to dissolve in both aqueous and oil phases and can show similar performance to surfactants in the water–oil interface. In this study, the effect of ethanol and methyl ethyl ketone solvents with and without a new nanocomposite on the reduction of interfacial tension (IFT) as a mechanism of the main EOR has been examined. The addition of these solvents to nanofluids is a new strategy that enhances the reactions at the interface of the two phases and improves the performance of the IFT mechanism. Also, diluted formation water samples were used as the simplest and most accessible smart water and synergistic effects on the system were investigated. Mutual solvents were tested at 5, 10, and 15 % by volume with and without nanocomposite at 25, 50 and 75 °C. In this way, different parameters of salinity, temperature, different concentrations of solvents and nanocomposite on IFT reduction were investigated. According to the results, each of these processes separately has positive effects in reducing IFT. But the combination of smart water - mutual solvent - nanocomposite showed the best effect in reducing IFT. The addition of solvents to water and nanofluids has a good potential to reduce IFT in reservoirs with high temperature and high salinity conditions. The optimum concentration of nanocomposite in the presence and absence of solvent was 1000 ppm, which shows that the optimum concentration NCs for IFT reduction is not affected by the presence of the solvent. But adding solvent to different concentrations of nanofluid has positive effects in reducing IFT. In general, methyl ethyl ketone has a stronger effect on reducing IFT than ethanol. Finally, the minimum IFT was observed for a mixture of 1000 ppm nanocomposite and 15 % methyl ethyl ketone with 50 % formation water as the base fluid at the temperature of 75 °C.

## 1. Introduction

According to projections of the International Energy Agency (IEA), by 2035, the global demand for fossil fuels would have increased by about one-third [1]. Also, many oil fields have reached their half-life and due to exploration problems, the discovery of new oil reservoirs has decreased [2,3]. Additionally, primary and secondary recovery methods

can produce about one-third of the original oil (OOIP) [3]. Thus, the development of new EOR methods is vital in oil industry to commercially recover more oil and to delay the abandonment of oil fields [3,4]. Combined EOR is a common method that can lead to the ideal EOR process by promoting and modifying one or more EOR methods and causes further loss of remaining saturated oil content [5].

One of the most important and efficient mechanisms for EOR is the

\* Corresponding author.

E-mail address: [khaksar@put.ac.ir](mailto:khaksar@put.ac.ir) (A. Khaksar Manshad).

<https://doi.org/10.1016/j.fuel.2023.127464>

Received 20 October 2022; Received in revised form 21 December 2022; Accepted 7 January 2023

Available online 24 January 2023

0016-2361/© 2023 Published by Elsevier Ltd.

IFT reduction between the oil and the injected fluid. The indicator of energy at the interface of two immiscible fluids is known as interfacial tension (IFT) [6]. The IFT value is a measure that shows the miscibility of fluids in the reservoir; the lower the IFT value, the closer the fluids are to miscibility. An IFT value of  $10^{-3}$  mN/m is considered ultra-low and indicative of a fully miscible fluid state, while the average IFT value between oil and water under standard conditions is 10–30 mN/m. A high IFT value between oil and water causes immiscible behavior between fluids and prevents the displacement of oil from the reservoir. By reducing the IFT, the capillary pressure decreases, and the extraction of the oil trapped in the reservoir's pore network is made easier [7]. Nanofluids, surfactants, polymers, and low-salinity water tend to reduce IFT and are successful agents in EOR processes [6].

Changing ion concentrations to increase beneficial ions and decrease harmful ions, as well as diluting or purifying saline samples to reduce total salinity, and generally changing water chemistry are known as smart water, engineered water, advanced ion management, and low salinity water [8–10]. The main mechanism of smart water is wettability alteration [11], and the effect of salinity on reducing or increasing IFT has not been well established. The results and trends vary based on the systems studied and the test conditions, which may depend on the composition of the crude oil and the thermodynamic conditions. Increasing or decreasing IFT can also be influenced by different brine formulations [12]. The utilization of water extracted from reservoir formation can be assessed when access to water is challenging or unavailable. Cost estimation may show that treating and controlling ion concentration will be less expensive than transferring water with lower salinity to the field [11].

Moreover, the use of nanotechnology as modern knowledge in EOR shows that it can be effective in reducing IFT. The use of nanofluids is also known as smart nanofluids [5,13,14]. Nanoparticles are small particles (1–100 nm) and are significant in EOR due to their chemical and physical properties [15]. The ability of these particles to provide a powerful driving force for diffusion due to their large surface area, especially at high temperatures, is one of their most interesting and important characteristics [16,17]. Also, due to the small size of nanoparticles, they can easily pass through the pore throat in a porous medium [18]. Some favorable results of the use of nanoparticles in EOR, such as IFT reduction [4,19,20], wettability alteration [21,22], asphaltene inhibition [23], reducing the viscosity of oil [24,25], increasing the viscosity of injecting fluid [26–28], disjoining pressure [29–31], pore channel plugging [32,33], and nano-emulsion creation [34]. Many research studies have reported that nanoparticles play important roles in chemical enhanced oil recovery (CEOR) processes [4,35]. smart water [36,37], surfactants [2,38–41], polymers [42,43], gas [44], and injection as carbonated [8,45] are chemical methods commonly used with nano enhanced oil recovery (NEOR) method [5]. In other words, hybrid nanocomposites can improve the performance of the CEOR process to increase the potential for wettability alteration and reduce the IFT by CEOR techniques [46–48]. Various liquids such as surfactant, alcohol, polymer, distilled water and brine with different salinities are used to disperse the nanoparticles and prepare the nanofluid for EOR [49,50]. Solvents with different mechanisms increase oil recovery compared to conventional water flooding [51] and are used as an independent or combined method with other methods [52]. Mutual solvents are soluble in both water and oil phases and include ethyl alcohol, isopropyl alcohol, tertiary butyl alcohol secondary butyl alcohol, *n*-amyl alcohol, methyl ethyl ketone, acetone [53], dimethyl ether [54], and others. In the first study, Holm et al. showed that by injecting a slug of mutual solvent, the oil in the porous medium is displaced. They found that the relative solubility of the solvent in oil and water, and the distance traveled by the flood are two factors influencing oil recovery efficiency [53]. Chernetsky et al. introduced Dimethyl Ether Enhanced Waterflood (DEW) as a novel EOR technology and they reported that the residual oil saturation by the solvent was significantly lower than the conventional waterflood [54,55]. Chahardowli et al. demonstrated that continuous

dimethyl ether/polymer (DMEP) flooding has a higher recovery than continuous dimethyl ether/brine (DMEB) flooding and shortens oil production time. Their results also show that combining polymer and dimethyl ether can reduce the viscosifying effect of the polymer [51]. Dehaghani and Badizad investigated the viscosity reduction by heptane, methanol, toluene, and gas condensate. The viscosity of heavy oil decreased with toluene, heptane and gas condensate, but methanol increased the viscosity due to the formation of hydrogen bonds [56]. Ratnakar et al. reported similar results for decreasing oil viscosity and increasing oil recovery by simulating the phase behavior of dimethyl ether, using experiments and the PVT model [57–59]. AlZayer et al. studied the behavior of two mutual solvents, diethyl ether and carbon dioxide (CO<sub>2</sub>) as carbonated water, and showed that oil recovery increases in carbonate plugs. The mass transfer of mutual solvents from the water phase (injection phase) to the oil phase, oil swelling and viscosity reduction mobilized the oil [60]. Javanmard et al. observed significant oil production by dimethyl ether in a fractured chalk reservoir core plug. The dimethyl ether is rapidly transferred from the brine solution to the oil, and partitions into the oil in the low permeability, eventually increasing oil production [61]. Nowrouzi et al. used methanol and acetone as mutual solvents in different volume ratios to investigate IFT and wettability alteration. Acetone was more effective than methanol in reducing IFT and contact angle. Decreased IFT was directly related to increased pressure and solvent concentrations of methanol and acetone and inversely related to increased salinity. Also, more hydrophilicity with increasing solvent concentration, increasing pressure, and increasing seawater salinity were directly related, but the presence of CO<sub>2</sub> showed an inverse relationship with increasing salinity [52,62]. Nowrouzi et al. evaluated the dynamic and equilibrium oil swelling under the influence of injected fluid containing soluble CO<sub>2</sub> and acetone at 75 °C and various pressures. They found that oil swelling increases over time to reach a near-constant value at equilibrium time and the presence of acetone could increase oil swelling. Acetone volume ratio, pressure and salinity were directly related to oil swelling [63]. Table 1 depicts a summary of literature findings on the effects of brine, nanocomposite materials, and solvents on IFT.

Regarding related literature, the effect of adding different percentages of mutual solvents to nanofluids to reduce the IFT of oil has not been investigated. In other words, the combined method of smart water - mutual solvent - nanocomposite has not been done so far and the NEOR and CEOR methods are performed separately and in combination to investigate the reduction of IFT. Moreover, in most studies of CEOR by solvents, the mechanisms of oil swelling and viscosity reduction have been tested and the ability of solvents to reduce IFT has not been fully investigated. Current work focuses on the reduction of IFT by ethanol and methyl ethyl ketone solvents with and without smart water and nanofluids. In order to evaluate the effect of nanocomposites on IFT reduction, three concentrations of 500, 1000 and 1500 ppm nanocomposite were dispersed with distilled water, formation water with initial concentration and diluted formation water. After measuring IFT and determining the optimum concentration of nanocomposite, the effect of adding different volume ratios of both solvents on reducing IFT was investigated to maximize the benefits of these nanocomposites. Various parameters such as salinity, temperature, and different concentrations of solvents and nanocomposite on IFT were evaluated based on pendant drop experiments.

## 2. Materials and equipment

### 2.1. Brine and crude oil

Asmari formation water was used to prepare the solution, the analysis of which is shown in Table 2, and we used distilled water to dilute the formation water. The dead crude oil used in the Iranian Gachsaran reservoir was supplied and its properties are presented in Table 3.

**Table 1**  
Summary of literature findings on the effects of brine, nanocomposite materials, and solvents on IFT.

| EOR technique       | Type of materials   | Outcome   | References |
|---------------------|---|---|------------|
| Smartwater          | Formation-brine/[NaCl & CaCl <sub>2</sub> ]   | IFT decreases with increasing salinity.   | [64]       |
|                     | Complex reservoir brine   | IFT increased with increasing salinity, pressure and temperature  | [65]       |
|                     | Formation-brine + seawater/[NaCl & CaCl <sub>2</sub> ]  | IFT decreased with increasing salinity.   | [12]       |
|                     | Seawater  | IFT increased with increasing salinity.   | [52]       |
|                     | Yates reservoir brine   | IFT decreased with increasing salinity.   | [66]       |
|                     | Deionized-water + sweater/[NaCl]  | There is no clear relationship between IFT and crude oil properties.  | [67]       |
| Nanofluids          | Different complex brine systems   | IFT reduced with no clear prediction of the correlation for pure hydrocarbons.                                    | [68]       |
|                     | TiO <sub>2</sub> , MgO & $\gamma$ -Al <sub>2</sub> O <sub>3</sub> + smartwater                | IFT reduction from 25.677 to 12.818, 12.785 and 9.332 mN/m, respectively. IFT increased with increasing salinity. | [5]        |
|                     | ZnO/SiO <sub>2</sub> /bentonite + smartwater  | IFT reduced from 21.18 to 2.59 mN/m. IFT increased with increasing salinity.                                      | [49]       |
|                     | TiO <sub>2</sub> /Quartz + smartwater   | IFT reduced from 36.4 to 3.5 mN/m.  | [48]       |
|                     | ZnO@ PAM NCs + DTAB surfactant  | IFT reduced from 29.16 to 1.354 mN/m.   | [3]        |
|                     | SiO <sub>2</sub> /Montmorilant/Xanthan + deionized water                                      | IFT reduced from 36 to 15.42 mN/m.  | [15]       |
|                     | NiO/SiO <sub>2</sub> + distilled water & seawater   | IFT reduced from 28 to 1.84 mN/m.   | [69]       |
|                     | SiO <sub>2</sub> + SDS surfactant   | IFT reduced from 20 to 1.87 mN/m.   | [70]       |
|                     | SiO <sub>2</sub> + surfactant   | IFT reduced from 35 to 10.9 mN/m.   | [19]       |
|                     | SiO <sub>2</sub> , TiO <sub>2</sub> & Al <sub>2</sub> O <sub>3</sub> + 3 wt% NaCl brine       | IFT reduced from 19.2 to 17.5, 15.2 and 12.8 mN/m, respectively.  | [71]       |
|                     | Al <sub>2</sub> O <sub>3</sub> , Fe <sub>2</sub> O <sub>3</sub> & SiO <sub>2</sub> + propanol | IFT reduced from 38.5 to 2.25, 2.75 and 1.45 mN/m, respectively.  | [34]       |
|                     | SiO <sub>2</sub> + 5 wt% NaCl water   | IFT reduced from 26.5 to 1.95 mN/m.   | [72]       |
|                     | SiO <sub>2</sub> & FSPNs + ethanol  | IFT reduced from 37.5 to 22.1 and 13 mN/m, respectively.  | [73]       |
| HLP & NWP + ethanol | IFT reduced from 26.3 to 1.75 and 2.55 mN/m, respectively.                                    | [20]  |            |

## 2.2. Ethanol and methyl ethyl ketone solvents

Ethanol and methyl ethyl ketone with  $\geq 99\%$  purity were purchased from Merck Company. Ethanol with the chemical formula C<sub>2</sub>H<sub>6</sub>O has densities of 0.790–0.793 and methyl ethyl ketone with the chemical formula C<sub>4</sub>H<sub>8</sub>O has densities of 0.804–0.805 g/cm<sup>3</sup>, at 20 °C.

**Table 2**  
Composition of formation water used in the study.

| Na <sup>+</sup> | K <sup>+</sup> | Mg <sup>2+</sup> | Ca <sup>2+</sup> | Fe <sup>2+</sup> | Cl <sup>-</sup> | HCO <sub>3</sub> <sup>-</sup> | SO <sub>4</sub> <sup>2-</sup> | TDS [mg/L] |
|-----------------|----------------|------------------|------------------|------------------|-----------------|-------------------------------|-------------------------------|------------|
| 57,031          | 57,031         | 1701             | 9000             | 0                | 108,275         | 220                           | 768                           | 176,995    |

## 2.3. Synthesis of SiO<sub>2</sub>/KCl/Xanthan nanocomposites

In this study, a new nanocomposite called SiO<sub>2</sub>/KCl/Xanthan was used to prepare nano-suspensions. The composition of this nanocomposite includes KCl (as a common salt), SiO<sub>2</sub> (as nanoparticles) and xanthan gum (as a natural stabilizing polymer). Na<sub>2</sub>SiO<sub>3</sub>, euphorbia condylocarpa plant extract, xanthan gum, KCl and ethanol are needed to synthesize this nanocomposites, and NaOH was added during this process, to adjust pH. Sodium silicate (Na<sub>2</sub>SiO<sub>3</sub>) was purchased from Sigma-Aldrich Company and other chemical additives for nanocomposite synthesis were provided from Petrochem Company.

In order to synthesize the nanocomposite, 100 mL of euphorbia condylocarpa plant extract was first mixed with 5 gm of Na<sub>2</sub>SiO<sub>3</sub> while stirring at 80 °C for 10 hr at 10 pH as shown in Fig. 1. After the components were mixed together thoroughly, precipitation was obtained. Then the obtained precipitation was separated and added to an ethanolic suspension of 10 gm of the xanthan substrate at 80 °C for 5 hr under reflux conditions. Further, after drying and milling of the precipitate, the milled SiO<sub>2</sub>-xanthan nanocomposite was mixed with 100 mL KCl-hydroalcoholic solution at 100 °C and stirred for 4 hr. Finally, the SiO<sub>2</sub>/KCl/Xanthan nanocomposite was produced by drying and milling of the final precipitate [74].

### 2.3.1. Characterization of SiO<sub>2</sub>/KCl/Xanthan nanocomposites

X-ray Diffraction (XRD), Fourier-Transform Infrared Spectroscopy characterization test (FTIR), and scanning electron microscope (SEM) analytical approaches have been performed to determine the crystalline phases, functional groups, and surface morphology of NCs. The XRD spectrum of Fig. 2 includes all peaks with crystalline planes of all three components Xanthan, SiO<sub>2</sub>, and KCl, and is related to their crystallinity and phase limpidness of silica NPs and KCl on the xanthan surface. The three main peaks indicate the presence of SiO<sub>2</sub> and KCl in the synthesized NCs. The nanocomposite has a high phase purity because the XRD pattern shows no diffraction peak caused by other impurities. In general, there is a typical broad peak in the XRD pattern, which is related to the amorphous phase SiO<sub>2</sub> and shows the associated small particles and their inner structure, and thus high purity. According to Fig. 3 the NCs FTIR spectrum is in the wavelength range of 400 to 4000 cm<sup>-1</sup> which contain several main peaks [a-e] and shows existing compound bond systems. The main peaks around 600 (a), 1050 (b), 1450 (c), 1600 (d), 2800 (e), and 3420 (f) cm<sup>-1</sup> are related to C—C, stretching C—O, sp<sup>2</sup>-stretching C=C, stretching C=O, sp<sup>3</sup>-stretching C—H, and stretching O—H bonds, respectively. Based on the above spectrum, the presence of organic functional groups of phytochemicals adsorbed on the surface of NCs, and indicates the proper synthesis and good performance of the nanocomposite. SEM analysis has been used to the study surface morphology of the nanocomposite images taken by Scanning Electron Microscopy. According to Fig. 4, the SiO<sub>2</sub> nanoparticles and KCl were continuously distributed on the surface of the xanthan substrate. SEM micrographs show that the particle size of the nanocomposite is in the range of nanometers and has a homogeneous and spherical structure, which indicates the successful synthesis of green NCs [74].

### 2.4. Density, conductivity and pH measurements

Density measuring device model DA-640 made by KEM company is used to measure density at different temperatures (in the range of 0–90 °C). Its measurement range is 0 to 3 g/cm<sup>3</sup> with an accuracy of 0.0001 g/cm<sup>3</sup>. This apparatus measures the density of fluid based on the

Table 3

The composition and main properties of crude oil used in the study.

| Component   | C <sub>1</sub> | C <sub>2</sub> | C <sub>3</sub> | iC <sub>4</sub> | nC <sub>4</sub> | iC <sub>5</sub> | nC <sub>5</sub> | C <sub>6</sub> | C <sub>7</sub> | C <sub>8</sub> | C <sub>9</sub> | C <sub>10</sub> | C <sub>11</sub> | C <sub>12</sub> <sup>+</sup> | Total |
|---|----------------|----------------|----------------|-----------------|-----------------|-----------------|-----------------|----------------|----------------|----------------|----------------|-----------------|-----------------|------------------------------|-------|
| Molar percent   | 0.00           | 0.08           | 0.73           | 0.72            | 2.22            | 1.10            | 1.10            | 8.66           | 9.32           | 6.60           | 7.14           | 5.36            | 5.01            | 51.96                        | 100.0 |
| Molecular weight(MW) = 247  |                |                |                |                 |                 |                 |                 |                |                |                |                |                 |                 |                              |       |
| Molecular weight of C <sub>12</sub> <sup>+</sup> = 380              |                |                |                |                 |                 |                 |                 |                |                |                |                |                 |                 |                              |       |
| Specific gravity of C <sub>12</sub> <sup>+</sup> @15.55 °C = 0.9369 |                |                |                |                 |                 |                 |                 |                |                |                |                |                 |                 |                              |       |
| Saturation pressure of reservoir fluid @60.6 °C = 14.04 MPa         |                |                |                |                 |                 |                 |                 |                |                |                |                |                 |                 |                              |       |

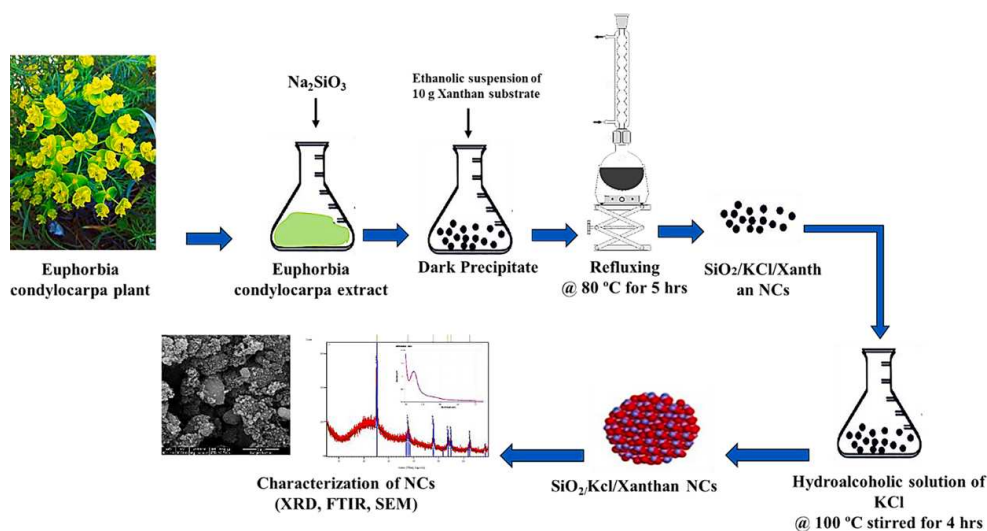


Fig. 1. Schematic illustrates the procedural steps of developing NCs [74,75].

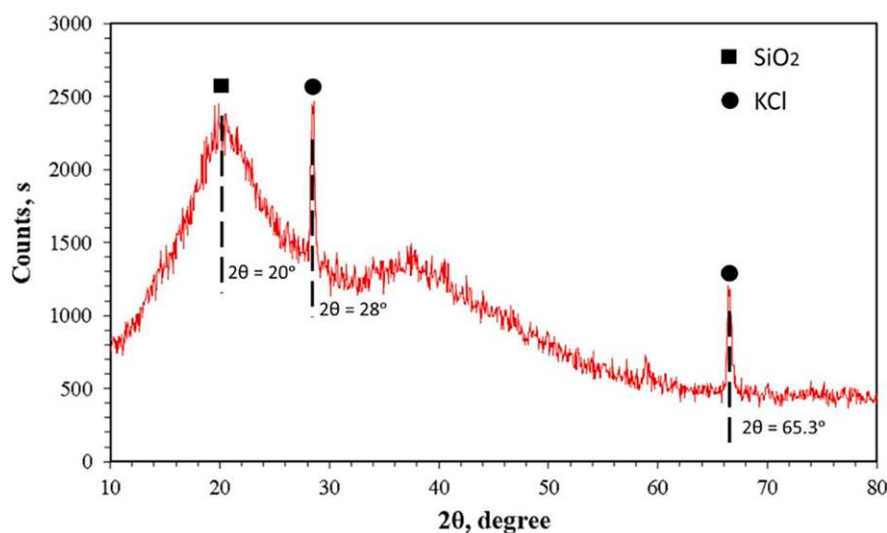


Fig. 2. XRD spectrum pattern of the nanocomposite [74,75].

resonant frequency oscillation method. Before each use of the device, it is washed with water and acetone and then dried. Also, Mettler Toledo S230, and WTW<sup>TM</sup> inoLab<sup>TM</sup> Cond 7310 were used to measure conductivity and pH, respectively.

### 2.5. IFT measurement

IFT measurement between oil and different types of solutions was performed using the pendant drop method. A VIT-6000 device (manufactured by Fars, accuracy 99 %) includes ISCO pumps, a chamber with glass windows, a metal needle (needle is closed in the bottom of the chamber), a light projection, a camera and a computer with an image

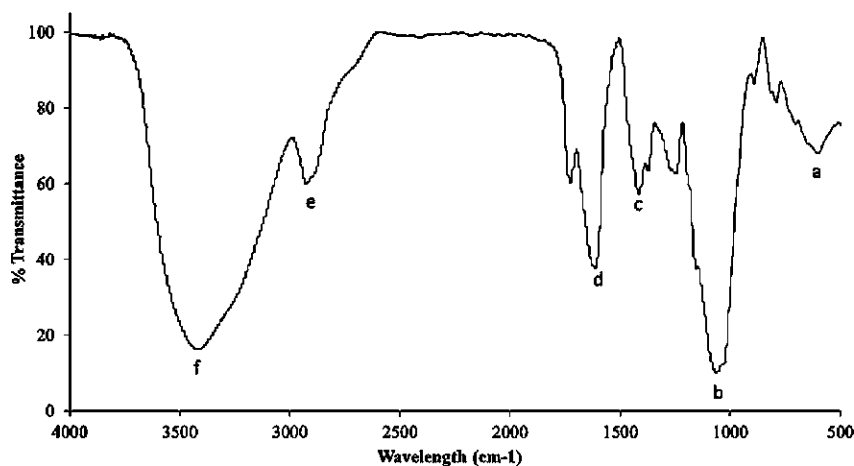


Fig. 3. FTIR spectrum pattern of the nanocomposite [74,75].

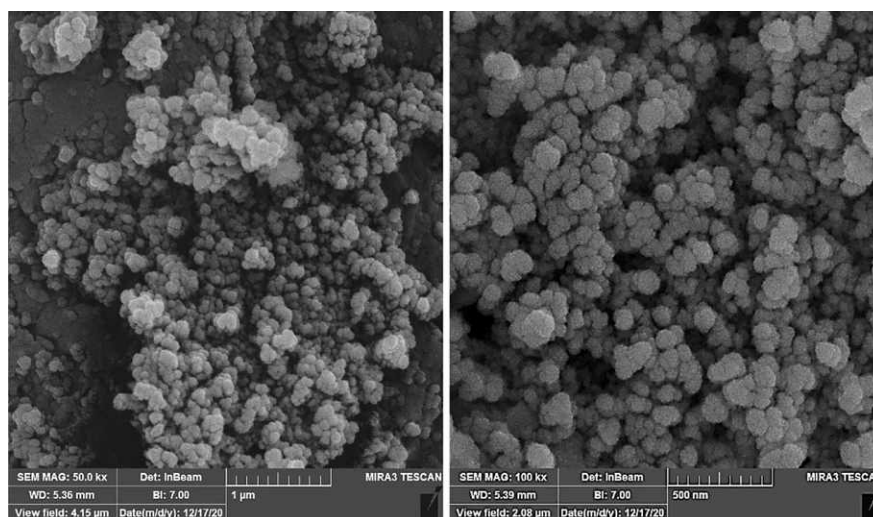


Fig. 4. SEM photographic of nanocomposites at 200Kx magnify [74,75].

processing software, which is used to measure the value of IFT in both static and dynamic conditions. In this method, for measuring IFT between two liquids, after pouring the solution into the experimental chamber, a drop of crude oil is suspended from the needle in the presence of the solution (filled in the main chamber). Crude oil drop is controlled by ISCO pump (Teledyne ISCO, Model D – 500, pressure accuracy 0.1 %) and with a digital camera, images of oil droplets are recorded at various time stages. Software according to Eq. (1) calculates the IFT between oil droplets and aqueous solution, and IFT is measured at three different temperatures, which are regulated by a temperature regulator. Fig. 5 shows the illustration of this device [15,76].

$$\gamma = \frac{gDe^2\Delta\rho}{H} \quad (1)$$

Where “ $\gamma$ ” is the interfacial tension (mN/m), “ $g$ ” is the gravity force, “ $De$ ” is the equatorial diameter of the drop (cm), “ $\Delta\rho$ ” is the density difference between two immiscible liquids ( $\text{g}/\text{cm}^3$ ) and “ $H$ ” is the coefficient of the drop shape [15].

## 2.6. Ultrasonic agitation system

The Hielscher Ultrasonic Mixer (UP200) was used to disperse nanoparticles in base fluids and has a power of 200 W and a frequency of 24 kHz and its amplitude can vary between 20 and 100 %. Ultrasonic agitation device creates a homogeneous solution by converting electric current into mechanical vibration and creating waves of intense pressure in a liquid medium. The applications for this device are extremely varied. The important applications of this type of agitator include the uniform mixing of fluids used in nanotechnology, as well as the blending of various types of nanomaterials with basic fluids.

## 3. Experimental methods

Fig. 6 shows the experimental procedure of this study. First, formation water in different ratios (50 % of formation water + 50 % distilled water), (25 % formation water + 75 % distilled water), (10 % formation water + 90 % distilled water), and (3 % formation water + 97 % water Distilled) was diluted and were tested as smart water. Then methyl ethyl ketone and ethanol were added to the base fluids separately at three

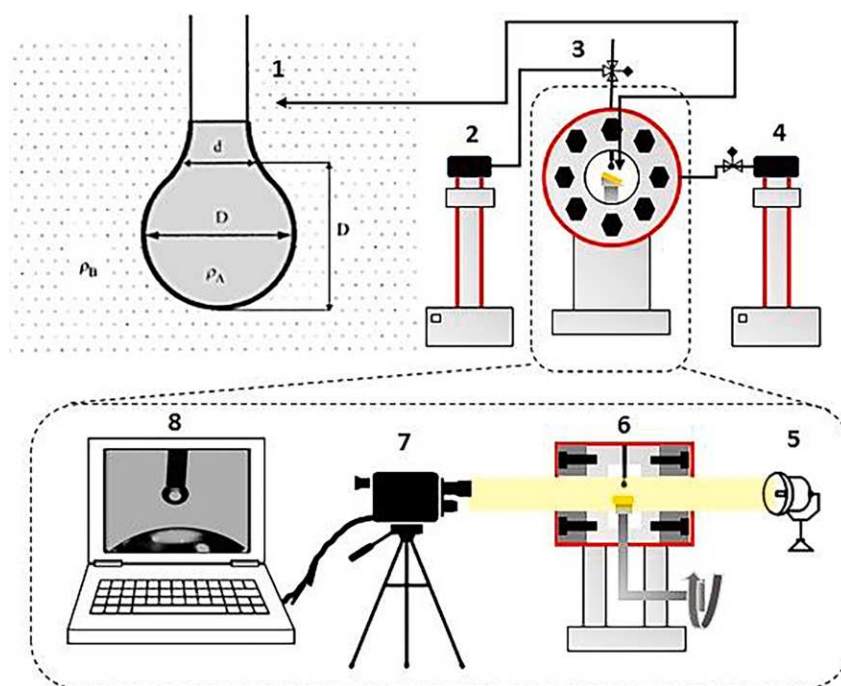


Fig. 5. Illustration of IFT setup, (1) Illustration of digital drop of liquid shape (crude oil in this case), (2) ISCO pump for controlling crude oil droplet, (3) Main chamber for the IFT measurement, front view, (4) ISCO pump for filling the main chamber with fluid, (5) Light projection, (6) Main chamber, side view, (7) Video camera for recording, (8) computer software for interpretation [15].

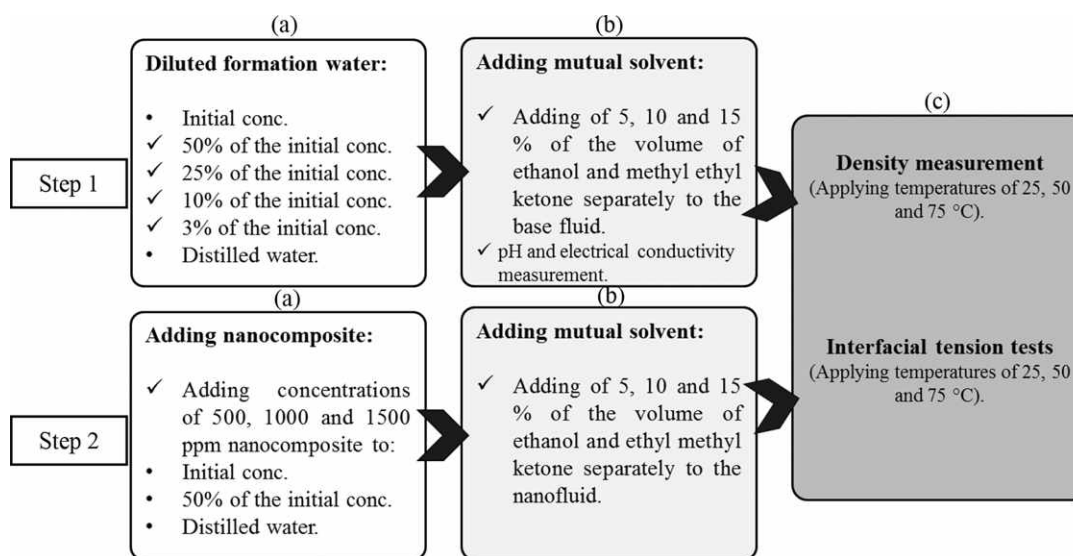


Fig. 6. The flowchart of the experiment steps in the study. Step 1: (a) formation water in different ratios was diluted, (b) MEK and ethanol were added to the base fluids, (c) Density and IFT tests were performed (at three temperatures of 25, 50, and 75 °C). Step 2: (a) preparation of the nanofluid, (b) solvents were added to the nanofluids (c) Density and IFT tests were performed.

concentrations of 5, 10 and 15 % by volume and mixed. Density and IFT tests were performed at three temperatures of 25, 50, and 75 °C. The pH and conductivity of the prepared chemical solutions (15 % of solvent within water at different salinity levels) were reported. In the next step, concentrations of 500, 1000, and 1500 KCl-SiO<sub>2</sub>-xanthan nanocomposites were selected for the preparation of the nanofluid. After

adding the nanocomposite to the base fluids (formation water with initial concentration, diluted formation water and distilled water), it dispersed by an ultrasonic device for half an hour. After the optimum concentration of the nanocomposite was determined, different percentages of solvents were added separately to the nanofluids (optimum concentration) and mixed. Finally, the density and IFT of nanofluids

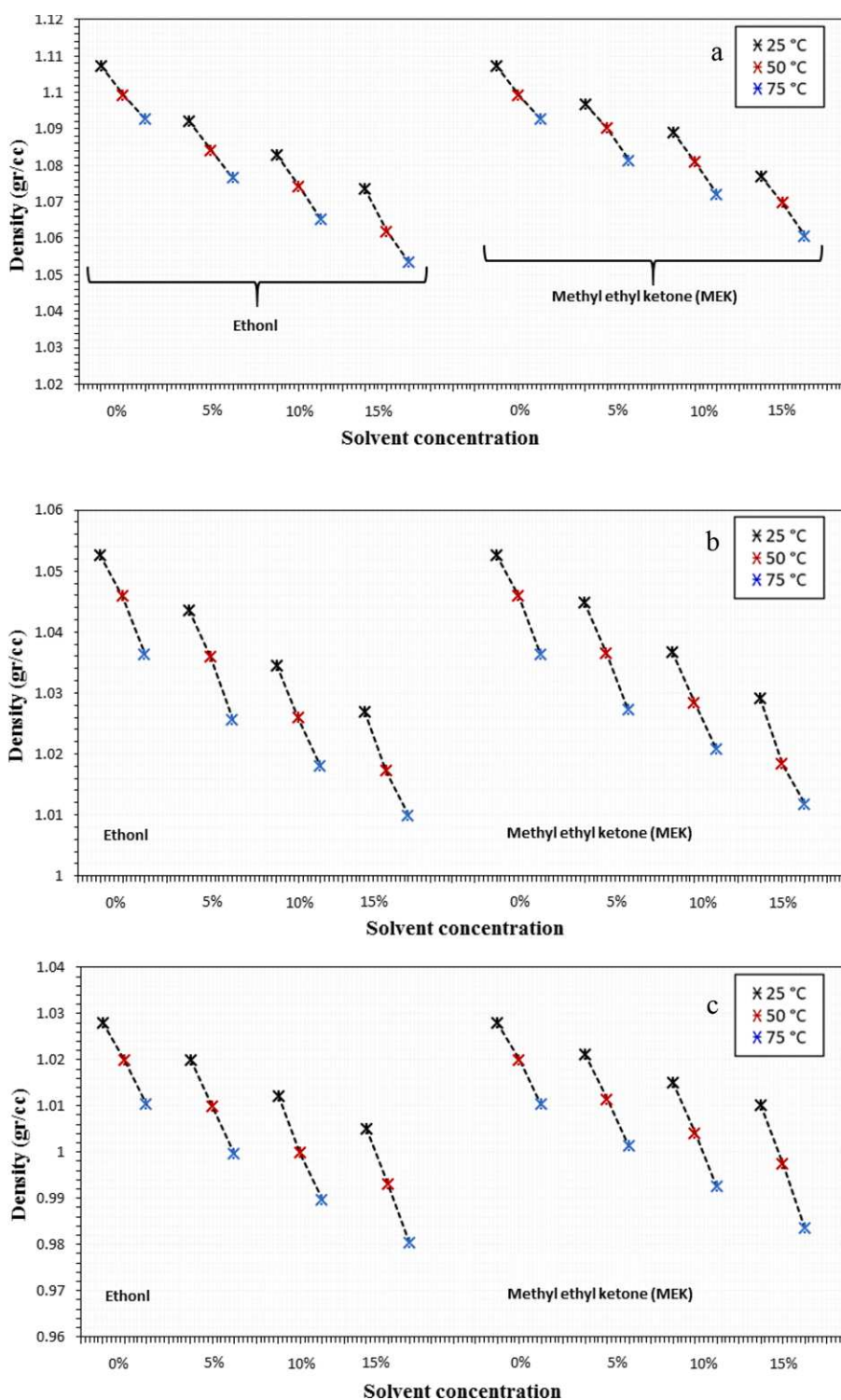


Fig. 7. Density graphs for binary solutions of formation water at different salinities/distilled water and ethanol/ methyl ethyl ketone (MEK) solvents at temperatures of 25, 50 and 75 °C; a) formation water, b) formation water 50 %, c) formation water (25 %), d) formation water (10 %), e) formation water (3 %), and f) distilled water.

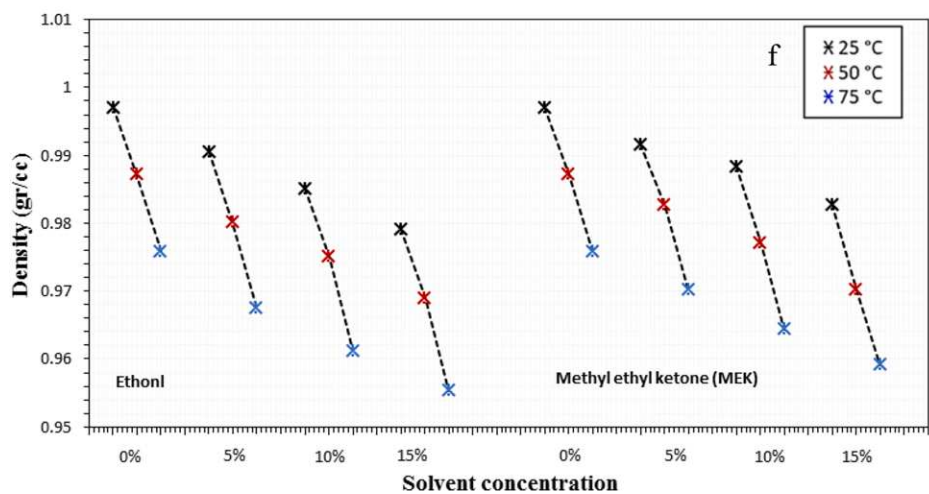
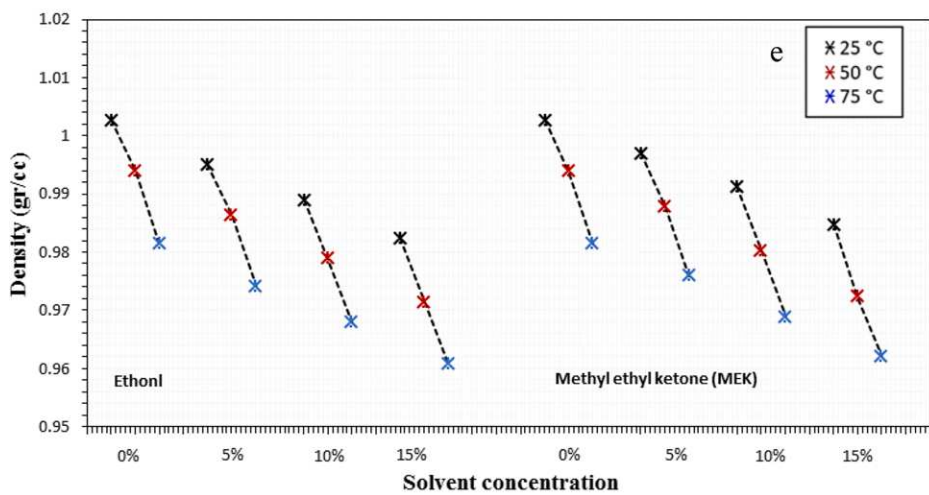
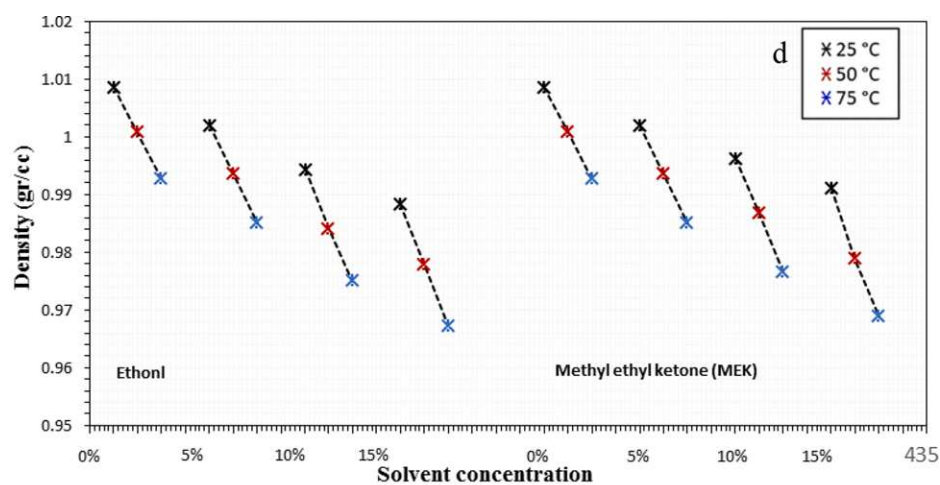


Fig. 7. (continued).

with and without solvent were measured at three temperatures of 25, 50 and 75 °C. Also, IFTs of various concentrations (500, 1000 and 1500 ppm) nanofluids with various concentrations (5, 10 and 15 %) solvents at optimal salinity were measured.

## 4. Results and discussion

### 4.1. Mutual solvents

#### 4.1.1. Density of the mutual solvents

Fig. 7 shows the density changes due to the increase in solvent percentage, salinity and temperature, and density data are used to measure IFT. As the concentration of ethanol and methyl ethyl ketone increases, the density of the solvents decreases because the density of the solvents is lower than that of the base fluid. As the system temperature increases, the density decreases.

#### 4.1.2. Effect of the mutual solvents on water–oil IFT

Fig. 9 shows the equilibrium IFT values of binary solutions including formation water with initial concentration, ratios of 50, 25, 10, 3 % of formation water, and distilled water with and without 5, 10 and 15 % ethanol and methyl ethyl ketone solvents at different temperature. By increasing the concentration of ethanol and methyl ethyl ketone solvents in the binary mixture of water + solvent, the reduction of IFT increases. This decrease in IFT can be due to the structure of these two solvents. The structure of ethanol is a polar hydrophilic (OH) and a non-polar hydrophobic (C<sub>2</sub>H<sub>5</sub>). Ethanol dissolves in water because ethanol and water have hydrogen bonds, the ethanol–water hydrogen bond is placed between the water and weakens the water hydrogen bond, thus reducing surface tension. Methyl ethyl ketone also has a polar and non-polar sections and can act as a co-surfactant in aqueous solutions and be absorbed in the liquid–liquid interface so that this structure can explain the reduction of IFT by methyl ethyl ketone. By increasing the concentration of solvents, the thin layer formed on the interface is strengthened as shown in Fig. 8. In addition, ethanol and methyl ethyl ketone have

lower densities than water and as shown in Fig. 7, the addition of solvents to water causes a smaller density difference between the solution and the oil. According to Eq. (1), IFT is affected by the difference in density of solutions and oils [52,62].

#### 4.1.3. Effect of the salinity on water–oil IFT

Examining different levels of formation water salinity to reduce IFT showed that the change in formation water salinity has little effect on IFT reduction. The lowest IFT was obtained for the mixture of 50 % formation water and 50 % distilled water as shown in Fig. 10. In general, less IFT was observed in higher formation water salinities. The IFT values for the initial concentration of 50, 25, 10, 3 % of formation water and distilled water were obtained 18.11, 17.38, 18.32, 20.32, 22.06 and 25.65 mN/m, respectively. By diluting the formation water, the low concentration of divalent cations (i.e., Ca<sup>2+</sup>, Mg<sup>2+</sup>, and SO<sub>4</sub><sup>2-</sup>) decreases and in this situation, the effect of the salting-out mechanism of high salinity FW has a greater effect on reducing IFT than the salting-in of low salinity FW [77]. The mechanism of salting-out in high salinity water is the phenomenon that organic components are more likely to move in the oil phase because the solubility of polar organic components decreases in the aqueous phase, but the mechanism of salting-in is a phenomenon that is the tendency of organic particles to dissolve in water [5,77]. In pure water, the water molecules form a strong structure on one side of the aqueous phase interface, so that any interface disturbance is low [78]. IFT increase with the decrease of formation water salinity is consistent with the results of Rao et al. [66], and Xu et al. [64].

There is a synergistic effect on IFT reduction when both solvent and soluble ions are present in the solution. As shown in Fig. 8, adsorption of solvents at the water–oil interface creates a layer that can adsorb ions and increase the layer, so the oil–solvent–ion layer is thicker than the oil–ion layer. With increasing salinity, the solubility of solvents in aqueous solution decreases, which leads to an increase in solvent mass transfer from the aqueous phase to the oil phase [52,63]. At high salinity, the activity coefficient of alcohols increases, and the solubility in the aqueous phase decreases, thus increasing the effect of solvents [79]. We

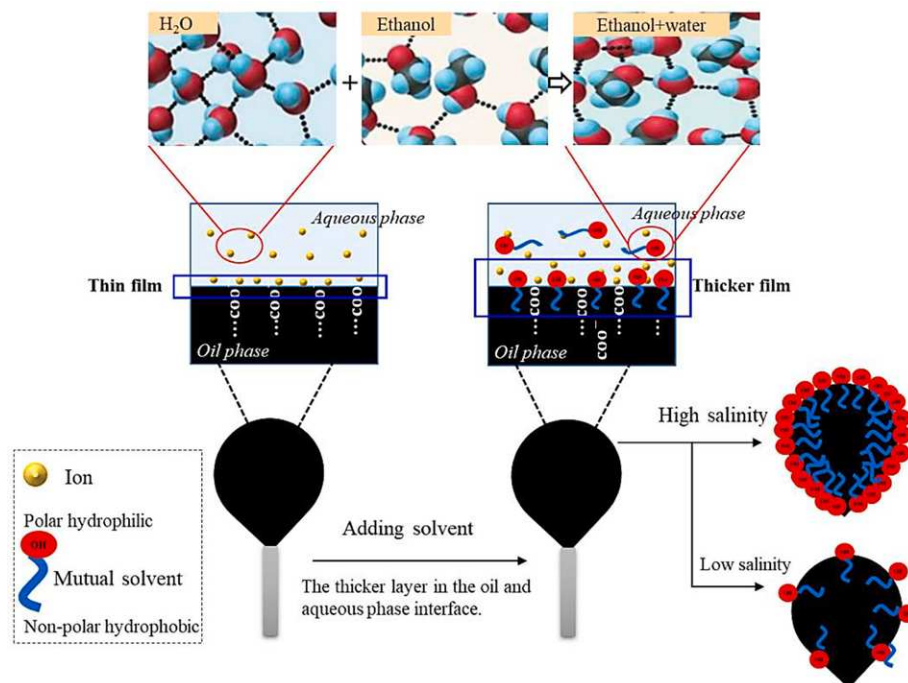


Fig. 8. Schematic of the mechanism reduction of IFT between oil and aqueous phase by mutual solvents.

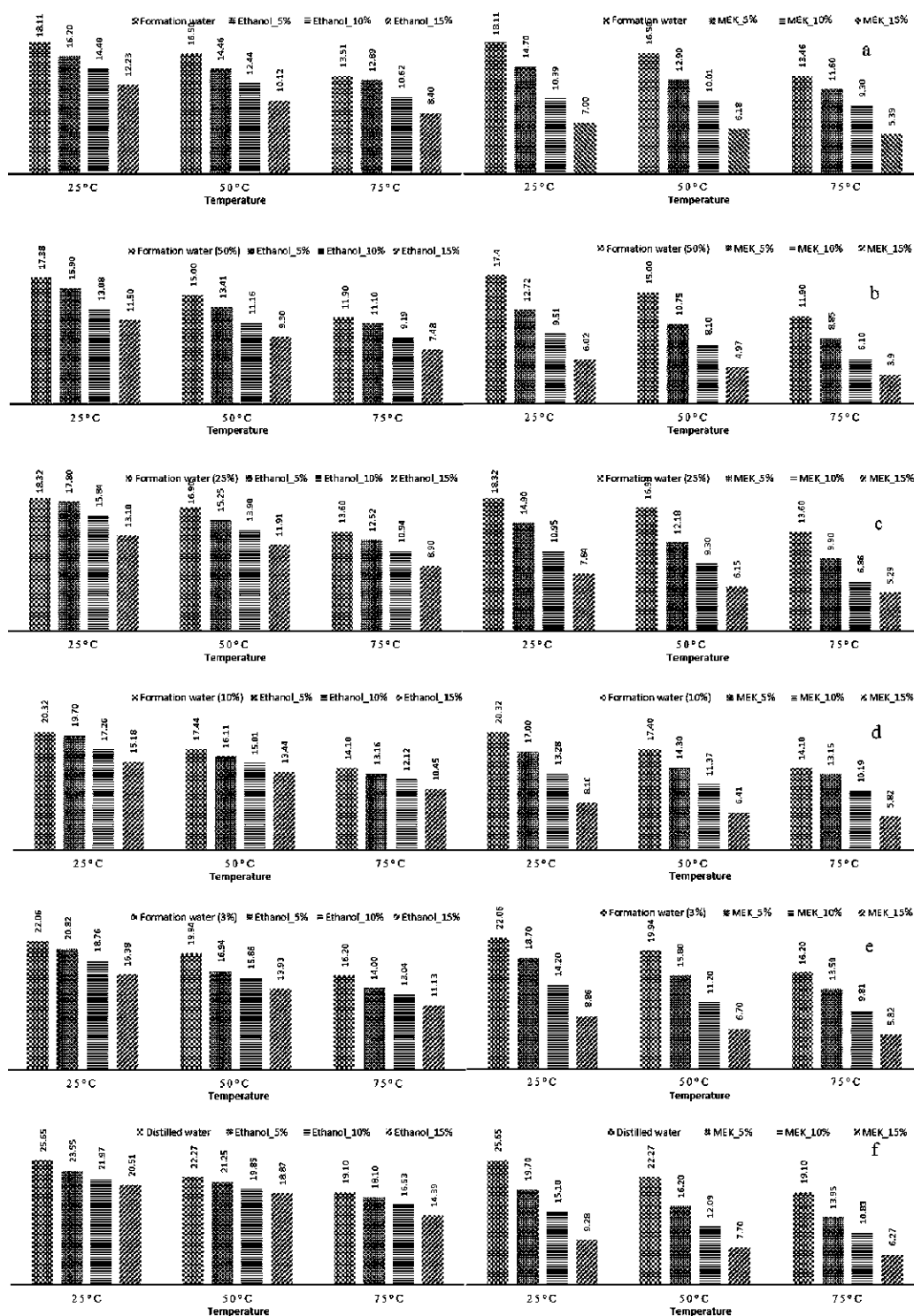


Fig. 9. IFT values of crude-oil/aqueous phase under different conditions of temperature (25, 50 and 75 °C), solvents (ethanol and methyl ethyl ketone (MEK) and water salinity; a) formation water, b) formation water 50 %, c) formation water (25 %), d) formation water (10 %), e) formation water (3 %), and f) distilled water.

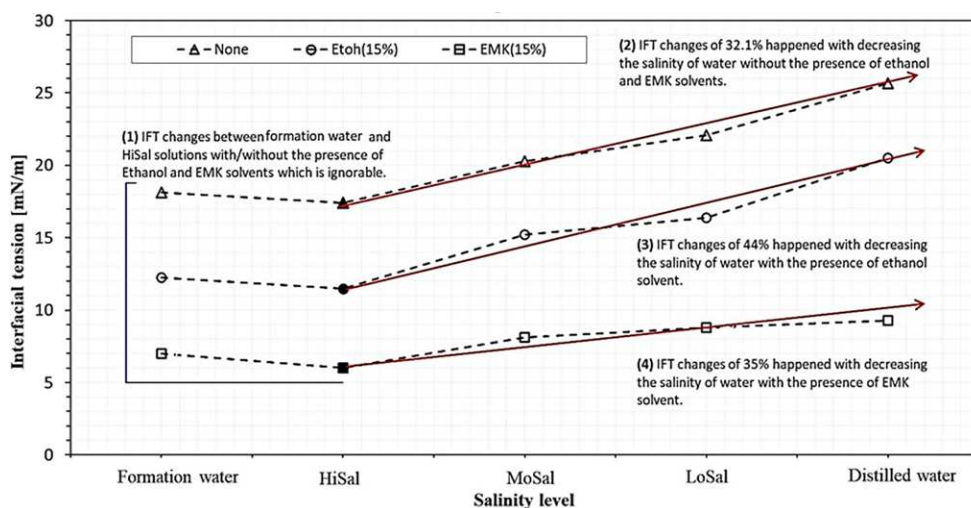


Fig. 10. IFT of crude-oil/solvents systems under the effect of water salinity (formation water, HiSal (formation water 50%), MoSal (formation water 10%), LoSal (formation water 3%) and distilled water).

observed that when 15 % methyl ethyl ketone is added to formation water with initial concentration, a heterogeneous layer is formed on the surface of the solution (in the presence and absence of NCs). Of course, it should be noted that the minimum amount of IFT in the presence and absence of solvents was obtained for 50 % formation water, so IFT in the presence of solvent can depend on the IFT of the base fluid (see Fig. 10). Fig. 11 shows the dynamic graph of IFT for the binary solution of 50 % formation water and 15 % methyl ethyl ketone, which the IFT decreases with increasing test time until reaches a constant equilibrium value. This decrease in IFT over time can be due to the solvent mass transfer from the aqueous phase to the oil phase. According to laboratory observations, methyl ethyl ketone dissolves faster in oil than ethanol, but to some extent, it dissolves in formation water. In other words, the further reduction of IFT by methyl ethyl ketone compared to ethanol could be due to their partitioning coefficient.

Fig. 10 shows a comparison of IFT results for different levels of

salinity in the absence and presence of 15 % of solvents. Various parameters such as brine salinity, type and concentration of ions affect the IFT value between crude oil and brine. Measurements of pH and electrical conductivity were used to evaluate the effects of salinity (Fig. 12a and b). It is clear from the comparison of Figs. 12 and 10, formation water with higher pH reduces IFT to a greater extent and 50 % formation water shows the highest pH and the lowest IFT compared to others in the presence and absence of solvent.

#### 4.1.4. Effect of temperature on water–oil IFT

Comparing the equilibrium IFT graphs at temperature increased from 25 to 75 °C in Fig. 13, shows that with increasing temperature from 25 to 75 °C, IFT decreases in the presence and absence of solvents. In fact, increasing temperature is effective in reducing IFT. This phenomenon can be explained by the fact that increasing temperature, decreases the number of hydrogen bonds formed among water molecules and, the

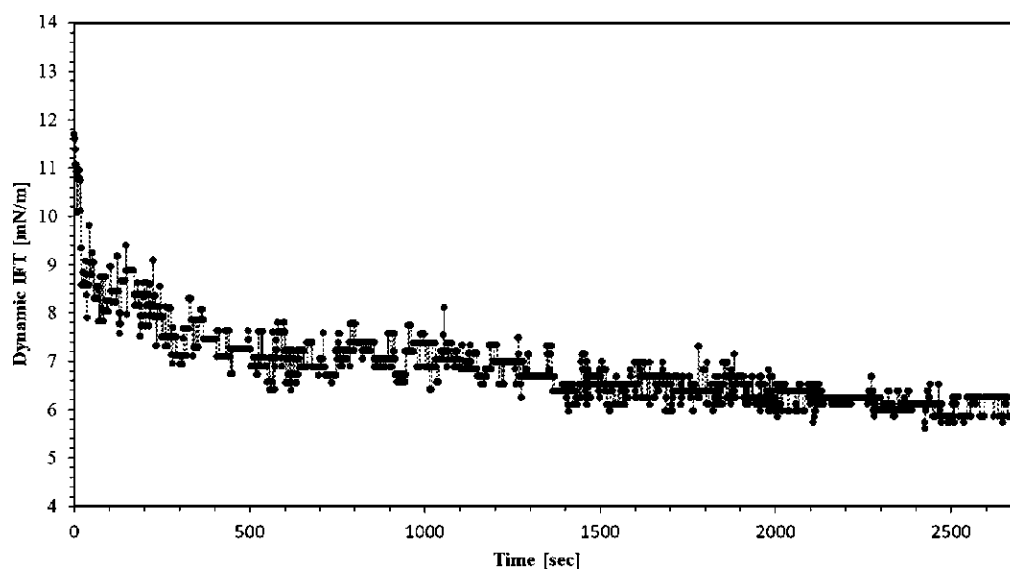


Fig. 11. Dynamic IFT change for binary solution of 50% formation water and 15% methyl ethyl ketone.

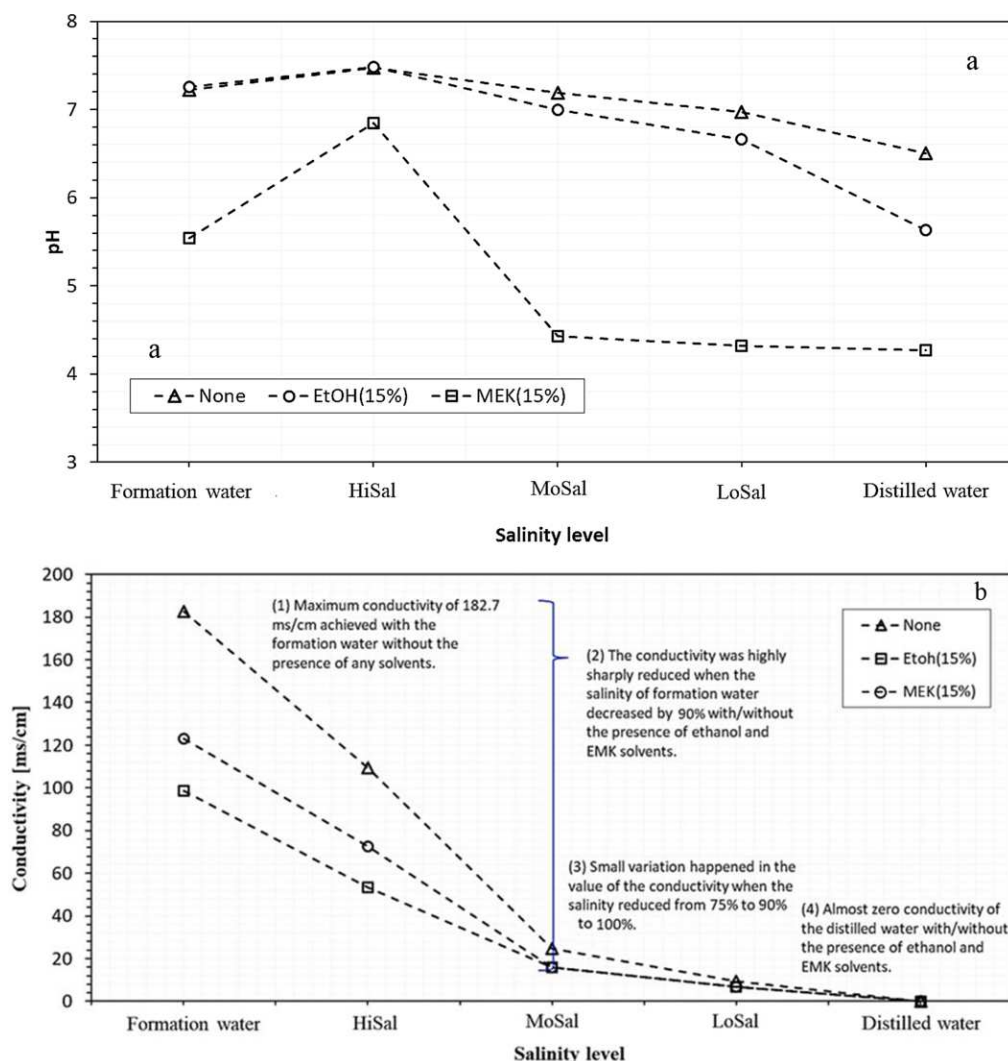


Fig. 12. (a) pH and (b) electrical conductivity graphs for binary solutions of formation water at different salinities/ distilled water and ethanol/ methyl ethyl ketone.

energy required to create a unit area of free water is reduced. Therefore, leading to a decreased IFT. Moreover, at higher temperatures, the miscibility of water and solvent is increased, which helps to further reduce the IFT [80]. It should also be noted that when the temperature is low, the reduction of IFT is not as high as the temperature because the thermal motion of the solvent molecules is much weaker [81].

#### 4.2. SiO<sub>2</sub>/KCl/Xanthan nanocomposites

##### 4.2.1. Density of the nanofluids

As seen in Fig. 14, that when ethanol and methyl ethyl ketone are added to nanofluids, the density decreases as they have a lower density than nanofluids. As the system temperature increases, the density decreases and at all three temperatures of 25, 50 and 75 °C, the density of the solutions decreases with increasing concentration of solvents. It should be noted that by adding nanocomposite to the base fluids, the density increases slightly.

##### 4.2.2. Effect of the synthesized NCs on water–oil IFT

To understand the behavior of IFT reduction by nanofluid and also to

determine the optimum nanofluid concentration, IFT test between crude oil and nanofluid at different concentrations of KCl-SiO<sub>2</sub>-xanthan nanocomposite with formation water, 50 % formation water and distilled water were measured. Fig. 15 illustrates the equilibrium IFT graph for the crude oil in the presence of the KCl-SiO<sub>2</sub>-xanthan nanocomposite in the different base fluids at 25 °C. By adding concentrations of 500, 1000 and 1500 ppm nanocomposite, IFT formation water decreased from 18.11 mN/m to 17.14, 15.40 and 16.93 mN/m. The 50 % formation water IFT value decreased from 17.38 mN/m to 16.44, 14.59 and 16.10 mN/m. Finally, the distilled water IFT value decreased from 25.65 mN/m to 23.52, 19.51 and 21.61 mN/m. Therefore, the concentration of 1000 ppm nanocomposite showed optimum effectiveness for maximum reduction of IFT in base fluids. Li et al. [82] and Dahle et al. [83], explained the general mechanism of IFT reduction by nanomaterials forming a layer at the interface between nano-fluid and crude oil (see Fig. 16). This layer-like structure acts as a mediator between immiscible fluids and, like surfactants, can reduce IFT in the interface between crude oil and fluid [46]. In other words, since the nanoparticles are confined to one surface, they form a thin layer around the crude oil. Therefore, the decrease in IFT between the two liquids is

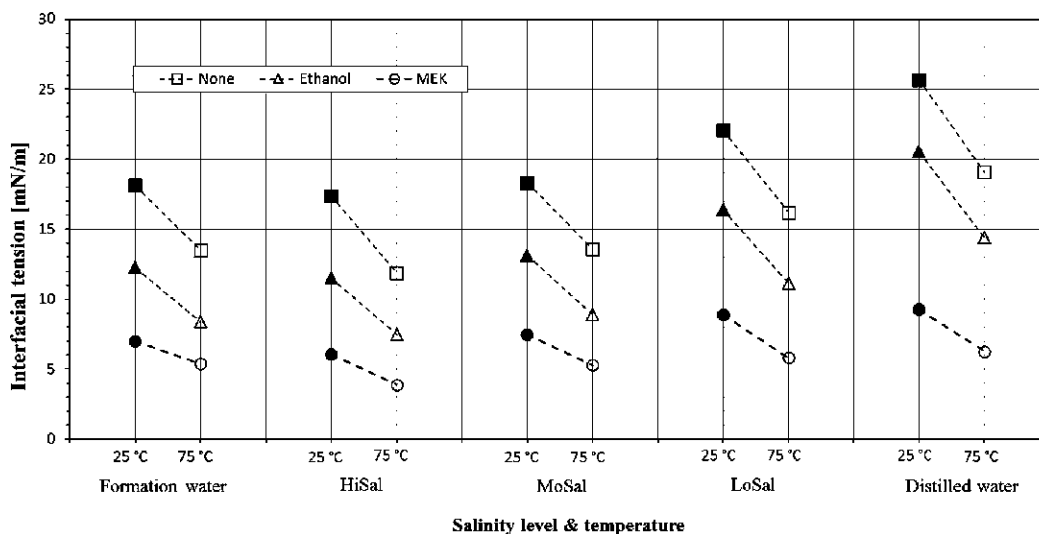


Fig. 13. IFT graphs for binary solutions of formation water at different salinities/distilled water and ethanol/ methyl ethyl ketone at; a) 25 °C, and b) 75 °C.

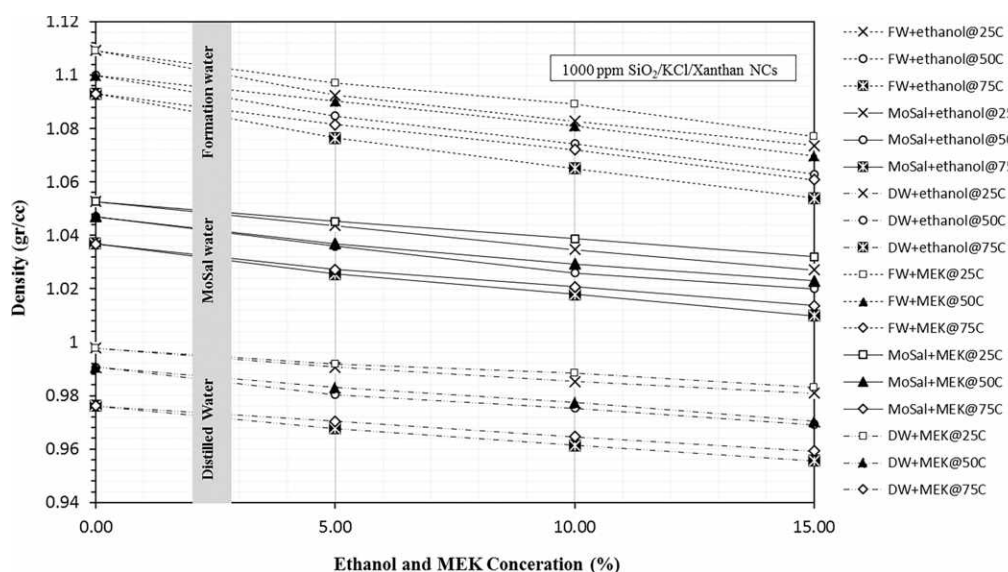


Fig. 14. Density graph for ternary solutions of formation water at different salinities/ distilled water and concentration of 1000 ppm nanocomposite with different concentrations of ethanol/ methyl ethyl ketone at 25, 50 and 75 °C.

due to the increase in entropy, mobility and adsorption of nanoparticles on the surface of crude oil, which leads to an increase in pressure relative to volume (disjoining pressure) [15]. Brownian motion and electrostatic repulsion between nanoparticles lead to this pressure. Factors affecting the strength of this profile include pressure, temperature, particle size and salinity of the base fluid [5,84]. Generally, the lowest IFT value was obtained when 1000 ppm NC was dispersed in 50 % formation water (simultaneous presence of ions and NCs). Although the percentage of reduction of IFT in distilled water is higher than in formation water. With dispersing 1000 ppm KCl-SiO<sub>2</sub>-xanthan NC in formation water, 50 % formation water and distilled water, their IFT decreased by 14.96 %, 16.05 % and 23.94 %, respectively. When both ions and NPs are present in the solution (regardless of the synergistic effect between ions and NPs), repulsive-repulsive interactions between ions and NPs occur. In

the competition between ions and NPs to occupy the interface, eventually, particles with kinetic energy and higher concentrations can be absorbed in the interface [85]. Consequently, ions can reduce the areas that are absorbed by nanoparticles on the interface, and increasing the concentration of ions decreases the absorption of nanoparticles [5]. In another different mechanism that considers interactions between active ions and NPs, ions are absorbed by the NPs as charged particles and are coupled with polar components of crude oil. As a result, ions and nanoparticles form more active particles that reinforce the layer at the interface thus IFT reduction increases (see Fig. 16) [85].

#### 4.2.3. Effect of the synthesized NCs on water–oil IFT with the presence of the mutual solvents

After determining the concentration of 1000 ppm as the optimum

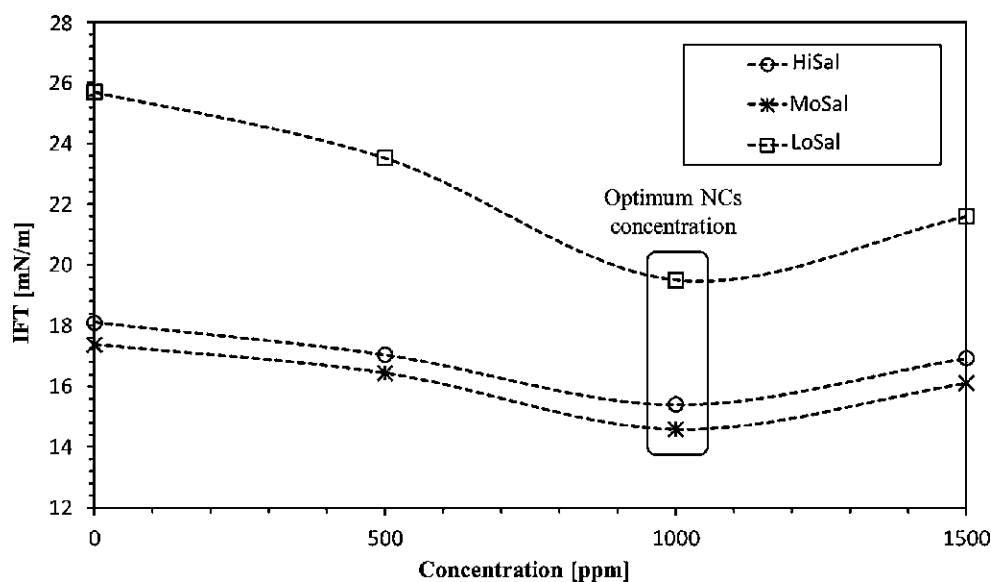


Fig. 15. IFT values measured for the crude oil in the presence of the  $\text{SiO}_2/\text{KCl}/\text{Xanthan}$  NCs in the different base fluids at 25 °C. Schematic of the effect mechanism of synthesized NCs on oil–water IFT.

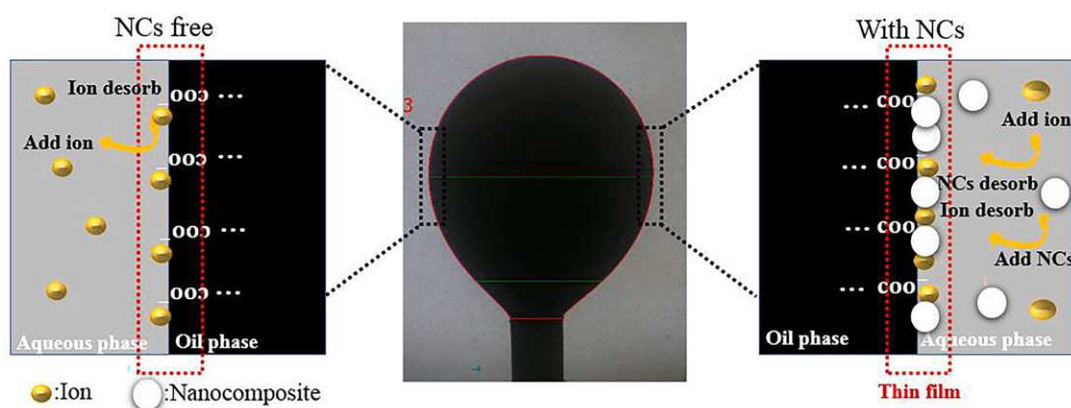


Fig. 16. Schematic of the effect mechanism of ions and NCs on oil–water IFT.

concentration of the synthesized NCs in the base fluids, 5, 10 and 15 % ethanol and methyl ethyl ketone were added to the nanofluids and the effect of solvents on reducing IFT at three temperatures of 25, 50 and 75 °C was investigated. Fig. 17 shows the IFT of the nanofluids prepared from mixing 1000 ppm  $\text{SiO}_2/\text{KCl}/\text{Xanthan}$  NCs within the formation water, 50 % formation water and distilled water in the presence and absence of ethanol and methyl ethyl ketone (MEK) solvents. When solvents are added to the nanofluid, the IFT decreases with increasing solvent concentration. The minimum IFT is 1.51 mN/m obtained for a nanofluid composed of 50 % formation water (MoSal) and 1000 ppm NCs with 15 % methyl ethyl ketone under 75 °C (see Fig. 17c). The reduction in IFT of nanofluids by methyl ethyl ketone is greater than that of ethanol. In previous sections of the study, IFT reduction by solvents and nanocomposite was observed separately.

As is clear, with increasing temperature, IFT decreases which shows that nanocomposites are more effective at higher temperatures (see Fig. 17). This is also in agreement with Manshad et al. [49], who observed a further decrease in IFT by nanocomposites with increasing temperature. The mechanism of IFT reduction by nanocomposite and

solvents has better performance at higher temperatures. In all three NCs concentrations, with increasing solvent concentration, IFT decreased, but the best NCs performance was obtained at 1000 ppm (see Fig. 18). It is noteworthy that with the addition of solvents, the concentration of 1000 ppm has a better performance in reducing IFT and the optimal concentration of nanocomposite in the presence of solvent does not shift to a concentration of 500 or 1500 ppm NCs. Although solvents alone lead to IFT reduction at the interface between phases, the presence of NPs at the interface between oil and solvent/water causes a further decrease. As indicated, IFT decreases with increasing concentration of solvents and nanocomposites (up to 1000 ppm).

Nanocomposites reduce IFT by forming a layer at the interface between water and crude oil [82].  $\text{SiO}_2$  NPs are placed in the interface between two phases and lead to a decrease in IFT (like surfactants) [7]. On the other hand, mutual solvents can act as surfactants in the oil–water interface [52]. Surfactants and nanoparticles exhibit more complex behaviors when they are at the oil–water interface in comparison with when they are alone at the interface. Furthermore, the extra interactions between them can change the IFT [86]. Various studies on the

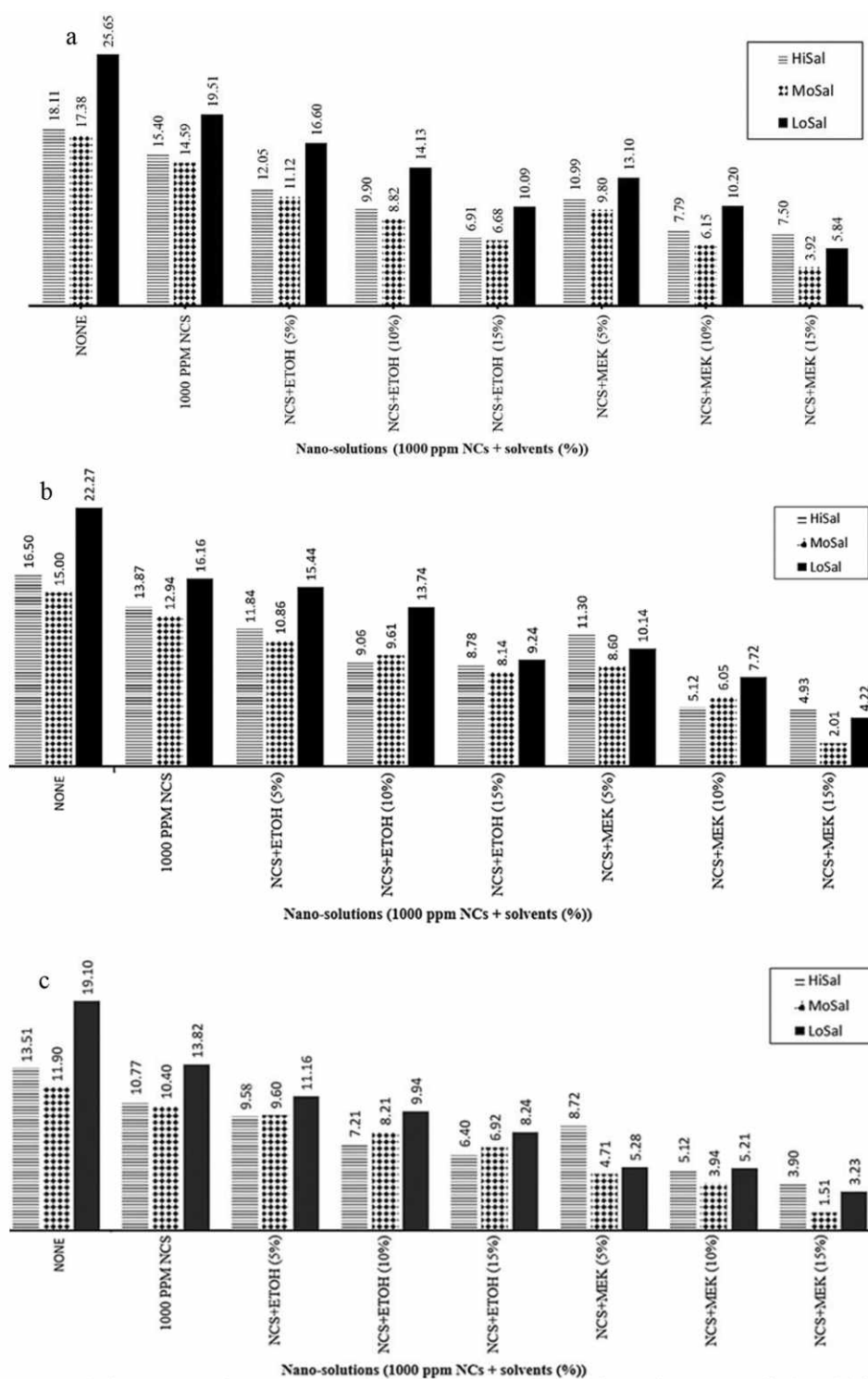


Fig. 17. IFT graph for concentration 1000 ppm of the synthesized NCs with formation water (HiSal), 50 % formation water (MoSal), and distilled water (LoSal) in the presence and absence of different concentrations of ethanol/ methyl ethyl ketone under different temperature ranges of; a) 25 °C, b) 50 °C and c) 75 °C.

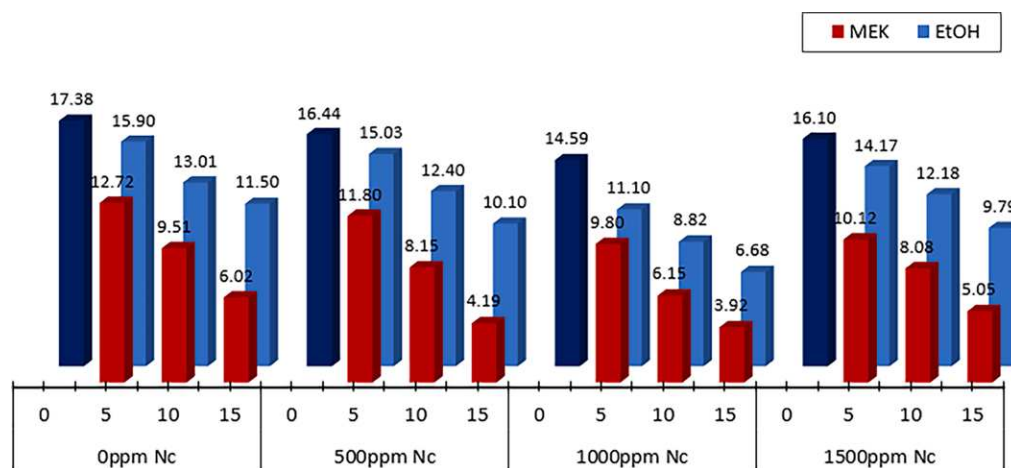


Fig. 18. IFT values of the used solvents (ethanol and methyl ethyl ketone) different concentrations of 5, 10 and 15% within the MoSal water with/without the presence of the synthesized NCs.

combination of surfactants and NPs have reported different effects of increasing or decreasing IFT [3,78,87]. Even in some cases, adding the combination of surfactants and NPs has not changed the IFT value [88]. In other words, the localization of NPs at the interface, which is influenced by the nature of NPs and the interaction between NPs and surfactant molecules, can reduce IFT [86]. Since nanoparticles can reduce the contact area and surfactants can reduce IFT, sufficient adsorption of surface-active agents at the interface causes further reduce IFT [89].

The combination of solvents with nanofluids shows a synergistic effect in reducing IFT, which is superior to when tested separately and activates an extra cooperative. Dispersion of nanoparticles in ethanol was done by Ogolo et al. [90] and Onyekonwu and Ogolo. [91]. Simultaneous use of nanoparticles and ethanol can be an additional advantage for EOR because nanoparticles change the properties of the solvent to a very good surfactant and the IFT is further reduced [91]. Ethanol is more prone to strong covalent bonds with hydrocarbons than nanoparticles in the solution state, which leads to the transforming of the viscous and dense hydrocarbon compound to a lighter form dominated by single hydrogen bonds. As a result, the addition of solvent to the nanofluid due to the molecular chemistry of the solvent can cause covalent bonding and make it possible to mix with the oil. Finally, IFT is reduced to a greater extent, and the oil changes from dead to mobile oil with lower density (see Fig. 19) [92].

In general, the findings showed that each factor (ions, NCs, and

solvents) has a complementary effect in reducing IFT. As mentioned earlier, the mechanism of nanoparticles and mutual solvents in reducing IFT is similar to surfactant molecules, they accumulate on the liquid surface and form a film at the interface [49,62]. Also, ions absorbed in the interface (due to polar components in crude oil) reduce IFT by forming a thin film at the interface [85]. In fact, the synergistic role of ions and NCs with mutual solvents in the aqueous phase has an important effect in reducing IFT due to the evolution of active agents at the interface resulting from the chemical reaction [52,92]. In this case, the further IFT reduction is due to activating an extra cooperative by ions/NCs/solvents interaction at the water–oil interface [52,91].

## 5. Conclusions

In this study, a series of IFT tests were performed to improve oil recovery by smart water, mutual solvent, and nanocomposite in different ranges of salinity and temperature were investigated. In general, ethanol, methyl ethyl ketone and KCl-SiO<sub>2</sub>-xanthan nanocomposite separately showed the ability to reduce IFT, but the combination of these two methods increases IFT reduction. Based on the results:

- The mixture of 50 % formation water and 50 % distilled water showed the lowest IFT and with the increasing dilution of formation water, the relationship was reversed and the IFT increased.

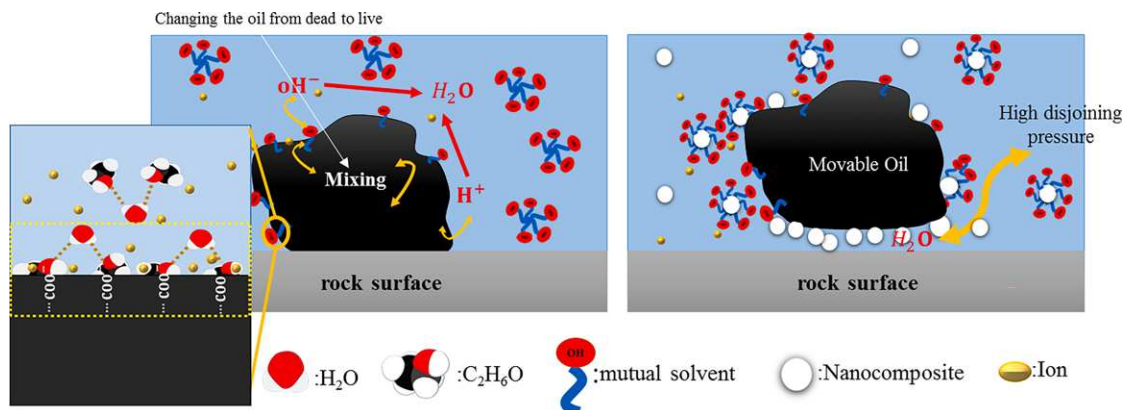


Fig. 19. Schematic of IFT reduction in the presence of nanocomposites and the used solvents.

- IFT decreases with increasing concentration of solvents in the base fluid and methyl ethyl ketone further reduces IFT than ethanol.
- The mutual solvent reduces the IFT at different salinity levels. But in general, in high salinity brine, less IFT was observed by solvents.
- The lowest IFT for the binary solution is 50 % formation water and 15 % methyl ethyl ketone value 6.02 mN/m is obtained as well as temperature increase from 25 °C to 50 and 75 °C, reduced IFT to 4.97 and 3.88 mN/m.
- Optimum NCs concentrations with and without solvents were obtained at a concentration of 1000 ppm.
- The addition of solvents to the nanofluid improves performance. The lowest IFT was obtained for nanofluid in the presence of 15 % by volume of methyl ethyl ketone with 50 % formation water as the base fluid at 75 °C.
- Ethanol, methyl ethyl ketone and the KCl-SiO<sub>2</sub>-xanthan NCs can be suitable candidates for high salinity and high temperature reservoirs where chemical agents in CEOR such as surfactants may not be compatible.

#### CRedit authorship contribution statement

**Fatemeh Motraghi:** Data curation, Formal Analysis, Writing - original draft. **Abbas Khaksar Manshad:** Supervision, Methodology, Writing - review & editing. **Majid Akbari:** Supervision. **Jagar A. Ali:** Writing - review & editing. **S. Mohammad Sajadi:** Writing - review & editing. **Stefan Iglauer:** Writing - review & editing. **Alireza Keshavarz:** Writing - review & editing.

#### Declaration of Competing Interest

The authors declare that they have no known competing financial interests or personal relationships that could have appeared to influence the work reported in this paper.

#### Data availability

Data will be made available on request.

#### References

- [1] Medina OE, Olmos C, Lopera SH, Cortés FB, Franco CA. Nanotechnology applied to thermal enhanced oil recovery processes: a review. *Energies* 2019;12(24):4671. <https://doi.org/10.3390/en12244671>.
- [2] Asl HF, Zargar G, Manshad AK, Takassi MA, Ali JA, Keshavarz A. Experimental investigation into I-Arg and I-Cys eco-friendly surfactants in enhanced oil recovery by considering IFT reduction and wettability alteration. *Pet Sci* 2020;17(1):105–17. <https://doi.org/10.1007/s12182-019-0354-2>.
- [3] Asl FO, Zargar G, Manshad AK, Iglauer S, Keshavarz A. Experimental investigation and simulation for hybrid of nanocomposite and surfactant as EOR process in carbonate oil reservoirs. *Fuel* 2022;319:123591. <https://doi.org/10.1016/j.fuel.2022.123591>.
- [4] Ali JA, Kolo K, Manshad AK, Mohammadi AH. Recent advances in application of nanotechnology in chemical enhanced oil recovery: effects of nanoparticles on wettability alteration, interfacial tension reduction, and flooding. *Egypt J Pet* 2018;27(4):1371–83. <https://doi.org/10.1016/j.ejpe.2018.09.006>.
- [5] Nowrouzi I, Manshad AK, Mohammadi AH. Effects of TiO<sub>2</sub>, MgO, and γ-Al<sub>2</sub>O<sub>3</sub> nano-particles in carbonated water on water-oil interfacial tension (IFT) reduction in chemical enhanced oil recovery (CEOR) process. *J Mol Liq* 2019;292:111348. <https://doi.org/10.1016/j.molliq.2019.111348>.
- [6] Razavirad F, Shahrabadi A, Babakhani Dehkordi P, Rashidi A. Experimental pore-scale study of a novel functionalized iron-carbon nanohybrid for enhanced oil recovery (EOR). *Nanomaterials* 2021;12(1):103. <https://doi.org/10.3390/nano12010103>.
- [7] Davoodi S, Al-Shargabi M, Wood DA, Rukavishnikov VS, Minaev KM. Experimental and field applications of nanotechnology for enhanced oil recovery purposes: a review. *Fuel* 2022;324:124669. <https://doi.org/10.1016/j.fuel.2022.124669>.
- [8] Manshad AK, Olad M, Taghipour SA, Nowrouzi I, Mohammadi AH. Effects of water soluble ions on interfacial tension (IFT) between oil and brine in smart and carbonated smart water injection process in oil reservoirs. *J Mol Liq* 2016;223:987–93. <https://doi.org/10.1016/j.molliq.2016.08.089>.
- [9] Manshad AK, Nowrouzi I, Mohammadi AH. Effects of water soluble ions on wettability alteration and contact angle in smart and carbonated smart water injection process in oil reservoirs. *J Mol Liq* 2017;244:440–52. <https://doi.org/10.1016/j.molliq.2017.09.011>.
- [10] Ali JA, Kolo K, Khaksar Manshad A, Stephen K, Keshavarz A. Modification of LoSal water performance in reducing interfacial tension using green ZnO/SiO<sub>2</sub> nanocomposite coated by xanthan. *Appl Nanosci* 2019;9(3):397–409. <https://doi.org/10.1007/s13204-018-0923-5>.
- [11] Nowrouzi I, Manshad AK, Mohammadi AH. Effects of ions and dissolved carbon dioxide in brine on wettability alteration, contact angle and oil production in smart water and carbonated smart water injection processes in carbonate oil reservoirs. *Fuel* 2019;235:1039–51. <https://doi.org/10.1016/j.fuel.2018.08.067>.
- [12] Sauerer B, Al-Hamad M, Ma SM, Abdallah W. Effect of formation water salinity on interfacial tension of reservoir fluids. *J Pet Sci Eng* 2021;204:108700. <https://doi.org/10.1016/j.petrol.2021.108700>.
- [13] El-Diasty AI, Ragab AM. Applications of nanotechnology in the oil & gas industry: Latest trends worldwide & future challenges in Egypt. *North Africa Technical Conference and Exhibition*. OnePetro; 2013. <https://doi.org/10.2118/164716-MS>.
- [14] Omidi A, Manshad AK, Moradi S, Ali JA, Sajadi SM, Keshavarz A. Smart-and nano-hybrid chemical EOR flooding using Fe<sub>3</sub>O<sub>4</sub>/eggshell nanocomposites. *J Mol Liq* 2020;316:113880. <https://doi.org/10.1016/j.molliq.2020.113880>.
- [15] Nazarahari MJ, Manshad AK, Ali M, Ali JA, Shafiei A, Sajadi SM, et al. Impact of a novel biosynthesized nanocomposite (SiO<sub>2</sub>@ Montmorillonite@ Xanthan) on wettability shift and interfacial tension: Applications for enhanced oil recovery. *Fuel* 2021;210:120773. <https://doi.org/10.1016/j.fuel.2021.120773>.
- [16] Chegenizadeh N, Saeedi A, Xie Q. Application of nanotechnology for enhancing oil recovery—A review. *Petroleum* 2016;2(4):324–33. <https://doi.org/10.1016/j.petlm.2016.10.002>.
- [17] Al-Anssari S, Barifcani A, Keshavarz A, Iglauer S. Impact of nanoparticles on the CO<sub>2</sub>-brine interfacial tension at high pressure and temperature. *J Colloid Interface Sci* 2018;532:136–42. <https://doi.org/10.1016/j.jcis.2018.07.115>.
- [18] Rodriguez Pin E, Roberts M, Yu H, Huh C, Bryant SL. Enhanced migration of surface-treated nanoparticles in sedimentary rocks. *SPE annual technical conference and exhibition*. Society of Petroleum Engineers; 2009. <https://doi.org/10.2118/124418-MS>.
- [19] Emadi S, Shadizadeh SR, Manshad AK, Rahimi AM, Mohammadi AH. Effect of nano silica particles on Interfacial Tension (IFT) and mobility control of natural surfactant (Cedr Extraction) solution in enhanced oil recovery process by nano-surfactant flooding. *J Mol Liq* 2017;248:163–7. <https://doi.org/10.1016/j.molliq.2017.10.031>.
- [20] Roustaei A, Moghadasi J, Iran A, Bagherzadeh H, Shahrabadi A. An experimental investigation of polysilicon nanoparticles' recovery efficiencies through changes in interfacial tension and wettability alteration. *SPE international oilfield nanotechnology conference and exhibition*. OnePetro; 2012. <https://doi.org/10.2118/156976-MS>.
- [21] Karimi A, Fakhroueian Z, Bahramian A, Pour Khiabani N, Darabad JB, Azin R, et al. Wettability alteration in carbonates using zirconium oxide nanofluids: EOR implications. *Energy Fuel* 2012;26(2):1028–36. <https://doi.org/10.1021/ef201475u>.
- [22] Moslan M, Sulaiman WRW, Ismail A, Jaafar M. Applications of aluminium oxide and zirconium oxide nanoparticles in altering dolomite rock wettability using different dispersing medium. *Chem Eng Trans* 2017;56:1339–44. <https://doi.org/10.3303/CET1756224>.
- [23] Mohammadi M, Akbari M, Fakhroueian Z, Bahramian A, Azin R, Arya S. Inhibition of asphaltene precipitation by TiO<sub>2</sub>, SiO<sub>2</sub>, and ZrO<sub>2</sub> nanofluids. *Energy Fuel* 2011;25(7):3150–6. <https://doi.org/10.1021/ef2001635>.
- [24] Taborda EA, Franco CA, Lopera SH, Alvarado V, Cortés FB. Effect of nanoparticles/nanofluids on the rheology of heavy crude oil and its mobility on porous media at reservoir conditions. *Fuel* 2016;184:222–32. <https://doi.org/10.1016/j.fuel.2016.07.013>.
- [25] Mohammadi M, Dadvar M, Dabir B. TiO<sub>2</sub>/SiO<sub>2</sub> nanofluids as novel inhibitors for the stability of asphaltene particles in crude oil: mechanistic understanding, screening, modeling, and optimization. *J Mol Liq* 2017;238:326–40. <https://doi.org/10.1016/j.molliq.2017.05.014>.
- [26] Ehtesabi H, Ahadian MM, Taghikhani V. Enhanced heavy oil recovery using TiO<sub>2</sub> nanoparticles: investigation of deposition during transport in core plug. *Energy Fuel* 2015;29(1):1–8. <https://doi.org/10.1021/ef5015605>.
- [27] Salem Ragab AM, Hannora AE. A Comparative investigation of nano particle effects for improved oil recovery—experimental work. *SPE Kuwait oil and gas show and conference*. Society of Petroleum Engineers; 2015. <https://doi.org/10.2118/175395-MS>.
- [28] Al-Anssari S, Ali M, Alajmi M, Akhondzadeh H, Khaksar Manshad A, Kalantariasi A, et al. Synergistic effect of nanoparticles and polymers on the rheological properties of injection fluids: implications for enhanced oil recovery. *Energy Fuel* 2021;35(7):6125–35.
- [29] Chengara A, Nikolov AD, Wasan DT, Trokhymchuk A, Henderson D. Spreading of nanofluids driven by the structural disjoining pressure gradient. *J Colloid Interface Sci* 2004;280(1):192–201. <https://doi.org/10.1016/j.jcis.2004.07.005>.
- [30] McElfresh P, Olguin C, Ector D. The application of nanoparticle dispersions to remove paraffin and polymer filter cake damage. *SPE International Symposium and Exhibition on Formation Damage Control*. OnePetro; 2012. <https://doi.org/10.2118/151848-MS>.
- [31] Al-Anssari S, Arain Z-U-A, Barifcani A, Keshavarz A, Ali M, Iglauer S. Influence of pressure and temperature on CO<sub>2</sub>-nanofluid interfacial tension: Implication for enhanced oil recovery and carbon geosequestration. *Abu Dhabi International Petroleum Exhibition & Conference*. OnePetro; 2018. <https://doi.org/10.2118/192964-MS>.
- [32] Zamani A, Maini B, Pereira-Almao P. Flow of nanodispersed catalyst particles through porous media: Effect of permeability and temperature. *Can J Chem Eng* 2012;90(2):304–14. <https://doi.org/10.1002/cjce.20629>.

- [33] Skauge T, Hetland S, Spildo K, Skauge A. Nano-sized particles for EOR. *SPE improved oil recovery symposium*. OnePetro; 2010. <https://doi.org/10.2118/129933-MS>.
- [34] Anganaei H, Pourabdollah K, Rostami A. Experimental improvement of nano-enhanced oil recovery using nano-emulsions. *Arab J Sci Eng* 2014;39(8):6453–61. <https://doi.org/10.1007/s13369-014-1258-5>.
- [35] de Castro Dantas TN, de Souza TTC, Neto AAD, de Alencar Moura MCP, de Barros Neto EL. Experimental study of nanofluids applied in EOR processes. *J Surfactant Deterg* 2017;20(5):1095–104. <https://doi.org/10.1007/s11743-017-1992-2>.
- [36] Assef Y, Arab D, Pourafshary P. Application of nanofluid to control fines migration to improve the performance of low salinity water flooding and alkaline flooding. *J Pet Sci Eng* 2014;124:331–40. <https://doi.org/10.1016/j.petrol.2014.09.023>.
- [37] Sadatshojaei E, Jamialahmadi M, Esmailzadeh F, Ghazanfari MH. Effects of low-salinity water coupled with silica nanoparticles on wettability alteration of dolomite at reservoir temperature. *Pet Sci Technol* 2016;34(15):1345–51. <https://doi.org/10.1080/10916466.2016.1204316>.
- [38] Ahmadi MA, Shadizadeh SR. Nano-surfactant flooding in carbonate reservoirs: a mechanistic study. *Eur. Phys. J. Plus* 2017;132(6):1–13. <https://doi.org/10.1140/epjp/i2017-11488-6>.
- [39] Kothari N, Raina B, Chandak K, Iyer V, Mahajan H. Application of ferrofluid for enhanced surfactant flooding in EOR. *SPE EUROPEC/EAGE Annual Conference and Exhibition*. OnePetro; 2010. <https://doi.org/10.2118/131272-MS>.
- [40] Asl HF, Zargar G, Manshad AK, Takassi MA, Ali JA, Keshavarz A. Effect of SiO<sub>2</sub> nanoparticles on the performance of L-Arg and L-Cys surfactants for enhanced oil recovery in carbonate porous media. *J Mol Liq* 2020;300:112290. <https://doi.org/10.1016/j.molliq.2019.112290>.
- [41] Eslahati M, Mehrabianfar P, Isari AA, Bahraminejad H, Manshad AK, Keshavarz A. Experimental investigation of Alfalfa natural surfactant and synergistic effects of Ca<sup>2+</sup>, Mg<sup>2+</sup>, and SO<sub>4</sub><sup>2-</sup> ions for EOR applications: interfacial tension optimization, wettability alteration and imbibition studies. *J Mol Liq* 2020;310:113123. <https://doi.org/10.1016/j.molliq.2020.113123>.
- [42] Khalilnezhad SS, Cheraghian G, Roayaei E, Tabatabaee H, Karambeigi MS. Improving heavy oil recovery in the polymer flooding process by utilizing hydrophilic silica nanoparticles. *Energy Sources Part A* 2017. <https://doi.org/10.1080/15567036.2017.1302521>.
- [43] Cheraghian G. Effect of nano titanium dioxide on heavy oil recovery during polymer flooding. *Pet Sci Technol* 2016;34(7):633–41. <https://doi.org/10.1080/10916466.2016.1156125>.
- [44] Moradi B, Pourafshary P, Jalali F, Mohammadi M, Emadi M. Experimental study of water-based nanofluid alternating gas injection as a novel enhanced oil-recovery method in oil-wet carbonate reservoirs. *J Nat Gas Sci Eng* 2015;27:64–73. <https://doi.org/10.1016/j.jngse.2015.07.009>.
- [45] Yang D, Tontiwachuthikul P, Gu Y. Interfacial tensions of the crude oil+ reservoir brine+ CO<sub>2</sub> systems at pressures up to 31 MPa and temperatures of 27 C and 58 C. *J Chem Eng Data* 2005;50(4):1242–9. <https://doi.org/10.1021/je0500227>.
- [46] Bahraminejad H, Khaksar Manshad A, Riazi M, Ali JA, Sajadi SM, Keshavarz A. CuO/TiO<sub>2</sub>/PAM as a novel introduced hybrid agent for water–oil interfacial tension and wettability optimization in chemical enhanced oil recovery. *Energy Fuel* 2019;33(11):10547–60. <https://doi.org/10.1021/acs.energyfuels.9b02109>.
- [47] Ali J, Manshad AK, Imani I, Sajadi SM, Keshavarz A. Greenly synthesized magnetite@ SiO<sub>2</sub>@ xanthan nanocomposites and its application in enhanced oil recovery: IFT reduction and wettability alteration. *Arab J Sci Eng* 2020;45(9):7751–61. <https://doi.org/10.1007/s13369-020-04377-x>.
- [48] Zargar G, Arabpour T, Khaksar Manshad A, Ali JA, Mohammad Sajadi S, Keshavarz A, et al. Experimental investigation of the effect of green TiO<sub>2</sub>/Quartz nanocomposite on interfacial tension reduction, wettability alteration, and oil recovery improvement. *Fuel* 2020;263:116599. <https://doi.org/10.1016/j.fuel.2019.116599>.
- [49] Manshad AK, Ali JA, Haghighi OM, Sajadi SM, Keshavarz A. Oil recovery aspects of ZnO<sub>2</sub>/SiO<sub>2</sub> nano-clay in the carbonate reservoir. *Fuel* 2022;307:121927. <https://doi.org/10.1016/j.fuel.2021.121927>.
- [50] Jia H, Dai J, Miao L, Wei X, Tang H, Huang P, et al. Potential application of novel amphiphilic Janus-SiO<sub>2</sub> nanoparticles stabilized O/W/O emulsion for enhanced oil recovery. *Colloids Surf A Physicochem Eng Asp* 2021;622:126658. <https://doi.org/10.1016/j.colsurfa.2021.126658>.
- [51] Chahardowli M, Farajzadeh R, Bruining H. Experimental investigation of the use of the dimethyl ether/polymer hybrid as a novel enhanced oil recovery method. *J Ind Eng Chem* 2016;38:50–60. <https://doi.org/10.1016/j.jiec.2016.04.008>.
- [52] Nowrouzi I, Mohammadi AH, Manshad AK. Utilization of methanol and acetone as mutual solvents to reduce interfacial tension (IFT) in enhanced oil recovery process by carbonated smart water injection. *J Mol Liq* 2020;304:112733. <https://doi.org/10.1016/j.molliq.2020.112733>.
- [53] Holm L, Csaszar A. Oil recovery by solvents mutually soluble in oil and water. *Soc Pet Eng J* 1962;2(02):129–44. <https://doi.org/10.2118/117-PA>.
- [54] Chernetsky A, Masalmeh S, Eikmans D, Boerrigter P, Fadili A, Parsons C, et al. A novel enhanced oil recovery technique: experimental results and modelling workflow of the DME enhanced waterflood technology. *Abu Dhabi International Petroleum Exhibition and Conference*. OnePetro; 2015. <https://doi.org/10.2118/177919-MS>.
- [55] Parsons C, Chernetsky A, Eikmans D, Te Riele P, Boersma D, Sersic I, et al. Introducing a novel enhanced oil recovery technology. *IOR 2017-19th European Symposium on Improved Oil Recovery*. 2017. European Association of Geoscientists & Engineers; 2017:1–9. <https://doi.org/10.3997/2214-4609.201700313>.
- [56] Dehaghani AHS, Badizad MH. Experimental study of Iranian heavy crude oil viscosity reduction by diluting with heptane, methanol, toluene, gas condensate and naphtha. *Petroleum* 2016;2(4):415–24. <https://doi.org/10.1016/j.petlm.2016.08.012>.
- [57] Ratnakar RR, Dindoruk B, Wilson L. Experimental investigation of DME–water–crude oil phase behavior and PVT modeling for the application of DME-enhanced waterflooding. *Fuel* 2016;182:188–97. <https://doi.org/10.1016/j.fuel.2016.05.096>.
- [58] Ratnakar R, Dindoruk B, Wilson L. Use of DME as an EOR agent: experimental and modeling study to capture interactions of DME, brine and crudes at reservoir conditions. *SPE Annual Technical Conference and Exhibition*. OnePetro; 2016. <https://doi.org/10.2118/181515-MS>.
- [59] Ratnakar RR, Dindoruk B, Wilson LC. Phase behavior experiments and PVT modeling of DME-brine-crude oil mixtures based on Huron-Vidal mixing rules for EOR applications. *Fluid Phase Equilib* 2017;434:49–62. <https://doi.org/10.1016/j.fluid.2016.11.021>.
- [60] AlZayer A, Sanaei A, Mohanty K, Sepehrmoori K. Experimental and numerical investigation of mutual solvents for EOR applications. *J Pet Sci Eng* 2019;177:224–35. <https://doi.org/10.1016/j.petrol.2019.02.048>.
- [61] Javanmard H, Seyyedi M, Nielsen SM. On oil recovery mechanisms and potential of DME–brine injection in the North Sea chalk oil reservoirs. *Ind Eng Chem Res* 2018;57(46):15898–908. <https://doi.org/10.1021/acs.energyfuels.9b02600>.
- [62] Nowrouzi I, Mohammadi AH, Manshad AK. Effects of methanol and acetone as mutual solvents on wettability alteration of carbonate reservoir rock and imbibition of carbonated seawater. *J Pet Sci Eng* 2020;195:107609. <https://doi.org/10.1016/j.petrol.2020.107609>.
- [63] Nowrouzi I, Mohammadi AH, Manshad AK. Effects of a ketone mutual solvent on the dynamic and equilibrium behaviors of crude oil swelling in enhanced oil recovery process by carbonated seawater flooding. *J Pet Sci Eng* 2021;196:108005. <https://doi.org/10.1016/j.petrol.2020.108005>.
- [64] Xu W. Experimental investigation of dynamic interfacial interactions at reservoir conditions. 2005. [https://digitalcommons.lsu.edu/gradschool\\_theses/968](https://digitalcommons.lsu.edu/gradschool_theses/968).
- [65] Okasha TM, Alshaiwash A. Effect of brine salinity on interfacial tension in Arab-D carbonate reservoir, Saudi Arabia. *SPE Middle East oil and gas show and conference*. OnePetro; 2009. <https://doi.org/10.2118/119600-MS>.
- [66] Vijapurapu CS, Rao DN. Compositional effects of fluids on spreading, adhesion and wettability in porous media. *Colloids Surf A Physicochem Eng Asp* 2004;241(1–3):335–42. <https://doi.org/10.1016/j.colsurfa.2004.04.024>.
- [67] Fan T, Buckley J. Crude Oil IFT Measurements by the Pendant Drop Method. *Semi Annual Report for 2004*;1:04–19.
- [68] Firoozabadi A, Ramey HJ. Surface tension of water-hydrocarbon systems at reservoir conditions. *J Can Pet Technol* 1988;27(03). <https://doi.org/10.2118/88-03-03>.
- [69] Dahkaee KP, Sadeghi MT, Fakhroueian Z, Esmailzadeh P. Effect of NiO/SiO<sub>2</sub> nanofluids on the ultra interfacial tension reduction between heavy oil and aqueous solution and their use for wettability alteration of carbonate rocks. *J Pet Sci Eng* 2019;176:11–26. <https://doi.org/10.1016/j.petrol.2019.01.024>.
- [70] Zargartalebi M, Barati N, Kharat R. Influences of hydrophilic and hydrophobic silica nanoparticles on anionic surfactant properties: Interfacial and adsorption behaviors. *J Pet Sci Eng* 2014;119:36–43. <https://doi.org/10.1016/j.petrol.2014.04.010>.
- [71] Hendraningrat L, Torsæter O. Metal oxide-based nanoparticles: revealing their potential to enhance oil recovery in different wettability systems. *Appl Nanosci* 2015;5(2):181–99. <https://doi.org/10.1007/s13204-014-0305-6>.
- [72] Roustaei A, Saffarzadeh S, Mohammadi M. An evaluation of modified silica nanoparticles' efficiency in enhancing oil recovery of light and intermediate oil reservoirs. *Egypt J Pet* 2013;22(3):427–33. <https://doi.org/10.1016/j.ejpe.2013.06.010>.
- [73] Azarshin S, Moghadasi J, A Aboosadi Z. Surface functionalization of silica nanoparticles to improve the performance of water flooding in oil wet reservoirs. *Energy Exploration & Exploitation* 2017;35(6):685–97. <https://doi.org/10.1177/2F0144598717716281>.
- [74] Ali JA, Hamadamin AB, Ahmed SM, Mahmood BS, Sajadi SM, Manshad AK. Synergistic effect of nano-inhibitive drilling fluid on the shale swelling performance at high temperature and high pressure. *Energy Fuel* 2022;36(4):1996–2006. <https://doi.org/10.1021/acs.energyfuels.1c03804>.
- [75] Ahmadi A, Manshad AK, Ali JA, Iglauer S, Sajadi SM, Keshavarz A, et al. Insight into nano-chemical enhanced oil recovery from carbonate reservoirs using environmentally friendly nanomaterials. *ACS Omega* 2022;7(41):36165–74. <https://doi.org/10.1021/acscomega.2c03076>.
- [76] Drelich J, Fang C, White C. Measurement of interfacial tension in fluid-fluid systems. *Encyclop Surf Colloid Sci* 2002;3:3158–63.
- [77] Esfandiarian A, Maghsoudian A, Shirazi M, Tamsilian Y, Kord S, Sheng JJ. Mechanistic investigation of the synergy of a wide range of salinities and ionic liquids for enhanced oil recovery: fluid–fluid interactions. *Energy Fuel* 2021;35(4):3011–31. <https://doi.org/10.1021/acs.energyfuels.0c03371>.
- [78] Nourinia A, Manshad AK, Shadizadeh SR, Ali JA, Iglauer S, Keshavarz A, et al. Synergistic efficiency of zinc oxide/montmorillonite nanocomposites and a new derived saponin in liquid/liquid/solid interface-included systems: application in nanotechnology-assisted enhanced oil recovery. *ACS Omega* 2022;7(29):24951–72.
- [79] Al Maskari NS, Saeedi A, Xie Q. Alcohol-assisted waterflooding in carbonate reservoirs. *Energy Fuel* 2019;33(11):10651–8. <https://doi.org/10.1021/acs.energyfuels>.
- [80] Jian C, Poopari MR, Liu Q, Zepa N, Zeng H, Tang T. Mechanistic understanding of the effect of temperature and salinity on the water/toluene interfacial tension. *Energy Fuel* 2016;30(12):10228–35. <https://doi.org/10.1021/acs.energyfuels.6b01995>.

- [81] Chen Z, Zhao X. Enhancing heavy-oil recovery by using middle carbon alcohol-enhanced waterflooding, surfactant flooding, and foam flooding. *Energy Fuel* 2015;29(4):2153–61. <https://doi.org/10.1021/ef502652a>.
- [82] Li S, Hendraningrat L, Torsaeter O. Improved oil recovery by hydrophilic silica nanoparticles suspension: 2 phase flow experimental studies. *IPTC 2013: International Petroleum Technology Conference*. European Association of Geoscientists & Engineers; 2013:cp-350-00212. <https://doi.org/10.3997/2214-4609-pdb.350.iptc16707>.
- [83] Dahle G. The effect of nanoparticles on oil/water interfacial tension. Project thesis, NTNU 2013.
- [84] Aveyard R, Binks BP, Clint JH. Emulsions stabilised solely by colloidal particles. *Adv Colloid Interface Sci* 2003;100:503–46. [https://doi.org/10.1016/S0001-8686\(02\)00069-6](https://doi.org/10.1016/S0001-8686(02)00069-6).
- [85] Nowrouzi I, Khaksar Manshad A, Mohammadi AH. Effects of MgO,  $\gamma$ -Al<sub>2</sub>O<sub>3</sub>, and TiO<sub>2</sub> nanoparticles at low concentrations on interfacial tension (IFT), rock wettability, and oil recovery by spontaneous imbibition in the process of smart nanofluid injection into carbonate reservoirs. *ACS Omega* 2022;7(26):22161–72. <https://doi.org/10.1021/acsomega.1c07134>.
- [86] Vu TV, Papavassiliou DV. Synergistic effects of surfactants and heterogeneous nanoparticles at oil-water interface: insights from computations. *J Colloid Interface Sci* 2019;553:50–8. <https://doi.org/10.1016/j.jcis.2019.05.102>.
- [87] Ranatunga RU, Nguyen CT, Wilson BA, Shinoda W, Nielsen SO. Molecular dynamics study of nanoparticles and non-ionic surfactant at an oil–water interface. *Soft Matter* 2011;7(15):6942–52. <https://doi.org/10.1021/jp105355y>.
- [88] Luo M, Dai LL. Molecular dynamics simulations of surfactant and nanoparticle self-assembly at liquid–liquid interfaces. *J Phys Condens Matter* 2007;19(37):375109. <https://doi.org/10.1088/0953-8984/19/37/375109>.
- [89] Xu F, Zhong X, Li Z, Cao W, Yang Y, Liu M. Synergistic Mechanisms Between Nanoparticles and Surfactants: Insight Into NP-Surfactant Interactions. 10. FRONTIERS MEDIA SA AVENUE DU TRIBUNAL FEDERAL 34, LAUSANNE, CH-1015, SWITZERLAND; 2022. <https://doi.org/10.3389/fenrg.2022.913360>.
- [90] Ogolo N, Olafuyi O, Onyekonwu M. Enhanced oil recovery using nanoparticles. *SPE Saudi Arabia section technical symposium and exhibition*. OnePetro; 2012. <https://doi.org/10.2118/160847-MS>.
- [91] Onyekonwu MO, Ogolo NA. Investigating the use of nanoparticles in enhancing oil recovery. *Nigeria Annual international conference and exhibition*. OnePetro; 2010. <https://doi.org/10.2118/140744-MS>.
- [92] Ejeh C, Afgan I, AlMansob H, Brantson E, Fekala J, Odiator M, et al. Computational fluid dynamics for ameliorating oil recovery using silicon-based nanofluids and ethanol in oil-wet reservoirs. *Energy Rep* 2020;6:3023–35. <https://doi.org/10.1016/j.egyrs.2020.10.028>.

